

AD-A055 891 PRATT AND WHITNEY AIRCRAFT GROUP WEST PALM BEACH FL 6--ETC F/G 1/3  
TF30 THIRD-STAGE COMPOSITE FAN BLADE SERVICE PROGRAM. (U)  
MAY 78 D G RANDALL

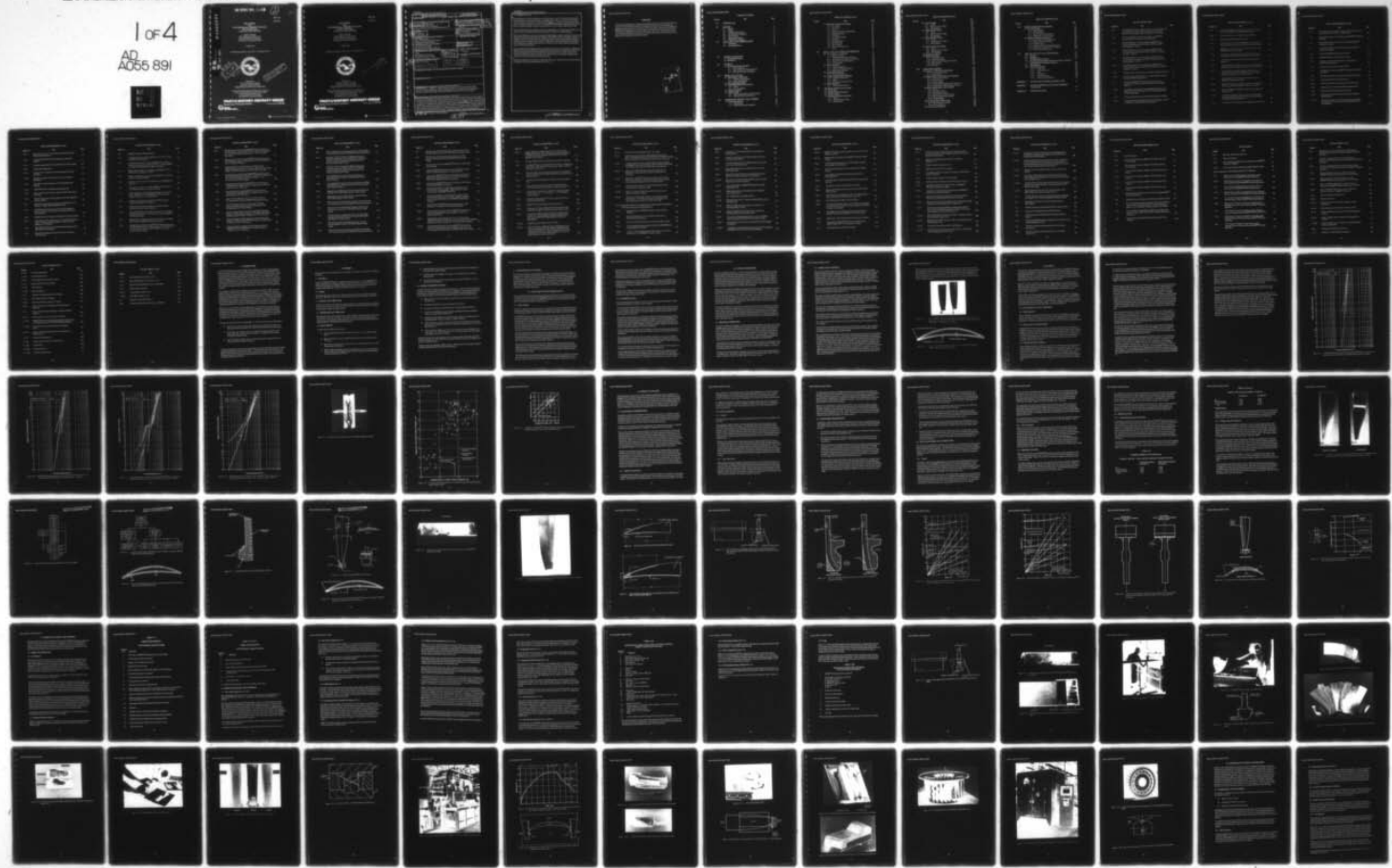
F33657-70-C-0624

NL

UNCLASSIFIED

PWA-5141

1 of 4  
AD  
A055 891



AD No. AD A 055891  
JDC FILE COPY

FOR FURTHER TRAN *JK*

2  
*JK*

PWA-5151

FR-10097

FINAL REPORT  
FOR  
TF30 THIRD-STAGE COMPOSITE FAN BLADE  
SERVICE PROGRAM  
Contract No. F33657-70-C-0624

David G. Randall  
Pratt & Whitney Aircraft Group  
United Technologies Corporation  
East Hartford, Connecticut 06108

15 May 1978

Final Report for Period 1 July 1970 – 31 December 1977



This document has been approved  
for public release and sale; its  
distribution is unlimited.

Prepared for  
Air Force Systems Command  
Aeronautical Systems Division  
Wright-Patterson Air Force Base, Ohio 45433

Air Force Plant Representative Office (OL-AA, Det. 4)  
Air Force Contract Management Division (AFSC)  
Pratt & Whitney Aircraft Group  
East Hartford, Connecticut 06108

**PRATT & WHITNEY AIRCRAFT GROUP**

Government Products Division



P. O. Box 2691  
West Palm Beach, Florida 33402

5



PWA-5151

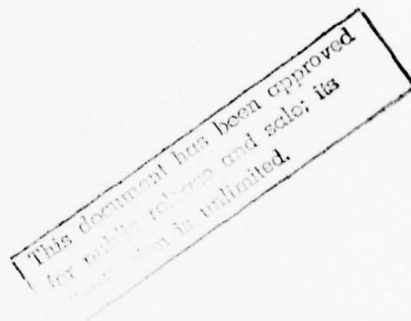
FR-10097

**FINAL REPORT  
FOR  
TF30 THIRD-STAGE COMPOSITE FAN BLADE  
SERVICE PROGRAM  
Contract No. F33657-70-C-0624**

David G. Randall  
Pratt & Whitney Aircraft Group  
United Technologies Corporation  
East Hartford, Connecticut 06108

15 May 1978

Final Report for Period 1 July 1970 – 31 December 1977



Prepared for  
Air Force Systems Command  
Aeronautical Systems Division  
Wright-Patterson Air Force Base, Ohio 45433

Air Force Plant Representative Office (OL-AA, Det. 4)  
Air Force Contract Management Division (AFSC)  
Pratt & Whitney Aircraft Group  
East Hartford, Connecticut 06108

**PRATT & WHITNEY AIRCRAFT GROUP**

Government Products Division



P. O. Box 2691  
West Palm Beach, Florida 33402



Unclassified

SECURITY CLASSIFICATION OF THIS PAGE (When Data Entered)

REPORT DOCUMENTATION PAGE		READ INSTRUCTIONS BEFORE COMPLETING FORM
1. REPORT NUMBER	2. GOVT ACCESSION NO.	3. RECIPIENT'S CATALOG NUMBER
6. TITLE (and Subtitle) Final Report for TF30 Third-Stage Composite Fan Blade Service Program	7. TYPE OF REPORT & PERIOD COVERED Final Technical Report, 1 Jul 1978 - 31 Dec 1979	8. PERFORMING ORG. REPORT NUMBER PWA-5141
9. AUTHOR(s) 10. David G. Randall	11. CONTRACT OR GRANT NUMBER(s) F33657-78-C-0624	12. PROGRAM ELEMENT, PROJECT, TASK AREA & WORK UNIT NUMBERS
13. PERFORMING ORGANIZATION NAME AND ADDRESS Pratt & Whitney Aircraft Division of United Technologies Corporation East Hartford, Connecticut 06108	14. CONTROLLING OFFICE NAME AND ADDRESS Air Force Systems Command Aeronautical Systems Division, ASD/YZI Wright-Patterson Air Force Base, Ohio 45433	15. REPORT DATE 15 May 1978
16. MONITORING AGENCY NAME & ADDRESS (if different from Controlling Office) AFPRO Pratt & Whitney Aircraft Group East Hartford, Connecticut 06108	17. NUMBER OF PAGES 12368 p	18. SECURITY CLASS. (of this report) Unclassified
19. DECLASSIFICATION/DOWNGRADING SCHEDULE	20. DISTRIBUTION STATEMENT (of this Report) PWA-5141 PWA-FR-10897	
21. DISTRIBUTION STATEMENT (of the abstract entered in Block 20, if different from Report) DISTRIBUTION STATEMENT A Approved for public release Distribution Unlimited		
22. SUPPLEMENTARY NOTES		
23. KEY WORDS (Continue on reverse side if necessary and identify by block number) BORSIC® fibers, BORSIC® material; composite material; fan; fan blade; airfoil; blade attachment; blade leading edge; blade trailing edge; blade root; blade tip; disk; foreign object damage; combined stress/fatigue; diffusion bonding/hot pressing; finite element analysis.		
24. ABSTRACT (Continue on reverse side if necessary and identify by block number) The successful application of advanced composites as the structural material for aircraft jet engine rotating parts will significantly reduce engine weight and improve engine performance characteristics. To solve the component design, manufacturing, and quality assurance problems associated with such an application, a program was conducted to design and develop BORSIC®/Aluminum third-stage fan blades, which would operate satisfactorily in the TF30-P-7 or P-9 engine models. Program objectives were to improve the existing design of a composite material fan blade, manufacture the blade, and demonstrate its quality by bench and engine environment testing. The scope of the program required to successfully meet these objectives included establishing design and fabrication procedures.		

Unclassified

SECURITY CLASSIFICATION OF THIS PAGE(When Data Entered)

20. ABSTRACT (Cont'd)

developing special tooling, evaluating current nondestructive inspection techniques and adapting these techniques to composite materials, establishing quality assurance criteria, and developing comprehensive bench and engine environment test programs to adequately demonstrate fan-blade quality. During the program, several sets of BORSIC/Aluminum blades weighing 40 percent less than comparable TF30 bill of material titanium blades were successfully produced and tested.

Based on this extensive test program, and with the establishment of quality control criteria and repair procedures, the blades were deemed acceptable for evaluation in a flight program.

One full set of blades was selected, reinspected to flight quality standards, assembled, balanced and shipped to Edwards Air Force Base for installation in a TF30 P-9 engine. The engine was then installed in an F111-D aircraft, which was in service at Edwards. Over a period of approximately 17 months, this blade set amassed a total of 184.1 flight hours in 90 separate flights. No restrictions were imposed on the flight envelope; however, a periodic 25-hour on-the-wing borescope inspection of the blades was required.

At the completion of this flight evaluation, the blade set was removed and returned to P&WA East Hartford, for a full bench inspection, including both non-destructive and destructive testing. The only blade degradation found by this inspection program was surface cracking of some of the blades in the root area of the airfoil. These cracks were confined to the surface cross-ply layers, and did not extend to the main load-bearing core plies.

During the total program, 246 engine-configuration blades were manufactured and non-destructively inspected; with an overall acceptance rate of 92.3%.

Unclassified

SECURITY CLASSIFICATION OF THIS PAGE(When Data Entered)

**FOREWORD**

This report describes the work performed during the period 1 July 1970 through 31 December 1977 by Pratt & Whitney Aircraft Group, United Technologies Corporation, East Hartford, Connecticut under Contract No. F33657-70-C-0624, as amended by Modification P00005 dated 10 January 1977, with the Air Force Systems Command, Aeronautical Systems Division, Wright-Patterson Air Force Base, Ohio. This report is submitted in compliance with the requirements of Sequence No. A008 of the Contract Data Requirements List, DD Form 1423 attached to the above contract.

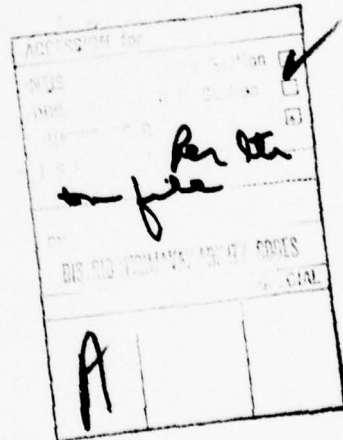


## TABLE OF CONTENTS

Section	Title	Page
1.0	INTRODUCTION	1
2.0	SUMMARY	2
2.1	Material	2
2.2	Design	2
2.3	Tooling and Fabrication	2
2.4	Non Destructive Inspection	2
2.5	Bench Testing	2
2.6	Environment Testing	3
2.7	Flight Service Evaluation	4
3.0	CONCLUSIONS & RECOMMENDATIONS	4
3.1	Conclusions	4
3.2	Recommendations	5
4.0	GENERAL BACKGROUND	6
4.1	Mechanical Properties	6
4.2	Fabrication	7
5.0	MATERIAL	9
5.1	Raw Material Quality Assurance	9
5.1.1	Visual Inspection	9
5.1.2	Fiber Content and Characterization	9
5.1.3	Mechanical Property Evaluation	9
6.0	DESIGN AND ANALYSIS	19
6.1	Blade Design Considerations	19
6.1.1	Vibration Considerations	19
6.1.2	Stress Considerations	20
6.2	Blade Design Methodology	21
6.3	Final Blade Design and Construction	22
6.3.1	Airfoil	22
6.3.2	Root Attachment	23
6.4	Vibration Analyses	23
6.5	Stress Analysis	24
6.5.1	Airfoil Steady Stress and Test Analyses	24
6.5.2	Titanium Dovetail Attachment	25
7.0	FABRICATION, TOOLING, AND EQUIPMENT	41
7.1	Fabrication Processes	41
7.1.1	Development	41
7.1.2	Finalized Fabrication Sequence	41

## TABLE OF CONTENTS (Cont'd)

Section	Title	Page
<b>7.2 Fabrication Tooling and Techniques</b>		43
7.2.1 Ply Cutting		43
7.2.2 Root Blocks		44
7.2.3 Wedge		44
7.2.4 Preforming and Spot Welding Plies		44
7.2.5 Diffusion Bonding		45
7.2.6 Deflashing		46
7.2.7 Leading Edge Plating		46
7.2.8 Shuttling		46
7.2.9 Root Machining		46
7.2.10 Tip Machining		48
7.2.11 Heat Treating		48
7.2.12 Dimensional Inspection		48
7.2.13 Disk		49
<b>8.0 NONDESTRUCTIVE TESTING AND INSPECTION</b>		67
<b>8.1 Methodology of Development</b>		67
8.1.1 Defect Detection		67
8.1.2 Radiographic Detection of Defects		68
8.1.3 Acoustic Emission Detection of Defects		68
8.1.4 Elastic Property Determination		68
8.1.5 Test Specimens		68
<b>8.2 Defect Detection</b>		69
8.2.1 Ultrasonic Methods		69
8.2.2 Advanced Ultrasonic Methods		70
8.2.3 Miscellaneous Methods		70
<b>8.3 Radiographic Inspection</b>		70
8.3.1 Film Enhancement		71
<b>8.4 Acoustic Emission Defect Detection</b>		72
8.4.1 Tensile Test Specimens		72
8.4.2 Blades		72
8.4.3 Monitoring Equipment Used		73
<b>8.5 Elastic Properties</b>		73
8.5.1 Modulus Determination		73
<b>9.0 MATERIAL SERVICE EVALUATION</b>		79
<b>9.1 Test Program</b>		79
<b>9.2 Specimen Damage Procedures</b>		80
<b>9.3 Test Procedures</b>		87
<b>9.4 Undamaged Specimens (Base Line)</b>		89
9.4.1 Tensiles		89
9.4.2 High Frequency Fatigue		91
9.4.3 Metallography		94

## TABLE OF CONTENTS (Cont'd)

Section	Title	Page
9.5	<b>Erosion Damage</b>	103
9.5.1	Tensile	103
9.5.2	High Frequency Fatigue	103
9.5.3	Metallography	106
9.6	<b>Ballistic Impact Damage</b>	110
9.6.1	Tensile	110
9.6.2	High Frequency Fatigue	111
9.6.3	Metallography	117
9.7	<b>Thermal Fatigue Damage</b>	122
9.7.1	Tensile	122
9.7.2	High Frequency Fatigue	122
9.7.3	Metallography	125
9.8	<b>Salt Stress-Corrosion Damage</b>	129
9.8.1	Tensile	129
9.8.2	High Frequency Fatigue	129
9.8.3	Metallography	133
9.9	<b>Discussion of Results</b>	133
9.10	<b>Repair Technology</b>	138
9.10.1	Repair Procedures	138
9.10.2	Tensile Test Results	139
9.10.3	High Frequency Fatigue Test Results	147
9.10.4	Metallography	152
9.10.5	Summary	158
10.0	<b>BLADE BENCH TESTING</b>	159
10.1	<b>Summary of Blade Bench Test Results</b>	159
10.1.1	Environmental Testing	159
10.1.2	Stress Testing	160
10.2	<b>Environmental Tests, Results, and Conclusions</b>	160
10.2.1	Salt Corrosion Testing	160
10.2.2	Thermal Shock	162
10.2.3	Erosion Testing	163
10.2.4	Foreign Object Damage (gravel, rivets, etc.)	164
10.2.5	Foreign Object Damage (massive objects)	166
10.3	<b>Stress Testing, Results, and Conclusions</b>	168
10.3.1	Untwist	168
10.3.2	Static Stress Survey	169
10.3.3	Spin-Pit Burst Testing	170
10.3.4	High Frequency Fatigue Testing	174
10.3.5	Internal Damping Investigation	177
10.3.6	Tip Rub Testing	178
10.4	<b>Combined Stress Fatigue Testing</b>	179
10.4.1	Methodology and Results	180
10.4.2	Recommendation	180
10.5	<b>Goodman Type Diagrams</b>	182

## TABLE OF CONTENTS (Cont'd)

Section	Title	Page
<b>11.0</b>	<b>ENGINE ENVIRONMENTAL TESTING</b>	229
<b>11.1</b>	<b>Sea Level Testing</b>	229
11.1.1	Engine Buildup	230
11.1.2	Instrumentation	231
11.1.3	Test Program and Engine Run	233
11.1.4	"Piggyback" Sea Level Testing	246
<b>11.2</b>	<b>Supersonic/Altitude Test Program</b>	248
11.2.1	Engine X-433-26 Build Summary	252
11.2.2	Altitude Endurance Testing	255
11.2.3	Test Procedures	261
11.2.4	Vibratory Stress and Temperature Survey	262
11.2.5	Destructive Examination of Test Blade	268
11.2.6	Nondestructive Inspection	270
<b>12.0</b>	<b>AIRCRAFT FLIGHT EVALUATION PROGRAM</b>	292
<b>12.1</b>	<b>Summary</b>	292
<b>12.2</b>	<b>Introduction</b>	292
<b>12.3</b>	<b>Pre-Flight Quality Assurance</b>	292
<b>12.4</b>	<b>Field Inspection Procedures and Rework Limits for TF30-P-9</b>	
3rd Stage Borsic®/Aluminum Fan Rotor		298
<b>12.5</b>	<b>Flight Program</b>	301
<b>12.6</b>	<b>Post Flight Inspection</b>	301
12.6.1	Weight Loss	301
12.6.2	Visual Inspection	302
12.6.3	X-Ray	303
12.6.4	Dimensional	303
12.6.5	Natural Frequency	303
12.6.6	Destructive Examination	303
<b>APPENDIX A</b>	<b>BLADE MANUFACTURING LEARNING CURVE</b>	A-1
<b>APPENDIX B</b>	<b>QUALITY CONTROL PLAN FOR TF30 COMPOSITE FAN BLADES</b>	B-1
<b>APPENDIX C</b>	<b>PROGRAM REVIEWS</b>	C-1

## LIST OF ILLUSTRATIONS

Figure No.	Title	Page
4.2-1	These BORSIC®/Aluminum Blades Show the Complex Shape That Can Be Fabricated From Composite Materials; Left, Finished – Machined Root and Blade; Right, Unfinished Root and Blade	8
4.2-2	The Core and Shell Construction Selected for the BORSIC®/Aluminum Blades Fabricated Under This Program	8
5.1-1	Weibull Distribution of Tensile Strength of BORSIC® Fiber Extracted From Monolayer Tape Which Yielded Acceptable Panel Strength (> 140 ksi)	12
5.1-2	Weibull Distribution of Tensile Strength of BORSIC® Fiber Extracted From Composite Panel Which Exhibited Acceptable Strength (> 140 ksi)	13
5.1-3	Weibull Distribution of Tensile Strength of BORSIC® Fiber Extracted From Monolayer Tape Which Yielded Unacceptable Panel Strength (< 140 ksi)	14
5.1-4	Weibull Distribution of Tensile Strength of BORSIC® Fiber Extracted From Composite Panel Which Exhibited Unacceptable Strength (< 140 ksi)	15
5.1-5	Monolayer Tape Tensile Specimen and Gripping Alignment Fixture	16
5.1-6	In General, Panel Strengths Were Less Than One-Half of the Tape Strength of Higher Strength Tapes	17
5.1-7	Correlation of BORSIC®/Aluminum Monolayer Tape and Composite Panel Tensile Strength for Union Carbide Supplied Material	18
6.0-1	Comparison of Shroudless TF30-P-9 BORSIC®/Aluminum Fan Blade Designed and Fabricated Under This Program With B/M Titanium Alloy Blade	26
6.1-1	Typical Logic Network Used in Designing Composite Fan Blades	27
6.1-2	Computerized Techniques Developed by Pratt & Whitney Aircraft to Optimize Composite Blade Structural Design	28

## LIST OF ILLUSTRATIONS (Cont'd)

Figure No.	Title	Page
6.1-3	Core and Shell Blade Design as Shown in This Cross Section is Used to Meet Stiffness and Strength Requirements	28
6.1-4	Typical Finite Element of a Blade Attachment Design	29
6.2-1	Typical Composite Blade Design Concept	30
6.3-1	Cross Section View of TF30-P-9 BORSIC®/Aluminum Third-Stage Fan Blade Designed and Fabricated Under This Program	30
6.3-2	Relative Sizes of the 44 Plies Used in the Construction of the BORSIC®/Aluminum Fan Blade	31
6.3-3	Composite Fan Blade Showing Nickel-Cobalt Leading Edge Protection Extending From Tip to Within One-Inch of Root	32
6.3-4	Cross Section View Showing Nickel-Cobalt Leading Edge Protection	33
6.3-5	Alternate Design of Leading Edge Protection; This Design Was Not Pursued Because of High Cost and Fabrication Difficulty	33
6.3-6	The Low-Wedge, Small-Splay Radius, Titanium Dovetail Attachment Selected for the BORSIC®/Aluminum Blades Designed and Fabricated Under This Program	34
6.3-7	The Candidate Dovetail Geometries Considered for the BORSIC®/Aluminum Fan Blades	35
6.4-1	Resonance Diagram and Measured Frequencies of BORSIC®/Aluminum Third-Stage Fan Blade at Room Temperature	36
6.4-2	Resonance Diagram of BORSIC®/Aluminum Third-Stage Fan Blade at 450°F	37
6.4-3	Comparison of Disk Rim Thickness Needed for Blades With Titanium FOD Protection With Thickness Needed for Blades With Nickel-Cobalt FOD Protection	38
6.5-1	Cross Section View Showing Point of Maximum Shell Stress (A)	39

## LIST OF ILLUSTRATIONS (Cont'd)

Figure No.	Title	Page
6.5-2	Plot of Maximum and Average Interlaminar Shear Stresses in the Cross-Ply Layers as a Function of Splay Radius	40
7.1-1	Titanium Root Blocks Used in Design of the BORSIC®/Aluminum Fan Blades	50
7.2-1	Roll-Cutting Templates for TF30-P-9 Third-Stage BORSIC®/Aluminum Fan Blade	51
7.2-2	Roll-Cutting Sandwich for TF30-P-9 Third-Stage BORSIC®/Aluminum Fan Blade	51
7.2-3	Roll-Cutting BORSIC®/Aluminum Ply Shapes	52
7.2-4	BORSIC®/Aluminum Plies After Roll-Cutting	53
7.2-5	Schematic of Numeric Keller Cutting Tool Showing the Modified Head and Shank	53
7.2-6	Ring Section Used to Form a Simple Wedge	54
7.2-7	Plies Required to Fabricate BORSIC®/Aluminum Third-Stage Fan Blade	54
7.2-8	Preforming Tool Used to Assemble the Plies Into Blade Form	55
7.2-9	Spotwelding the Plies in the Preform Tool	56
7.2-10	Three Packages of Plies are Produced to Form Each Blade	57
7.2-11	Cross-Section View of the Blade Diffusion Bonding Tool	58
7.2-12	Preforming Tool With Ply Package in Position	59
7.2-13	The Vacuum Retort/Press Facilities Used in the Diffusion Bonding Process	60
7.2-14	The Heat and Cooling Cycles Which Comprise the Diffusion Bonding Process; The Total Cycle Required Between Nine- and Ten-Hours	60

## LIST OF ILLUSTRATIONS (Cont'd)

Figure No.	Title	Page
7.2-15	Schematic View of the "Flash" Which was Formed During the Diffusion Bonding Process	61
7.2-16	Composite Blade With Nickel-Cobalt Plating Tool Partially Installed	61
7.2-17	Composite Blade With Nickel-Cobalt Plating Tool Fully Installed	62
7.2-18	Nickel-Cobalt Plating Tank	62
7.2-19	Schematic View of Shuttle Used to Position Blades for Final Machining	63
7.2-20	The Blade Lock Slots Were Produced by Electro-Discharge Machining	63
7.2-21	The Blade Lock Was Produced by Conventional Machining Methods	64
7.2-22	Slotted Rack Used to Hold Blades During Heat Treat	65
7.2-23	Electric Heat Treat Oven Used to Apply the 800°F Stress Relief Heat Treat	66
7.2-24	TF30-P-9 Third-Stage Fan Disk Adapted for Use With BORSIC®/ Aluminum Blades	66
8.2-1	Ultrasonic C-Scan Inspection of Bulk of Airfoil With 0.25 Inch Diameter, 1.0 MHz, Sperry Wheel Search Units	75
8.2-2	Areas Near Edges of Airfoil and Just Above Root Platform Inspected Using 0.25 Inch Diameter Transducers With Lucite Shoes Attached	76
8.2-3	Modified Fixture for Ultrasonic C-Scanning of Composite Airfoils	77
8.2-4	Root Sections Ultrasonically Inspected by Through-Transmission Using $\frac{1}{2}$ " Diameter Transmitter With $\frac{1}{4}$ " Diameter Receiver Masked to $1/32$ " Diameter	77
8.4-1	Blade Deflection Rig and Acoustic Monitoring Equipment With Blade Mounted for Inspection	78
8.5-1	Equipment for Measuring Ultrasonic Velocity in Composite Panel Specimens	78

## LIST OF ILLUSTRATIONS (Cont'd)

Figure No.	Title	Page
9.1-1	BORSIC® Damage Evaluation Program	79
9.2-1	Composite Specimen Configuration Showing Location of Erosion and Ballistic Impact Damage	80
9.2-2	Typical Erosion Effect on 20-Layer BORSICAL® Test Panels of a Nine-Second Exposure to 0.14 g/sec Flow at 27-Micron Alumina in 60 Psig Air at an Impingement Angle at 20 Degrees	81
9.2-3	Ballistic Impact Damage on a Unidirectional BORSICAL® Test Panel Specimen, SAR-B s/A-3A/u-H2	82
9.2-4	Ballistic Impact Damage on a Component BORSICAL® Test Panel Specimen, SAR-Bs/A-7B/B-H3	83
9.2-5	Ultrasonic C-Scan Traces of Typical Ballistic Impact BORSICAL® Specimens	84
9.2-6	Typical Corrosive Effect on 20-Layer BORSICAL® Test Panels of a 100-Hour Exposure to a Humid Salt Spray	85
9.2-7	Surface Appearance of Unidirectional Component, and Cross-Ply (Left to Right, Respectively) BORSICAL® Specimens After 100-Hour Salt Stress - Corrosion Exposure	86
9.3-1	Equipment and Specimen Arrangement for High Frequency Fatigue Testing at Room Temperature	87
9.3-2	Equipment and Specimen Arrangement for High Frequency Fatigue Testing at Elevated Temperature	88
9.4-1	Effect of High Frequency Fatigue Exposure on the 70°F Tensile Strength of Undamaged 50 Volume-Percent 20-Layer BORSIC®/Aluminum Specimens	91
9.4-2	High Frequency Fatigue Test Results for Undamaged 50 Volume-Percent 20-Layer BORSIC®/Aluminum Specimens	94
9.4-3	Microstructure of Unidirectional BORSIC®/Aluminum Specimens That Were High Frequency Fatigue Tested at 70°F and 2450 $\mu$ in./in. for 10 <sup>7</sup> Cycles (1C/u-H2 at Left) and 2900 $\mu$ in./in. for 10 <sup>6</sup> Cycles (2D/u-H3 at Right)	95

## LIST OF ILLUSTRATIONS (Cont'd)

Figure No.	Title	Page
9.4-4	Microstructure of Unidirectional BORSIC®/Aluminum Specimens That Were High Frequency Fatigue Tested at 70°F and 3100 $\mu$ in./in. for 2 x 10 <sup>6</sup> Cycles (2E/u-H2 at Left) and 3 x 10 <sup>6</sup> Cycles (1D/u-H4 at Right)	96
9.4-5	Microstructure of Unidirectional BORSIC®/Aluminum Specimens That Were High Frequency Fatigue Tested at 70°F and 3100 $\mu$ in./in. for 5 x 10 <sup>6</sup> Cycles (1E/u-H3)	97
9.4-6	Surface Appearance and Microstructure of Unidirectional BORSIC®/Aluminum Specimens That Were High Frequency Fatigue Tested at 450°F and 2180 $\mu$ in./in. for 10 <sup>6</sup> Cycles (11F/u-H1)	99
9.4-7	Microstructure of Unidirectional BORSIC®/Aluminum Specimens That Were High Frequency Fatigue Tested at 450°F and 2100 $\mu$ in./in. for 5 x 10 <sup>6</sup> Cycles (3D/u-H3 at Left) and 2200 $\mu$ in./in. for 2 x 10 <sup>6</sup> Cycles (11E/u-H3 at Right)	100
9.4-8	Microstructure of Component BORSIC®/Aluminum Specimen (7F/B-H4) That Was High Frequency Fatigue Tested at 450°F and 1755 $\mu$ in./in. for 2 x 10 <sup>6</sup> Cycles	101
9.4-9	Microstructure of Cross-Ply BORSIC®/Aluminum Specimen (12D/C-H4) That Was High Frequency Fatigue Tested at 450°F and 1265 $\mu$ in./in. for 10 <sup>7</sup> Cycles	102
9.5-1	Effect of Erosion Damage on the 70°F Tensile Strength of 50 Volume-Percent 20-Layer BORSIC®/Aluminum Specimens	103
9.5-2	Typical Unidirectional Erosion Test Specimen Following Erosion and High Frequency Fatigue Testing Showing Lack of Delamination in the Eroded Region	107
9.5-3	Surface of Deeply Eroded Unidirectional BORSIC®/Aluminum Specimen (3E/u-H3) Before (Left) and After (Right) 450°F High Frequency Fatigue Testing at 2100 $\mu$ in./in. for 5 x 10 <sup>6</sup> Cycles.	108
9.5-4	Surface Appearance and Microstructure of Eroded Component Specimen (7A/B-H2) After 450°F High Frequency Fatigue Testing at 1575 $\mu$ in./in. for 5 x 10 <sup>6</sup> Cycles	109
9.5-5	Surface Appearance of Deeply Eroded Component Specimen (4D/B-H4) After 450°F High Frequency Fatigue Testing at 1710 $\mu$ in./in. for 5 x 10 <sup>6</sup> Cycles	110

## LIST OF ILLUSTRATIONS (Cont'd)

Figure No.	Title	Page
9.6-1	Effect of Ballistic Impact Damage on the 70°F Tensile Strength of 50 Volume-Percent 20-Layer BORSIC®/Aluminum Specimens	111
9.6-2	Ultrasonic C-Scan Test Results for Ballistically Impacted Unidirectional Specimen (3A/u-H2) Before and After High Frequency Fatigue Testing Showing Delamination That Occurred During Fatigue Testing	115
9.6-3	Ultrasonic C-Scan Test Results for Ballistically Impacted Component Specimen (7B/B-H4) Before and After High Frequency Fatigue Testing Showing Delamination That Occurred During Fatigue Testing	116
9.6-4	Typical Ballistically Impacted Unidirectional Specimen After High Frequency Fatigue Testing Showing Extensive Matrix Cracking	118
9.6-5	Typical Ballistically Impacted Component Specimen (7B/B-H4) After High Frequency Fatigue Testing at 450°F Showing Only Limited Matrix Cracking	119
9.6-6	Microstructure at Ballistically Impacted Component Specimen (7D/B-H2) After 450°F High Frequency Fatigue Testing	120
9.6-7	Ballistically Impacted Cross-Ply Specimen (9E/C-H4) After 450°F High Frequency Fatigue Testing	121
9.7-1	Effect of Thermal Fatigue Damage on the 70°F Tensile Strength of 50 Volume-Percent 20-Layer BORSIC®/Aluminum Specimens	122
9.7-2	Microstructure of Thermal Fatigue Damaged Unidirectional Specimen (11A/u-H2) After 70°F High Frequency Fatigue Testing	126
9.7-3	Surface Appearance and Microstructure of Thermal Fatigue Damaged Unidirectional Specimen (11D/u-H2) After 450°F High Frequency Fatigue Testing	127
9.7-4	Microstructure of Thermal Fatigue Damaged Component Specimen (8B/B-H1) After 450°F High Frequency Fatigue Testing	128
9.8-1	Effect of Salt-Corrosion Damage on the 70°F Tensile Strength of 50 Volume-Percent 20-Layer BORSIC®/Aluminum Specimens	130

## LIST OF ILLUSTRATIONS (Cont'd)

Figure No.	Title	Page
9.8-2	Microstructure of Salt Stress-Corrosion Damaged Unidirectional Specimen (6B/u-H2) After 70°F High Frequency Fatigue Testing	134
9.8-3	Microstructure of Salt Stress-Corrosion Damaged Cross-Ply Specimen (12D/C-H1) After 450°F High Frequency Fatigue Testing	135
9.10-1	Impacted Area of 20-Layer BORSIC®/Aluminum Test Specimens Prior to Repair	140
9.10-2	Impacted BORSIC®/Aluminum 20-Layer Test Specimens After Removal of Damaged Material by Leaching With HCl	141
9.10-3	Twenty-Layer BORSIC®/Aluminum Test Specimen as Repaired With Aluminum/Silicone Resin (Left), and After 100 Hours at 500°F in Air. Slight Discoloration is Apparent	145
9.10-4	Twenty-Layer BORSIC®/Aluminum Test Specimen After Repair With Polyimide/Graphite Composite	146
9.10-5	Summary of the Effect of Various Repair Techniques on the 70° and 450°F Tensile Strength of Ballistic-Impact Damaged 50 Volume-Percent BORSIC®/Aluminum	147
-6	Summary of the Effect of Various Repair Techniques on the 70° and 450°F High Frequency Fatigue Capability of Ballistic-Impact Damaged 50 Volume-Percent BORSIC®/Aluminum ns Specimens	152
9.10-7	Typical 20-Layer BORSIC®/Aluminum Test Specimens After Testing in the As-Impacted Condition Without Repair	153
9.10-8	Typical Unidirectional (0°) 20-Layer BORSIC®/Aluminum Test Specimen as Repaired With Aluminum/Silicone (Top Left), and as Tensile Tested	154
9.10-9	Typical Component Configuration ( $\pm 45^\circ$ , $0^\circ$ , $\pm 45^\circ$ ), 20-Layer BORSIC®/Aluminum Test Specimen as Repaired With Aluminum/Silicone (upper Left), and After Tensile Test. No Leaching Prior to Repair.	155
9.10-10	Typical Unidirectional (0°) 20-Layer BORSIC®/Aluminum Test Specimen as Repaired With Aluminum/Silicone and After Tensile Test. Damaged Area Removed by Leaching With HCl Prior to Repair.	156

## LIST OF ILLUSTRATIONS (Cont'd)

Figure No.	Title	Page
9.10-11	Typical Component Configuration ( $\pm 45^\circ$ , $0^\circ$ , $\pm 45^\circ$ ) 20-Layer BORSICAL® Test Specimen as Repaired With Aluminum/Silicone and After Tensile Test. Damaged Area Removed by Leaching With HC1 Prior to Repair.	157
10.1-1	Goodman Diagram for Room Temperature and 450°F Conditions	183
10.2-1	The BORSIC®/Aluminum Blade Showed No Evidence of Significant Salt Corrosion After An Elevated Temperature (500°F), 100-Hour Salt-Stress-Corrosion Test	184
10.2-2	Inspection Showed No Discernable Degradation of the BORSIC®/Aluminum Blades After a 100-Hour Salt-Stress-Corrosion Test Under Humid Conditions	185
10.2-3	Fluidized Bed Thermal Fatigue Test Rig Used for Thermal Shock Tests	186
10.2-4	Nickel/Cobalt Leading Edge of Blade S-20 After 80 Thermal Cycles Showing Crack Caused by Pit in Leading Edge; Mag = 7X	187
10.2-5	Concave Side of Composite Fan Blade D-17 Showing Condition After FOD Spin Test. N = 10,360 rpm, T = 70°F, FOD With 75 grams of Sand	188
10.2-6	Particulate Erosion Rig Used For Static Testing at Both Room and Elevated Temperatures	189
10.2-7	BORSIC®/Aluminum Blades Following Erosion Tests	190
10.2-8	Comparison of Composite Blades With Nickel-Cobalt Leading Edge Protection; Blade on Right Has Increased Protected Area	191
10.2-9	Comparison of Blades Subjected to High-Temperature Static Erosion Test: Composite Blade With Nickel-Cobalt Leading Edge (Left); Titanium TF30 Bill-of-Material Third-Stage Blade (Right)	192
10.2-10	Small Object Static Ballistic Impact Test Rig	193
10.2-11	Post-Test Condition of Ballistic Impacted Fan Blades; (A) Unprotected Composite Blade, (B) Composite Blade With Hard Nickel Leading Edge; (C) Composite Blade With Nickel-Cobalt Leading Edge, (D) TF30-6-4 Titanium Blade; (E) Composite Blade With Boron Carbide Leading Edge	194

## LIST OF ILLUSTRATIONS (Cont'd)

Figure No.	Title	Page
10.2-12	Small Object Dynamic Ballistic Impact Test Facility	195
10.2-13	Comparison of Concave Sides of Bill-of-Material Titanium Fan Blades and BORSIC®/Aluminum Fan Blades After 66 Strikes per Blade With $\frac{1}{4}$ Inch Quartz Gravel at Room Temperature and 10,360 rpm	196
10.2-14	Comparison of Concave Sides of Bill-of-Materials Titanium Blades and BORSIC®/Aluminum Fan Blades After 66 Strikes Per Blade With $\frac{1}{4}$ Inch Quartz Gravel at Room Temperature and 10,360 rpm	197
10.2-15	Appearance of Bill-of-Material Titanium Fan Blade After 23 Strikes With $\frac{1}{2}$ -Gram Steel Rivet at Room Temperature and 10,360 rpm	198
10.2-16	Appearance of BORSIC®/Aluminum Fan Blade After 23 Strikes With $\frac{1}{2}$ -Gram Steel Rivet at Room Temperature and 10,360 rpm. Lost Material Was About Twice That of Titanium Blade	199
10.2-17	Damage Sustained by Blade E-216 After Being Impacted With a Single One-Inch Tempered Ice Ball	200
10.2-18	Blade E-227 Sustained This Damage After Three Impacts of One-Inch Tempered Ice Balls	201
10.2-19	The Effect of Leading Edge Thickness on FOD Blade at Right Had 0.025-Inch L.E. Radius and Sustained Only Slight Dents When Impacted by Six One-Inch Tempered Ice Balls	202
10.2-20	Single Blade FOD Tests - Multiple Impact Drop Mechanism Configuration. (A) Object Drop Mechanism, (B) Wind Screen	203
10.2-21	Damage Sustained by BORSIC®/Aluminum Blade in Massive FOD Test	204
10.3-1	Spin-Pit Test Rig Used to Conduct Blade Untwist Tests at Engine Operating Conditions	205
10.3-2	Location of Proximity Probes Used to Determine Blade Untwist	206
10.3-3	Experimentally Determined Angle of Untwist for BORSIC®/Aluminum Fan Blade D-2 at 450°F	207
10.3-4	Location of Strain Gages Used to Conduct Test One of the Static Stress Survey on the BORSIC®/Aluminum Blades	208

## LIST OF ILLUSTRATIONS (Cont'd)

Figure No.	Title	Page
10.3-5	Comparison of Actual and Predicted P/A and Restrained Warping Stresses	209
10.3-6	Location of Strain Gages on the Blade Airfoil for Test Two of the Static Stress Survey	210
10.3-7	Location of Strain Gages in the Blade Platform Area for Test Two of the Static Stress Survey	211
10.3-8	Strain Gage Instrumentation on Disk for Test Two of the Static Stress Survey	212
10.3-9	Elastic Strain Gage Data From Vacuum Spin Pit Testing of Blade E-92 at Room Temperature and 10,000 rpm	213
10.3-10	Blade R-10, an Early Development Blade Survived a Spin-Pit Proof Test in Excellent Condition	214
10.3-11	Typical Failure Mode of BORSIC®/Aluminum Fan Blade During Burst Tests	214
10.3-12	E-Blade Root Sections Following Burst Test, Arranged in Order of Burst Speed	215
10.3-13	Plot of Burst Speed Versus Blade Density	216
10.3-14	Damping/Fatigue Test of Composite Fan Blade With Leading Edge Protection	216
10.3-15	Results of High Frequency Fatigue Test Conducted on Undamaged Blades at 450°F	217
10.3-16	Results of High Frequency Fatigue Tests Conducted on Undamaged Blades at Room Temperature	217
10.3-17	A Five Percent First Bending Frequency Loss at $\pm 18,500$ psi at Room Temperature Was Selected as a Failure Criterion	218
10.3-18	Instrumentation Locations For Conducting the Internal Damping Investigation	218
10.3-19	Comparison of the Damping Log Decrement Versus Tip Amplitude of BORSIC®/Aluminum and Titanium B/M Blades	219

## LIST OF ILLUSTRATIONS (Cont'd)

Figure No.	Title	Page
10.3-20	BORSIC®/Aluminum Airfoil Temperature as a Function of Tip Amplitude and Span	220
10.3-21	Bending Fatigue Testing Increased BORSIC®/Aluminum Blade Damping	221
10.4-1	E-Services Blade With Aluminum Tip Pads Diffusion Bonded to the Airfoil for CSF Testing	222
10.4-2	Blade Gripping Technique Used for Combined Stress Fatigue Testing	223
10.4-3	Static Radial Load Required to Duplicate Blade Stress at Operating Speeds	223
10.4-4	Composite Blade Root Block Holding Fixture Showing Heating Elements	224
10.4-5	Test Rig for Combined Stress Application to Blades	224
10.4-6	Approximate Instrumentation Locations for Combined Stress/Fatigue Testing	225
10.4-7	Ideal Chordwise Stress Distribution Just Above Blade Platform; Areas Above and Below the Neutral Axis are Equal	226
10.4-8	Strain Distribution on Blade E-166 in CSF Rig	227
10.5-1	Data From Spit-Pit Burst Fatigue, and Combined Stress/Fatigue Tests Were Used to Generate the Room Temperature and 450°F Goodmap Type Diagrams	228
11.0-1	The Vehicle for Conducting Engine Environmental Tests on BORSIC®/Aluminum Fan Blades Was a TF30-P-9 Engine	273
11.0-2	Blade Set No. 2 Used in the Supersonic/Altitude Test Program	274
11.1-1	Comparison of the BORSIC®/Aluminum TF30-P-9 Third-Stage Fan Blade With the B/M Titanium Fan Blade	275
11.1-2	Pratt & Whitney Aircraft TF30-P-9 Engine	276

## LIST OF ILLUSTRATIONS (Cont'd)

Figure No.	Title	Page
11.1-3	Schematic Showing Location and Type of Strain-Gage Instrumentation on Second- and Third-Stage Fan Blades for Sea-Level Engine Environment Test	276
11.1-4	Schedule for 100-Hour Subsonic Engine Test Program (Blade Set No. 1)	277
11.1-5	TF30-P-9 Six-Hour Endurance Cycle	277
11.2-1	Flight Envelope of the F-111A Aircraft	278
11.2-2	The 200-Hour Supersonic Altitude Test Program in Which Blade Set No. 2 Was Used	279
11.2-3	TF30-P-9 Engine Installed in X-210 Test Stand	279
11.2-4	0.090-Inch Deep Tip Rub Area on TF30-P-9 Engine Fan Case	280
11.2-5	Installation of Strain-Gage Instrumentation on BORSIC®/Aluminum Third-Stage Fan Blades	281
11.2-6	Installation of Thermocouple Instrumentation on BORSIC®/Aluminum Third-Stage Fan Blades	282
11.2-7	Data From the Preliminary Stress Survey Yielded the Data for These Plots of Representative Stress Versus Fan Speed	283
11.2-8	Maximum Vibratory Stresses Which Occurred at Significant Engine Operating Conditions During Altitude Stress Survey	284
11.2-9	The Schedule for Running Military and Maximum Endurance Tests. This Schedule Was Subsequently Changed to Encompass Approximately 10.5-Hours at Military Power	285
11.2-10	The Cycle Schedule for Conducting the Mn 2.2 Endurance Portion of the Supersonic/Altitude Tests	286
11.2-11	Damaged Area at Blade Tip Convex Side, Due to Rubbing Contact With Compressor Case	287
11.2-12	Location of Crack at Concave Side of Airfoil Root	288
11.2-13	Close-Up View of Crack at Concave Side of Root. Crack Extends Around Leading Edge to Convex Side.	288

## LIST OF ILLUSTRATIONS (Cont'd)

Figure No.	Title	Page
11.2-14	Vertical Plane Cross-Sectional View Shows the Misalignment of Root Blocks at Upstream End of Blade as Well as Deformation of Plies Just Above Root Blocks	289
11.2-15	Nominal Dimensions of Sections Examined by Microexamination and Leaching/Crossply Removal; Dashed Lines Represent the Extent of Damage Due to Overstressing at the Blade Root; Shaded Area Indicates Probable Damage in Microsection	289
11.2-16	Correlation of Crack Length and Fiber Layer on Concave Side of Blade	290
11.2-17	Convex Side of Blade With Surface Aluminum Layer Removed Shows Relatively Little Damage (Arrow) and Damage Was Limited to First Crossply Layer	290
11.2-18	Fractured Fibers in First Crossply of Concave Side After Leaching and Removing Leading Edge Piece; Damage Was More Extensive Than on Convex Side	291
11.2-19	First Longitudinal Fiber Layer on Concave Side Shows Only Slight Damage Above Plane of Dominant Crack	291
12-1	TF30-P-9 3rd Rotor Assembly as Received at Edwards AFB Prior to Installation F111-D Aircraft (BORSIC®/Aluminum Blades)	308
12-2	Bill-of-Material TF30-P-9 3rd Rotor Assembly (Titanium Alloy Blades)	309
12-3	TF30-P-9 2nd Stator Assembly With Borescope Inspection Port	310
12-4	Areas Used to Establish Damage and Rework Limits	311
12-5	TF30 Composite Fan Flight Program (Cumulative Hours by Month)	312
12-6	TF30-P-9 BORSIC®/Aluminum Fan Blades After 184-Hr. F111-D Flight Program (Rear View)	313
12-7	TF30-P-9 3rd Rotor After Removal From F111-D Aircraft (Rear View)	314
12-8	TF30-P-9 3rd Rotor After Removal From F111-D Aircraft (Front View)	315

## LIST OF ILLUSTRATIONS (Cont'd)

Figure No.	Title	Page
12-9	Root Deformation	316
12-10	Concave (Pressure) Surface of Blade E-169 as Removed From F111-D Aircraft	317
12-11	Convex (Suction) Surface of Blade E-169 as Removal From F111-D Aircraft	317
12-12	Concave (Pressure) Surface of Blade E-169 with 2nd Ply Layer Exposed	318
12-13	Convex (Suction) Surface of Blade E-169 with 2nd Ply Layer Exposed	318
12-14	Concave (Pressure) Surface of Blade E-169 with 7th Ply Layer Exposed	319
12-15	Convex (Suction) Surface of Blade E-169 with 7th Ply Layer Exposed	319
A-1	Manufacturing Learning Curve for TF30-P-9 3rd Stage BORSIC®/ Aluminum Fan Blades	A-1
B-1	Modified Fixture for Ultrasonic C-Scanning of Composite Airfoils	B-8
B-2	Root Sections Ultrasonically Inspected by Through-Transmission Using $\frac{1}{2}$ " Diameter Transmitter With $\frac{1}{4}$ " Diameter Receiver Masked to $1/32$ " Diameter. Operating Frequency is 5.0 MHZ.	B-8
B-3	Areas Near Blade Leading Edge, Trailing Edge, and Adjacent to Root Are Inspected With This Ultrasonic Through Transmission Equipment	B-9
B-4	Example of Root Bond Defect Readily Detected By C-Scan Inspection	B-10

## LIST OF TABLES

Number	Title	Page
6.5-I	Maximum Airfoil Static Stress (psi)	24
7.1-I	Fabrication Sequence	42
7.2-II	Process for Plating Nickel/Cobalt Leading Edges on BORSIC®/Aluminum Fan Blades	47
7.2-III	Processing Information Recorded on Blade Operation Sheets	49
8.5-I	Comparison of Young's Modulus Data for 0° Orientation	74
9.4-I	Base-Line 70°F Tensile Results for Undamaged 20-Layer 50 Percent-Volume BORSIC®/Aluminum Specimens	90
9.4-II	High Frequency Fatigue Test Results for Undamaged 20-Layer 50 Percent-Volume BORSIC®/Aluminum Specimens	92
9.5-I	70°F Tensile Test Results for Erosion Damaged 20-Layer 50 Percent-Volume BORSIC®/Aluminum Specimens	104
9.5-II	High Frequency Fatigue Test Results For Erosion Damaged 20-Layer 50 Percent-Volume BORSIC®/Aluminum Specimens	105
9.6-I	70°F Tensile Test Results For Ballistic Impact Damaged 20-Layer 50 Percent-Volume BORSIC®/Aluminum Specimens	112
9.6-II	High Frequency Fatigue Test Results For Ballistic Impact Damaged 20-Layer 50 Percent-Volume BORSIC®/Aluminum Specimens	113
9.7-I	70°F Tensile Test Results For Thermal Fatigue Damaged 20-Layer 50 Percent-Volume BORSIC®/Aluminum Specimens	123
9.7-II	High Frequency Fatigue Test Results For Thermal Fatigue Damaged 20-Layer 50 Percent-Volume BORSIC®/Aluminum Specimens	124
9.8-I	70°F Tensile Test Results For Salt Stress-Corrosion Damaged 20-Layer 50 Percent-Volume BORSIC®/Aluminum Specimens	131

## LIST OF TABLES (Cont'd)

Number	Title	Page
9.8-II	High Frequency Fatigue Test Results For Salt-Corrosion Damaged 20-Layer 50 Percent-Volume BORSIC®/Aluminum Specimens	132
9.9-I	Summary of Damaged Effects on 70°F Tensile Test Properties of 20-Layer 50 Percent-Volume BORSIC®/Aluminum Specimens	136
9.9-II	Summary of Damaged Effects on High Frequency Fatigue Properties of 20-Layer 50 Percent-Volume BORSIC®/Aluminum Specimens	137
9.10-I	Tensile Test Results for 20-Layer 50 Percent-Volume BORSIC®/Aluminum Specimens Before and After Repair	142
9.10-II	HFF Test Results for 20-Layer 50 Percent-Volume BORSIC®/Aluminum Specimens Before and After Repair	148
10.2-I	Effect of 100-Hour Humid Salt Corrosion on Natural Frequencies of BORSIC®/Aluminum Blades S-36 and S-43	161
10.2-II	Effect of 2000 Thermal Cycles (-65°F to 5000°F) on Natural Frequencies of BORSIC®/Aluminum	163
10.3-I	Maximum Airfoil Static Stress (psi)	169
10.3-II	Blade R-10 Spin Test	170
10.3-III	Burst Performance of Stress Relieved Blades at Room Temperature	172
10.3-IV	Burst Performance of Stress Relieved Blades at 450°F	173
10.3-V	Results of High Frequency Fatigue Test Undamaged Blades at 450°F	175
10.3-VI	Results of High Frequency Fatigue Test Damaged Blades at 450°F	176
10.3-VII	Results of High Frequency Fatigue Test Undamaged Blades at Room Temperature	177
10.4-I	Combined Stress/Fatigue Test Results	181
11.1-I	Deviations to TF30-P-9 B/M Configuration	230

## LIST OF TABLES (Cont'd)

Number	Title	Page
11.1-II	TF30 CIP Engine Blades	232
11.1-III	TF30 CIP Blade Set #1	242
11.1-IV	TF30 CIP Blade Set #1 Frequency Shift	243
11.1-V	Blade Set #1 Post Test Airfoil Data	244
11.1-VI	X-Ray Results	246
11.1-VII	Natural Frequencies	247
11.2-I	Summary of Supersonic Engine Test Program	249
11.2-II	TF30 Altitude Engine Test Blades	251
11.2-III	Blades Installed After Tip Rub at 57 Hours	253
11.2-IV	Strain Gage Summary Third-Stage Fan Blade Simulated Flight Test	255
11.2-V	Thermocouple Summary Third-Stage Fan Blade Simulated Flight Test	256
11.2-VI	Maximum Stresses at Sea Level Static Conditions	257
11.2-VII	BORSIC®/Aluminum Third-Stage Blades Max Stress Summary TF30 Engine X-433-26 In X-210 Stand Altitude Running	258
11.2-VIII	Maximum Airfoil Temperatures Measured at Military-Thrust	259
11.2-IX	Maximum Slip Ring Bearing and Cavity Temperatures at Military Thrust	260
11.2-X	Ducting Cable Displacement	260
11.2-XI	Quality Assurance Data Service Blade E-184	268
11.2-XII	X-Ray Results	270
11.2-XIII	Natural Frequencies	271
11.2-XIV	TIP Station Chord Angle	272

LIST OF TABLES (Cont'd)

Number	Title	Page
12.3-I	Rejected Blades From Set Nos. 1 and 2	295
12.3-II	Flight Quality Blades From Set Nos. 1 and 2	297
12.4-I	Maximum Allowable Blended Crack or Nick Limits	299
12.6-I	Blade Permanent Untwist	304
12.6-II	Average Blade Frequency Loss	305
12.6-III	Worst Blade Frequency Loss	306
B-I	Summary of Inspection Results	B-6
B-II	Variation of Blade Density, Frequency, and Weight	B-6

## 1.0 INTRODUCTION

The TF30 Third-Stage Composite Fan Blade Service Program was a major effort directed toward early service evaluation of the TF30-P-9 third-stage fan blades made of BORSIC®/Aluminum composite material. The program was initiated to further refine and develop existing composite fan blade designs and fabricating techniques which were developed under the Advanced Composite Engine Program (ACE), Air Force Contract F-33615-69-C-1651, conducted by Pratt & Whitney Aircraft for the Air Force Materials Laboratory and Aero Propulsion Laboratory, Wright-Patterson Air Force Base, Ohio. Advantages associated with using advanced composites as the structural material for aircraft jet engine fan blades include a significant reduction in engine weight, improved performance, and the potential for increasing fan tip speed.

The Composite Fan Blade Service Program was conducted in two phases. Phase I was a diversified effort in which the blade designs initiated under the ACE Program were finalized; prototype advanced composite test specimens, blades and peculiar engine parts were designed, fabricated, and rig tested; tools required to fabricate the prototype components were designed and fabricated; and fan blades were fabricated and structurally tested. Concurrent with these efforts fabricating techniques were developed and refined and a program was initiated to develop effective nondestructive inspection (NDI) procedures for the blades. Procurement of composite material for use in Phase II of the Fan Blade Service Program was initiated.

Phase II was a specific effort in which tooling, blades, and adapting parts for an engine environment test program were fabricated; blades and adapting parts were tested in an engine at simulated sea level subsonic and altitude supersonic conditions; and engine environment test results were thoroughly evaluated. Fabricating processes and NDI procedures developed in Phase I of the Program were further refined as well. The final task was a successful 184-hour flight service demonstration in F111-D aircraft at Edwards AFB, Cal.

The choice of the TF30 engine as the hardware test vehicle was based on these considerations:

- The TF30 is a modern turbofan engine which powers operational supersonic aircraft and in which the fan blades are subjected to high temperatures and tip speed.
- TF30 engines were available for use in experimental testing and included those funded under this contract and those available on a 'piggyback' basis from Product Support Program engines.
- The TF30, being currently in service, affords the immediate opportunity of evaluating the blades in a flight environment.

The effort was directed toward the third-stage blade because the third-stage provides the highest possible fan temperature environment (470°F). A further benefit is that the first and second stages of the fan protect the third from massive foreign object ingestion such as birds and ice. This protection from foreign object damage (FOD) increases the safety factor making immediate flight evaluation more feasible.

## 2.0 SUMMARY

All major objectives of the program were accomplished. Paragraphs 2.1 through 2.6 summarize the results:

### 2.1 MATERIAL

A source of BORSIC®/Aluminum composite material was found from which BORSIC®/Aluminum monolayer tape could be procured at a set price and within a reasonable lead time. The tape was purchased to a P&WA material specification which resulted in procurement of a uniform, high quality tape. The tape acceptance rate was over 95 percent.

### 2.2 DESIGN

The blade design which evolved fully meets structural and aerodynamic flight requirements and can be consistently fabricated to a high quality standard in a normal shop environment.

### 2.3 TOOLING AND FABRICATION

Tools and processes were developed by which 246 blades were fabricated with an acceptance rate in excess of 92 percent. Blade dies exhibited a life of at least 168 parts, and are adequate for fabrication of flight evaluation hardware.

### 2.4 NONDESTRUCTIVE INSPECTION

Nondestructive inspection procedures were developed which enabled the engine environment test program to be conducted with no blade failures. NDI procedures included ultrasonic C-scan, X-ray, visual, acoustic emission and eddy current, as well as determining density and natural frequency. All blades were proof spin-tested.

### 2.5 BENCH TESTING

Composite blade bench tests showed that:

- No blade degradation resulted from salt corrosion or a -65° to 500°F thermal shock.
- Blades lost frequency in pure bending fatigue tests but did not otherwise fail in  $10^7$  cycles.
- Burst speeds, demonstrated in spin pit tests were at least 30 percent above normal red line speed (10,550 rpm).
- Blades withstood the highest engine operating stresses (except for surge stresses) during combined stress/fatigue testing, as shown in modified Goodman diagrams (at room temperature and 450°F).

- Composite blades with a nickel-cobalt leading edge had slightly better resistance to sand erosion than titanium blades.
- Composite blades were slightly less resistant to small FOD (gravel, rivets) than titanium blades.
- Composite blades had relatively poor resistance to massive FOD (birds, ice) compared with titanium blades.

## 2.6 ENGINE ENVIRONMENT TESTING

A total of 564 hours of testing in an engine environment were conducted. Of these, 300 hours took place in a funded engine, while 264 hours were "piggyback" tested during CIP/PSP testing. Tests were conducted on two full sets of composite blades and included 444 hours of cyclic endurance testing at sea level and supersonic conditions. Test results showed that:

- Blade vibratory stresses were within acceptable levels, both with a clean inlet and with distortion.
- Aerodynamic performance and stall margin were unaffected.
- As many as 19 surges were performed with no apparent detrimental effects.
- A severe tip rub (0.090 in.) caused no blade catastrophic failure but did induce cracks in 7 of the 36 blades (20 percent).
- Leading edge FOD, blended to maximum limits, resulted in no blade damage during approximately 50 hours of subsequent engine operation.
- Blade performance could be evaluated in all portions of the flight envelope including high altitude, high Mach number; high altitude, low Mach number; and sea level, Mach number 1.2.
- After test times of 100 hours or more, X-ray inspection indicated small cracks in some blades at the leading edge near the root. However, these cracks did not grow appreciably in test time to 364 hours.

During the testing in the engine environment, the maximum blade temperature was 470°F; maximum blade tip speed was 1500 ft/sec; and maximum blade stresses were 8,000 psi (non-surge) and 30,000 psi (surge).

Because of the crack indications, P&WA imposed a 200-hour limit on blade engine operation during the flight program before a full bench inspection.

## 2.7 FLIGHT SERVICE EVALUATION

One full set of previously ground engine-tested blades was installed in an F111-D aircraft at Edwards AFB, California, and subjected to 184.1 hours of unrestricted flight over a span of 90 flights in 17 months. This was the first flight of an advanced composite material applied to an engine primary structural component, i.e., the 3rd stage fan. No serious composite blade problems occurred during this time. Bench inspection of the blades following the flight program revealed no damage except for surface cracks in the root region of several blades. The flight program was conducted entirely by the USAF and program details are to be reported in a separate ASD report.

## 3.0 CONCLUSIONS AND RECOMMENDATIONS

This component improvement program was directed toward early service testing of TF30-P-9 third-stage fan blades fabricated of BORSIC®/Aluminum composite material. The blade attachment roots were fabricated of BORSIC®/Aluminum material with titanium dovetail section, and aluminum wedges to splay the fibers.

### 3.1 CONCLUSIONS

From the overall results of the program, it is concluded that TF30-P-9 BORSIC®/Aluminum third-stage fan blades, designed, fabricated and inspected according to the procedures developed during this program, will be acceptable for flight service subject to periodic inspection.

The BORSIC®/Aluminum composite material selected consisted of silicon-carbide coated boron fiber filaments affixed to AA6061 aluminum foil by plasma spraying AA6061 aluminum powder. When made to procurement specifications, BORSIC®/Aluminum Tape Specification PWA 437 and BORSIC® Filament Specification PWA 438, this material exhibited the required properties to meet fan-blade application requirements. (These two specifications are included in Appendix B, Quality Control Plan for TF30 Composite Fan Blades, to show the standards that were imposed on tape and filament fabrication.) Results of quality assurance tests indicated that random sampling was not sufficient to assure quality.

The blades fabricated under this program were designed to meet all stress and vibratory conditions consistent with their application as third-stage fan blades in a TF30-P-9 engine. Analysis indicated that core (unidirectional fibers) and shell (fibers at  $\pm 45^\circ$ ) construction would provide both the strength and stiffness requirements for these blades. Titanium dovetail root attachments provided ample shear and bearing strength.

The tools and fabricating procedures developed during this program were specifically developed for a low production run application. Fabrication process parameters were held to tight tolerances to ensure program success. Subsequent test results indicated that the blades fabricated using the tools and processes developed during the program exhibited superior performance characteristics.

The NDI procedures developed during this program demonstrated the capability of detecting all known significant material and/or fabrication defects. The blades flight tested did not have any cracks detected by these procedures prior to installation in the flight test engine.

Bench testing provided the evidence that the BORSIC®/Aluminum third-stage fan blades had sufficient structural integrity to successfully undergo evaluation in an operating engine environment. It was further concluded that neither salt corrosion nor thermal shock had significant effect on blade structure. The blades exhibited sufficient FOD resistance to perform satisfactorily in a third-stage fan environment.

During both simulated sea-level static and altitude/supersonic testing, the BORSIC®/Aluminum blades exhibited the capability of performing well in a flight environment. Engine performance was in no way degraded by incorporating advanced composite blades in the fan third-stage.

The 184 hours of flight service operation was highly successful, but did result in surface cracking of several blades. In future designs, this can probably be avoided by improved filament orientation and blade processing.

### 3.2 RECOMMENDATIONS

It is recommended that the blades in service be evaluated at 200-hour intervals by a bench inspection including 10x visual and x-ray techniques.

It is recommended that the blades be service evaluated in a flight program. However, due to x-ray indications of small cracks in some ground engine test blades at the leading edge near the root, a 200-hour limit should be imposed on flight test blade operation before a full bench inspection is conducted.

It is further recommended that all tape lots be tested and the strength of each tape lot be evaluated. Tape lots exhibiting average filament strengths of more than 340,000 psi would result in panels having the required 140,000 psi strength. Tape lots exhibiting filament strengths of less than 340,000 psi must be qualified by demonstrating that panels pressed from the tape exhibit at least 140,000 psi composite strength. If possible, the tape vendor should be required to guarantee the final tape properties.

A future study should be conducted to investigate the effects of imposing less stringent production controls on blade quality and also to optimize tools for use in long production run applications.

The procedures outlined in this report; specifically, ultrasonic C-scan, contact ultrasonic through-transmission, x-ray, determination of natural frequency and density, fluorescent penetrant inspection, visual inspection, and proof spin testing should be adopted as the quality assurance procedures in future advanced composite programs.

It is recommended that a program be conducted to improve methods of FOD protection to expand the use of composite materials in jet engine fan applications.

Future designs should also utilize improved filament orientations and tooling/processing techniques to minimize filament breakage which can lead to cracking of the composite structure. Potential residual stress problems should be identified. Spin-pit burst testing can be a useful tool for this purpose, by establishing actual burst speeds vs. predicted values.

#### 4.0 GENERAL BACKGROUND

The term "advanced composites", as used in this report, applies to materials made up of high strength, high modulus, low density fibers combined with a matrix material which holds the fibers in proper conformation and distributes the loads among them. It has been recognized for several years that, if these materials could be successfully applied to aircraft jet engines, significant weight and performance benefits would result. Development programs conducted to date have thoroughly demonstrated this potential and reinforced the desirability of refining the production and inspection techniques required to produce high quality, advanced composite, jet engine aircraft parts economically and consistently.

Although silicon-carbide and sapphire show promise for future use as fiber materials in advanced composites, current interest is centered on graphite and boron. These are available in a wide variety of fiber forms. For example, graphite can be obtained in high strength or high modulus forms in either short lengths or as a continuous filament. It can also be obtained as yarn composed of several hundred filaments, woven yarn, or tow. Boron fiber can be obtained either as uncoated or coated with silicon-carbide and in sizes ranging from four mils to eleven mils in diameter. The term BORSIC®, as used herein, refers to Boron Silicon Carbide coated fibers under United Technologies trademark.

The matrix materials can be either metal or organic. Standard alloys of aluminum or titanium are the usual metal matrix materials and they may start out in the form of foil, plasma spray, molten metal, or powder. Organic matrix materials can be characterized as low temperature (epoxy resin) or high temperature (polyimide resin) materials. Boron fiber can be combined with either metal or organic matrix materials while graphite fiber is normally used with an organic matrix material. Development efforts are currently underway to combine graphite fiber with an aluminum matrix.

#### 4.1 MECHANICAL PROPERTIES

Advanced composite materials have extremely high specific strengths and moduli. Fiber tensile strengths range as high as 500,000 psi and moduli up to 60 million psi, while densities are 0.1 lb/in<sup>3</sup> for boron fibers and 0.05 lb/in<sup>3</sup> for graphite fibers. When combined with a matrix to form a composite material, the strength in the direction of fiber orientation is generally proportional to the volume percentage of fiber in the composite. Density of the composite on the other hand, may remain the same as that of the fiber, or increase slightly. Consequently, their specific properties are superior to those of titanium, which is currently favored for jet engine structural use where the engine temperature environment is less than 800°F.

The properties of advanced composite materials are anisotropic, however. The strength of composites transverse to the fiber direction is far less than in the axial direction of the fibers. The anisotropic characteristic can be overcome to a great extent by proper design (i.e., cross-plying) and fabrication of the component.

Temperatures at which advanced composites can be used as structural materials are limited by the matrices used. These limits are generally 200-300°F for epoxy matrices, 600°F for polyimide or aluminum matrices, and 800-1,000°F for titanium matrices.

## 4.2 FABRICATION TECHNIQUES

Structural components made from advanced composites are laminar, built from successive layers of advanced composite tape (sheet) or broad goods. The tape or broad goods can be purchased in either monolayer or multilayer form. Those composite materials having an organic matrix are called "prepreg" because they are usually impregnated with the matrix material. Composites with a metal matrix sometimes contain an organic "fugitive" binder by which the manufacturer holds the fibers in position while applying the metal matrix. If present, the fugitive binder must be driven off by heat and vacuum during processing, otherwise occlusions result, thereby weakening the material.

Composite materials can be used to make shapes as simple as flat panels or forms as complicated as turbine engine fan blades which have a two-dimensional taper, curvature, and twist plus a root attachment at one end (Figure 4.2-1).

Processing of the part, whether simple or complex, is usually similar. Plies of the proper shape and size are cut, stacked with the proper fiber orientation, loaded into a mold (for organic matrices) or die (for metal matrices), and subjected to heat and pressure for a specified period of time. This last operation, normally performed in a vacuum, is called a "cure" cycle when used with organics, and a "bonding" cycle when used with metal matrices.

The cure cycle is performed at moderate pressure levels. The characteristics of organic materials however, often dictate that more than one temperature level be applied during the cure cycle and that the time/temperature relationships be closely controlled.

The bonding cycle for metals, on the other hand, is a diffusion bonding process, and requires less stringent control of time-temperature relationships. It does, however, require high pressures, in the range of 3500-5000 psi for aluminum and up to 25,000 psi for titanium.

The vacuum environment for either cycle can be provided by the use of autoclaves, retorts, or by bagging.

After molding and bonding, finishing operations are performed as required. The composite materials can be machined, but in the case of boron the only effective finishing techniques are grinding and electrodisscharge machining (EDM).

Most composite parts require more than one fiber orientation in their structure to meet strength and stiffness requirements. This is a consequence of the anisotropic properties of composites. In fan blades, for example, the most critical structural design requirements are those of bending and torsional stiffness, tensile strength in the radial direction, and sometimes torsional creep strength. These requirements usually cannot be met by a unidirectional fiber orientation, but necessitate a "cross-ply" layup where the fibers are alternately arranged at some angle to the radial axis of the airfoil. Another possible solution is to incorporate a "core-shell" construction (Figure 4.2-2), wherein the bending and radial load requirements are satisfied by the core of radial fibers, and the torsional stiffness and creep requirements are satisfied by  $\pm 45^\circ$  cross-ply shell. The latter arrangement is the one used in the TF30 fan blades designed, fabricated and tested under this program.

The most common problems which occur in manufacturing composite parts are voids in the matrix material, delamination of the plies, cracking, misorientation of fibers, and broken fibers. All of these defects, however, can be detected with high assurance by proper application of NDI techniques such as X-ray and ultrasonic C-scan. In addition, the effects of flaws in advanced composites are reduced because composite materials are less notch sensitive than most metals, including titanium.

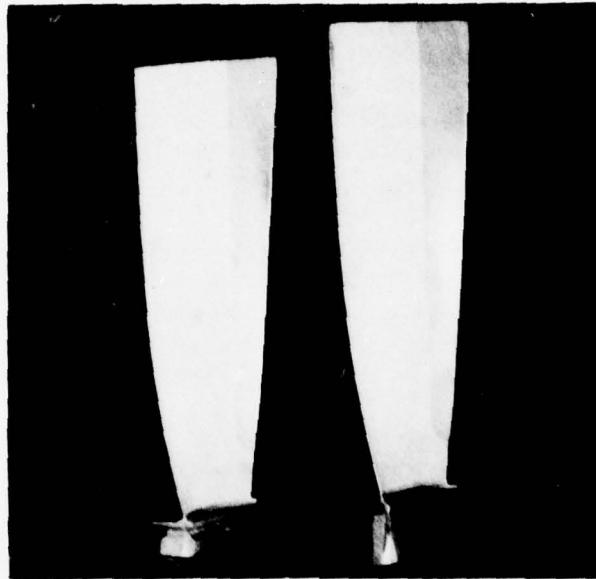


Figure 4.2-1 *These BORSIC®/Aluminum Blades Show the Complex Shape That Can Be Fabricated From Composite Materials; Left, Finished - Machined Root and Blade; Right, Unfinished Root and Blade*

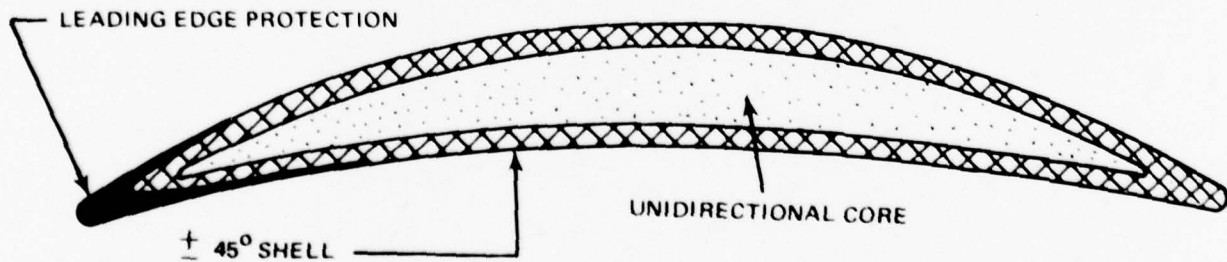


Figure 4.2-2 *The Core and Shell Construction Selected for the BORSIC®/Aluminum Blades Fabricated Under This Program*

## 5.0 MATERIAL

The advanced composite material selected for use in this program was BORSIC®/Aluminum consisting of silicon-carbide coated boron filaments affixed to AA6061 aluminum foil by plasma spraying (PWA 437-1) AA6061 aluminum powder. The material, ordered to Specification PWA 437-1, Rev. D, was procured as a monolayer tape from two sources; the Hamilton Standard Division of United Technologies Corporation, Broadbrook, Connecticut and the Materials System Division of Union Carbide, Indianapolis, Indiana.

The choice of 6061 aluminum as the matrix material was made on the basis of Pratt & Whitney Aircraft experience in prior programs. BORSIC®(silicon-carbide coated boron) fibers were chosen rather than uncoated boron fibers because of fabricability: the coated fibers allow the composite material to be processed at higher temperatures and over a greater range of temperatures.

Upon delivery, the advanced composite was inspected to ensure conformance to the procurement specifications, BORSIC®/Aluminum Tape Specification PWA 437 and BORSIC® Filament Specification PWA 438 which are included in this document as Appendix A. The inspections, described in Paragraph 5.1, showed that the composite material tape purchased was consistently uniform and of high quality. The tape acceptance rate was in excess of 95 percent for the Union Carbide tape, which incorporated HSD fiber.

### 5.1 RAW MATERIAL QUALITY ASSURANCE

#### 5.1.1 Visual Inspection

All raw material received was visually inspected for loose or missing fibers, fiber crossover, creases or wrinkles in the back-up foil and other visually discernible defects. Minor defects which were confined to a small area and would have no degrading effect on component fabrication or composite material physical properties were not a cause for material rejection.

#### 5.1.2 Fiber Content and Characterization

A sample taken from a corner of each tape was weighed and measured to determine the weight per unit area. The aluminum matrix was then removed by leaching. Fiber spacing, diameter, and content were then determined from the remaining material. Slight deviations in weight per unit area, fiber diameter, and excessive fiber content were expected to have no effect on the program and, consequently, tapes with such deviations were judged to be acceptable. On the other hand, material in which the fiber content was less than that specified in PWA 437 was rejected.

#### 5.1.3 Mechanical Property Evaluation

Initial mechanical property testing was conducted on unidirectional test panels fabricated from a randomly selected tape for each 100 square feet of material received. The test panels, fabricated in accordance with paragraph 3.2.1 of Specification PWA 437, consisted of ten layers of composite material pressed together for 1.5 hours in a vacuum of  $10^{-4}$  Torr or less, at a temperature of  $1040^{\circ} \pm 10^{\circ}$ F and a pressure of 5000 psi. Properties determined included longitudinal ultimate tensile strength and modulus (filaments parallel to applied load) and transverse ultimate tensile strength (filaments perpendicular to applied load).

Test results of the initial panels showed strengths as low as 53,900 psi, significantly below the minimum specification requirement of 140,000 psi.

An additional panel was fabricated from a tape which had exhibited a strength of 92,900 psi. This test panel was laminated at 950°F and tensile tested to determine whether the low strength was the result of insufficient silicon-carbide coating. Tensile strength improved only slightly to 100,600 psi which indicated that the coating was sufficient.

Weibull analysis of single-filament tensile test results on fiber extracted from as-received tapes and from fabricated test panels revealed that panel fabrication had no observable effect on filament strength. However, there was a significant difference between fibers extracted from material which exhibited an acceptable strength greater than 140,000 psi, and those fibers from materials which did not meet strength specifications. Figures 5.1-1 through 5.1-4 show that the incidence of fibers having a strength less than 200,000 psi or fibers having defects was significantly greater for the weak material. Despite this demonstrated difference in fibers, however, the results of filament testing are not always consistent with panel testing. Sufficient inconsistencies existed to indicate that mean fiber strength values may not provide a valid criterion of filament quality, and fiber testing only a small sample may be insufficient to detect unacceptable material. The variability in tape-to-tape composite strength demonstrated the advisability of evaluating the strength of all tape lots rather than a random sampling.

The cost and time involved to evaluate the strength of each tape lot by extensive panel or fiber testing led to developing tensile test specimens of monolayer tapes as qualitative predictors of subsequent composite (panel or component) strength. Test specimens contained 40-45 filaments and were 0.250 inches wide by 4.0 inches long with a 2.0 inch gage length and 1.0 inch long aluminum doublers attached by epoxy adhesive to the gripping areas. A gripping alignment fixture, used to avoid bending stresses, and a monolayer tape tensile test specimen are shown in Figure 5.1-5.

Strength values were estimated using the total fiber cross sectional area only because the load carrying capability of the uncompacted matrix was negligible. The rule of mixtures; i.e., the strength of the composite is directly proportional to the volume percentage of filament, indicated that the composites, having approximately 50 percent filament, would exhibit about half the strength indicated by the tests.

Correlation of tape test results and composite panel properties, Figure 5.1-6, showed that in general, panel strengths were less than half of the tape strength for the higher strength material. Tape strength above approximately 415,000 - 420,000 psi correlated with acceptable composite panel strengths, while tapes with strengths less than 260,000 psi yielded unacceptable composite panels. Experience on this and other programs conducted at Pratt & Whitney Aircraft indicated that material containing BORSCIC® filament prior to mid-January, 1971, and exhibiting average strength above 415,000 psi would have acceptable panel strength. Tapes that exhibited strengths less than 420,000 psi required panel fabrication and testing to assure that the composites would have the required tensile strength of 140,000 psi.

It was judged that exceptions to the correlation were due to significant strength differences between fiber lots which were revealed during testing. Initially, three specimens were obtained from a single edge of each tape. This selection of test specimen locations had the result that only one of the two or three fiber lots used to fabricate a tape was actually tested. Consequently, tensile test results were highly consistent. When test specimens from different edges of the tape were selected, however, some tapes exhibited large differences in strength. This was attributed to the fact that different fiber lots were used to fabricate a single tape. This is shown in Figure 5.1-6 where tape lots, J, K and X are indicated.

Subsequent testing was expanded so that specimens selected were representative of more than 75 percent of the tape area. This provided a more accurate assessment of the tape's strength.

Testing of Union Carbide material received between July, 1971 and mid-November 1971 revealed an apparent improvement in manufacture. Test results showed that the composite panel strength was approximately 50 percent of the tape strength. Figure 5.1-7, shows the correlation of tape and composite panel strengths for this material. The lower line in this figure represents a panel strength 50 percent of that of the tape based on the rule of mixtures. The upper line, parallel to the 50 percent line and located at the top of the strength band, crosses the composite specification minimum of 140,000 psi near the 340,000 psi tape strength level, indicating that a tape strength of 340,000 psi would ensure acceptable composite strength. Therefore, when panel testing of one randomly selected tape from each 100 square feet of tape received was resumed, panels from tapes with strengths of 340,000 psi or greater were not tested providing that the monolayer tensile tests from different locations of the same tape exhibited no significant decrease in strength.

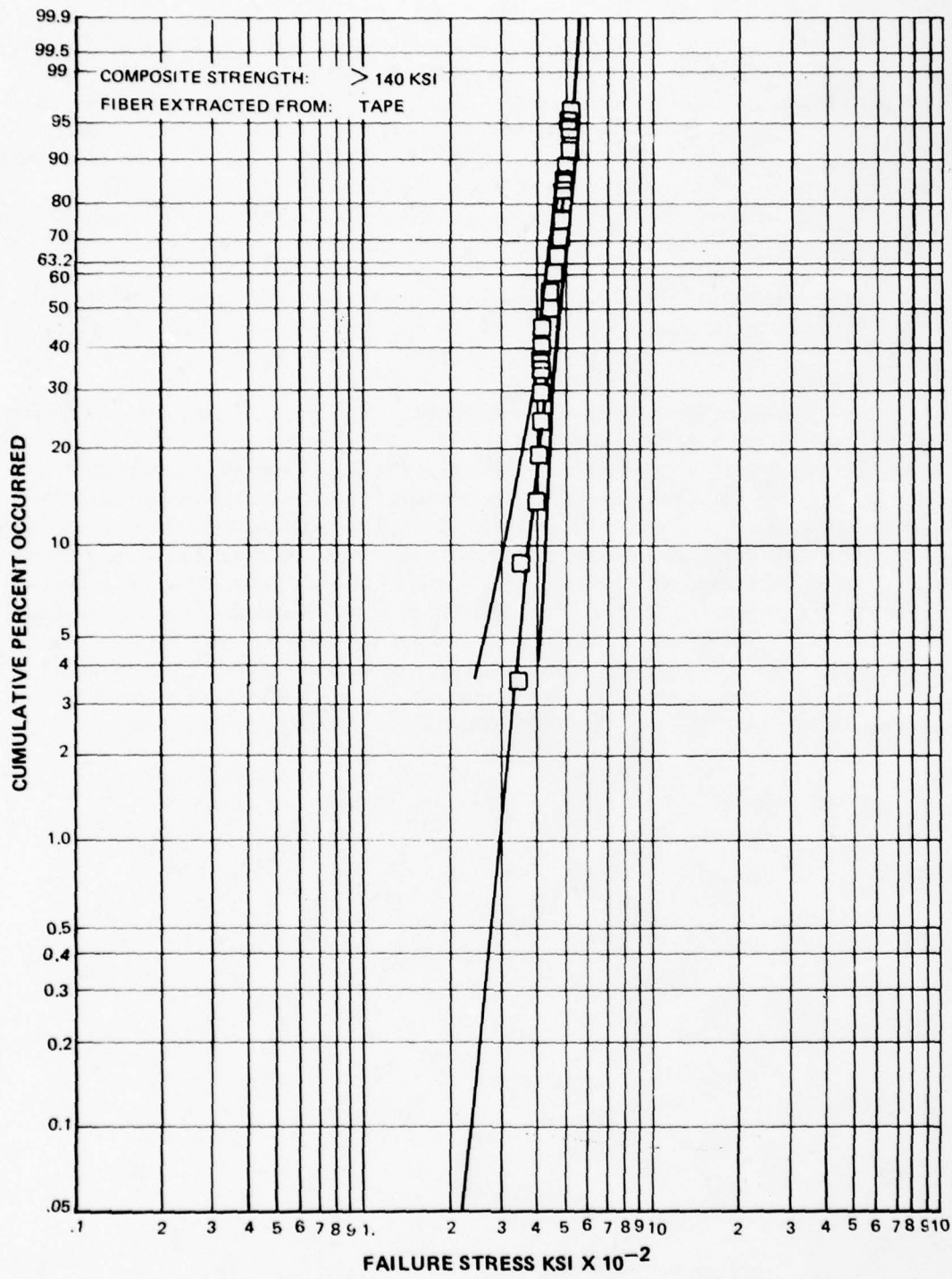


Figure 5.1-1 Weibull Distribution of Tensile Strength of BORSIC® Fiber Extracted From Monolayer Tape Which Yielded Acceptable Panel Strength (> 140 ksi)

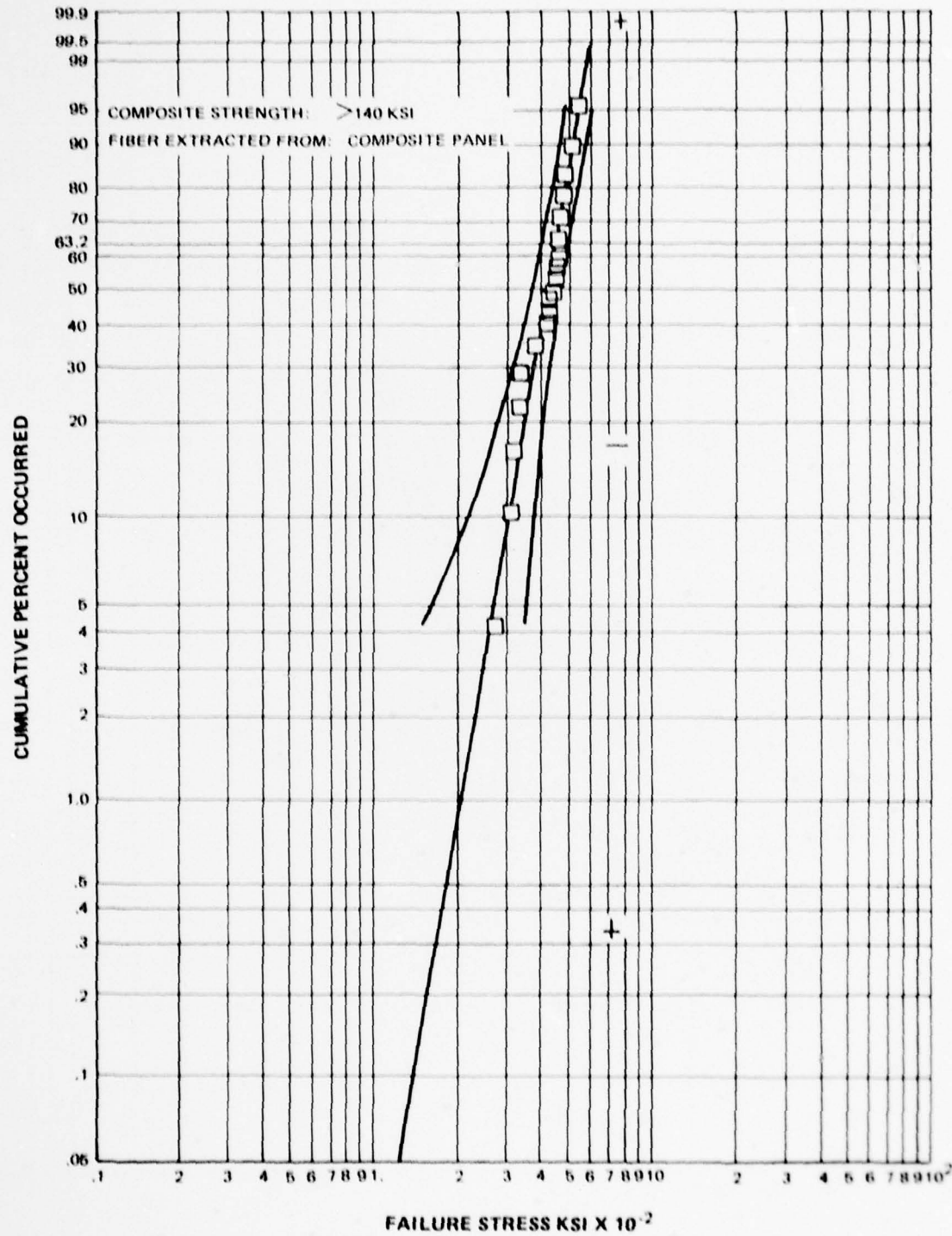


Figure 5.1-2 Weibull Distribution of Tensile Strength of BORSIC® Fiber Extracted From Composite Panel Which Exhibited Acceptable Strength ( $> 140$  ksi)

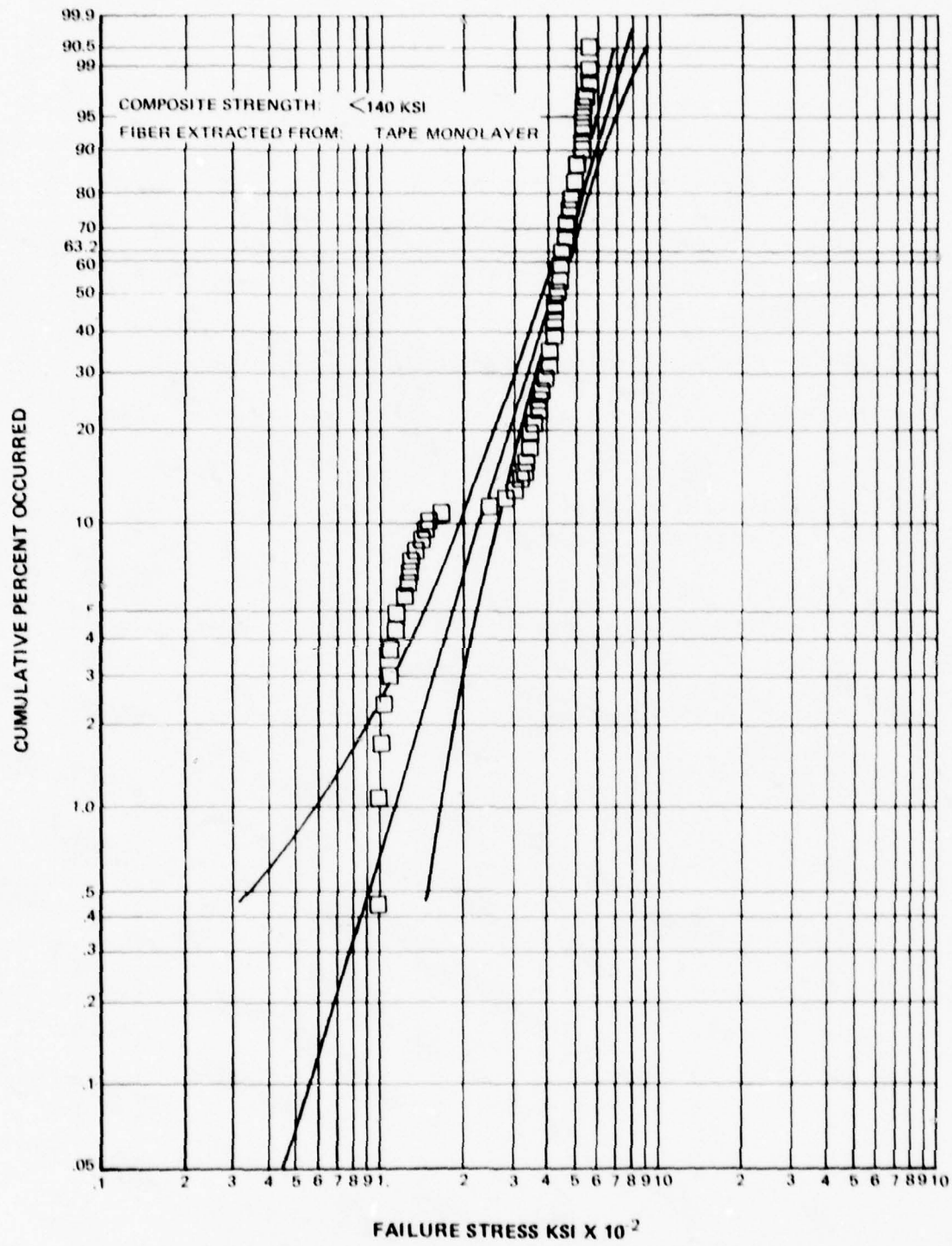


Figure 5.1-3 Weibull Distribution of Tensile Strength of BORSIC® Fiber Extracted From Monolayer Tape Which Yielded Unacceptable Panel Strength (<140 ksi)

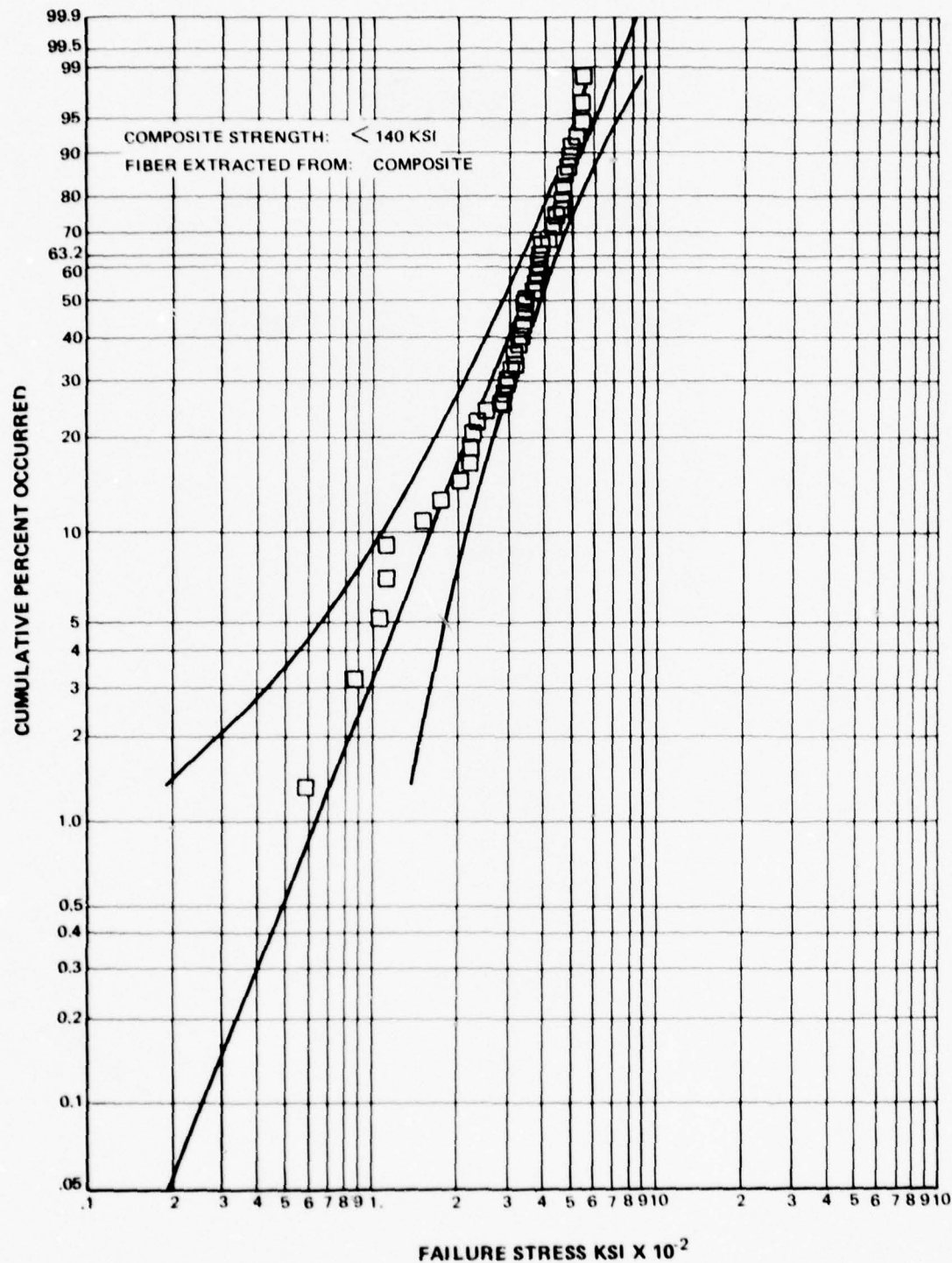
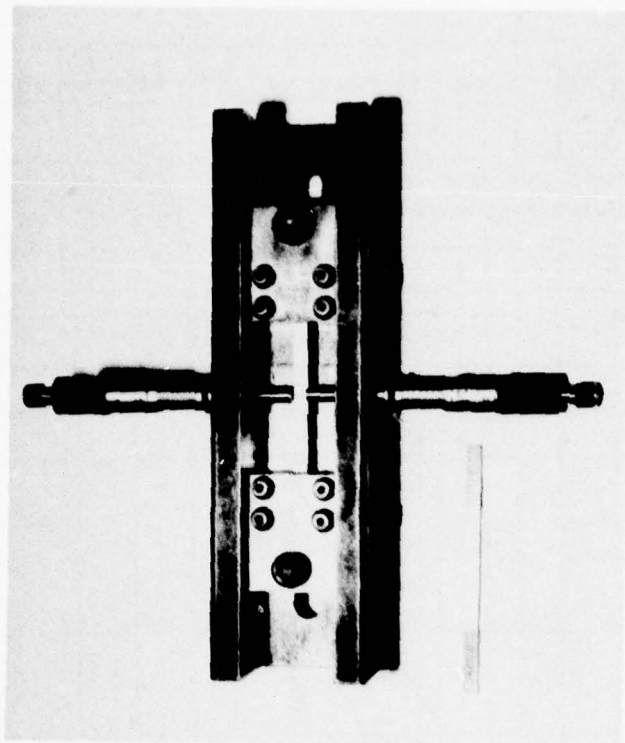


Figure 5.1-4 Weibull Distribution of Tensile Strength of BORSIC® Fiber Extracted From Composite Panel Which Exhibited Unacceptable Strength (< 140 ksi)



*Figure 5.1-5 Monolayer Tape Tensile Specimen and Gripping Alignment Fixture*

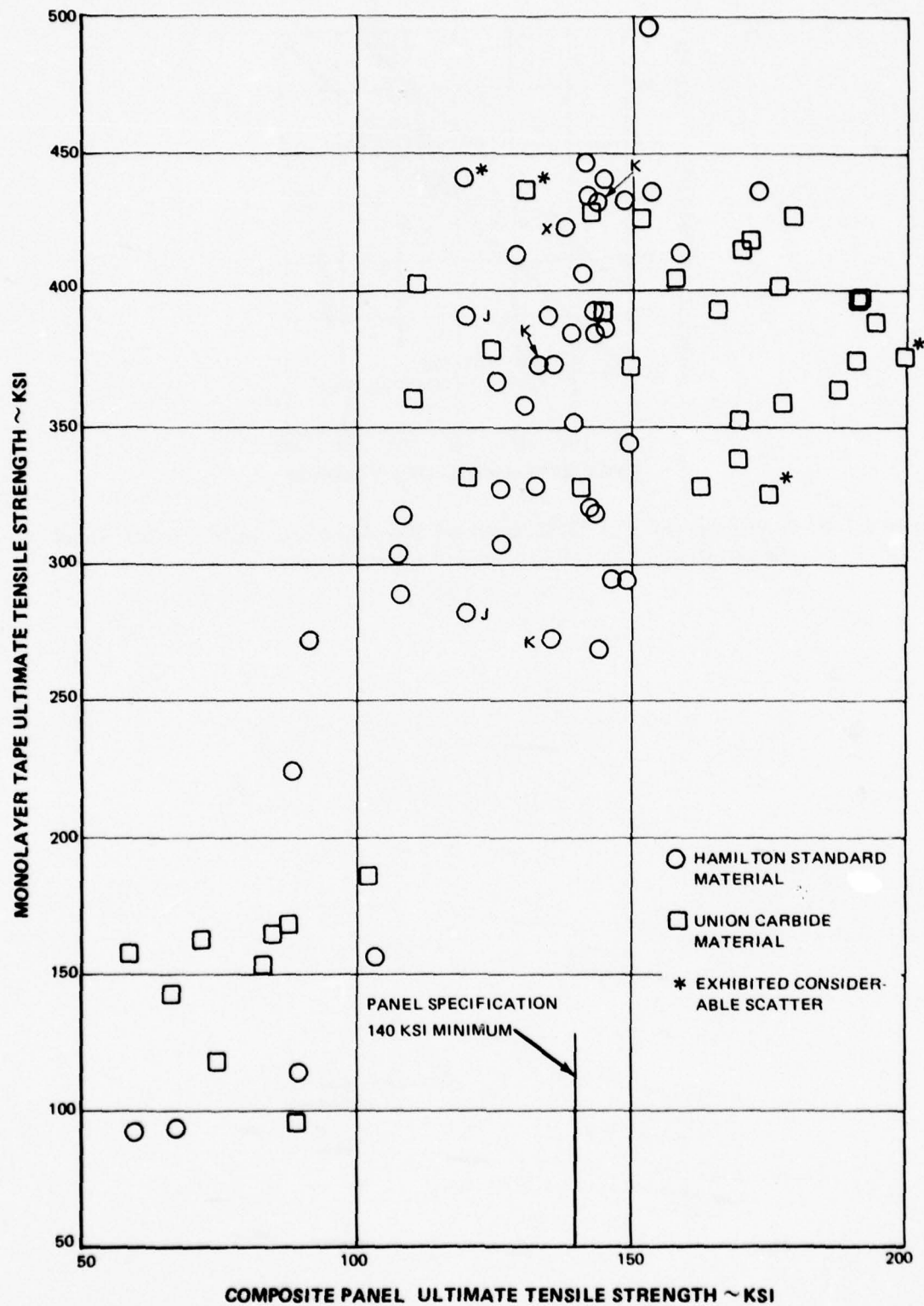


Figure 5.1-6 In General, Panel Strengths Were Less Than One-Half of the Tape Strength of Higher Strength Tapes

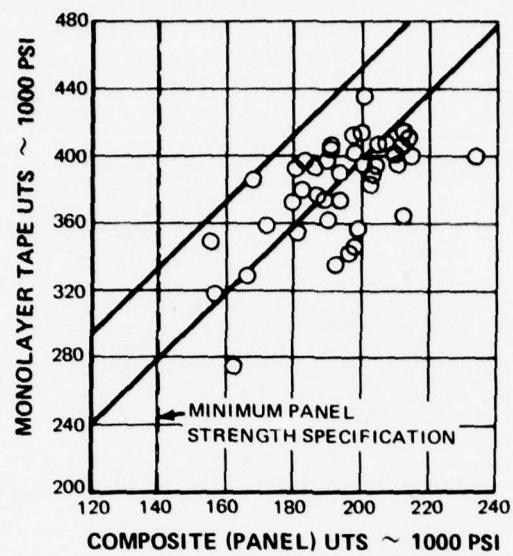


Figure 5.1-7 Correlation of BORSIC<sup>®</sup>/Aluminum Monolayer Tape and Composite Panel Tensile Strength for Union Carbide Supplied Material

## 6.0 DESIGN AND ANALYSIS

The airfoil shape of the third-stage blades designed and fabricated under this program was established by the contract commitment that the blades would be service evaluated in a Pratt & Whitney Aircraft TF30-P-9 engine. Except for the part-span shroud, which was eliminated, the blade airfoil shape is identical to that of the TF30-P-9 bill of material (B/M) titanium alloy blade. As a consequence of removing the shroud, the blade shape was smoothly blended to eliminate the chordwise notches and local thickening at the shroud locations. Figure 6.0-1 shows a comparison of the advanced composite blade with the B/M titanium alloy blade.

### 6.1 BLADE DESIGN CONSIDERATIONS

Fan blades must satisfy both vibration and static stress requirements. The vibratory design criteria are primarily concerned with the second order engine excitation (2E) of lower order bending frequencies and avoiding torsional flutter. The stress criteria of both the airfoil and attachment sections of the blade are imposed to ensure that the blade will be able to withstand the loading to which it will be subjected during engine operation.

In addition to the vibration and stress requirements, the blades must also be able to withstand foreign object damage (FOD) due to ingestion of foreign objects into the engine.

Because of the inherent anisotropic properties of advanced composite blades and the significant interdependence of fabrication techniques on mechanical and physical properties, the design procedure for advanced composite blades is highly sophisticated. In general, the composite-blade design process requires more iterations than the design process for isotropic material blades. Figure 6.1-1 is a typical logic network used in the design of composite fan blades and illustrates the complexity of the process. This has resulted in the development of advanced, computerized techniques to analyze the stress state and vibration characteristics of nonhomogenous and anisotropic material fan blades. These techniques, developed by P&WA and outlined in Figure 6.1-2, were used extensively to optimize the fan blade design.

Although the procedures are more complex, the structure of composite blades does allow a certain amount of design flexibility not available when designing with isotropic materials. The lay-up pattern of the laminates can be varied in an effort to meet specific design criteria. The shell and core construction shown in Figure 6.1-3 can be used to advantage in meeting bending and torsional frequency requirements as well as stress requirements. The shell provides the torsional stiffness to meet torsional frequency requirements and keep the angle of untwist at an acceptable level. The core, on the otherhand, provides the bending stiffness to satisfy the bending frequency requirements as well as providing the P/A load carrying and gas bending and restrained warping stress capability.

#### 6.1.1 Vibration Considerations

The high modulus-to-density of advanced composite materials is not sufficient to compensate completely for the reduced bending frequency which resulted from eliminating the part-span shroud. Consequently, first bending resonance by 2E excitation was unavoidable. To resolve

in this condition the composite fibers must be oriented and distributed so as to reduce the first bending frequency to a level where 2E excitation would have little adverse effect. However, the blade stiffness must not be decreased to a level where the second coupled bending frequency is reduced to a point where it will undergo 2E excitation in the engine operating range.

An additional consideration is that the torsional frequency of the blade must be maintained at a sufficiently high level to achieve an adequate torsional flutter parameter. This parameter is defined as  $b\omega_t$  where  $b$  is the chord length in feet and  $\omega_t$  is the first torsional blade frequency in radians/sec.

### 6.1.2 Stress Considerations

#### 6.1.2.1 Airfoil

The general stress criteria used in fan blade design include yield stress, low cycle fatigue (LCF), and creep.

Low magnitude vibratory stresses, combined with high level steady state stresses, create a potential fatigue problem in fan blades. In addition to stress due to aerodynamic loading, steady state stresses result from centrifugal forces (P/A stress), blade untwist, and restrained warping. Under centrifugal loads, large torsional moments are developed in the rotating blades because of blade pretwist and the asymmetric blade geometry with respect to the plane of rotation. The fixed condition of the hub prevents warping and results in longitudinal (restrained warping) stresses. Blade untwist and camber variation due to torsion cause additional longitudinal stresses.

Vibration of the blades induces torques and moments resulting in high frequency stresses. The magnitude and frequency of these vibratory stresses depends upon the natural frequency of the blades and disks and are a function of the torsional and bending rigidities of the systems. A yield strength criterion is traditionally applied to metallic fan blades because experience has shown that vibratory fatigue failures are avoided by limiting the steady stress to a fraction of the yield strength. With composites, the criterion is to limit the steady stress to a fraction of the composite ultimate strength since yield strength essentially coincides with the ultimate strength.

#### 6.1.2.2 Root Attachment

Blade attachments transmit tensile, bending, bearing, shear, and torsional loads from the airfoil to the disk. A design constraint is that the attachment must be stronger than the airfoil so that, in the event of failure, the failure will occur in the airfoil section of the blade rather than the more massive attachment section, thereby minimizing secondary damage. The blade attachment must have sufficient strength to withstand the high induced inertial loads and in addition, must be designed so that stress concentrations are reduced to a level where they will not be adversely affected by the vibratory loading environment.

To design the blade attachments, P&WA has developed a computerized finite-element technique by which the stresses in this attachment can be accurately analyzed. In this technique, the elastic continuum is replaced by a mesh of interconnected quadrilateral elements of known stiffness. Equilibrium and compatibility conditions at the nodal points are then satisfied and a system of simultaneous equations is generated. The solution to these equations approximates the exact elasticity solution.

Figure 6.1-4 is a schematic of a typical finite element model of a blade attachment design. Because of symmetry, only one-half of the design need be considered provided appropriate boundary conditions are specified along the axis of symmetry. As can be seen, the element size can be varied throughout the body – small elements in areas of rapid stress variation and larger elements where stresses vary more slowly. This provides the means to more accurately determine stress profiles and stress concentration factors.

## 6.2 BLADE DESIGN METHODOLOGY

A disciplined, orderly design procedure was implemented to ensure a successful fan blade and rotor design as well as to provide a cost effective design effort which would minimize duplication of effort and optimize the analytical iterations required. An outline of the procedure is as follows:

1. Fan flowpath and blade airfoil contour technical data were determined. These data were based on the TF30-P-9 engine B/M blade data.
2. Fiber volume percent, airfoil weight, and centrifugal pull were determined based on the required fan speed plus ten percent. This data identified the root load carrying requirements.
3. The blade attachment was designed taking into account the design constraints described in Section 6.1.2.2 of this report as well as manufacturing considerations. Although blade root and disk lug attachment stresses were calculated in the same way as for a metal blade, particular attention was paid to tooth shear and bearing stresses as well as the bonded root joint shear stress because of the anisotropic properties of composites materials. In addition, the broach-angle of the blade root attachment was optimized so as to produce the smoothest flow of fibers into the root.

To form the root section, the fiber plies which make up the blade were translated from the aerodynamic airfoil section into a rectangular wedge shaped root and splayed into two fiber bundles. An aluminum wedge was inserted between the bundles, and titanium root pads were bonded to the outer surface of the fiber bundles. The root pads provided the surface necessary to carry the bearing loads produced by the interaction of centrifugal force and the restraining lug of the disk. Figure 6.2-1 shows a cross-section of this design.

The rectangular shape of the root simplifies manufacturing the aluminum wedges and titanium root pads. To achieve maximum shear strength of the bonded joint, the mating surfaces were matched as closely as possible. The design aim is to obtain the smoothest possible transition in the shortest radial length. This will minimize overall blade length and consequent vibratory problems as well as avoiding the possibility of imposing more stringent pitch limitations on the disk lug design.

Although the design criteria are not identical to those for metal blades, every effort was made to adhere to proven disk and blade design relationships.

4. Concurrent with the design effort which provided the basic configuration, the fiber orientation of the plies was optimized so that the vibratory and stress criteria would be adequately met. The core and shell construction was selected as the best means of meeting all design criteria, including torsional creep (untwist) of the airfoil.
5. After determining the fiber orientation and both the radial and axial blade tilt, a computer program was developed to determine the flat pattern shape of each ply to be used in the blade construction. The airfoil taper established the overall span length of each ply.
6. Finished tolerances were determined to be those expected of a titanium blade; consequently, techniques to calculate the blade tip clearance and root balance were those used for titanium blades. However, it was expected that actual clearances might differ due to changes in the coefficient of expansion and density of the composite material, plus lower airfoil stiffness.

### 6.3 FINAL BLADE DESIGN AND CONSTRUCTION

The blade has an overall length, including root attachment, of approximately ten inches; chord length is approximately three inches. The blade weight is only 6.6 ounces, 40 percent lighter than the TF30-P-9 engine B/M blade. The airfoil has a maximum twist of 49° and a maximum camber of 68°. Its leading and trailing edges are a maximum of 26.4 mils thick. The blade is designed to operate at a maximum tip speed of 1500 ft/sec and at a maximum temperature of 470°F.

#### 6.3.1 Airfoil

The airfoil is constructed of 6061 aluminum alloy matrix material reinforced with a 50 percent volume of 4.2 mil BORSIC® fiber (boron fiber coated with silicon carbide). The aluminum alloy matrix material was chosen because of its superior fabricability and good corrosion resistance as well as Pratt & Whitney Aircraft experience with the material. Coated boron fiber, rather than uncoated, was chosen also because of fabricability; the BORSIC® fiber allows a greater range of, and higher, processing temperatures.

Figure 6.3-1 shows a cross section of the core and shell blade construction as well as the fiber orientation in each element. The inner core is composed of all-radially oriented fibers to provide both bending stiffness and strength in the radial (root-to-tip) direction. In the shell the alternate fiber layers are oriented  $\pm 45^\circ$  to the radially oriented core fibers. The orientation of the fibers in the shell provides the required torsional stiffness and creep strength.

The ratio of shell-core-shell thickness is 20 percent-60 percent-20 percent based on the maximum thickness at a given airfoil cross section. This thickness ratio is maintained from blade root to tip. A total of 44 plies is used in the root area, only 13 of which extend to the tip. The 44 ply shapes at the root were established by computer after the airfoil aerodynamic parameters were established. The inner most radial ply is the smallest and the outermost "cross" ply is the largest. Figure 6.3-2 shows the relative sizes of the plies.

To provide protection against sand/dust/rain erosion and the types of FOD encountered in a fan's third stage (normally gravel and small metal objects) the airfoil has a nickel-cobalt leading edge extending from the tip to within one inch of the root. Figure 6.3-3 shows this protection while Figure 6.3-4 shows a cross section of the leading edge. Nickel-cobalt (Ni-Co) alloy was selected rather than hardened nickel for the leading edge because it exhibits superior hardness above 350°F.

An alternate leading edge design consisting of a two-piece titanium alloy sheath was developed but was abandoned because of substantially higher cost and fabrication difficulty. Figure 6.3-5 shows the alternate design.

### 6.3.2 Root Attachment

Figure 6.3-6 shows the low-wedge, one inch splay radius, titanium dovetail attachment selected for the advanced composite fan blade, while Figure 6.3-7 is a sketch of the titanium dovetail attachment geometries considered. The low wedge attachment was selected and fabricated under this program. The selected design has several advantages over the aluminum double-dovetail attachment design developed and tested under the Advanced Composite Engine Program, Phase I, Air Force Contract F33615-69-C-1651 and discussed in Technical Report AFML-TR-70-89, J. A. Mangiapane, April, 1970. The prime advantage is the ample shear strength of the titanium pads; a ratio of maximum titanium shear stress at redline speed and 450°F to allowable titanium shear stress at the same conditions is 0.53. Other advantages include simpler geometry, superior wear resistance and a high bearing strength throughout the operating temperature range.

## 6.4 VIBRATION ANALYSIS

Blade vibration analyses, using BORSIC®/Aluminum composite material properties at both room temperature and 450°F, were conducted. The effect of the Ni-Co leading edge was included in the analysis. Figures 6.4-1 and 6.4-2 are resonance diagrams showing the results of these analyses.

The analyses indicated that, at both room temperature and 450°F the TF30-P-9 BORSIC®/Aluminum fan blade with FOD protection will be excited in first bending by 2E engine frequency at about 5000 rpm. This rpm is just above idle in the engine operating range which would occur only during rapid descent from high altitude. The 5000 rpm speed does not coincide with any potential operating speed of extended duration.

The coupled blade-disk second mode 2-nodal diameter frequency satisfies the Pratt & Whitney Aircraft imposed ten percent margin requirement on 2E excitation at redline engine speed. To meet this requirement for a Ni-Co FOD protected blade, the disk design incorporates a live-rim thickness 0.1 inch larger than the rim thickness of a disk designed for a blade with titanium FOD protection. Figure 6.4-3 is a sketch which compares the two disks.

The shroudless BORSIC®/Aluminum blade with FOD protection exhibits a flutter parameter, ( $b \omega_t = 1187$  ft/sec) such that torsional flutter is not anticipated. This conclusion is reinforced by the results of a rig test conducted on shroudless third stage titanium blades having a  $b \omega_t$  of 1120 ft/sec. Test results indicated that the blades were flutter free.

## 6.5 STRESS ANALYSIS

### 6.5.1 Airfoil Steady Stress and Test Analyses

A gas-bending and blade tilt analysis was conducted on the BORSIC®/Aluminum blade in order to equalize the maximum shell stresses. The shell stresses are a maximum at two points on the blade airfoil root, on the convex side at the leading edge, and at point A as shown in Figure 6.5-1. The maximum shell stress (combined P/A, restrained warping, and gas-bending stresses) at the leading edge is reduced by tilting the blade to create a moment which acts against the gas-bending moment. The level of stress reduction which can be achieved in this way is limited because, as the leading edge stress is reduced, the stress at point A increases. The optimum tilt is attained when the leading edge shell stress with maximum gas loading equals the shell stress at the three-fourth chord position on the convex surface with minimum gas loading.

This analysis indicated that the recommended stack line offsets (tilt) were 0.2 inches tangential and 0.0319 inches axial at the blade tip. Table 6.5-1 lists the elastically calculated longitudinal stress components and their vector sum at the locations of peak stress at the airfoil root section ( $r = 7.01$  in.). Values are:

TABLE 6.5-I  
MAXIMUM AIRFOIL STATIC STRESS (psi)

Conditions: Mach No. 1.2, Sea Level, Max Afterburner, Fan Speed 10,355 rpm

	Core ( $0^\circ$ fiber orientation) 3/4 Chord (CV)	Shell ( $\pm 45^\circ$ fiber orientation) Leading Edge
P/A (p)	32,170	18,000
Restrained Warping	21,000	24,500
Tilt and Gas Bending	2,406	1,410
Total	55,576	43,910*

TABLE 6.5-I (Cont'd)

Conditions: Min. Gas Load, Fan Speed = 10,350 rpm

	3/4 Chord (CV)	3/4 Chord (CV)
P/A	32,170	18,000
Restrained Warping	21,000	19,450
Tilt and Gas Bending	7,070	6,920
Total	60,240	44,370*

**\* Balanced Stresses**

The recommended stack line offsets (tilt) were determined by balancing the total longitudinal stress at the leading edge of the shell (maximum gas loads, Mach No. 1.2, sea level, maximum afterburner flight conditions) against the total longitudinal stress at the three-fourth chord position on the convex shell surface (minimum gas load at fan speed of 10,350 rpm).

### 6.5.2 Titanium Dovetail Attachment

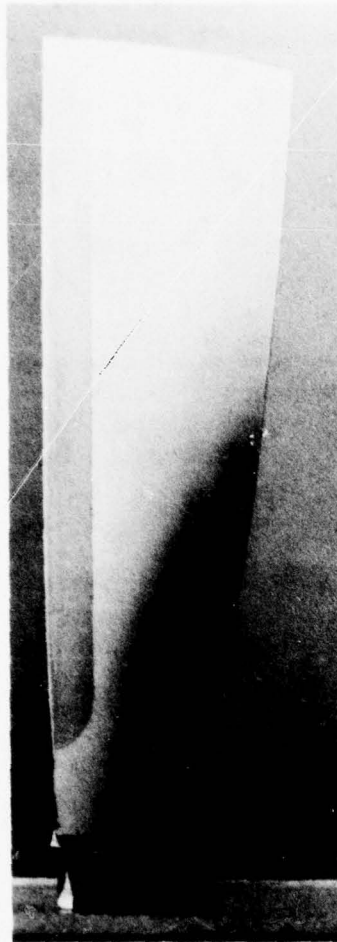
The titanium dovetail attachment was optimized by using a finite element method of analysis to determine the combination of fiber splay radius and wedge height which would result in minimum interlaminar shear stress in the  $\pm 45^\circ$  oriented fiber cross-ply. Two wedge heights were considered, and several splay radii were analyzed for each wedge configuration. Figure 6.5-2 shows a plot of maximum and average interlaminar shear stress in the cross-ply layers versus the splay radius for the "high" and "low" wedge designs. The optimum design is indicated to be a low wedge combined with a small splay radius.

The minimum bend radius to which the fibers can be subjected is limited by the maximum allowable bending stress induced in the fibers by curvature. Unidirectionally oriented fibers (core) may be bent about a minimum radius of 0.75 in. while the cross ply fibers (shell) may be bent about a minimum radius of 0.375 in. Bending about these minimum radii will induce a maximum 160,000 psi bending stress in the fibers. Figure 6.5-2 shows that the interlaminar shear stresses for the cross ply layers of the optimized dovetail design are less than the allowable value of 5,300 psi or 66.6 percent of the shear strength.

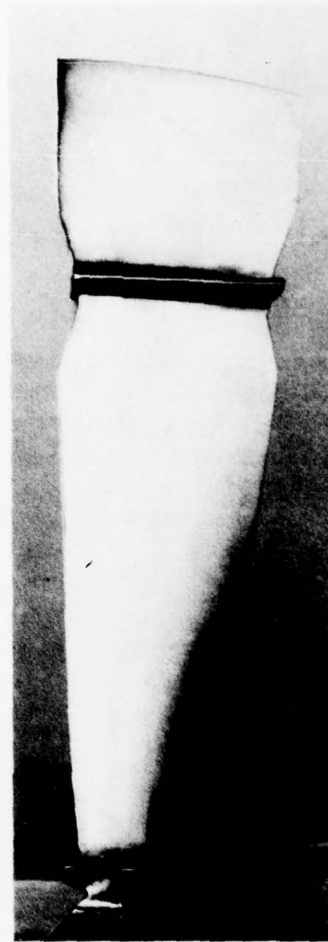
In the optimized configuration the fibers are splayed by a single aluminum wedge which produces a minimum splay radius of 0.75 in. in the unidirectionally oriented fibers. The titanium pads provide ample shear and bearing strength throughout the operating temperature range.

The root design point shown in Figure 6.5-2 was based on fabricability and inspectability considerations as well as laminar shear strength. Although the stress optimized design results in a slightly lower shear stress, the larger bend radius of the actual design point (one inch vs three-fourths inch) reduces fabrication difficulties at the root and facilitates ultrasonic inspection. In either case, the average shear stress is well below the allowable value and the maximum shear stress is not affected at all.

PRAITT & WHITNEY AIRCRAFT GROUP



**BORSIC®/ALUMINUM**



**B/M TITANIUM**

*Figure 6.0-1 Comparison of Shroudless TF30-P-9 BORSIC®/Aluminum Fan Blade Designed and Fabricated Under This Program With B/M Titanium Alloy Blade*

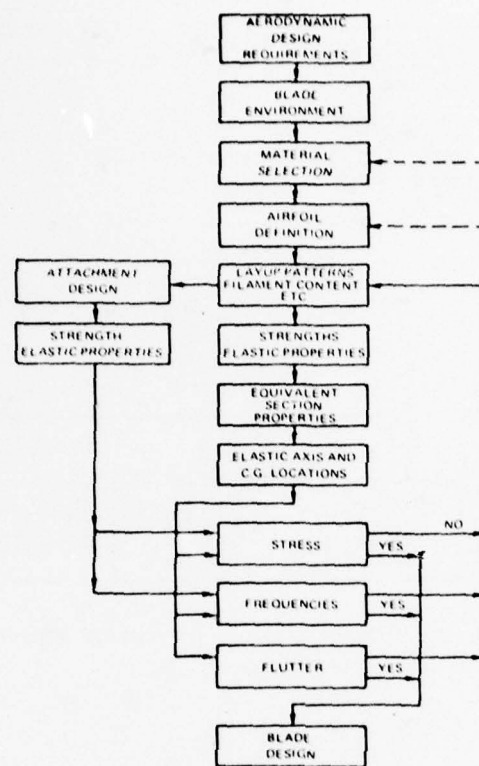


Figure 6.1-1 Typical Logic Network Used in Designing Composite Fan Blades

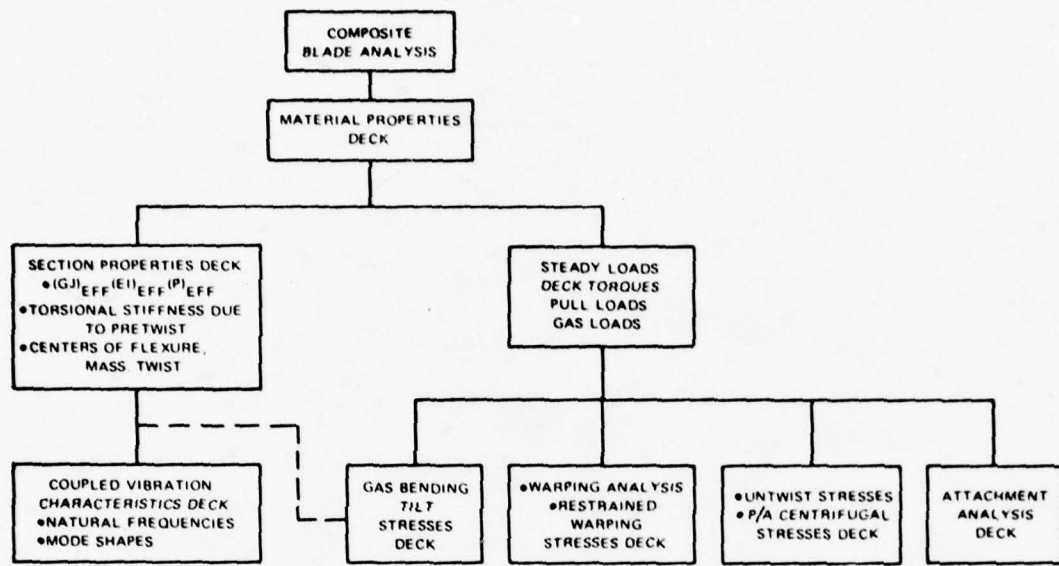


Figure 6.1-2 Computerized Techniques Developed by Pratt & Whitney Aircraft to Optimize Composite Blade Structural Design

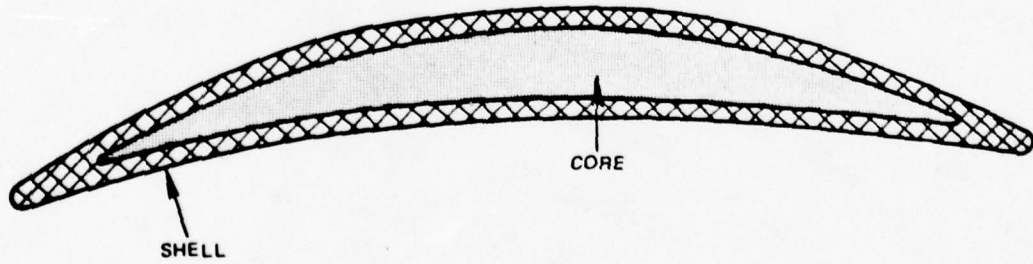


Figure 6.1-3 Core and Shell Blade Design As Shown in This Cross Section is Used to Meet Stiffness and Strength Requirements

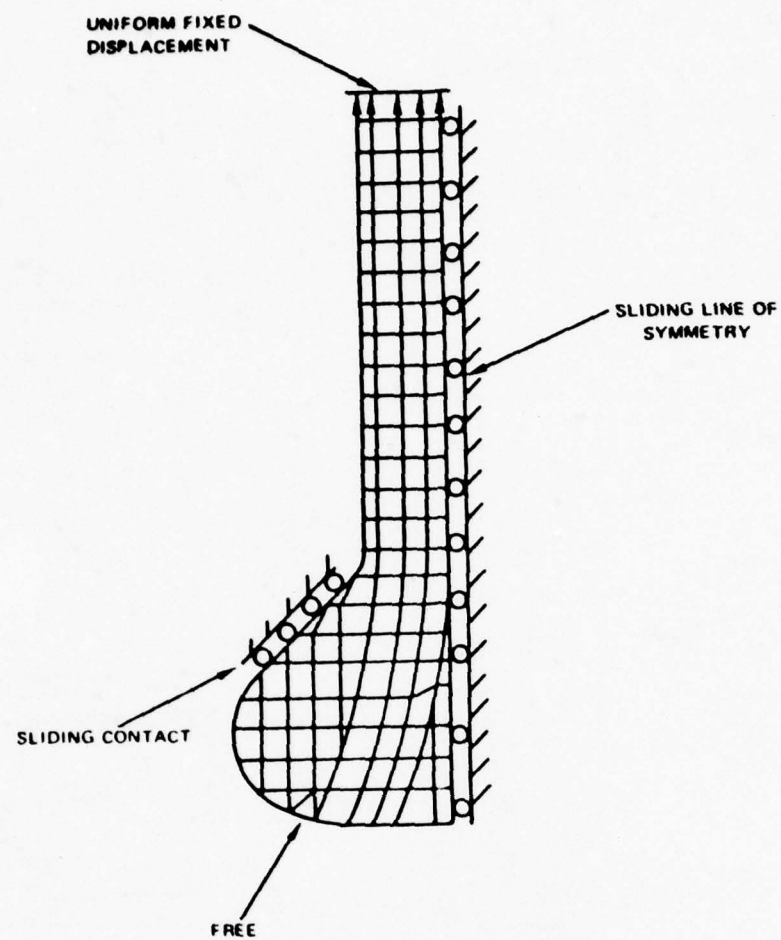


Figure 6.1-4 Typical Finite Element of a Blade Attachment Design

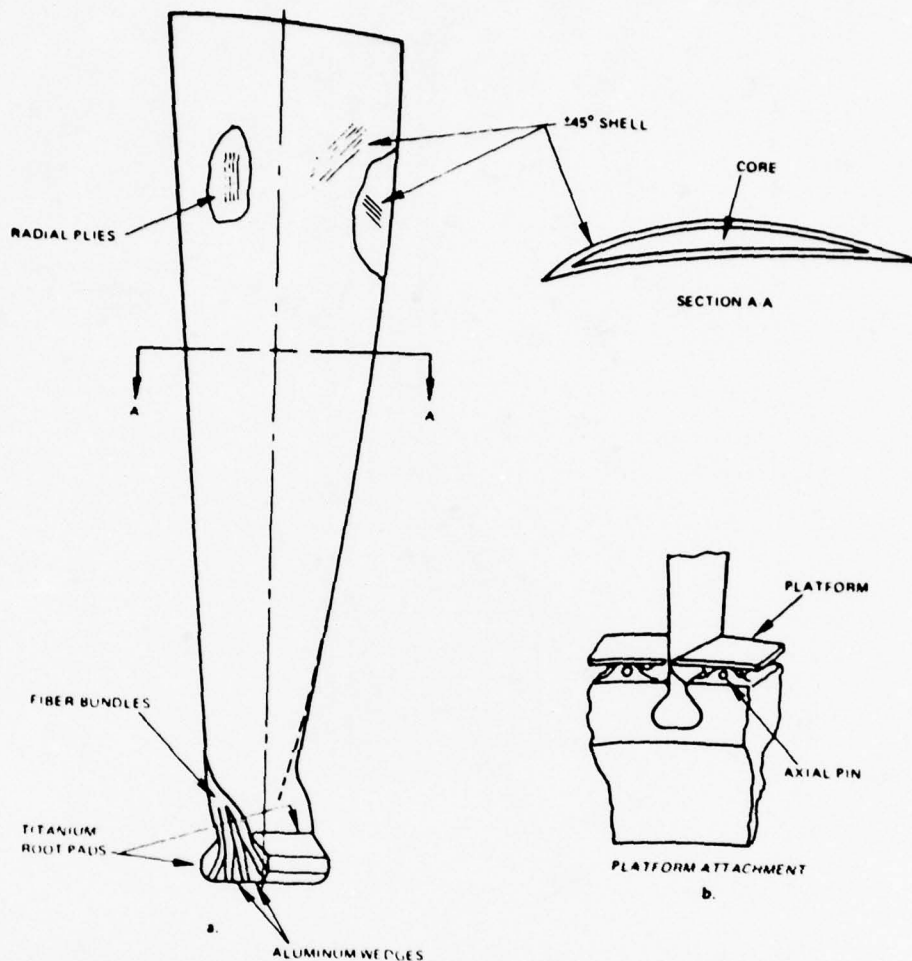
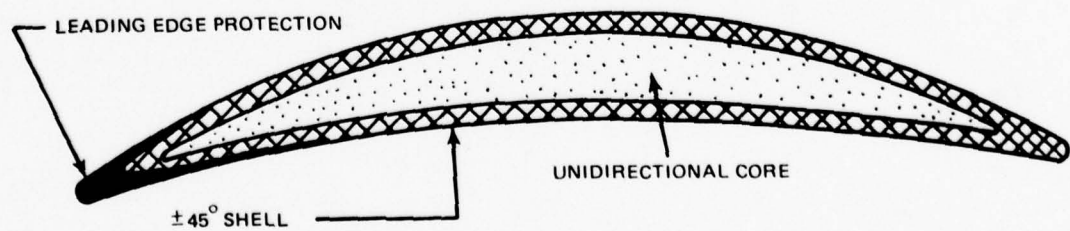
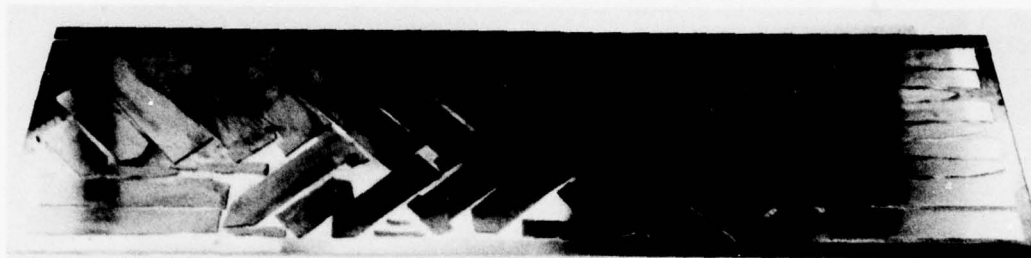


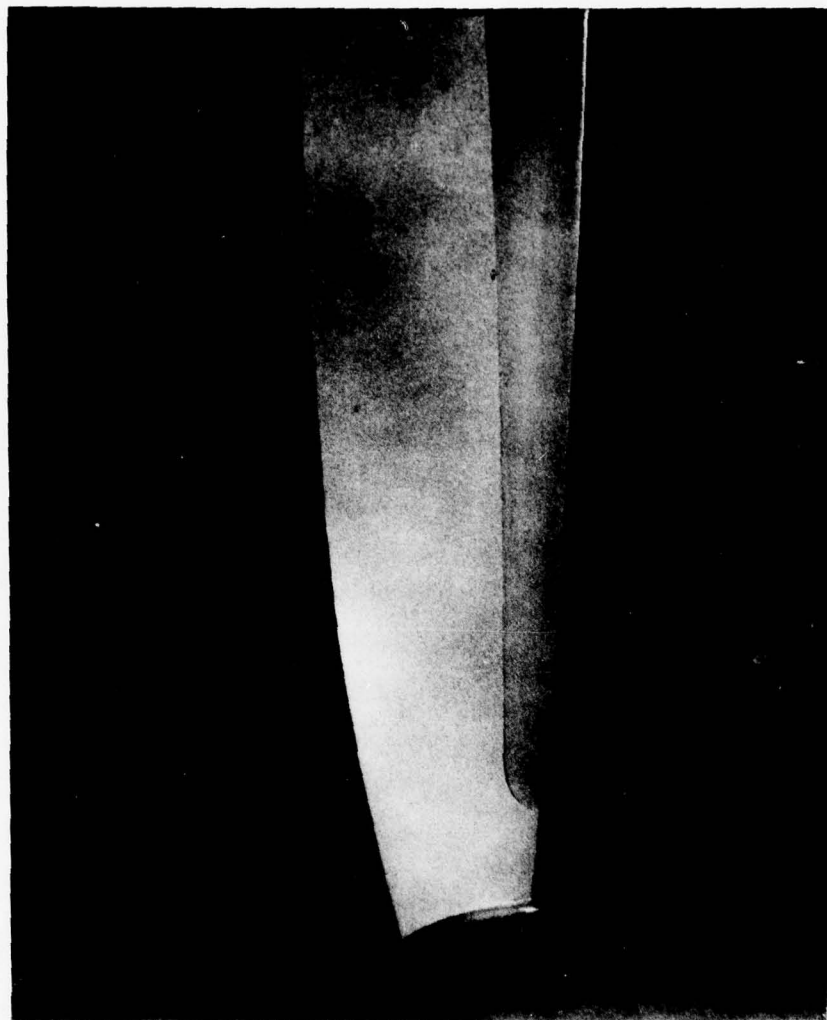
Figure 6.2-1 Typical Composite Blade Design Concept

Figure 6.3-1 Cross Section View of TF30-P-9 BORSIC®/Aluminum Third-Stage Fan Blade  
Designed and Fabricated Under This Program

44 PLY SHAPES



*Figure 6.3-2 Relative Sizes of the 44 Plies Used in the Construction of the BORSIC®/Aluminum Fan Blade*



*Figure 6.3-3 Composite Fan Blade Showing Nickel-Cobalt Leading Edge Protection Extending From Tip to Within One-Inch of Root*

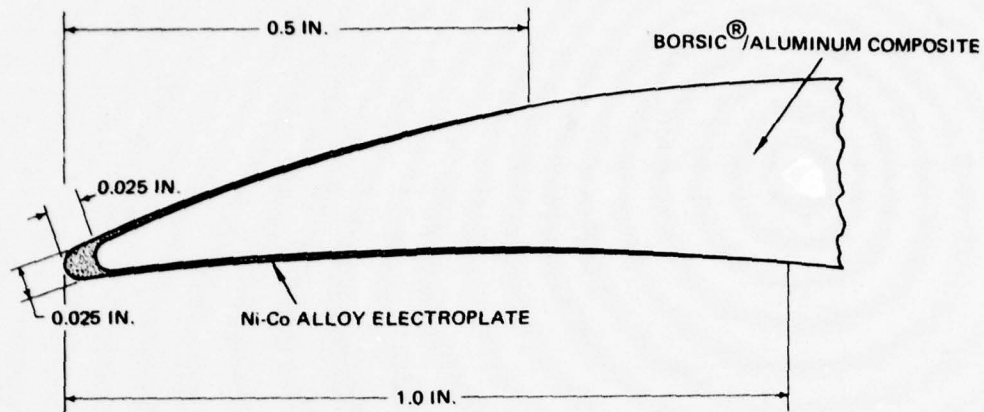


Figure 6.3-4 Cross Section View Showing Nickel-Cobalt Leading Edge Protection

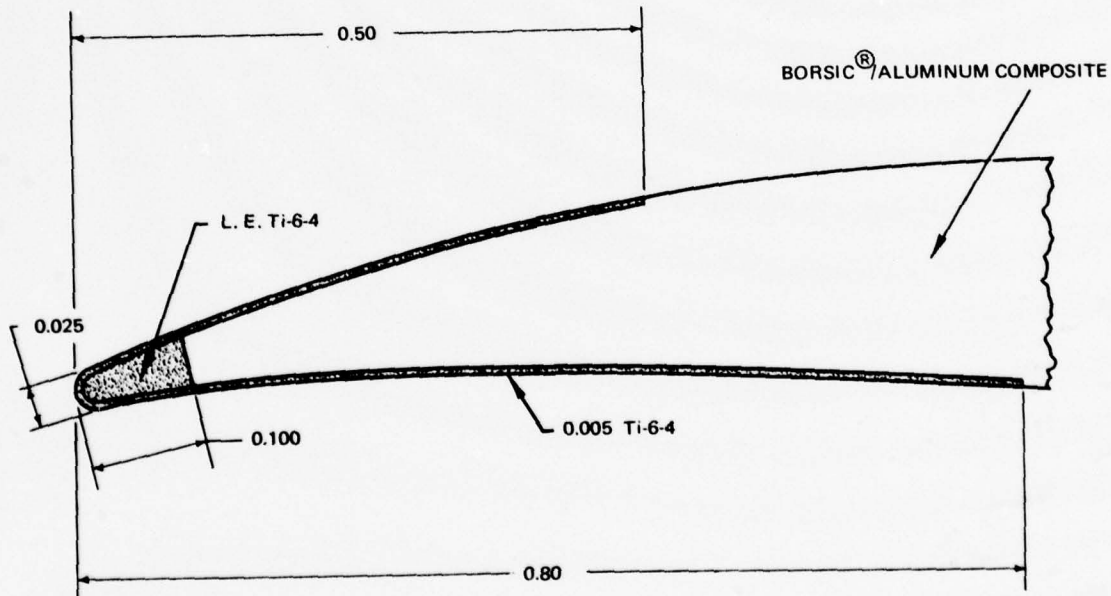
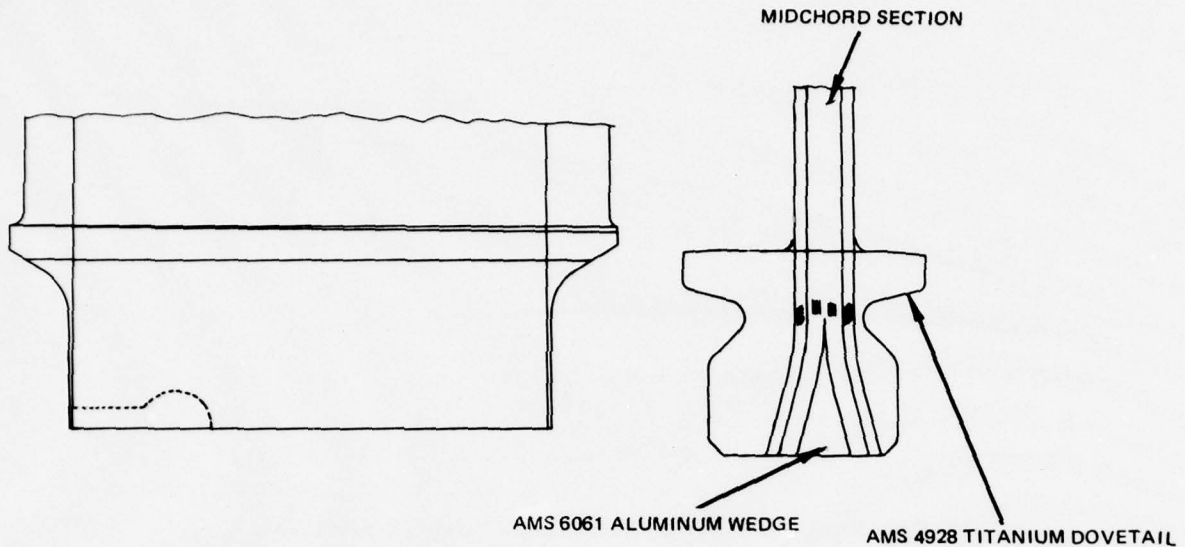


Figure 6.3-5 Alternate Design of Leading Edge Protection; This Design Was Not Pursued Because of High Cost and Fabrication Difficulty



*Figure 6.3-6 The Low-Wedge, One-Inch Splay Radius, Titanium Dovetail Attachment Selected for the BORSIC®/Aluminum Blades Designed and Fabricated Under This Program*

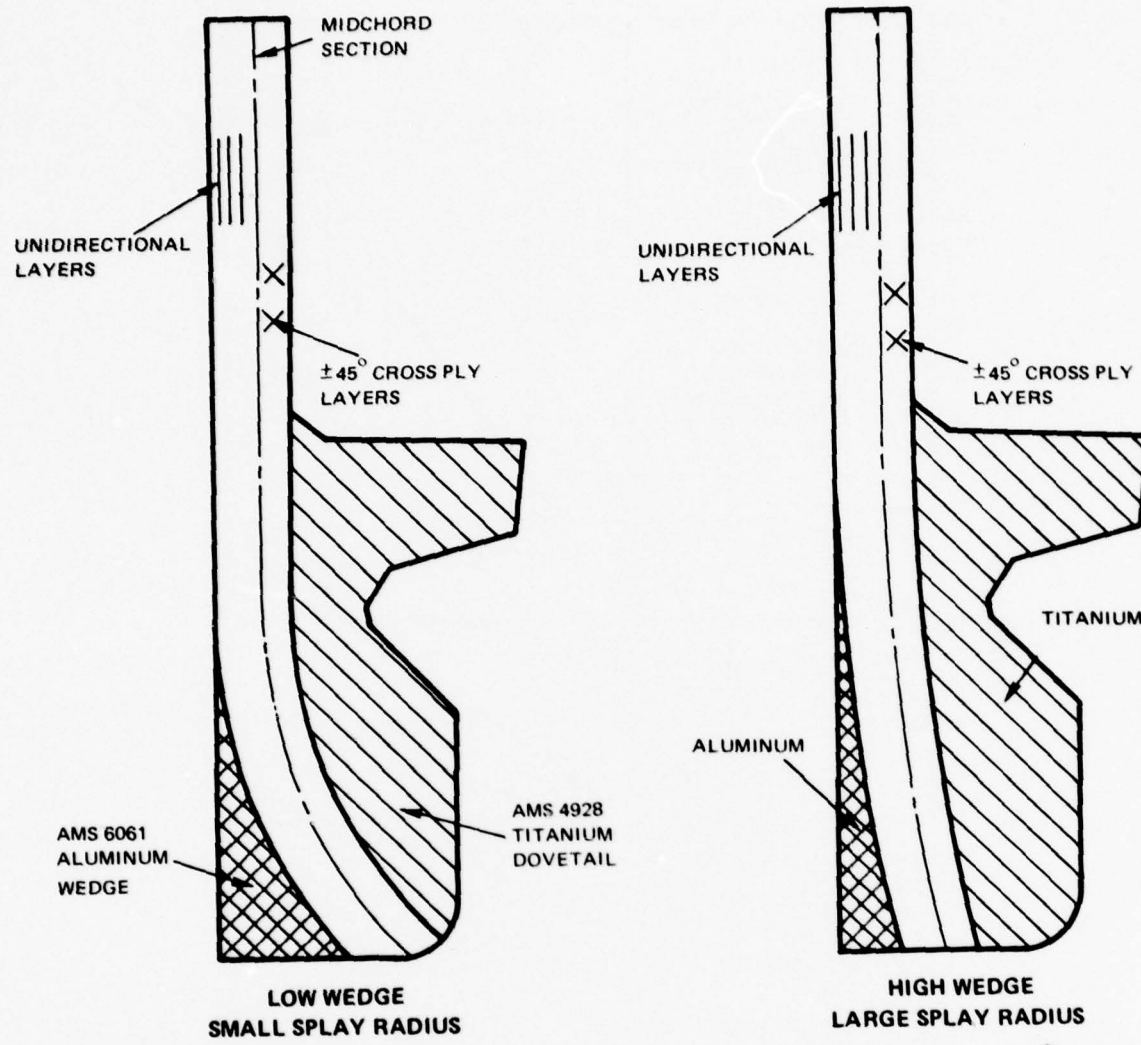


Figure 6.3-7 The Two Candidate Dovetail Geometries Considered for the BORSIC®/Aluminum Fan Blades

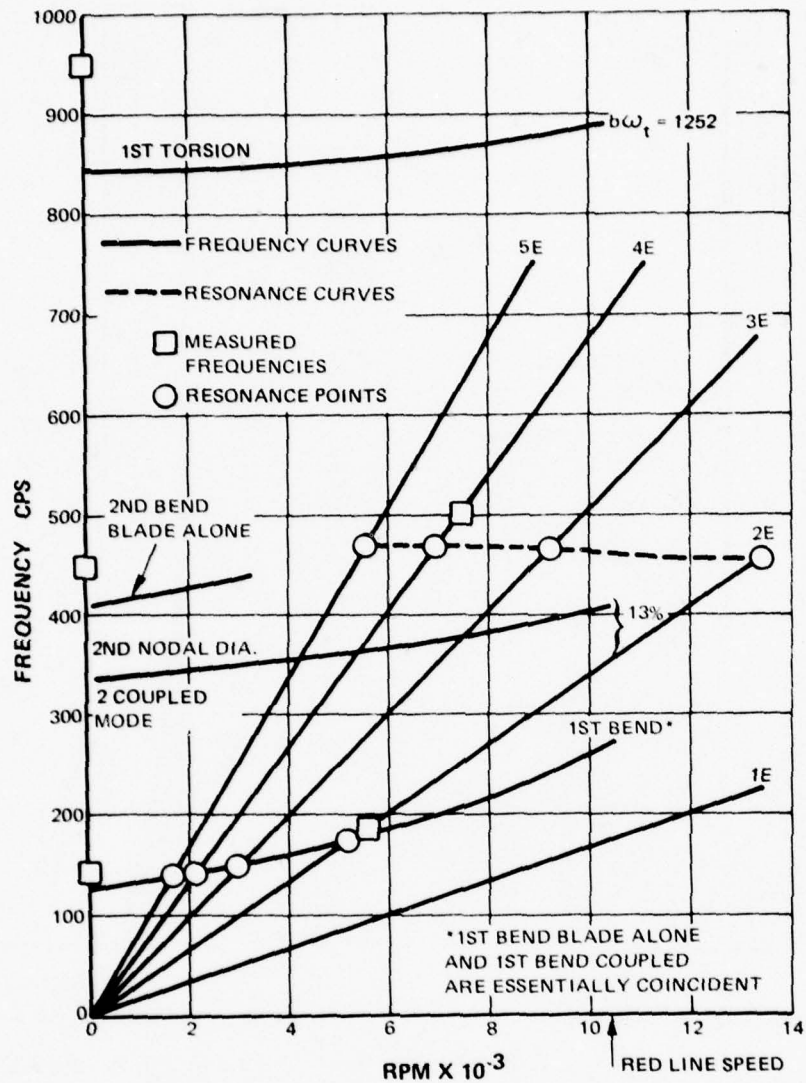


Figure 6.4-1 Resonance Diagram and Measured Frequencies of BORSIC®/Aluminum Third-Stage Fan Blade at Room Temperature

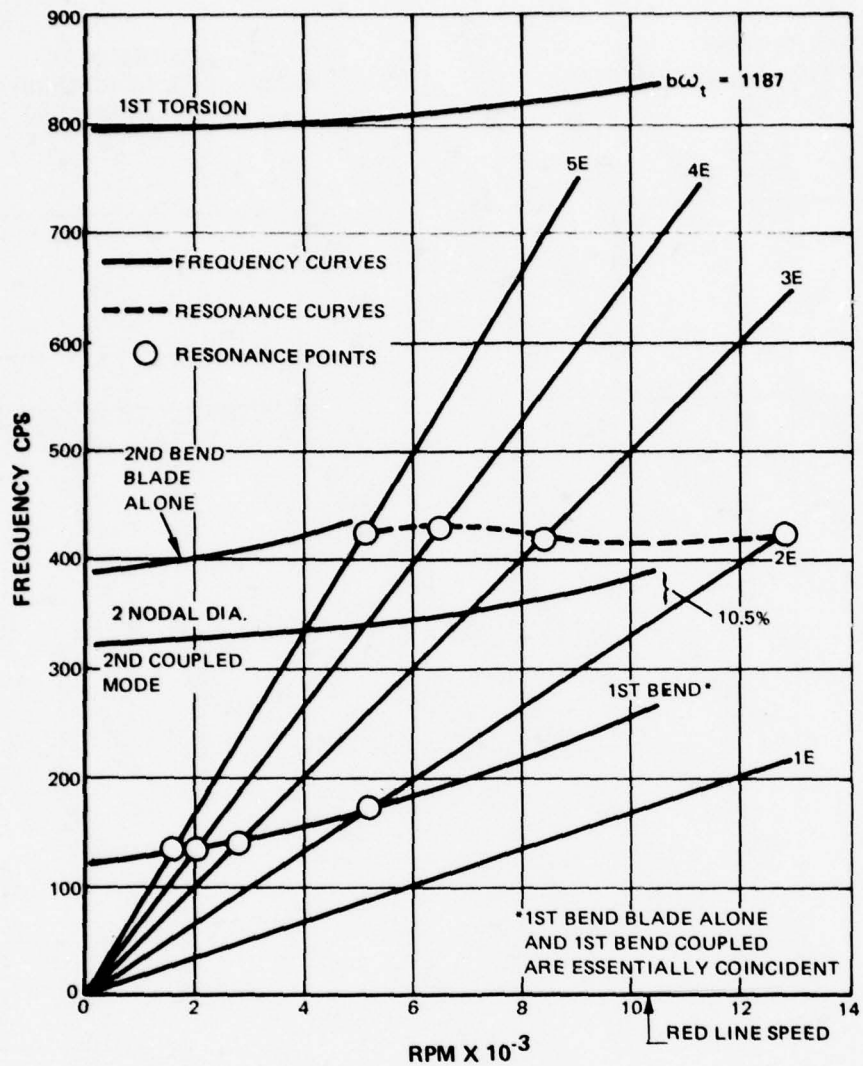


Figure 6.4-2 Resonance Diagram of BORSIC®/Aluminum Third-Stage Fan Blade at 450°F

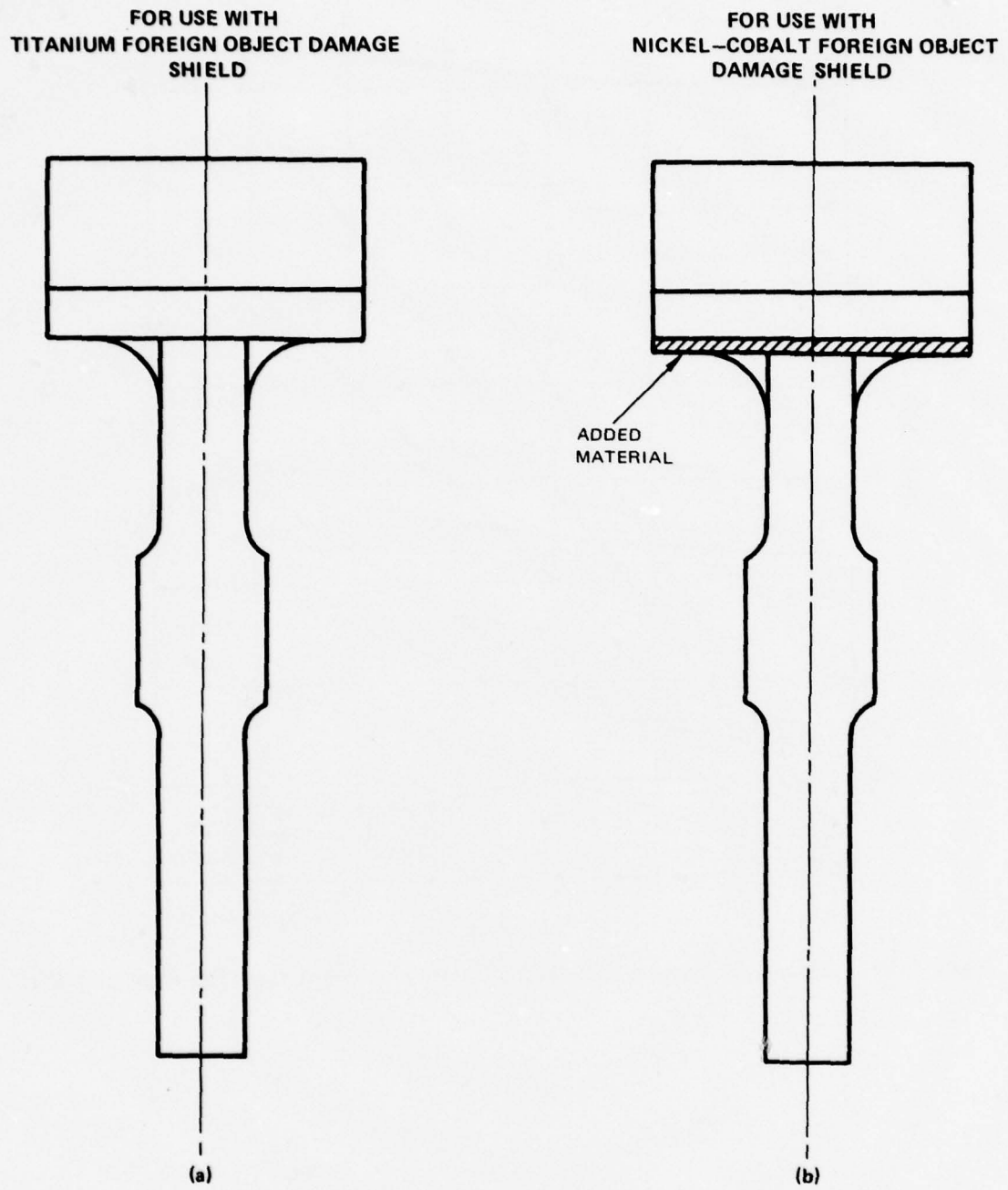


Figure 6.4-3 Comparison of Disk Rim Thickness Needed for Blades With Titanium FOD Protection With Thickness Needed for Blades With Nickel-Cobalt FOD Protection

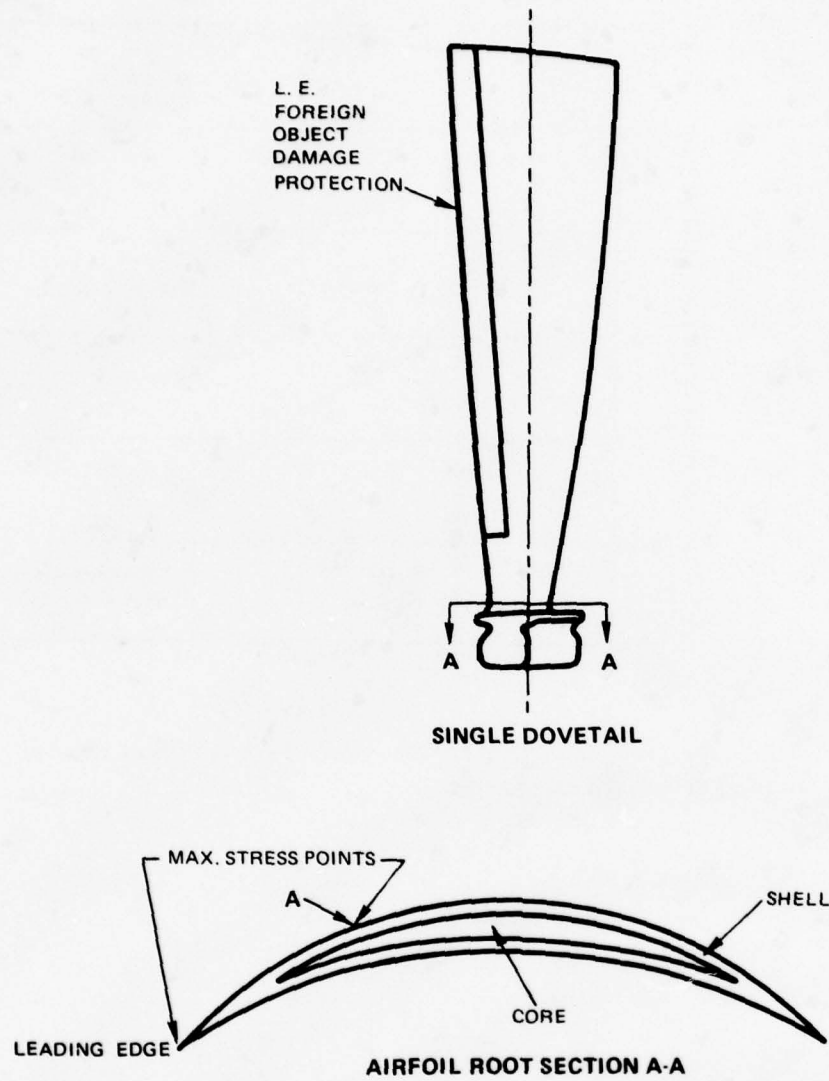


Figure 6.5-1 Cross Section View Showing Points of Maximum Shell Stress

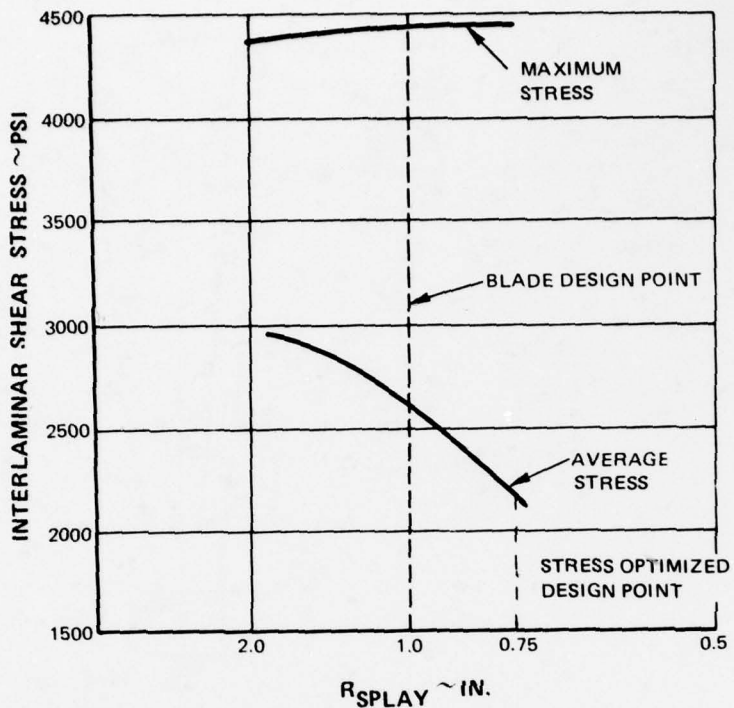
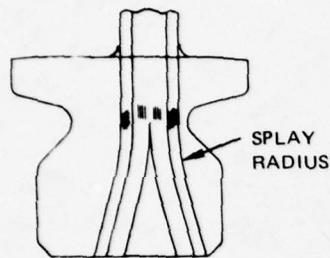


Figure 6.5-2 Plot of Maximum and Average Interlaminar Shear Stresses in the Cross-Ply Layers as a Function of Splay Rodius

## 7.0 FABRICATION, TOOLING AND EQUIPMENT

The fabrication processes and tooling used in producing the BORSIC®/Aluminum third-stage fan blades under this contract were developed specifically to meet the needs of this program; i.e., a short production run application. Emphasis was placed on developing the techniques and tools necessary to ensure technical success rather than conducting an effort directed toward possible future long production run cost optimization.

### 7.1 FABRICATION PROCESSES

#### 7.1.1 Development

Stringent process control parameters were established and adhered to throughout the program. These parameters will form the basis for fabricating flight quality hardware. In the blade bonding-diffusion process the atmospheric pressure in the retort was reduced to a maximum of  $10^{-4}$  Torr, the dies were heated to  $1050^\circ \pm 10^\circ\text{F}$ , and a load of 5000 psi was applied for 1.5 hours. Although holding these parameters was relatively difficult, it was an effective method of ensuring that the technical success of the program would not be compromised. Lowering the standards could have resulted in such a compromise.

During the development stages of the process, two problems were defined which had to be solved before fabricating parts of high quality.

The first involved fabricating the titanium root blocks to a  $\pm 0.002$  in. tolerance. Figure 7.1-1 shows these blocks. Machining was chosen over casting or forming as the most feasible method of producing the blocks. Both tracer machining (from a master) and numerical tape control (NC) machining were possible. The NC tape approach was tried unsuccessfully. Subsequent trials using the tracer technique were even less successful. Improved tooling was then developed and the NC approach again tried. This resulted in the successful and consistent production of engine quality parts.

The presence of a second problem area was recognized when initial spin-pit proof testing of the blades resulted in several failures at 115 percent design speed. It was determined that high residual stresses induced in the fibers during the hot-pressing operation were causing the failures. Initial remedial action was to relieve the stresses by adjusting the cool-down rate of the die. Success by this method was inconsistent, so an  $800^\circ\text{F}$  heat-treat was applied to the blades in their finished configuration. This procedure solved the problem and no further blade failures were experienced either in spin-pit or engine environment testing.

During this developmental period 59 blades, E-1 through E-59, were either not processed by optimum procedures or destroyed in spin-pit testing.

#### 7.1.2 Finalized Fabrication Sequence

Table 7.1-1 outlines the sequence of operations used in producing the blades from which all engine test blades were selected. This sequence was used to fabricate 189 blades (E-60 through E-248).

**TABLE 7.1-I**  
**FABRICATION SEQUENCE**  
**TF30 Third-Stage Composite Fan Blade**

<b>Sequence No.</b>	<b>Operation</b>
1.	Cut 44 plies of BORSIC <sup>®</sup> /Aluminum tape to correct shapes.
2.	Cut three plies of .005" 6061 Al foil.
3.	Machine two 6-4 titanium root blocks.
4.	Machine one 6061 Al wedge.
5.	Stack, preform, and tack-weld plies together into three packages.
6.	Record weight of blade components.
7.	Tack-weld together three ply packages, wedge, and root blocks.
8.	Load assembly into closed die.
9.	Transfer die to vacuum retort/press facility.
10.	Reduce pressure in retort to $10^{-4}$ Torr or lower, induction heat die to $1050^{\circ} \pm 10^{\circ}$ F, load blade to 5000 psi (78.5 tons), hold for 1.5 hrs., cool down.
11.	Remove compacted blade from die, deflash edges, and clean blade.
12.	Perform in-process, non-destructive inspection (density determination, ultrasonic C-scan, acoustic emission).
13.	Electroplate nickel-cobalt leading edge protection on airfoil.
14.	Shutting
15.	Machine root form, platform, and undercut, by grinding.
16.	Machine blade lock slot by electro-discharge machining (EDM).
17.	Machine blade tip by EDM (rough) and grinding (finish).
18.	Clean and heat treat at $800^{\circ}$ F for 3 hours (two cycles).
19.	Check airfoil twist.

**TABLE 7.1-I (Cont.)**  
**FABRICATION SEQUENCE**  
**TF30 Third-Stage Composite Fan Blade**

<b>Sequence No.</b>	<b>Operation</b>
20.	Mark blade with proper identification.
21.	Inspect blade dimensions.
22.	Inspect blade root by fluorescent penetrant inspection (FPI).
23.	Determine blade natural frequencies in first and second bending, and first torsional modes.
24.	Proof spin to 12,150 rpm (5 cycles).
25.	X-ray blade airfoil.
26.	Mark blade with appropriate experimental flight quality mark.

## 7.2 FABRICATION TOOLING AND TECHNIQUES

### 7.2.1 Ply Cutting (Sequence Nos. 1 and 2)

After establishing the final ply shapes to be used in this program, a ply cutting tool\* was designed and fabricated. Figures 7.2-1 through 7.2-4 show the tool and illustrate its operation.

The tool consists of 44 steel, ply-shaped templates, one for each of the required ply shapes. The templates were assembled into a single tool by adhesively mounting on a steel backing plate. Sharp upper corners were produced on the templates by means of a "skim" cut on the upper surface of the template assembly. To operate the tool, a sheet of BORSIC®/Aluminum tape was placed on the cutting surfaces of the tool. A sheet of reinforced cork, approximately one-half inch thick was then placed on top of the tape. This "sandwich"-tool, BORSIC®/Aluminum, and cork – was then passed through a set of rubber rollers. The pressure applied by the rollers was transmitted through the cork, thereby pressing the composite sheet against the templates which punched out the ply shapes.

In this program, approximately 50 sets of plies could be produced before another skim cut was needed to sharpen the tool.

\*A similar tool was used in Phase II of the Advanced Composite Engine Program, Air Force Contract F-33615-69-C-1651.

### 7.2.2 Root Blocks (Sequence No. 3)

Two titanium root blocks, shown in Figure 7.1-1, are used in each blade. Each of the blocks has one contoured surface with compound curvature; the remaining surfaces are flat. The contoured surface was machined in a Numeric Keller, and airfoil-section charts were used to prepare the numerical control tape. To maintain the dimensional tolerance of  $\pm 0.002$  in. required for this surface, special procedures had to be developed and implemented. These were:

- Parts were machined one at a time to assure optimum control, even though the Numeric Keller used is a three-spindle machine.
- A special tapered-shank cutting tool was designed which provided precise tool location.
- The cutting-tool head, shown in Figure 7.2-5, was made non-spherical in order to provide a more uniform cutting rate as the tool moved up or down the shoulders of the contoured surface of the block.

Tapped holes were provided in the surface of the blocks opposite the contoured surface to allow bolting to the Numeric Keller mounting plate. During final machining of the blade root these holes were eliminated.

### 7.2.3 Wedge (Sequence No. 4)

Each blade requires an aluminum (6061 aluminum alloy) wedge to splay the fibers in the blade root. To fabricate this wedge, a full ring having the required cross section was turned on a lathe. The ring was then cut into three sections, each of which was sufficiently long to form a single wedge. Figure 7.2-6 shows one of these sections. Because the tip of the wedge was designed to be as close as possible to a knife edge, it had to be supported by a back-up tool when the final cut was made.

### 7.2.4 Preforming and Spot Welding Plies (Sequence No. 5)

To facilitate loading the plies into the forming die, a preforming tool was designed and fabricated in order to assemble the 44 plies required for each blade. Figure 7.2-7 shows the plies required to fabricate a blade. The tool, shown in Figure 7.2-8 was contoured to duplicate the airfoil twist and camber. The tool was used to assemble the 44 plies into three separate packages. The assembly operation consisted of manually pressing the individual plies against the contoured surface of the tool and then spot welding them to a five mil 6061 aluminum alloy foil sheet and/or to each other in non-critical areas. To facilitate the welding operation, shown in Figure 7.2-9, the preform tool was made of copper.

Figure 7.2-10 shows the three packages of plies produced for each blade during the preforming and spot welding process.

### 7.2.5 Diffusion Bonding (Sequence Nos. 8, 9, 10)

Figures 7.2-11 and 7.2-8 show the blade bonding tool. This tool is a closed die consisting of a contoured upper punch and lower die, two tapered side plates, two tapered end plates, and a retaining ring. The retaining ring both aligned and contained the internal die components as well as acting as a susceptor (heat generating body) during the induction heating process. The tool is referred to as a "balanced" die because the root and tip chord angles are equal relative to the line of action of the punch.

Rectangular cavities at the root end of the punch accommodate the titanium root blocks. Three thermocouples, which pass through the upper surface of the punch, measure root, midspan, and tip temperatures during the diffusion bonding process. A fourth thermocouple measures the temperature of the susceptor ring.

Water-cooled induction heating coils, made of copper tubing, are wound around the susceptor ring, as well as around the upper flange of the punch and the lower flange of the die. Die stops between the punch flange and the end and sideplates limit the downward travel of the punch during the pressing operation.

In operation, the die was placed in a 42-inch diameter vacuum retort which was mounted in a 150-ton hydraulic press. A ten-inch, high-speed, vacuum diffusion pump, connected to the retort, had the capability to reduce the retort pressure to  $10^{-5}$  Torr. Supplementary controls and load, temperature, and vacuum recording instrumentation completed the installation. Figure 7.2-12 shows the vacuum retort/press facilities used.

Figure 7.2-13 is a chart showing the heat-up, hold, and cool-down cycle which comprised the total diffusion bond process. The heating cycle took about five hours normally and was performed as rapidly as possible, consistent with maintaining a vacuum of  $10^{-4}$  Torr or better. The hold, or bonding cycle, was accomplished in 1.5 hours at a temperature of  $1040^{\circ}\text{F}$ - $1060^{\circ}\text{F}$ , a ram pressure of 5000 psi, and a vacuum of  $10^{-4}$  Torr or more. Halting the induction heating initiated the cool-down cycle. The system was then allowed to cool at its natural rate to  $600^{\circ}\text{F}$  while the vacuum of  $10^{-4}$  Torr was maintained. When  $600^{\circ}\text{F}$  was reached, the retort was opened, argon was introduced into the retort and air cooling continued. At  $400^{\circ}\text{F}$ , the die was removed from the retort and disassembled. As Figure 7.2-13 shows, the cooling cycle took approximately three hours and the total diffusion bonding cycle required between nine and ten hours.

The die was then disassembled and the blade was visually examined. The final punch position was determined by measuring the height of the rivets above the die stops. The die components were then cleaned and prepared for the next bonding cycle.

A total of 168 blades were pressed in a single die with no significant die wear or distortion.

Artificially retarded cool-down cycles were tried early in the program in an effort to reduce blade residual stresses. The effectiveness of this approach proved inconsistent and a heat-treat cycle, described in a subsequent paragraph of this report, was far more successful.

#### 7.2.6 Deflashing (Sequence No. 11)

Because the blades were pressed in a closed die, the aluminum flash at the leading and trailing edges was a "vertical" flash as shown in Figure 7.2-14. This flash was removed by hand filing; no special tools were used.

#### 7.2.7 Leading Edge Plating (Sequence No. 13)

Electroplating of the Ni-Co leading edge was accomplished using the tooling shown in Figures 7.2-15, -16, and -17. The tool was shaped to control the amount of fluid available to the leading edge regions, so that a heavy build-up of plate would occur at the edge and a lesser thickness of plate would occur in the regions farther from the edge. This resulted in the tapered configuration shown in Figure 4.3-4, Section 4.3. The plating fluid was forced to circulate past the leading edge from tip to root in order to sweep away gas bubbles which tend to cling to the leading edge and cause pitting. Forced circulation decreased plating time as well.

A taper at the inboard (root) end of the leading edge plate was also required. This was accomplished by using a "thief" wire at that location. This wire captured current normally available to the blade, and as a result reduced the plating thickness in the local area around the wire.

Standard electroplating tanks and current controls were used for this process. The current controls were constructed to handle three blades simultaneously. Table 7.2-II outlines the plating process sequence.

#### 7.2.8 Shuttling (Sequence No. 14)

To prepare for final machining, the blades were fixed in shuttles which are short, thick-walled tubes (usually square or hexagonal) with ends and outer surfaces machined flat. The blades were inserted in the shuttle to a point just above the root as shown in Figure 7.2-18. A comparator image of an airfoil section near the root was used to properly orient the blade with respect to a reference surface on the shuttle. Originally, Cerrobend was used to fill the shuttle cavity in order to fix the blades firmly in place. Toward the end of the program Cerrobend was replaced by Rigidax WINF yellow, a reinforced wax, to position the blades. The last 50 blades (approximately) were shuttled with the Rigidax WINF yellow.

#### 7.2.9 Root Machining (Sequence Nos. 15 and 16)

Due to the presence of BORSIC®/Aluminum on some of the root surfaces, the root shape was produced by grinding. Conventional titanium grinding tools were used. The blade lock slot, shown in Figure 7.2-19, was produced by EDM again using conventional tools. Figure 7.2-20 shows the blade locks which were also produced by conventional means.

TABLE 7.2-II

PROCESS FOR PLATING NICKEL/COBALT LEADING EDGES ON  
BORSIC®/ALUMINUM FAN BLADES

Sequence No.	Operation
1.	Weigh blade and record
2.	Tape leading edges with Mylar tape
3.	Mask (five coats PMC 1801)
4.	Trim maskant
5.	Vapor blast (35 to 40 psi)
6.	Water rinse
7.	Fixture
8.	Check continuity
9.	PS48 dip - fifteen seconds ( $\text{HNO}_3$ -HF)
10.	Water rinse
11.	PS30 dip - fifteen seconds (zincate)
12.	Water rinse
13.	PS11 dip - ten seconds ( $\text{HNO}_3$ )
14.	Water rinse
15.	PS30 dip - fifteen seconds (zincate)
16.	Water rinse
17.	1 percent sulfuric dip - five to ten seconds
18.	Water rinse
19.	Nickel/cobalt plate - three hours with agitation on with current of 1.5 amp, nickel anode and 1.0 amp, cobalt anode
20.	Water rinse
21.	Remove from fixture
22.	Visually inspect - if acceptable, remove maskant - if not acceptable, strip with 50 percent $\text{HNO}_3$ , and replate
23.	Weigh blade and record weight
24.	Bake at 300° to 350°F, two hours*
25.	Polish
26.	Cut one-half inch off tip for hardness check and analysis (as necessary)

\*The 350°F bake improved the bond between the plate and the substrate and would also reveal a poor bond by causing blisters. The 50 percent cobalt, 50 percent nickel solution provided a plate hardness greater than that of 6-4 titanium alloy.

#### **7.2.10 Tip Machining (Sequence No. 17)**

Using the finished root as a position reference, the blade tip was rough machined by EDM, and finish ground. Conventional tooling was used.

#### **7.2.11 Heat Treating (Sequence No. 18)**

Blades were heat treated at 800°F by suspending them from a slotted rack shown in Figure 7.2-21 and heating them in the electric oven shown in Figure 7.2-22. This heat-treat was successful in relieving the residual stresses induced during the diffusion bonding cycle. These residual stresses had caused premature spin-pit proof testing failures in early blades (Section 10.3.3, Spin-Pit Burst Testing).

#### **7.2.12 Dimensional Inspection (Sequence No. 21)**

Blade root form was inspected in process using a 10X shadowgraph. Airfoil contour was inspected by use of a New England Plotter which produced a permanent 10X plot of any desired airfoil station.

Sequences 12, 22, 23, 24 and 25 refer to non-destructive inspection, which is covered in Section 8.0.

### 7.2.13 Disk

Figure 7.2-23 shows the third-stage disk which was produced by conventional means with the exception of the blade slots. Because the slots had to be deeper than normal, they were broached with two sets of broach cutters, one producing the upper portion of the slot, and the other the lower portion (Figure 7.2-24). The two-cut approach was taken to eliminate the expense of a new broach.

A full set of process operation sheets, describing the various operations in detail, accompanied each blade through its manufacturing cycle. At the completion of the cycle, these sheets were filed for future reference. Critical data items were recorded on the sheets as well. These items are listed in Table 7.2-III.

**TABLE 7.2-III**  
**PROCESSING INFORMATION RECORDED**  
**ON BLADE OPERATION SHEETS**

1. BORSIC®/Aluminum tape lot number(s)
2. Total weight of ply package, including:
  - Titanium root blocks
  - Aluminum wedge
  - BORSIC®/Aluminum plies
  - Aluminum foils
  - Shim
3. Weight of bonded blade
4. Root block shim thickness
5. Bonding temperature
6. Vacuum level during bonding
- \*7. Height of aluminum rivets above stops
- \*8. Height of aluminum rivets above die flange surface
9. Die used

\*These measurements indicate the position of the punch after the load has been applied.

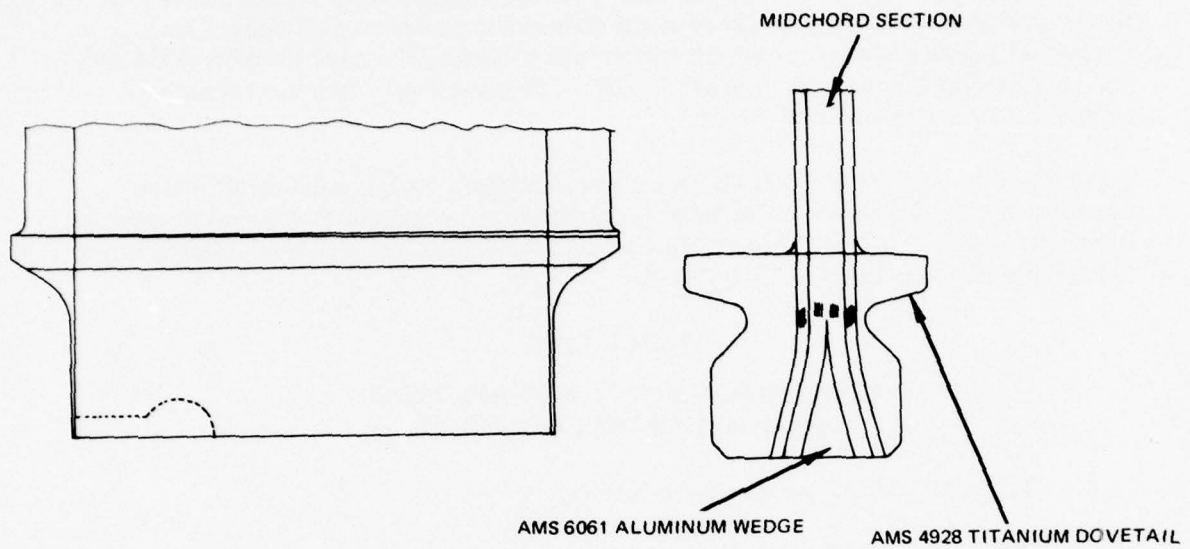


Figure 7.1-1 Titanium Root Blocks Used in Fabrication of the BORSIC®/Aluminum Fan Blades

44 PLY SHAPES



Figure 7.2-1 Roll-Cutting Templates for TF30-P-9 Third-Stage BORSIC®/Aluminum Fan Blade

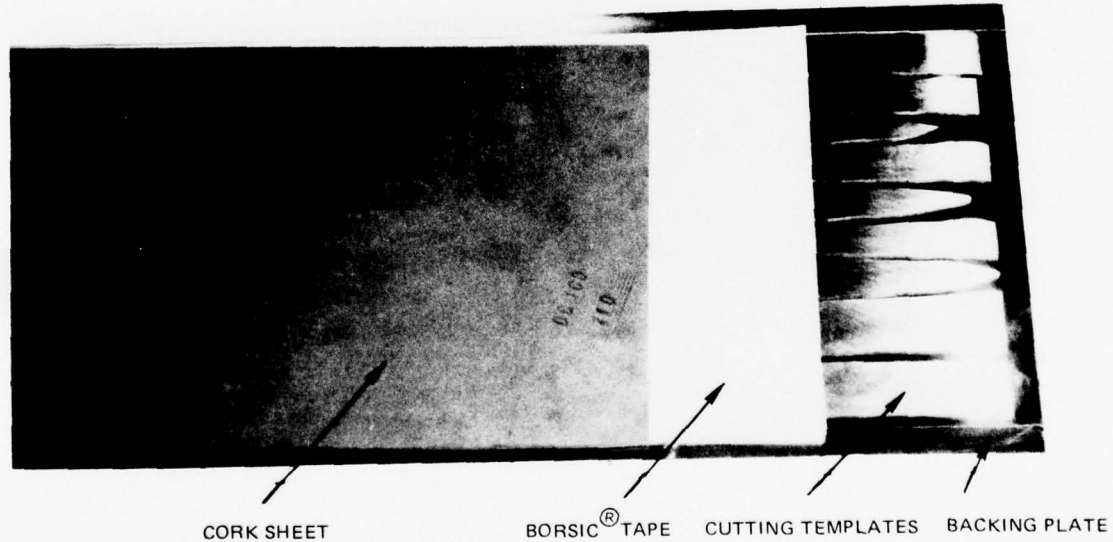


Figure 7.2-2 Roll-Cutting Sandwich for TF30-P-9 Third-Stage BORSIC®/Aluminum Fan Blade

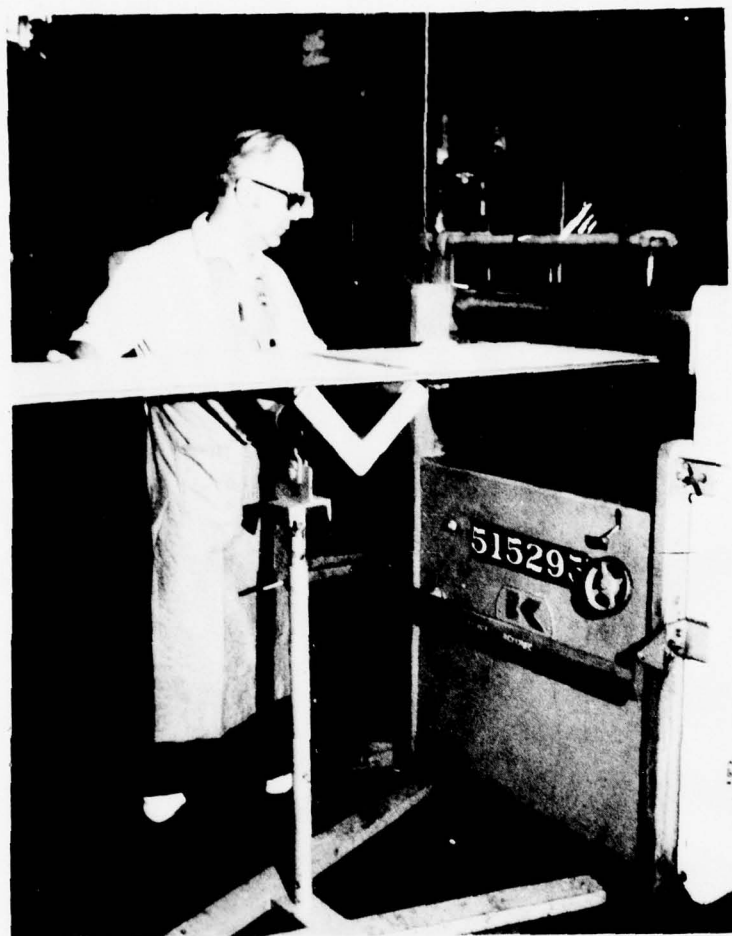


Figure 7.2-3 Roll-Cutting BORSIC®/Aluminum Ply Shapes



Figure 7.2-4 BORSIC®/Aluminum Plies After Roll-Cutting

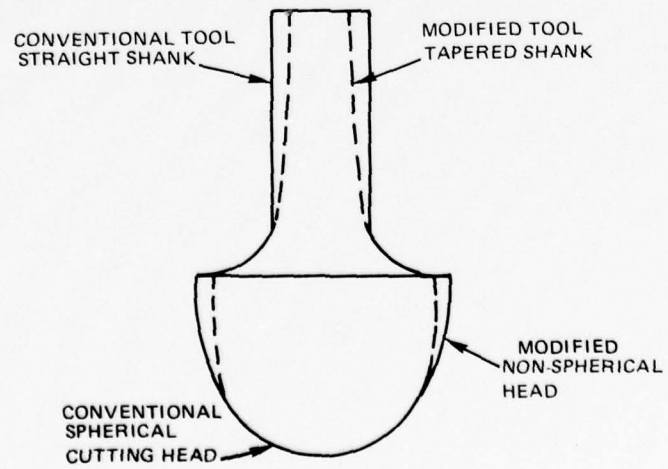
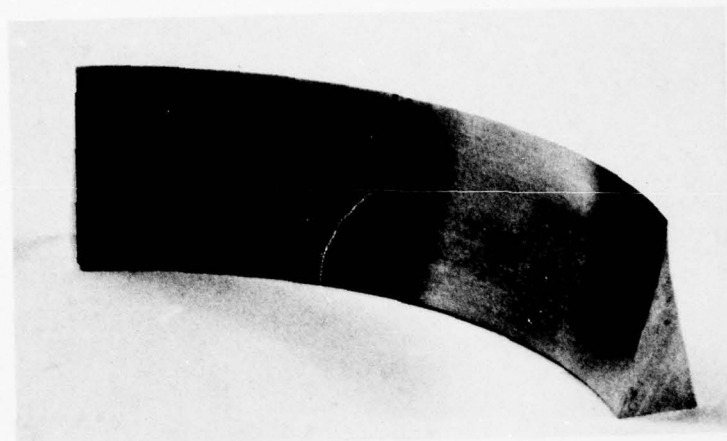
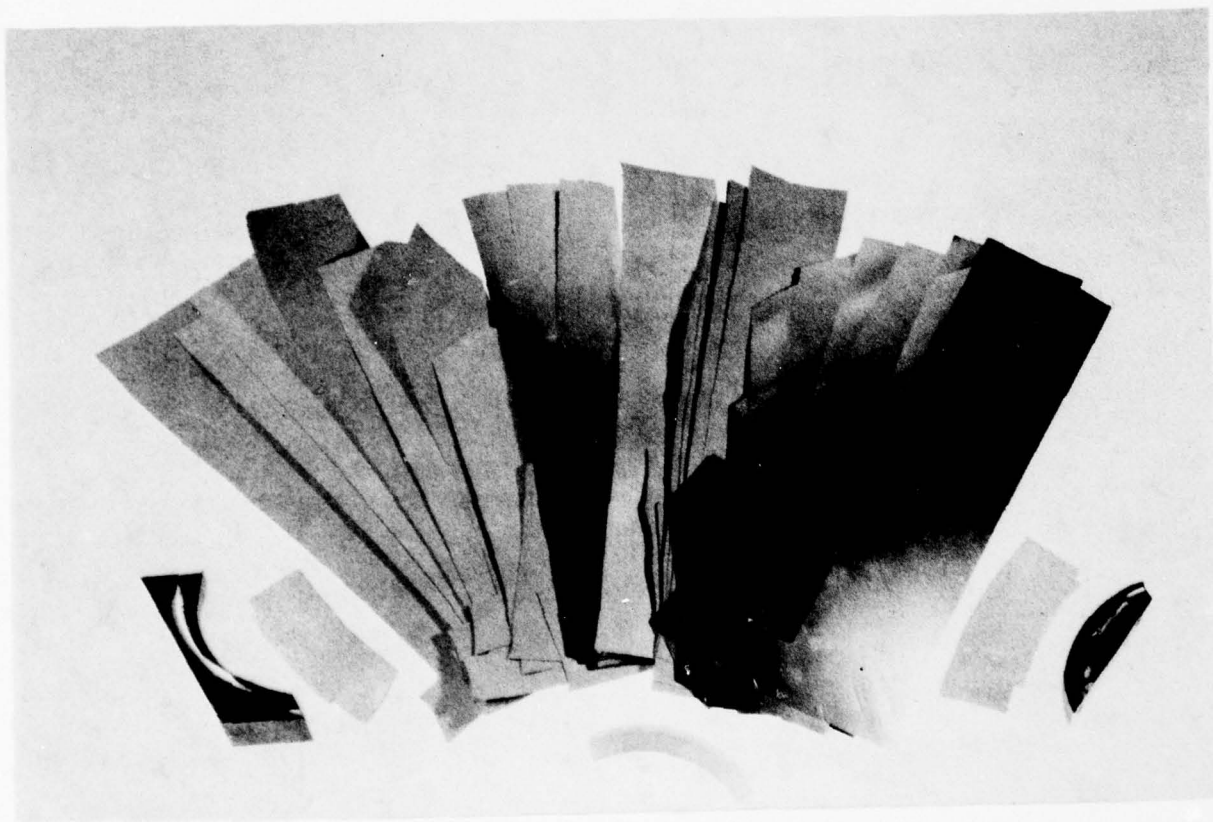


Figure 7.2-5 Schematic of Numeric Keller Cutting Tool Showing the Modified Head and Shank



*Figure 7.2-6 Ring Section Used to Form a Single Wedge*



*Figure 7.2-7 Plies Required to Fabricate BORSIC®/Aluminum Third-Stage Fan Blade*

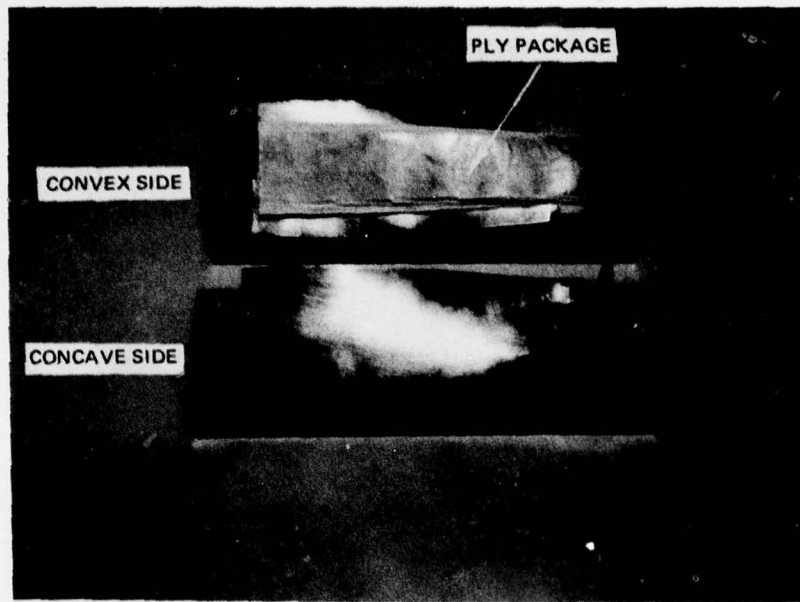


*Figure 7.2-8 Preforming Tool, with Ply Package in Position, Used to Assemble the Plies Into Blade Form*



*Figure 7.2-9 Spotwelding the Plies in the Preform Tool*

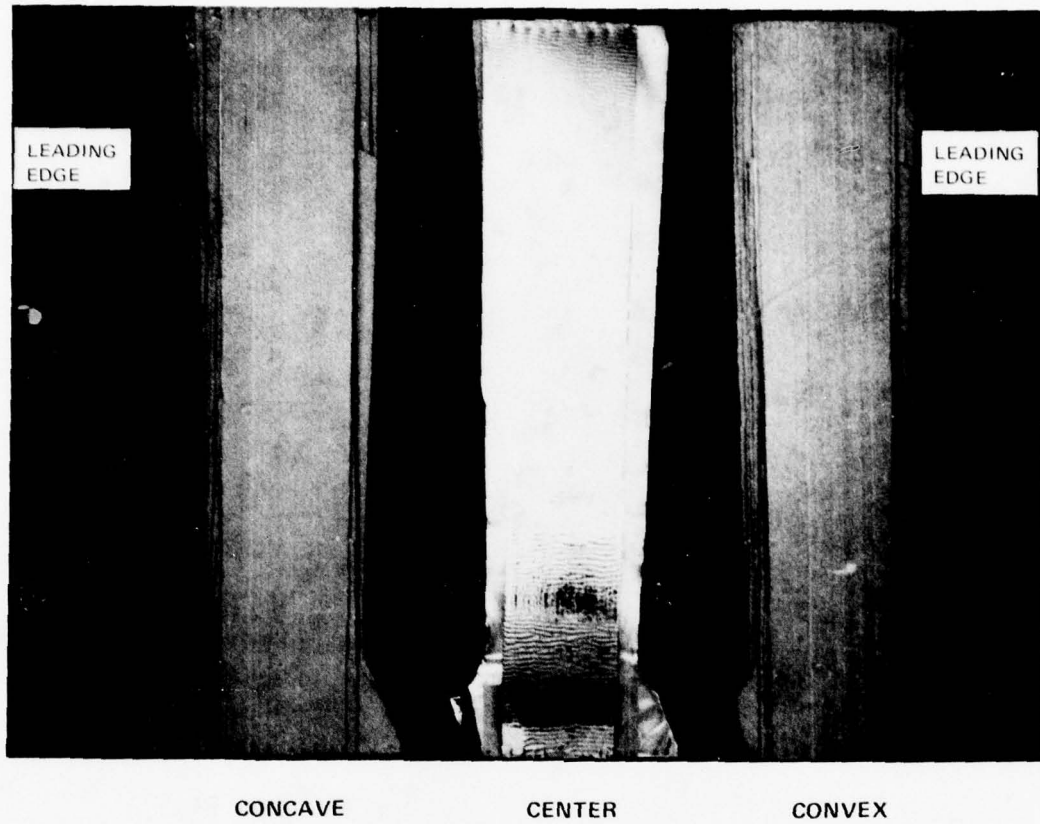


Figure 7.2-10 Three Packages of Plies are Produced to Form Each Blade

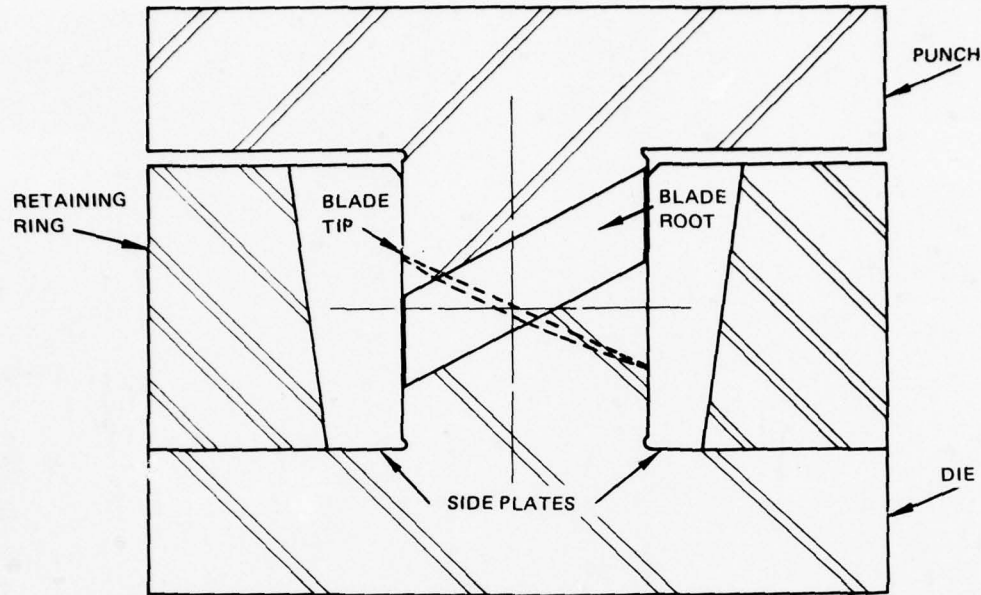


Figure 7.2-11 Cross-Section View of the Blade Diffusion Bonding Tool

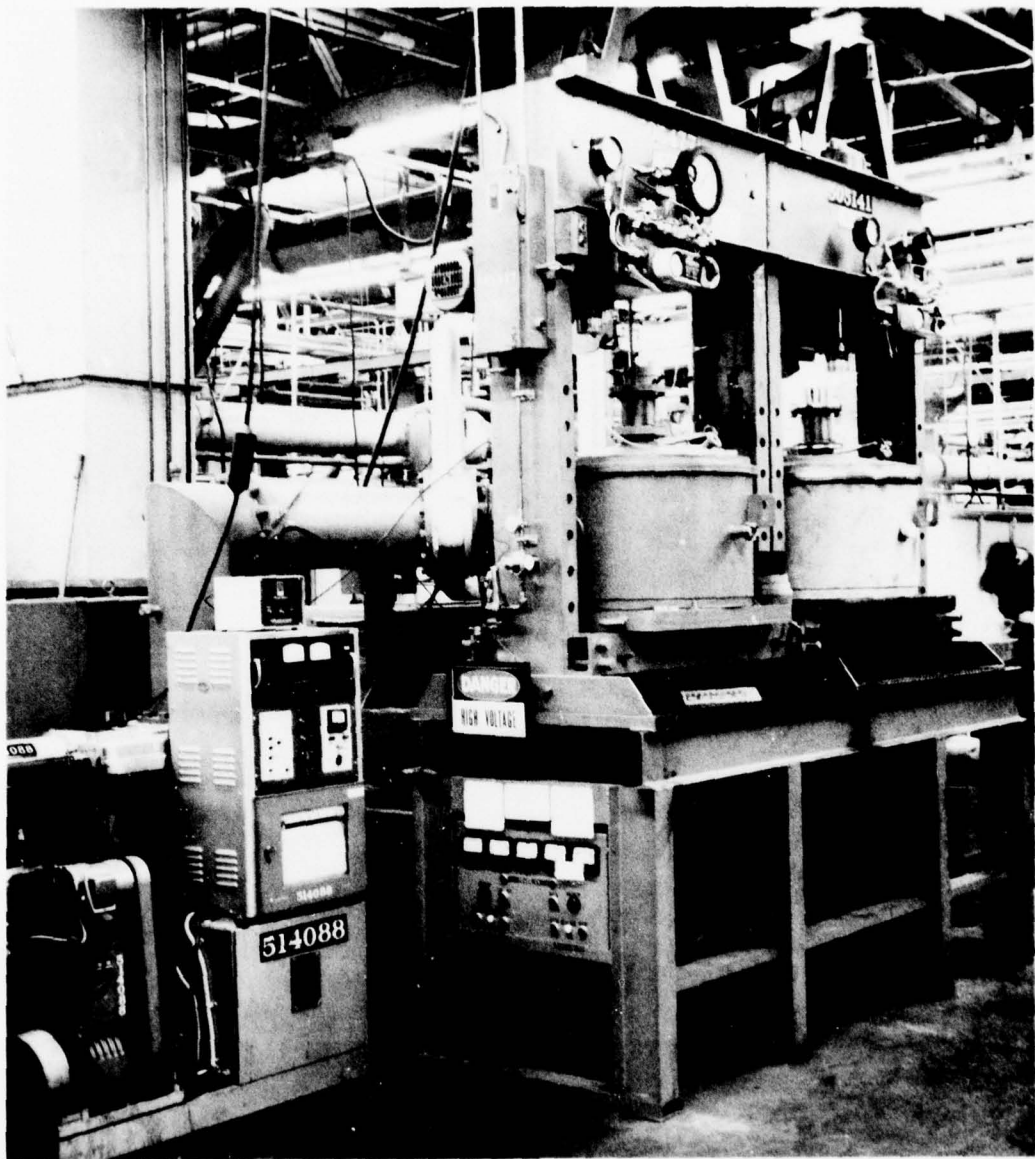


Figure 7.2-12 The Vacuum Retort/Press Facilities Used in the Diffusion Bonding Process

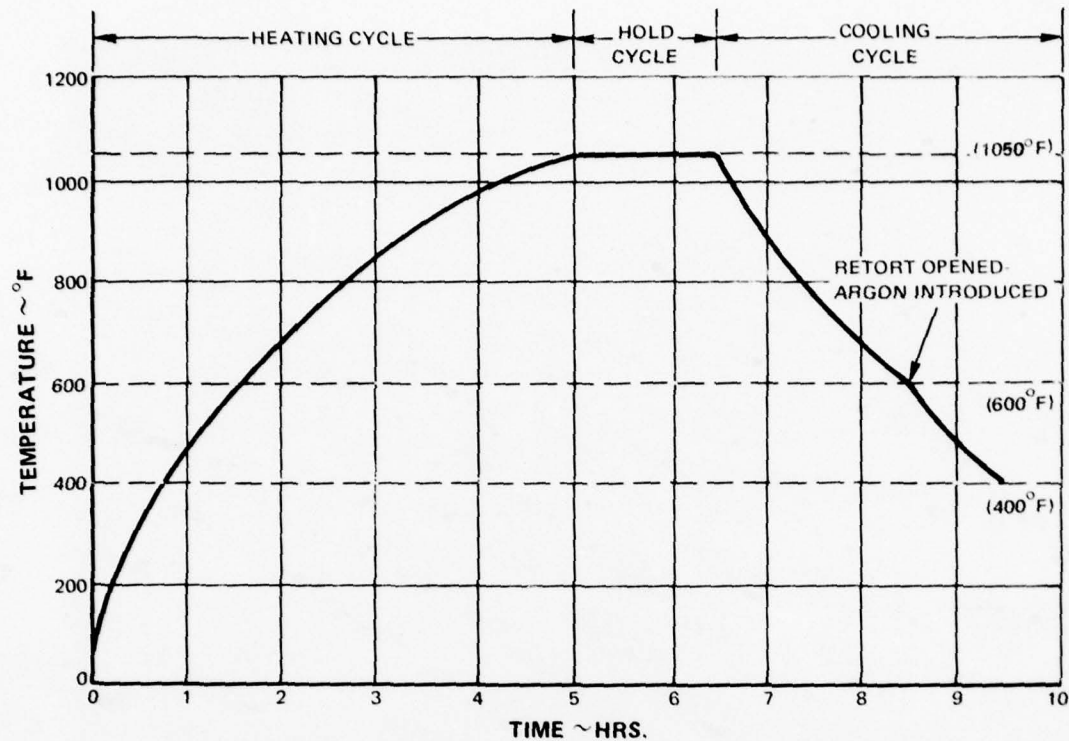


Figure 7.2-13 The Heat and Cooling Cycles Which Comprise the Diffusion Bonding Process; The Total Cycle Required Between Nine- and Ten-Hours

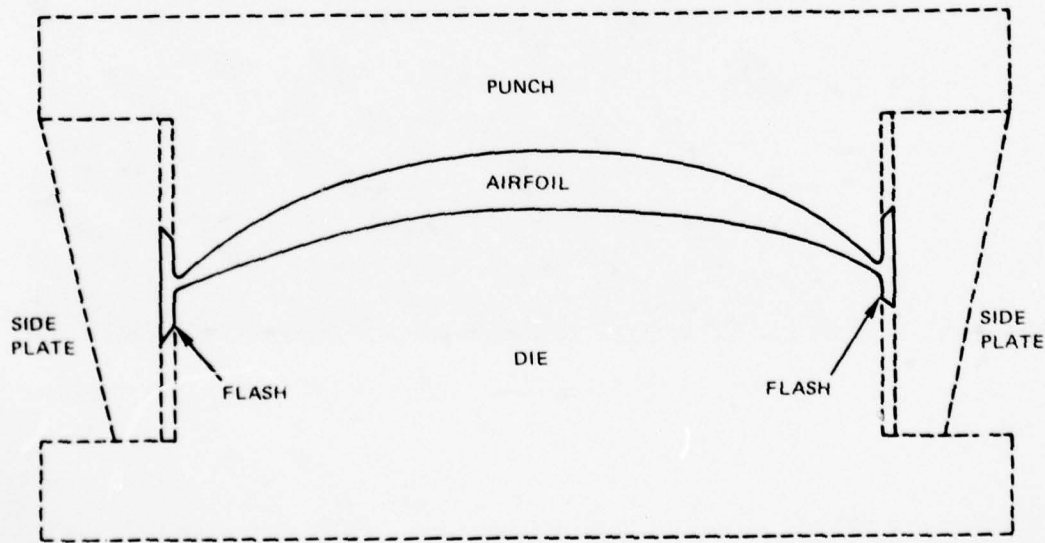


Figure 7.2-14 Schematic View of the "Flash" Which was Formed During the Diffusion Bonding Process (Exaggerated)

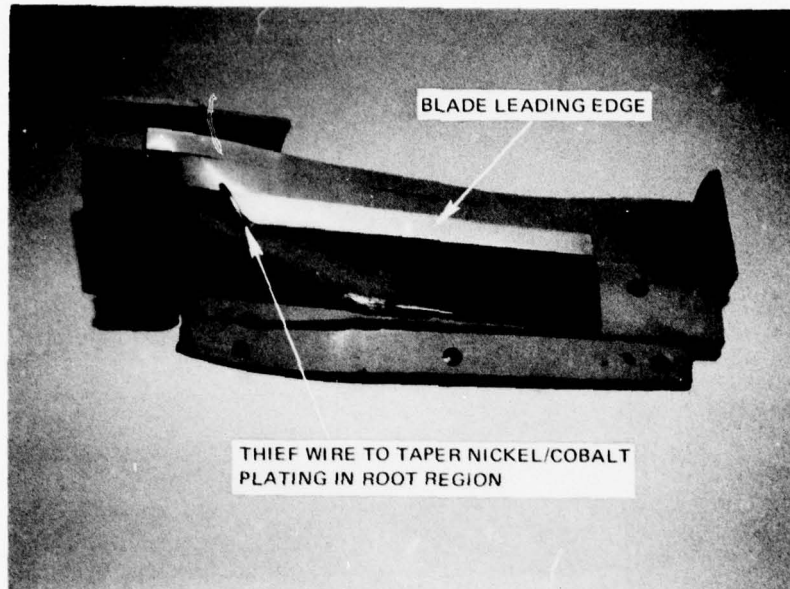


Figure 7.2-15 Composite Blade With Nickel-Cobalt Plating Tool Partially Installed

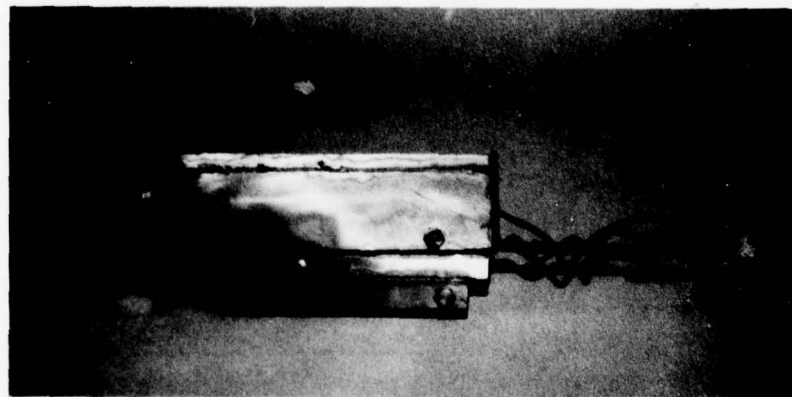


Figure 7.2-16 Composite Blade With Nickel-Cobalt Plating Tool Fully Installed



Figure 7.2-17 Nickel-Cobalt Plating Tank

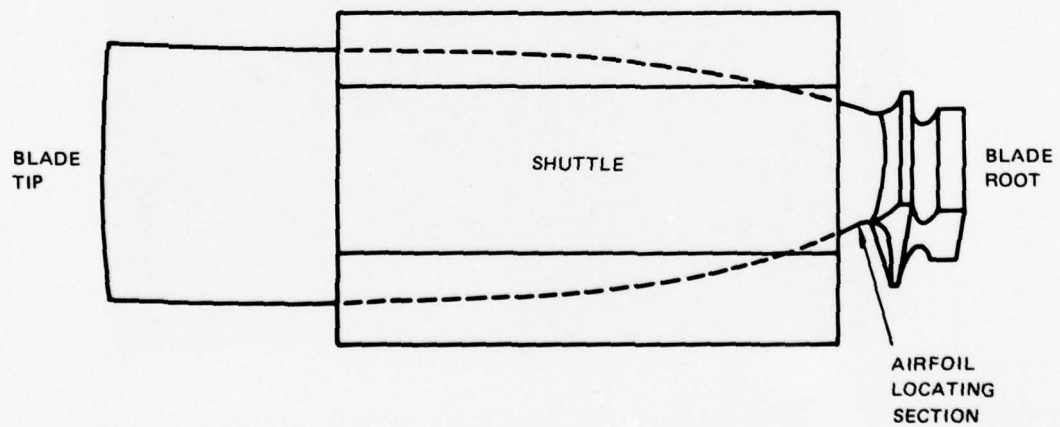


Figure 7.2-18 Schematic View of Shuttle Used To Position Blades for Final Machining

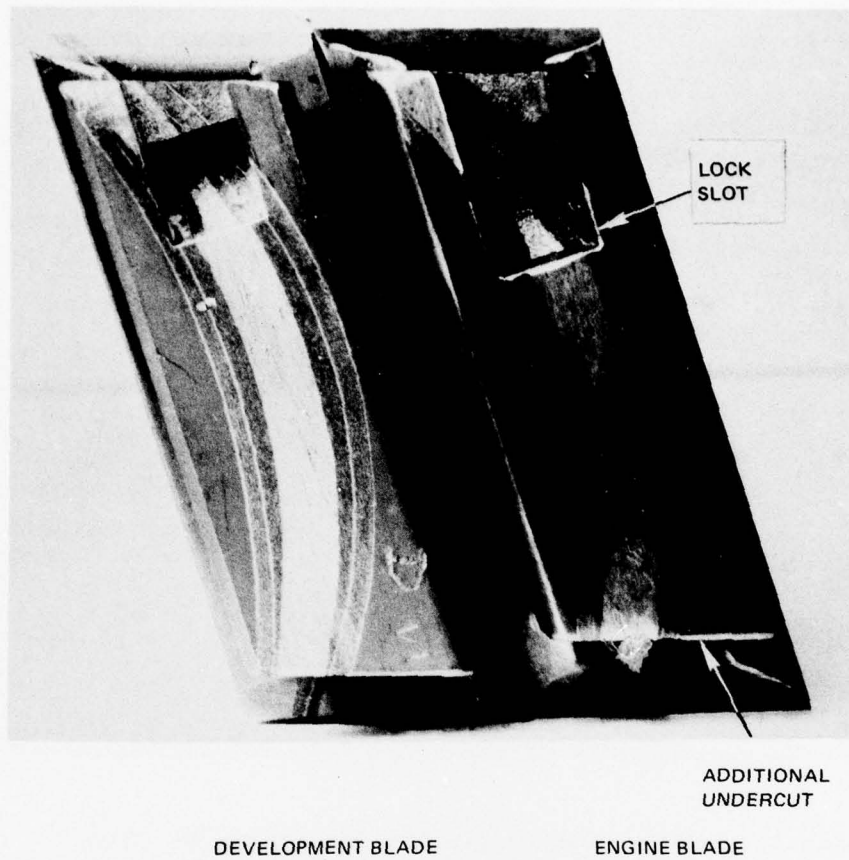


Figure 7.2-19 The Blade Lock Slots Were Produced By Electro-Discharge Machining

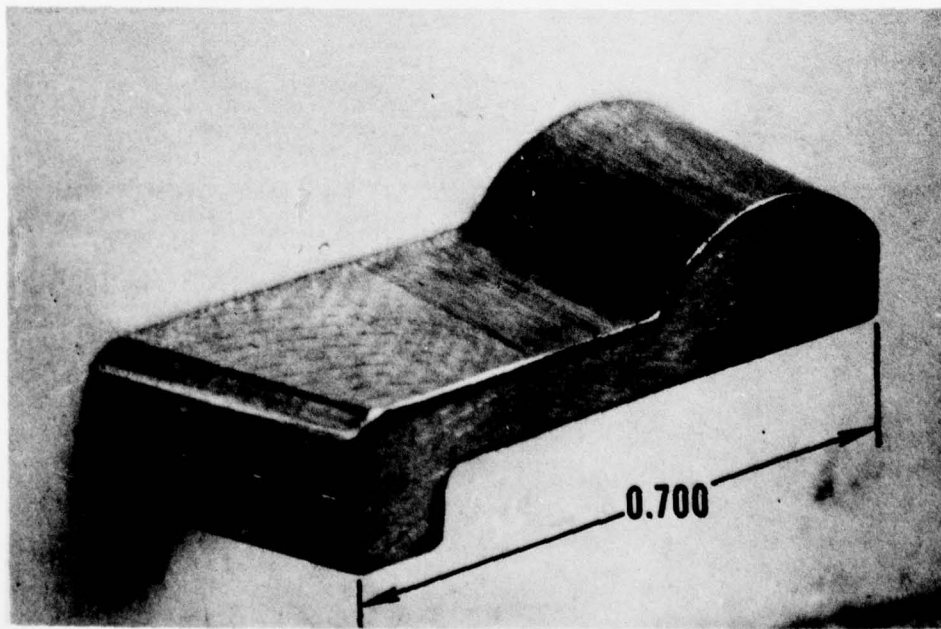
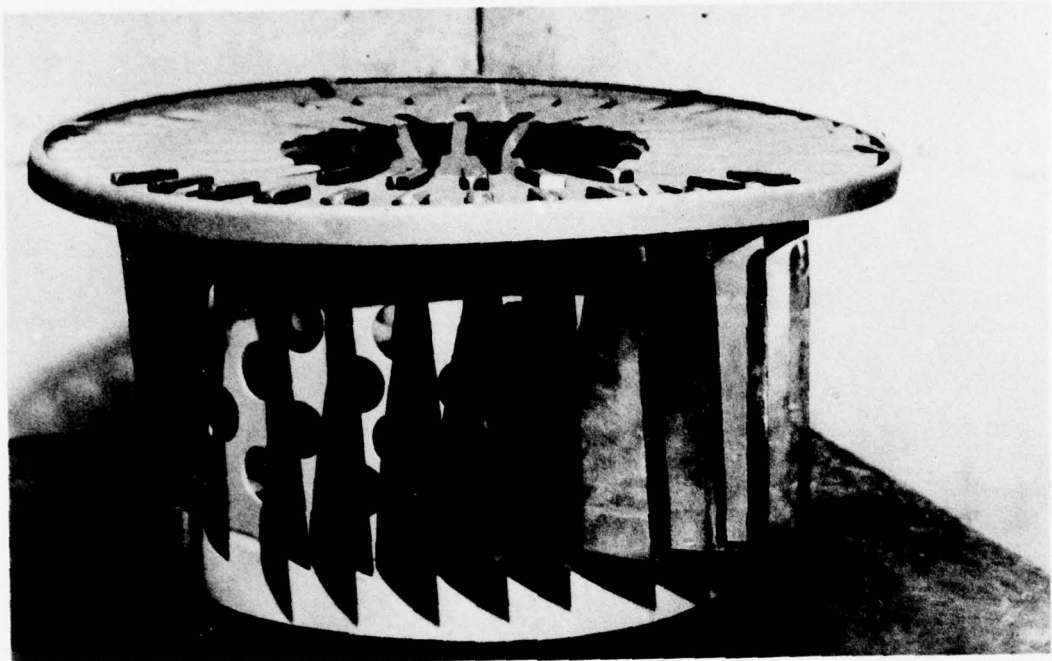


Figure 7.2-20 The Blade Lock Was Produced By Conventional Machining Methods



*Figure 7.2-21 Slotted Rack Used to Hold Blades During Heat Treat*



Figure 7.2-22. Electric Heat Treat Oven Used to Apply the 800° F Stress Relief Heat Treat

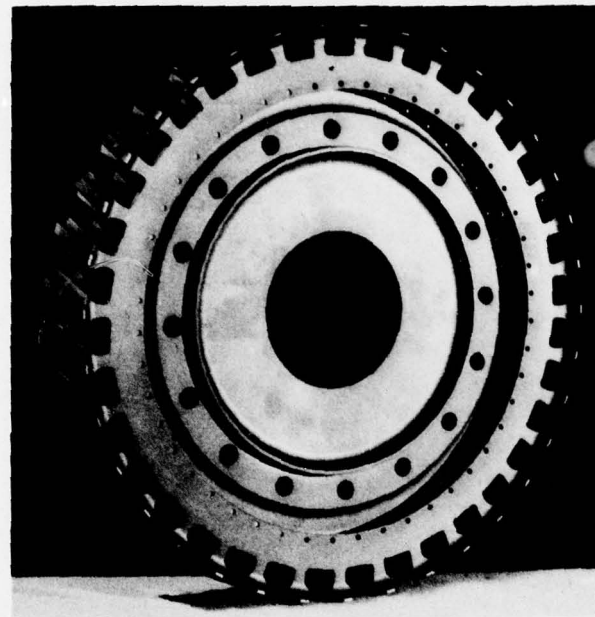


Figure 7.2-23 TF30-P-9 Third-Stage Fan Disk Adapted for Use With BORSIC®/Aluminum Blades

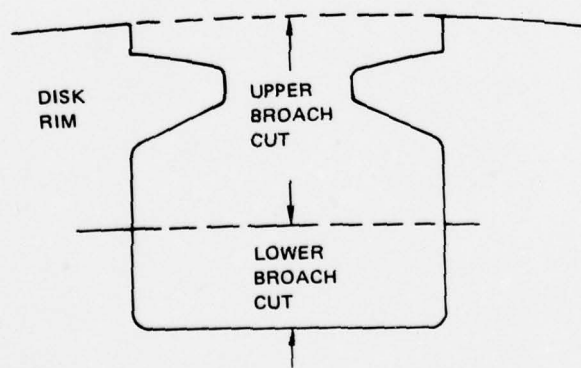


Figure 7.2-24 Two Cuts Were Required to Broach the Blade Slots of the Third-Stage Disk

## 8.0 NONDESTRUCTIVE TESTING AND INSPECTION

Because of the nonhomogeneous, anisotropic nature of BORSIC®/Aluminum composites, the inspection techniques and procedures existing at the start of this program would not provide valid, dependable results. Consequently, a comprehensive nondestructive inspection (NDI) development and evaluation effort was included in the program which was directed toward establishing reliable quality control techniques and procedures for the production of advanced composite fan blades. In addition to establishing the methods to detect defects, the program included developing nondestructive methods for determining both the elastic properties and composition of the materials as well. The latter two quality control parameters were investigated because nonhomogeneous composites are composed of structural elements which can vary in amount, quality, and in this program, in fiber orientation. These variations can result in substantial changes in the physical properties of the composite.

### 8.1 METHODOLOGY OF DEVELOPMENT

The program as originally structured consisted of a literature search and three independent development activities:

- Methods to detect defects
- Radiographic methods of inspection
- Methods to determine elastic properties

Radiography was the subject of independent study because experience indicated that it represented the greatest potential for fiber distress detection. As the program progressed, acoustic emission methods of detecting defects evolved into a fourth independent development activity, whereas it was originally included under the general methods to detect defects category.

To evaluate the methods being developed to detect defects and material elastic properties, composite test panels and blades were used. Those methods which appeared to be most reliable were further evaluated by applying them to the engine test blades produced in the program.

#### 8.1.1 Defect Detection

Advanced methods of defect detection generated at other facilities, as well as those developed at Pratt & Whitney Aircraft, were evaluated under this program. To evaluate the methods developed outside P&WA, blades with programmed defects were provided to the outside facilities. The reports of findings were submitted to P&WA and compared to the actual defects; the specific defect detection system was also evaluated.

### **8.1.2 Radiographic Detection of Defects**

This activity was conducted similarly to that described in paragraph 8.1.1. However, with the radiographic methods the basic X-ray exposure and film reading were conducted at P&WA facilities. Film enhancement and evaluation were usually conducted at a vendor's site using his commercial equipment. Duplicate radiographs of a blade defect were provided to each radiographic equipment manufacturer for enhancement. For methods of radiographic defect detection which did not produce a permanent record, P&WA personnel visited the vendor's site in order to evaluate the methods used. Each method of detection was evaluated on the reports received.

### **8.1.3 Acoustic Emission Detection of Defects**

The acoustic emission development program included both smooth and notched tensile specimens as well as correlating blade emissions with combined stress fatigue. Spectrum response and pulse height analysis were evaluated. However, the total energy emitted proved to be the most effective parameter and was the one used in these studies.

### **8.1.4 Elastic Property Determination**

The amount, quality and fiber orientation of the components in a composite material can adversely affect its physical properties; defect detection alone is not a sufficient criterion for determining the suitability of a batch of composite material for structural purposes. Consequently, a program was conducted to develop the most reliable method for determining material modulus and analyzing material composition.

### **8.1.5 Test Specimens**

Two production configuration blades were produced with programmed defects. These defects represented conditions that might occur during fabrication and included varying degrees of cut fibers, unbonds, wrinkled plies and areas cut from plies. The defects were located in various parts of the blades to study the effect of location on detectability.

Four 4-in. x 6-in. panels were fabricated with defects simulating varying amounts of porosity. Panels were 20 layers thick with one-quarter inch and one-half inch diameter defects. Some defects were created by removing areas of tape, while others were created by removing just the foil backing from the tape. Each panel had defects with material removed from one ply and from two plies. To ensure porosity would occur, two panels were pressed at a reduced pressure and temperature of 3500 psi and 970°F for 1.5 hours. The other two panels were pressed at 1050°F and 5000 psi for 1.5 hours in accordance with the fabrication specification.

Thirteen 4-in x 6-in panels representing various fiber contents, number of plies and fiber orientation schemes were obtained for elastic property studies. Fiber contents of 30, 40 and 50 percent volume; ply counts of 10, 20 and 40; and five different ply orientation schemes were included among the panels.

All samples fabricated for this program were made from five mil BORSIC®/Aluminum tape, utilizing 4.2 mil dia. fiber.

AD-A055 891 PRATT AND WHITNEY AIRCRAFT GROUP WEST PALM BEACH FL G--ETC F/G 1/3  
TF30 THIRD-STAGE COMPOSITE FAN BLADE SERVICE PROGRAM. (U)  
MAY 78 D G RANDALL F33657-70-C-0624  
UNCLASSIFIED PWA-5141 NL

2 of 4  
AD  
A055 891



## 8.2 DEFECT DETECTION

### 8.2.1 Ultrasonics

The use of ultrasonics proved to be the most effective inspection technique to detect unbond or delamination defects. The characteristic straight-line transmission of energy with the lack of diffusion and the high impedance represented by an unbond area all favor this method as an inspection technique. Because of the many reflective surfaces in a composite structure, a pulse echo ultrasonic method can be difficult. However, through-transmission methods are not hampered by extraneous reflections. Because of the almost total inability to transmit across an unbond area, we can look for large losses in the transmitted signal to indicate defective areas. The effectiveness of this method was proven during this program and four separate procedures utilizing ultrasonic through-transmission have been applied.

#### 8.2.1.1 Procedure One

The first procedure utilizes two-wheel search units slightly spring loaded against each other. The spring load assists in ultrasonic coupling and maintains the blade in the correct orientation for the ultrasonic transmission. Additional coupling is obtained by wetting the surface of the wheels. The particular system used in this program had a 0.75-in. diameter transmitter and 0.25-in. diameter receiver operating at 1 MHz. The frequency was low because the unit was also used for graphite/epoxy blades which have an excessively high attenuation at higher frequencies. Delaminations approaching the size of the receiver have been detected with this system. Advantages of the system are that it is easy to set up, requires only a small area, and provides a very fast inspection method. However, because of the size of the wheels, it is not effective at the airfoil edges or within the root platform radius. Figure 8.2-1 shows this method.

#### 8.2.1.2 Procedure Two

A second procedure was developed to inspect the areas which the wheel search units missed. Two 0.25-in. diameter transducers fitted with radiused plastic adaptors were mounted to allow a contact through-transmission inspection of the airfoil. Although not as fast, a rapid inspection of the area missed by the wheel units can be made with a greater sensitivity to smaller defects. Figure 8.2-2 shows this method.

#### 8.2.1.3 Procedure Three

A third procedure was developed to obtain an inspection less susceptible to human error and one with an increased sensitivity to porosity as well as delaminations or unbonds. With a dummy blade and follower system to act as a positioning device, a "C" scan recording is made of the airfoil. The setup, shown in Figure 8.2-3, uses a 0.50-in. diameter SIL transmitter on a 0.1870-in. diameter SIL receiver operating at 2.25 MHz. It provides a complete inspection of the blade airfoil and produces a permanent record. The method has excellent resolution with a capability of varying sensitivity by recording different levels of transmittal signal.

#### 8.2.1.4 Procedure Four

The fourth procedure was applied to inspecting the root attachment area. In fabricating the root, the two titanium alloy blocks and the aluminum wedge are attached to the composite structure by diffusion bonding. The blocks are later machined to obtain the proper blade root configuration. To ensure a bond has been achieved, an ultrasonic through-transmission "C" scan of the root is made before the roots are machined. Using a 0.5-inch diameter SIL transmitter and a 0.62 in. diameter SIL receiver operating at 5 MHz, broken fibers at the wedge tip as well as unbond areas have been detected. Figure 8.2-4 shows a root section being inspected.

#### 8.2.2 Advanced Ultrasonic Methods of Defect Detection

Two advanced methods of ultrasonic through-transmission imaging were evaluated at vendor's sites. Acoustic holography by Holosonics, Inc., Richland, Washington, and Acoustic Optical by TRW, Redondo Beach, California, were applied to the defect samples. Both methods present real time images of ultrasonic signals; however, neither appears to have the resolution of present scanning methods. They are much more complicated and require a combination of optical and ultrasonic systems as well as being affected by blade curvature. Because of this it was decided to continue with standard scanning methods rather than to pursue either of the imaging systems.

#### 8.2.3 Miscellaneous Methods of Defect Detection

Fluorescent penetrant and eddy current methods were evaluated for crack detection. Both methods proved effective but were not thought to be production inspection procedures. They appear to be more applicable as fatigue detection methods during service.

Several methods were evaluated which proved ineffective or otherwise unacceptable. Thermal methods (infrared) were unsuccessful because the high thermal conductivity of the blade diffused the heat and destroyed resolution. Holographic methods proved excellent for shallow defects but were unable to effectively detect defects at any significant depth. This method might have application for bonded leading edge protection schemes or for thin composites. Application of Krypton exposure methods by Industrial Nucleonics utilizing radioactive Krypton 85 gas was unacceptable because the inherent porosity of the composite made the blade extremely difficult to degas.

### 8.3 RADIOGRAPHIC INSPECTION

Although it is ineffective in detecting bond and delamination defects, X-ray radiography is the most effective method of detecting other composite blade defects. Not only does this method provide the widest type of defect detection range but it has also proved useful for determining ply orientation. Ply orientation is clearly distinguishable with high quality radiographs.

As examples of the effectiveness of X-ray radiography for defect detection, the following defects were detected using standard production equipment (Norelco OEG-50):

- Single fiber skewed 10°
- Single ply of cut fibers in a ten-ply layup
- 0.375 in. diameter hole in one ply of 30 plies
- Five broken plies in the root section

These sensitivities were obtained by using low KV outputs (20-35), a target-to-film distance of 36 inches, and a beryllium window tube with a small focal spot size (1.5mm target). With a 1500 MAS exposure and Eastman Kodak M film, blade radiographs had sufficient resolution and contrast to permit inspection with 20X magnification.

Further improvements in the resolution and sensitivity were achieved by using a Picker Minishot system with a 0.5mm focal spot and by placing a single emulsion, extra fine grain film in direct contact with the subject. Eliminating the film holder allowed the film to be placed closer to the subject in areas where geometry was a problem. The Minishot proved to be ideal for this application as it is a self-contained cabinet unit which requires no special facilities. With this unit, adequate contrast and resolution were obtained on single-ply composites to allow identification of the tungsten filament, the BORSIC® fiber, and the aluminum matrix at magnifications of 30X.

The most difficult fiber discontinuity to detect was a small number of broken plies in the root area. The thickness of the root, the uneven cross section, and the subject-to-film distance created resolution problems. However, by using 0.005 inch lead screens, five broken plies at the root wedge tip were detectable. Although using lead screens at these low KV's ( $\approx 35$ ) is unusual, in this case they were effective in reducing scatter and were needed to produce the required image sharpness.

### 8.3.1 Film Enhancement

In an attempt to improve defect detectability on radiographs, nine methods of film enhancement were evaluated. None of the nine improved defect detectability any more than the detectability provided by a 20x magnification of the original radiograph. However, three of the nine methods, the Philco Ford color derivation, the Dupont film contrast method, and printing on lithographic film in the P&WA photographic laboratory, made defects more obvious. These methods were expensive and time consuming; therefore, it was decided to use relatively high magnification only for radiographic image enhancement when inspecting the flight evaluation fan blades.

## 8.4 ACOUSTIC EMISSION DEFECT DETECTION

Unlike homogeneous materials, boron/aluminum composites generate a large number of emissions when stressed. Many of these emissions are sufficiently large to be heard without electronic amplification. The emissions occur at stress levels well below the yield stress and even may occur while the material is cooling or aging. An attempt was made in this program to measure the emission output and correlate it with mechanical test results.

### 8.4.1 Tensile Test Specimens

The initial attempt to determine the effectiveness of acoustic emissions as a defect detection tool was to monitor the emissions from both center-notched and smooth specimens during tensile test.

The center-notched specimens exhibited a drastic change in emission rate just prior to failure. This phenomenon was used to time the triggering of high-speed cameras in an attempt to photograph the specimen at the instant of failure. Using a film speed of 2,500 to 5000 frames per second, a maximum of eight seconds of film was available to conduct the photography. By monitoring the emission rates, an accurate warning of impending failure was received and the camera was triggered successfully. However, despite the high frame speed, the failure was so rapid that the event occurred between frames.

Investigations conducted in monitoring the acoustic emissions of smooth tensile specimens showed that by loading them to less than 50 percent of the failure load, the specimen could be used to predict the ability of the specimen to meet specifications. At a load of 50,000 psi an acceptable specimen had a total emission energy of 1.6, whereas a specimen with an unacceptable ultimate tensile strength of less than 140,000 psi had a total emission energy of 70 at the same loading.

### 8.4.2 Blades

The blades manufactured during this program were subjected to a 200 mil tip deflection while acoustic emissions were monitored. Figure 8.4-1 shows the blade deflection rig and acoustic emission monitoring equipment used. A wide range of emission levels was noted. Three of these blades were tested in combined stress fatigue at 450°F. The blade with the lowest amount of acoustic emission (7.4) failed at 54,000 cycles with severe fabrication damage noted. The blade with the highest acoustic emission (130) failed at 5,240,000 cycles and had no apparent fabrication damage. The third blade had acoustic emission energy of 72 and failed at 1,540,000 cycles with evidence of minor fabrication damage. The correlation with cycle life and acoustic emission is the reverse of what would be expected at first glance. However, these blades were given a controlled deflection rather than applying a controlled load, and the emission level may be a function of the relative stress created. A blade with fabrication damage would deflect more easily, have less stress generated, and, consequently, exhibit a smaller emission output.

#### 8.4.3 Monitoring Equipment Used

The equipment used for these studies was a Nortec Acoustic Emission Monitor NDT-200 with a Krohn-Hite filter model 3202 and a Mosely 7100B strip chart recorder. The pickup used was a Nortec 1.5 MHz longitudinal wave 0.75 in. diameter lithium-sulfate transducer. The correlations described above were made by measuring total energy output. Additional efforts to relate spectrum and pulse height analysis proved unsuccessful.

### 8.5 ELASTIC PROPERTIES

The elastic properties of a component made of advanced composite material depend largely on the procedures used to fabricate the component. Consequently, quality assurance procedures are unique in that they must not only detect "normal" defects with a high degree of confidence but also must provide information relative to the adequacy of the components physical properties as well as the correctness of the fabrication procedures used. If adequate elastic properties can be confirmed by measurement, then it is possible to ensure that the fabrication procedures were correct.

In this program, two elastic properties, natural frequency and modulus, were measured as potential parameters by which to characterize the BORSIC®/Aluminum blades designed and fabricated under this contract. The natural frequency measurements proved to be sensitive only to gross changes however, and, as a result, this characterization technique was not aggressively pursued.

#### 8.5.1 Modulus Determination

Three separate methods of modulus determination were evaluated on specimens to establish correlations. Ultrasonic velocity measurements, elastomat dynamic modulus measurements, and strain gage data from tensile specimens were compared. Specimens with various ply orientation, fiber volume percent and specimen thickness were used for the comparison. Results indicated that, in every case, the experimentally determined data was lower than analytically determined values. This difference increased as the percent fiber increased. Table 8.5-I lists the data for the 0° orientation samples with various fiber volume percent. A mean value and a standard deviation value is included for the experimental results. It is evident from this data that the experimental methods for determining modulus give fairly consistent values.

##### 8.5.1.1 Ultrasonic Velocity Measurements

To apply ultrasonic velocity measurement techniques requires that the measurement be made from a surface parallel to the direction of measurement. The fixture shown in Figure 8.5-1 was designed and fabricated to accomplish this. The fixture positions a sending transducer and two accurately spaced receiving transducers on the surface of composite panels. By rotating the fixture, velocity measurements can be made in any direction relative to the ply layups. The results obtained on 0° ply direction panels with this fixture are included in Table 8.5-I discussed above and were part of the good correlation exhibited. Two additional fixtures were made to fit the blade airfoil near the tip and near the root. They were designed to measure velocity in only one direction along the length of the blade. They have been successfully used to measure acoustic velocities on production blades.

The purpose of determining blade modulus with ultrasonic velocity measurements was to insure correct fiber modulus, fiber content and correct ply layups. However, the modulus only varied from approximately  $30 \times 10^6$  psi in the  $0^\circ$  ply direction to approximately  $20 \times 10^6$  in the  $90^\circ$  direction. Consequently, only large ply layup discrepancies are detectable. Ply layup can be verified better on x-ray radiographs. Fiber modulus is spot inspected with tensile tests before the airfoil is made to ensure fabrication efforts are not wasted. Fiber content can be determined within 3% with an eddy current method that is presented in the next section. For these reasons, it was impractical to expect ultrasonic velocity measurements to produce any new or useful information and the method was discontinued. Although it has little value for BORSIC®/Aluminum composites, it may have more use for other systems where substitute inspection methods are not as successful.

In conjunction with elastic property measurements, three methods for determining volume percent fibers were evaluated. They included eddy current conductivity measurement, beta backscatter, and radiation gaging. Using conductivity values measured with a Magnaflux FM 100 conductivity meter, it was possible to predict the percent fiber content within  $\pm 3$  percent. Beta backscatter methods utilizing promethium and thallium probes could not match the accuracy attained with conductivity measurements. Other attempts to utilize radiation gaging were unsuccessful. Even using measurements made with three different energy sources, the absorption of aluminum and boron could not be separated. The tungsten represents too small a volume percent to make accurate measurements. The sources used were americium 241 (60 kev), cadmium 109 (22.2 kev) and cobalt 57 (122 kev).

TABLE 8.5-1  
COMPARISON OF YOUNG'S MODULUS DATA FOR  $0^\circ$  ORIENTATION

Panel	Percent Fiber	Elastomat*		Ultrasonic Velocity*			Tensile Test*		Mean*	Standard Deviation	Analytical*
		E1	E2	S1	S2	Panel	T1	T3			
SSV3E	30	22.5	21.7	23.0	22.2	23.8	24.1	21.2	22.6	0.99	24.0
SSV3C	30	23.8	23.0	22.1	22.8	24.0	22.8	22.4	23.0	0.64	
SSV3A	30	23.1	21.3	20.9		22.7	20.4	18.6	21.2	1.49	
SSU3E	40	26.6	25.4	26.2	27.0	27.2	27.8	28.4	27.0	0.93	28.8
SSU3C	40	28.3	27.7	24.8	26.8	28.0	23.8		26.6	1.69	
SSU3A	40	26.0	26.4	24.2	23.2	25.0	21.8	23.8	24.4	1.49	
SST9E	50	28.8	29.4	30.5	29.8	29.6	31.4	29.8	29.9	0.78	33.6
SST9C	50	29.0	29.3	29.9	29.9	29.7	28.0	27.2	29.0	0.96	32.8
SST9A	50	28.4	28.2	27.7	26.4	27.7	25.6	26.8	27.3	0.95	30.1

\*Young's Modulus,  $10^6$  psi

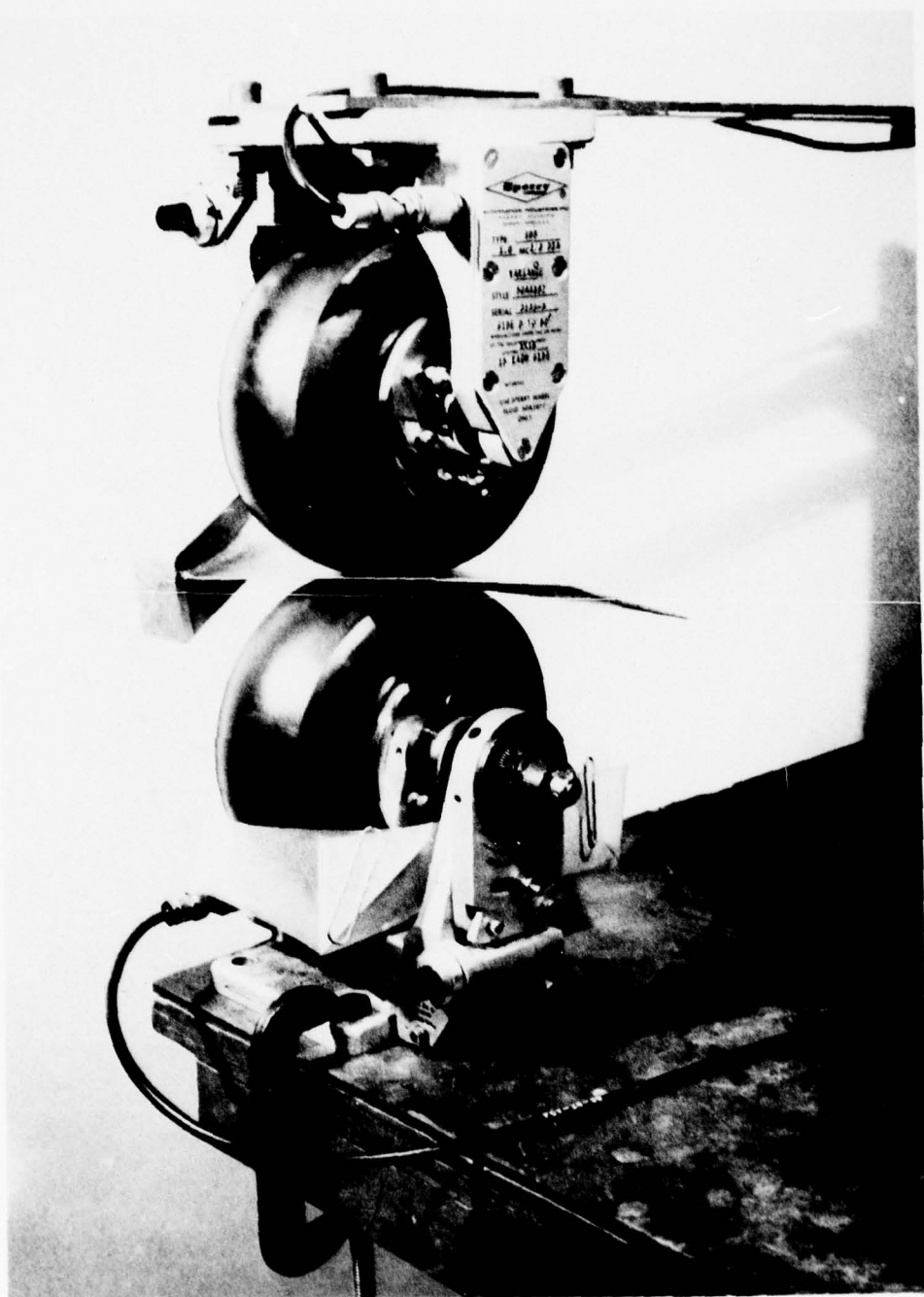


Figure 8.2-1     Ultrasonic C-Scan Inspection of Bulk of Airfoil With 0.25 Inch Diameter, 1.0 MHZ, Sperry Wheel Search Units

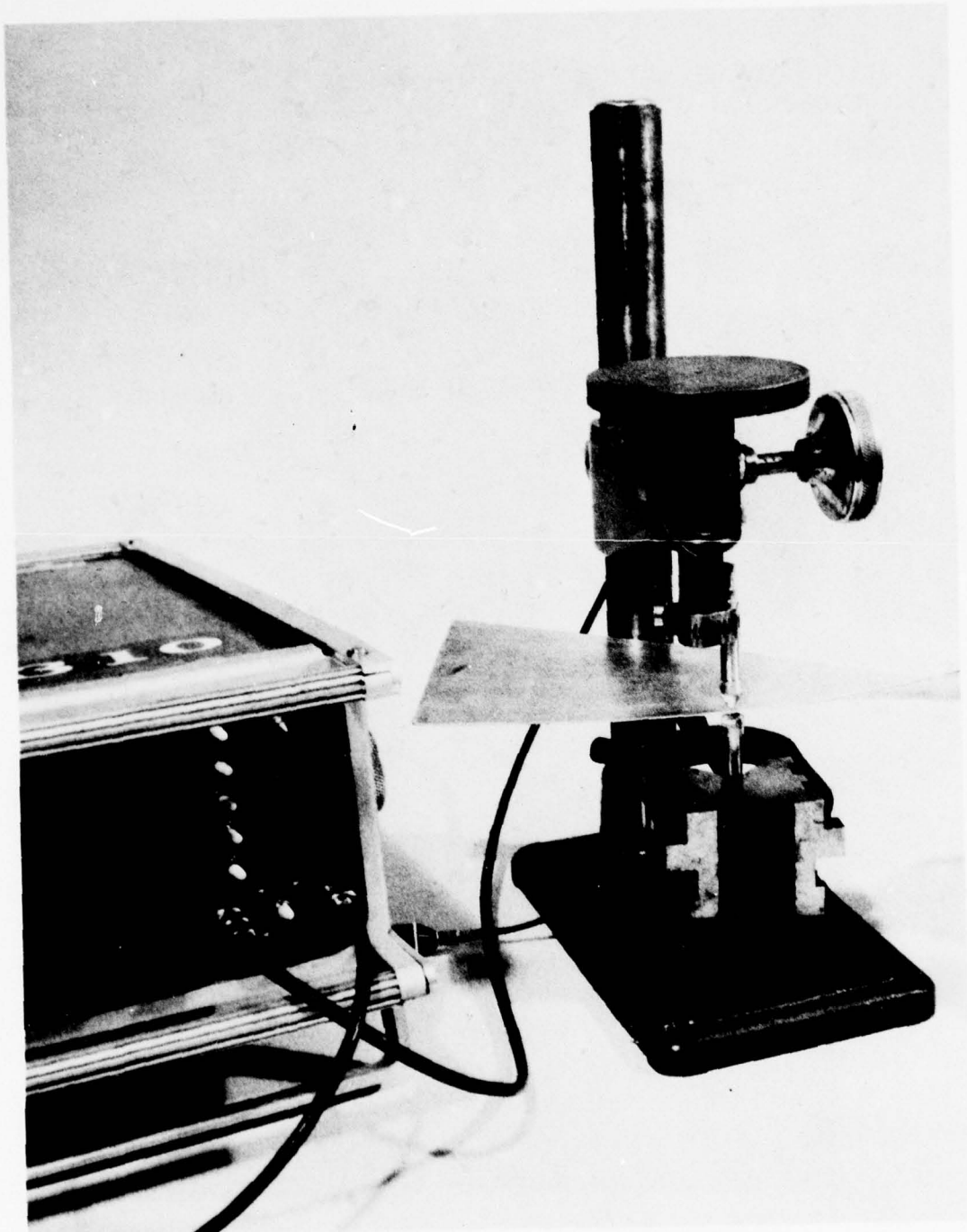


Figure 8.2-2      *Areas Near Edges of Airfoil and Just Above Root Platform Inspected Using 0.25 Inch Diameter Transducers With Lucite Shoes Attached*

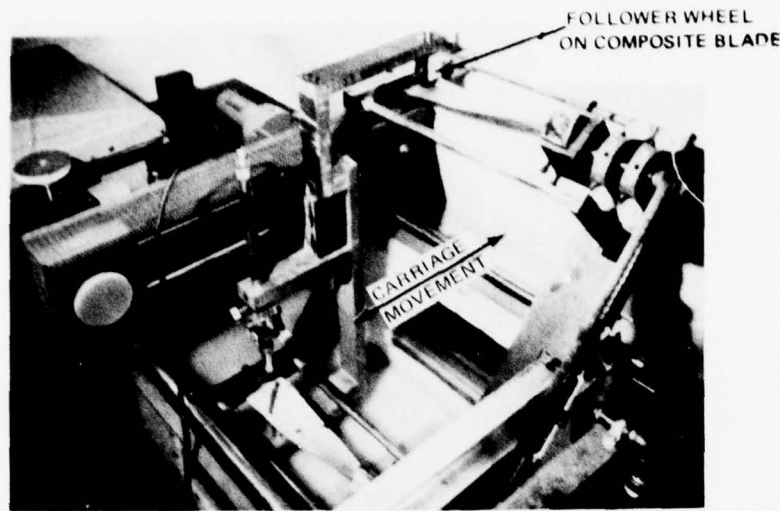


Figure 8.2-3 Modified Fixture for Ultrasonic C-Scanning of Composite Airfoils

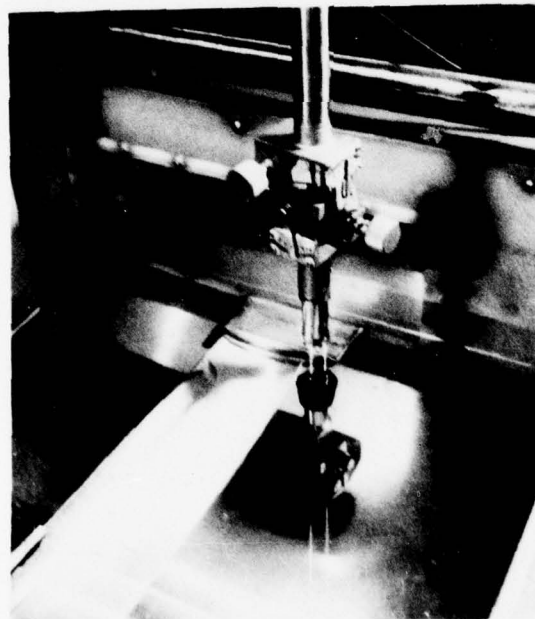
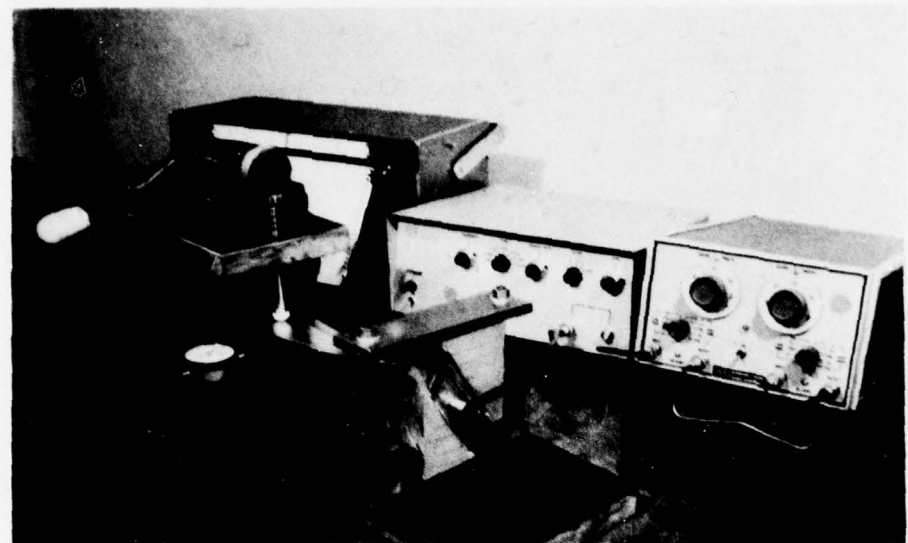
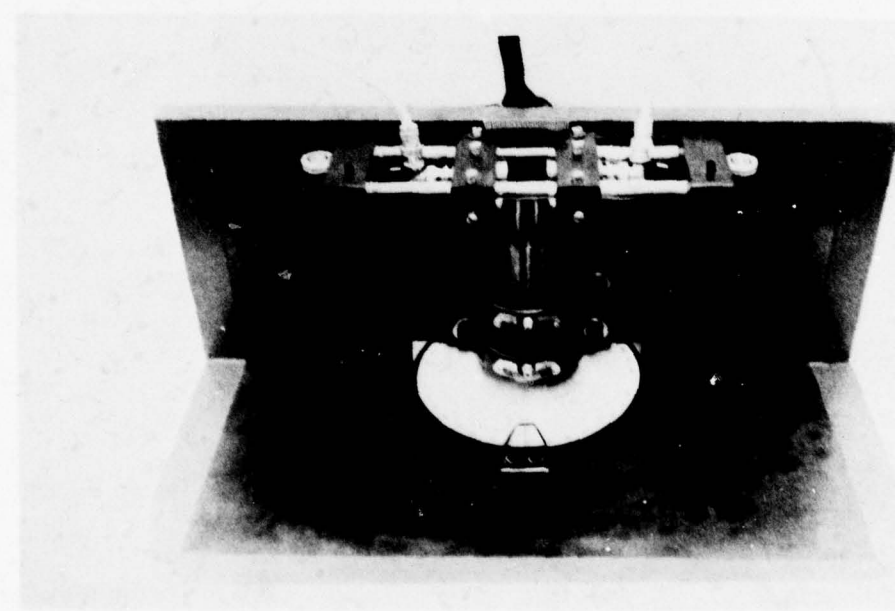


Figure 8.2-4 Root Sections Ultrasonically Inspected by Through-Transmission Using  
1/2" Diameter Transmitter With 1/4" Diameter Receiver Masked to 1/32"  
Diameter



*Figure 8.4-1 Blade Deflector Rig and Acoustic Monitoring Equipment With Blade Mounted For Inspection*



*Figure 8.5-1 Equipment For Measuring Ultrasonic Velocity in Composite Panel Specimens*

## 9.0 MATERIAL SERVICE EVALUATION

### 9.1 TEST PROGRAM

Turbine engine fan blades may incur damage from several possible sources in their operating environment. The general criterion for a serviceable part is that it be capable of continued service after sustaining minor damage until it is retired at a suitable inspection time. The objective of this program was to obtain knowledge concerning the potential serviceability of Borsical® for fan blade material. Specifically, the amount of static and high-frequency fatigue (HFF) property degradation resulting from foreign object damage (FOD), erosion, corrosion and thermal fatigue damage was established in this effort. Specimens, rather than actual components, were utilized to permit close control of test parameters and to facilitate a less ambiguous interpretation of test results.

The specimen panels were fabricated using identical parameters to those used for fabrication of the TF30 fan blades (1050 to 1080°F at 5000 psi in a vacuum of  $10^{-4}$  torr or better) and were 20 layers thick (approximately 0.100 inch). Three different ply configurations were used: unidirectional ( $0^\circ$ ), representing the blade core; cross ply ( $\pm 45^\circ$ ), representing the blade shell; and a sandwich configuration to represent the actual blade component and to reveal any core-shell interactions. The component configuration was 20 percent  $\pm 45^\circ$ ; 60 percent unidirectional, and 20 percent  $\pm 45^\circ$ . All material contained  $50 \pm 3$  volume percent Borsic® fiber. Specimens were electrodischarge machined and subjected to one of the four potential types of damage (except for the base-line specimens) followed by HFF, tensile, and post-HFF tensile testing. The high-frequency fatigue test program involved testing specimens to various fractions of their expected life, as shown in Figure 9.1-1. Upon completion of the high-frequency fatigue tests, microstructures were examined for evidence of fatigue and the effect of the controlled damage on the microstructure. Tensile properties of HFF-tested samples were determined to define the effect of the combination of fatigue and controlled damage on tensile strength.

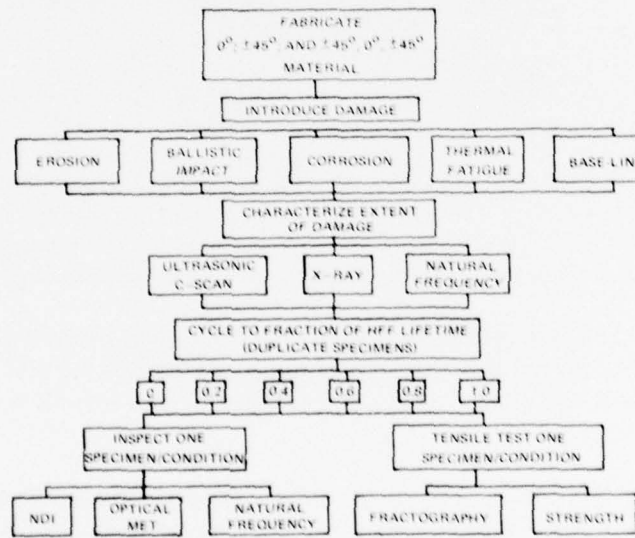


Figure 9.1-1 Borsical® Damage Evaluation Program

The high-frequency fatigue failure criterion was either visible delamination or a ten percent drop in first-bending natural frequency. Since no significant frequency drop occurred during tests of the unidirectional configuration, the condition of this material was estimated by observation of visible delamination. Cross ply HFF life was determined by a ten-percent drop in natural frequency with no evidence of delamination. Specimens of the component configuration exhibited frequency drops within  $5 \times 10^5$  cycles; however, visible delamination did occur later in the test and was used as the criterion for failure.

## 9.2 SPECIMEN DAMAGE PROCEDURES

Test specimens used to evaluate the various potential types of damage were straight-sided 0.8 x 5.0-inch sections taken from 20-layer composite panels. When local damage was inflicted (such as erosion or ballistic impact), the damaged area was located 2.0 inches from the specimen end. This location corresponds to the region adjacent to the grip edge during HFF testing (approximate point of maximum stress). Figure 9.2-1 depicts the specimen described, as well as the tensile specimen which was subsequently machined from the damaged sample. As illustrated, the most severely damaged area of each test specimen was located within the tensile specimen gage length.

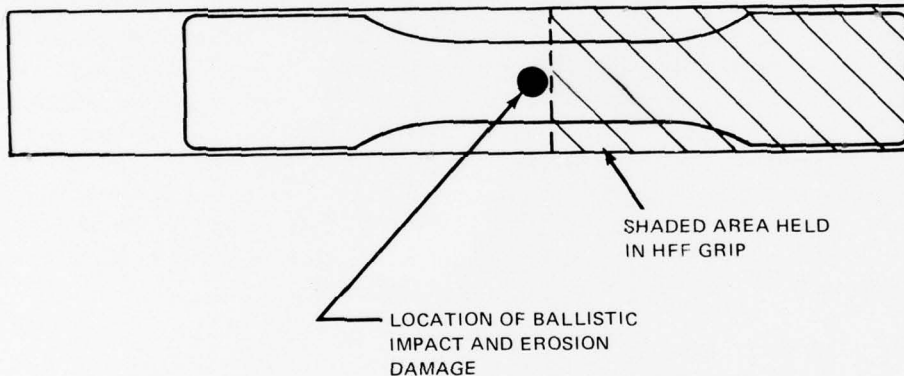


Figure 9.2-1 Composite Specimen Configuration Showing Location of Erosion and Ballistic Impact Damage

The erosion of test samples was accomplished using an SS White Airbrasive Unit set at an abrasive flow rate of 0.14 gm/sec for a sufficient time to expose two layers of fiber in unidirectional material. The abrasive consisted of 27 micron alumina impinging the sample surface at an angle of 20 degrees. Typical eroded samples are shown in Figure 9.2-2.

Ballistic impact damage was achieved with a 0.67 gm pellet fired from an air pistol at a velocity of 500 ft/sec. The resulting damage is shown in Figures 9.2-3 and 9.2-4. To assess the extent of damage produced by impacting, ultrasonic C-scan inspection was performed, as illustrated by Figure 9.2-5.

Thermal fatigue exposure consisted of cycling Borsical® specimens for 2000 to 3000 cycles in fluidized sand beds. Each cycle consisted of one minute at 500°F followed by one minute at -65°F.

One hundred hours of exposure to a humid salt spray at 90°F was performed on Borsical® samples subjected to 1880 $\mu$  in./in. surface strain through the use of bend fixtures as shown in Figure 9.2-6. Typical exposed specimens are shown in Figure 9.2-7.

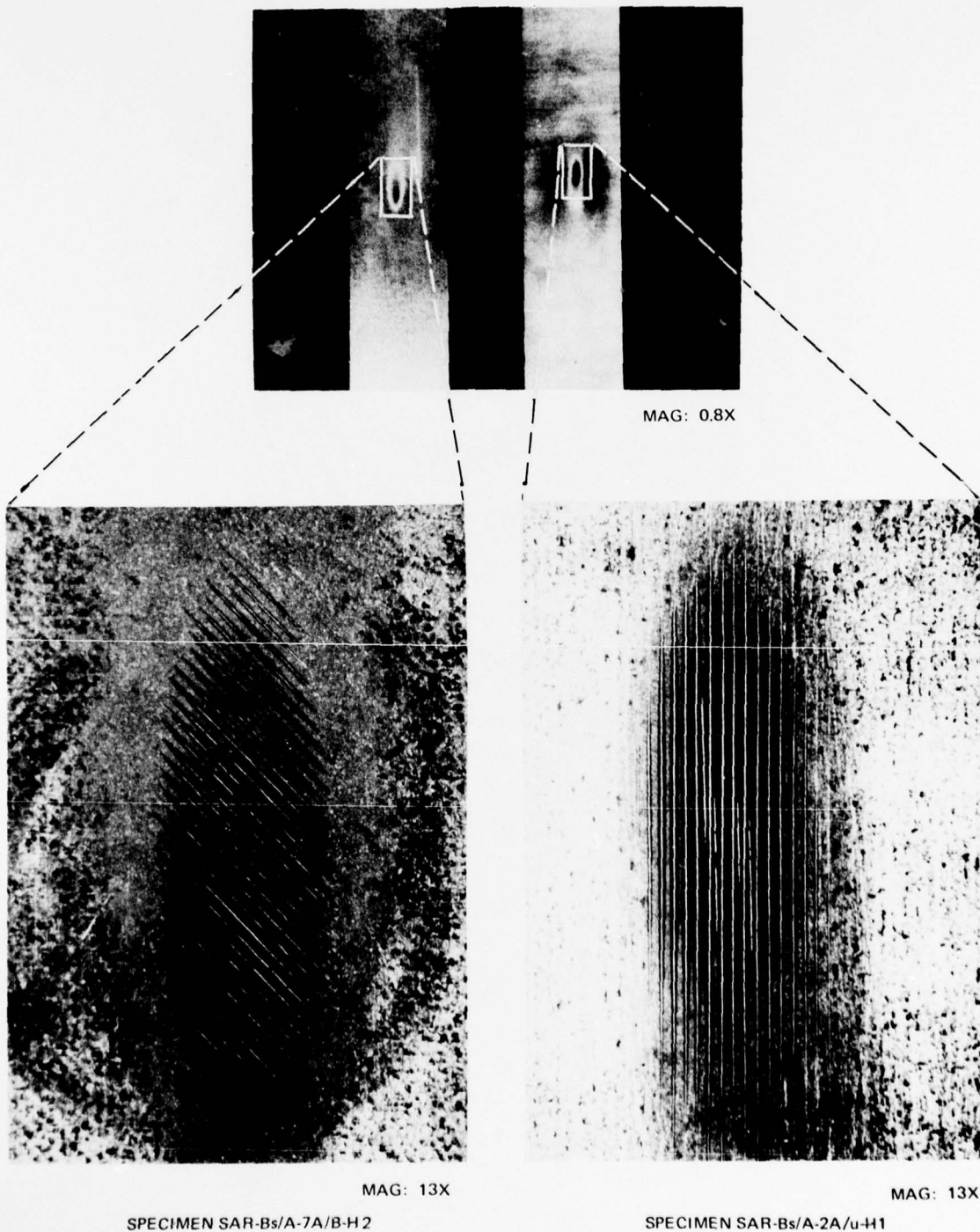
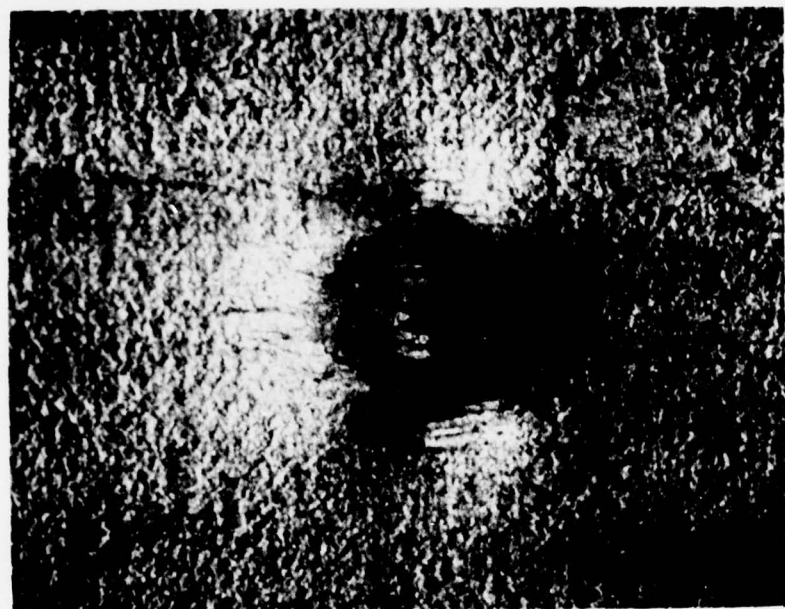
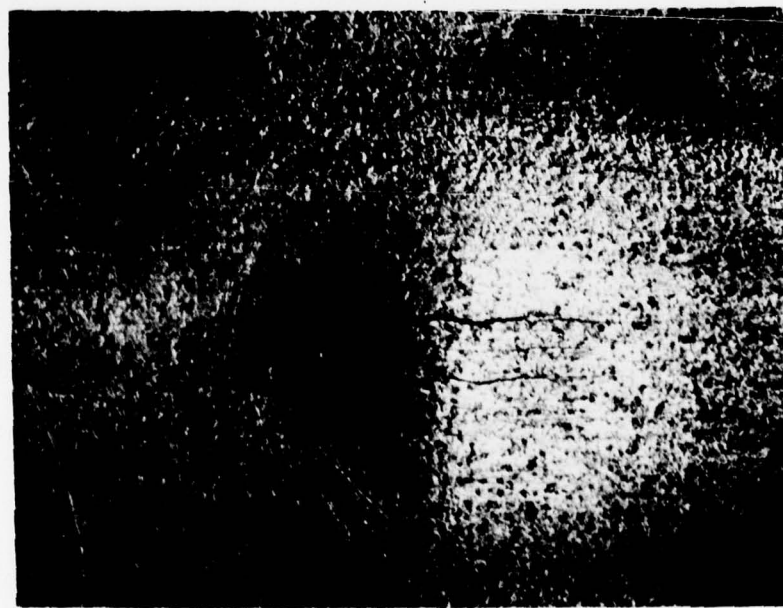


Figure 9.2-2 Typical Erosion Effect on 20-Layer Borsical<sup>®</sup> Test Panels of a Nine-Second Exposure to 0.14 g/sec Flow of 27-Micron Alumina in 60 psig Air at an Impingement Angle of 20 Degrees



FRONT

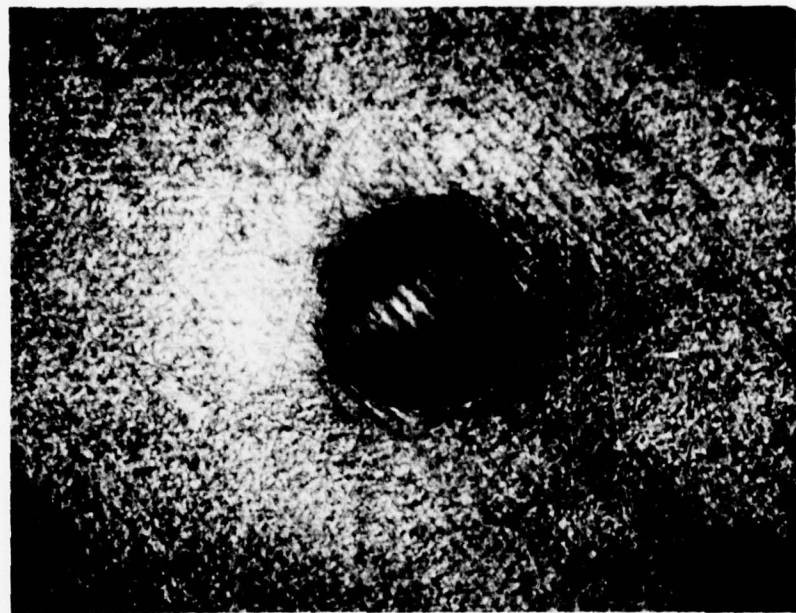
MAG: 13X



BACK

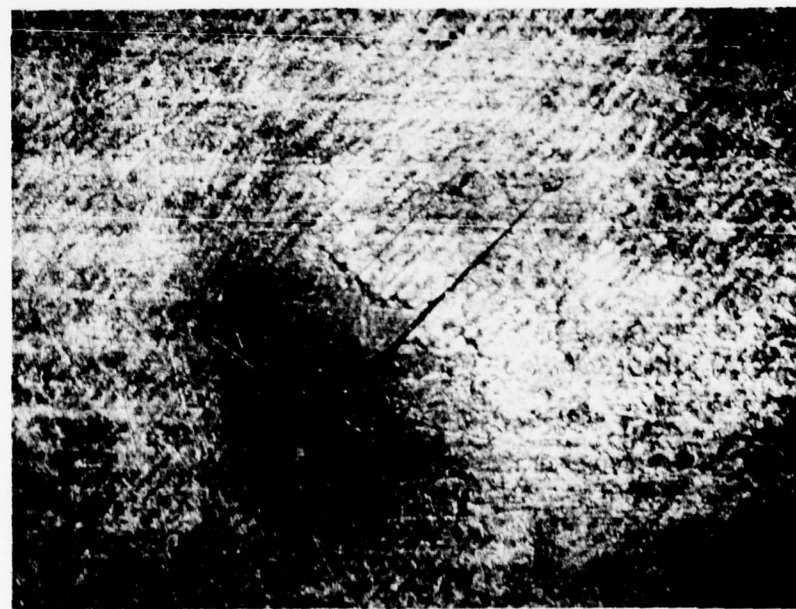
MAG: 13X

*Figure 9.2-3 Ballistic Impact Damage on a Unidirectional Borsical® Test Panel Specimen, SAR-Bs/A-3A/u-H2*



FRONT

MAG: 13X



BACK

MAG: 13X

*Figure 9.2-4 Ballistic Impact Damage on a Component Borsical® Test Panel Specimen,  
SAR-Bs/A-7B/B-H3*

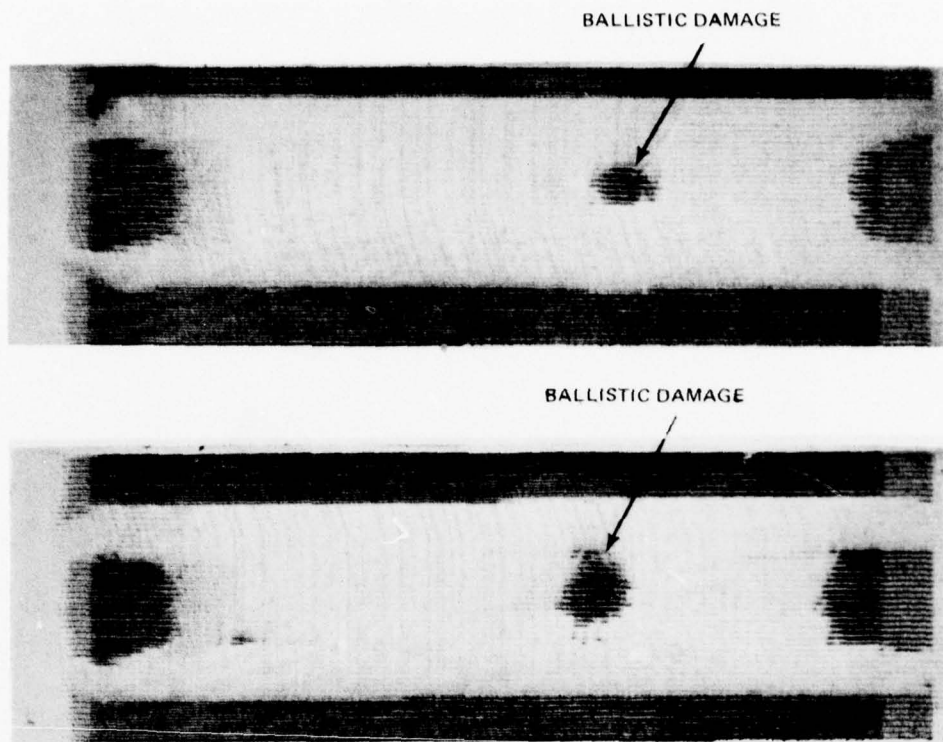


Figure 9.2-5 Ultrasonic C-Scan Traces of Typical Ballistic Impact Borsical® Specimens

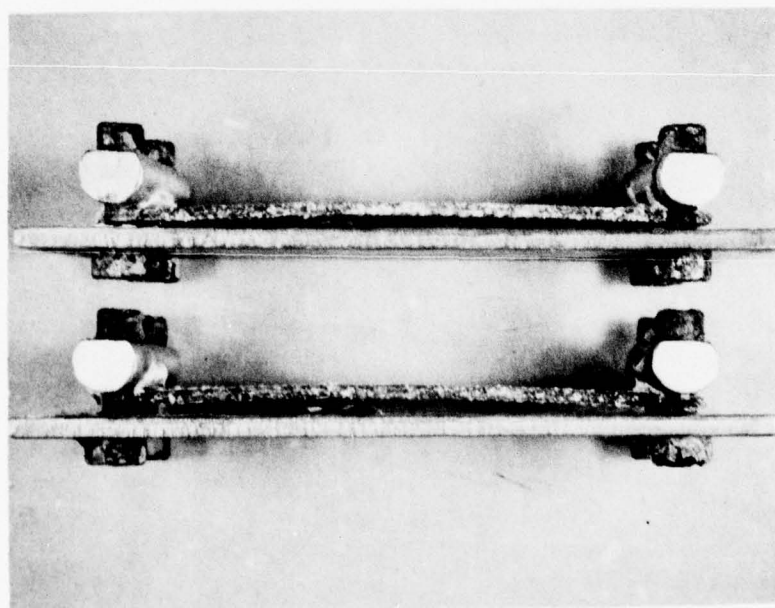


SPECIMEN  
SAR-Bs/A-6A/u-H3



SPECIMEN  
SAR-Bs/A-8E/B-H2

MAG: 0.75X



SPECIMEN  
SAR-Bs/A-6A/u-H3



SPECIMEN  
SAR-Bs/A-8A/B-H2

MAG: 0.75X

**Figure 9.2-6** Typical Corrosive Effect on 20-Layer Borsical<sup>®</sup> Test Panels of a 100-hour Exposure to a Humid Salt Spray; Maximum Strain at Fulcrum of the Test Fixture was 1880 microinches which is Equivalent to a Bending Stress of 60,000 psi for the Unidirectional Specimens and 35,000 psi for the Component Specimens

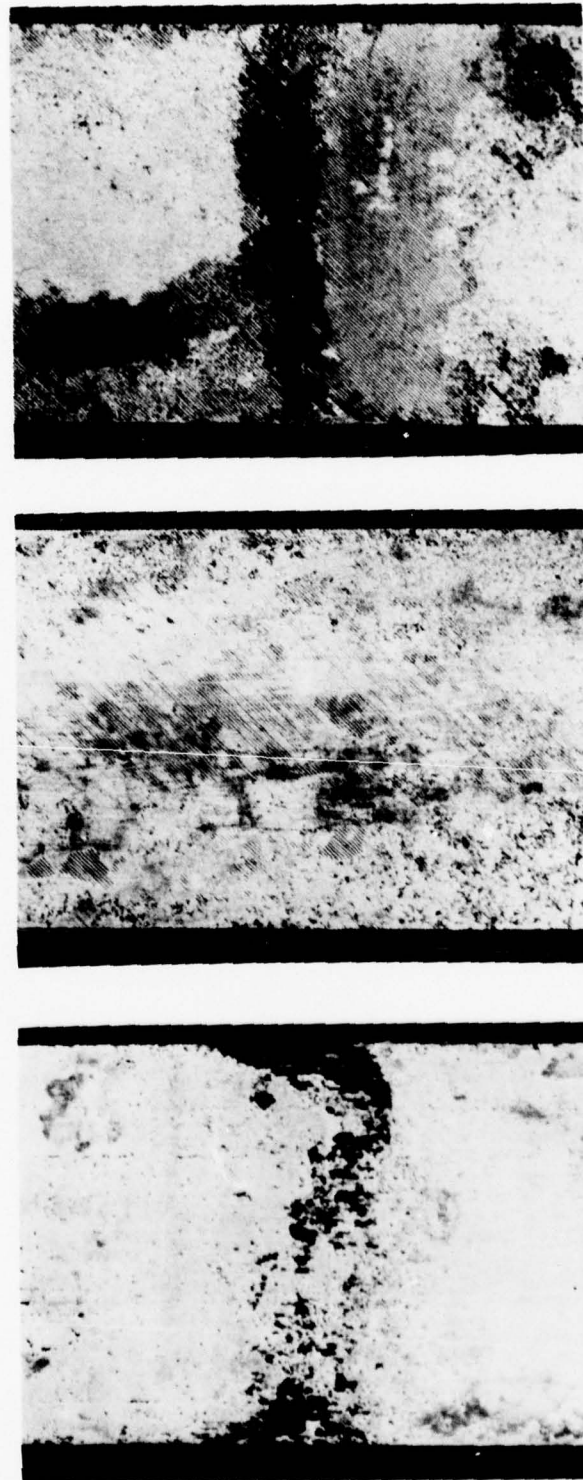


Figure 9.2-7   Surface Appearance of Unidirectional, Component, and Cross-Ply (Left to Right, Respectively) Borsicel (B) Specimens After 100-hour Salt Stress-Corrosion Exposure

### 9.3 TEST PROCEDURES

Twenty-layer tensile specimens with a 0.4-inch wide gage section were tested with either nickel-plated or epoxy-bonded aluminum doublers at the grip ends, depending on the expected failure load. These 4.0-inch long specimens were mounted in clamp-type grips using a micrometer alignment fixture. The grips had serrated faces to provide adequate gripping with minimum clamping force (30 in.-lb). The specimen-grip assembly was then installed in an Instron tensile machine using pin connections. Single-ball-pivot universal joints were located at both upper and lower grips to ensure minimum load-train induced bending. The load was applied to failure at 0.050 in./min cross-head speed. A plot of load versus cross-head displacement was obtained on the tensile machine recorder chart for a modulus determination of selected specimens. Also, back-to-back strain gages were used to detect any specimen bending during the tensile test.

High frequency fatigue testing was conducted in modified Krouse rigs, shown in Figure 9.3-1 at 60 cycles per second. Elevated temperatures were obtained by placing a resistance-wound furnace around the specimens, as shown in Figure 9.3-2. Thermocouples were located on the specimen surface near the maximum strain location. In general, duplicate specimens were run simultaneously with individual surface strains measured by strain gages located near the grip edge which is the maximum strain location. Periodic specimen inspections were conducted during fatigue testing to determine any natural frequency change and to observe any visible material degradation such as delamination. These inspections were accomplished without removing the specimens from the test rig.

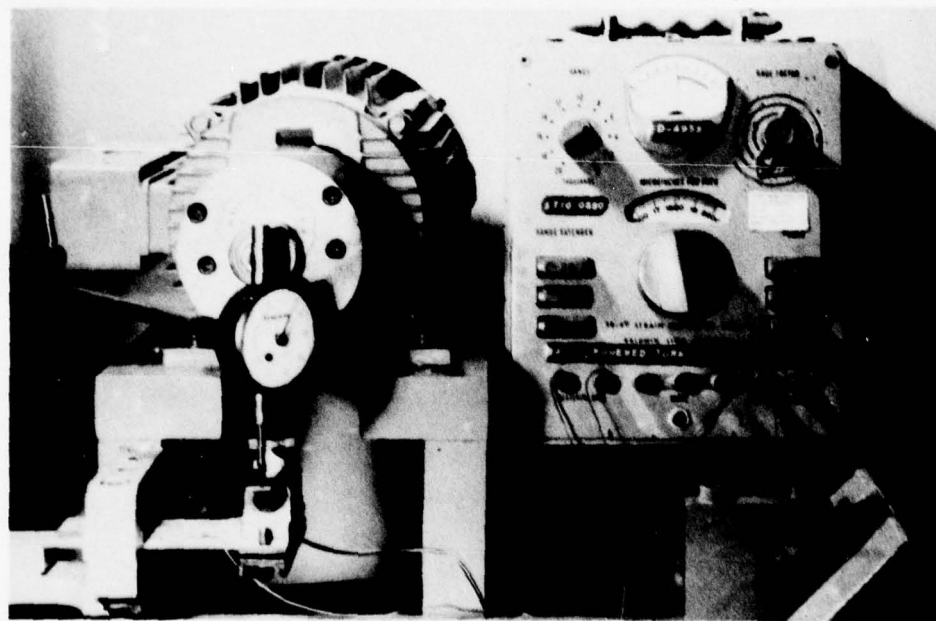
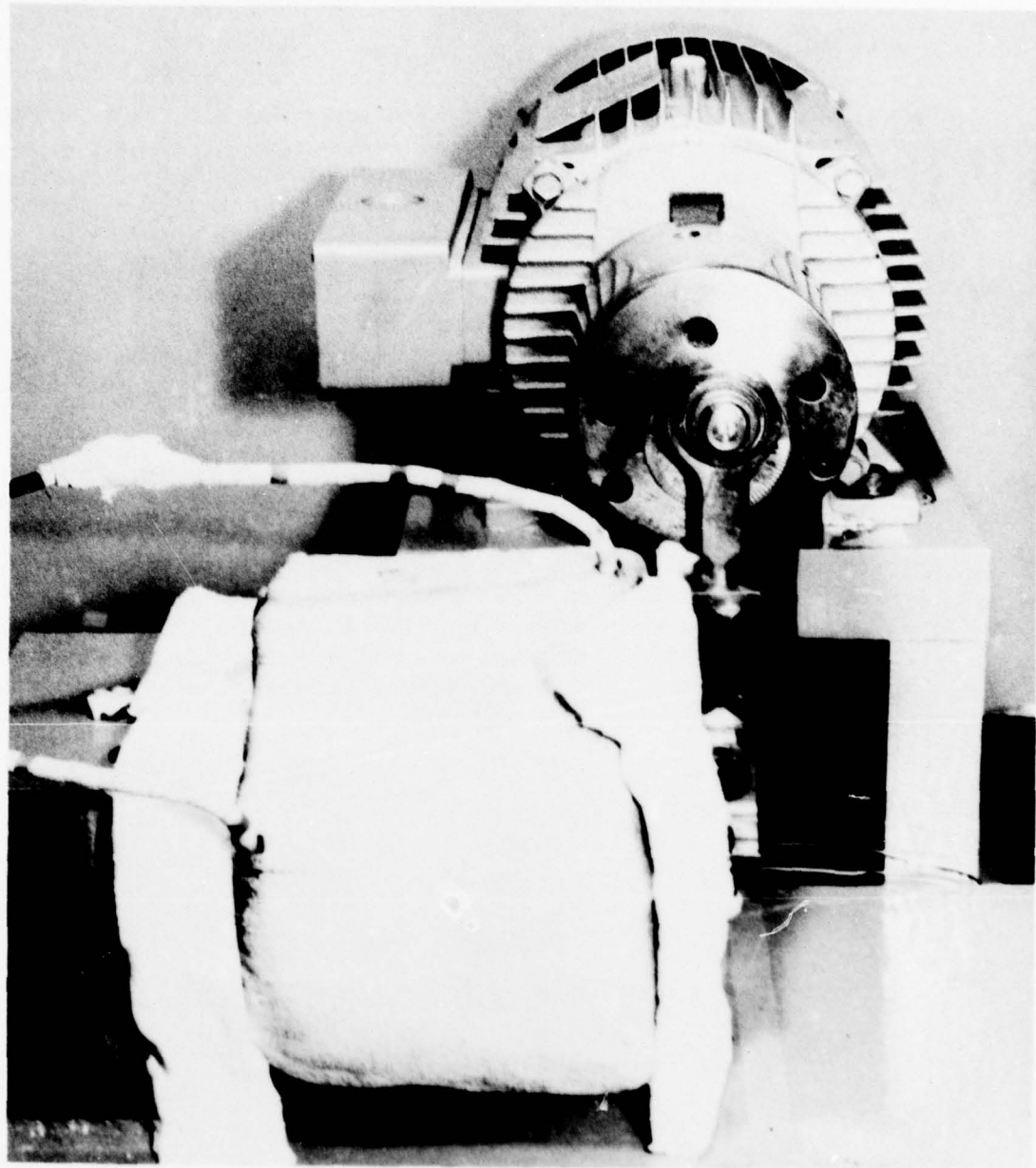


Figure 9.3-1 Equipment and Specimen Arrangement for High Frequency Fatigue Testing at Room Temperature



*Figure 9.3-2 Equipment and Specimen Arrangement for High Frequency Fatigue Testing at Elevated Temperature*

#### 9.4 UNDAMAGED SPECIMENS (Base-line)

The following conclusions were drawn from the results of the testing of undamaged specimens:

- HFF exposure at 450°F had no significant effect on the 70°F tensile strength of cross-ply or component laminates. Unidirectional laminates retained their strength after 70°F HFF exposure but appeared to lose about 25 percent of their strength after 450°F HFF exposure.
- Maximum strain HFF run-out ( $10^7$  cycles) levels were 2800  $\mu$ in./in. at 70°F for unidirectional material and 2100, 1500 and 700  $\mu$ in./in. for unidirectional, component, and cross-ply material, respectively, at 450°F.
- The mode of HFF damage for unidirectional specimens consisted of the formation of matrix cracks with delamination and fiber damage observed after exposure to high strains. Fiber splitting was observed in cross-ply material. The splitting orientation was parallel to the specimen surface for component laminates and normal to the surface for all cross-ply material.

##### 9.4.1 Tensile

Base-line tensile properties were determined for undamaged 50-percent Borsical<sup>®</sup> specimens with and without HFF exposure. Results shown in Table 9.4-1 and Figure 9.4-1 revealed no effect of 70°F HFF exposure on unidirectional material, or of 450°F HFF exposure on  $\pm 45^\circ$  material. HFF exposure at 450°F lowered the strength of component material slightly, and unidirectional material about 25 percent. Neither the HFF strain range nor the number of cycles over the range tested appeared to influence tensile strength except for component material where a trend of higher strength with lower strain range was observed (see Table 9.4-1).

TABLE 9.4-I

BASELINE 70° F TENILE RESULTS FOR UNDAMAGED 20-LAYER  
50 PERCENT - VOLUME BORSICAL® SPECIMENS

Specimen Number	Ply Config.	Prior HFF Exposure					
		Temp. (°F)	Strain (μin./in.)	Cycles to Failure	Total Cycles	UTS (10 <sup>3</sup> psi)	Modulus (10 <sup>6</sup> psi)
15B/u-T2	0°		None			166.5	35.5
15B/u-T3	0°		None			149.0	32.8
15B/u-T4	0°		None			153.0	30.7
15B/u-T5	0°		None			127.5	31.8
15E/u-T1	0°		None			155.3	34.0
15E/u-T2	0°		None			155.1	33.8
1C/u-H3	0°	70	3380	3x10 <sup>6</sup>	10 <sup>7</sup>	130.7	—
1C/u-H1	0°	70	3215	5x10 <sup>6</sup>	10 <sup>7</sup>	153.0	—
2D/u-H2	0°	70	2925	DNF*	10 <sup>6</sup>	157.1	—
2E/u-H3	0°	70	2900	DNF	10 <sup>6</sup>	157.5	—
1A/u-H1	0°	70	2830	DNF	10 <sup>7</sup>	169.1	—
1E/u-H2	0°	70	2000	DNF	10 <sup>7</sup>	139.5	—
6F/u-H2	0°	450	2330	2x10 <sup>6</sup>	3x10 <sup>6</sup>	103.5	—
5D/u-H4	0°	450	2200	5x10 <sup>6</sup>	5x10 <sup>6</sup>	138.0	—
6E/u-H3	0°	450	2170	3x10 <sup>6</sup>	4x10 <sup>6</sup>	92.7	—
3D/u-H4	0°	450	2030	DNF	5x10 <sup>6</sup>	93.5	—
2E/u-H1	0°	450	1500	DNF	10 <sup>7</sup>	138.0	—
4F/B-T1	±45°, 0°, ±45°		None			127.2	—
4F/B-T2	±45°, 0°, ±45°		None			125.0	28.0
4F/B-T3	±45°, 0°, ±45°		None			118.0	26.8
4F/B-T4	±45°, 0°, ±45°		None			101.0	26.8
8F/B-H3	±45°, 0°, ±45°	450	1700	3x10 <sup>6</sup>	3x10 <sup>6</sup>	93.6	—
8F/B-H1	±45°, 0°, ±45°	450	1695	2x10 <sup>6</sup>	2x10 <sup>6</sup>	99.1	—
8E/B-H4	±45°, 0°, ±45°	450	1630	5x10 <sup>6</sup>	5x10 <sup>6</sup>	111.5	—
8D/B-H4	±45°, 0°, ±45°	450	1620	DNF	4x10 <sup>6</sup>	110.0	—
8C/B-H3	±45°, 0°, ±45°	450	1540	DNF	5x10 <sup>6</sup>	113.2	—
5F/C-T1	±45°		None			21.6	16.0
5F/C-T3	±45°		None			21.8	12.6
5F/C-T4	±45°		None			22.3	14.9
5E/C-H4	±45°	450	975	DNF	3x10 <sup>6</sup>	22.6	—
5D/C-H1	±45°	450	910	DNF	10 <sup>6</sup>	21.9	—
5D/C-H3	±45°	450	870	DNF	5x10 <sup>6</sup>	21.7	—
5B/C-H3	±45°	450	760	DNF	4x10 <sup>6</sup>	24.5	—

\*DNF = Did not fail.

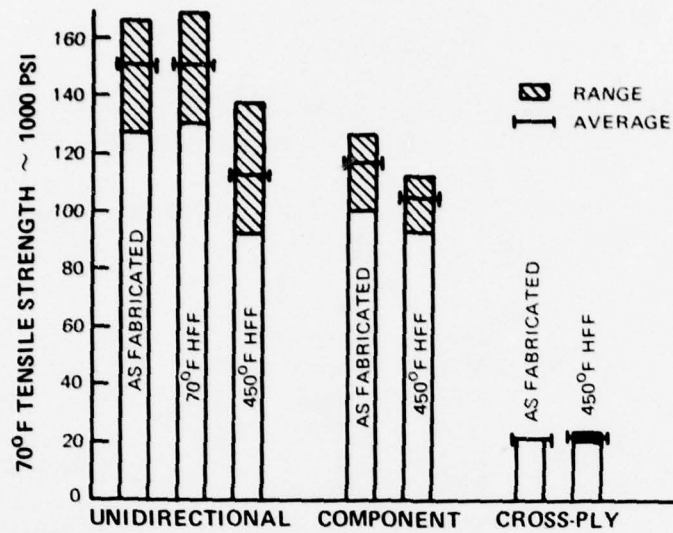


Figure 9.4-1 Effect of High Frequency Fatigue Exposure on the 70°F Tensile Strength of Undamaged 50 Volume-Percent 20-Layer Borsicel® Specimens

#### 9.4.2 High Frequency Fatigue

High frequency fatigue testing of damaged specimens was performed to establish base line levels for assessing the effects of damage on fatigue strength. Table 9.4-II contains the HFF data for unidirectional specimens at room temperature and for all three ply configurations at 450°F. The strain versus cycles-to-failure curves plotted in Figure 9.4-2 were determined using a least-squares analysis of the data in Table 9.4-II. The results indicate a  $10^7$  run-out strain of  $2800 \mu\text{in./in.}$  for the unidirectional material or approximately 81,000 psi based on interpolation from tensile stress-strain curves. Similarly, the run-out strain levels for the unidirectional and the  $\pm 45^\circ$  material at 450°F are  $2100 \mu\text{in./in.}$  (68,500 psi) and  $700 \mu\text{in./in.}$  (6500 psi), respectively. The component material run-out strain of  $1500 \mu\text{in./in.}$  corresponds to a shell surface stress of 8700 psi and a maximum stress of 31,500 psi which occurs in the core at the core-shell interface. This latter stress level was determined by estimating the strain at the core-shell interface, located approximately 0.3 inch from the neutral axis, and using tensile stress-strain curves to estimate the stress.

TABLE 9.4-II  
HIGH FREQUENCY FATIGUE TEST RESULTS FOR UNDAMAGED  
20-LAYER 50 PERCENT - VOLUME BORSICAL® SPECIMENS

Specimen Number	Ply Config.	Temp. (°F)	Strain (μin./in.)	Cycles to Failure*	Total Cycles	Failure Mode
1E/u-H2	0°	70	2000	DNF**	$10^7$	—
1E/u-H1	0°	70	2320	DNF	$10^7$	—
1C/u-H2	0°	70	2450	DNF	$10^7$	—
1A/u-H1	0°	70	2830	DNF	$10^7$	—
2D/u-H3	0°	70	2900	DNF	$10^6$	—
1A/u-H2	0°	70	2920	$10^7$	$10^7$	Delamination
2D/u-H2	0°	70	2925	DNF	$10^6$	—
1A/u-H4	0°	70	3000	$6 \times 10^6$	$6 \times 10^6$	Delamination
1D/u-H3	0°	70	3000	$5 \times 10^6$	$10^7$	Delamination
2E/u-H2	0°	70	3100	DNF	$2 \times 10^6$	—
2E/u-H3	0°	70	3100	DNF	$2 \times 10^6$	—
1D/u-H1	0°	70	3100	$3 \times 10^6$	$3 \times 10^6$	Delamination
1D/u-H4	0°	70	3100	$3 \times 10^6$	$3 \times 10^6$	Delamination
1E/u-H3	0°	70	3100	$5 \times 10^6$	$5 \times 10^6$	Delamination
1E/u-H4	0°	70	3100	$4 \times 10^6$	$5 \times 10^6$	Delamination
1C/u-H1	0°	70	3215	$5 \times 10^6$	$10^7$	Delamination
1C/u-H3	0°	70	3380	$3 \times 10^6$	$10^7$	Delamination
1B/u-H1	0°	450	1400	DNF	$10^7$	—
2E/u-H1	0°	450	1500	DNF	$10^7$	—
3D/u-H4	0°	450	2030	DNF	$5 \times 10^6$	—
1B/u-H2	0°	450	2100	DNF	$10^7$	—
3F/u-H1	0°	450	2105	$4 \times 10^6$	$5 \times 10^6$	Delamination
3D/u-H3	0°	450	2105	DNF	$5 \times 10^6$	—
3F/u-H4	0°	450	2130	$5 \times 10^6$	$5 \times 10^6$	Delamination
11E/u-H4	0°	450	2150	$10^6$	$10^6$	Delamination
6E/u-H3	0°	450	2170	$3 \times 10^6$	$4 \times 10^6$	Delamination
11F/u-H1	0°	450	2180	$10^6$	$10^6$	Delamination
2D/u-H4	0°	450	2200	$5 \times 10^6$	$5 \times 10^6$	Delamination
6E/u-H2	0°	450	2200	$2 \times 10^6$	$4 \times 10^6$	Delamination
11E/u-H1	0°	450	2220	$5 \times 10^5$	$2 \times 10^6$	Delamination
11E/u-H3	0°	450	2220	$5 \times 10^5$	$2 \times 10^6$	Delamination
6F/u-H1	0°	450	2280	$2 \times 10^6$	$3 \times 10^6$	Delamination
6F/u-H2	0°	450	2330	$2 \times 10^6$	$3 \times 10^6$	Delamination

TABLE 9.4-II (Cont'd)

Specimen Number	Ply Config.	Temp. (°F)	Strain (μin./in.)	Cycles to Failure*	Total Cycles	Failure Mode
7E/B-H1	±45°,0°,±45°	450	1300	10 <sup>7</sup>	10 <sup>7</sup>	Delamination
8C/B-H3	±45°,0°,±45°	450	1540	DNF	5x10 <sup>6</sup>	—
7E/B-H2	±45°,0°,±45°	450	1600	4x10 <sup>6</sup>	4x10 <sup>6</sup>	Delamination
4C/B-H4	±45°,0°,±45°	450	1600	10 <sup>6</sup>	10 <sup>7</sup>	Delamination
8E/B-H3	±45°,0°,±45°	450	1610	5x10 <sup>6</sup>	5x10 <sup>6</sup>	Delamination
8D/B-H1	±45°,0°,±45°	450	1615	DNF	4x10 <sup>6</sup>	—
8D/B-H4	±45°,0°,±45°	450	1620	DNF	4x10 <sup>6</sup>	—
8C/B-H2	±45°,0°,±45°	450	1630	DNF	5x10 <sup>6</sup>	—
8E/B-H4	±45°,0°,±45°	450	1630	5x10 <sup>6</sup>	5x10 <sup>6</sup>	Delamination
8F/B-H1	±45°,0°,±45°	450	1695	2x10 <sup>6</sup>	2x10 <sup>6</sup>	Delamination
8F/B-H3	±45°,0°,±45°	450	1700	3x10 <sup>6</sup>	3x10 <sup>6</sup>	Delamination
8F/B-H2	±45°,0°,±45°	450	1725	10 <sup>6</sup>	3x10 <sup>6</sup>	Delamination
4C/B-H3	±45°,0°,±45°	450	1750	3x10 <sup>6</sup>	6x10 <sup>6</sup>	Delamination
7F/B-H4	±45°,0°,±45°	450	1755	2x10 <sup>6</sup>	2x10 <sup>6</sup>	Delamination
4C/B-H2	±45°,0°,±45°	450	1950	5x10 <sup>5</sup>	10 <sup>7</sup>	Delamination
4D/B-H1	±45°,0°,±45°	450	3560	Failed on Loading		
5B/C-H4	±45°	450	730	8x10 <sup>6</sup>	4x10 <sup>6</sup>	10% f <sub>n</sub> Drop
5C/C-H4	±45°	450	740	11x10 <sup>6</sup>	5x10 <sup>6</sup>	10% f <sub>n</sub> Drop
5B/C-H3	±45°	450	760	8x10 <sup>6</sup>	4x10 <sup>6</sup>	10% f <sub>n</sub> Drop
5C/C-H3	±45°	450	770	11x10 <sup>6</sup>	5x10 <sup>6</sup>	10% f <sub>n</sub> Drop
5D/C-H3	±45°	450	870	6x10 <sup>6</sup>	5x10 <sup>6</sup>	10% f <sub>n</sub> Drop
5D/C-H4	±45°	450	870	6x10 <sup>6</sup>	5x10 <sup>6</sup>	10% f <sub>n</sub> Drop
9D/C-H2	±45°	450	900	4x10 <sup>6</sup>	10 <sup>6</sup>	10% f <sub>n</sub> Drop
5D/C-H1	±45°	450	910	4x10 <sup>6</sup>	10 <sup>6</sup>	10% f <sub>n</sub> Drop
5D/C-H2	±45°	450	935	3x10 <sup>6</sup>	5x10 <sup>6</sup>	10% f <sub>n</sub> Drop
9D/C-H4	±45°	450	960	5x10 <sup>6</sup>	3x10 <sup>6</sup>	10% f <sub>n</sub> Drop
5E/C-H4	±45°	450	975	5x10 <sup>6</sup>	3x10 <sup>6</sup>	10% f <sub>n</sub> Drop
12C/C-H3	±45°	450	1000	4x10 <sup>6</sup>	10 <sup>7</sup>	10% f <sub>n</sub> Drop
12D/C-H4	±45°	450	1265	2x10 <sup>6</sup>	10 <sup>7</sup>	10% f <sub>n</sub> Drop
12D/C-H2	±45°	450	1280	3x10 <sup>6</sup>	8x10 <sup>6</sup>	10% f <sub>n</sub> Drop
12F/C-H1	±45°	450	1325	2x10 <sup>6</sup>	10 <sup>7</sup>	10% f <sub>n</sub> Drop
12D/C-H3	±45°	450	1505	2x10 <sup>6</sup>	2x10 <sup>6</sup>	10% f <sub>n</sub> Drop

\* Number of cycles to failure for ±45° specimens determined from a plot of natural frequency drop versus cycles and, in some cases, extrapolated to the ten percent frequency drop.

\*\* DNF = Did not fail.

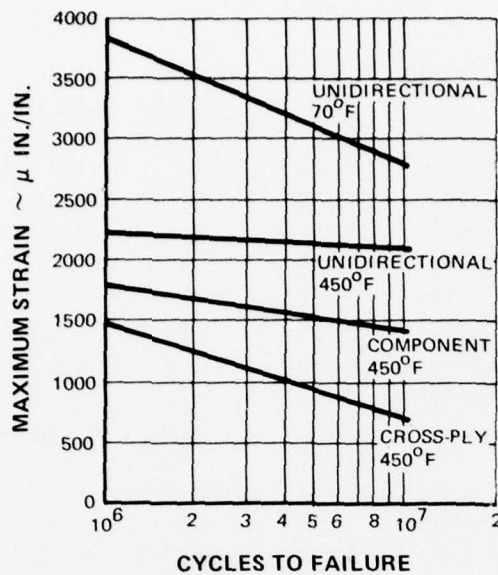


Figure 9.4-2 High Frequency Fatigue Test Results for Undamaged 50 Volume-Percent 20-Layer Borsical® Specimens

#### 9.4.3 Metallography

Room temperature HFF tests of unidirectional specimens resulted in microstructures of several distinct types. When run at low strain levels ( $< 2400 \mu\text{in./in.}$ ), no fatigue cracks or delaminations were observed. Between 2400 and approximately  $3000 \mu\text{in./in.}$  strain, the unidirectional specimens that were tested to  $10^7$  cycles developed internal fatigue cracks of the type shown in Figure 9.4-3 with no visible specimen delamination or appreciable frequency drop. Note that the cracks are not associated with the fiber-matrix and the ply-to-ply interfaces, indicating good bonding during panel fabrication. Specimens cycled at approximately  $3100 \mu\text{in./in.}$  and higher for up to  $5 \times 10^6$  cycles revealed that surface delamination occurred at about  $3 \times 10^6$  cycles with severe matrix and fiber damage near the specimen surface, as shown in Figure 9.4-4. Delamination with very few fatigue cracks and no significant natural frequency drop was detected in specimens tested at high strains (greater than  $3400 \mu\text{in./in.}$ ) for short times. An additional type of deterioration observed after testing at  $3100 \mu\text{in./in.}$  consisted of internal delamination between the ninth and tenth layers of the 20-layer composite, as shown in Figure 9.4-5. No fiber splitting was observed in any unidirectional specimens examined after room temperature HFF tests.

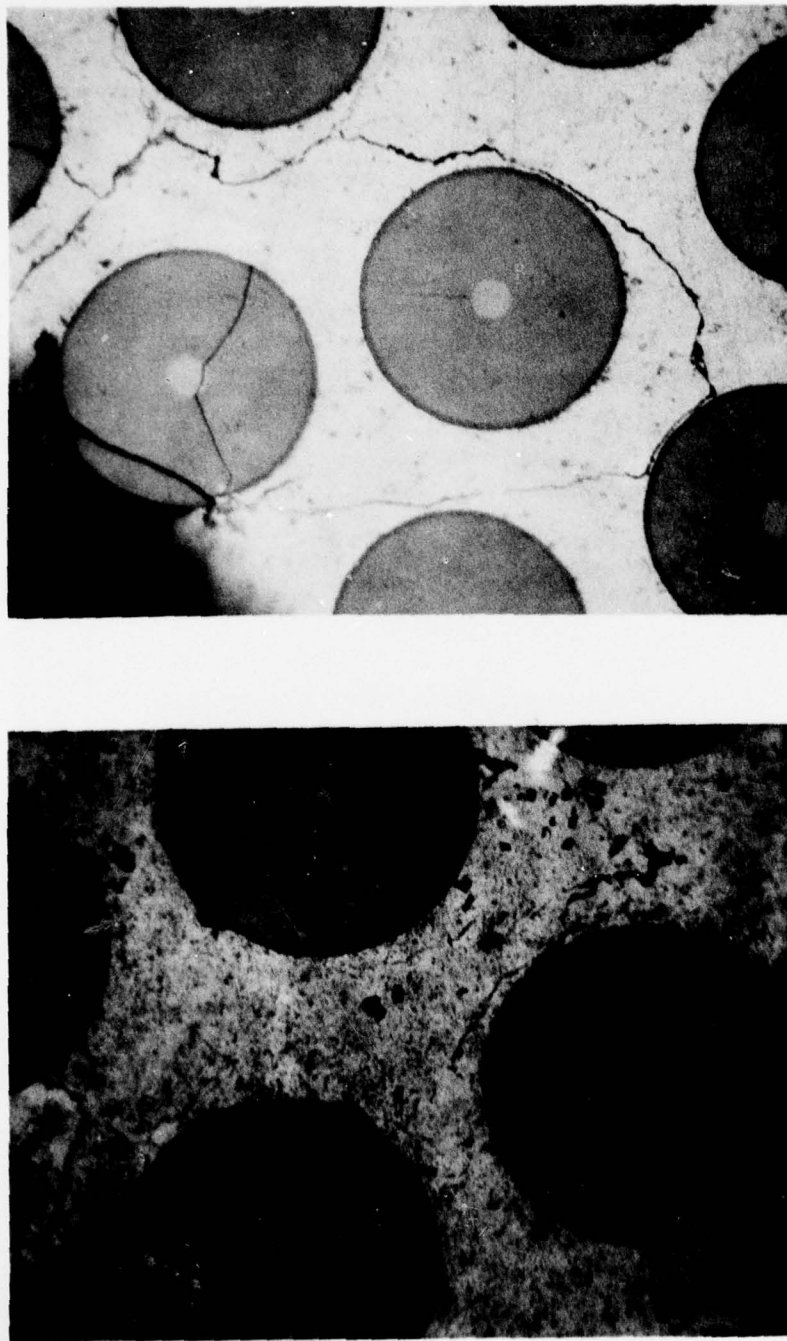


Figure 9.4-3 Microstructure of Unidirectional Borsicai® Specimens that were High Frequency Fatigue Tested at 70°F and 2450  $\mu$  in./in. for  $10^7$  cycles (1C/u-H2 at Left) and 2900  $\mu$  in./in. for  $10^6$  cycles (2D/u-H3 at Right)

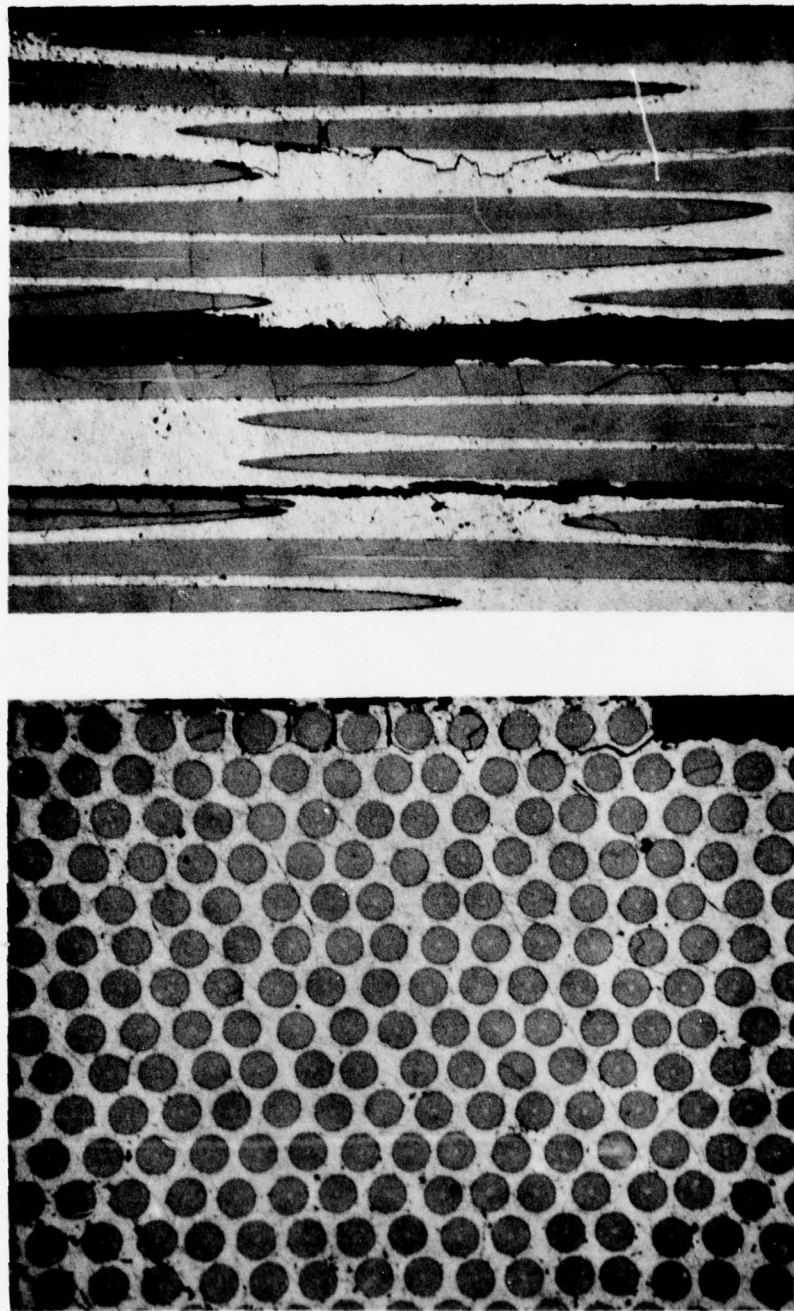


Figure 9.4-4 *Microstructure of Unidirectional Borsicaf® Specimens that were High Frequency Fatigue Tested at 70°F and 3100  $\mu$  in. in. for  $2 \times 10^6$  Cycles (2E/u-H2 at Left) and  $3 \times 10^6$  cycles (1D/u-H4 at Right)*

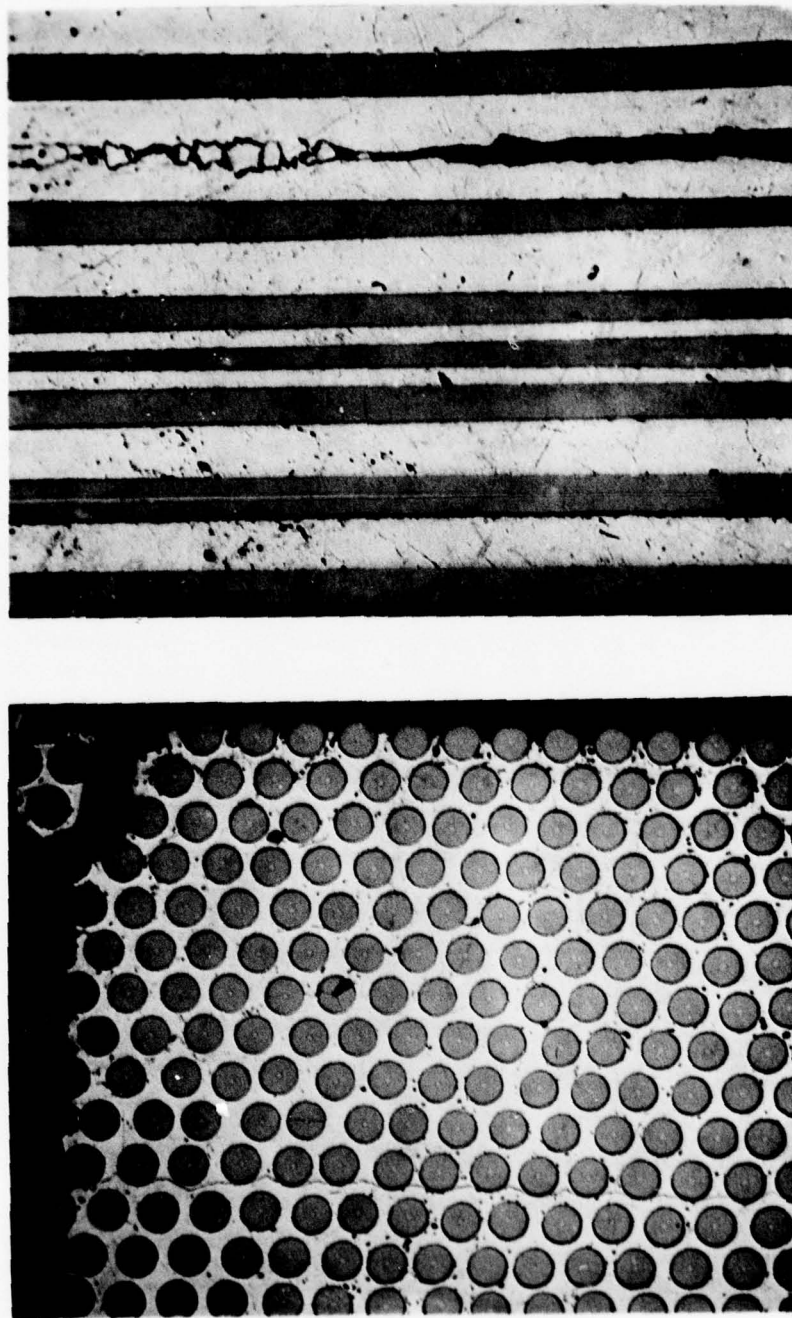
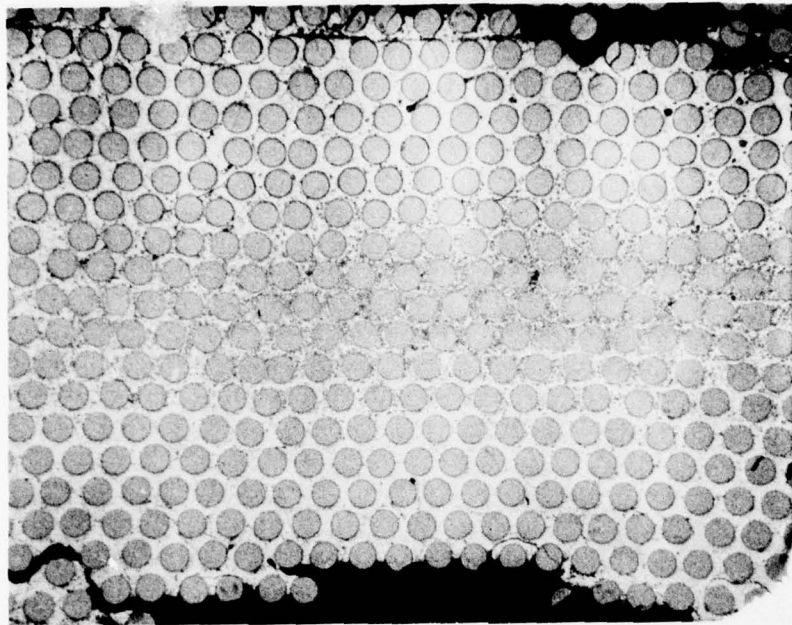


Figure 9.4-5 Microstructure of Unidirectional Borsicat® Specimens that were High Frequency Fatigue Tested at 70°F and 3100  $\mu$  in./in. for  $5 \times 10^6$  Cycles (1E/u-H3)

At 450°F the HFF failures of unidirectional specimens did not differ greatly from those tested at room temperature. At this higher test temperature, lower strain levels were used, but the basic failure modes were unchanged. Failures consisted mostly of surface delamination (Figure 9.4-6) with some internal delamination between middle layers, and a few cracks (Figure 9.4-7). Differences between microstructures for the various HFF life fractions were not found, and all unidirectional specimens had similar internal defects regardless of test temperature or percent of life exhausted.

The undamaged component configuration specimens which were HFF tested at 450°F exhibited a very distinctive failure mode in addition to surface delamination. Splitting of cross-ply fibers parallel to the plane of the specimen was detected in every component specimen tested (see Figure 9.4-8). Fatigue cracks and delaminations were noted in some but not all samples. The splitting is believed to contribute to the immediate natural frequency drop detected for all component specimens tested at approximately 1600  $\mu$ in./in. strain or greater. None of the unidirectional fibers in the core were split and no matrix deterioration was observed around the core fibers. As in the unidirectional material, no real microstructure differences were noted between specimens tested to 20 percent versus 100 percent of their expected HFF life.

Cross-ply samples that were HFF tested at 450°F contained numerous fatigue cracks which appeared to originate at split fibers (see Figure 9.4-9). The orientation of the splitting which occurred in the fibers of the cross-ply laminate was normal to the plane of the specimens rather than parallel as found in the component specimens. Stress analysis of cross-ply samples during HFF testing indicated that the tensile stresses in the plane of the samples could result in fiber splitting due to the low transverse strength of Borsic® filament. During fatigue testing, a ten percent drop in natural frequency occurred prior to delamination, and apparently the fiber splitting, as well as the growth of fatigue cracks in the matrix, produced that frequency drop. The orientation of fiber splitting directed the fatigue cracks into the specimen, preventing visual delamination.



*Figure 9.4-6 Surface Appearance and Microstructure of Unidirectional Borsica® Specimens that were High Frequency Fatigue Tested at 450°F and 2180  $\mu$  in./in. for  $10^6$  Cycles (11F/u-H1)*

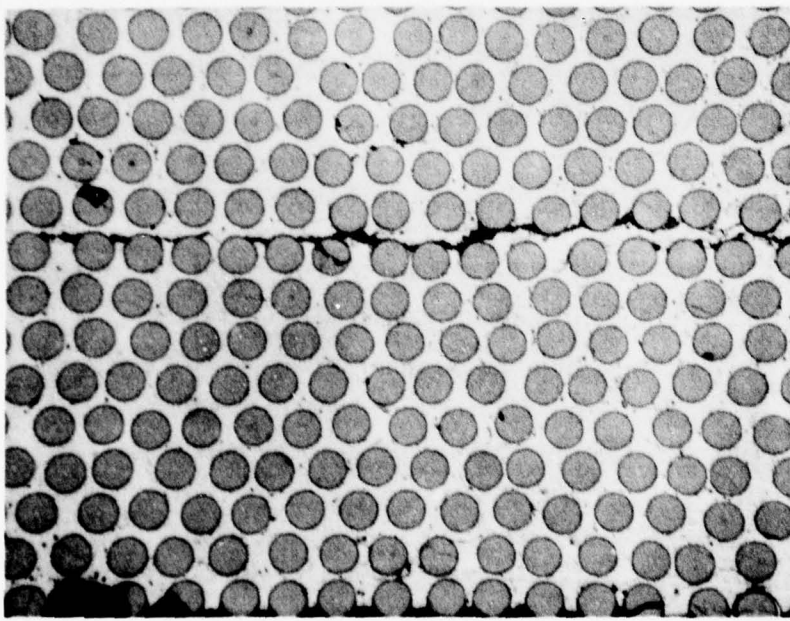
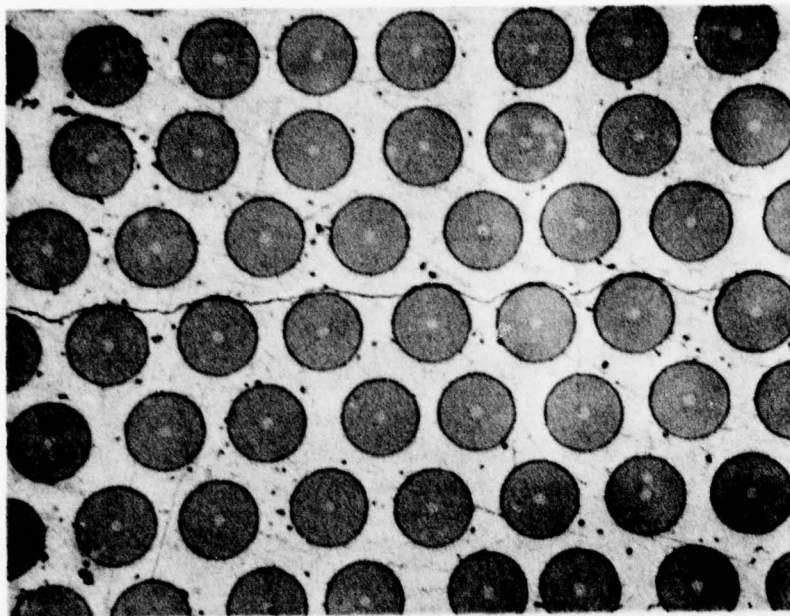
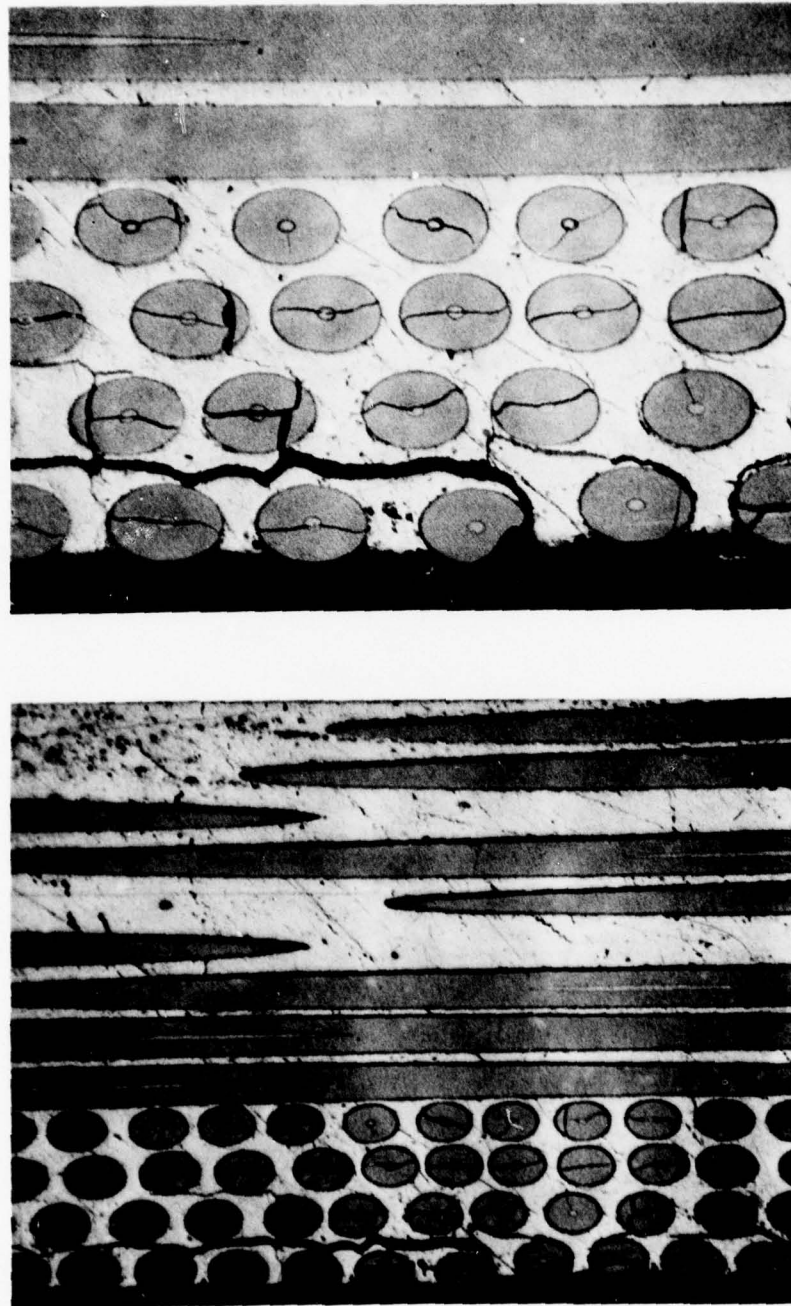


Figure 9.4-7 *Microstructure of Unidirectional Borsicaf® Specimens that were High Frequency Fatigue Tested at 450°F and 2100  $\mu$  in./in. for  $5 \times 10^6$  Cycles (3D/u-H3 at Left) and  $2220 \mu$  in./in. for  $2 \times 10^6$  Cycles (11E/u-H3 at Right)*



*Figure 9.4-8 Microstructure of Component Borsicai<sup>®</sup> Specimen (7F/B-H4) that was High Frequency Fatigue Tested at 450° F and 1755  $\mu$  in./in. for  $2 \times 10^6$  Cycles*

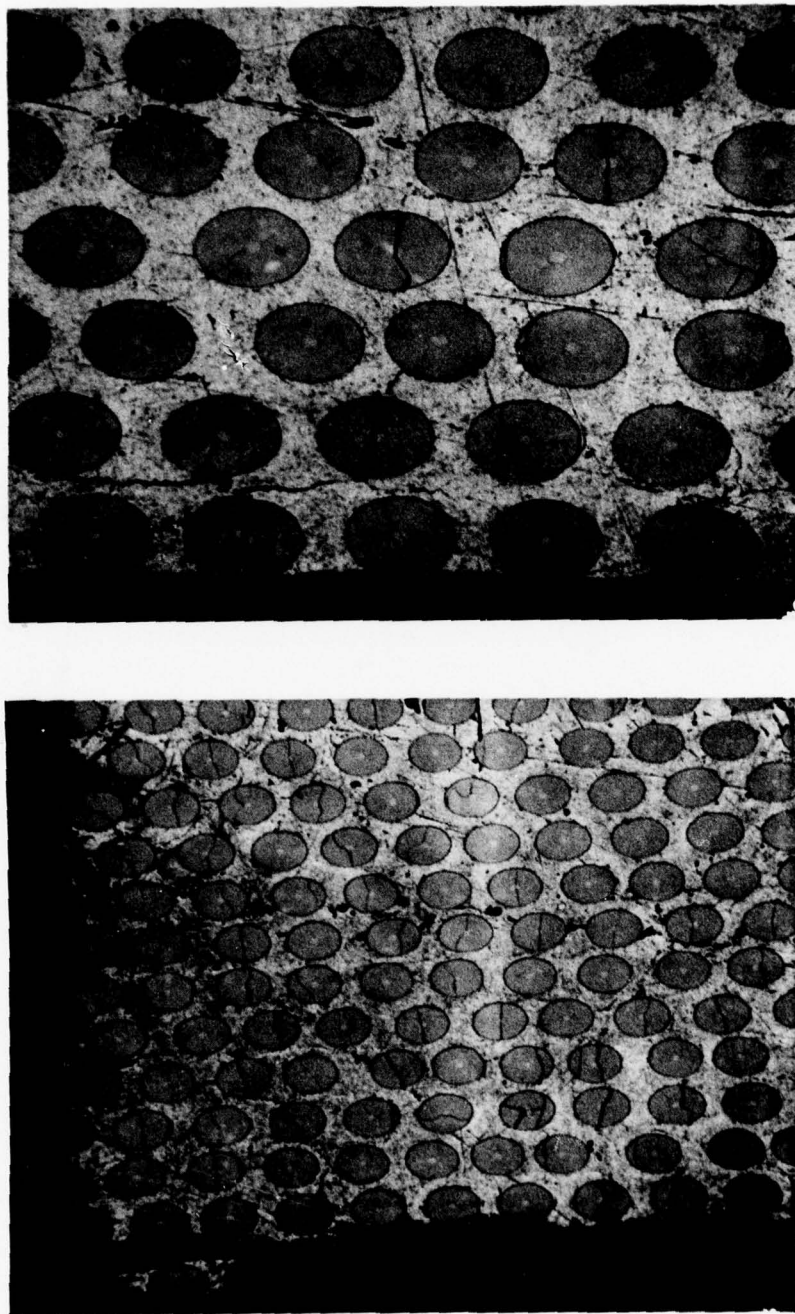


Figure 9.4-9 Microstructure of Cross-Ply Borsicaf® Specimen (12D/C-H4) that was High Frequency Fatigue Tested at 450°F and 1265  $\mu$  in./in. for  $10^7$  Cycles

## 9.5 EROSION DAMAGE

Tests conducted on erosion damaged specimens lead to the following conclusions:

- In order to reduce the 450°F HFF capability of unidirectional or cross-ply laminates, erosion damage must be severe enough to break the fibers.
- Erosion damage to break as many as four layers of cross-ply fibers does not reduce the 70°F tensile strength or 450°F HFF life of component material.
- Erosion damaged specimens subjected to HFF testing suffer a strength reduction equivalent to that for base-line undamaged specimens.

### 9.5.1 Tensile

Room temperature tensile properties of all three of the ply configurations were not significantly influenced by erosion exposure as illustrated in Figure 9.5-1 and Table 9.5-I. Eroded specimens which were HFF tested had tensile strengths comparable to undamaged HFF-tested samples.

### 9.5.2 High Frequency Fatigue

Erosion damage did not significantly reduce the HFF capability of any of the three ply configurations (Table 9.5-II). However, when severe erosion damage was inflicted to the extent of breaking fibers, both the unidirectional and the cross-ply configurations suffered reductions in HFF life similar to those of ballistically impacted samples (described below). On the other hand, the HFF life of the component configuration material was not reduced by severe erosion (again similar to the behavior of impacted samples). It is apparent that erosion of component material would have to damage the unidirectional fiber portion of the material to influence the HFF life.

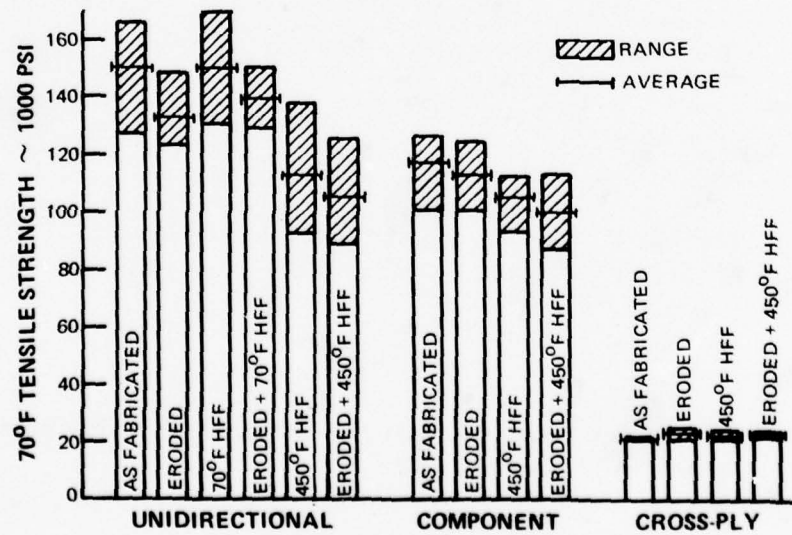


Figure 9.5-1  
Effect of Erosion Damage on the 70°F Tensile Strength of 50 Volume-Percent 20-Layer Borsical® Specimens

TABLE 9.5-1

70°F TENSILE TEST RESULTS FOR EROSION DAMAGED  
20-LAYER 50 PERCENT - VOLUME BORSICAL® SPECIMENS

Specimen Number	Ply Config.	Type of Prior Erosion*	Prior HFF Exposure				UTS (10 <sup>3</sup> psi)	Modulus (10 <sup>6</sup> psi)
			Temp. (°F)	Strain (μin./in.)	Cycles to Failure	Total Cycles		
2A/u-H3	0°	I		None			123.4	—
2A/u-H4	0°	I		None			148.2	—
2A/u-H1	0°	I		None			127.0	35.3
2C/u-H1	0°	I	70	3400	10 <sup>6</sup>	4x10 <sup>6</sup>	129.2	—
2C/u-H2	0°	I	70	3400	2x10 <sup>6</sup>	4x10 <sup>6</sup>	146.2	—
2A/u-H2	0°	I	70	3350	3x10 <sup>6</sup>	10 <sup>7</sup>	151.4	—
2B/u-H1	0°	I	70	3345	3x10 <sup>6</sup>	10 <sup>7</sup>	131.5	—
2C/u-H3	0°	I	450	2295	2x10 <sup>6</sup>	5x10 <sup>6</sup>	126.0	—
3E/u-H4	0°	I	450	2175	4x10 <sup>6</sup>	5x10 <sup>6</sup>	100.5	—
3E/u-H3	0°	II	450	2100	10 <sup>6</sup>	5x10 <sup>6</sup>	89.2	—
7A/B-H4	±45°,0°,±45°	I		None			101.2	—
7C/B-H2	±45°,0°,±45°	I		None			125.2	—
4B/B-H2	±45°,0°,±45°	I	450	1550	5x10 <sup>6</sup>	5x10 <sup>6</sup>	100.5	—
7A/B-H1	±45°,0°,±45°	I	450	1530	DNF**	5x10 <sup>6</sup>	87.4	—
4D/B-H4	±45°,0°,±45°	II	450	1710	5x10 <sup>6</sup>	5x10 <sup>6</sup>	113.7	—
9C/C-H2	±45°	I		None			20.9	—
9B/C-H4	±45°	I		None			25.0	—
9A/C-H2	±45°	I	450	970	5x10 <sup>6</sup>	5x10 <sup>6</sup>	23.8	—
5E/C-H2	±45°	I	450	875	5x10 <sup>6</sup>	5x10 <sup>6</sup>	22.8	—
9F/C-H3	±45°	I	450	860	DNF	4x10 <sup>6</sup>	22.9	—
5E/C-H1	±45°	II	450	980	2x10 <sup>6</sup>	5x10 <sup>6</sup>	22.4	—

\* Type I; sufficient erosion to expose two layers of fibers without fiber breakage.  
Type II; sufficient erosion to break fibers.

\*\* DNF = Did not fail.

TABLE 9.5-II

HIGH FREQUENCY FATIGUE TEST RESULTS FOR EROSION  
DAMAGED 20-LAYER 50 PERCENT - VOLUME BORSICAL® SPECIMENS

Specimen Number	Type of Erosion*	Ply Config.	Temp. (°F)	Strain (μin./in.)	Cycles to Failure	Total Cycles	Failure Mode
2B/u-H1	I	0°	70	3345	3x10 <sup>6</sup>	10 <sup>7</sup>	Delamination
2A/u-H2	I	0°	70	3350	3x10 <sup>6</sup>	10 <sup>7</sup>	Delamination
2C/u-H1	I	0°	70	3400	10 <sup>6</sup>	4x10 <sup>6</sup>	Delamination
2C/u-H2	I	0°	70	3400	2x10 <sup>6</sup>	4x10 <sup>6</sup>	Delamination
2B/u-H4	I	0°	70	3450	5x10 <sup>6</sup>	8x10 <sup>6</sup>	Delamination
2C/u-H4	I	0°	450	2160	4x10 <sup>6</sup>	5x10 <sup>6</sup>	Delamination
3E/u-H4	I	0°	450	2175	4x10 <sup>6</sup>	5x10 <sup>6</sup>	Delamination
2C/u-H3	I	0°	450	2295	2x10 <sup>6</sup>	5x10 <sup>6</sup>	Delamination
3E/u-H3	II	0°	450	2100	10 <sup>6</sup>	5x10 <sup>6</sup>	Delamination
7A/B-H1	I	±45°,0°,±45°	450	1530	DNF**	5x10 <sup>6</sup>	—
4B/B-H2	I	±45°,0°,±45°	450	1550	5x10 <sup>6</sup>	5x10 <sup>6</sup>	Delamination
7A/B-H2	I	±45°,0°,±45°	450	1575	5x10 <sup>6</sup>	5x10 <sup>6</sup>	Delamination
7B/B-H2	I	±45°,0°,±45°	450	1580	DNF	4x10 <sup>6</sup>	—
7A/B-H3	I	±45°,0°,±45°	450	1600	DNF	4x10 <sup>6</sup>	—
4D/B-H4	II	±45°,0°,±45°	450	1710	5x10 <sup>6</sup>	5x10 <sup>6</sup>	Delamination
9F/C-H3	I	±45°	450	860	5x10 <sup>6+</sup>	4x10 <sup>6</sup>	10% f <sub>n</sub> drop
5E/C-H2	I	±45°	450	875	5x10 <sup>6</sup>	5x10 <sup>6</sup>	10% f <sub>n</sub> drop
9F/C-H1	I	±45°	450	920	5x10 <sup>6+</sup>	4x10 <sup>6</sup>	10% f <sub>n</sub> drop
9B/C-H1	I	±45°	450	950	5x10 <sup>6</sup>	5x10 <sup>6</sup>	10% f <sub>n</sub> drop
9A/C-H2	I	±45°	450	970	5x10 <sup>6</sup>	5x10 <sup>6</sup>	10% f <sub>n</sub> drop
5E/C-H1	II	±45°	450	980	2x10 <sup>6+</sup>	5x10 <sup>6</sup>	10% f <sub>n</sub> drop

\* Type I: sufficient erosion to expose two layers of fibers without fiber breakage.

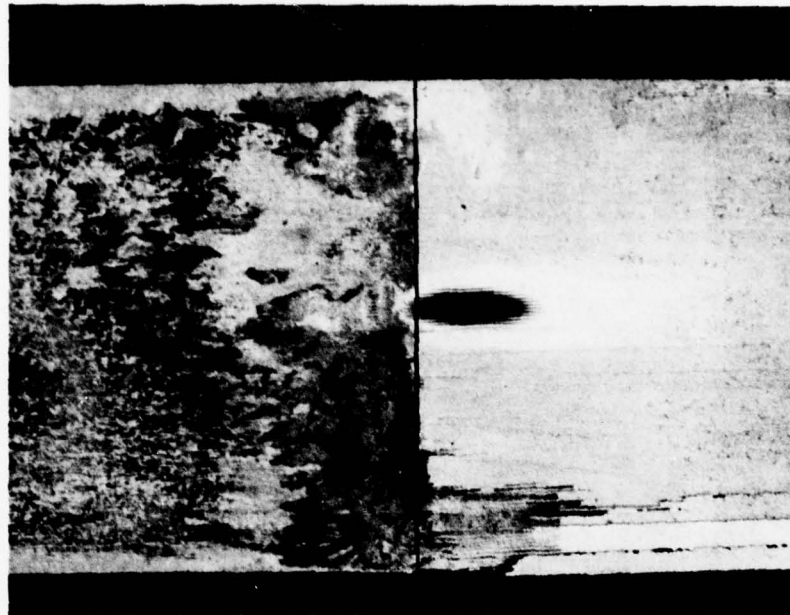
Type II: sufficient erosion to break fibers.

\*\* DNF = Did not fail.

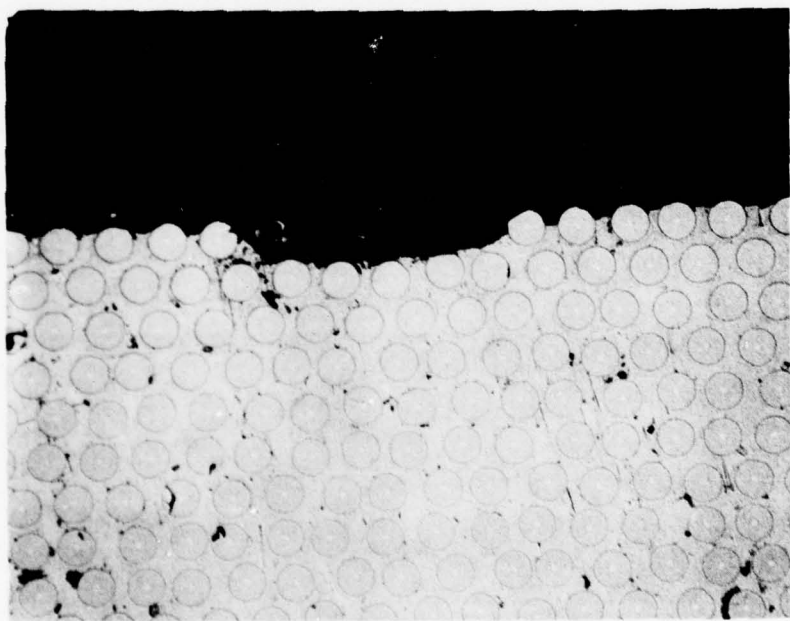
+ Estimated failure.

### 9.5.3 Metallography

The microstructure of eroded (exposed fibers) 70°F HFF-tested unidirectional specimens was similar to that for undamaged specimens. As shown in Figure 9.5-2, failure takes place by surface delamination with no internal fatigue cracks. Eroded unidirectional specimens HFF-tested at 450°F also looked identical to the undamaged specimens. The delamination did not occur preferentially at the eroded region even when cycled to 100 percent of life expectancy at either room temperature or 450°F. A deeply eroded sample with broken fibers was HFF tested at 450°F and did delaminate from the damaged area as shown in Figure 9.5-3. Erosion damage also did not alter the failure mode for component specimens. As with undamaged specimens, the 450°F HFF test resulted in splitting of the cross-ply layers and surface delamination as shown in Figure 9.5-4. It should be noted that, again, delamination did not originate in the eroded area of exposed fibers. A deeply eroded component specimen (fibers broken during erosion) behaved in a 450°F HFF test as though there were no broken fibers, and specimen delamination did not begin at the eroded area, as shown in Figure 9.5-5.



MAG: 3X



MAG: 50X

*Figure 9.5-2 Typical Unidirectional Erosion Test Specimen Following Erosion and High Frequency Fatigue Testing Showing Lack of Delamination in the Eroded Region.*

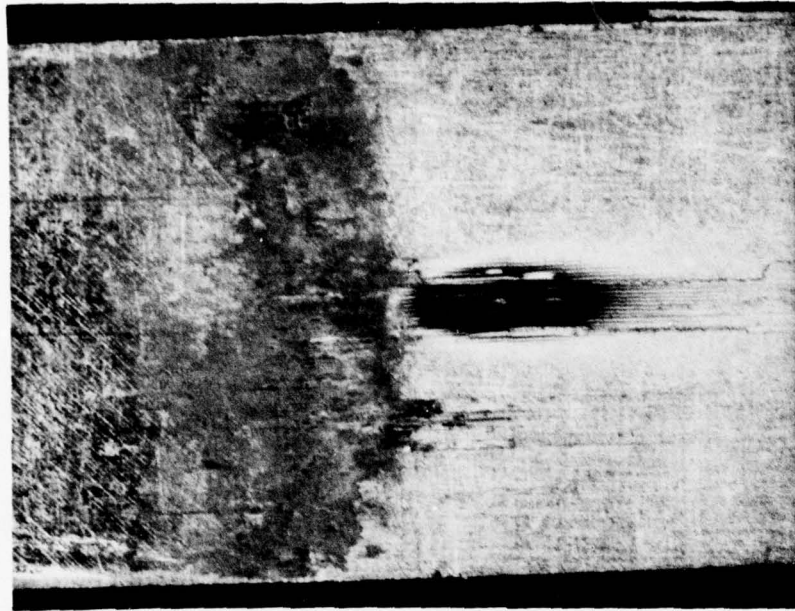


Figure 9.5-3      Surface of Deeply Eroded Unidirectional Borsicaf® Specimen (3E/u-H3) Before (Left) and After (Right) 450°F High Frequency Fatigue Testing at 2100  $\mu$  in./in. for  $5 \times 10^6$  Cycles

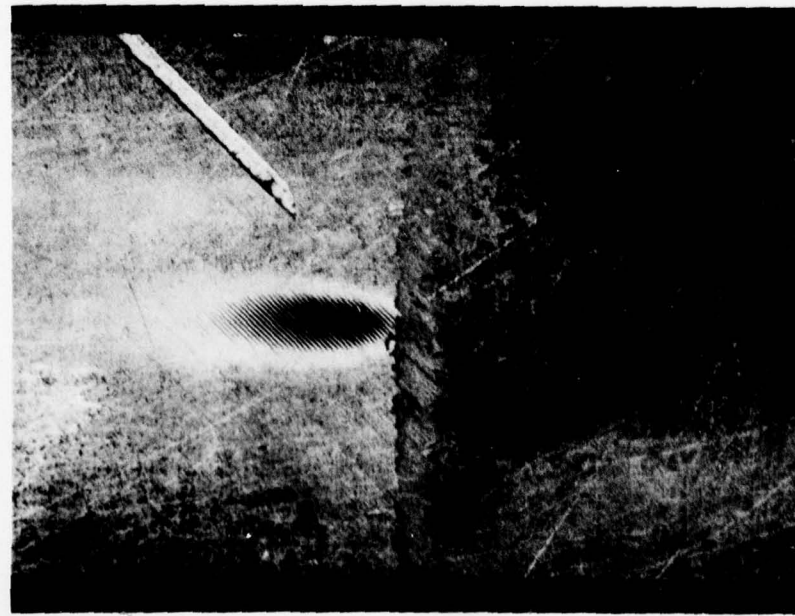
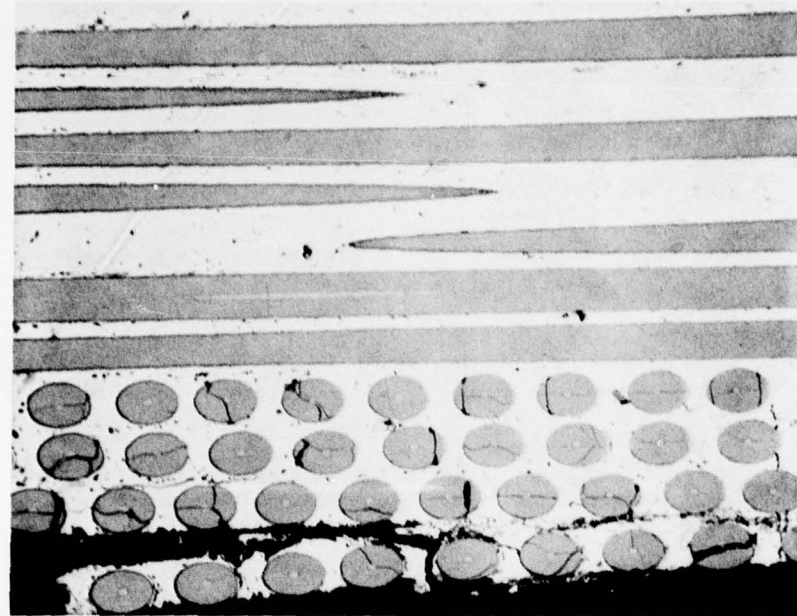
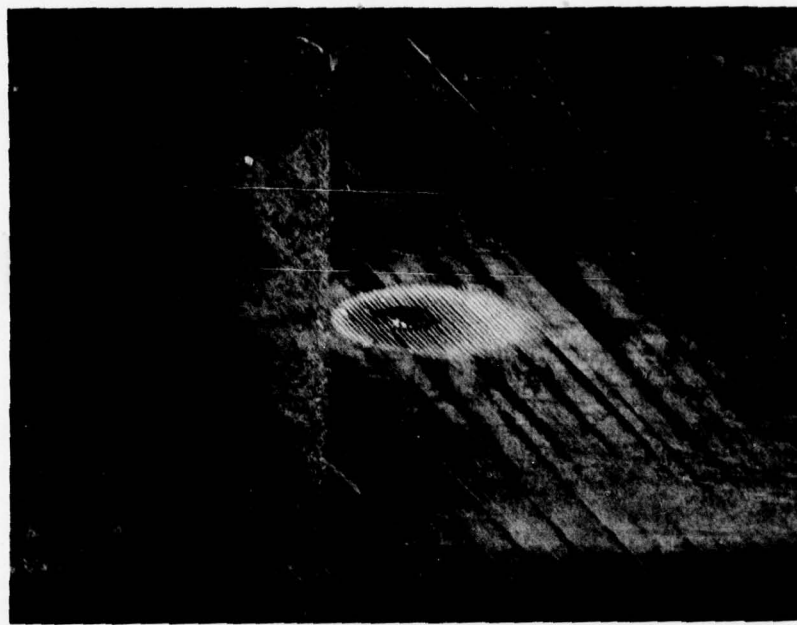


Figure 9.5-4 Surface Appearance and Microstructure of Eroded Component Specimen (7A/B-H2) After 450° F High Frequency Fatigue Testing at  $1575 \mu \text{in./in.}$  for  $5 \times 10^6$  Cycles



**Figure 9.5-5** Surface Appearance of Deeply Eroded Component Specimen (4D/B-H4) After 450°F High Frequency Fatigue Testing at  $1710 \mu \text{in./in.}$  for  $5 \times 10^6$  Cycles

## 9.6 BALLISTIC IMPACT DAMAGE

Specimens subjected to ballistic impact damage were tested and the following conclusions were drawn:

- Borsical® composites which sustain ballistic impact damage have their strength reduced proportionally to the cross-section area that was physically damaged during impact.
- The cross-ply structure exhibited the least strength reduction due to ballistic impact; however, all three configurations had about the same percentage reduction after subsequent 450°F HFF testing.
- HFF life for the unidirectional cross-ply specimens is reduced by ballistic impact damage; however, HFF life of component specimens is not affected by impact damage of the level evaluated.

### 9.6.1 Tensile

The impact evaluated in this program was sufficient to break fibers in all the ply configurations tested as evidenced by the reduced strength levels shown in Figure 9.6-1 and Table 9.6-1. Although all specimens had lower strengths after damage, the percent decrease in ultimate tensile strength varied from one ply configuration to another. The strength loss due to impact was 43.5, 42 and 18.7 percent for the unidirectional, component and cross-ply configurations.

respectively. The loss in strength due to ballistic impact followed by 450°F HFF testing was similar for all three configurations and was 53.8, 47.5 and 48.4 percent for unidirectional, component and cross-ply configurations, respectively.

### 9.6.2 High Frequency Fatigue

Ballistic impact damage drastically lowered the HFF life of the unidirectional and cross-ply configurations as shown in Table 9.6-II. However, impact damage did not significantly reduce the HFF life of the component material specimens. C-scan results, shown in Figures 9.6-2 and 9.6-3, show that delamination failures in the unidirectional specimens are initiated at the impact area while the delamination failures in the component specimens extend from the grip edge (similar to undamaged specimens) up through the impacted region. This would indicate that the failures do not emanate from the impact area in the component specimens. Cross-ply laminates suffer a drop in natural frequency due to impact damage but no delamination occurs.

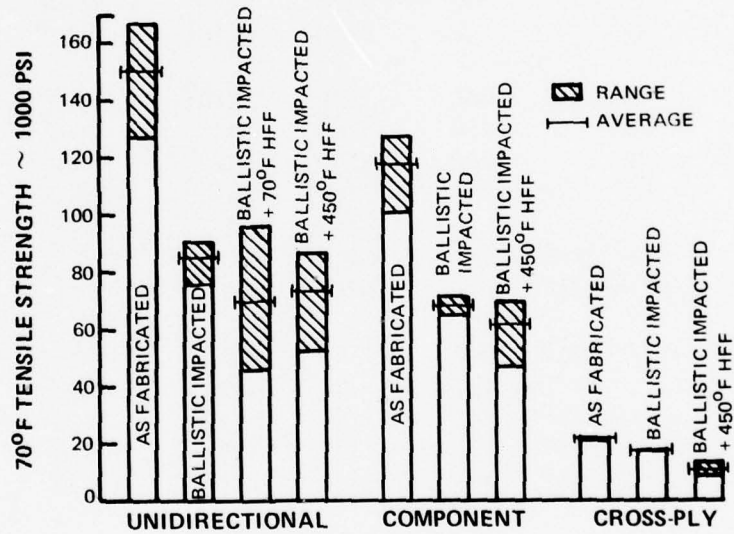


Figure 9.6-1 Effect of Ballistic Impact Damage on the 70°F Tensile Strength of 50 Volume-Percent 20-Layer Borsical® Specimens

TABLE 9.6-I

70°F TENSILE TEST RESULTS FOR BALLISTIC IMPACT DAMAGED  
20-LAYER 50 PERCENT - VOLUME BORSICAL® SPECIMENS

Specimen Number	Ply Config.	Prior HFF Exposure				
		Temp. (°F)	Strain (μin./in.)	Cycles to Failure	Total Cycles	UTS (10³ psi)
3A/u-H1	0°		None			75.6
3A/u-H4	0°		None			78.3
3B/u-H3	0°		None			88.5
3E/u-H1	0°		None			90.5
3B/u-H2	0°	70	3100	5x10 <sup>5</sup>	10 <sup>6</sup>	95.8
6E/u-H1	0°	70	3100	5x10 <sup>5</sup>	2x10 <sup>6</sup>	63.4
3C/u-H4	0°	70	3100	10 <sup>5</sup>	3x10 <sup>6</sup>	47.3
3C/u-H1	0°	70	3100	10 <sup>5</sup>	4x10 <sup>6</sup>	45.9
3B/u-H4	0°	70	3500	5x10 <sup>5</sup>	5x10 <sup>6</sup>	85.2
3E/u-H2	0°	70	3550	5x10 <sup>5</sup>	5x10 <sup>6</sup>	81.4
3B/u-H1	0°	450	2100	5x10 <sup>5</sup>	2x10 <sup>6</sup>	52.7
6C/u-H2	0°	450	2100	10 <sup>6</sup>	3x10 <sup>6</sup>	75.7
6D/u-H2	0°	450	2100	3x10 <sup>6</sup>	4x10 <sup>6</sup>	87.0
6D/u-114	0°	450	2100	4x10 <sup>6</sup>	5x10 <sup>6</sup>	78.5
7D/B-H3	±45°, 0°, ±45°		None			65.1
7D/B-H4	±45°, 0°, ±45°		None			71.7
4E/B-H1	±45°, 0°, ±45°	450	1700	10 <sup>6</sup>	10 <sup>6</sup>	69.3
4E/B-H3	±45°, 0°, ±45°	450	1700	2x10 <sup>6</sup>	2x10 <sup>6</sup>	64.1
7D/B-H1	±45°, 0°, ±45°	450	1700	3x10 <sup>6</sup>	3x10 <sup>6</sup>	60.7
7C/B-H3	±45°, 0°, ±45°	450	1700	4x10 <sup>6</sup>	4x10 <sup>6</sup>	69.8
7B/B-H3	±45°, 0°, ±45°	450	1700	3x10 <sup>6</sup>	5x10 <sup>6</sup>	47.4
9A/C-H1	±45°	450	None			17.7
9A/C-H3	±45°	450	None			17.9
9C/C-H3	±45°	450	900	10 <sup>6</sup>	10 <sup>6</sup>	11.4
9E/C-H2	±45°	450	900	2x10 <sup>6</sup>	2x10 <sup>6</sup>	11.6
9C/C-H1	±45°	450	900	3x10 <sup>6</sup>	3x10 <sup>6</sup>	10.8
9B/C-H2	±45°	450	750	DNF*	4x10 <sup>6</sup>	13.5
9E/C-H3	±45°	450	900	10 <sup>6</sup>	5x10 <sup>6</sup>	9.3

\* DNF = Did not fail.

## PRATT &amp; WHITNEY AIRCRAFT GROUP

TABLE 9.6-II

HIGH FREQUENCY FATIGUE TEST RESULTS FOR BALLISTIC IMPACT  
DAMAGED 20-LAYER 50 PERCENT - VOLUME BORSICAL® SPECIMENS

Specimen Number	Ply Config.	Temp. (°F)	Strain (μin./in.)	Cycles to Failure	Total Cycles	Failure Mode
3B/u-H2	0°	70	3100	5x10 <sup>5</sup>	10 <sup>6</sup>	Delamination
3D/u-H1	0°	70	3100	5x10 <sup>5</sup>	2x10 <sup>6</sup>	Delamination
6E/u-H1	0°	70	3100	5x10 <sup>5</sup>	2x10 <sup>6</sup>	Delamination
3C/u-H3	0°	70	3100	10 <sup>5</sup>	3x10 <sup>6</sup>	Delamination
3C/u-H4	0°	70	3100	10 <sup>5</sup>	3x10 <sup>6</sup>	Delamination
3C/u-H1	0°	70	3100	10 <sup>5</sup>	4x10 <sup>6</sup>	Delamination
3C/u-H2	0°	70	3100	10 <sup>5</sup>	4x10 <sup>6</sup>	Delamination
3A/u-H3	0°	70	3350	10 <sup>6</sup>	5x10 <sup>6</sup>	Delamination
3A/u-H2	0°	70	3480	3x10 <sup>6</sup>	10 <sup>7</sup>	Delamination
3B/u-H4	0°	70	3500	5x10 <sup>5</sup>	5x10 <sup>6</sup>	Delamination
3E/u-H2	0°	70	3550	5x10 <sup>5</sup>	5x10 <sup>6</sup>	Delamination
6C/u-H3	0°	450	2100	10 <sup>6</sup>	10 <sup>6</sup>	Delamination
3B/u-H1	0°	450	2100	5x10 <sup>5</sup>	2x10 <sup>6</sup>	Delamination
3D/u-H2	0°	450	2100	5x10 <sup>5</sup>	2x10 <sup>6</sup>	Delamination
6C/u-H1	0°	450	2100	10 <sup>6</sup>	3x10 <sup>6</sup>	Delamination
6C/u-H2	0°	450	2100	10 <sup>6</sup>	3x10 <sup>6</sup>	Delamination
6C/u-H4	0°	450	2100	3x10 <sup>6</sup>	4x10 <sup>6</sup>	Delamination
6D/u-H2	0°	450	2100	3x10 <sup>6</sup>	4x10 <sup>6</sup>	Delamination
6D/u-H3	0°	450	2100	3x10 <sup>6</sup>	5x10 <sup>6</sup>	Delamination
6D/u-H4	0°	450	2100	4x10 <sup>6</sup>	5x10 <sup>6</sup>	Delamination
4E/B-H1	±45°,0°,±45°	450	1700	10 <sup>6</sup>	10 <sup>6</sup>	Delamination
4E/B-H2	±45°,0°,±45°	450	1700	10 <sup>6</sup>	10 <sup>6</sup>	Delamination
4E/B-H3	±45°,0°,±45°	450	1700	2x10 <sup>6</sup>	2x10 <sup>6</sup>	Delamination
4E/B-H4	±45°,0°,±45°	450	1700	2x10 <sup>6</sup>	2x10 <sup>6</sup>	Delamination
7D/B-H1	±45°,0°,±45°	450	1700	3x10 <sup>6</sup>	3x10 <sup>6</sup>	Delamination
7D/B-H2	±45°,0°,±45°	450	1700	3x10 <sup>6</sup>	3x10 <sup>6</sup>	Delamination
7C/B-H3	±45°,0°,±45°	450	1700	4x10 <sup>6</sup>	4x10 <sup>6</sup>	Delamination
7C/B-H4	±45°,0°,±45°	450	1700	4x10 <sup>6</sup>	4x10 <sup>6</sup>	Delamination
7B/B-H3	±45°,0°,±45°	450	1700	3x10 <sup>6</sup>	5x10 <sup>6</sup>	Delamination
7B/B-H4	±45°,0°,±45°	450	1700	3x10 <sup>6</sup>	5x10 <sup>6</sup>	Delamination
9B/C-H2	±45°	450	750	6x10 <sup>6</sup> *	4x10 <sup>6</sup>	10% f <sub>n</sub> Drop
9B/C-H3	±45°	450	750	6x10 <sup>6</sup> *	4x10 <sup>6</sup>	10% f <sub>n</sub> Drop
9C/C-H3	±45°	450	900	10 <sup>6</sup>	10 <sup>6</sup>	10% f <sub>n</sub> Drop

TABLE 9.6-II

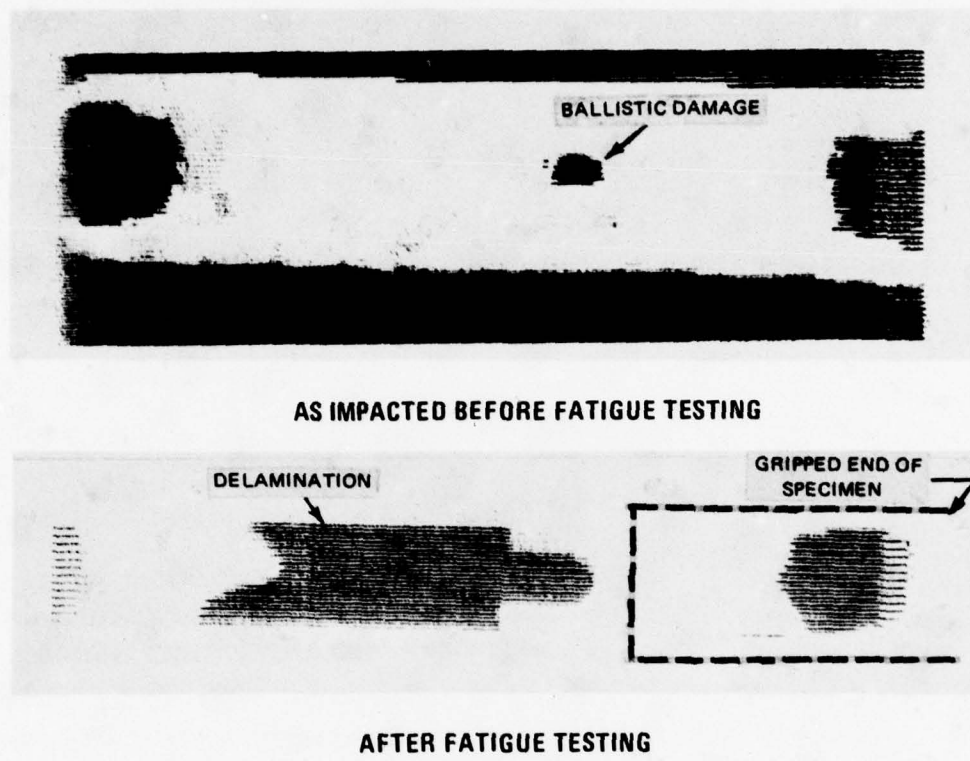
HIGH FREQUENCY FATIGUE TEST RESULTS FOR BALLISTIC IMPACT  
DAMAGED 20-LAYER 50 PERCENT - VOLUME BORSICAL® SPECIMENS

Specimen Number	Ply Config.	Temp. (°F)	Strain (μin./in.)	Cycles to Failure	Total Cycles	Failure Mode
3B/u-H2	0°	70	3100	5x10 <sup>5</sup>	10 <sup>6</sup>	Delamination
3D/u-H1	0°	70	3100	5x10 <sup>5</sup>	2x10 <sup>6</sup>	Delamination
6E/u-H1	0°	70	3100	5x10 <sup>5</sup>	2x10 <sup>6</sup>	Delamination
3C/u-H3	0°	70	3100	10 <sup>5</sup>	3x10 <sup>6</sup>	Delamination
3C/u-H4	0°	70	3100	10 <sup>5</sup>	3x10 <sup>6</sup>	Delamination
3C/u-H1	0°	70	3100	10 <sup>5</sup>	4x10 <sup>6</sup>	Delamination
3C/u-H2	0°	70	3100	10 <sup>5</sup>	4x10 <sup>6</sup>	Delamination
3A/u-H3	0°	70	3350	10 <sup>6</sup>	5x10 <sup>6</sup>	Delamination
3A/u-H2	0°	70	3480	3x10 <sup>6</sup>	10 <sup>7</sup>	Delamination
3B/u-H4	0°	70	3500	5x10 <sup>5</sup>	5x10 <sup>6</sup>	Delamination
3E/u-H2	0°	70	3550	5x10 <sup>5</sup>	5x10 <sup>6</sup>	Delamination
6C/u-H3	0°	450	2100	10 <sup>6</sup>	10 <sup>6</sup>	Delamination
3B/u-H1	0°	450	2100	5x10 <sup>5</sup>	2x10 <sup>6</sup>	Delamination
3D/u-H2	0°	450	2100	5x10 <sup>5</sup>	2x10 <sup>6</sup>	Delamination
6C/u-H1	0°	450	2100	10 <sup>6</sup>	3x10 <sup>6</sup>	Delamination
6C/u-H2	0°	450	2100	10 <sup>6</sup>	3x10 <sup>6</sup>	Delamination
6C/u-H4	0°	450	2100	3x10 <sup>6</sup>	4x10 <sup>6</sup>	Delamination
6D/u-H2	0°	450	2100	3x10 <sup>6</sup>	4x10 <sup>6</sup>	Delamination
6D/u-H3	0°	450	2100	3x10 <sup>6</sup>	5x10 <sup>6</sup>	Delamination
6D/u-H4	0°	450	2100	4x10 <sup>6</sup>	5x10 <sup>6</sup>	Delamination
4E/B-H1	±45°,0°,±45°	450	1700	10 <sup>6</sup>	10 <sup>6</sup>	Delamination
4E/B-H2	±45°,0°,±45°	450	1700	10 <sup>6</sup>	10 <sup>6</sup>	Delamination
4E/B-H3	±45°,0°,±45°	450	1700	2x10 <sup>6</sup>	2x10 <sup>6</sup>	Delamination
4E/B-H4	±45°,0°,±45°	450	1700	2x10 <sup>6</sup>	2x10 <sup>6</sup>	Delamination
7D/B-H1	±45°,0°,±45°	450	1700	3x10 <sup>6</sup>	3x10 <sup>6</sup>	Delamination
7D/B-H2	±45°,0°,±45°	450	1700	3x10 <sup>6</sup>	3x10 <sup>6</sup>	Delamination
7C/B-H3	±45°,0°,±45°	450	1700	4x10 <sup>6</sup>	4x10 <sup>6</sup>	Delamination
7C/B-H4	±45°,0°,±45°	450	1700	4x10 <sup>6</sup>	4x10 <sup>6</sup>	Delamination
7B/B-H3	±45°,0°,±45°	450	1700	3x10 <sup>6</sup>	5x10 <sup>6</sup>	Delamination
7B/B-H4	±45°,0°,±45°	450	1700	3x10 <sup>6</sup>	5x10 <sup>6</sup>	Delamination
9B/C-H2	±45°	450	750	6x10 <sup>6</sup> *	4x10 <sup>6</sup>	10% f <sub>n</sub> Drop
9B/C-H3	±45°	450	750	6x10 <sup>6</sup> *	4x10 <sup>6</sup>	10% f <sub>n</sub> Drop
9C/C-H3	±45°	450	900	10 <sup>6</sup>	10 <sup>6</sup>	10% f <sub>n</sub> Drop

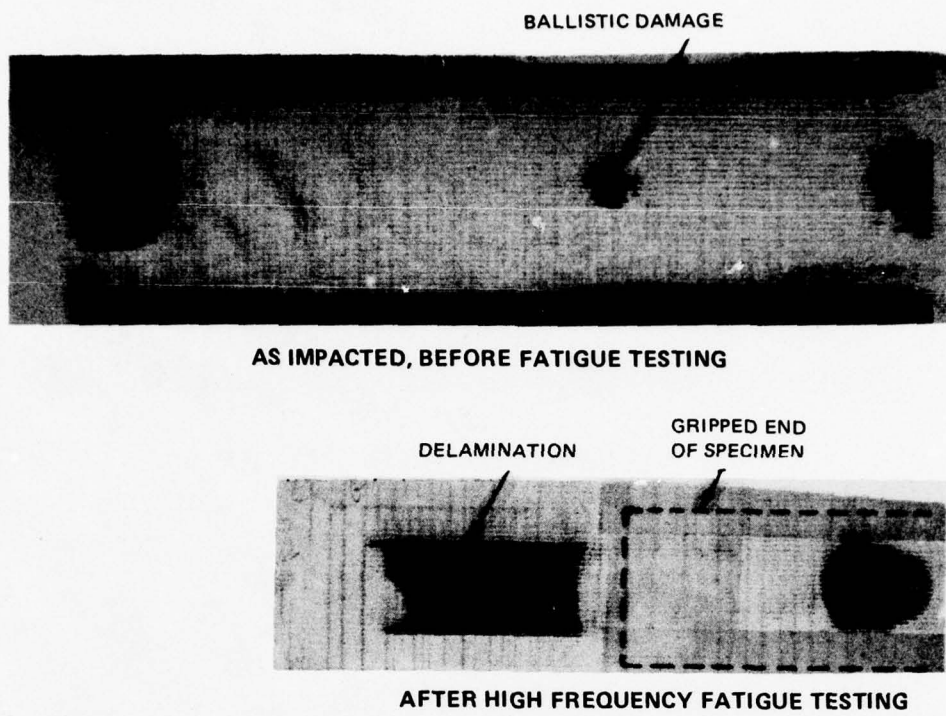
\*Fracture surface indicated defective specimens.

TABLE 9.6-II (Cont'd)

Specimen Number	Ply Config.	Temp. (°F)	Strain (μin./in.)	Cycles to Failure	Total Cycles	Failure Mode
9E/C-H1	±45°	450	900	10 <sup>6</sup>	10 <sup>6</sup>	10% f <sub>n</sub> Drop
9E/C-H2	±45°	450	900	2x10 <sup>6</sup>	2x10 <sup>6</sup>	10% f <sub>n</sub> Drop
9F/C-H2	±45°	450	900	2x10 <sup>6</sup>	2x10 <sup>6</sup>	10% f <sub>n</sub> Drop
9C/C-H1	±45°	450	900	3x10 <sup>6</sup>	3x10 <sup>6</sup>	10% f <sub>n</sub> Drop
9A/C-H4	±45°	450	900	3x10 <sup>6</sup>	3x10 <sup>6</sup>	10% f <sub>n</sub> Drop
9E/C-H3	±45°	450	900	10 <sup>6</sup>	5x10 <sup>6</sup>	10% f <sub>n</sub> Drop
9E/C-H4	±45°	450	900	10 <sup>6</sup>	5x10 <sup>6</sup>	10% f <sub>n</sub> Drop



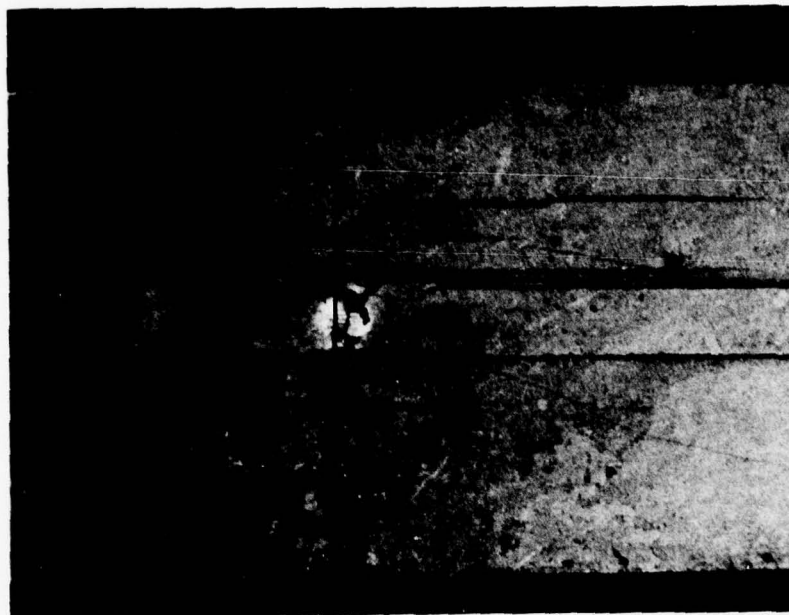
*Figure 9.6-2 Ultrasonic C-Scan Test Results for Ballistically Impacted Unidirectional Specimen (3A/u-H2) Before and After High Frequency Fatigue Testing Showing Delamination That Occurred During Fatigue Testing.*



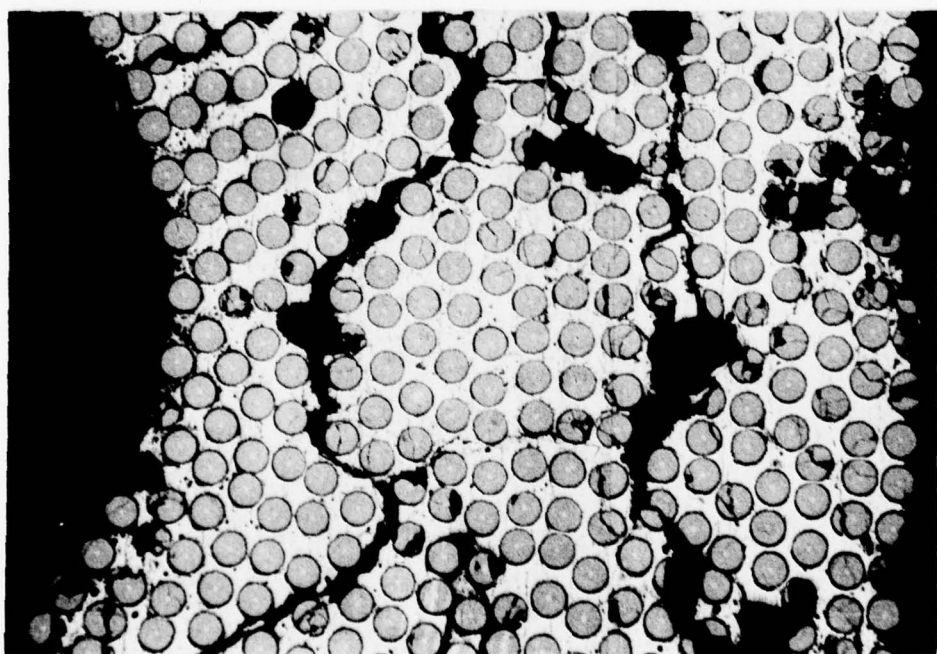
**Figure 9.6-3** Ultrasonic C-Scan Test Results for Ballistically Impacted Component Specimen (7B/B-H4) Before and After High Frequency Fatigue Testing Showing Delamination that Occurred During Fatigue Testing

### 9.6.3 Metallography

A large amount of matrix cracking was found in the unidirectional specimens after impact, plus 70°F or 450°F HFF testing, as shown in Figure 9.6-4. In contrast, the component specimens which were impacted and HFF tested at 450°F did not contain as much matrix damage as the unidirectional specimens, as shown in Figure 9.6-5. Note that although the cross-ply layers suffered extensive fiber breakage, the unidirectional core fibers remained intact and little matrix cracking occurred. At locations away from the immediate impact area, fiber splitting and surface delamination took place in these component specimens similar to the undamaged specimen behavior, as shown in Figure 9.6-6. Impact plus 450°F HFF damage of cross-ply material is illustrated in Figure 9.6-7. The excessive fiber and matrix damage shown are probably the cause of the early frequency drop observed.



MAG: 3X



MAG: 50X

**Figure 9.6-4** Typical Ballistically Impacted Unidirectional Specimen After High Frequency Fatigue Testing Showing Extensive Matrix Cracking

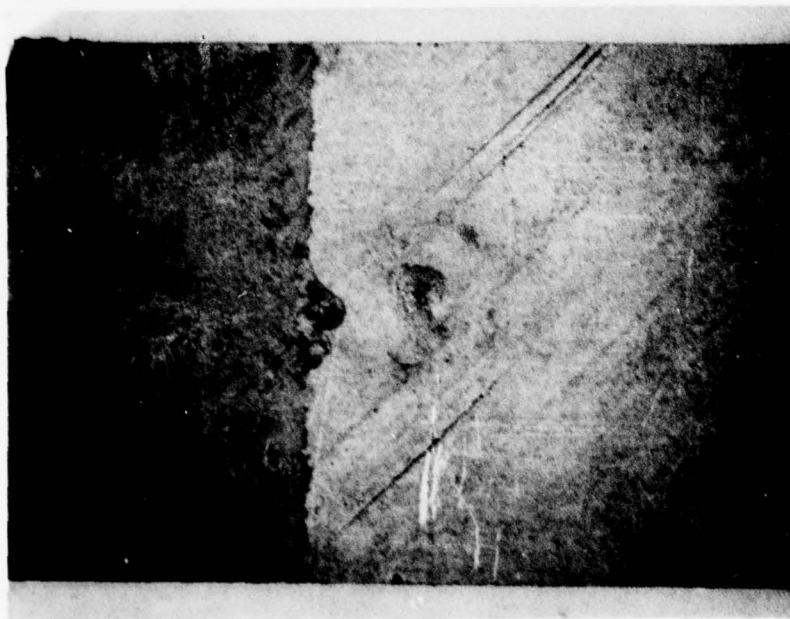
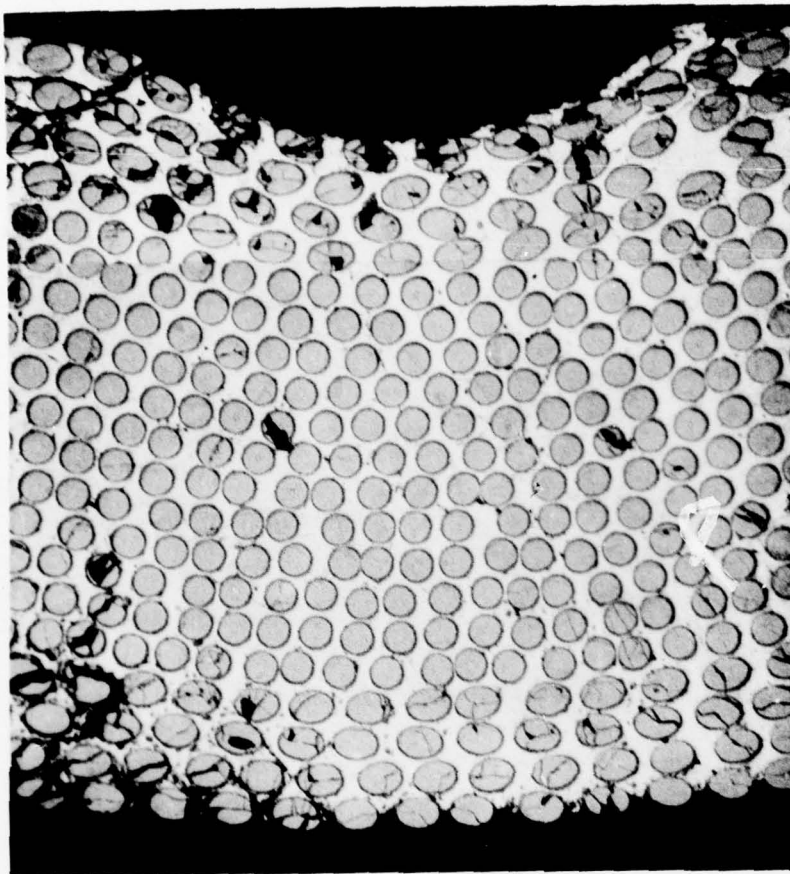


*Figure 9.6-5 Typical Ballistically Impacted Component Specimen (7B1B-H4) After High Frequency Fatigue Testing at 450°F Showing Only Limited Matrix Cracking*

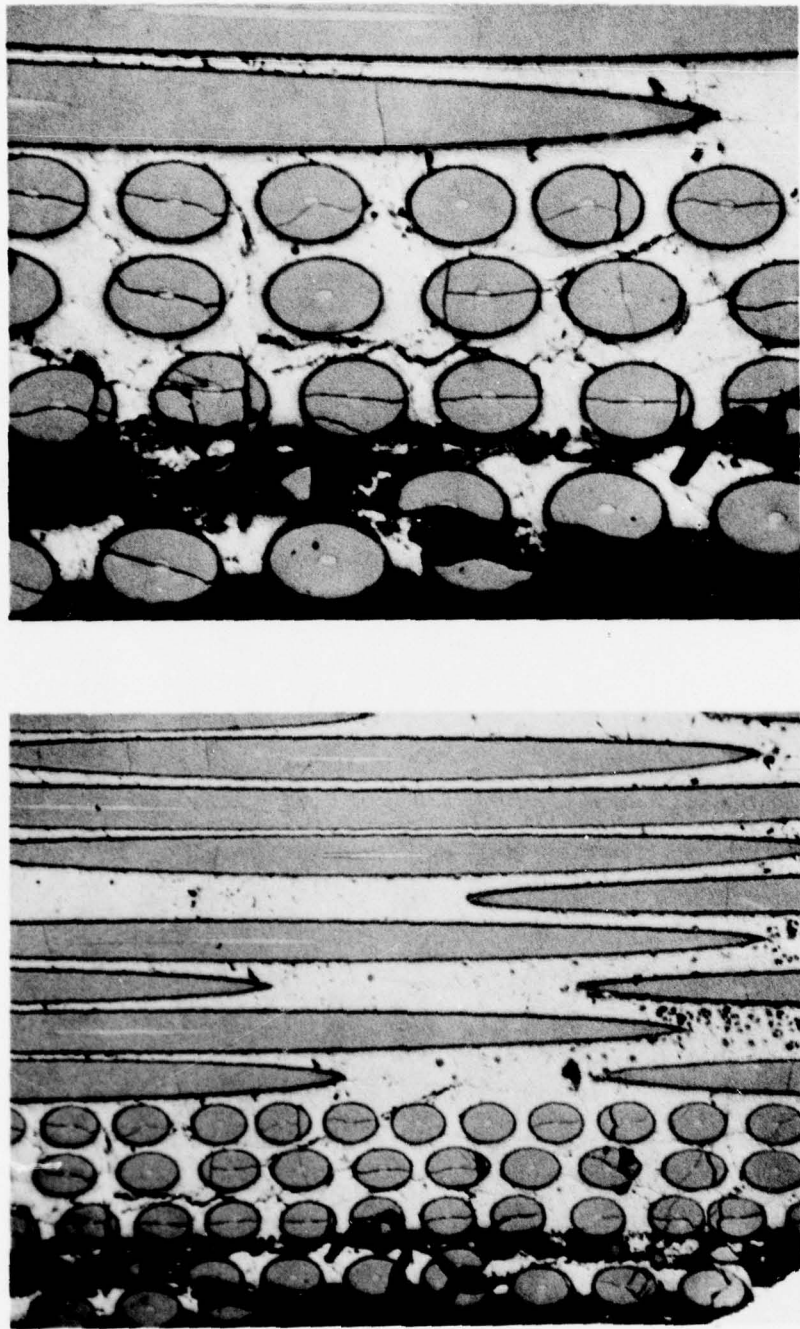


Figure 9.6-6 Microstructure of Ballistically Impacted Component Specimen (7D/B-H2) After 450°F High Frequency Fatigue Testing

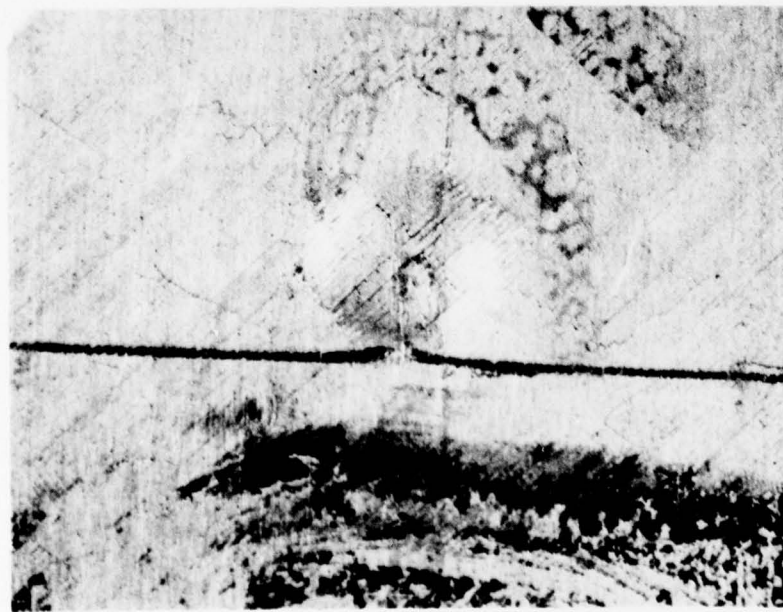
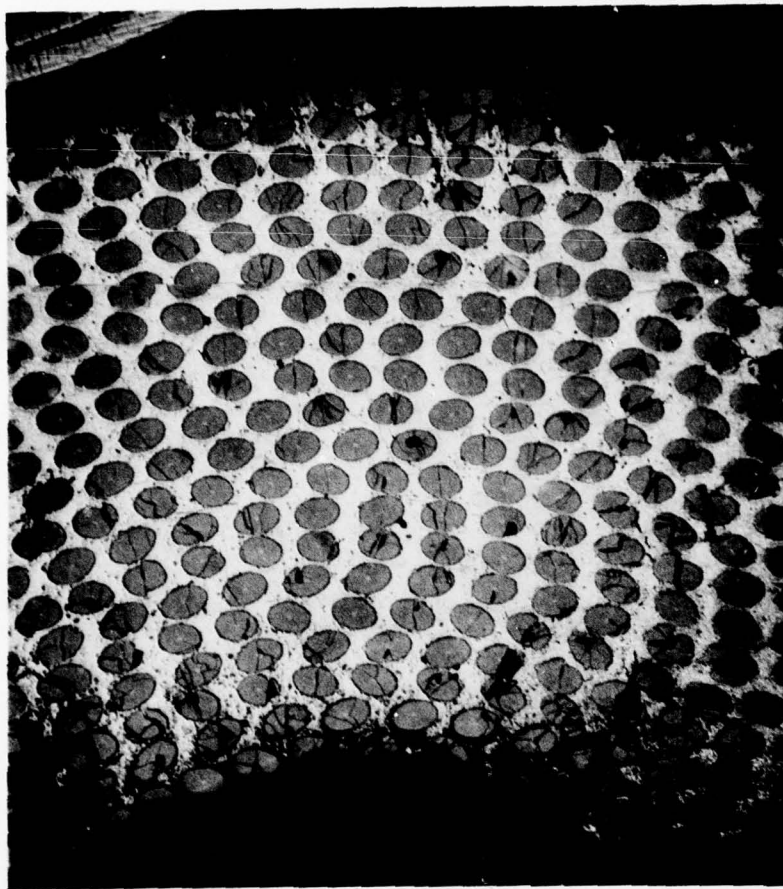


Figure 9.6-7 Ballistically Impacted Cross-ply Specimen (9E/C-H4) After 450° F. High Frequency  
Fatigue Testing

## 9.7 THERMAL FATIGUE DAMAGE

The following conclusions were drawn from the results of the thermal fatigue damage testing:

- Tensile strength of Borsical® composite unidirectional specimens is apparently lowered by thermal cycling.
- HFF damage at 450°F in addition to thermal cycling lowers the 70°F tensile strength of the component specimens beyond that of undamaged HFF specimens but does not affect the cross-ply composite strength.
- Component specimens did not suffer reduction in their HFF capability as a result of thermal fatigue exposure.

### 9.7.1 Tensile

The 70°F tensile strength (Figure 9.7-1 and Table 9.7-I) of cross-ply and component specimens was not significantly influenced by thermal cycling (-65 to 500°F). Subsequent HFF testing at 450°F reduced the strength of component specimens with no significant effect observed for cross-ply specimens. The strength of unidirectional material decreased as a result of thermal cycling followed by 70°F HFF exposure; however, considerable scatter was observed. HFF exposure at 450°F apparently lowered the tensile strength of unidirectional material; however, the anomalous behavior of thermal cycled specimens with no subsequent HFF exposure prevented a clear analysis.

### 9.7.2 High Frequency Fatigue

Unidirectional and cross-ply composite HFF capability was reduced by thermal fatigue cycling (Table 9.7-II). The component specimens did not suffer loss in HFF life after thermal fatigue.

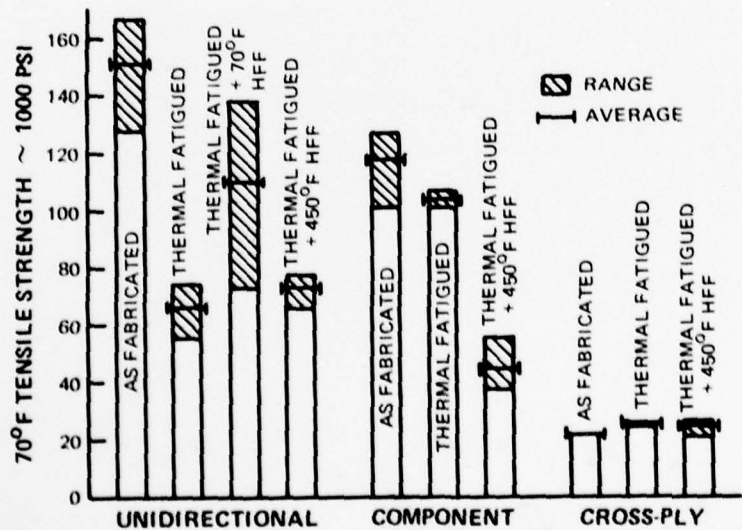


Figure 9.7-1 Effect of Thermal Fatigue Damage on the 70°F Tensile Strength of 50 Volume-Percent 20-Layer Borsical® Specimens

TABLE 9.7-I

70°F TENSILE TEST RESULTS FOR THERMAL FATIGUE  
DAMAGED 20-LAYER 50 PERCENT - VOLUME BORSICAL® SPECIMENS

Specimen Number	Ply Config.	Temp. (°F)	Prior HFF Exposure			UTS (10 <sup>3</sup> psi)	Modulus (10 <sup>6</sup> psi)
			Strain (μin./in.)	Cycles to Failure	Total Cycles		
11A/u-H1	0°		None			73.9	-
2F/u-H3	0°		None			60.7	-
2F/u-H4	0°		None			74.2	
11B/u-H1	0°		None			55.3	
11A/u-H4	0°	70	3140	10 <sup>5</sup>	5x10 <sup>6</sup>	116.0	
11F/u-H3	0°	70	3060	2x10 <sup>6</sup>	10 <sup>7</sup>	72.7	
11B/u-H2	0°	70	2900	DNF*	4x10 <sup>6</sup>	138.0	
2F/u-H2	0°	70	2540	DNF	10 <sup>7</sup>	121.7	
2F/u-H1	0°	70	2540	DNF	10 <sup>7</sup>	101.5	
11B/u-H3	0°	450	2150	4x10 <sup>6</sup>	4x10 <sup>6</sup>	75.7	-
11D/u-H1	0°	450	2090	2x10 <sup>6</sup>	5x10 <sup>6</sup>	65.7	-
11D/u-H3	0°	450	2080	2x10 <sup>6</sup>	3x10 <sup>6</sup>	77.7	-
8A/B-H1	±45°,0°,±45°		None			106.8	26.7
8A/B-H3	±45°,0°,±45°		None			100.8	28.5
8C/B-H1	±45°,0°,±45°	450	1770	3x10 <sup>6</sup>	3x10 <sup>6</sup>	37.3	-
8D/B-H2	±45°,0°,±45°	450	1655	3x10 <sup>6</sup>	4x10 <sup>6</sup>	41.2	-
8B/B-H3	±45°,0°,±45°	450	1565	3x10 <sup>6</sup>	5x10 <sup>6</sup>	55.8	-
12A/C-H4	±45°		None			25.9	
12B/C-H1	±45°		None			24.7	
12C/C-H1	±45°	450	915	5x10 <sup>5</sup>	3x10 <sup>6</sup>	25.8	
12B/C-H3	±45°	450	970	3x10 <sup>5</sup>	4x10 <sup>6</sup>	21.0	
12A/C-H1	±45°	450	885	5x10 <sup>5</sup>	5x10 <sup>6</sup>	26.8	

\* DNF = Did not fail.

TABLE 9.7-II

HIGH FREQUENCY FATIGUE TEST RESULTS FOR THERMAL FATIGUE  
DAMAGED 20-LAYER 50 PERCENT - VOLUME BORSICAL® SPECIMENS

Specimen Number	Ply Config.	Temp. (°F)	Strain (μin./in.)	Cycles to Failure	Total Cycles	Failure Mode
2F/u-H1	0°	70	2540	3x10 <sup>6</sup>	10 <sup>7</sup>	Delamination
2F/u-H2	0°	70	2540	6x10 <sup>6</sup>	10 <sup>7</sup>	Delamination
11B/u-H2	0°	70	2900	DNF*	4x10 <sup>6</sup>	—
11A/u-H3	0°	70	3025	DNF	5x10 <sup>6</sup>	—
11D/u-H3	0°	70	3060	2x10 <sup>6</sup>	10 <sup>7</sup>	Delamination
11A/u-H2	0°	70	3100	3x10 <sup>6</sup>	4x10 <sup>6</sup>	Delamination
11A/u-H4	0°	70	3140	10 <sup>5</sup>	5x10 <sup>6</sup>	Delamination
11F/u-H3	0°	70	3060	2x10 <sup>6</sup>	10 <sup>7</sup>	Delamination
2F/u-H2	0°	70	2540	DNF	10 <sup>7</sup>	—
11D/u-H4	0°	450	2065	2x10 <sup>6</sup>	3x10 <sup>6</sup>	Delamination
11D/u-H3	0°	450	2080	2x10 <sup>6</sup>	3x10 <sup>6</sup>	Delamination
11D/u-H1	0°	450	2090	2x10 <sup>6</sup>	5x10 <sup>6</sup>	Delamination
11B/u-H4	0°	450	2115	DNF	4x10 <sup>6</sup>	—
11B/u-H3	0°	450	2150	4x10 <sup>6</sup>	4x10 <sup>6</sup>	Delamination
11D/u-H2	0°	450	2220	3x10 <sup>6</sup>	5x10 <sup>6</sup>	Delamination
8B/B-H3	±45°,0°,±45°	450	1565	3x10 <sup>6</sup>	5x10 <sup>6</sup>	Delamination
8D/B-H2	±45°,0°,±45°	450	1655	3x10 <sup>6</sup>	4x10 <sup>6</sup>	Delamination
8C/B-H4	±45°,0°,±45°	450	1680	3x10 <sup>6</sup>	5x10 <sup>6</sup>	Delamination
8B/B-H4	±45°,0°,±45°	450	1705	3x10 <sup>6</sup>	3x10 <sup>6</sup>	Delamination
8E/B-H1	±45°,0°,±45°	450	1715	3x10 <sup>6</sup>	4x10 <sup>6</sup>	Delamination
8C/B-H1	±45°,0°,±45°	450	1770	3x10 <sup>6</sup>	3x10 <sup>6</sup>	Delamination
12A/C-H1	±45°	450	885	5x10 <sup>5</sup>	5x10 <sup>6</sup>	10% f <sub>n</sub> drop
12C/C-H1	±45°	450	915	5x10 <sup>5</sup> **	3x10 <sup>6</sup>	10% f <sub>n</sub> drop
12A/C-H2	±45°	450	920	5x10 <sup>5</sup>	5x10 <sup>6</sup>	10% f <sub>n</sub> drop
12B/C-H3	±45°	450	970	3x10 <sup>5</sup>	4x10 <sup>6</sup>	10% f <sub>n</sub> drop
12B/C-H4	±45°	450	980	3x10 <sup>5</sup>	4x10 <sup>6</sup>	10% f <sub>n</sub> drop

\* DNF = Did not fail.

\*\* Estimated Failure

### 9.7.3 Metallurgy

The unidirectional specimens which were thermal cycled and HFF tested at room temperature and approximately 3100  $\mu$ in./in. contained numerous fatigue cracks as shown in Figure 9.7-2. These fatigue cracks, which were not found to any significant amount in undamaged specimens tested at similar strains (shown in Figure 9.4-4), apparently resulted from a combination of thermal cycling and HFF testing. No fatigue cracks were detected in as-thermal-fatigue specimens. Microstructure variations after various amounts of HFF damage were undetectable. When HFF tested at 450°F, the unidirectional specimens exhibited severe internal delamination extending inward from the specimen surface and edge, as shown in (Figure 9.7-3).

The microstructure of thermal fatigue component specimens looked no different from undamaged specimens after a 450°F HFF test. Failures were characterized by splitting of the cross-ply fibers and surface delamination (Figure 9.7-4) with interconnected fatigue cracks. Cross-ply samples also appeared similar to undamaged specimens with fiber splitting normal to the specimen surface.

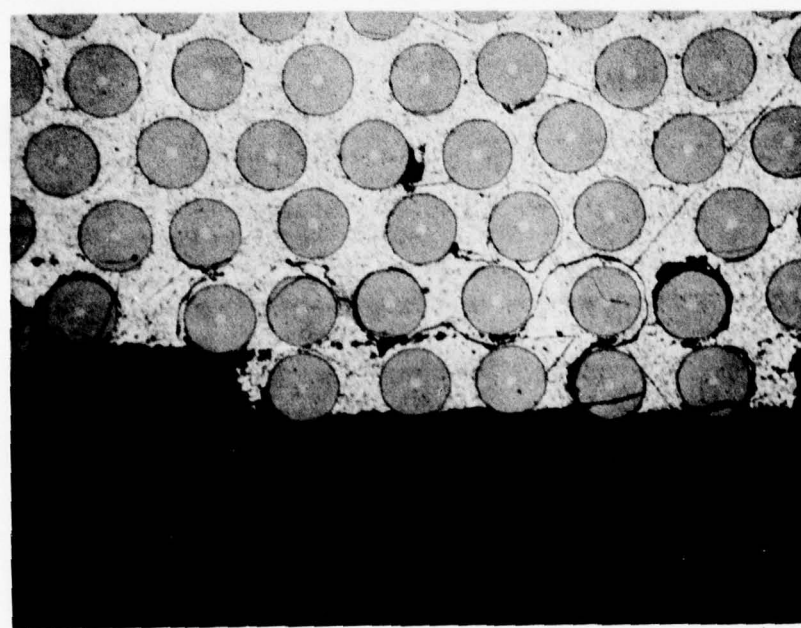
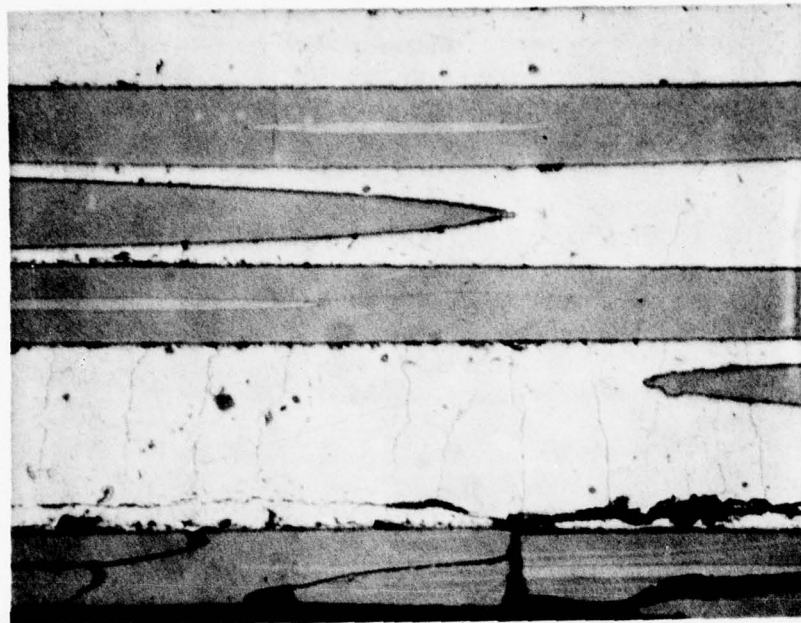


Figure 9.7-2 Microstructure of Thermal Fatigue Damaged Unidirectional Specimen (11A/u-H2)  
After 70° F High Frequency Fatigue Testing

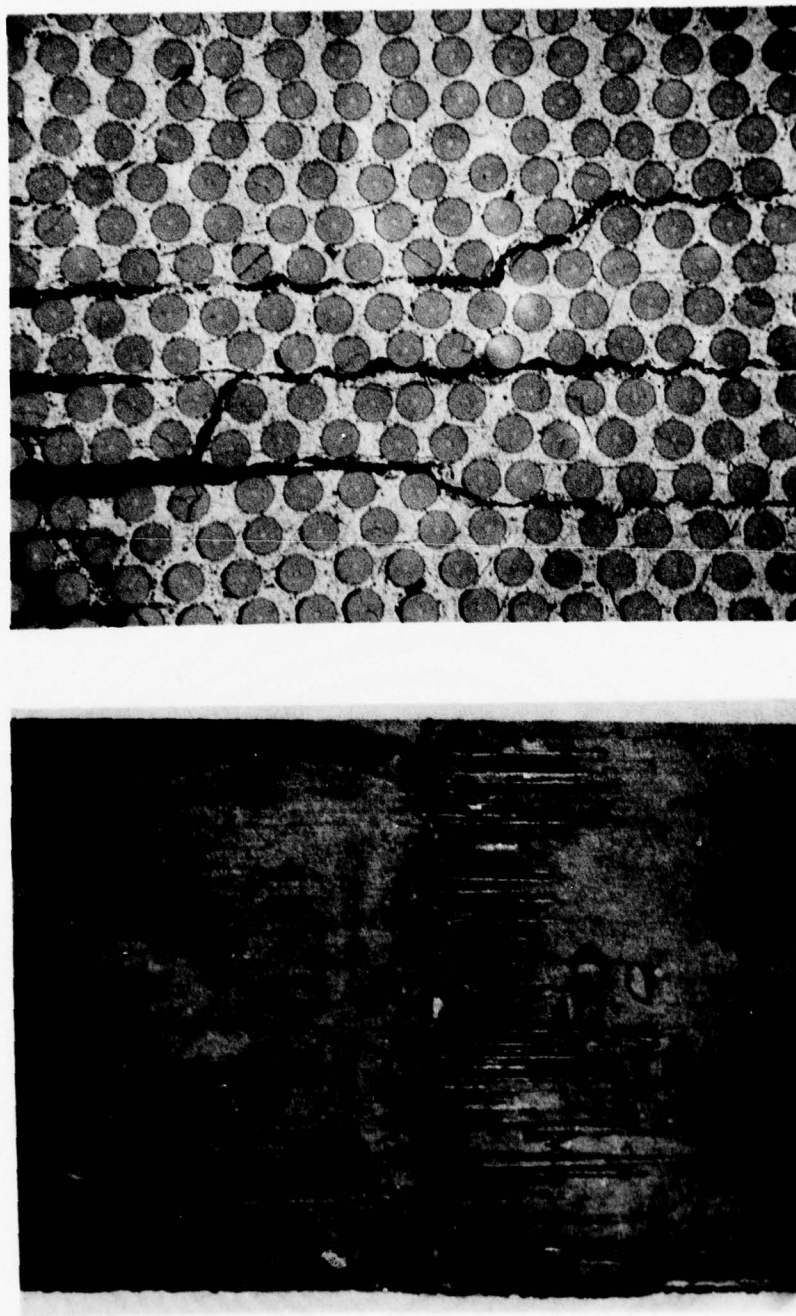


Figure 9.7-3 *Surface Appearance and Microstructure of Thermal Fatigue Damaged Unidirectional Specimen (11D/u-H2) After 450°F High Frequency Fatigue Testing*

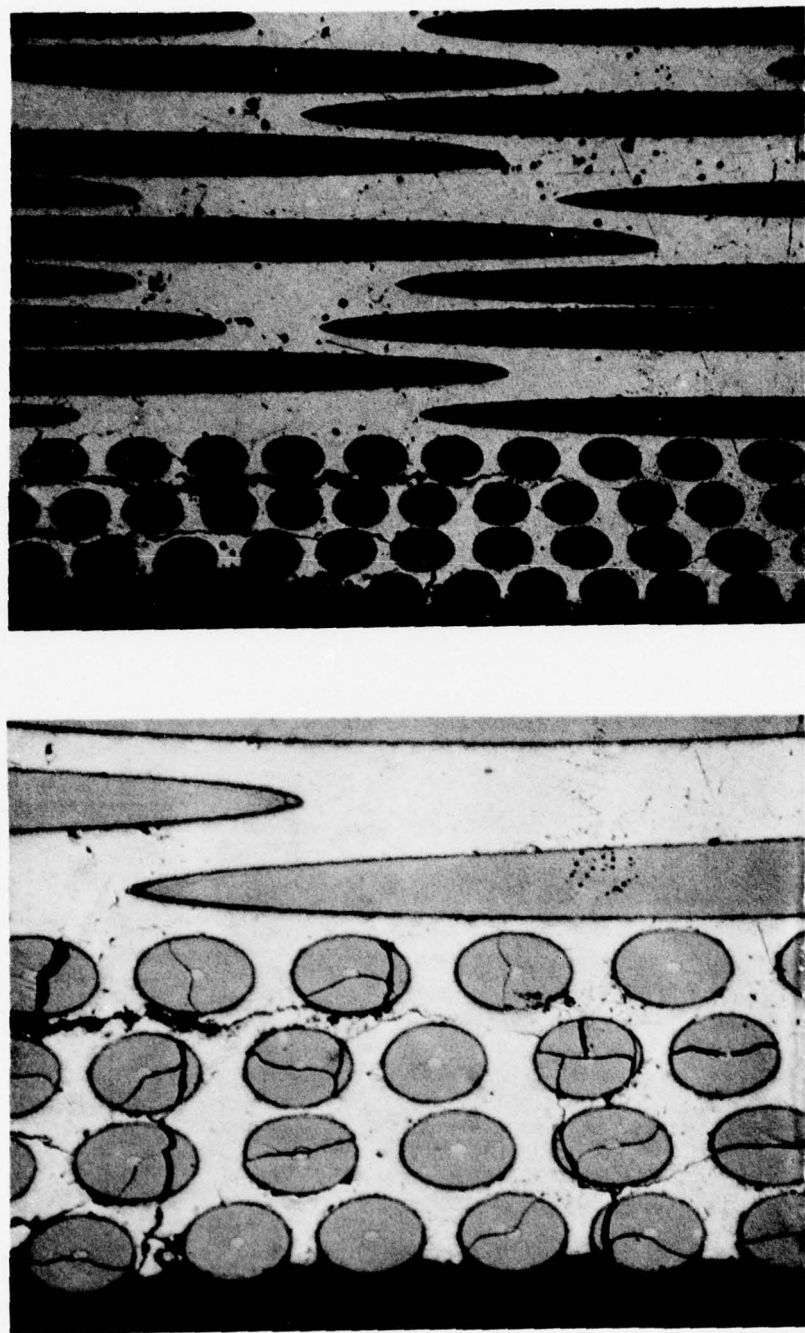


Figure 9.7-4 *Microstructure of Thermal Fatigue Damaged Component Specimen (8B/B-H1)  
After 450°F High Frequency Fatigue Testing*

## 9.8 SALT STRESS-CORROSION DAMAGE

The results from the salt stress-corrosion damaged specimen testing lead to the following conclusions:

- Salt stress corrosion had no affect on the 70°F strength of cross-ply or component Borsical® composites.
- HFF damage in addition to the corrosion did not reduce composite tensile strength in the crossply and component specimens.
- Component specimens retain their 450°F HFF capability even after 100 hours of salt stress corrosion; however, crossply and unidirectional layups do suffer a loss in HFF life at 450°F.

### 9.8.1 Tensile

Salt stress corrosion, with or without HFF testing, did not affect 70°F tensile strength of the cross-ply or the component specimens, as indicated in Figure 9.8-1 and Table 9.8-I. Unidirectional specimens exhibited an apparent decrease in strength due to salt stress corrosion followed by HFF exposure to 70 or 450°F; however, the anomalous behavior of exposed specimens with no subsequent HFF prevented a clear analysis.

### 9.8.2 High Frequency Fatigue

HFF tests on unidirectional and cross-ply specimens at 450°F indicated a slight reduction in HFF capability due to salt stress corrosion, as shown in Table 9.8-II. At the same time, unidirectional specimens HFF tested at 70°F and component specimens tested at 450°F were not influenced by the corrosion exposure. The lowering of the HFF life for the cross-ply specimens may be due to the fact that the exposure strain of 1880  $\mu$ in./in. was more than double the HFF test strain which resulted in matrix yielding, resulting in a permanent bend to the specimens.

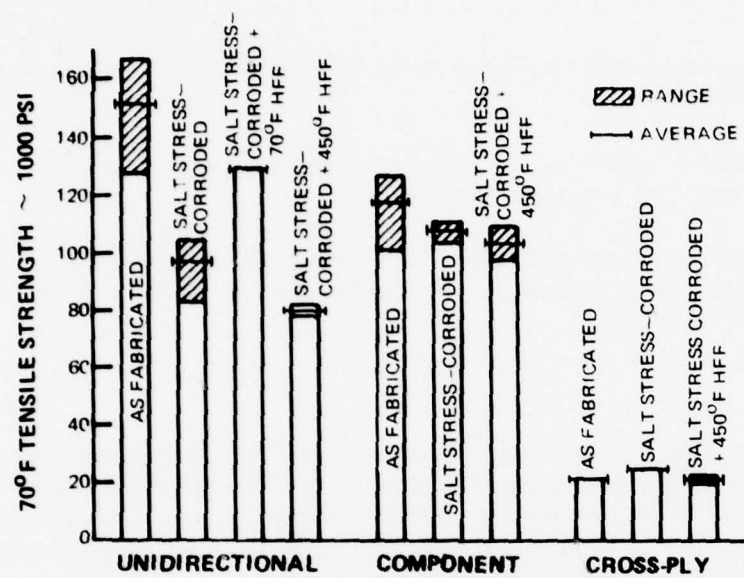


Figure 9.8.1 Effect of Salt Stress-Corrosion Damage on the 70°F Tensile Strength of 50 Volume-Percent 20-Layer Borsical® Specimens

TABLE 9.8-1

70°F TENSILE TEST RESULTS FOR SALT STRESS - CORROSION  
DAMAGED 20-LAYER 50 PERCENT - VOLUME BORSICAL® SPECIMENS

Specimen Number	Ply Config.	Temp. (°F)	Strain (μin./in.)	Prior HFF Exposure			
				Cycles to Failure	Total Cycles	UTS (10 <sup>3</sup> psi)	Modulus (10 <sup>6</sup> psi)
6A/u-H1	0°		None			83.2	—
6A/u-H2	0°		None			100.8	—
3F/u-H2	0°		None			103.5	—
3F/u-H3	0°		None			104.5	—
6A/u-H3	0°		None			100.2	—
6A/u-H4	0°		None			89.2	—
6B/u-H1	0°	70	3400	10 <sup>6</sup>	5x10 <sup>6</sup>	129.0	—
6B/u-H4	0°	70	3400	5x10 <sup>6</sup>	5x10 <sup>6</sup>	129.5	—
6D/u-H1	0°	450	2170	3x10 <sup>6</sup>	4x10 <sup>6</sup>	81.9	—
6F/u-H4	0°	450	2100	3x10 <sup>6</sup>	3x10 <sup>6</sup>	78.1	—
8A/B-H2	±45°,0°,±45°		None			103.8	28.8
8A/B-H4	±45°,0°,±45°		None			111.2	28.0
8E/B-H2	±45°,0°,±45°	450	1445	DNF*	5x10 <sup>6</sup>	110.0	—
8B/B-H1	±45°,0°,±45°	450	1450	DNF	5x10 <sup>6</sup>	103.1	—
7F/B-H3	±45°,0°,±45°	450	1730	DNF	3x10 <sup>6</sup>	98.0	—
12A/C-H3	±45°		None			25.2	—
12B/C-H2	±45°		None			24.8	—
9F/C-H4	±45°	450	995	3x10 <sup>6</sup>	3x10 <sup>6</sup>	22.4	—
12E/C-H1	±45°	450	920	2x10 <sup>6</sup>	5x10 <sup>6</sup>	23.1	—
9C/C-H4	±45°	450	860	3x10 <sup>6</sup>	4x10 <sup>6</sup>	20.6	—

\* DNF = Did not fail.

TABLE 9.8.II

HIGH FREQUENCY FATIGUE TEST RESULTS FOR SALT - CORROSION  
DAMAGED 20-LAYER 50 PERCENT - VOLUME BORSICAL® SPECIMENS

Specimen Number	Ply Config.	Temp. (°F)	Strain (μin./in.)	Cycles to Failure	Total Cycles	Failure Mode
6B/u-H3	0°	70	3400	3x10 <sup>6</sup>	5x10 <sup>6</sup>	Delamination
6B/u-H4	0°	70	3400	5x10 <sup>6</sup>	5x10 <sup>6</sup>	Delamination
6B/u-H1	0°	70	3400	10 <sup>6</sup>	5x10 <sup>6</sup>	Delamination
6B/u-H2	0°	70	3400	3x10 <sup>6</sup>	5x10 <sup>6</sup>	Delamination
6E/u-H4	0°	450	2055	4x10 <sup>6</sup>	4x10 <sup>6</sup>	Delamination
11F/u-H2	0°	450	2100	3x10 <sup>6</sup>	3x10 <sup>6</sup>	Delamination
6F/u-H4	0°	450	2100	3x10 <sup>6</sup>	3x10 <sup>6</sup>	Delamination
11F/u-H4	0°	450	2135	2x10 <sup>6</sup>	5x10 <sup>6</sup>	Delamination
11E/u-H2	0°	450	2150	2x10 <sup>6</sup>	5x10 <sup>6</sup>	Delamination
6D/u-H1	0°	450	2170	3x10 <sup>6</sup>	4x10 <sup>6</sup>	Delamination
8B/B-H2	±45°, 0°, ±45°	450	1445	DNF*	5x10 <sup>6</sup>	—
8B/B-H1	±45°, 0°, ±45°	450	1450	DNF	5x10 <sup>6</sup>	—
8F/B-H4	±45°, 0°, ±45°	450	1615	DNF	4x10 <sup>6</sup>	—
8E/B-H2	±45°, 0°, ±45°	450	1625	DNF	4x10 <sup>6</sup>	—
8D/B-H3	±45°, 0°, ±45°	450	1675	DNF	3x10 <sup>6</sup>	—
7F/B-H3	±45°, 0°, ±45°	450	1730	DNF	3x10 <sup>6</sup>	—
9C/C-H4	±45°	450	860	3x10 <sup>6</sup>	4x10 <sup>6</sup>	10% f <sub>n</sub> drop
12C/C-H4	±45°	450	900	2x10 <sup>6</sup>	5x10 <sup>6</sup>	10% f <sub>n</sub> drop
12E/C-H1	±45°	450	920	2x10 <sup>6</sup>	5x10 <sup>6</sup>	10% f <sub>n</sub> drop
12F/C-H3	±45°	450	925	3x10 <sup>6</sup>	4x10 <sup>6</sup>	10% f <sub>n</sub> drop
12E/C-H3	±45°	450	985	3x10 <sup>6</sup>	3x10 <sup>6</sup>	10% f <sub>n</sub> drop
9F/C-H4	±45°	450	995	3x10 <sup>6</sup>	3x10 <sup>6</sup>	10% f <sub>n</sub> drop

\* DNF = Did not fail.

### 9.8.3 Metallography

In general, salt stress corrosion had no apparent effect on the HFF failure mode of the three ply configurations that were tested. Unidirectional material had surface delamination and matrix cracking, Figure 9.8-2, and component specimens exhibited surface delamination and fiber splitting parallel to the specimen surface, as previously shown in Figure 9.4-8. Cross-ply material had surface delamination in addition to matrix cracking and fiber splitting, as shown in Figure 9.8-3. This surface delamination is apparently a result of the very high surface strain during the salt exposure.

## 9.9 Discussion of Results

None of the four types of damage evaluated in this program appear to result in rapid deterioration of component properties. A summary of the results, presented in Tables 9.9-I and 9.9-II, reveals no exposure effect on HFF life of component specimens with only ballistic impact and thermal fatigue showing any effect on tensile properties of this material. The effect of ballistic impact is directly proportional to the cross-sectional area physically damaged from impact which can be estimated from visual inspection. Erosion damage will apparently have an effect only when it penetrates into the blade core which, from actual component testing, is not anticipated.

Results of actual component testing, consisting of exposure to these four types of damage followed by 450°F HFF testing have been in agreement with the above results. Component testing consisting of thermal cycling followed by spin pit testing has shown that the decrease in tensile strength due to thermal cycling is insufficient to cause premature blade failure.

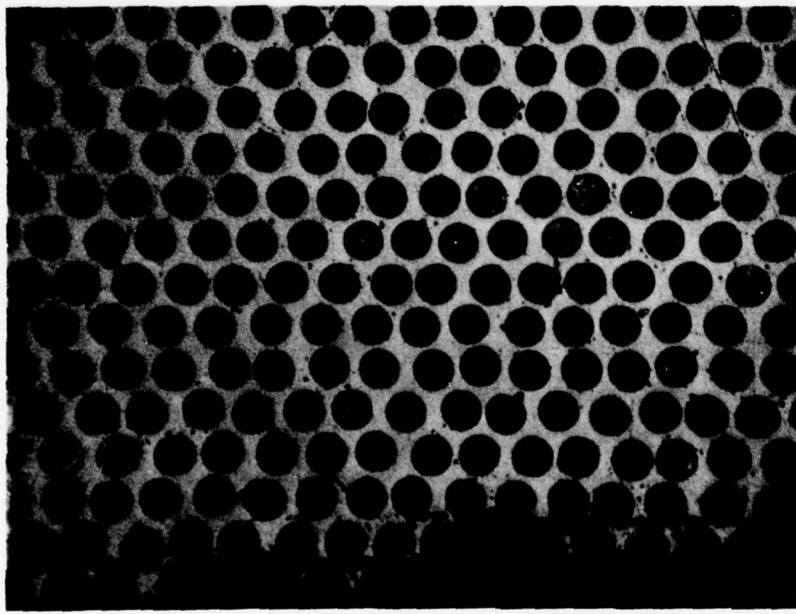
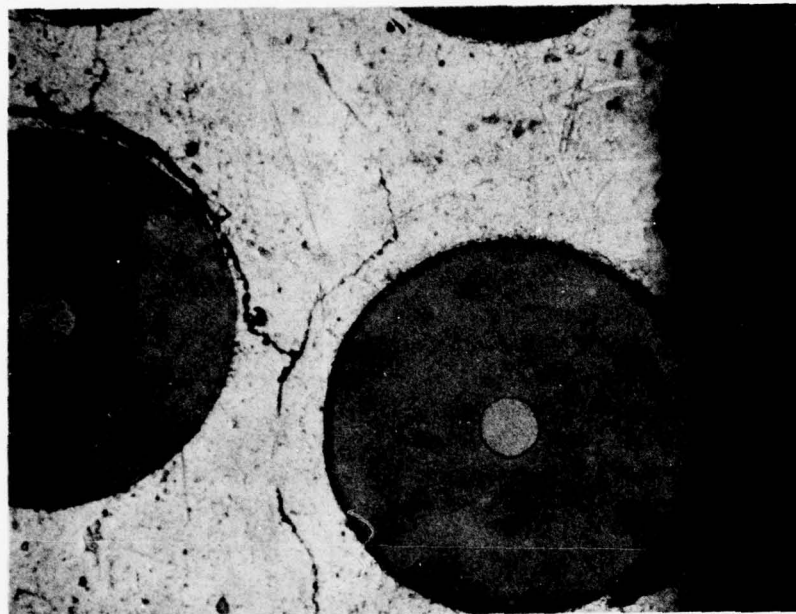
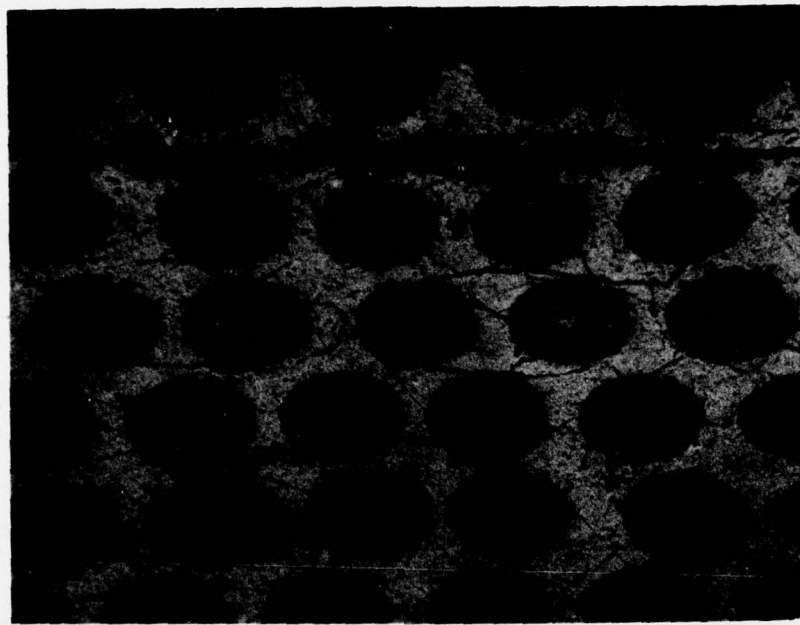


Figure 9.8-2 Microstructure of Salt Stress-Corrosion Damaged Unidirectional Specimen (6B/u-H2) After 70° F High Frequency Fatigue Testing



*Figure 9.8-3 Microstructure of Salt Stress-Corrosion Damaged Cross-Ply Specimen (12D/C-H1)  
After 450°F High Frequency Fatigue Testing*

TABLE 9.9-I

SUMMARY OF DAMAGE EFFECTS ON 70°F TENSILE TEST  
PROPERTIES OF 20-LAYER 50 PERCENT - VOLUME BORSICAL® SPECIMENS

<u>Damage Exposure</u>	<u>Ply Configuration</u>		
	<u>Unidirectional</u>	<u>Component</u>	<u>Cross-Ply</u>
70°F HFF	None		
450°F HFF	About 25% lower	Very slightly lower	None
Erosion	Nil*	None	None
Erosion +70°F HFF	Nil		
Erosion +450°F HFF	None	Nil	None
Ballistic Impact	Lower (43.5%)	Lower (42%)	Slightly Lower (18.7%)
BI + 70°F HFF	54% Lower		
BI + 450°F HFF	53.8% Lower	47.5% Lower	48.4% Lower
Thermal Fatigue	Lower	Nil	None
TF + 70°F HFF	Slightly Lower		
TF + 450°F HFF	Lower	Lower	None
Salt Stress-Corrosion	Lower	Nil	None
SSC + 70°F HFF	Slightly Lower		
SSC + 450°F HFF	Lower	Nil	None

\* Nil = Slightly lower properties but within material scatter band.

TABLE 9.9-II

SUMMARY OF DAMAGE EFFECTS ON HIGH FREQUENCY FATIGUE  
PROPERTIES OF 20-LAYER 50 PERCENT - VOLUME BORSICAL® SPECIMENS

Damage Exposure	Ply Configuration			
	Unidirectional (70°F HFF)	(450°F HFF)	Component (450°F HFF)	Cross-Ply (450°F HFF)
Erosion (I)*	None	None	None	None
Erosion (II)*	—	Lower	None	Lower
Ballistic Impact	Much Lower	Lower	None	Lower
Thermal Fatigue	Lower	Slightly Lower	None	Much Lower
Salt Stress-Corrosion	None	Slightly Lower	None	Lower

\*Type I; sufficient erosion to expose two layers of fibers without fiber breakage.

\*Type II; sufficient erosion to break fibers.

## 9.10 REPAIR TECHNOLOGY

In addition to establishing the service capability of Borsical® fan blades, a companion program was conducted to develop and evaluate schemes for the repair of damaged components. Specimens, rather than actual blades, were utilized to permit close control of test parameters and to facilitate a less ambiguous interpretation of test results. Techniques investigated for repair of surface damage included aluminum brazing, aluminum/silicone resin, zinc/aluminum soldering, polyimide resin filler, and resin filler with additives such as graphite or powdered aluminum. Tensile and high frequency fatigue tests were conducted at room temperature and at 450°F on both as-damaged and repaired specimens to evaluate the effectiveness of these schemes. Of the repair methods investigated, the most promising were the aluminum/silicone resin and the polyimide plus graphite filler. The procedures for repairing Borsical® test specimens using these repair schemes are described below. The other materials proved unsatisfactory because of poor bonding, undesirable thermal expansion coefficients, or, in the case of the aluminum braze, the high processing temperature (900°F) warped the specimen.

### 9.10.1 Repair Procedures

Twenty-layer unidirectional (0°) and component configuration ( $\pm 45^\circ$ , 0°,  $\pm 45^\circ$ ) specimens were impacted with a 0.67 gram pellet fired from an air pistol at a velocity of 500 feet per second. Both tensile and high frequency fatigue specimens were damaged in this manner (Figure 9.10-1). Repairs were made on specimens in both the as-damaged condition and after removal of damaged material (Figure 9.10-2).

Repair of specimens with aluminum/silicone resin was achieved by direct application of the resin to the damaged area. The aluminum/silicone resin was allowed to set in air at room temperature for approximately four hours and then sanded smooth. Multiple applications were required in some cases where the damaged material was removed prior to repair. To ensure that the aluminum/silicone resin repair would be usable at 450°F, a repaired test piece was exposed for 100 hours at 500°F and only slight discoloration resulted (Figure 9.10-3).

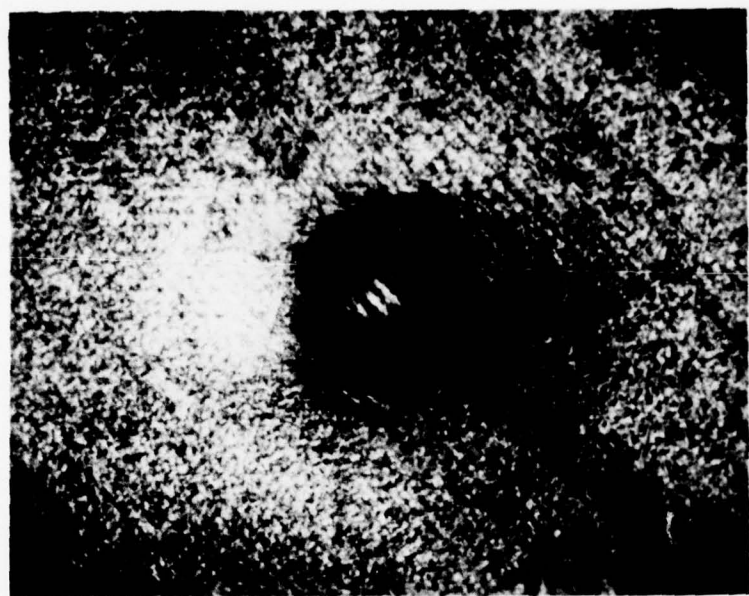
Polyimide/graphite repair was accomplished using a mixture (1:6) of chopped graphite tow (Morganite II) 1/16- to 1/4-inch long and polyimide powder (P13N). Preformed slugs of polyimide/graphite approximately 0.28-inch diameter by 0.2-inch thick were pressed at 550°F and 150 psi for 10 minutes. After removing the damaged area by drilling, specimens were repaired with these slugs by pressing the slug into the cleaned out hole at 550°F and 200 psi for 30 minutes. A 450°F cure for four hours completed the repair procedure (Figure 9.10-4).

### 9.10.2 Tensile Test Results

Room temperature and 450°F tensile tests were conducted on both unidirectional and component configuration specimens in the as-impacted and repaired condition with the results shown in Table 9.10-I. Some of the low strength values resulted from the off-center location of damage and repair on some test specimens. This condition causes non-uniaxial loading and excessive bending during test.

A summary of the effect of each kind of repair on tensile strength for the Borisical® composites is shown in Figure 9.10-5. The strength of impacted unidirectional specimens was lowered slightly at 450°F when samples were leached prior to either an aluminum/silicone resin or a graphite/polyimide repair. This five to ten percent strength reduction probably is due to the removal of matrix during leaching rather than an interaction between the composite and the filler material. The specific amount of matrix removed by leaching varied from specimen to specimen, and is believed to account for some low strength values for the component configuration specimens.

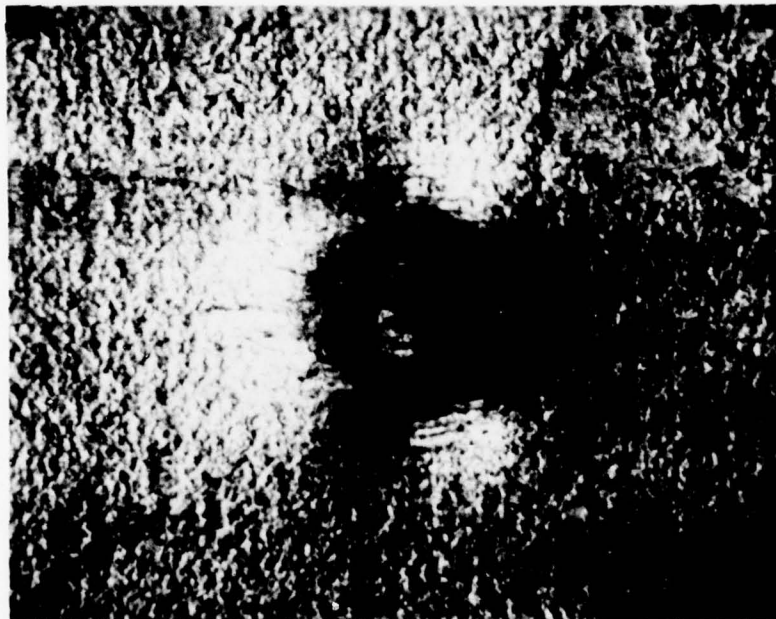
Based on the data in Table 9.10-I and Figure 9.10-5, both the graphite/polyimide and the aluminum /silicone resin repairs would not significantly reduce the as-damaged composite strength. However, leaching away damaged material followed by repair is not recommended for maintaining maximum strength.



ES4436-26

$\pm 45^\circ$ ,  $0^\circ$ ,  $\pm 45^\circ$

*Mag: 13X*

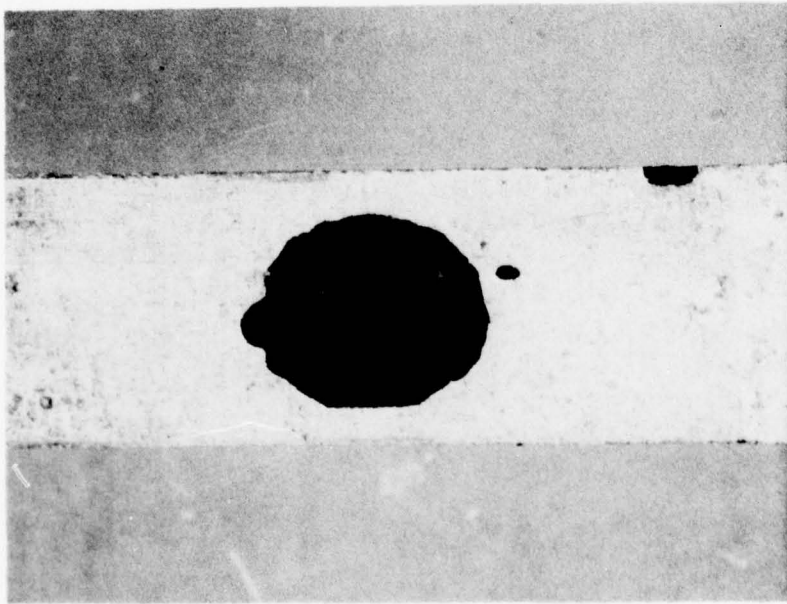


ES4436-24

*Unidirectional*

*Mag: 13X*

*Figure 9.10-1 Impacted Area of 20-Layer Borsicat® Test Specimens Prior to Repair*



M-1795

Unidirectional  
Mag: 4X

M-1764  
Mag: 4X

M-1764  
 $\pm 45^\circ, 0^\circ, \pm 45^\circ$   
Mag: 4X

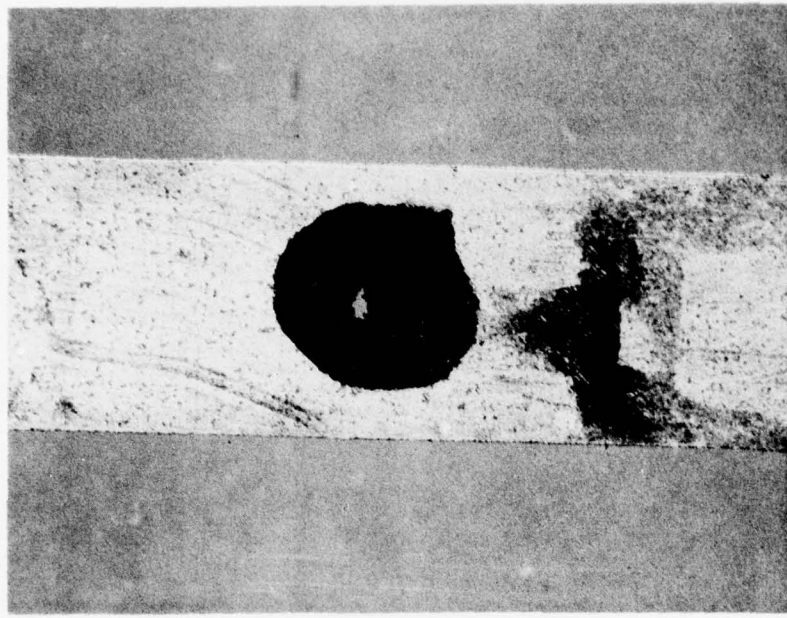


Figure 9.10-2    Impacted Borsicaf® 20-Layer Test Specimens After Removal of Damaged Material by Leaching with HCl

TABLE 9.10-I  
TENSILE TEST RESULTS FOR 20-LAYER 50 PERCENT VOLUME  
BORSICAL® SPECIMENS BEFORE AND AFTER REPAIR

Specimen Number	Ply Config.	Condition	Test Temp. (° F)	Tensile Strength (1000 psi)
3 A/U-H1	0°	As impacted	70	75.6
3 A/U-H4	0°	As impacted	70	78.3
3 B/U-H3	0°	As impacted	70	88.5
3 E/U-H1	0°	As impacted	70	90.5
15 A/U-T1	0°	As impacted	70	89.9
15 A/U-T2	0°	As impacted	70	95.3
15 A/U-T3	0°	As impacted	70	94.7
15 D/U-T4	0°	Leached-A1/Silicone Resin Repaired	70	77.0
15 A/U-T4	0°	As impacted	450	99.7
15 A/U-T5	0°	As impacted	450	76.0
15 A/U-T6	0°	As impacted	450	91.8
15 B/U-T6	0°	Unleached-A1/Silicone Resin Repaired	450	59.0*
15 D/U-T5	0°	Unleached-A1/Silicone Resin Repaired	450	82.0
15 D/U-T2	0°	Leached-A1/Silicone Resin Repaired	450	79.7
15 E/U-T6	0°	Leached-A1/Silicone Resin Repaired	450	72.7
15 E/U-T3	0°	Leached-Polyimide/Graphite Repaired	450	63.9

\* Low strength result due to bending caused by improper location of impact (too close to specimen edge).

TABLE 9.10-I (Cont'd)

<u>Specimen Number</u>	<u>Ply Config.</u>	<u>Condition</u>	<u>Test Temp. (°F)</u>	<u>Tensile Strength (1000 psi)</u>
7 D/B-H3	±45°,0°,±45°	As impacted	70	65.1
7 D/B-H4	±45°,0°,±45°	As impacted	70	71.7
16 B/B-T6	±45°,0°,±45°	Unleached-A1/Silicone Resin Repaired	70	37.0*
17 A/B-T3	±45°,0°,±45°	Unleached-A1/Silicone Resin Repaired	70	57.8
17 D/B-T1	±45°,0°,±45°	Unleached-A1/Silicone Resin Repaired	70	71.8
17 A/B-T2	±45°,0°,±45°	Leached-A1/Silicone Resin Repaired	70	49.7
17 B/B-T3	±45°,0°,±45°	Leached-A1/Silicone Resin Repaired	70	57.3
17 C/B-T2	±45°,0°,±45°	Leached-A1/Silicone Resin Repaired	70	38.2*
17 B/B-T1	±45°,0°,±45°	Leached-Polyimide/Graphite Repaired	70	67.1
17 B/B-T2	±45°,0°,±45°	Leached-Polyimide/Graphite Repaired	70	55.6
17 C/B-T3	±45°,0°,±45°	Leached-Polyimide/Graphite Repaired	70	67.2
16 A/B-T4	±45°,0°,±45°	As impacted	450	73.4
16 B/B-T1	±45°,0°,±45°	As impacted	450	63.8
16 B/B-T2	±45°,0°,±45°	As impacted	450	26.6*
16 B/B-T5	±45°,0°,±45°	As impacted	450	7.4*
16 B/B-T3	±45°,0°,±45°	Unleached-A1/Silicone Resin Repaired	450	51.4

TABLE 9.10-I (Cont'd)

<u>Specimen Number</u>	<u>Ply Config.</u>	<u>Condition</u>	<u>Test Temp. (°F)</u>	<u>Tensile Strength (1000 psi)</u>
16 C/B-T5	$\pm 45^\circ, 0^\circ, \pm 45^\circ$	Unleached-A1/Silicone Resin Repaired	450	72.2
16 C/B-T6	$\pm 45^\circ, 0^\circ, \pm 45^\circ$	Unleached-A1/Silicone Resin Repaired	450	63.1
16 A/B-T1	$\pm 45^\circ, 0^\circ, \pm 45^\circ$	Leached-A1/Silicone Resin Repaired	450	67.8
16 A/B-T2	$\pm 45^\circ, 0^\circ, \pm 45^\circ$	Leached-A1/Silicone Resin Repaired	450	68.3
16 A/B-T3	$\pm 45^\circ, 0^\circ, \pm 45^\circ$	Leached-A1/Silicone Resin Repaired	450	63.0
16 A/B-T5	$\pm 45^\circ, 0^\circ, \pm 45^\circ$	Leached-Polyimide/ Graphite Repaired	450	67.1
16 A/B-T6	$\pm 45^\circ, 0^\circ, \pm 45^\circ$	Leached-Polyimide/ Graphite Repaired	450	66.7
16 B/B-T4	$\pm 45^\circ, 0^\circ, \pm 45^\circ$	Leached-Polyimide/ Graphite Repaired	450	20.1*

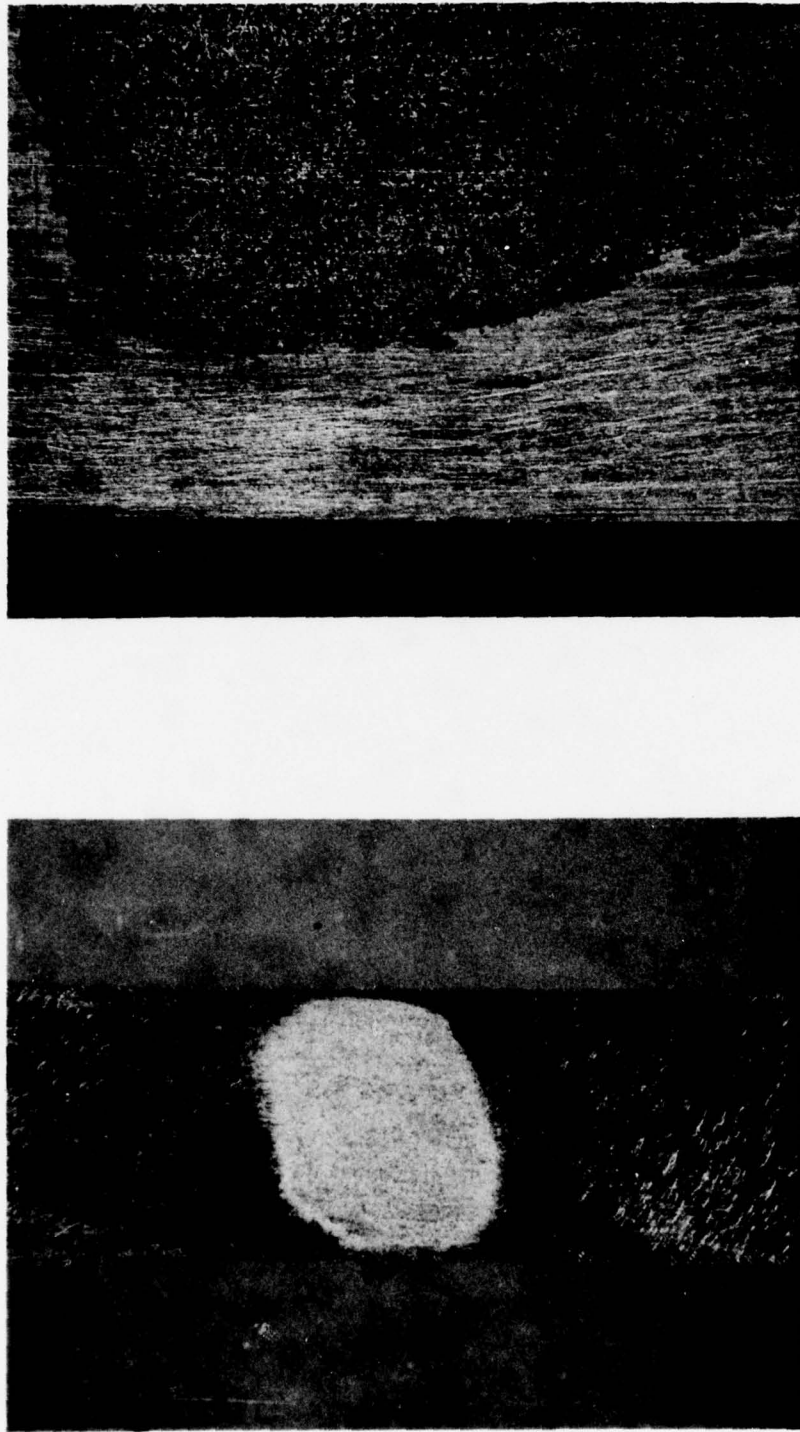
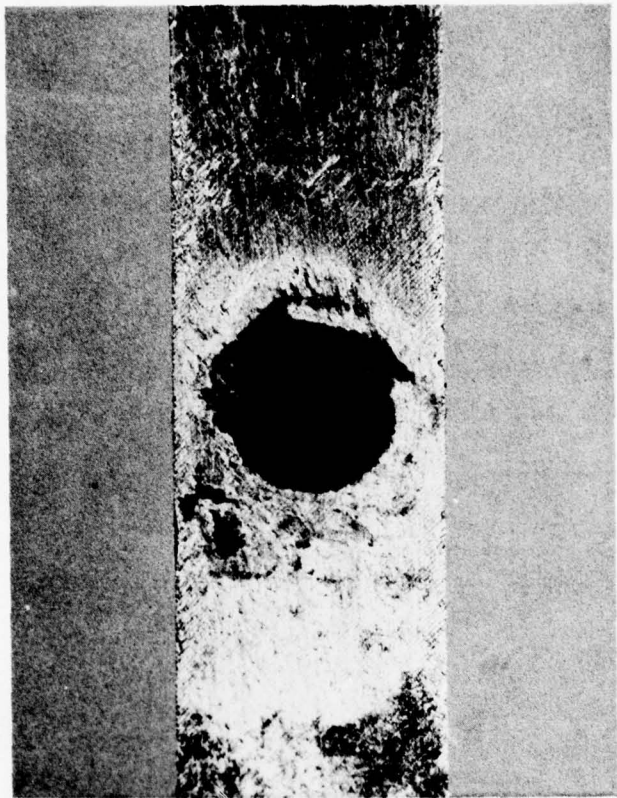


Figure 9.10-3      Twenty-Layer Borsicel® Test Specimen as Repaired with Aluminum/Silicone Resin (Left), and After 100 Hours at 500°F in Air. Slight Discoloration is Apparent



M-1952

Mag: 4X

**Figure 9.10-4**    *Typical 20-Layer Borsical<sup>®</sup> Test Specimen After Repair with Polyimide/Graphite Composite*

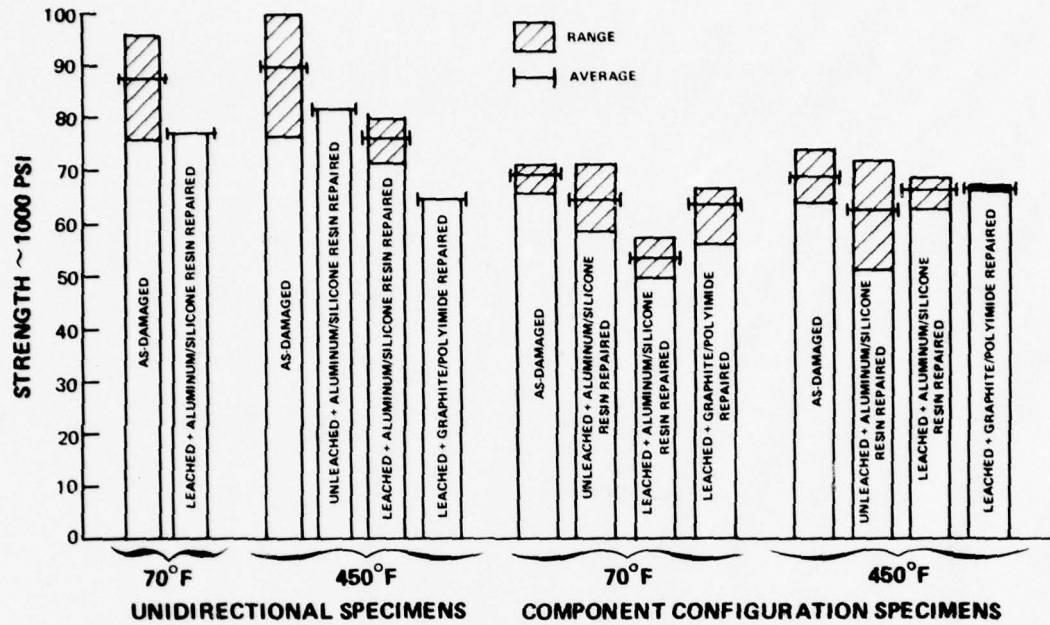


**Figure 9.10-5** Summary of the Effect of Various Repair Techniques on the 70 and 450°F Tensile Strength of Ballistic-Impact Damaged 50 Volume Percent Borsical® Specimens

### 9.10.3 HFF Test Results

Results of high frequency fatigue (HFF) testing of impacted and repaired specimens are shown in Table 9.10-II. The as-impacted test results are from the service capability portion of this program. The criterion for failure of the unidirectional and component configuration specimens was delamination or cracking.

As shown in Figure 9.10-6, the leaching or drilling of specimens prior to repair resulted in generally shorter HFF lives than for the as-impacted condition. The only exception was the component configuration specimens HFF tested at 450°F which suffered no decrease in HFF capability when repaired with aluminum/silicone resin. As with the tensile specimens described previously, leaching prior to repair removes excess matrix aluminum and can result in accelerated delamination even after specimen repair. The drilling out of damaged matrix and fibers also caused rapid specimen delamination during HFF testing.

TABLE 9.10-II

HFF TEST RESULTS FOR 20-LAYER 50 PERCENT VOLUME  
BORSICAL<sup>®</sup> SPECIMENS BEFORE AND AFTER REPAIR

<u>Specimen Number</u>	<u>Ply Config.</u>	<u>Condition</u>	<u>Test Temp. (°F)</u>	<u>Strain (μ-in/in)</u>	<u>Cycles to Failure</u>
3 D/U-H2	0°	As impacted	70	3100	5x10 <sup>5</sup>
3 D/U-H1	0°	As impacted	70	3100	5x10 <sup>5</sup>
6 E/U-H1	0°	As impacted	70	3100	5x10 <sup>5</sup>
3 C/U-H3	0°	As impacted	70	3100	10 <sup>5</sup>
3 C/U-H4	0°	As impacted	70	3100	10 <sup>5</sup>
3 C/U-H1	0°	As impacted	70	3100	10 <sup>5</sup>
3 C/U-H2	0°	As impacted	70	3100	10 <sup>5</sup>
23 A/U-H4	0°	Leached-Al/ Silicone Resin Repaired	70	3100	10 <sup>5</sup>
23 A/U-H6	0°	Leached-Al/ Silicone Resin Repaired	70	3100	10 <sup>5</sup>
6 C/U-H3	0°	As impacted	450	2100	10 <sup>6</sup>
3 B/U-H1	0°	As impacted	450	2100	5x10 <sup>5</sup>
3 D/U-H2	0°	As impacted	450	2100	5x10 <sup>5</sup>
6 C/U-H1	0°	As impacted	450	2100	10 <sup>6</sup>
6 C/U-H2	0°	As impacted	450	2100	10 <sup>6</sup>
6 C/U-H4	0°	As impacted	450	2100	3x10 <sup>6</sup>
6 D/U-H2	0°	As impacted	450	2100	3x10 <sup>6</sup>
6 D/U-H3	0°	As impacted	450	2100	3x10 <sup>6</sup>

TABLE 9.10-II (Cont'd)

<u>Specimen Number</u>	<u>Ply Config.</u>	<u>Condition</u>	<u>Test Temp. (°F)</u>	<u>Strain (μ-in/in)</u>	<u>Cycles to Failure</u>
6 D/U-H4	0°	As impacted	450	2100	4x10 <sup>6</sup>
23 A/U-H1	0°	Leached-Al/ Silicone Resin Repaired	450	2100	5x10 <sup>5</sup>
23 A/U-H3	0°	Leached Al/ Silicone Resin Repaired	450	2100	5x10 <sup>5</sup>
23 A/U-H5	0°	Leached Al/ Silicone Resin Repaired	450	2100	5x10 <sup>5</sup>
17 A/B-H3	±45°,0°,±45°	As impacted	70	2700	10 <sup>7</sup>
17 A/B-H4	±45°,0°,±45°	As impacted	70	2700	10 <sup>7</sup>
17 D/B-H2	±45°,0°,±45°	Leached-Al/ Silicone Resin Repaired	70	2700	2x10 <sup>5</sup>
17 D/B-H5	±45°,0°,±45°	Leached-Al/ Silicone Resin Repaired	70	2700	2x10 <sup>5</sup>
17 E/B-H3	±45°,0°,±45°	Leached-Al/ Silicone Resin Repaired	70	2700	5x10 <sup>5</sup>
17 B/B-H2	±45°,0°,±45°	Drilled-Polyi- mide/Graphite Repaired	70	2700	5x10 <sup>5</sup>
17 C/B-H4	±45°,0°,±45°	Drilled Polyi- mide/Graphite Repaired	70	2700	5x10 <sup>5</sup>
4 E/B-H1	±45°,0°,±45°	As impacted	450	1700	10 <sup>6</sup>
4 E/B-H2	±45°,0°,±45°	As impacted	450	1700	10 <sup>6</sup>

TABLE 9.10-II (Cont'd)

<u>Specimen Number</u>	<u>Ply Config.</u>	<u>Condition</u>	<u>Test Temp. (°F)</u>	<u>Strain (μ-in/in)</u>	<u>Cycles to Failure</u>
4 E/B-H3	$\pm 45^\circ, 0^\circ, \pm 45^\circ$	As impacted	450	1700	$2 \times 10^6$
4 E/B-H4	$\pm 45^\circ, 0^\circ, \pm 45^\circ$	As impacted	450	1700	$2 \times 10^6$
7 D/B-H1	$\pm 45^\circ, 0^\circ, \pm 45^\circ$	As impacted	450	1700	$3 \times 10^6$
7 D/B-H2	$\pm 45^\circ, 0^\circ, \pm 45^\circ$	As impacted	450	1700	$3 \times 10^6$
7 C/B-H3	$\pm 45^\circ, 0^\circ, \pm 45^\circ$	As impacted	450	1700	$4 \times 10^6$
7 C/B-H4	$\pm 45^\circ, 0^\circ, \pm 45^\circ$	As impacted	450	1700	$4 \times 10^6$
7 B/B-H3	$\pm 45^\circ, 0^\circ, \pm 45^\circ$	As impacted	450	1700	$3 \times 10^6$
7 B/B-H4	$\pm 45^\circ, 0^\circ, \pm 45^\circ$	As impacted	450	1700	$3 \times 10^6$
17 A/B-H1	$\pm 45^\circ, 0^\circ, \pm 45^\circ$	As impacted	450	1700	$4 \times 10^6$
17 A/B-H2	$\pm 45^\circ, 0^\circ, \pm 45^\circ$	As impacted	450	1700	$4 \times 10^6$
17 D/B-H1	$\pm 45^\circ, 0^\circ, \pm 45^\circ$	Unleached-A1/ Silicone Resin Repaired	450	1700	$3 \times 10^6$
17 D/B-H3	$\pm 45^\circ, 0^\circ, \pm 45^\circ$	Unleached-A1/ Silicone Resin Repaired	450	1700	$4 \times 10^6$
17 F/B-H5	$\pm 45^\circ, 0^\circ, \pm 45^\circ$	Unleached-A1/ Silicone Resin Repaired	450	1700	$3 \times 10^6$
17 D/B-H4	$\pm 45^\circ, 0^\circ, \pm 45^\circ$	Leached-A1/ Silicone Resin Repaired	450	1700	$2 \times 10^6$
17 E/B-H1	$\pm 45^\circ, 0^\circ, \pm 45^\circ$	Leached-A1/ Silicone Resin Repaired	450	1700	$10^6$

TABLE 9.10-II (Cont'd)

<u>Specimen Number</u>	<u>Ply Config.</u>	<u>Condition</u>	<u>Test Temp. (°F)</u>	<u>Strain (μ-in/in)</u>	<u>Cycles to Failure</u>
17 E/B-H2	$\pm 45^\circ, 0^\circ, \pm 45^\circ$	Leached-A1/ Silicone Resin Repaired	450	1700	$2 \times 10^6$
17 B/B-H1	$\pm 45^\circ, 0^\circ, \pm 45^\circ$	Drilled-Polyimide/ Graphite Repaired	450	1700	$5 \times 10^5$
17 C/B-H3	$\pm 45^\circ, 0^\circ, \pm 45^\circ$	Drilled-Polyimide/ Graphite Repaired	450	1700	$5 \times 10^5$

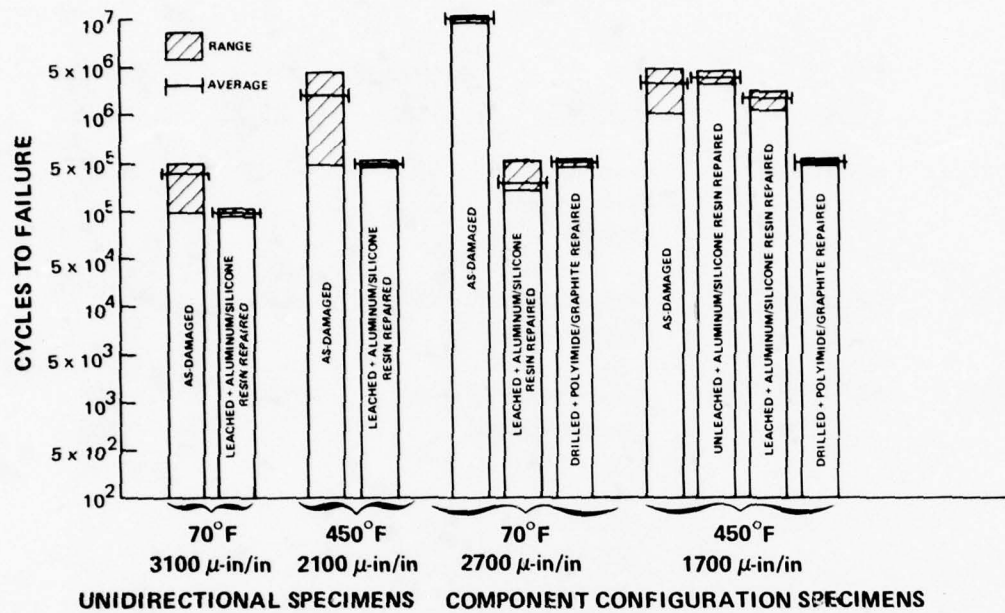


Figure 9.10-6 Summary of the Effect of Various Repair Techniques on the 70 and 450°F High-Frequency Fatigue Capability of Ballistic-Impact Damaged 50 Volume Percent Borsical® Specimens

#### 9.10.4 Metallography

The fracture surfaces of post-tensile test as-damaged specimens versus damaged and aluminum/silicone resin repaired specimens are shown in Figures 9.10-7 through 9.10-11. Examination of these fractures revealed that complete filling with aluminum/silicone is more difficult when the damaged material is leached away. Also note that the failures of the leached and repaired samples resulted in extensive pull-out of the aluminum/silicone filler compared with the samples repaired in the as-damaged condition. Based on ease of repair and retention of the aluminum/silicone filler, no leaching should be done prior to repair.

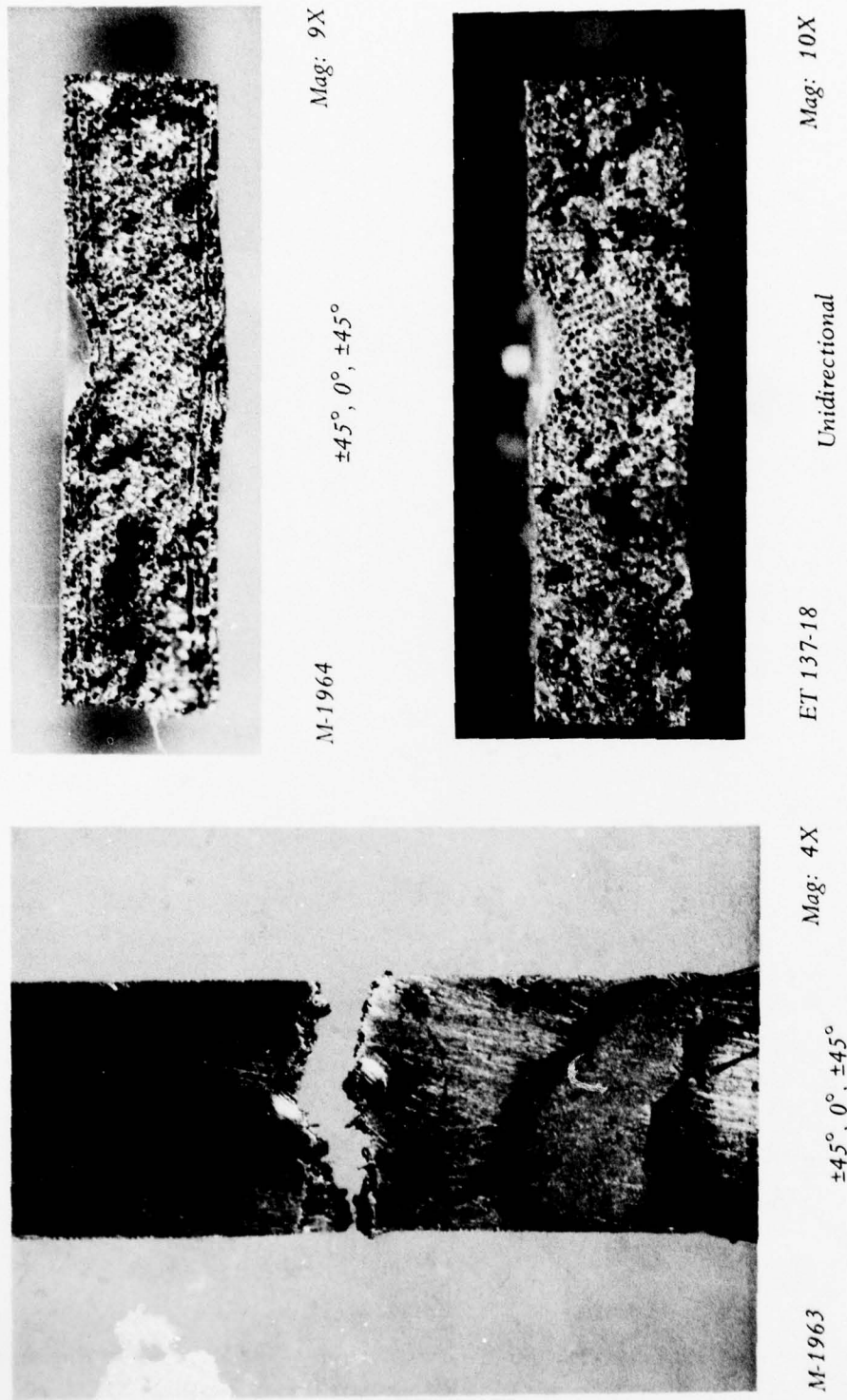
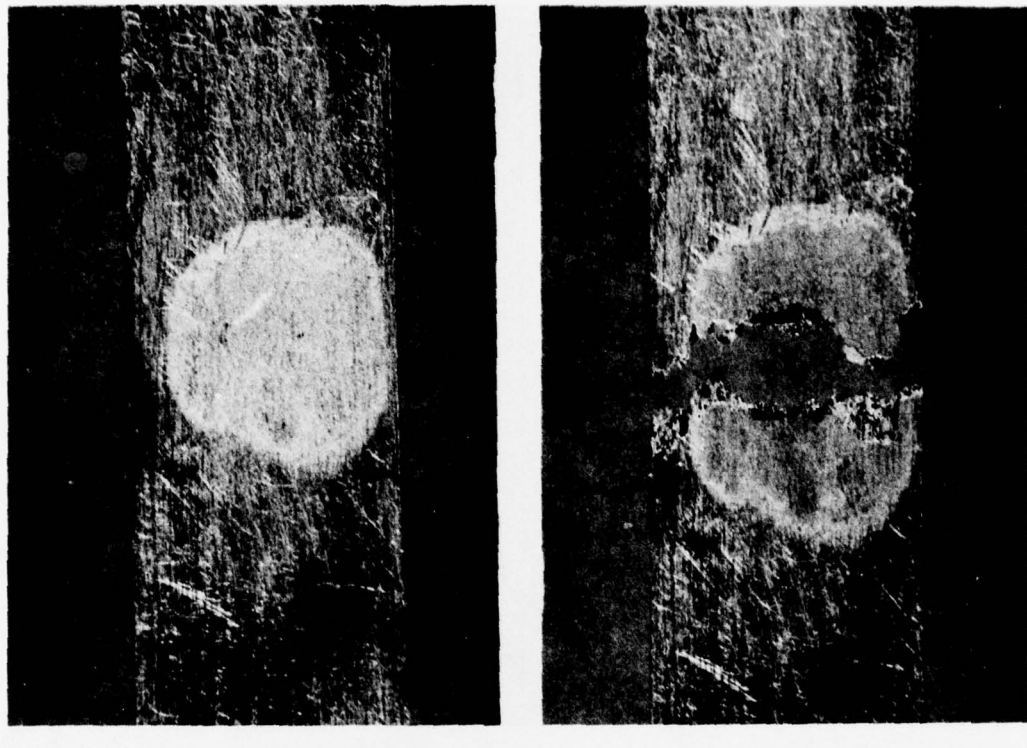
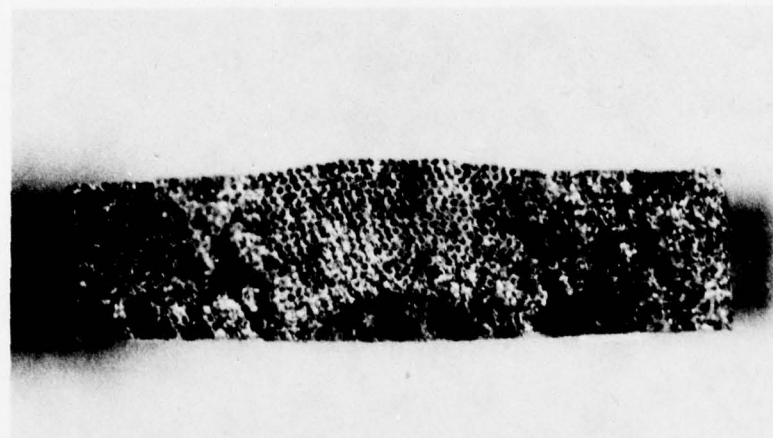


Figure 9.10-7 Typical 20-Layer Borsicat® Test Specimens After Testing in the As-Impacted Condition Without Repair

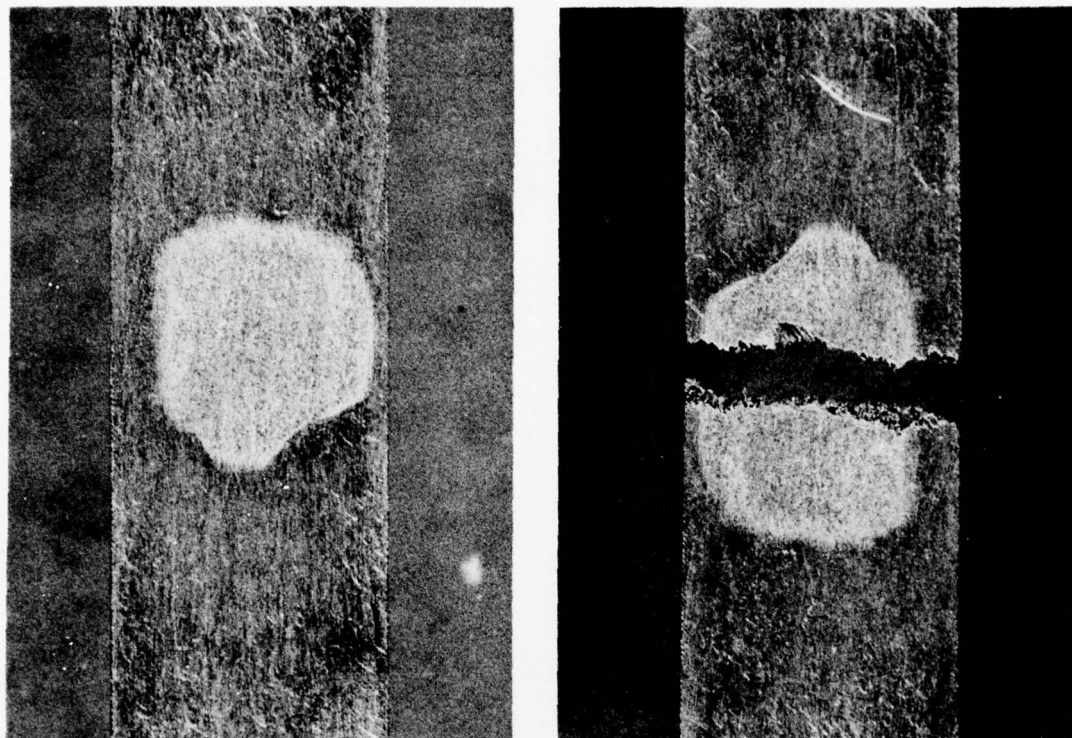


M-1814      As Repaired      Mag: 4X      M-1889      Tensile Tested      Mag: 4X



M-1907      Tensile Tested      Mag: 9X

**Figure 9.10-8**    *Typical Unidirectional (0°) 20-Layer Borsical® Test Specimen as Repaired with Aluminum/Silicone (Top Left), and as Tensile Tested*



M-1855

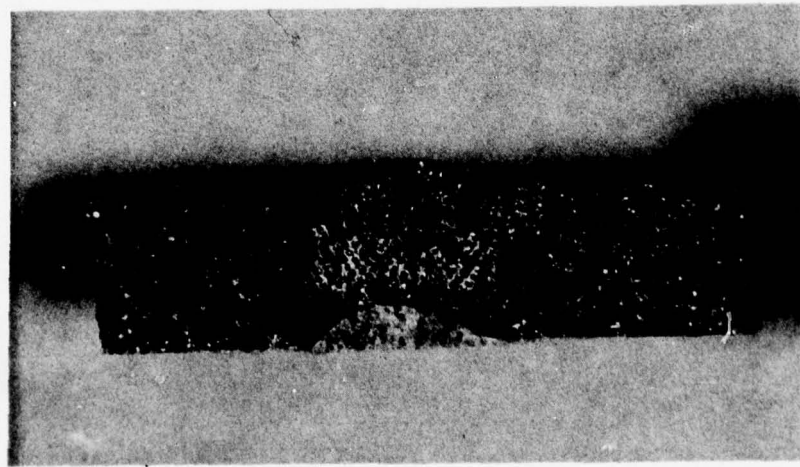
As Repaired

Mag: 4X

M-1893

Tensile Tested

Mag: 4X

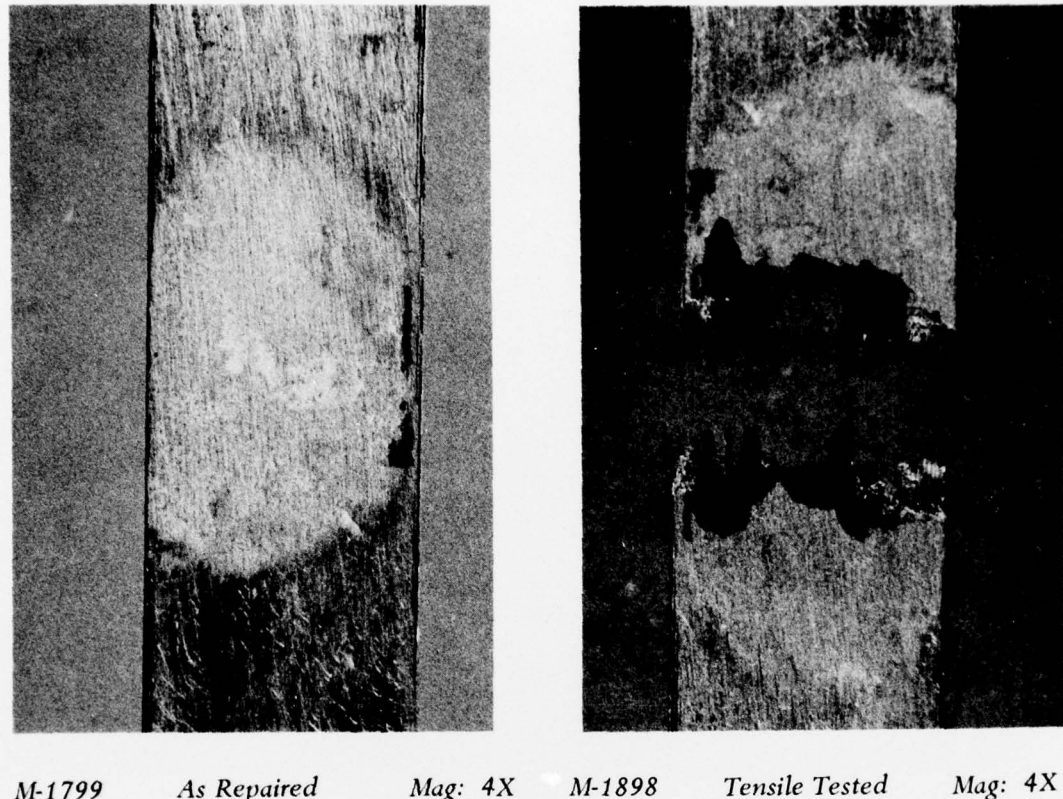


M-1910

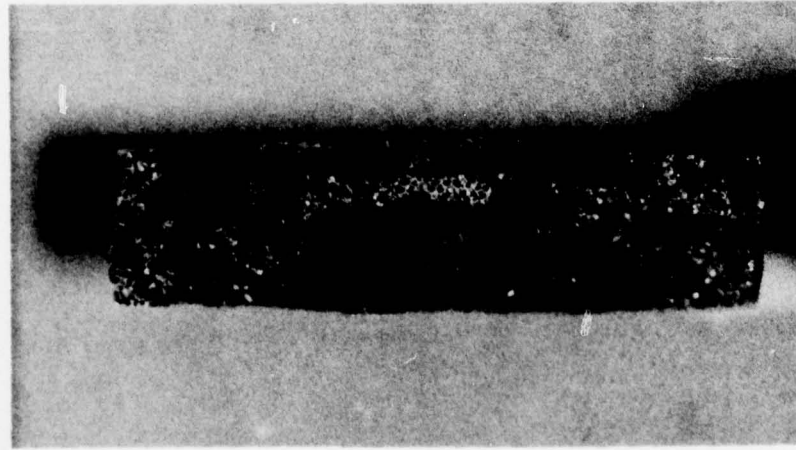
Tensile Tested

Mag: 9X

**Figure 9.10-9** Typical Component Configuration ( $\pm 45^\circ$ ,  $0^\circ$ ,  $\pm 45^\circ$ ), 20-Layer Borsical<sup>®</sup> Test Specimen as Repaired with Aluminum/Silicone (Upper Left), and After Tensile Test. No Leaching Prior to Repair



M-1799      As Repaired      Mag: 4X      M-1898      Tensile Tested      Mag: 4X



M-1914      Tensile Tested      Mag: 9X

Figure 9.10-10      Typical Unidirectional (0°) 20-Layer Borsical® Test Specimen as Repaired with Aluminum/Silicone and After Tensile Test. Damaged Area Removed by Leaching with HCl Prior to Repair

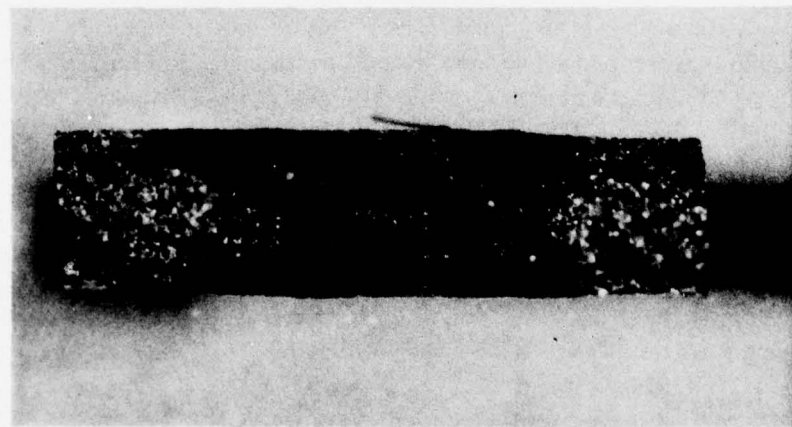
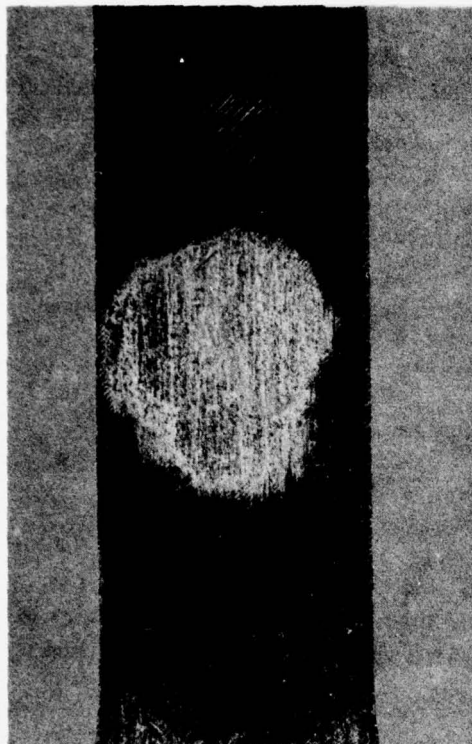


**Figure 9.10-11** Typical Component Configuration ( $\pm 45^\circ$ ,  $0^\circ$ ,  $\pm 45^\circ$ ), 20-Layer Borsical® Test Specimen as Repaired with Aluminum/Silicone and After Tensile Test. Damaged Area Removed by Leaching with HCl Prior to Repair

### 9.10.5 Summary

The following tabulation summarizes the results of the damage repair evaluations.

<u>Repair</u>	<u>Results of Evaluation</u>
Aluminum/silicone resin	Most acceptable repair scheme.
Polyimide resin and graphite tow	Satisfactory but requires leaching or drilling prior to repair which lowers strength and HFF capability.
713 Aluminum brazing	Brazing temperatures too high (900° F+) caused specimens to warp.
95 Zn-5 Sn solder	Inadequate wetting of composite resulted in poor bond.
95 Zn-5 Al solder	Only slightly better wetting than 95 Zn-5 Sn solder; required ultrasonics to achieve any bond.
Polyimide resin	Thermal expansion mismatch resulted in cracking and separation at bond.
Polyimide resin and aluminum filler	Thermal expansion mismatch resulted in cracking and bond separation.

The repair techniques described above were selected for investigation primarily for ease of repair. Improving strength over as-impacted material was not a criterion for satisfactory repairs; achieving and maintaining proper airfoil contour for aerodynamic considerations was the primary concern.

Other repair methods such as repressing Borsical® tape into damaged composites could also be employed. However, these approaches would require hot pressing facilities which are not readily available in the field and were therefore not evaluated. If service requirements make it necessary to recoup the strength loss due to impact damage, then careful examination of repressing-type repairs would need to be made.

## 10.0 BLADE BENCH TESTING

Before beginning engine environmental testing, approximately 142 BORSIC®/aluminum TF30-P-9 third-stage fan blades fabricated under this program were evaluated in a series of bench tests. In the test program, individual blades were subjected to various environmental and stress loading conditions typical of those which would be encountered in operating service.

The externally applied environmental conditions to which the blades were subjected were:

- Salt corrosion
- Thermal shock
- Erosion
- Foreign object damage from small, hard objects such as gravel and rivets
- Foreign object damage from massive objects such as birds and ice.

The foreign object damage (FOD) tests were categorized into small and massive in order to properly evaluate third-stage fan blade performance under conditions which they probably would encounter, i.e. small object ingestion and those conditions which would not be expected to occur, i.e. massive object ingestion.

In the stress tests, the blades were subjected to the several types of internal static and dynamic stresses which would be encountered under typical engine operating conditions.

Stress tests included:

- Blade untwist
- Stress survey
- Spit-pit burst tests
- Bending fatigue
- Combined stress fatigue

The object of the stress tests was to generate data which, when combined with stress data generated in the engine environment test program, can be used to help predict blade survival under engine operating conditions.

### 10.1 SUMMARY OF BLADE BENCH TEST RESULTS

Results of the bench test program indicated that the BORSIC®/aluminum third-stage fan blades fabricated under this program would survive in an engine operating environment but blade life could not be precisely determined. This aspect of blade performance will be addressed in Engine Environment Testing, Section 11, of this document.

#### 10.1.1 Environmental Testing

The results of the series of environmental tests indicated that BORSIC®/aluminum blades are entirely adequate for a third-stage fan environment but would not meet first-stage FOD requirements where the blades might encounter the ingestion of massive foreign objects.

In general, neither salt corrosion nor a -65°F to +500°F thermal shock adversely affected the BORSIC®/aluminum blades. Erosion resistance, with the nickel-cobalt leading edge FOD protection, was slightly superior to titanium blades, although small object FOD was slightly inferior. Resistance to massive FOD was significantly inferior to that exhibited by titanium blades.

#### 10.1.2 Stress Testing

Figure 10.1-1 is a Goodman-type diagram constructed from data generated during bench stress testing. It is so called because, unlike a true Goodman diagram, it incorporates variable criteria of failure. Diagrams of this type, together with stress data generated in engine environmental tests would be used to predict the probability of blade survival in an engine environment.

On the diagram, point B reflects the combined stress-fatigue test data, while Point C reflects the steady stress test data. Both stress modes specify separation of the airfoil from the root as the criterion of failure. Point A, vibratory test data, takes an arbitrary five percent frequency loss in  $10^7$  cycles as the failure criterion. Establishing an arbitrary failure criterion was necessary because no blades could be failed by separation in pure fatigue tests, while on the other hand, blade frequency degradation could not be tracked in the combined fatigue stress tests because of the configuration of the test blades. Burst testing induced no frequency loss prior to separation.

Goodman type diagrams were generated for blades tested at both room temperature and 450°F. The 450°F temperature is the maximum temperature the blade root area will reach at operating conditions of Mach No. (Mn) 2.2, 56,000 ft. This was confirmed during the engine environment test program.

Comparison of the generated diagrams with engine test stress surveys indicated that the blades would survive the engine test. The only operating stresses subsequently encountered outside the diagram were engine surge stresses, which were of short duration.

Fatigue testing in the second bending and first torsional modes was also attempted, but inherent damping in the blade structure prevented generating significant stresses in these modes, even with our larger shake tables. Water erosion testing was not conducted because it is not considered to be a problem with metal-matrix composites.

The results of spin-pit blade untwist testing confirmed the analytical predictions within the limits of experimental error. A spin-pit static stress survey revealed no stresses higher than predicted.

### 10.2 ENVIRONMENTAL TESTS, RESULTS, AND CONCLUSIONS

#### 10.2.1 Salt Corrosion Testing

Three blades (S-16, S-36, and S-43) having unfinished root attachments and incorporating nickel-cobalt leading edge (LE) protection electroplated directly to the airfoils were subjected to salt corrosion in a stressed condition for 100-hour periods. Post test NDI revealed no significant degradation of any of the three blades and indicated that BORSIC®-6061 aluminum alloy blades are not subject to salt-stress corrosion either at elevated temperature or humid conditions.

## 10.2.1.1 Elevated Temperature Testing

Blade S-16 was mechanically prestressed to 60,000 psi and then soaked at 500°F for 100 hours with a salt solution applied directly to the blade surfaces. Figure 10.2-1 shows the post-test condition of the blade. Nondestructive inspection and visual examination showed no evidence of significant salt corrosion. High frequency fatigue testing was not feasible for this blade because the bending stress/temperature/time cycle produced a permanent/set in the blade.

## 10.2.1.2 Humid Environment Testing

Blade S-36 was prestressed to 60,000 psi maximum by deflecting the tip 0.78 inch in a bend fixture. The blade was then exposed to a humid salt spray at 90°F for 100 hours. Figure 10.2-2 depicts the post-test condition of the blade. Blade S-43 was similarly tested, except that it was prestressed to 15,000 psi by deflecting the tip 0.2 inch. Following the corrosion testing, both blades were examined visually and non-destructively. No significant degradation was discernible.

The effects of the tests on blade natural frequency are presented in Table 10.2-1. The minor variations in pre-and post-test natural frequencies in the first bending and first torsional modes are considered to be within the limits of errors due to accuracy of measurement. The frequency losses in the second bending mode, although apparently real, are of insignificant magnitude.

TABLE 10.2-1

## EFFECT OF 100-HOUR HUMID SALT CORROSION ON NATURAL FREQUENCIES OF BORSIC®/ALUMINUM BLADES S-36 AND S-43

Blade	Mode	Pre-Test Natural Frequency (Hz)	Post-test Natural Frequency (Hz)	% Loss
S-36	1st Bending	131	131	---
	2nd Bending	426	420	1.4
	1st Torsion	884	895	---
S-43	1st Bending	130	128	1.5
	2nd Bending	425	418	1.6
	1st Torsion	868	864	0.5

Both blades were then high frequency fatigue (HFF) tested in the first bending mode at a temperature of 450°F and stressed to  $\pm 15,000$  psi. After  $10^7$  cycles, blade S-36 exhibited a first bending frequency loss of 3.5 percent and 2.0 percent when measured at room temperature and 450°F, respectively. Blade S-43 exhibited similar frequency losses of 3.2 and 2.7 percent when measured at the same temperatures. These slight frequency losses compare well to frequency losses suffered by composite blades not subjected to salt corrosion tests.

### 10.2.2 Thermal Shock

Five blades (S-3, S-20, E-24, S-40, and S-46) were subjected to thermal shock and then fatigue tested to determine the effect, if any, on the blades. The three main areas of concern were the BORSICAL® composite material, the nickel-cobalt leading edge bond, and the titanium root pad bond.

The thermal shock was administered by immersing the blade in a -65°F fluidized bed for two minutes, removing it and immediately immersing it in a +500°F fluidized bed for two minutes. This cycle was repeated 2000 times on four of the blades and 2450 times on the remaining one. To test the leading edge bond and the BORSIC® material the airfoil section of the blade was immersed. To test the titanium root bond, the root area was immersed. Figure 10.2-3 shows the fluidized beds used.

Results of the tests indicated that, although there was a slight decrease in natural frequency, composite blade structural integrity was not degraded.

#### 10.2.2.1 Composite Material/Leading Edge Testing

The airfoil section of three blades, S-3, S-20, and S-40, were subjected to 2000 cycles each of -65°F to +500°F thermal shock. The results indicated that:

- No delamination or change in the composite material density was observed.
- No degradation of the bond between the electroplated nickel-cobalt LE and the composite material airfoil occurred.
- Some cracking of the nickel-cobalt LE occurred. This, however, was associated with LE pits which were subsequently eliminated, or with the root end of the LE plate where thin areas of plating existed. The LE pits are shown in Figure 10.2-4.
- Subsequent HFF testing at 450°F indicated that the thermal fatigue testing had no effect on the rate of decay of the blade natural frequency in  $10^7$  cycles.

#### 10.2.2.2 Titanium Root Bond Testing

The root of blade E-24 was subjected to 2540 cycles of -65°F thermal shock. Nondestructive inspection and density checks showed that the blade suffered no degradation.

After the thermal shock, blade E-24 was subjected to five proof spin cycles to 12,150 rpm. It was then deliberately run to destruction and burst at 13,886 rpm. This burst speed is comparable to that of blades which weren't thermal cycled and indicates that thermal cycling does not significantly affect BORSIC® composite tensile strength or root bond shear strength.

Blade S-46 was subjected to 2000 cycles of -65°F to +500°F and showed no signs of degradation. It was then HFF tested. The pre-test and post-test results of HFF testing are presented in Table 10.2-II. The slight frequency degradation noted is well within design limits.

TABLE 10.2-II

**EFFECT OF 2000 THERMAL CYCLES (-65°F to 5000°F) ON NATURAL FREQUENCY  
DEGRADATION OF BORSIC®/ALUMINUM BLADE S-46**

Mode	Pre-HFF Natural Frequency (Hz)	Post-HFF Natural Frequency (Hz)	% Loss
1st Bending	132	131	0.8
2nd Bending	432	419	3.0
1st Torsion	885	854	3.5

### 10.2.3 Erosion Testing

Six blades (S-14, S-28, S-51, S-60, D-17, D-20), all incorporating nickel-cobalt leading edge protection, were exposed to sand erosion tests. Static tests were performed at both room temperatures and 450°F. The sand used for all tests conformed to MIL-E-5007C specification. Control blades of bill of material (B/M) titanium alloy were tested with the BORSICAL® blades to provide baseline data.

Results of the tests indicated that:

- No effects detrimental to the basic structural integrity of the blades were observed
- Surface matrix material on the unprotected portion of the airfoil eroded rapidly but as the fibers became exposed, the erosion rate diminished rapidly
- A precise weight loss split between the nickel cobalt leading edge and the rest of the blade was virtually impossible to determine. Consequently, total blade loss only was measured
- None of the tests achieved the desired impingement pattern. Figure 10.2-5 shows the condition of blade D-17 after the dynamic erosion test. The anticipated service-induced pattern would correspond closely to the shape of the leading edge sheath on the pressure side of the blade
- Although results were somewhat obscured by the unexpected sand impingement patterns achieved, it is evident that the harder nickel-cobalt provided excellent sand erosion protection and can be interpreted as being superior to that provided by titanium alloys.
- It would be desirable to perform an erosion test with the nickel-cobalt leading edge protection in an engine environment in order to achieve more realistic erosion patterns.

AD-A055 891 PRATT AND WHITNEY AIRCRAFT GROUP WEST PALM BEACH FL G--ETC F/G 1/3  
TF30 THIRD-STAGE COMPOSITE FAN BLADE SERVICE PROGRAM. (U)  
MAY 78 D G RANDALL

F33657-70-C-0624

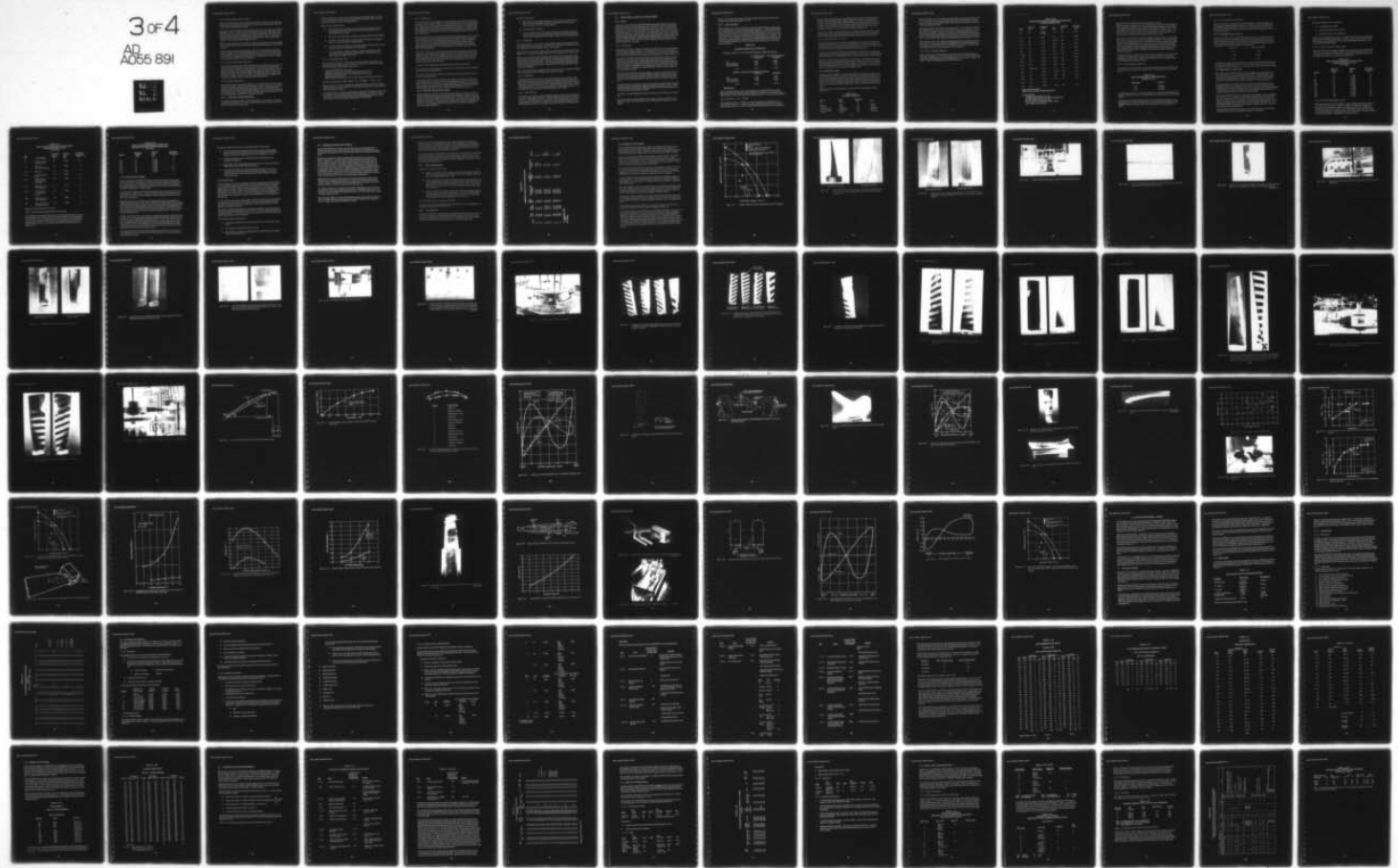
NL

UNCLASSIFIED

PWA-5141

3 of 4

AD  
A055 891



#### 10.2.3.1 Room Temperature Static Testing

The test rig shown in Figure 10.2-6 was used for static testing. In this rig, the test blade was mounted in the test chamber at the desired angle of attack. Pressurized air picked up erosive material which impinged against the blade.

The initial tests were performed on blades S-14 and S-28, as well as base line tests on titanium B/M blades in each case. Blade S-14 and its base line blade were eroded with 100 pounds of sand at a rate of 3 lb/min. The blades experienced similar weight losses. Blade S-28 and its base line blades were eroded with 360 pounds of sand at a rate of 1 lb/min. In this test, the weight loss of the titanium blade was 70 percent higher than that of the composite blade. Figure 10.2-7 shows both composite blades after test.

Blade S-14 was then subjected to HFF testing. The results indicated that the erosion damage had no significant effect on the rate of decay of the blade natural frequency in the first bending mode.

Analysis of blade S-28 indicated that more than 90 percent of its weight loss was from the composite material, not the nickel-cobalt leading edge. As a result, the leading edge protection was redesigned to cover a greater portion of the composite surface as shown in Figure 10.2-8. This new configuration extended back to one-third chord at the tip, and conforms to erosion patterns experienced on service blades.

#### 10.2.3.2 Elevated Temperature Static Testing

Two blades, S-51 and S-60, were subjected to sand erosion at 450°F in the static test rig. To provide the elevated temperatures, the entering air is mixed with fuel and ignited before picking up the sand. Gas velocity as high as Mach No. 1.0 is attainable upstream of the test chamber. Both blades had the original leading edge configuration, and were subjected to 100 pounds of sand at a feed rate of 0.1 lb/min. Total weight loss of the composite blade was less than 1 percent (1.8 gm), but was greater than that of the base line titanium blade. The post-test condition of one set of blades is shown in Figure 10.2-9.

#### 10.2.3.3 Dynamic Erosion Testing

Dynamic sand erosion of two composite blades, D-17 and D-20, and one base line titanium blade was performed in a spin pit at room temperature. The three blades were individually brought up to 10,360 rpm and impacted with 75 grams of sand. The weight loss of the composite blades was twice that of the titanium blade; but, most of the eroded material was the aluminum matrix. The visual appearance of the nickel-cobalt leading edge was excellent. The composite blades incorporated the redesigned leading edge.

#### 10.2.4 Foreign Object Damage (Small Objects)

Although the third-stage fan blade of the TF30-P-9 engine is not anticipated to encounter massive foreign objects such as ice or birds, small hard objects such as gravel or rivets can be expected to penetrate to the third stage.

In order to evaluate the resistance of the TF30 third-stage composite fan blades to this type of FOD, both static and dynamic testing was performed using 30-caliber bullets, 0.25 inch gravel, and 0.5 gram steel rivets as the foreign objects.

Results of the tests indicated that:

- The damage caused by small, hard objects impacting at high velocity will cause local damage ranging from moderate to severe, but will not degrade the basic structural integrity of the blade.
- The nickel-cobalt leading edge is effective in minimizing small object FOD damage.
- The nickel-cobalt leading edge is extremely tough and adherent and exhibits no tendency to crack or peel off the composite airfoil.
- Further improvement is required in the composite blade structure to make it equal to titanium blades in FOD resistance to massive objects.
- The composite blades fabricated under this program and having nickel-cobalt leading edge protection will survive a flight evaluation program without undue risk of catastrophic failure due to FOD.

#### 10.2.4.1 Static Ballistic Impact Tests

The test rig, shown in Figure 10.2-10 was used to impact five blades with 30-caliber, 110 grain steel projectiles traveling at 1300 - 1500 ft./sec. Figure 10.2-11 shows the five blades tested and the results. Blade configurations included:

- Unprotected BORSIC®/aluminum blade,
- BORSIC®/aluminum blade with hard nickel leading edge protection,
- BORSIC®/aluminum blade with nickel-cobalt leading edge protection,
- Bill of Material titanium blade
- BORSIC®/aluminum blade with boron-carbide leading edge protection at the tip only.

Each blade was impacted at incidence angles of Tip - 0°, Midspan - 15°, Root - 40°.

Damage was severe in all cases, but apparently completely localized. There was no tendency of the leading edge to peel off. Post-test X-ray and ultrasonic inspection confirmed that only localized damage was sustained.

Two of these blades, S-1 and S-4, were subsequently subjected to  $10^7$  HFF cycles with a total tip amplitude of 0.4 inch at 450°F. Blade S-1 had a nickel-plated LE and blade S-4 had no LE protection. The fatigue testing indicated that the leading edge damage had no adverse effect on the decay rate of the blade natural frequency in first bending.

#### 10.2.4.2 Dynamic Tests

Two series of FOD tests were performed in a spin pit facility, one using 0.25 inch gravel and the other 0.5 gram steel rivets. Figure 10.2-12 shows the test facility. These tests duplicated the rotating speed (10,360 rpm) and blade stiffening effects that occur in an engine environment. Blade tip speed in all of these tests was approximately 1500 ft/sec. In all cases, B/M titanium alloy blades were tested one-for-one with the composite blades to provide baseline data. Videotape was used for all tests to record and verify adequate impact events and to observe blade reaction.

The first series of tests used 0.25 inch quartz gravel as the impacting medium. Two composite blades with nickel-cobalt leading edges, and two B/M titanium alloy blades, rotating at the speed of 10,360 rpm, were each impacted with 66 pieces of gravel. As shown in Figures 10.2-13 and 10.2-14, the composite blades and the titanium blades suffered moderate leading-edge damage. Although the total amount of material damaged on the composite blades was approximately 25 percent greater than that on the titanium blades, none of the nicks exceeded blend limits.

Figures 10.2-13 and -14 show that the unprotected portion of the composite blade leading edge near the root suffered severe damage in these tests, even though the impact velocity is relatively low in this region. This emphasizes the efficiency and the necessity of the nickel-cobalt leading edge. In an engine environment, however, foreign objects tend to be forced radially toward the blade tips. This fact tends to reduce the importance of the root area damage sustained when evaluating results.

No tendency of the leading edge to peel off the blade was observed in these tests.

The second series of tests was identical to the first, except that 0.5 gram steel rivets replaced the gravel as the impacting medium.

These rivets are representative of the type of engine hardware which might be encountered in future service applications.

Each blade was subjected to approximately 23 rivet strikes at 10,360 rpm. The results are shown in Figures 10.2-15 and 10.2-16. Leading edge damage was severe for both the composite and the titanium blades with the amount of damaged or lost material in the composite blade estimated to be twice that of the titanium blades. Blend limits were exceeded in the composite blades, but again there was no tendency for the leading edge to peel off.

#### 10.2.5 Foreign Object Damage (Massive Objects)

Dynamic testing was conducted on TF30-P-9 third-stage advanced composite fan blades to evaluate their FOD performance in an engine first-stage environment. These tests were conducted in the spin pit test facility shown in Figure 10.2-12. The tests consisted of impelling one-inch ice balls, three ounce birds, or six ounce gelatin "birds" against the fan blades. The fan blades were rotating at 10,360 rpm with an equivalent blade tip speed of approximately 1500 ft/sec. The impingement angle of the impacting objects was similar to that which exists in an engine environment.

Test results indicated that:

- While the nickel-cobalt leading edge did not prevent damage to the blades, neither did it exhibit the undesirable characteristic of breaking up or peeling off and thereby becoming a source of secondary damage.
- No root damage was observed.
- In order to perform well in a first-stage FOD environment, the impact resistance of the composite structure must be increased. Possible methods of achieving this increase are by using improved fiber, matrix material, and/or reorienting the fibers.

#### 10.2.5.1 Ice Ball Tests

Two composite blades, E-216 and E-227, and two B/M titanium blades were impacted with one-inch diameter, tempered ice balls. The ice balls were tempered by freezing them at sub-zero temperatures, then holding them at 30°F for several hours.

Blade E-216 was impacted with a single ice ball and sustained the fracture damage shown in Figure 10.2-17. The fracture boundary followed the  $\pm 45^\circ$  orientation of the surface fibers.

Blade E-227 was similarly tested but absorbed three impacts before sustaining the damage shown in Figure 10.2-18. Both of these blades had a leading edge maximum radius of .013 inch, which was the design requirement. The effect of the leading edge thickness on FOD resistance can be seen in Figure 10.2-19. The blade on the right had a leading edge radius of .025 inch and sustained six one-inch ice ball impacts with no damage other than a slight dent in the leading edge.

The two titanium alloy blades, similarly tested to obtain base line data, exhibited only slight dents in the leading edge after sustaining impacts from five ice balls.

#### 10.2.5.2 Starling Tests

Two composite blades, E-44 and E-228, were impacted with 3.25 ounce starlings. High-speed movies were taken of these tests which were conducted using the test rig shown in Figure 10.2-20. The movies showed that the birds had insufficient acceleration to penetrate far enough into the blade path so that "bites" of appreciable size could be taken. Consequently many small bites were taken from each bird and no blade damage resulted. To achieve valid results the acceleration of the birds would have to be increased.

#### 10.2.5.3 "Jelly" Bird Tests

In the final, massive FOD test, a spherical gelatine ball, approximately three inches in diameter was impelled against blade E-243. The ball weighed six ounces and had a density of 1.12 gm/cc. Two impacts occurred and removed 1.5 ounces from the ball. A piece of the blade leading edge was broken out. Figure 10.2-21 shows the damage sustained. The titanium blade tested under the same conditions sustained a slight dent on the leading edge.

## 10.3 STRESS TESTING, RESULTS, AND CONCLUSIONS

### 10.3.1 Untwist

Because the TF30-P-9 third-stage BORSIC®/aluminum fan blades designed and fabricated under this program had no part-span shrouds, they would exhibit a greater untwist at high rotating speeds than the titanium alloy B/M blades. The added untwist was calculated to be approximately one degree at the design speed. The analysis indicated that the total untwist of the blade would be 2.14 degrees at 450°F. The total untwist consists of two components, elastic untwist and plastic untwist (primary creep). Because the angle of attack of the blade leading edge significantly affects the blade aerodynamic performance, theoretical blade twist had to be verified empirically. Deviation from the predicted value, upon which the aerodynamic performance was calculated, can then be compensated for by altering the broach angle of the disk slots if necessary.

#### 10.3.1.1 Untwist Test

The spin-pit test rig shown in Figure 10.3-1 was used to conduct the tests to determine blade untwist at engine operating conditions. To determine the untwist, two proximity probes were mounted just outboard of the blade tip. One probe was mounted directly opposite the tip leading edge and the other directly opposite the tip trailing edge as shown in Figure 10.3-2.

In operation, as the blade rotates past the probes, each probe transmits a signal to an oscilloscope-camera read-out system. The time gap between the signals is calibrated in milliseconds and varies with the rpm and blade angle of attack ( $\alpha$ ). As the speed increases, the blade untwists thereby increasing  $\alpha$  and decreasing the time gap. Knowing the blade chord, speed, and original  $\alpha$ , the difference in the time gaps at two different speeds permits computing the change in  $\alpha$ . Readings were taken during both acceleration and deceleration at room temperature and 450°F.

The first two blades developed under this program, D-1 and D-2, were selected for this test. In their fabrication, both blades underwent a faulty processing procedure which was subsequently corrected during the development program. Blade D-1 failed during the 450°F test because of the processing procedure. Blade D-2, however, successfully completed the test.

For the test, blade D-2 was instrumented at the root, midspan, and tip with thermocouples. The blade was run through the speed range and incremental readings were taken at 4000, 6000, 8000, 9000, and 10,360 rpm. Readings were taken both during acceleration and deceleration and at room temperature and 450°F.

A minimum of four photographs was taken at each test point to minimize system inaccuracies.

The results of the test, shown in Figure 10.3-3, indicate a total untwist at 450°F of two degrees  $\pm 0.5$  degree. The experimental accuracy of these results is considered to be  $\pm 0.5$  degrees.

Because the test results agree closely with analytical design predictions, the disk slots were broached at the original design angle of  $17^\circ 30'$ .

### 10.3.2 Static Stress Survey

Maximum static stresses occur in the airfoil at its junction with the platform, and are made up of centrifugal (P/A), restrained warping, and gas bending stresses. Their predicted magnitude at peak stress locations in the most severe flight conditions is presented in Table 10.3-I. In order to confirm these stress levels, and their chordwise distribution, a static stress survey was performed on two blades in a vacuum spin pit at rotating speeds up to 12,150 rpm. Because of the vacuum environment of the spin pit, gas bending stresses were not present. Tilt stresses were also eliminated by compensating for airfoil tilt in the disk slot. Thus, only the P/A and restrained warping stresses which compose at least 84 percent of the major stress peaks were induced.

TABLE 10.3-I

## MAXIMUM AIRFOIL STATIC STRESS (psi)

Conditions: Mach No. 1.2, Sea Level, Max Afterburner, Fan Speed 10,355 rpm

	Core ( $0^\circ$ fiber orientation % Chord (CV))	Shell ( $\pm 45^\circ$ fiber orientation Leading Edge)
P/A	32,170	18,000
Restrained Warping	21,000	24,500
Tilt and Gas Bending	2,406	1,410
Total	55,576	43,910*

Conditions: Min. Gas Load, Fan Speed = 10,350 rpm

	% Chord (CV)	Leading Edge
P/A	32,170	18,000
Restrained Warping	21,000	19,450
Tilt and Gas Bending	7,070	6,920
Total	60,240	44,370*

\*Balanced Stresses

The data compiled during the stress survey indicates that the BORSIC®/aluminum blade design developed in this program has ample capability to withstand P/A and restrained warping stresses up to 10,350 rpm and that the predicted stresses were on the conservative (high) side.

#### 10.3.2.1 Static Stress Survey – Test One

The first test was conducted on blade E-23, which was instrumented with fourteen 0.125 inch grid static strain gages. The gages were radially aligned and positioned at the locations shown in Figure 10.3-4. All gages were located on the airfoil directly adjacent to the platform.

Room temperature strain levels were recorded both during acceleration and deceleration at speeds of 1000, 4000, 6000, 8000, 10,000, 11,000 and 12,150 rpm. The data indicated excellent strain gage linearity through 10,000 rpm, but above this speed the gage output was nonlinear. The nonlinearity was presumed due to plastic deformation (Blade E-23 was not stress relieved by the 800° F heat treat during fabrication, which might account for the deformation.) All gages except one performed satisfactorily during the test.

Figure 10.3-5 is a plot of the reduced data for the 10,000 rpm data point as well as the analytically predicted P/A and restrained warping stresses for the same rpm. This comparison shows that the actual leading edge stress peak did not develop as analytically predicted.

#### 10.3.2.2 Static Stress Survey – Test Two

The second stress survey test was conducted using blade E-92. In this test the blade was instrumented with 18 strain gages adjacent to the platform plus six gages in the platform area. The gages were 0.0625 inch grid and located as shown in Figures 10.3-6 and -7. Figure 10.3-8 shows the blade and disk combination with instrumentation completed.

The test procedure was identical to that used for blade E-23 in the first test. All 18 airfoil gages showed excellent linearity throughout the speed range. However, the 6 platform gages performed nonlinearly. Consequently, their data is suspect and not included in this document.

Figure 10.3-9 presents the reduced data from the airfoil gages at 10,000 rpm as well as the analytical prediction for the same speed for comparison. These data are in close agreement with the data obtained on Blade E-23, (Figure 10.3-5). In both surveys, the severe leading edge stress peak predicted did not develop. Although the peak stresses were lower than predicted, the average stress was very close to the analytical value.

#### 10.3.3 Spin-Pit Burst Testing

Although spin-proof-testing to 115 percent design speed (12,150 rpm) was included as a requirement in Item 5c, Phase 1 of the contract work statement, blade burst testing was not a specific contract stipulation. However, since several early blades failed at speeds below the required 115 percent proof capability, burst speed margin became of great concern. Consequently, once the blade residual stress problem was resolved (see below), several deliberate burst tests were performed (with no change to the contract) to firmly establish blade burst margin.

Blade R-10, an early development blade, was spin tested to the schedule presented in Table 10.3-II.

TABLE 10.3-II  
BLADE R-10 SPIN TEST

Type of Test	Speed (rpm)	Temperature (°F)	Time
Endurance	9,000	450	50 hours
Endurance	10,360	375	10 hours
Low Cycle Fatigue	4,000-9,000	450	1000 cycles
Low Cycle Fatigue	4,000-10,360	300	2000 cycles
Overspeed	11,400	350	15 seconds

As shown in Figure 10.3-10, the blade survived this engine oriented test in excellent condition. It was considered to be fully acceptable from a static stress standpoint for engine testing. It was also concluded that the fabrication processes were satisfactory and capable of producing high quality blades.

Subsequently, however, more than 27 percent of the early "E" series (engine test blades) spin proof-tested failed. One failure was at a speed of 10,782 rpm. Figure 10.3-11 shows the failure mode exhibited. The failures were traced to residual stresses induced in the fibers during the diffusion bonding process. These stresses were relieved and the problem solved by introducing an 800°F three-hour heat treat cycle in the fabrication process (see para. 7.2.11). No further blade failures occurred during spin proof-testing to 12,150 rpm.

A further direct result of these failures was initiating spin-pit burst tests into the test program. In these tests, the rotational speed is gradually increased until the test blade fails. In addition to conducting burst tests at room temperature, a burst test at 450° and a low cycle fatigue burst test at room temperature were also conducted.

#### 10.3.3.1 Room Temperature Burst Test

Spin-pit burst testing of 31 blades that were stress relieved by heat treating resulted in burst speeds ranging from 13,772 rpm to speeds in excess of 15,553 rpm. Because of the heat treat the minimum burst speed was increased from 10,782 rpm to 13,772 rpm or 28 percent. Table 10.3-III summarizes the results of these tests.

**TABLE 10.3-III**  
**BURST PERFORMANCE OF STRESS RELIEVED BLADES**  
**AT ROOM TEMPERATURE**

Blade	Heat Treat Cycle	Burst Speed (rpm)	Blade	Heat Treat Cycle	Burst Speed (rpm)
E-72	B-5	No Burst @ 15,500	E-124	B-6	15,553*
E-75	B-5	15,448	E-91	B-6	15,550+
E-71	B-6	15,338	E-152**	B-6	15,522+
E-66	B-3	15,270	E-84	B-6	15,119
E-77	B-5	15,230	E-142	B-6	15,014
E-67	B-3	15,210	E-112	B-6	14,935
E-100*	B-6	15,137	E-97	B-6	14,642
E-135	B-6	15,100	E-108	B-6	14,611
E-70	B-3	14,883	E-122	B-6	14,541
E-173	B-6	14,850	E-116	B-6	14,453
E-117	4 S/R Cycles	14,740	E-151	B-6	14,181
E-69	B-3	14,680	E-150**	B-6	14,177
E-68	B-3	14,650	E-88	B-6	14,174
E-104	B-6	14,560	E-102	B-6	13,797
E-153	B-6	14,270			
E-83	B-6	14,260	E-118	B-6	13,772

\* Blade E-100 had no platform

\* Blades E-152 and E-150 had no leading edge protection

**Heat Treat Cycle Key**

B-3 Single 800°F stress relief cycle - oven

B-5 800°F oven stress relief cycle plus 800° die stress relief cycle

\*B-6 Double 800°F stress relief cycle - oven

\*B-6 Stress relief cycle was applied to all blades used in the flight evaluation program (Appendix )

Figure 10.3-12 shows the results of the first 24 spin-pit burst tests.

The burst blades are arranged in order of descending burst speed from left to right with the blade leading edge toward the camera. The blades exhibiting the highest burst speeds had a more random failure than those which failed at lower speeds. The failure of the "lower-speed" blades occurred at the junction of the root and airfoil, the high stress plane. This indicates that they retained a greater level of residual stresses even after the 800°F heat treat stress relief cycle than the blades having a random failure pattern.

Figure 10.3-11 is a side view of a burst blade with the leading edge at the left. Both Figure 10.3-11 and -12 show that, in general, the leading edge fractures are closer to the platform fillet than are the trailing edge fractures. This indicates that failure initiated at the leading edge, because the leading edge fracture coincides more closely with the plane of highest stress. No contradictory evidence indicating a different point of failure initiation could be found. Examination of the fracture surfaces indicated that the composite structure was well oriented and well compacted, although there were some local areas of fabrication-induced broken fibers.

An attempt was made to correlate blade burst speed with parameters such as tape strength, composite panel strength, blade acoustic emission, blade serial number (to establish chronology) and blade density. Of these, only blade density showed a consistent trend. This correlation is shown in Figure 10.3-13.

#### 10.3.3.2 Elevated Temperature Burst Test

Three blades, E-96, E-147, and E-186, were spin pit burst tested at 450°F to provide data to establish a 450°F Goodman type diagram. Table 10.3-IV presents the results of these tests.

**TABLE 10.3-IV**  
**BURST PERFORMANCE OF STRESS RELIEVED**  
**BLADES AT 450°F**

Blade Number	Burst Speed
E-96	12,900 rpm
E-147	12,360 rpm
E-185	12,270 rpm

The minimum burst speed, 12,270 rpm, corresponds to maximum predicted shell stress of 63,000 psi. This value was used to establish the steady stress point on the 450°F Goodman diagram.

This minimum burst speed is nearly 90 percent of that established for the blade at room temperature (13,772 rpm) and compares very well with the predicted strength loss of the BORSIC®/aluminum composite blade when its temperature is increased from 70°F to 450°F.

### 10.3.3.3 Room Temperature LCF Burst Test

Blade E-92 was low cycle fatigue tested at room temperature. In this test, the blade was accelerated from 4000 rpm (engine idle speed) to 12,150 rpm (115 percent design speed) and maintained at the high speed for one minute. The blade survived 549 such cycles before bursting. This one test, however, is an insufficient statistical sampling upon which to base a valid conclusion.

### 10.3.3.4 Post-Engine Operation Burst Tests

Following the 364-hr. engine sea-level test program (Section 11.1), a total of 12 blades exhibited LE cracks above the platform. Following the ground engine tests and prior to the flight evaluation program, three of the blades with LE cracks were spin-pit burst tested at room temperature to assess the effect on burst speed of the 364-hour engine test, and the presence of the cracks. The test results are presented below:

Blade No.	Burst Speed (RPM)
E-105	12,966
E-130	13,980
E-156	13,687

Comparing these results with Table 10.3-III, it can be seen that the minimum burst speed of the engine-tested blades decreased from 13,772 rpm for new blades to 12,966 rpm, or approximately 6%, but still retained a 22.5% margin of safety over red-line speed (10,550 rpm).

### 10.3.4 High Frequency Fatigue Testing

Thirty blades were bench fatigue tested in the first bending mode during this test series. Tests were conducted at both room temperature and 450°F. An electrodynamic exciter system (shake table) rated at 2000 pounds was used to drive the blades at their natural frequency in the first bending mode. Physical characteristics of the test system limited acceleration of the blade to 33 g's. Figure 10.3-14 shows the system in operation.

The 33 g-load applied to the blades resulted in a maximum total tip deflection (double amplitude) of 0.8 inch. This deflection corresponds to a maximum blade shell stress of  $\pm 22,000$  psi, which occurs at the leading edge. The comparatively low tip deflections attained with this blade are the result of the high level of internal damping which results from the composite material and the fiber orientations used in the blade.

Four generations of blades were used in the fatigue testing program. They were designated "R", "D", "S", and "E". The R-, D-, and S-blades were developmental configurations while the E-blades were the final configuration used for engine testing. The R-, D-, and S-blades had similar airfoils but, while the R-, and D-blades had finished titanium roots, the S-blade was designed for airfoil testing only and had an unfinished aluminum root. The E-blade differed in that the dovetail root attachment was slightly shorter fore and aft and the airfoil edges were somewhat thinner.

The blades differed significantly in quality as well. The E-blades were of uniform high quality while the quality of the developmental blades was inconsistent.

Three series of fatigue tests were conducted:

- Undamaged blades at 450°F
- Deliberately damaged blades at 450°F
- Undamaged blades at room temperature

All of the tests established runout as  $10^7$  cycles, and the failure criterion was established to be five percent loss in first bending frequency. This is a realistic criterion because, should the frequency drop approximately ten percent, potentially dangerous resonances would occur in the engine operating range.

#### 10.3.4.1 Testing of Undamaged Blades at 450°F

Thirteen blades were tested at 450°F through  $10^7$  cycles at various values of tip deflection in this test. The results are presented in Table 10.3-V and plotted in Figure 10.3-15. The wide scatter exhibited at the  $\pm 16,500$  psi level is attributed to variations in blade quality. No engine-quality blades were included in this series of tests.

TABLE 10.3-V  
RESULTS OF HIGH FREQUENCY FATIGUE TEST  
UNDAMAGED BLADES AT 450°F  
( $10^7$  Cycles)

Blade No.	Double Tip Amplitude (inch)	Maximum Stress (psi)	First Bending Frequency Loss (%)
R-7	0.4	$\pm 11,000$	4.8
	0.6	$\pm 16,500$	6.8
R-8	0.4	$\pm 11,000$	3.7
D-8	0.6	$\pm 16,500$	2.8
D-10	0.6	$\pm 16,500$	7.0
D-19	0.6	$\pm 16,500$	1.7
S-10	0.6	$\pm 16,500$	5.2
S-11	0.2	$\pm 5,500$	0
S-19	0.4	$\pm 11,000$	4.3
S-44	0.6	$\pm 16,500$	10.5
S-49	0.6	$\pm 16,500$	9.6
S-58	0.6	$\pm 16,500$	9.0
S-59	0.6	$\pm 16,500$	10.3

#### 10.3.4.2 Testing of Damaged Blades at 450°F

Nine blades were tested at 450°F through  $10^7$  cycles at a double amplitude tip deflection of 0.4 inch. This corresponds to a stress of 11,000 psi. The blades were deliberately damaged prior to test by ballistic impact, sand erosion, salt corrosion, or thermal shock, as outlined in Table 10.3-VI. Frequency loss is also presented in this table and compares very favorably with that of undamaged blades at the same stress level. The blades used were development-type blades, consequently not of optimum quality.

**TABLE 10.3-VI**  
**RESULTS OF HIGH FREQUENCY FATIGUE TEST**  
**DAMAGED BLADES AT 450°F**  
 $(10^7 \text{ Cycles})$

Blade No.	Type of Damage	Double Tip Amplitude (in.)	Maximum Stress (psi)	First Bending Frequency Loss (%)
S-1	30 caliber, 110 grain steel bullets 1300-	0.4	11,000	3.2
S-4	1500 ft./sec. 3 locations on leading edge	0.4	11,000	3.2
S-14	Sand erosion	0.4	11,000	1.7
S-15	One-inch ice ball 900 ft./sec.	0.4	11,000	1.7
S-16*	Dry salt corrosion 500°F, 100 hrs. 60 ksi prestress	0.4	11,000	3.9
S-20	Thermal shock -65 to 500°F 2000 cycles	0.4	11,000	2.8
S-36	Salt corrosion 100 hr., humid 60 ksi prestress	0.4	11,000	1.6
S-40	Thermal shock -65 to 500°F 2000 cycles	0.4	11,000	2.4
S-43	Salt corrosion 100 hr. humid 15 ksi prestress	0.4	11,000	2.6

\*Blade S-16 was severely deformed in corrosion test.

#### 10.3.4.3 Testing of Undamaged Blades at Room Temperature

Seven E-blades and one S-blade were tested at room temperature through  $10^7$  cycles at various tip deflections. The test results are tabulated in Table 10.3-VII and plotted in Figure 10.3-16. The curve presented in Figure 10.3-16 was the basis for establishing a five percent loss criterion at  $\pm 18,500$  psi, the value subsequently selected as the pure vibratory Point "A" on the room temperature Goodman type diagram presented in Figure 10.3-17.

**TABLE 10.3-VII**  
**RESULTS OF HIGH FREQUENCY FATIGUE TEST**  
**UNDAMAGED BLADES AT ROOM TEMPERATURE**  
 $(10^7 \text{ Cycles})$

Blade No.	Double Tip Amplitude (inch)	Maximum Stress (psi)	First Bending Frequency Loss (%)
S-10	0.4	$\pm 11,000$	1.8
E-101	0.6	$\pm 16,500$	3
E-89	0.7	$\pm 19,300$	7
E-78	0.7	$\pm 19,300$	6
E-149	0.8	$\pm 22,000$	9
E-74	0.8	$\pm 22,000$	10
E-113	0.8	$\pm 22,000$	10
E-125	0.8	$\pm 22,000$	8

### 10.3.5 Internal Damping Investigation

The lack of response of the BORSIC®/aluminum TF30-P-9 third-stage fan blade to mechanical excitation at its first bending natural frequency indicates a high level of internal damping. This phenomenon was investigated in conjunction with the HFF blade test program. The damping logarithmic decrement was experimentally determined for several blades, along with airfoil temperature rise and blade damage.

To conduct this investigation, each blade was instrumented with accelerometers and thermocouples as shown in Figure 10.3-18. Each blade was then excited at room temperature on a shaker table up to 0.6-inch double tip amplitude, and the damping log decrement and temperature were determined.

Figure 10.3-19 presents a comparison of the damping log decrement vs tip amplitude of BORSIC®/aluminum blade R-5, with that of a titanium alloy TF30-P-9 bill-of-material blade. The damping of the composite blade is an order of magnitude greater than that of the titanium blade. This increased damping probably evolves from the interaction of the BORSIC® filaments, at both  $0^\circ$  and  $\pm 45^\circ$  orientations, with the aluminum matrix. Figure 10.3-20 presents the composite airfoil temperature as a function of tip amplitude and span. These data are typical of all blades tested.

A history of 1st-bending HFF cycles apparently increased blade damping. This is illustrated in Figure 10.3-21. The damping log decrement of blade R-8 was determined both before and after HFF testing (0.4 inch double tip amplitude at  $450^\circ\text{F}$  for  $10^7$  cycles). The physical evidence of damage after HFF testing consisted of fluorescent penetrant indications of matrix cracks between the  $\pm 45^\circ$  surface filaments, in an area from the blade platform to midspan. These cracks increased in severity as the HFF testing proceeded, and were most severe at the blade edges and at midchord on the convex surface.

This damage apparently increased the blade damping log decrement by a factor of up to  $2\frac{1}{2}$ , and is assumed to be a result of the effect of the matrix cracks on elastic wave propagation through the blade structure.

The following conclusions were drawn from the high frequency fatigue testing:

- The room temperature bending fatigue limit of the advanced composite blades designed and fabricated under this program has been established as  $\pm 18,500$  psi based on a five percent natural frequency loss in first bending in  $10^7$  cycles.
- The high temperature,  $450^{\circ}\text{F}$ , bending fatigue limit of the blades has been established as 14,000 psi.
- Blade damage such as leading edge ballistic impact, erosion, corrosion and thermal fatigue has no apparent effect on blade fatigue life.
- Composite blades exhibit an internal damping characteristic that is an order of magnitude greater than that exhibited by titanium alloy blades. This, plus an inherent lack of notch sensitivity, greatly enhances their capability to endure a service environment.

#### 10.3.6 Tip Rub Testing

An internal P&WA review team recommended the addition of rig/engine tip rub tests (Section 11.3.1) to ascertain possible detrimental blade effects due to this phenomenon. Before this testing could be incorporated, however, a severe accidental tip rub occurred in the 200-hr. altitude engine test program. This tip rub was discovered after 57 hours of engine test time (following 10.5 hrs. of sea-level Mn 1.2), and was attributed to fan exit case deformation during the high Mn, low altitude testing. It caused several blades to contact the fiberglass rub-strip, and in one area to penetrate to a depth of .090 inch (through the rubstrip and into the titanium case).

As a result of this incident, seven blades exhibited cracks in the fillet area above the platform, and were replaced for the balance of the altitude test program. Several blades also lost approximately  $\frac{1}{4}$  inch of material at the trailing edge tip. This damage was blended, and the blades were reinstalled in the engine.

One of the seven blades having most severe fillet-area cracks (Blade E-184) was subjected to destructive examination to determine the extent of the crack. This investigation is described in detail in Section 11.2.5; it revealed that the crack was confined to the outer crossply layers, and did not penetrate to the radial core plies.

The conclusions drawn from this test are:

- The tip rub was probably more severe than would ever be encountered in normal service.
- No immediate catastrophic blade failure occurred.
- Blade damage was confined to insignificant loss of material at the tip and surface cracks in the airfoil root area.

#### 10.4 COMBINED STRESS/FATIGUE TESTING

Thirteen BORSIC®/aluminum blades were stress/fatigue tested by subjecting them to a vibratory load imposed over a steady radial load. The steady radial load produced the P/A and restrained warping stresses. The total stress field is referred to as combined stress fatigue (CSF).

The blades were prepared by diffusion bonding aluminum alloy pads to the tip area as shown in Figure 10.4-1. A channel parallel to, and equidistant from, the blade stacking line was machined on each surface. A plate was then inserted into each channel and adhesively bonded in position. A third plate, slotted at the free end to accept a cable, was then inserted between the free ends of the two plates bonded to the pad. With the cable in place, steady state loads in excess of 12,000 pounds can be applied to the blade by means of a pneumatic cylinder. Figure 10.4-2 shows the arrangement of the test fixture. The desired chordwise static stress distribution pattern can be achieved by adjusting the location of the cable in the slot. Figure 10.4-3 is a curve which shows the load required to duplicate the static stress levels which would occur at various blade rotating speeds.

During testing, the root of the blade is gripped in a broach block shown in Figure 10.4-4. This fixture can be equipped with as many as six Calrod-type electrical resistance heaters, which are capable of heating the blade root to the 500°F range. To augment the electrical heating, preheated air is blown over the blade root surfaces as well.

The vibratory bending stress was imposed on the blade by vibrating the root about the blade root centerline. This was accomplished mechanically by a 3600 RPM electric motor, acting through a camshaft to provide the required reciprocating motion to the broach block. Figure 10.4-5 shows the test rig used.

Before testing, the blades were instrumented with strain gages to measure the stress distribution on the airfoil. When elevated temperature testing was scheduled, thermocouples were also used. Figure 10.4-6 shows the instrument locations.

Although the test rig allowed adjusting the load and load distribution it was difficult to attain a "balanced" stress distribution in all cases. This is considered to be the primary reason for the scatter in the test data. Figure 10.4-7 presents the ideal (theoretical) chordwise stress distribution just above the blade platform. In the ideal distribution the integrated areas above and below the neutral axis should be equivalent.

A typical stress pattern which resulted in the CSF rig is shown in Figure 10.4-8 and represents the measured strain levels on blade E-166 at room temperature. Despite the skewness of the pattern, this blade performed well in CSF testing as evidenced by the test data. Similar strain patterns were developed for all blades tested, even though they were balanced as well as possible before initiating the test.

#### 10.4-1 Methodology and Results

The blades were divided into three groups:

- Group A consisted of four early development blades, which were tested at 450°F, 100 percent equivalent speed, and vibratory stress levels of 10,000 or 20,000 psi. None of these blades ran out to  $10^7$  cycles.
- Group B consisted of four engine-quality blades tested at room temperature, 100 percent equivalent speed, and at various levels of vibratory stress. The results were quite consistent. The two lowest stressed blades ran out to  $10^7$  cycles, the next blade showed a small crack after  $10^7$  cycles, and the highest stressed blade failed in  $9 \times 10^6$  cycles.
- Group C consisted of five blades tested at 450°F, either 90 or 100 percent equivalent speed, and at various levels of vibratory stress. Results show that all blades stressed to 100 percent equivalent speed failed, two at zero cycles. The blades stressed to 90 percent equivalent speed ran out to  $10^7$  cycles.

The results of these tests are presented in Table 10.4-1.

These data were used to help establish Goodman type diagrams. The resulting diagrams are discussed in paragraph 10.5 of this document.

#### 10.4.2 Recommendation

Because of the difficulty in obtaining uniform blade loading in this purely mechanical type of test rig, it is strongly recommended that future CSF testing be performed in a spin-pit. In a spin-pit environment the steady load will be of a centrifugal nature, and the vibratory stresses can be imposed by exciting the blade at a resonance point with air jets.

TABLE 104-I  
COMBINED STRESS FATIGUE TEST RESULTS

Group	Temp. (°F)	Blade Number	Equiv. Speed (%)	Static Stress (KSI) Core/Shell	Vibratory Stress (KSI)	Number of Cycles (10 <sup>6</sup> )	Result*
A	450	R-12	100	53/42.5	±20	0.36	F
A	450	D-3	100	53/42.5	±10	0.054	F
A	450	D-4	100	53/42.5	±10	1.5	F
A	450	D-12	100	53/42.5	±10	5.24	C
B	RT	E-136	100	53/42.5	±7	10	RO
B	RT	E-140	100	53/42.5	±10	10	RO
B	RT	E-138	100	53/42.5	±12	10	0.3°C
B	RT	E-73	100	53/42.5	±15	9.0	F
C	450	E-154	100	53/42.5	±6	0	F
C	450	E-191	100	53/42.5	±10	0	F
C	450	E-164	100	53/42.5	±10	2.25	F
C	450	E-166	90	43/34.5	±10	10	RO
C	450	E-186	90	43/34.5	±12	10	RO

\*F - Catastrophic Failure

C - Crack

RO - Runout

### 10.5 GOODMAN TYPE DIAGRAMS

The data obtained from the spin-pit burst, fatigue, and combined stress/fatigue tests were used to generate modified Goodman diagrams for the composite blades at both room temperature and 450°F conditions. The latter condition represents the highest temperature the TF30-P-9 third-stage fan blade will encounter at supersonic, high altitude conditions.

Figure 10.5-1 presents the resulting Goodman diagrams. The pure vibratory stress points, plotted on the ordinate, use a five percent loss in first bending frequency as a failure criterion (Reference Figures 10.3-15, -16). The other data points take separation of the airfoil from the root as the failure criterion. The diagrams were based on a total of 73 blade tests, 43 conducted at room temperature and 30 at 450°F.

The room temperature, shell vibratory stress limit was established at 18,500 psi. This value was based on data obtained from eight fatigue tests which were previously discussed in paragraph 10.3.4 of this section. The 450°F, shell vibratory stress limit was established at 14,000 psi and was based on 22 fatigue tests, discussed in the same paragraph.

The room temperature shell steady stress limit was established at 78,000 psi and based on 31 spin pit burst tests. The 450°F shell steady stress limit was established at 63,000 psi and was based on three spin pit tests. The spin-pit burst tests were discussed in paragraph 10.3.3 of this section.

The room temperature combined stress/fatigue limits were established at 42,500 psi steady stress and 12,000 psi vibratory stress and were based on four tests. The 450°F limits were established at 34,500 psi steady stress and 12,000 psi vibratory stress and were based on five tests. These tests were discussed in paragraph 10.3.4 of this section.

Developing the Goodman diagrams prior to engine environmental testing was a requirement of the Aeronautical Systems Division. The diagrams were to be used to accurately assess the probability of the blades successfully passing the simulated sea level and altitude flight tests.

The prediction that the blades would survive the engine environment tests was proved accurate in the subsequent 564-hour engine test program (Section 11.0).

The two engine test data points plotted represent the highest combination of vibratory and steady stress encountered in the sea level engine test program, fully described in Report PWA-4730, "100 Hour Sea Level Subsonic Engine Test of TF30 3rd Stage BORSIC®/Aluminum Fan Blades," with the exception of engine surge conditions where the vibratory stress went as high as 30,000 psi. These stresses were not exceeded in the altitude engine test program, where blade temperature reached 450°F. That program is described in Section 11.0 of this report. With the exception of short-time surge conditions, the highest blade stresses encountered in the entire flight envelope are contained well within the Goodman diagram.

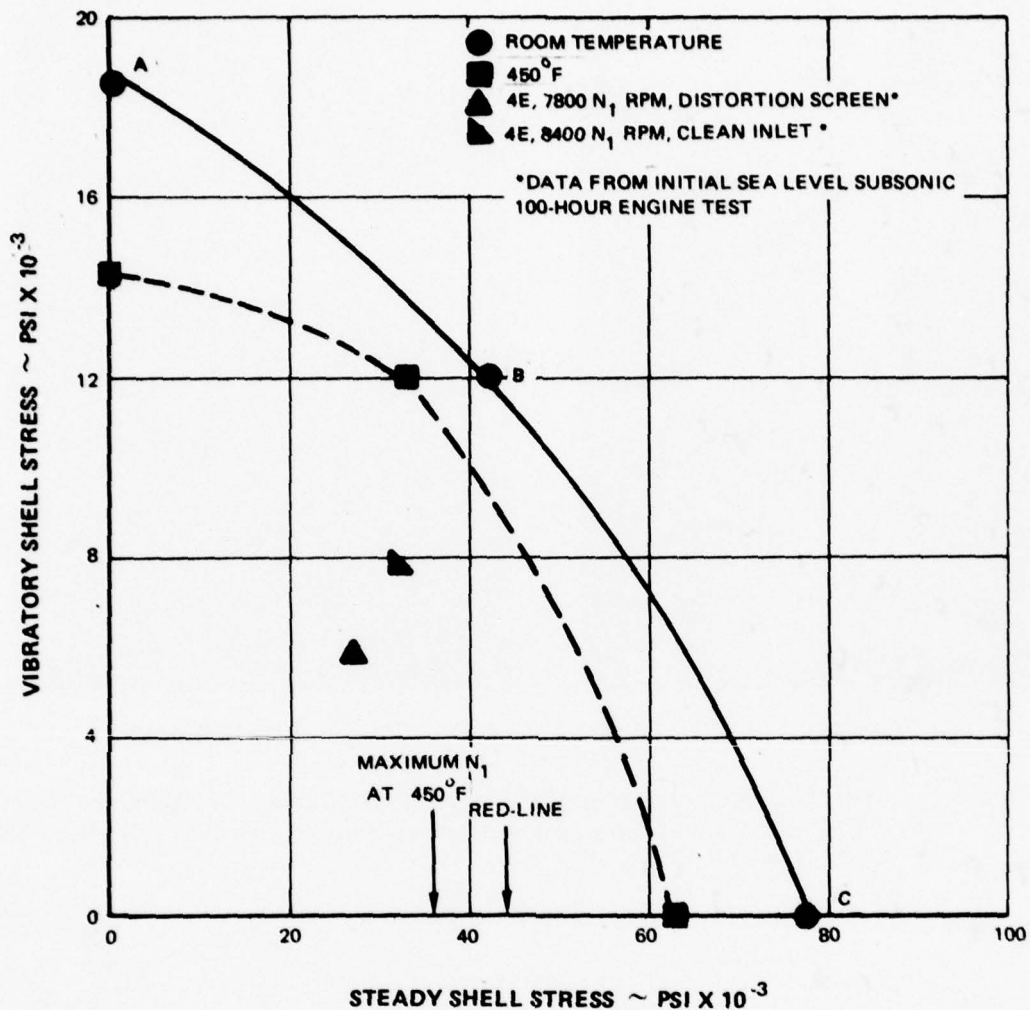
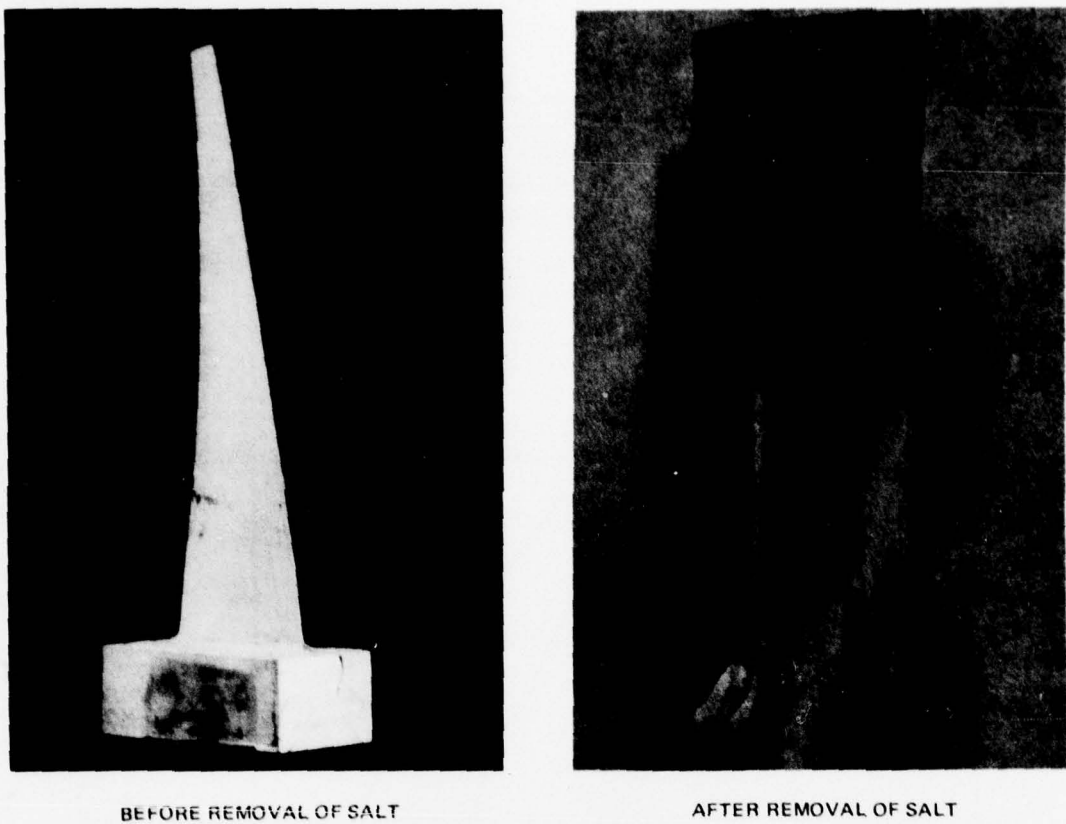


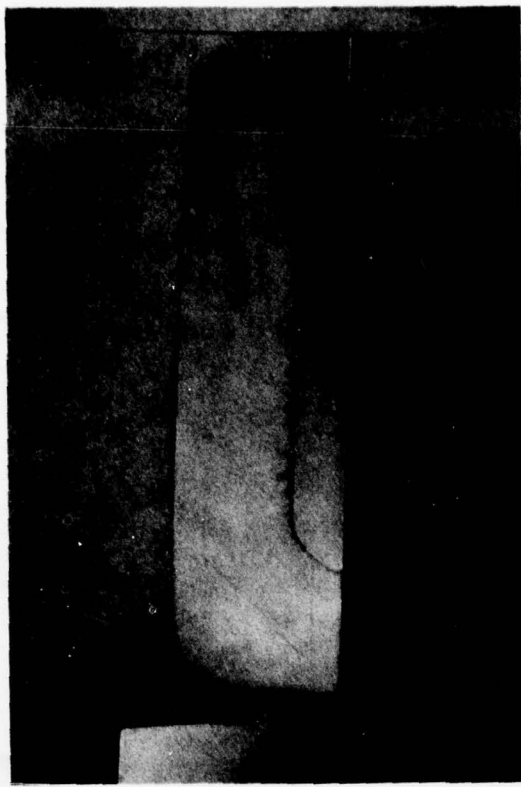
Figure 10.1-1 Goodman Diagram for Room Temperature and 450°F Conditions



*Figure 10.2-1 The BORSIC®/Aluminum Blade Showed No Evidence of Significant Salt Corrosion After an Elevated Temperature (500°F), 100-Hour Salt-Stress-Corrosion Test*



BEFORE REMOVAL OF SALT



AFTER REMOVAL OF SALT

*Figure 10.2-2      Inspection Showed No Discernable Degradation of the BORSIC®/Aluminum Blades After a 100-Hour Salt-Stress-Corrosion Test Under Humid Conditions at 90°F*

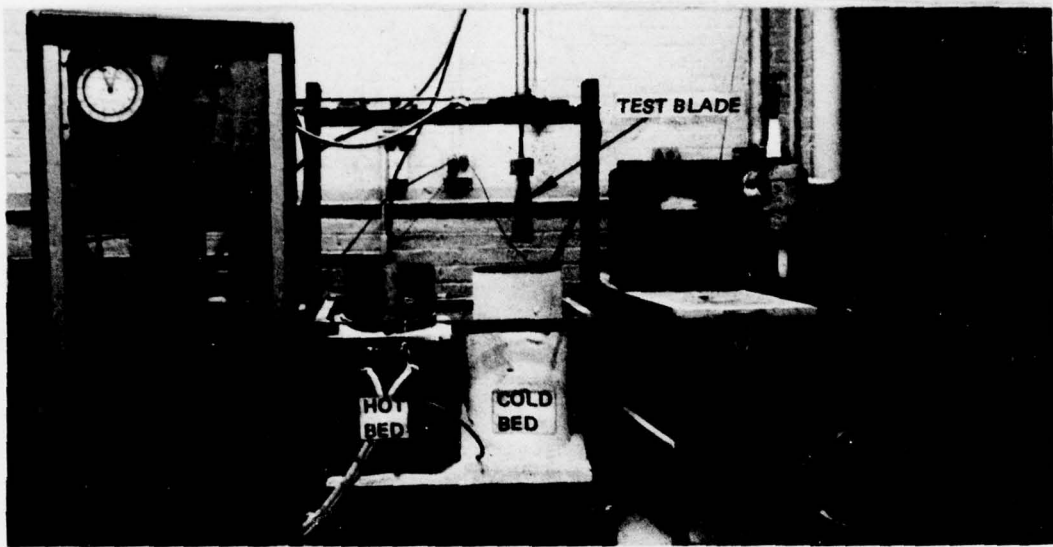
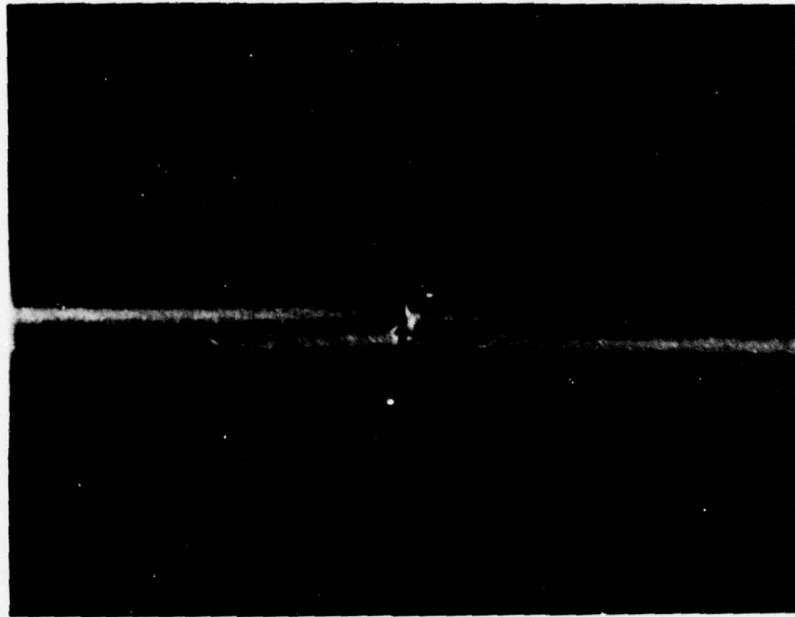
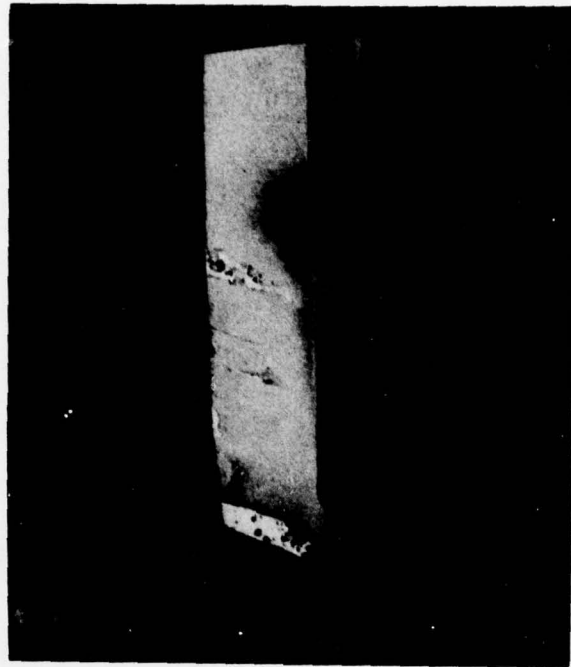


Figure 10.2-3 Fluidized Bed Thermal Fatigue Test Rig Used for Thermal Shock Tests



*Figure 10.2-4 Nickel/Cobalt Leading Edge of Blade S-20 After 80 Thermal Cycles Showing Crack Caused By Pit in Leading Edge; Mag =7X*



**Figure 10.2-5** Concave Side of Composite Fan Blade D-17 Showing Condition After FOD Spin Test.  $N = 10,360$  rpm,  $T = 70^{\circ}\text{F}$ , FOD With 75 grams of Sand  
(XPN-26814)

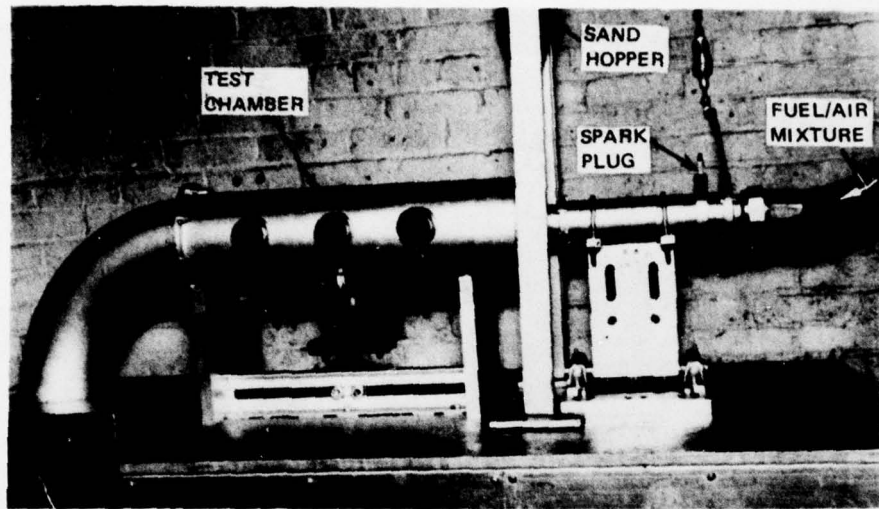
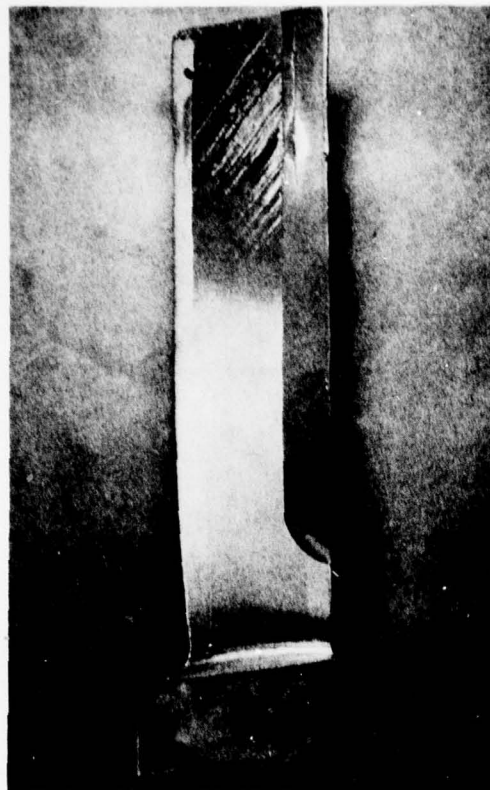
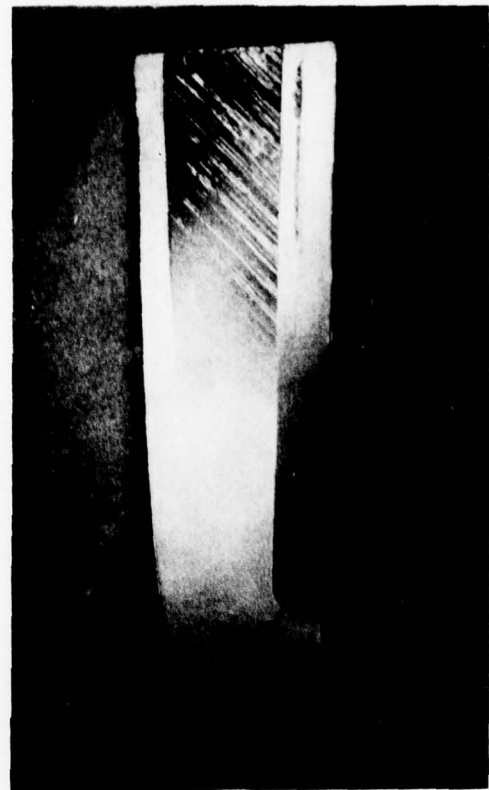


Figure 10.2-6 *Particulate Erosion Rig Used for Static Testing at Both Room and Elevated Temperatures*



BLADE S-14 ERODED WITH 100 LB  
SAND AT 3 LB/MIN



BLADE S-28 ERODED WITH 360 LB  
SAND AT 1 LB/MIN

*Figure 10.2-7 BORSiC®/Aluminum Blades Following Erosion Tests*

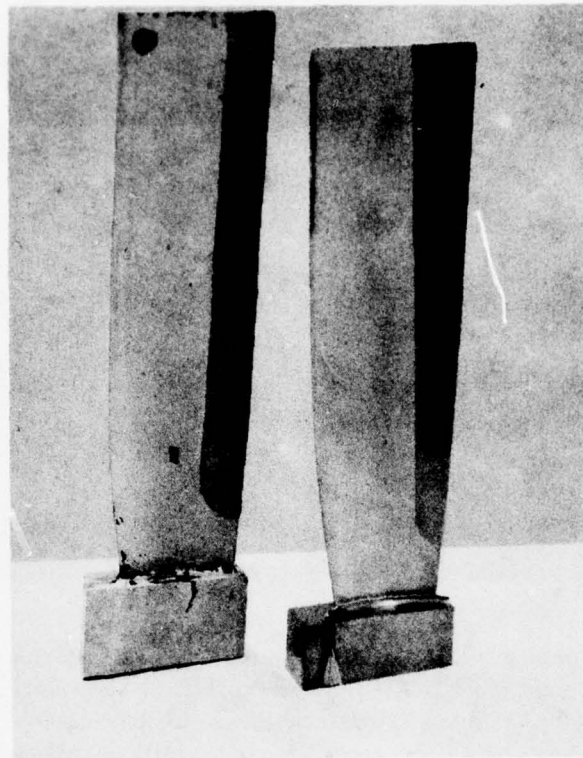


*Figure 10.2-8 Comparison of Composite Blades With Nickel-Cobalt Leading Edge Protection;  
Blade on Right Has Increased Protected Area*

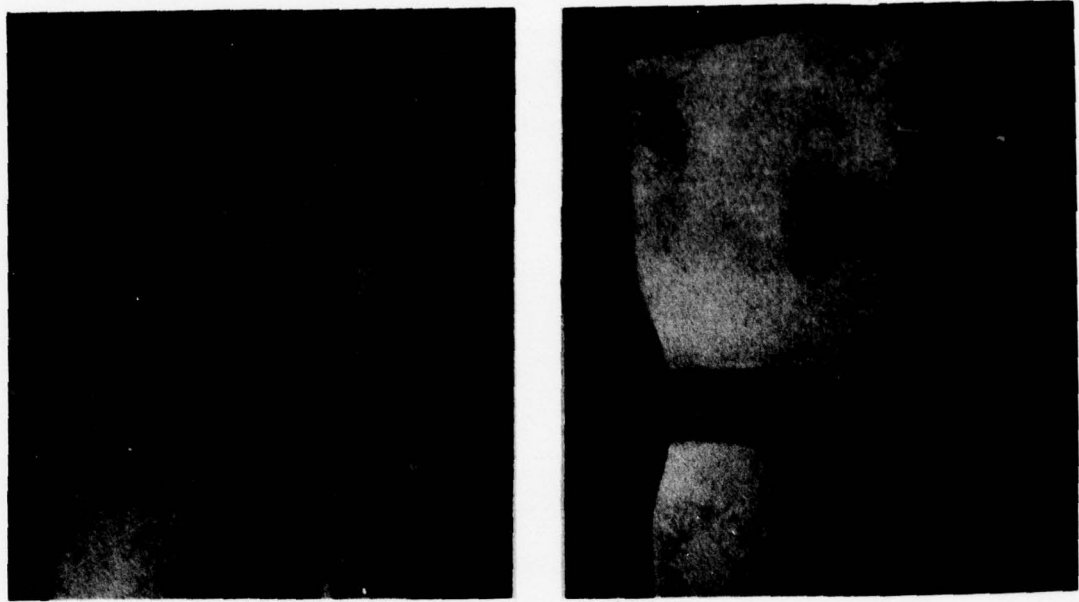


*Figure 10.2-9 Comparison of Blades Subjected to High-Temperature Static Erosion Test:  
Composite Blade With Nickel-Cobalt Leading Edge (Left); Titanium TF30  
Bill-of-Material Third-Stage Blade (Right)*

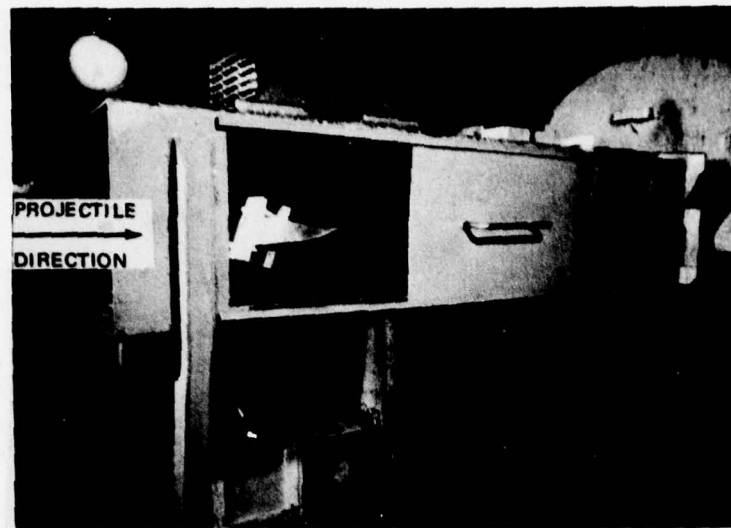


*Figure 10.2-10 Small Object Static Ballistic Impact Test Rig*

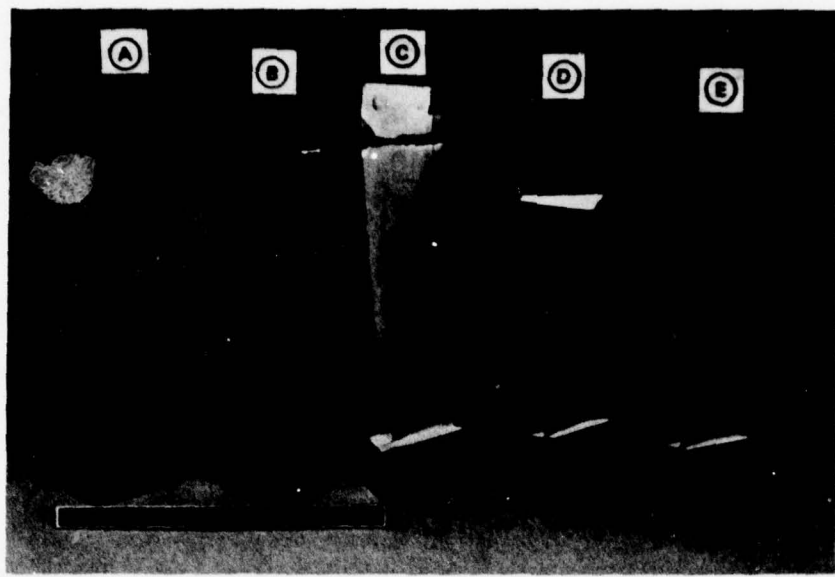


**Figure 10.2-11** Post-Test Condition of Ballistic Impacted Fan Blades; (A) Unprotected Composite Blade, (B) Composite Blade With Hard Nickel Leading Edge, (C) Composite Blade With Nickel-Cobalt Leading Edge, (D) TF30-P-9 Titanium Blade; (E) Composite Blade With Boron Carbide Leading Edge  
(CN-29585)

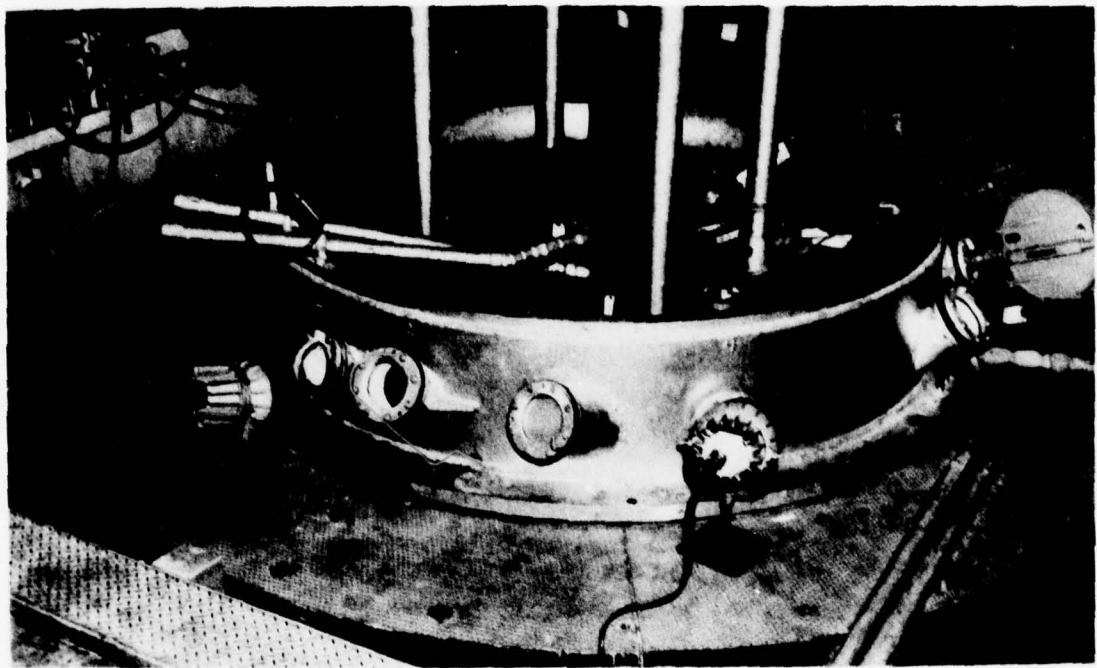


*Figure 10.2-12 Small Object Dynamic FOD Impact Test Facility*

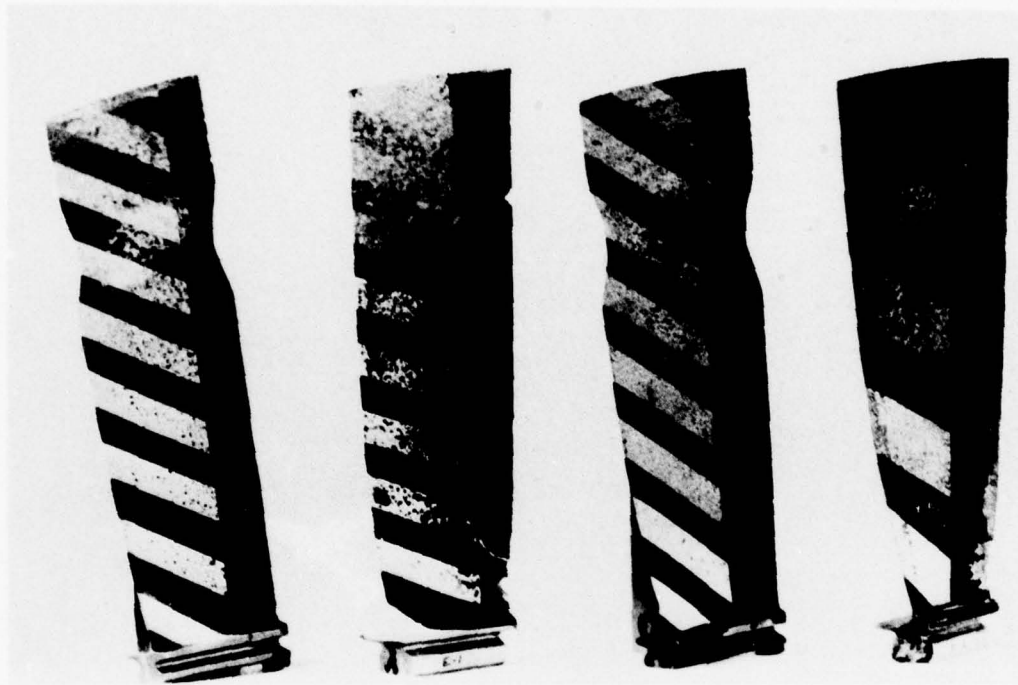


*Figure 10.2-13 Comparison of Concave Sides of Bill-of-Material Titanium Fan Blades and BORSIC® Fan Blades After 66 Strikes per Blade With 1/4-Inch Quartz Gravel at Room Temperature and at 10,360 rpm*

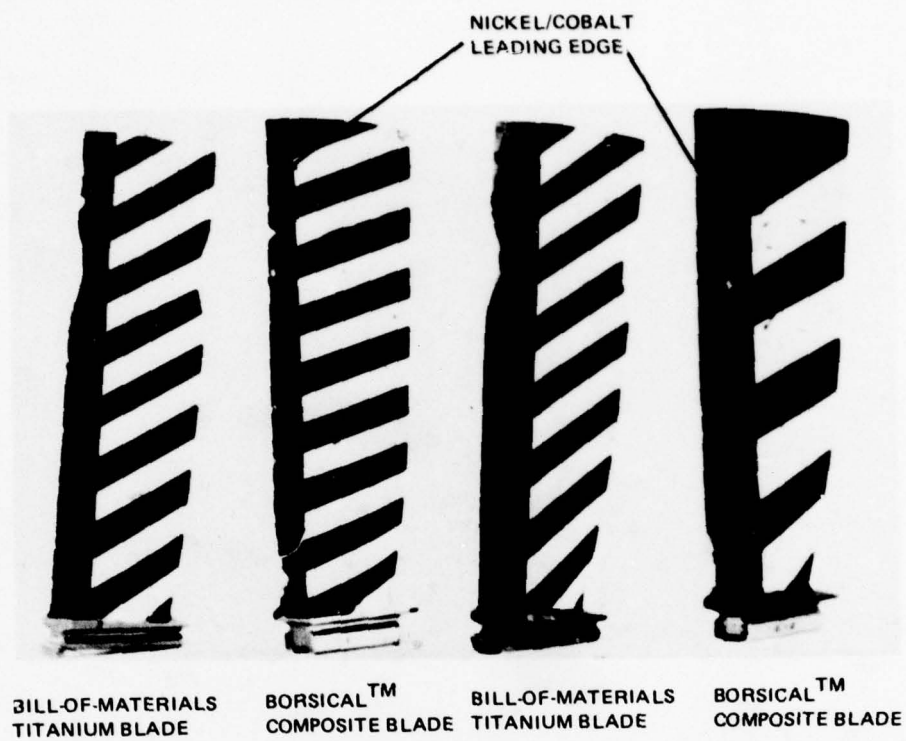
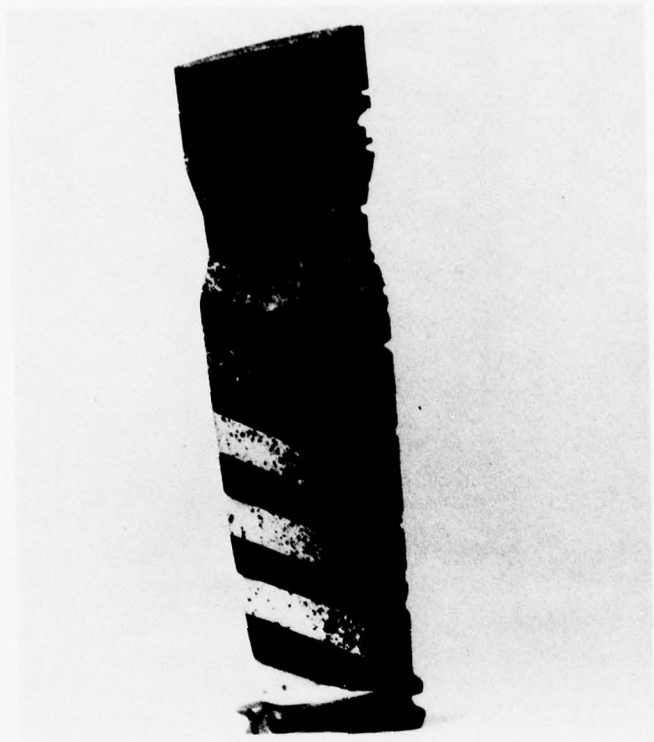


Figure 10.2-14 Comparison of Concave Sides of Bill-of-Materials Titanium Blades and BORSICAL<sup>®</sup> Fan Blades After 66 Strikes per Blade With  $\frac{1}{4}$ -Inch Quartz Gravel at Room Temperature and 10,360 rpm



*Figure 10.2-15      Appearance of Bill-of-Material Titanium Fan Blade After 23 Strikes With 1/2-Gram Steel Rivet at Room Temperature and at 10,360 rpm.*



Figure 10.2-16      Appearance of BORSiC<sup>®</sup>/Aluminum Fan Blade After 23 Strikes With 1/2-Gram Steel Rivet at Room Temperature and 10,300 rpm. Lost material was about twice that of titanium blade.



*Figure 10.2-17 Damage Sustained by Blade E-216 After Being Impacted With a Single One-Inch Tempered Ice Ball*

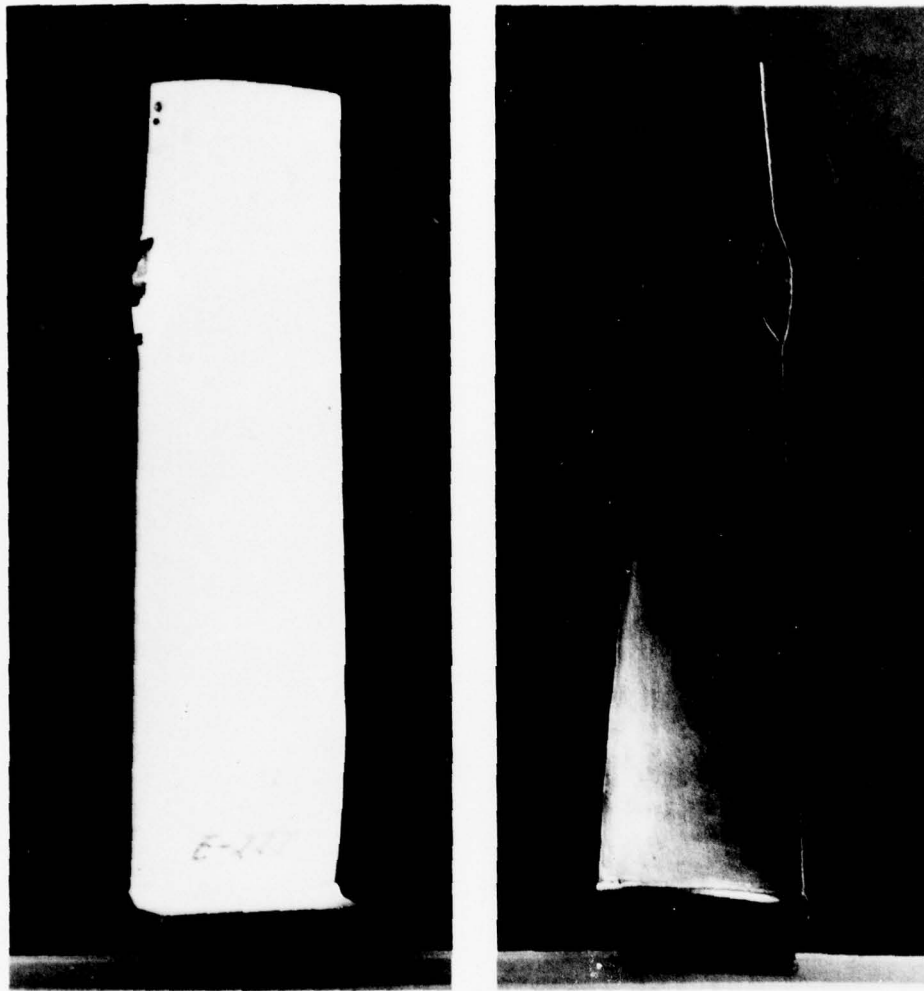


Figure 10.2-18      *Blade E-227 Sustained This Damage After Three Impacts of One-Inch Tempered Ice Balls*



*Figure 10.2-19 The Effect of Leading Edge Thickness on FOD. Blade at Right Had 0.025-inch L.E. Radius and Sustained Only Slight Dents When Impacted by Six One-Inch Tempered Ice Balls. Blade at left had 0.015-inch L.E. radius and sustained damage shown after three such impacts.*

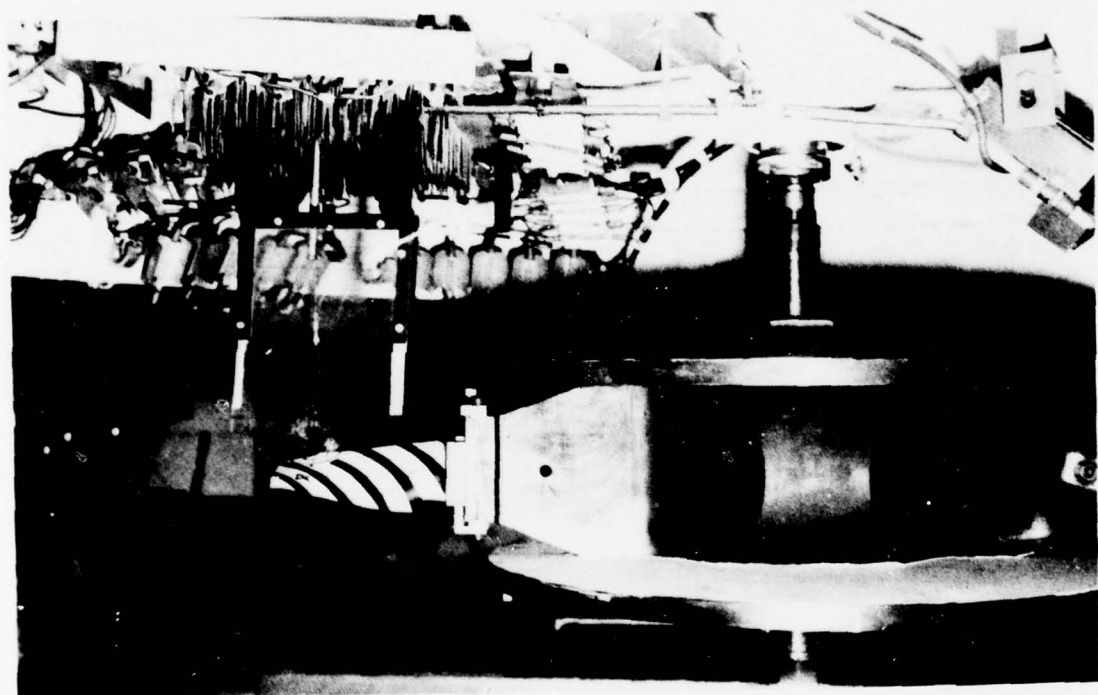


Figure 10.2-20 Single Blade FOD Tests – Multiple Impact Drop Mechanism Configuration.  
(A) Object Drop Mechanism, (B) Wind Screen.

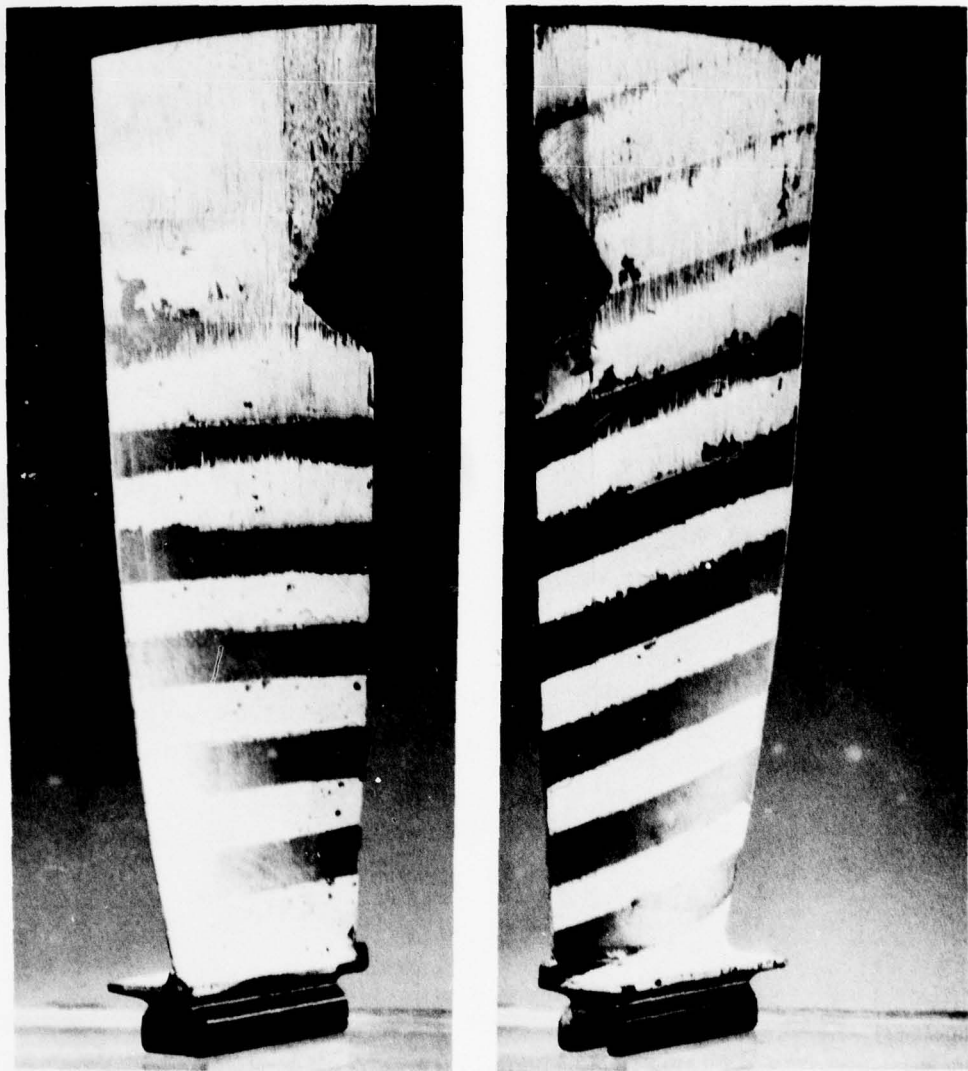
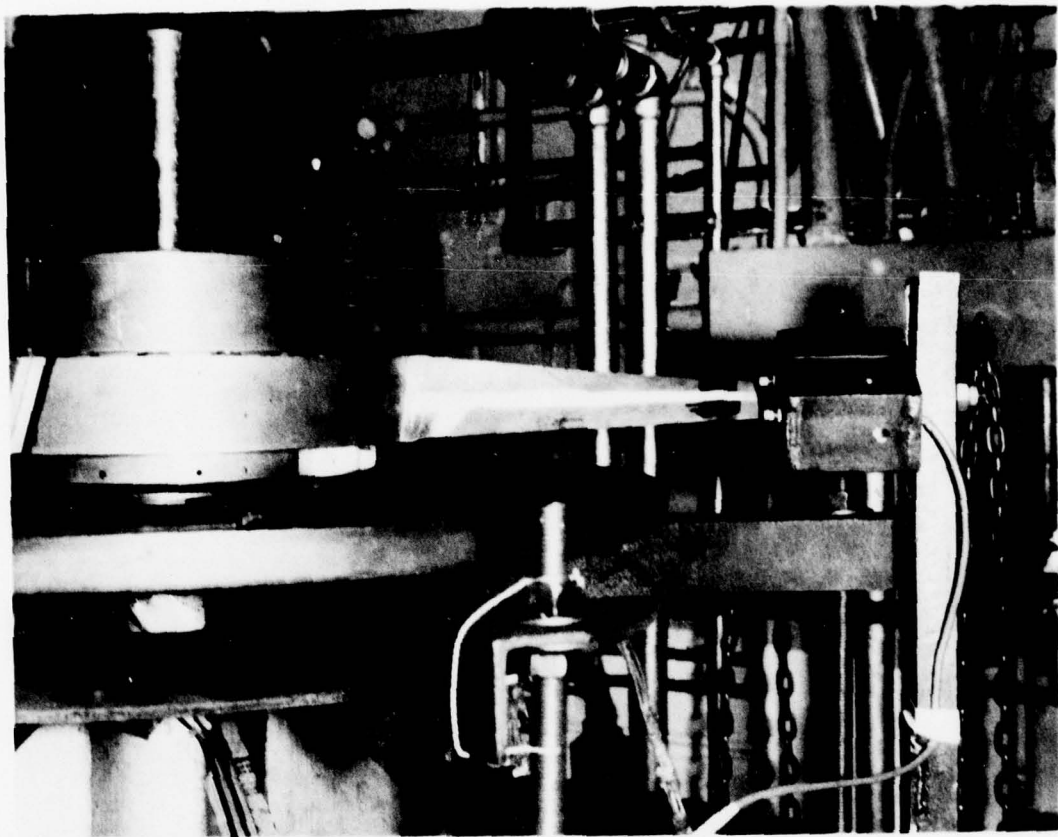


Figure 10.2.21     Damage Sustained by BORSIC<sup>®</sup>/Aluminum Blade in Massive FOD Test. Projectile  
was 6 oz. jelly ball.



*Figure 10.3-1 Spin-Pit Test Rig Used to Conduct Blade Unit twist Tests at Engine Operating Conditions*

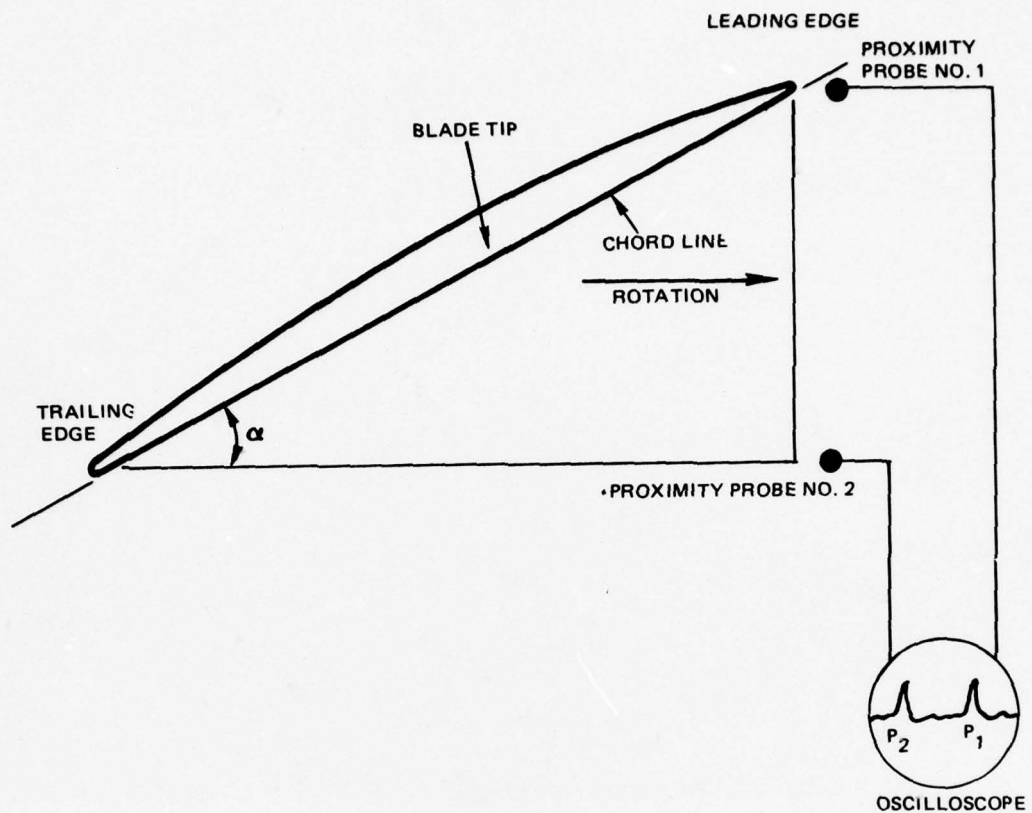


Figure 10.3-2 Location of Proximity Probes Used to Determine Blade Untwist

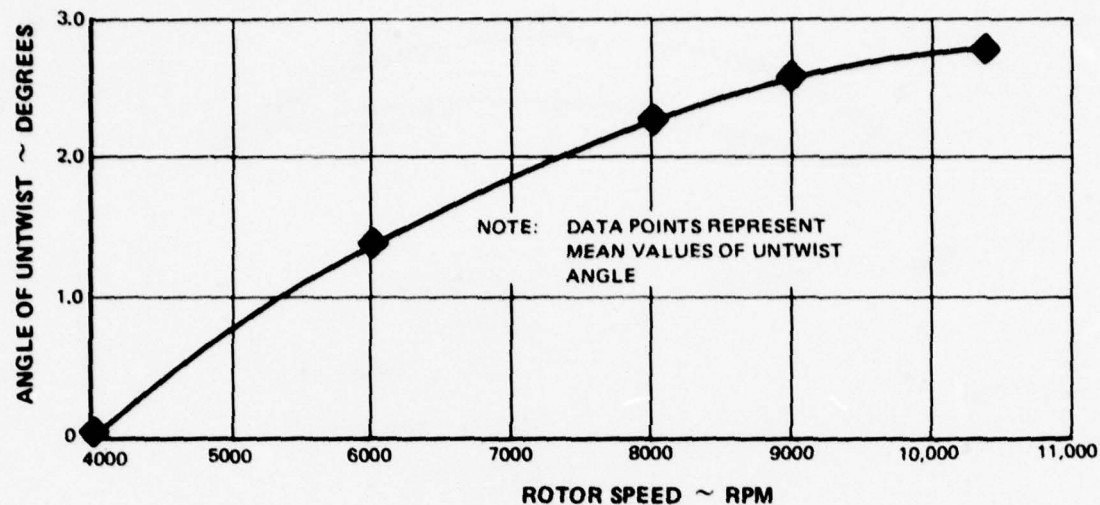
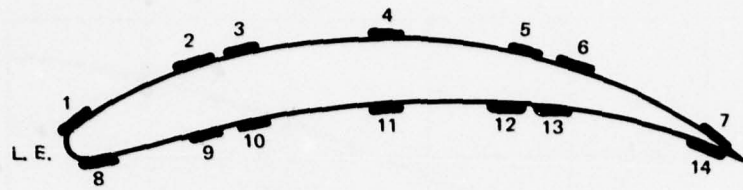


Figure 10.3-3    *Experimentally Determined Angle of Untwist for BORSIC<sup>®</sup> Fan Blade D-2 at 450°F*

PRATT & WHITNEY AIRCRAFT GROUP



<u>GAGE NO.</u>	<u>GAGE LOCATION</u>
1	CONVEX L.E.
2	CONVEX .6" (FROM L.E.)
3	CONVEX (NEAR .6" GAGE)
4	CONVEX RMT
5	CONVEX (NEAR .6" GAGE)
6	CONVEX .6" (FROM T.E.)
7	CONVEX T.E.
8	CONCAVE L.E.
9	CONCAVE .6" (FROM L.E.)
10	CONCAVE NEAR .6" GAGE
11	CONCAVE RMT
12	CONCAVE NEAR .6" GAGE
13	CONCAVE .6" (FROM T.E.)
14	CONCAVE T.E.

Figure 10.3-4 Location of Strain Gages Used to Conduct Test One of the Static Stress Survey on the BORSIC®/Aluminum Blades

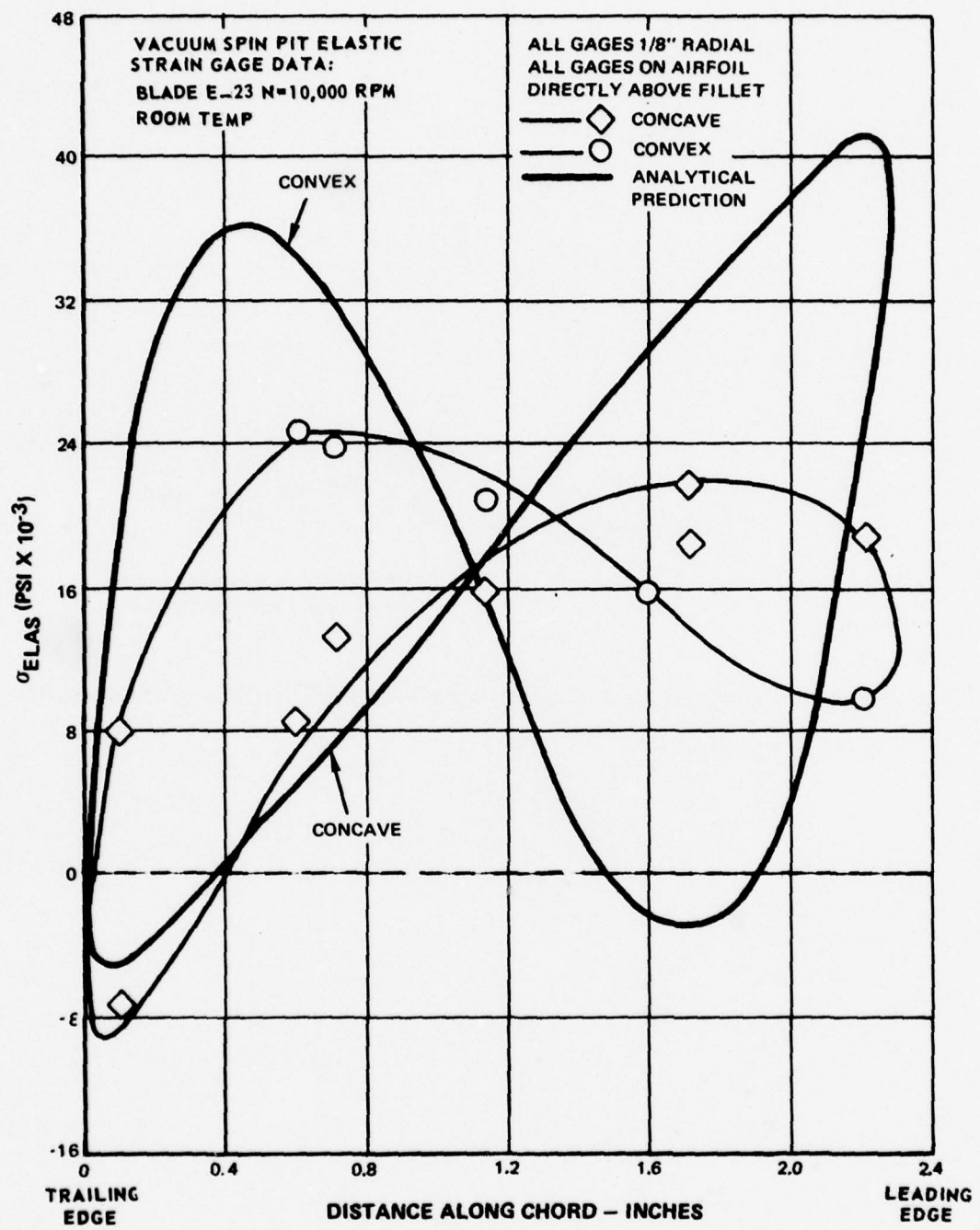


Figure 10.3-5 Comparison of Actual and Predicted  $P/A$  and Restrained Warping Stresses

PRATT & WHITNEY AIRCRAFT GROUP

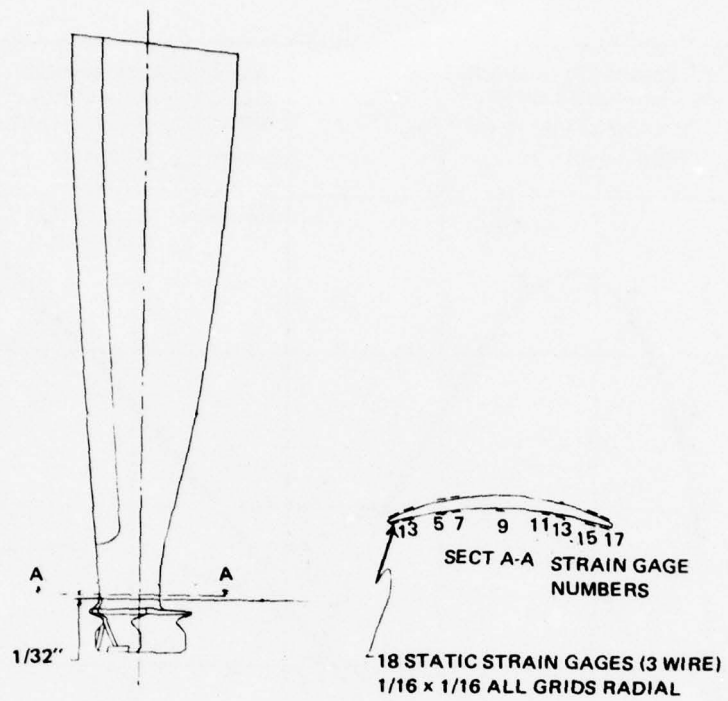


Figure 10.3-6 Location of Strain Gages on the Blade Airfoil Test Two of the Static Stress Survey

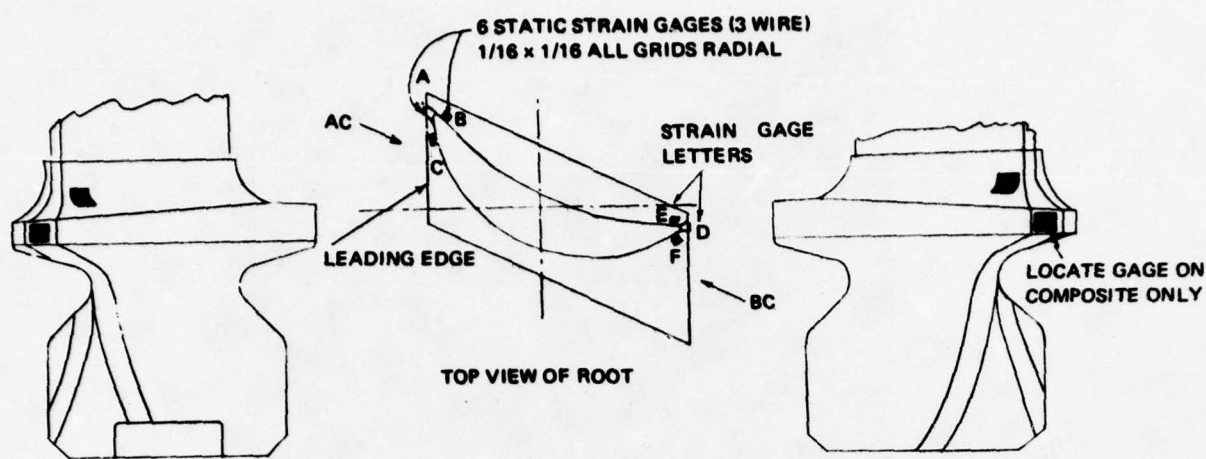
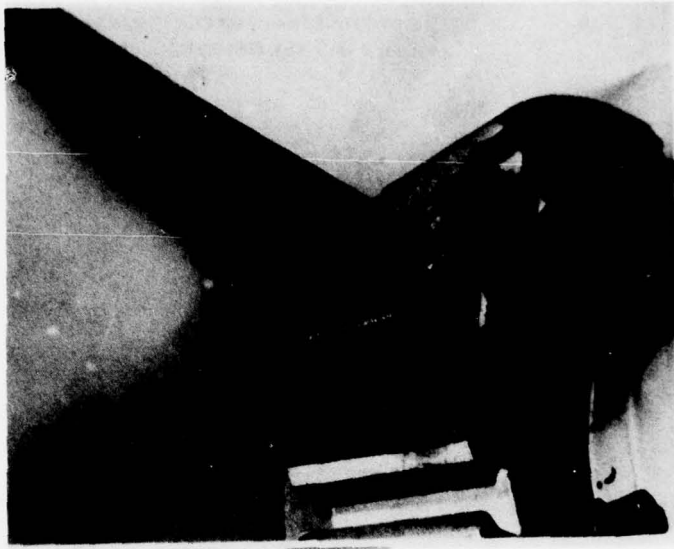


Figure 10.3-7 Location of Strain Gages in the Blade Platform Area for Test Two of the Static Stress Survey



*Figure 10.3-8 . Strain Gage Instrumentation Leads on Disk for Test Two of the Static Stress Survey*

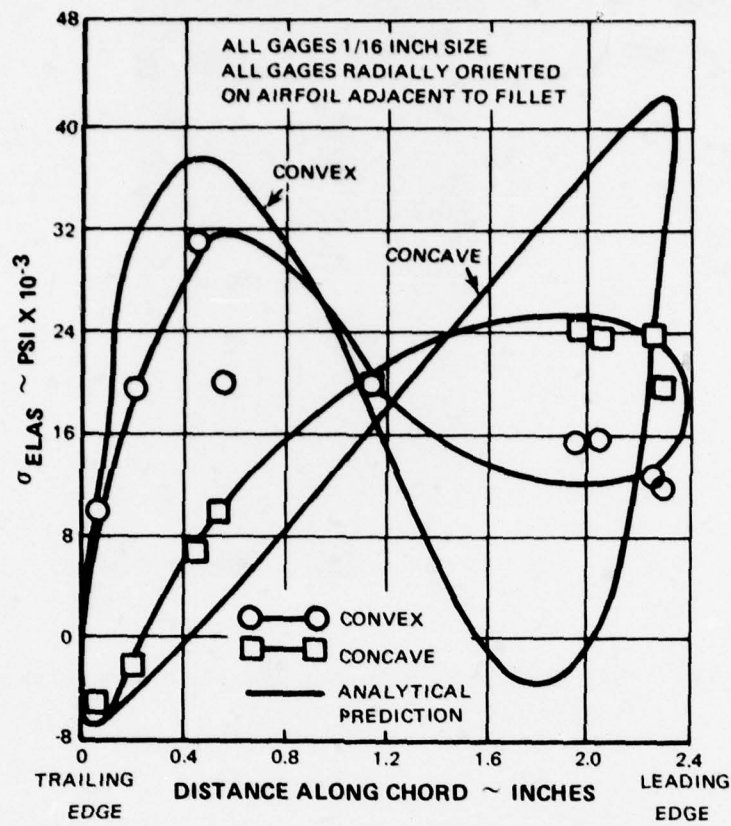
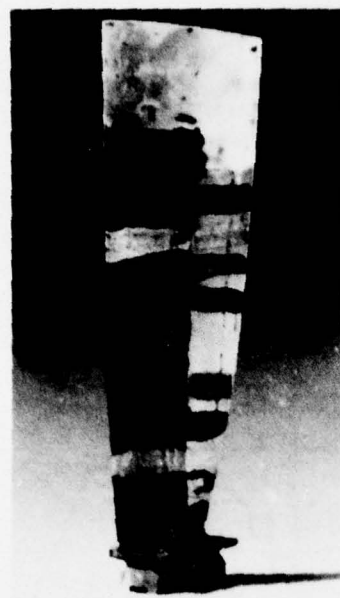
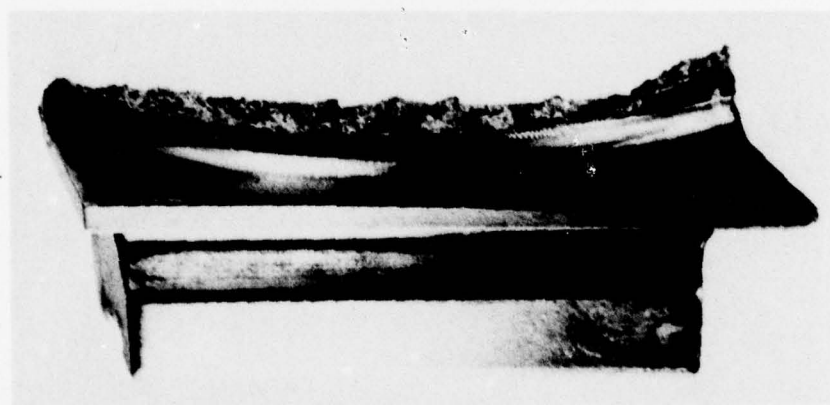


Figure 10.3-9 Elastic Strain Gage Data From Vacuum Spin Pit Testing of Blade E-92 at Room Temperature and 10,000 rpm



*Figure 10.3-10 Blade R-10, an Early Development Blade, Survived an Extensive Spin-Pit Proof Test in Excellent Condition*



*Figure 10.3-11 Typical Failure Mode of BORSIC®/Aluminum Fan Blade During Burst Tests*

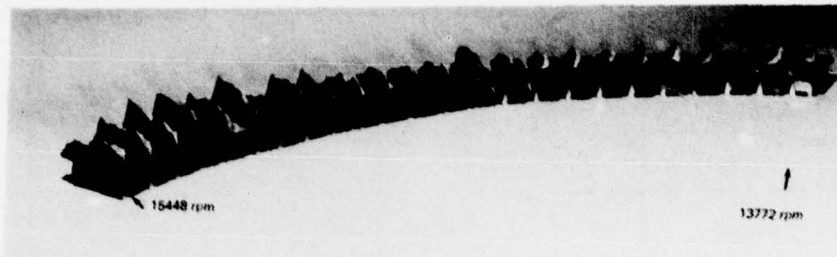


Figure 10.3-12 E-Blade Root Sections Following Burst Test, Arranged in Order of Burst Speed (XPN-31709)

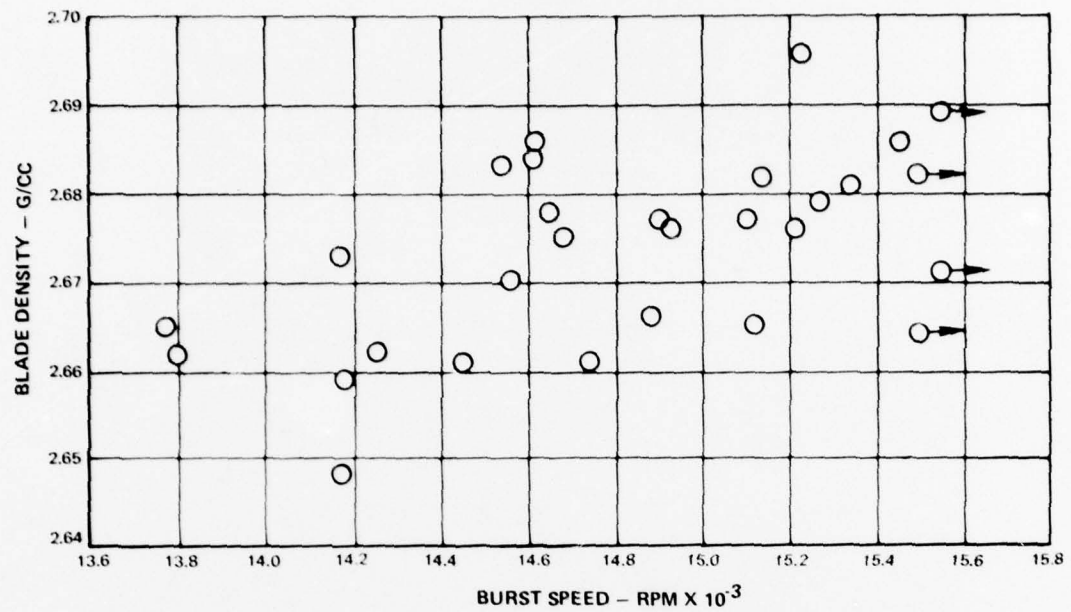


Figure 10.3-14 Plot of Burst Speed Versus Blade Density

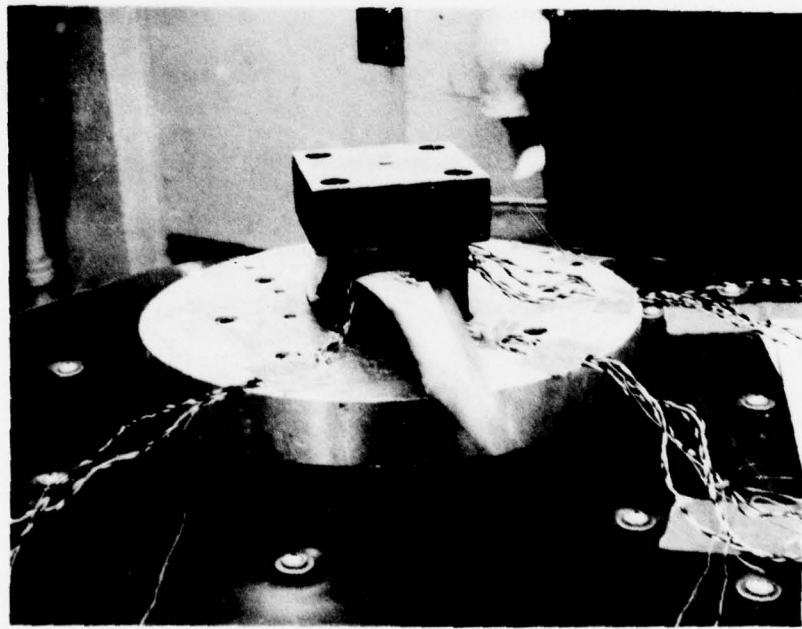


Figure 10.3-14 Damping/Fatigue Test of Composite Fan Blade With Leading Edge Protection

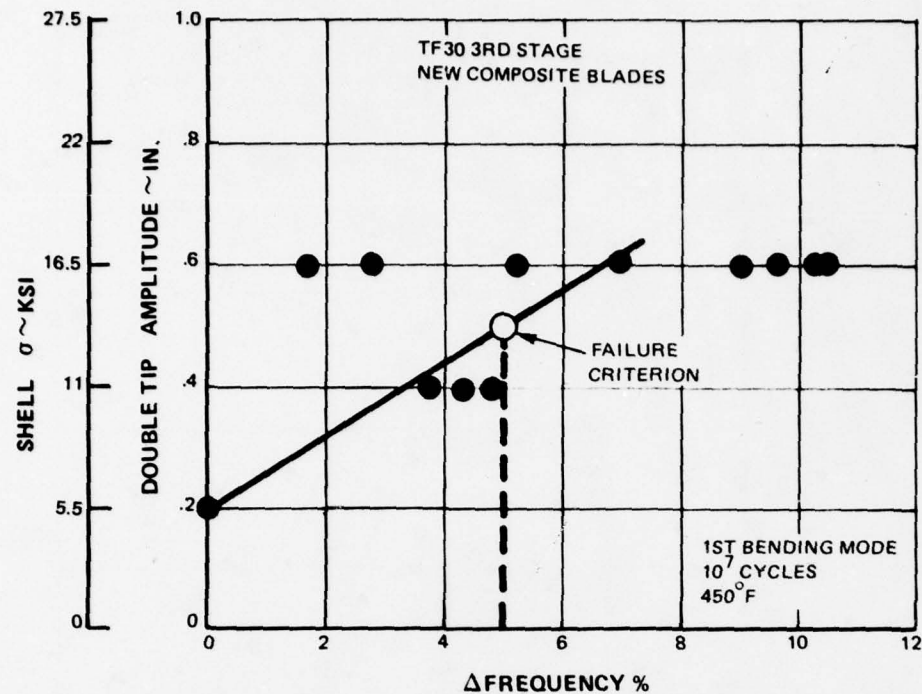


Figure 10.3-15 Results of High Frequency Fatigue Test Conducted on Undamaged Blades at 450°F

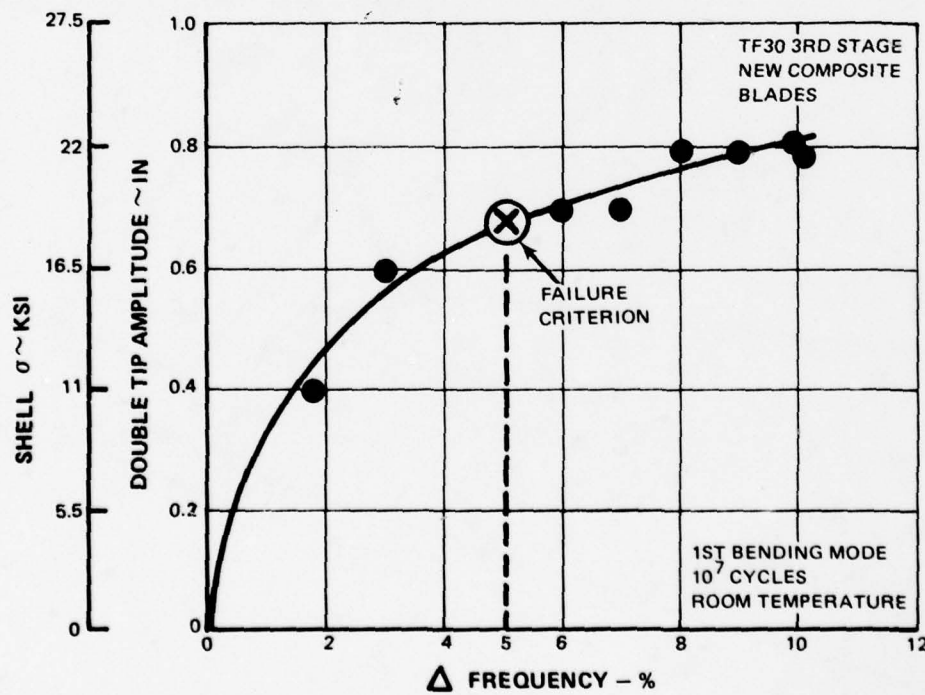


Figure 10.3-16 Results of High Frequency Fatigue Tests Conducted on Undamaged Blades at Room Temperature

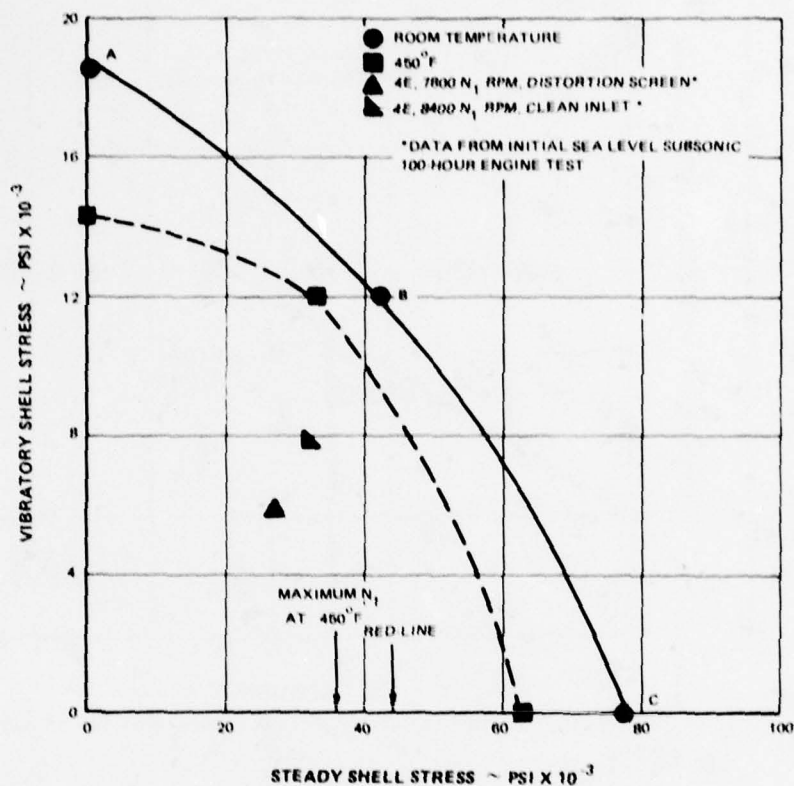


Figure 10.3-17 A Five Percent First Bending Frequency Loss at  $\pm 18,500$  psi at Room Temperature Was Selected as a Failure Criterion

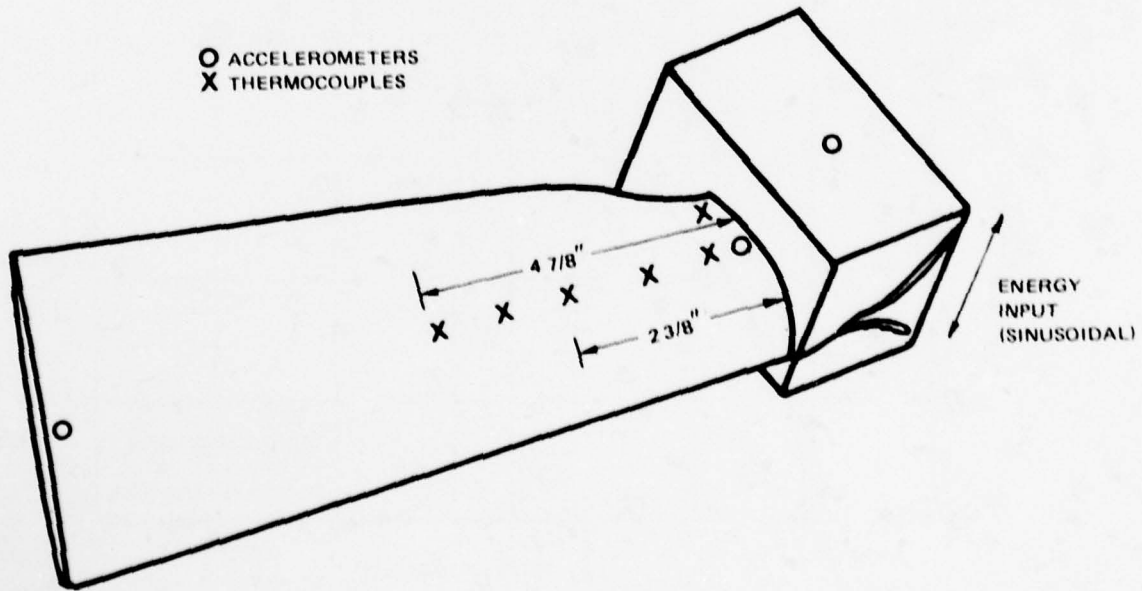


Figure 10.3-18 Instrumentation Locations for Conducting the Internal Damping Investigation

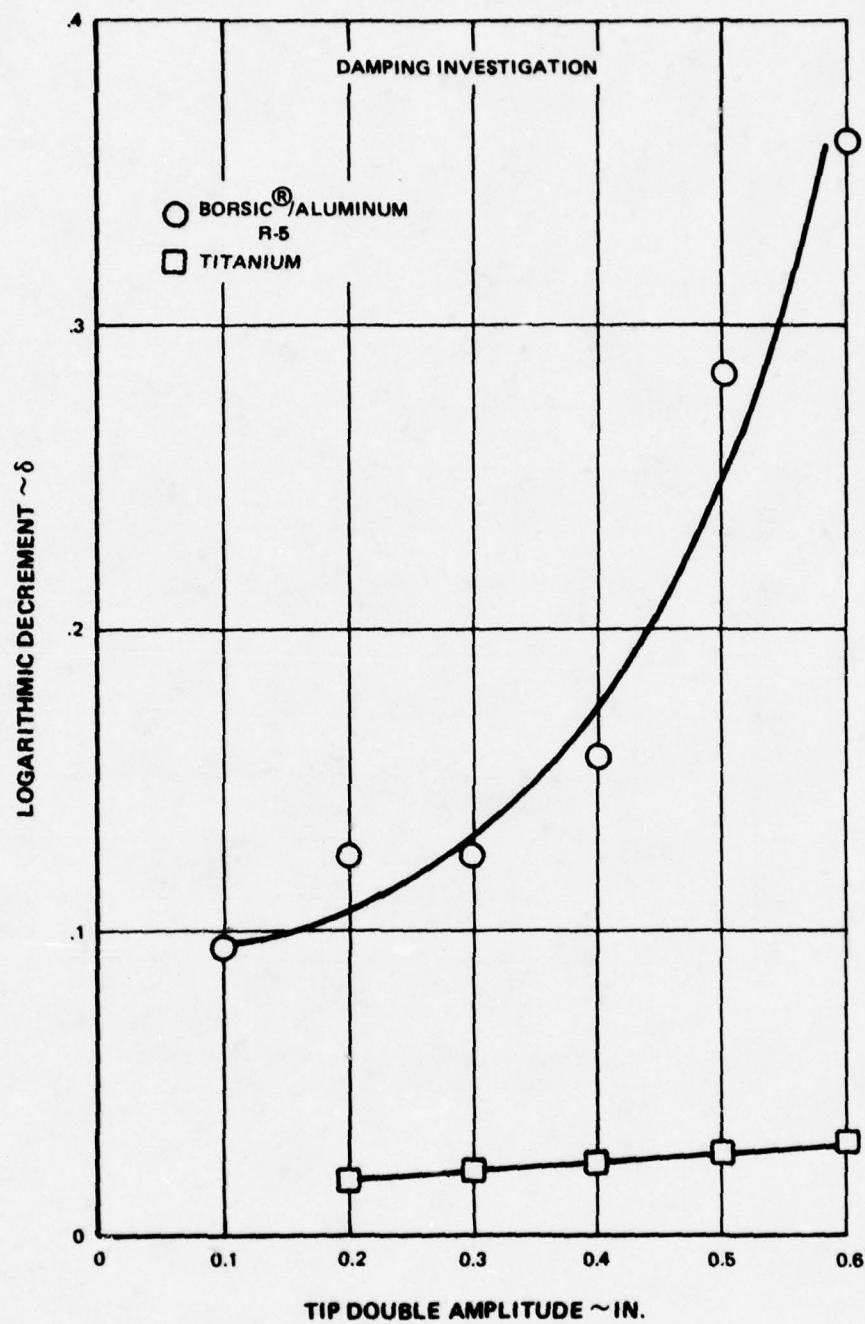


Figure 10.3-19 Comparison of the Damping Log Decrement Versus Tip Amplitude of BORSIC®/Aluminum and Titanium B/M Blades

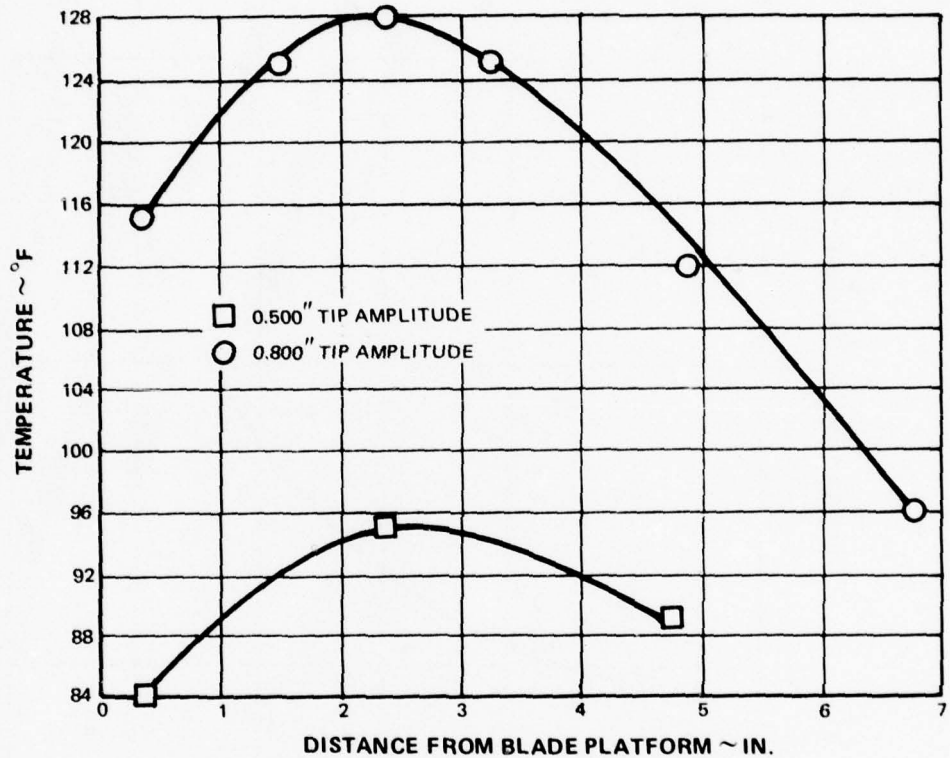


Figure 10.3-20 BORSIC®/Aluminum Airfoil Temperature as a Function of Total Tip Amplitude and Span (Room Temperature Shake Table Tests)

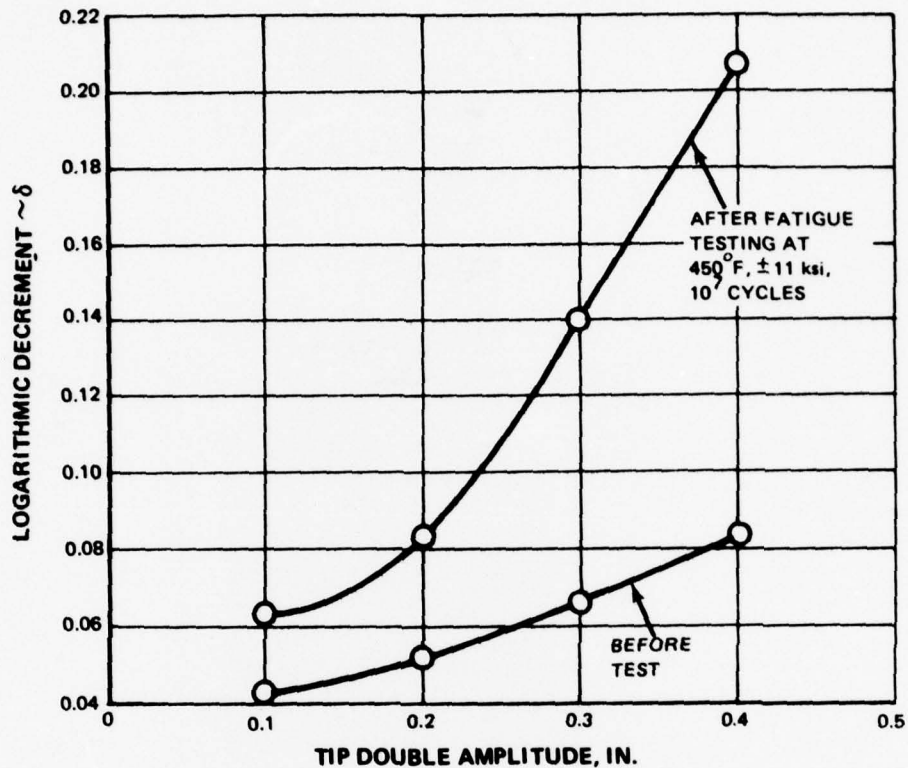
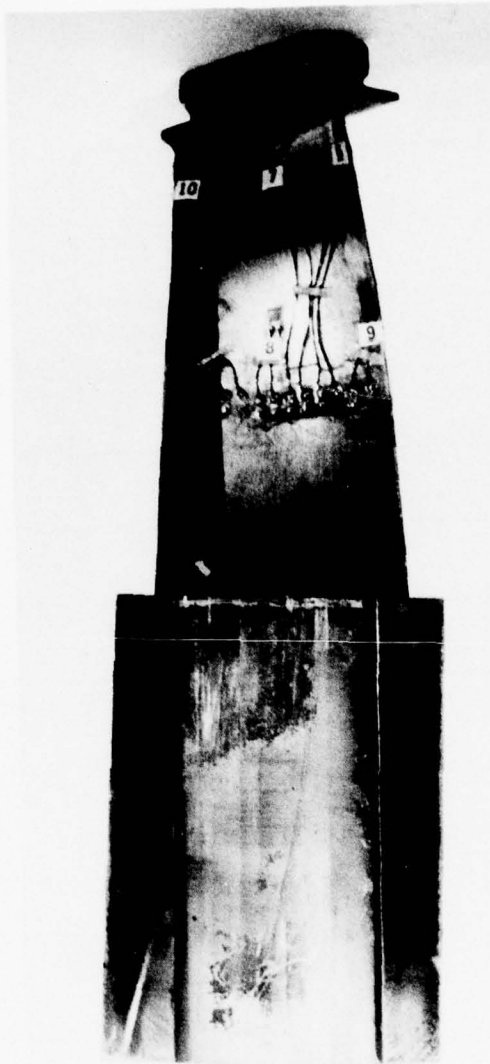


Figure 10.3-21 Bending Fatigue Testing Increased BORSIC®/Aluminum Blade Damping



*Figure 10.4-1 E-Series Blade with Aluminum Tip Pads Diffusion Bonded to the Airfoil for  
CSF Testing (XPN-31707)*

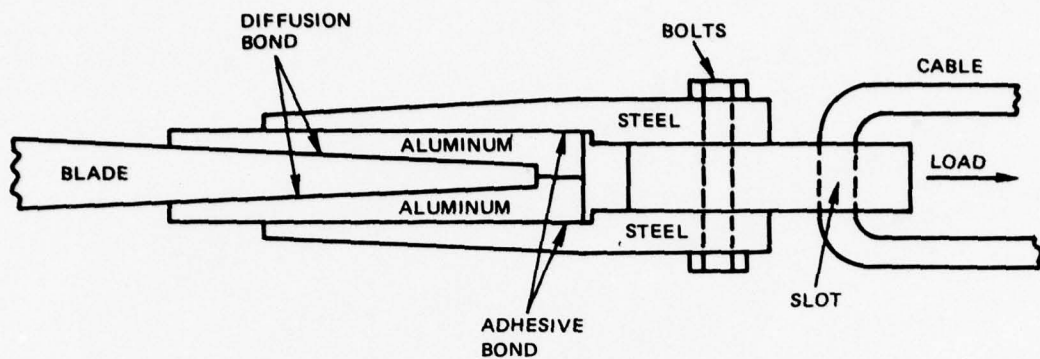


Figure 10.4-2 Blade Gripping Technique Used for Combined Stress Fatigue Testing

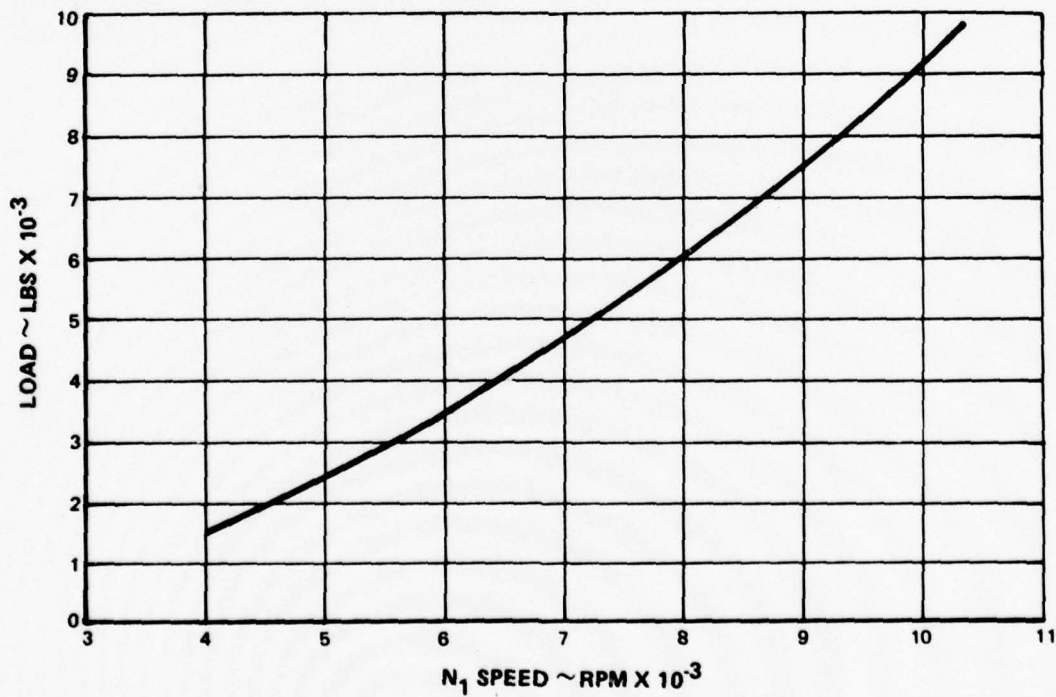


Figure 10.4-3 Static Radial Load Required to Duplicate Blade Stress at Operating Speeds

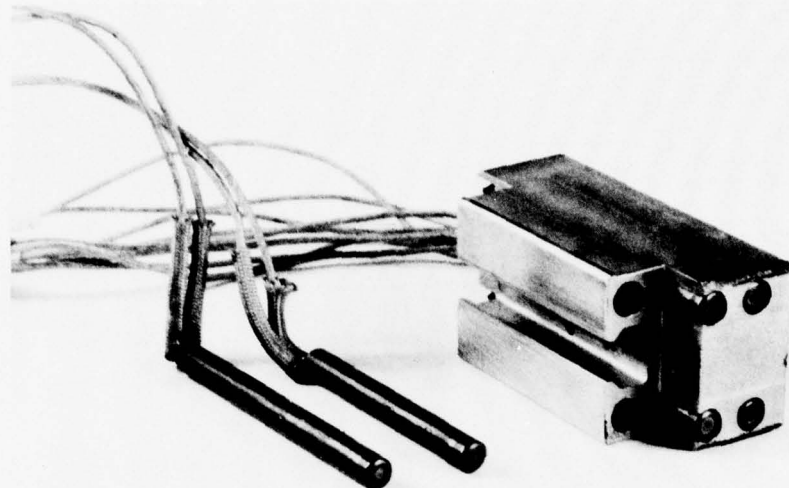


Figure 10.4-4     Composite Blade Root Block Holding Fixture Showing Heating Elements  
(XPN-12856)

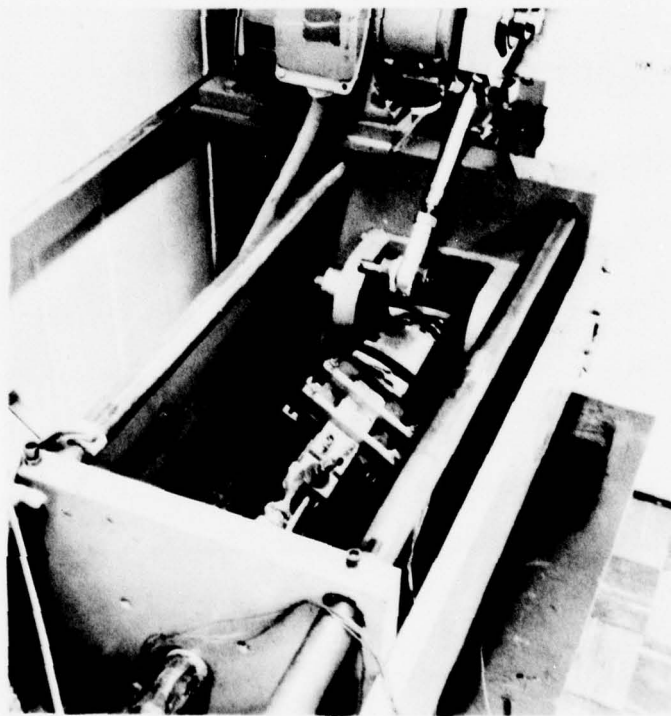


Figure 10.4-5     Test Rig for Combined Stress Application to Blades     (X-32242)

PRATT & WHITNEY AIRCRAFT GROUP

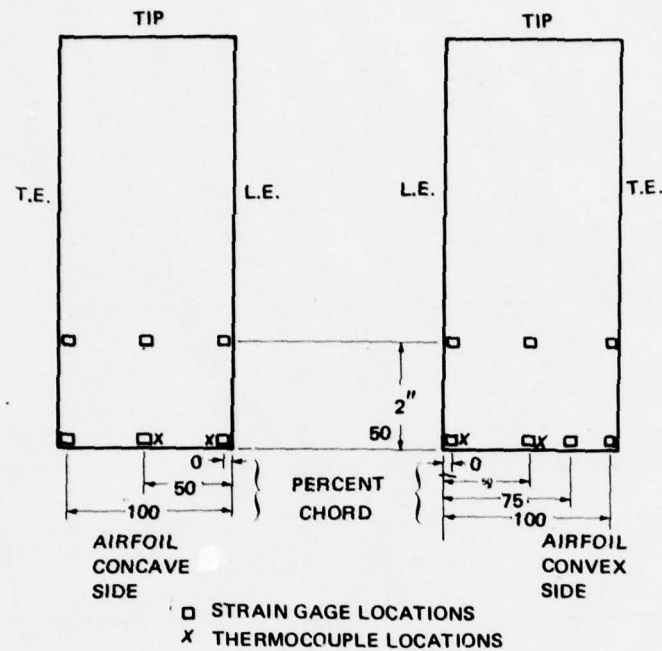


Figure 10.4-6 Approximate Instrumentation Locations for Combined Stress/Fatigue Testing

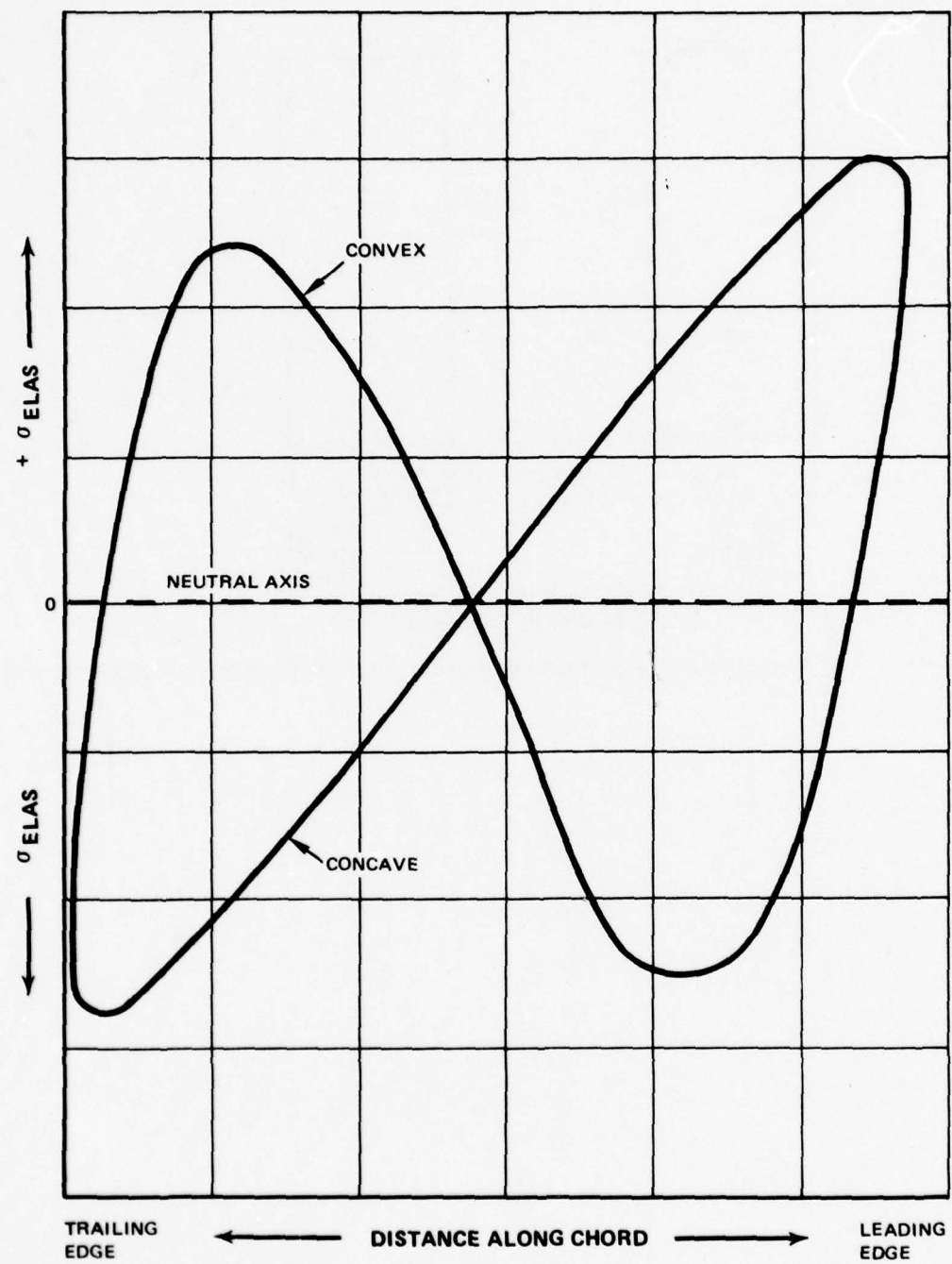


Figure 10.4-7    Ideal Chordwise Stress Distribution Just Above Blade Platform; Areas Above and Below the Neutral Axis Are Equal

PRATT & WHITNEY AIRCRAFT GROUP

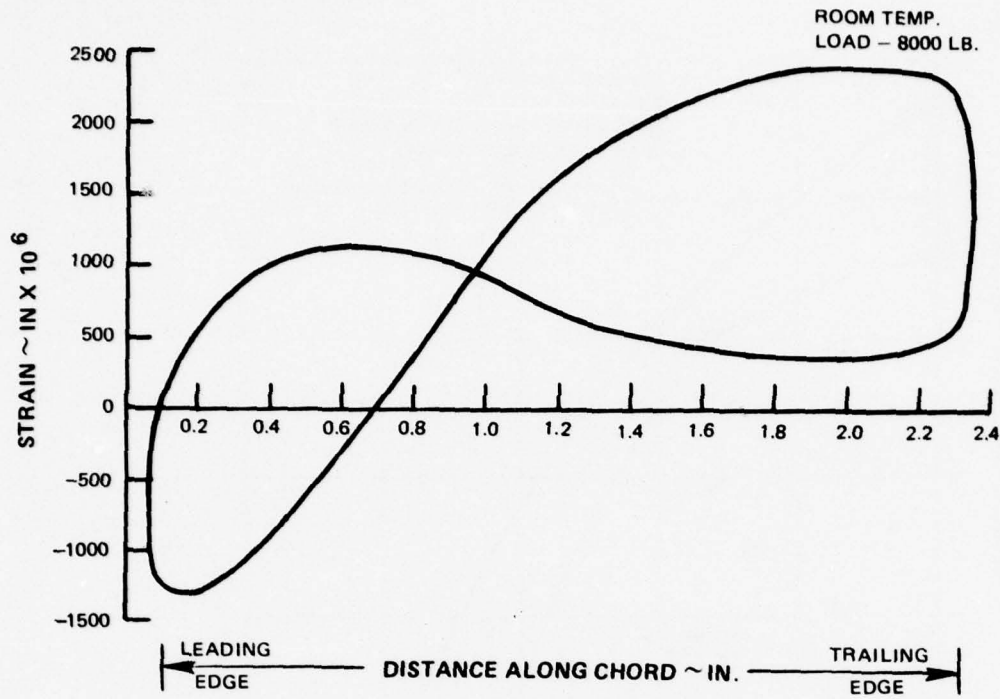


Figure 10.4-8 Strain Distribution on Blade E-166 in CSF Rig

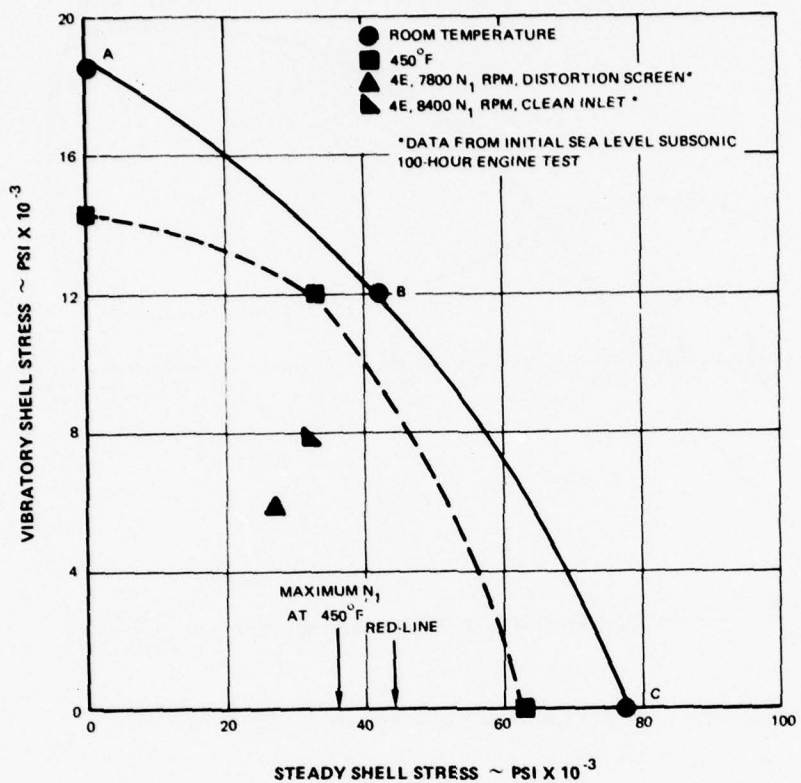


Figure 10.5-1 Data From Spin-Pit Burst, Fatigue, and Combined Stress/Fatigue Tests Were Used to Generate the Room Temperature and 450°F Goodman Type Diagrams

## 11.0 ENGINE ENVIRONMENTAL TESTING

The test vehicle used to conduct engine environmental testing of the BORSIC®/aluminum blades designed and fabricated under this program was a TF30-P-9 engine. Figure 11.0-1 shows the engine. A total of 564 hours engine environmental testing was conducted on two full sets of third-stage composite fan blades. Operation of the blades throughout the entire flight envelope, including supersonic and altitude conditions, was investigated and the blades performed well at all operating conditions.

The first set of blades (Set No. 1) underwent 364 hours of testing at sea-level conditions which included 314 hours of cyclic endurance testing. The first 100 hours of this test were fully documented in the interim report, PWA-4730, 100 Hours Sea-Level Subsonic Engine Test of TF30 3rd Stage Borsic-Aluminum® Fan Blades, dated 14 May 1973. A summary of this report as well as a description of an additional 264 hours of sea level endurance testing is presented in Section 11.1.

The second set of blades (Set No. 2) shown in Figure 11.0-2, was tested for 200 hours at supersonic/altitude conditions, including 120 hours at Mn 2.2, 56,000 ft. and 10 hours at Mn 1.2, sea level. This testing, completed in August 1973, is fully reported in section 11.2 below.

In September 1973, a joint P&WA/AF review of the entire engine test program was held, and as a result the blades were judged acceptable for use in a flight evaluation program in F-111 aircraft, with the stipulation that the blades must be removed and inspected on the bench after the initial 200 hours of operation. A summary of this review, plus the findings of a previous P&WA internal review in the 1st quarter of 1973, is presented in Section 11.3.

### 11.1 SEA LEVEL TESTING

In January, 1973, a full set of 36 TF30-P-9 third-stage fan blades, constructed of BORSIC®/aluminum composite material, successfully completed a 100 hour engine test at sea-level subsonic conditions. No special limitations were imposed on the test parameters or the test program, which included stress surveys, performance calibration, distortion and stall tolerance, as well as 50 hours of endurance testing. A total of 19 deliberate stalls were induced during the program.

Maximum vibratory stress peak recorded on the blades was 7,900 psi at the blade root leading edge (LE) except during surge when transient stresses as high as 33,000 psi were seen. Maximum rotor speed was 10,500 rpm and maximum recorded blade temperature was 214°F.

Aerodynamically, the shroudless rotor exhibited performance parameters equivalent to those of the bill-of-materials (B/M) rotor. Its stall margin with seventh-stage bleeds closed was also equivalent to that of the B/M rotor. With seventh-stage bleeds open there was possibly a slight loss of stall margin at the higher speeds. However, it is extremely difficult to pinpoint a stall setting with the seventh-stage bleeds open, a fact which must be considered when interpreting this data.

Structurally, the type of shroudless blade design used, shown in Figure 11.1-1, does have resonances in the operating range-specifically 2E/first bending mode at about 5000 rpm and 3E and 4E/second bending mode at higher speeds. However, the stress survey revealed no resonant stress peaks above 8,000 psi and no flutter, even with distortion. Surge stresses of approximately 33,000 psi occurred, which is comparable to those seen on B/M blades.

The 50-hour endurance program included engine operation at normal, military and maximum power, plus many snap accelerations and decelerations, including nearly 200 from idle to maximum power.

Following the 100-hour test, the composite blades were thoroughly inspected by NDI techniques. The only effect seen was a loss of natural frequency of approximately two percent which does not affect the capability of the blades to operate in an engine environment. No cracking, splitting, or delamination occurred, nor were any dimensional changes seen. The blades were judged to be completely acceptable for further engine operation.

It is emphasized that no special limitations were placed on the test program because of the presence of the composite fan blades. The entire practical subsonic operating envelope of the engine was explored, with limits imposed only by the capabilities of the test stand or of the engine itself.

#### 11.1.1 Engine Buildup

A TF30 experimental engine, No. X-433, was assembled to the P-9 configuration for this program although several deviations from the P-9 B/M were incorporated to accommodate the third-stage composite blades and required instrumentation. The deviations are presented in Table 11.1-I.

**TABLE 11.1-I**  
**DEVIATIONS TO TF30-P-9 B/M CONFIGURATION**

<u>Part Name</u>	<u>Part Number</u>	<u>Bill of Material</u>
*2nd-Stage Disk	559502B SKL555117	559502D
*2-3 Spacer	562058 SKL55118	562058
2-3 Air Seal	713246 SKL55119	562054
3rd-Stage Fan Blades (36)	713603	616503
3rd-Stage Disk	713703	569503 SKL43888
3rd-Stage Fan Blade Locks (36)	661920	NA

\*Slotted to accommodate instrumentation leads

Table 11.1-II presents pertinent data about Blade Set No. 1 including raw material used, physical characteristics, and NDI results. At the time of the engine build, listed as build No. 24 for this engine, the majority of the engine parts had a total of 1380 hours previous run-time including 969 hours of endurance. A completed TF30-P-9 engine is shown in Figure 11.1-2.

### 11.1.2 Instrumentation

#### 11.1.2.1 Stress Survey

In order to determine composite blade operating characteristics during engine operation and to evaluate the effect of the composite blades on fan stage operation, four second- and seven third-stage fan blades were strain gaged for the composite blade engine test. Strain gage locations were established, as shown in Figure 11.1-3. Figure 11.1-3 also shows the circumferential location of the strain-gaged blades in the disk. This placement facilitates determining the magnitude and direction of travel of nonintegral-order engine excitations throughout the engine operating range. Two third-stage blades were also equipped with thermocouples to verify engine operating temperatures.

Thirty-eight M-M WD-DY-125AD-350-B87 strain gages were installed with M-610 adhesive. Kapton leads were soldered to the strain gage leads and routed down the airfoil using GA-60 cement. Four chromel-alumel thermocouples were fabricated by tackwelding the junction and then cementing it down with 3012 silver epoxy. The five mil C/A wires were routed along the airfoil using GA-60 cement to the splice area, where they were tackwelded to C/A duplex wire.

#### 11.1.2.2 Performance

Instrumentation was added to the build of X-433 to evaluate engine performance. The following measurements were made:

1. Low compressor entrance total temperature
2. Low compressor entrance static and total pressures
3. Low compressor discharge total pressure
4. Low compressor discharge total temperature
5. Fan duct entrance total pressure
6. Fan duct entrance total temperature
7. High compressor discharge total pressure
8. High compressor discharge total temperature
9. Primary burner discharge total temperature
10. Turbine discharge total temperature
11. Turbine discharge/fan duct discharge mixed total pressure
12. Low rotor speed
13. High rotor speed
14. Low compressor discharge static pressure
15. High compressor discharge static pressure
16. Burner pressure
17. Primary burner fuel flow
18. Total (primary and afterburner) fuel flow

TABLE 11.1-II  
TF30 COMPOSITE ENGINE TEST BLADES  
(Set No. 1)  
Listed in Order of Disk Location

Blade No.	Density $\frac{\text{lb}}{\text{in.}^3}$	Natural Frequency $\frac{1}{\text{Hz}}$	<u>1B</u>	<u>2B</u>	<u>1T</u>	Acoustic Emission $\frac{\text{CCV}}{\text{C.C.V.}}$	Tape Strength KSI	Tape Panel	Ultrasonic C-Scan Root	Airfoil.	X-P <sub>25%</sub>	FPI	Heat Treat.	Proof Spin	Weight oz.	Remarks
79	2.679	142	457	979	13/11	590/131	181.7	OK	OK	OK	OK	OK	B-6	OK	6.63	
105	2.658	140	441	948	51/13	590/100	347/197.3	OK	OK	OK	OK	OK	B-6	OK	6.62	
123	2.674	144	455	979	125/63	590/112	393	OK	OK	OK	OK	OK	B-6	OK	6.60	
110	2.675	139	445	957	56/67	590/92	376/193.2	OK	OK	OK	OK	OK	B-6	OK	6.63	
109	2.685	141	452	967	94/30	590/149	387	OK	OK	OK	OK	OK	B-6	OK	6.65	
95	2.669	138	445	956	95/73	590/151	415	OK	OK	OK	OK	OK	B-6	OK	6.57	
120	2.668	139	453	955	120/86	590/161	425	OK	OK	OK	OK	OK	B-6	OK	6.60	
165	2.681	140	439	941	62/29	590/96	386	OK	OK	OK	OK	OK	B-6	OK	6.73	
143	2.681	141	456	953	145/106	3004/48	413	OK	OK	OK	OK	OK	B-6	OK	—	Thermocouple Blade.
137	2.680	137	437	953	150/60	590/172	358	OK	OK	OK	OK	OK	B-6	OK	—	Strain Gage Blade.
145	2.683	138	452	941	123/66	3064/17	416/183.4	OK	OK	OK	OK	OK	B-6	OK	6.54	
162	2.680	138	441	945	110/9	3004/32	398/210.6	OK	OK	OK	OK	OK	B-6	OK	6.63	
99	2.675	143	462	983	81/43	590/126	405	OK	OK	OK	OK	OK	B-6	OK	6.68	
107	2.681	138	443	968	80/26	590/94	376/188.7	OK	OK	OK	OK	OK	B-6	OK	6.62	
158	2.669	140	444	975	222/129	3004/39	385	OK	OK	OK	OK	OK	B-6	OK	6.73	
133	2.683	140	444	955	154/71	590/115	406	OK	OK	OK	OK	OK	B-6	OK	—	Strain Gage Blade.
111	2.666	143	460	985	131/146	590/145	414	OK	OK	OK	OK	OK	B-6	OK	6.72	
121	2.668	143	462	981	179/126	590/105	373	OK	OK	OK	OK	OK	B-6	OK	6.70	
131	2.682	141	444	966	89/23	590/175	362	OK	OK	OK	OK	OK	B-6	OK	—	Strain Gage Blade.
130	2.674	139	442	957	115/48	590/176	352	OK	OK	OK	OK	OK	B-6	OK	—	Strain Gage Blade.
160	2.676	143	443	969	110/56	3004/34	399	OK	OK	OK	OK	OK	B-6	OK	6.71	
98	2.676	142	458	982	33/26	590/79	402/214	OK	OK	OK	OK	OK	B-6	OK	6.76	
128	2.669	134	432	929	95/50	3004/4	343/148.6	OK	OK	OK	OK	OK	B-6	OK	—	Strain Gage Blade.
156	2.672	143	443	964	170/60	3004/22	438	OK	OK	OK	OK	OK	B-6	OK	6.79	
157	2.671	140	441	952	176/119	3004/21	412	OK	OK	OK	OK	OK	B-6	OK	6.67	
139	2.675	137	442	931	132/54	3004/19	380	OK	OK	OK	OK	OK	B-6	OK	—	Thermocouple Blade.
127	2.679	137	434	968	170/76	3004/5	343/146	OK	OK	OK	OK	OK	B-6	OK	—	Strain Gage Blade.
126	2.666	140	443	946	79/63	590/107	375	OK	OK	OK	OK	OK	B-6	OK	—	Strain Gage Blade.
80	2.676	139	451	966	27/6	590/102	378	OK	OK	OK	OK	OK	B-6	OK	6.67	
144	2.684	140	456	953	141/145	3004/38	444	OK	OK	OK	OK	OK	B-6	OK	6.78	
119	2.675	141	456	964	80/79	590/167	443	OK	OK	OK	OK	OK	B-6	OK	6.62	
81	2.667	141	449	957	81/18	590/140	418	OK	OK	OK	OK	OK	B-6	OK	6.68	
103	2.666	139	455	962	8/5	590/103	343/196	OK	OK	OK	OK	OK	B-6	OK	6.63	
106	2.685	140	453	963	83/20	590/150	364	OK	OK	OK	OK	OK	B-6	OK	6.67	
161	2.677	141	442	969	110/56	3004/34	399	OK	OK	OK	OK	OK	B-6	OK	6.70	
86	2.684	142	443	965	6/3	590/134	393	OK	OK	OK	OK	OK	B-6	OK	6.72	

### 11.1.3 Test Program and Engine Run

The engine test program required a stress survey, performance evaluation, endurance testing, and distortion and stall tolerance evaluation for a total test time of 100 hours. Figure 11.1-4 shows the test program schedule. The instruction sheet used during the test program is outlined below:

#### 11.1.3.1 Stress Survey

The following tests were conducted for each tail-pipe and bleed combination:

- A stress survey for an engine start from light-off to idle thrust.
- A 30-second acceleration/30-second deceleration cycle from idle thrust to maximum low-pressure compressor operating speed and back to idle. Maximum operating limits were not exceeded. Maximum vibratory stress limits for composite fan blades are:
  - Transient condition - 15,000 psi (excluding surge)
  - Steady state condition - 5,000 psi
- A transient vibration survey.
- Repeated peak-stress points as considered desirable.

The tail-pipe/bleed/inlet combinations are tabulated below:

Run No.	Tail-Pipe Area (ft <sup>2</sup> ); Config.	7th-Stage Bleeds	12th-Stage Bleeds	Inlet Config.
1	B/M A/B	Closed	Closed	Clean
2	3.50; Conv-Div	Closed	Open	Clean
3	3.50; Conv-Div	Closed	Closed	Clean
4	3.00; Convergent	Closed	Open	Clean
5	3.00; Convergent	Closed	Closed	Clean
8	4.10; Conv-Div	Closed	Open	Clean
9	4.10; Conv-Div	Closed	Closed	Clean
10	3.50; Conv-Div	Closed	Open	58 A*
11	3.50; Conv-Div	Closed	Closed	58 A*

\* 58 A Distortion Screen

#### 11.1.3.2 Endurance Program

The engine endurance program consisted of repeated six-hour cycles as shown in Figure 11.1-5. Engine shutdowns were made as required. The following requirements were observed during these tests:

- Recorded all engine discrepancies.
- Took an oil sample at the first idle point of each cycle except for Cycle 1.
- Kept a record of all oil samples taken and all oil added.
- Inlet temperature was ambient.
- All power settings were within the trim and power setting curve, Figure 1 of the TF30 P-9 Test Instruction Sheet.
- Recorded all parameters included on the engine instrumentation sheet.

The six-hour endurance cycle was repeated until a total of 50 hours of endurance time had been accumulated.

#### 11.1.3.3 Performance Calibration

Required back-to-back for B/M and composite fan blade configurations. An engine performance calibration was conducted according to the following procedure:

- a. The engine was started according to normal procedures.
- b. The idle thrust was set at 710 to 720 pounds.
- c. The Military power level angle was set at 65 to 68 degrees and trimmed, if necessary, to the thrust trim curve.
- d. Nominal suppression was set in Mid Zone 3.
- e. The idle thrust was rechecked.
- f. Recorded tell data readings at the following points. Stabilized seven minutes before each reading. Wet and dry bulb thermometers and the barometer were recorded each hour. A vibration survey was conducted in conjunction with the calibration.
  - Idle
  - Maximum 12th-stage bleeds open
  - Maximum 12th-stage bleeds closed

For the remaining nonafterburning data points, the procedure described below was followed.

- The desired thrust (data points as listed below) was set with the seventh-stage bleeds closed, locked power lever angle; recorded readings.
- With the power lever angle locked in the seventh stage bleeds-closed position, the seventh-stage bleed was opened and the readings recorded.
- Closed the seventh-stage bleeds, unlocked the power lever angle, and the next data point was set (data points as listed below)
- 6000 pounds thrust
- 8000 pounds thrust
- 9000 pounds thrust
- 10,000 pounds thrust
- 11,000 pounds thrust
- 12,000 pounds thrust
- Military trim
- Minimum Zone 1
- Mid Zone 2
- Maximum Zone 5

g. When the above program had been satisfactorily completed, the engine was brought to idle thrust, allowed to cool, and shut down.

## 11.1.3.4 Distortion Tolerance and Stall Testing

Required back-to-back for Bill of Materials and composite fan blade configurations.

A series of tests was conducted to evaluate the engine and/or blade tolerance of various degrees of inlet distortion and the stall characteristics of the engine. The following procedures were observed during these tests:

## Distortion Valve Part No. XLR-46153

- Removed the Station 3 probes for the distortion testing.
- Installed the flame-out protection (FOP) system.
- Made a check run to evaluate proper functioning of the instrumentation and FOP systems. Actuated the FOP solenoid to assure that the surge protection system was functioning properly. Checked the engine for possible vibration shifts.
- Conducted the distortion test. Stabilized the engine for five minutes before recording data.
- At every ten hours of engine operation, the screens in the distortion valve were inspected and replaced if cracked.
- When the seventh-stage bleeds were open, the  $T_{t7}$  limit which was defined by the performance calibration was observed.
- With the base line configuration, conducted tests at the conditions shown in the following table.

X-433-24 Distortion Valve Program				
<u>Point</u>	<u>A/B</u>	<u>7th Bleeds</u>	<u>Conditions</u>	<u><math>N_1 \sqrt{\theta}</math></u>
1	No	Closed	Stall VOS** VOS-10 VOS-20 Full Open	9500
2	No	Closed	Stall VOS VOS-10 VOS-20 Full Open	9000

PRATT & WHITNEY AIRCRAFT GROUP

3	No	Closed	Stall VOS VOS-10 VOS-20 Full Open	8500
4	No	Closed	Stall VOS VOS-10 VOS-20 Full Open	7500
5	No	Open	Stall VOS VOS-10 VOS-20 Full Open	9000
X-433-24 Distortion Valve Program				
Point	A/B	7th Bleeds	Conditions	$N_1 \sqrt{\theta}$
6	No	Open	Stall VOS VOS-10 VOS-20 Full Open	8500
7	No	Open	Stall VOS VOS-10 VOS-20 Full Open	8000
8	No	Open	Stall VOS VOS-10 VOS-20 Full Open	7500
9	Z-1*	Closed	VOS-10	9500
10	Z-1*	Open	VOS-10	9000

\* Afterburner Zones

\*\*on verge of stall

## PRATT &amp; WHITNEY AIRCRAFT GROUP

Engine Run:

The actual engine test program which was run is detailed below in chronological order:

<u>Date</u>	<u>Event</u>	<u>Composite Blade Total Run Time To Date (Hrs)</u>	<u>Remarks</u>
9-22-72	Completed Engine Building	0	Engine Built to TF30 P-9 Configuration with Deviations as Noted in Section III.
			Installed in Sea Level Test Stand X-234
9-25-72	Baseline Blade Inspection		On-stand Blade Inspection Performed
			All Blades OK
9-27-72	Initiated Strain Gage Program	0	Strain Gage Data Recorded
9-29-72	Shutdown for Minor Engine Repair	1.58	2.8 Mil Max Inlet Vibration Reduced by Trim Balance to Acceptable Level of 1.6 Mil.
			Completed On-stand Blade Inspection OK
10-2-72	Restarted Strain Gage Program	1.58	
10-3-72	Shutdown for Minor Engine Repair	3.58	Strain Gage Leads Repaired
			Permanent Trim Balance Wgts. Added to Engine
			3rd Stage Removed From Engine
			Fan Stage Reassembled
10-12-72	Restarted Strain Gage Program	3.83	Installed Distortion Screen 58A

## PRATT &amp; WHITNEY AIRCRAFT GROUP

<u>Date</u>	<u>Event</u>	<u>Composite Blade Total Run Time To Date (Hrs)</u>	<u>Remarks</u>
10-23-72	Completed Strain Gage Program	8.24	Remove Distortion Screen
			Install Performance Instrumentation
10-26-72	Initiated Performance Calibration	8.24	Single 10th Compressor Blade Failed Prematurely
10-27-72	10 C Blade Failure	18.74	Single 10th Compressor Blade Failed Prematurely
			Not Composite Blade Related
			Initiated Complete Teardown and Rebuild of Engine
			Replaced Following Parts:

<u>Name</u>	<u>P/N</u>	<u>Quantity</u>
I/C	616154	1
10th Bld.	576710A	73
10th Sta.	581950D	1
Trans. Duct	594334	-
Heat Shield	589642	8
Combust. Chamber	SKL 56785	2
	635790	1
	635791	1
	SKL 56770	4
1st Turb. Vane	667451	15
	SKL 56324	
	SKL 57181	
1st Turb. Blade	679301	
	SKL 52963	
	674301	
	SKL 51525	
	674301	108
2nd Turb. Blade	597401	
	569502	5

## PRATT &amp; WHITNEY AIRCRAFT GROUP

<u>Date</u>	<u>Event</u>	<u>Composite Blade Total Run Time To Date (Hrs)</u>	<u>Remarks</u>
			3rd Turb. 651103 2 Blade
			Bench Blade Inspection OK
12-12-72	Completed Engine Rebuild	18.74	Installed X-433 Build 25 in X-234 Test Stand
12-14-72	Initiated Short Performance Calibration	18.74	Post-build Performance Check-out OK
12-15-72	Initiated Endurance Testing	23.16	
12-20-72	Completed Endurance Testing	73.16	Installed Performance Instrumentation
12-20-72	Completed Compressor Blade Portion of Back-to-Back Full Performance Calibration	79.82	Replaced Composite 3rd Rotor with B/M 3rd Rotor Performance Data Recorded in Section V
12-28-72	Completed B/M Portion of Back-to-Back Performance Calibration	79.82	Removed Performance Instrumentation Installed Distortion Valve
			Bench Composite Blade Inspection OK
1-4-73	Completed B/M Blade Portion of Stall Tolerance Program	79.82	Stall Tolerance Data Recorded Reinstalled Composite 3rd Rotor
1-10-73	Completed Composite Portion of Stall Tolerance Program	94.80	
1-11-73	Completed Steady State Cruise Condition (75% Normal Rated Power)	100.05	Initiated Post Test Inspection

The final inspection conducted on the engine blades was performed at the completion of 100 hours of engine testing. The inspection procedure included visual, ultrasonic, and eddy current inspection as well as frequency checks, x-ray, and dimensional inspection. This inspection was performed with the blades removed from the disk.

Post test visual, ultrasonic, eddy current and X-ray evaluation of the complete set of engine blades revealed no degradation. Post test frequency results were compared to pre-test data for the individual blades with the following results:

<u>Frequency</u>	<u>Max % Frequency Drop</u>	<u>Avg. % Frequency Drop</u>
1st Bending	2.8	1.36
2nd Bending	4.1	2.06
1st Torsion	2.3	1.37

The individual blade data are recorded in Table 11.1-III.

It should be noted that in general the nine instrumented blades (E-143, -137, -133, -131, -130, -128, -139, -127, -126) exhibit above average frequency drops in all three modes. Since pre-to-post-test evaluation of these nine blades required an additional stripping operation to remove the instrumentation adhesive, this operation may have affected the results (possible incomplete stripping resulting in change of mass) and would tend to make the reported averages conservative.

The data recorded in Table 11.1-III does not include the results recorded for eight blades (E-119, -145, -123, -107, -144, -95, -100, -79). The eight blades required epoxy coating to replace the outer aluminum layer inadvertently removed during fabrication, thus changing their stiffness/mass configuration and invalidating pre-test frequency results. All blade pre and post test frequencies are within blueprint specification limits, including the epoxy coated blades (Table 11.1-IV). Post-test dimensional evaluation of the engine blade set consisted of measurement of stacking point offset and chord angle at blade radial station J-J, located near the blade tip.

Since blade charting was not a standard part of the blade selection process when this blade set was compiled, pretest measurement data was not available for comparative analysis. The post-test measurement results are recorded in Table 11.1-V. However, subsequent pretest data compiled for later blades in this program show similar results, indicating negligible dimensional deviations due to engine test conditions. About 20 percent of all blades fabricated under this program were charted subsequently.

TABLE 11.1-III  
**TF30 COMPOSITE BLADE SET #1**  
**Frequency Shift**  
**Due to 100 Hr. Subsonic Engine Test**

Blade No.	1st Bending				2nd Bending				1st Torsion			
	Before Test	After Test	$\Delta$	% $\Delta$	Before Test	After Test	$\Delta$	% $\Delta$	Before Test	After Test	$\Delta$	% $\Delta$
105	140	138	2	1.4	441	439	2	0.4	948	940	8	0.8
109	141	140	1	0.7	452	439	13	2.8	967	956	11	1.1
120	139	138	1	0.7	453	435	18	3.9	955	943	12	1.2
143	141	139	2	1.4	456	439	17	3.7	953	940	13	1.3
137	137	134	3	2.1	437	428	9	2.0	953	931	22	2.3
162	138	138	0	0	441	434	7	1.5	945	935	10	1.0
99	143	141	2	1.3	462	443	19	4.1	983	968	15	1.5
158	140	141	0	0	444	443	1	0.2	975	958	17	1.7
133	140	136	4	2.8	444	434	10	2.0	955	937	18	1.8
111	143	142	1	0.6	460	445	14	3.0	985	971	14	1.4
121	143	141	2	1.3	462	448	14	3.0	981	967	14	1.4
131	141	139	2	1.4	444	435	9	2.0	966	952	14	1.4
130	139	136	3	2.0	442	431	11	2.4	957	942	15	1.5
160	143	140	3	2.0	443	441	2	0.4	969	949	20	2.0
98	142	141	1	0.7	458	440	18	3.9	982	968	14	1.4
128	134	132	2	1.4	432	424	8	1.8	929	919	10	1.0
156	143	141	2	1.3	443	445	0	0	961	960	4	0.4
157	140	138	2	1.4	441	440	1	0.2	952	937	15	1.5
139	137	134	3	2.1	442	431	9	2.0	931	919	12	1.2
127	137	134	3	2.1	434	423	11	2.5	968	952	16	1.6
126	140	136	4	2.8	443	433	10	2.0	946	934	12	1.2
80	139	138	1	0.7	451	437	14	3.1	966	953	13	1.3
81	141	138	3	2.1	449	441	8	1.7	957	945	12	1.2
103	139	137	2	1.4	455	442	13	2.8	962	950	12	1.2
106	140	138	2	1.4	453	435	17	3.7	963	950	13	1.3
161	141	141	0	0	442	439	3	0.6	969	952	17	1.7
86	142	140	2	1.4	443	436	7	1.5	965	950	15	1.5
165	140	138	2	1.4	439	437	2	0.4	941	926	15	1.5
	Avg.	2.0	1.36			Avg.	9.54	2.06		Avg.	13.68	1.37

Blueprint Tolerance 130±15

410 min.

850 min.

**TABLE 11.1-IV**  
**TF30 COMPOSITE BLADE SET #1 FREQUENCY SHIFT**  
**Due to 100 Hr. Subsonic Engine Test**  
**Epoxy Coated Blades Only**

Blade No.	1st Bending				2nd Bending				1st Torsion			
	Before Test	After Test	$\Delta$	% $\Delta$	Before Test	After Test	$\Delta$	% $\Delta$	Before Test	After Test	$\Delta$	% $\Delta$
119	141	135	6	4.2	456	423	33	7.2	964	932	32	3.3
145	138	132	6	4.3	452	417	35	7.7	941	905	36	3.8
123	144	137	7	4.8	455	431	24	5.2	979	945	34	3.4
107	138	133	5	3.5	443	412	31	6.9	968	935	33	3.4
144	140	134	6	4.2	458	426	32	6.9	953	925	28	2.9
95	138	132	6	4.3	445	416	29	6.5	956	926	30	3.1
110	139	133	6	4.3	445	413	32	7.1	957	925	32	3.3
79	142	136	6	4.2	457	427	30	6.5	979	949	30	3.0
	Avg.	6	4.24			Avg.	30.75	6.75		Avg.	31.88	3.28

TABLE 11.1-V

## BLADE SET #1

## POST TEST AIRFOIL DATA

<u>Blade</u>	<u>Section J-J</u>			
	<u>Stack Pt. Offset</u>	<u>Chord Angle</u>	<u>Δ Offset</u>	<u>Δ Angle Minutes</u>
135	+.44	22°	-.08	+80
137	+.49	21° 34'	-.03	+54
158	-.72	20° 52'	+.20	+12
156	+.10	21° 22'	-.42	+42
128	+.55	22° 24'	+.03	+104
98	+.63	21° 24'	+.11	+44
110	+.31	18° 34'	-.21	-126
95	+.67	20° 52'	+.15	+12
162	+.37	21° 54'	-.15	+74
139	+.94	23° 40'	+.42	+180
120	+.66	22° 34'	+.14	+114
81	+.62	22°	+.10	+80
126	+.36	21° 30'	-.16	+50
105	+.75	23° 12'	+.23	+152
127	+.93	21° 24'	+.41	+54
103	+.58	22° 46'	+.06	+126
86	+.50	20°	-.02	-40
107	+.48	20°	-.04	-40
144	+.59	22° 18'	+.07	+98
109	+.80	20° 46'	+.28	+6
123	+.06	20° 46'	-.46	+6

TABLE 11.1-V (Cont'd)

Blade	Stack Pt. Offset	Chord Angle	$\Delta$ Offset	$\Delta$ Angle Minutes
121	+.98	21° 14'	+.46	+34
131	+.48	21° 52'	-.04	+72
130	+.50	22° 14'	-.02	+94
80	+.78	20° 40'	+.26	+0
79	+.59	20° 36'	+.07	-4
165	+.46	21° 38'	-.06	+58
111	+.49	20° 52'	-.03	+12
161	+.35	20° 38'	-.17	-2
119	+.48	21° 24'	-.04	+44
99	+.70	21° 40'	+.18	+60
160	+.48	21° 40'	-.04	+60
145	+.60	22° 26'	+.08	+106
157	+.76	22° 50'	+.24	+130
99	+.83	21° 22'	+.31	+42
143	Not Charted			
		Average Deviation	.17	51
		Tolerance	.45	42'
		<u>Ave. Dev.</u> Tol.	.38	1.21
		<u>Max. Dev.</u> Tol.	1.02	4.30

#### 11.1.4 "Piggyback" Sea-Level Testing

In the period June-August, 1973, Blade Set No. 1 was installed in TF30-P-9 experimental engine X-467 and subjected to a total of 264 hours of piggyback\* cyclic endurance testing. The test cycles were standard P-9 six-hour endurance cycles, shown in Figure 11.1-5. For a standard 150-hour endurance test, 25 such cycles would be performed. Set No. 1 was subjected to one such 150-hour test. After 114 hours of the second test, the test was terminated due to an engine problem unrelated to the blades.

At this point Blade Set No. 1 had a total of 364 hours of sea-level test time, all but 50 being cyclic endurance. Non-destructive inspection of the blades at this time revealed 12 blades to have leading edge cracks just above the platform; the maximum length of these cracks was 3/8 inch (Table 11.1-VI). Because of the presence of these small cracks, the contractor recommended that any blades involved in subsequent flight programs be bench inspected after 200 hours of flight time. Table 11.1-VII presents the 364-hour frequency loss of these blades; all remained within design tolerances.

Before starting the piggyback testing, one blade was deliberately damaged by impacting it with 1/4 inch gravel in a spin pit at 100 percent speed. The damaged area was then blended to maximum blend limits allowed for B/M blades. After 264 hours of testing this blade exhibited no distress.

TABLE 11.1-VI  
X-RAY RESULTS  
SET NO. 1 AFTER 364 HOURS

##### Fillet Area Cracks Only

Blade No.	Pretest	Post Test
81	None	1/8 inch LE
105	None	1/8 inch LE
109	None	1/16 inch LE
111	None	3/16 inch LE 1/4 above fillet
126	None	3/16 inch LE
130	None	1/8 inch LE
144	None	3/8 inch LE
145	None	3/8 inch LE
156	None	1/8 inch LE
157	None	1/4 inch LE
162	None	1/8 inch LE
165	None	3/32 inch LE

\*"Piggyback" refers to blade testing performed as an adjunct to other engine testing, at no direct charge to this contract. In this case, the engine was being used to investigate improvements under the Product Support Program (PSP). These items are presented in paragraph 11.1.4.

TABLE 11.1-VII

## NATURAL FREQUENCIES

## SET NO. 1 AFTER 364 HOURS

Blade No.	1st Bending			2nd Bending			1st Torsion		
	Pretest	Post Test	% Change	Pretest	Post Test	% Change	Pretest	Post Test	% Change
79	142	137	3.5	457	429	6.1	979	959	2.0
80	139	139	0.0	451	436	3.3	966	962	0.4
81	141	139	1.4	449	439	2.2	957	954	0.3
86	142	140	1.4	443	436	1.6	965	961	0.4
95	138	133	3.5	445	417	6.1	956	937	2.0
98	142	142	0.0	458	442	3.5	982	978	0.4
99	143	142	0.7	462	446	3.5	983	978	0.5
103	139	138	0.7	455	441	3.1	962	960	0.2
105	140	139	0.7	441	440	0.2	948	952	+0.4
106	140	139	0.7	453	437	3.5	963	959	0.4
107	138	133	3.5	443	415	6.1	968	946	2.3
109	141	140	0.7	452	437	3.3	967	963	0.4
110	139	134	3.5	445	416	6.5	957	937	2.0
111	143	143	0.0	460	446	3.1	985	988	+0.3
119	141	135	4.3	456	422	7.5	964	943	2.3
120	139	139	0.0	453	437	3.5	955	954	0.1
121	143	142	0.7	462	450	2.6	981	979	0.2
123	144	137	4.9	455	432	5.1	979	958	2.2
126	140	137	2.1	443	434	2.0	946	946	0.0
127	137	135	1.4	434	428	1.4	968	965	0.3
128	134	132	1.4	432	424	1.9	929	929	0.0
130	139	137	1.4	442	436	1.4	957	954	0.3
131	141	139	1.4	444	437	1.5	966	964	0.2
133	140	137	2.1	444	435	2.0	955	948	0.7
137	137	135	1.4	437	428	2.0	953	945	0.8
139	137	135	1.4	442	433	2.0	931	929	0.2
143	141	139	1.4	456	438	3.9	953	950	0.3
144	140	135	3.5	458	429	6.5	953	936	1.8
145	138	133	3.5	452	422	6.6	941	920	2.1
156	143	143	0.0	443	445	+0.4	964	973	+0.9
157	140	139	0.7	441	437	0.9	952	949	0.3
158	140	141	+0.7	444	422	5.0	957	968	+1.1
160	143	141	1.4	443	444	+0.1	969	960	0.0
161	141	140	0.7	442	437	1.0	961	961	0.0
162	138	140	+1.4	441	437	0.9	945	947	+0.2
165	140	139	0.7	439	439	0.0	941	939	0.2
Avg. Change			1.4				3.0		

B/P Tol. 1st Bending Mode  $130 \pm 15$  cycles/sec  
 2nd Bending Mode  $410 \pm 10$  min cycles/sec  
 1st Torsion Mode  $850 \pm 50$  min cycles/sec

## 11.2 SUPERSONIC/ALTITUDE TEST PROGRAM

Blade Set No. 2 was used for engine testing at supersonic and altitude conditions. The flight envelope, shown in Figure 11.2-1, of the F-111A aircraft was explored at its three "corners", Mn 0.7, 33,000 ft.; Mn 2.2, 56,000 ft; and Mn 1.2, sea level. These represent, respectively, the highest blade speed, the highest blade temperature, and the highest blade loading. All three conditions were checked out in a stress survey, and the latter two were performed under endurance conditions.

Maximum blade speed was 10,550 rpm; maximum blade temperature was 467°F (tip) and 406°F (root); maximum blade vibratory stress was 6,000 psi, except for a stand-connected nonintegral acoustic rumble occurring at Mn 1.2, sea-level conditions.

A total of 200 hours was imposed on this blade set, as shown in Figure 11.2-2, which included the following basic elements:

- Stress survey at Mn 1.2, sea level, with and without inlet distortion.
- Stress survey at Mn 0.7, 33,000 feet altitude, with and without distortion.
- Stress survey at Mn 2.2 56,000 feet altitude, with clean inlet.
- 10-hour endurance test at Mn 1.2, sea level.
- 120-hour endurance test at Mn 2.2, 56,000 feet altitude.

} 31-hours total

The additional 39 hours not accounted for were required to set altitude conditions while the engine was operating. Testing started in February, 1973; and the 200-hour program was completed in July, 1973.

Table 11.2-I presents a chronological summary of the progress of this program.

TABLE 11.2-I  
SUMMARY OF SUPERSONIC ENGINE TEST PROGRAM

<u>Date</u>	<u>Event</u>	<u>Composite Engine Blade Set No. 2 Total Run Time To Date (Hours)</u>	<u>Remarks</u>
2-19-73	Complete engine building	0	Deliver to sea level test stand for installation
2-23-73	Complete sea level check-out	4.51	Initiated installation in capsule for altitude running
			Further delayed pending completion of 450°F Goodman Diagram
3-26-73	Complete Goodman diagram - OK to run engine program	4.51	Deliver to altitude test stand for installation.
4-5-73	Baseline blade inspection	4.51	
4-9-73	Initiate strain gage program	4.51	
4-11-73	Shutdown for distortion screen installation	14.34	Complete on-stand blade inspection - OK
4-13-73	Continue strain gage program	14.34	
4-26-73	Complete strain gage program	31.34	Complete on-stand blade inspection OK
			Set up for Mn 1.2 endurance program
4-30-73	Initiate Mn 1.2 sea level endurance	35.59	
5-3-73	Completed 10.5 hrs. of Mn 1.2 sea level endurance	57.23	Initiate engine hot section inspection
5-8-73	Remove fan stage for composite blade bench inspection	57.23	Severe composite blade tip rub noted - caused by test setup mount scheme
5-18-73	Completed composite blade bench inspection	57.23	Replaced seven blades exhibiting fillet cracks

TABLE 11.2-I (Cont'd)

<u>Date</u>	<u>Event</u>	<u>Composite Engine Blade Set No. 2 Total Run Time To Date (Hours)</u>	<u>Remarks</u>
5-24-73	Completed engine rebuild	57.23	Further testing delayed pending availability of test facility
6-14-73	Initiate short performance calibration	57.23	
6-18-73	Initiate Mn 2.2, 56,000 feet altitude endurance	62.73	
7-25-73	Completed Mn 2.2, 56,000 feet altitude endurance	200	End of test

The engine was mounted in altitude test stand X-210 shown in Figure 11.2-3. This stand has provisions for controlling the inlet temperature and pressure, and discharge pressure to simulate the various flight altitudes and Mach numbers at which the TF30 engine operates.

The 36 blades selected for this set are listed in Table 11.2-II, along with pertinent inspection and test data about the BORSIC®/aluminum tape and blades. After approximately 57 hours of running, evidence of a severe blade tip rub was discovered and seven blades were damaged, as described below.

After running 10.5 hours of sea-level endurance, the engine was opened for a hot section inspection and composite third-stage fan blade inspection. When the third-stage rotor was removed, inspection revealed that severe blade tip rubbing had occurred between the third-stage blades and the fan exit case fiberglass rubstrip. The most severe rub (approximately 0.090 inch deep) occurred at the 10 o'clock (clockwise from the rear) position on the fan exit case shown in Figure 11.2-4. This point is just forward of the thrust puck which absorbs engine thrust and transmits it to the mount hardware. Since the blade rubbed most severely at this point, the fan exit case had to be deformed during some engine operating condition. Most likely the Mn 1.2, sea level, afterburning condition was the point at which the tip rubbing occurred because the engine thrust and rotor speeds were at the maximum. There was also evidence that the axial clearance between the engine inlet hardware and the bellmouth was reduced to zero, since the bellmouth had a large axial crack at the same angular location as the thrust puck. Assuming clearance was zero, the bellmouth could transmit a compressive load to the fan exit case, thus causing it to distort. This compressive load in combination with the thrust puck load caused the most severe distortion at the thrust puck location, which is close to the third-stage fan blade fiberglass rubstrip.

Since there are areas of the third-stage blade rubstrip which exhibited no blade rub at all, the rubbing was not caused by the third-stage blades. The fault apparently lies with the mount system which distorted the third-stage blade rubstrip at some running condition.

TABLE II  
SET NO. 2

TF30 ALTITUDE ENGINE TEST BLADES

Blade No.	Density g/cc	Natural Frequency 1B	Natural Frequency 2B	1T	Acoustic Emission CC/CV	Tape Lot KSI	Tape Strength KSI	Ultrasonic C-Scan Root	X-Ray Airfoil	Heat Treat	FPI	Proof Spin	Remarks
					Tape/Panel								
* 82	2.666	141	447	961	2/31	590/101	392	OK	OK	OK	B-6	OK	
* 85	2.665	140	443	943	13/19	590/136	349	OK	OK	OK	B-6	OK	
87	2.667	144	462	983	13/10	590/159	404	OK	OK	OK	B-6	OK	
* 89	2.682	143	457	985	16/19	590/153	380	OK	OK	OK	B-6	OK	
114	2.664	143	462	989	94/67	590/166	423	OK	OK	OK	B-6	OK	
115	2.666	144	459	967	177/75	590/165	346	OK	OK	OK	B-6	OK	
* 148	2.669	140	461	972	103/42	300/29	380	OK	OK	OK	B-6	OK	
155	2.663	139	438	957	87/15	3004/23	423	OK	OK	OK	B-6	OK	
163	2.674	139	451	944	99/72	3004/30	341/149	OK	OK	OK	B-6	OK	
167	2.676	139	447	966	122/105	590/99	415	OK	OK	OK	B-6	OK	
168	2.670	141	456	970	100/63	3004/14	390	OK	OK	OK	B-6	OK	
169	2.667	137	449	946	168/96	3004/27	457	OK	OK	OK	B-6	OK	
170	2.669	137	450	941	90/41	590/45	372	OK	OK	OK	B-6	OK	
171	2.665	138	449	974	102/51	3004/6	250/191	OK	OK	OK	B-6	OK	
172	2.646	134	438	941	50/36	3004/13	330/161	OK	OK	OK	B-6	OK	
174	2.644	137	445	968	41/32	3004/77	362	OK	OK	OK	B-6	OK	
175	2.663	141	456	974	59/48	3004/82	454	OK	OK	OK	B-6	OK	
176	2.683	143	460	976	66/43	3004/20	326/214	OK	OK	OK	B-6	OK	
178	2.666	139	452	964	113/57	3004/80	427	OK	OK	OK	B-6	OK	
179	2.660	140	460	955	121/126	3004/81	431	OK	OK	OK	B-6	OK	
180	2.663	139	456	954	190/137	3004/83	432/201	OK	OK	OK	B-6	OK	
181	2.680	137	447	945	145/19	3004/89	436	OK	OK	OK	B-6	OK	
182	2.676	137	449	945	152/37	3004/86	436	OK	OK	OK	B-6	OK	
183	2.666	141	459	965	138/63	3004/92	426	OK	OK	OK	B-6	OK	
* 184	2.668	139	452	952	120/64	3004/91	425	OK	OK	OK	B-6	OK	
187	2.679	136	443	941	123/120	3004/85	392	OK	OK	OK	B-6	OK	
188	2.652	140	455	967	148/116	3004/84	362	OK	OK	OK	B-6	OK	
189	2.667	137	445	950	164/97	3004/98	488/185	OK	OK	OK	B-6	OK	
190	2.652	139	455	964	130/65	3004/100	385	OK	OK	OK	B-6	OK	
192	2.669	138	447	962	155/80	3004/97	394	OK	OK	OK	B-6	OK	
193	2.567	136	444	945	100/75	3004/95	341	OK	OK	OK	B-6	OK	
195	2.666	138	447	947	162/72	3004/93	418	OK	OK	OK	B-6	OK	
* 196	2.644	139	455	967	137/81	445/10	345	OK	OK	OK	B-6	OK	
197	2.664	139	453	957	162/64	3004/96	347/178	OK	OK	OK	B-6	OK	
199	2.654	139	453	967	90/67	445/13	370	OK	OK	OK	B-6	OK	
200	2.660	136	440	937	126/23	590/65	420	OK	OK	OK	B-6	OK	

\*Damaged during tip rubs. See Table II-XIII.

Non-destructive examination of the third-stage fan blades revealed seven blades which exhibited fillet cracks due to the severe tip rub. The results of a complete destructive examination of one of these blades are contained in Section 11.2.5. The seven blades (Nos. 82, 85, 89, 148, 163, 184, 196) were replaced with seven new blades, which are listed in Table 11.2-III.

After rebuilding, the engine completed Mn 2.2, 56,000 feet altitude endurance testing, which was the final element of the program.

### 11.2.1 Engine X-433-26 Build Summary

The subject engine was assembled to the TF30-P-9 configuration in order to run endurance at Mach 1.2 sea level and Mach 2.2 altitude on the BORSIC®/aluminum composite material third-stage fan blades. In addition to the endurance program, a strain gage stress survey was made with and without distortion screens.

The build started on January 30, 1973, and was completed and delivered to X-231 stand for sea-level checkout on February 19, 1973.

The engine had been disassembled only for third fan replacement, hot section repair, and tailcone replacement. A list of major part changes and reoperations follows.

#### 11.2.1.1 Low-Pressure Compressor

<u>Name</u>	<u>Part Added</u>	<u>From</u>	<u>Time</u>	<u>Part Cancelled</u>	<u>Sent To</u>	<u>Time</u>
3rd Blades	713603	F/S	0	713603	U/S	100.31
Cover	SKL57492	F/S	0	(covers fan inspection part)		

#### Reoperations

1. 2-3 airseal was reoped to machine radii into strain gage lead out slots.
2. 7 third fan blades were strain gaged.

#### 11.2.1.2 Turbine

<u>Name</u>	<u>Part Added</u>	<u>From</u>	<u>Time</u>	<u>Part Cancelled</u>	<u>Sent To</u>	<u>Time</u>
Oil Filter	692385	X-541		9382-4175	X-467	98.66
Cover						
Oil Filter	SKL55546	F/S		SKL55546	X-467	98.66
High Tension	516021	Lab		516021 S/N	Lab	
Lead	S/N296					
Igniters	519348C	Lab		519348C	Lab	
	S/N137,156			S/N117, 249		

TABLE 11.2-III  
BLADES INSTALLED AFTER TIP RUB AT 57 HOURS  
SET #2

Blade No.	Density g/cc	Natural Frequency 1B	Frequency 2B	Frequency 1T	Acoustic Emission CC/CV	Tape Lot	Tape Strength KSI	Root Tape/Panel	Ultrasonic C-Scan Airfoil	X-Ray	FPI	Heat Treat	Proof Spin
194	2.675	136	433	930	152/103	3004/94	421	OK	OK	OK	OK	B-6	OK
201	2.676	135	429	920	152/41	445/51	384	OK	OK	OK	OK	B-6	OK
205	2.666	132	420	920	58/23	445/58	356	OK	OK	OK	OK	B-6	OK
206	2.662	133	427	915	137/53	445/57	420	OK	OK	OK	OK	B-6	OK
212	2.666	133	425	917	68/30	445/48	339/158	OK	OK	OK	OK	B-6	OK
223	2.679	138	435	947	196/92	445/70	365	OK	OK	OK	OK	B-6	OK
225	2.672	140	443	960	121/51	445/76	434	OK	OK	OK	OK	B-6	OK

## Reoperations

1. Weld repaired outer transition duct on engine.
2. Weld repaired burner cans #1, 2, 3, 8.

## 11.2.1.3 Afterburner

<u>Name</u>	<u>Part Added</u>	<u>From</u>	<u>Time</u>	<u>Part Cancelled</u>	<u>Sent To</u>	<u>Time</u>
Tailcone	596820B SKL57470	F/S	0	596820	U/S	618.56
Z-5 Spray Ring	576775, SKL55951	F/S	0	576775	U/S	1491.29

## 11.2.1.4 PSP Items Incorporated

1. "1st Turbine Blade Life Improvement", Item C-68; Evaluation of PWA 1459 blades compared to PWA 663 and PWA 1455 blades.
2. "1st Stage Turbine Nozzle Vane Cracking", Item C-7A; Full O.D. cap vanes reoperated with cooling holes for increased air movement to be compared with full cap vanes without cooling holes.
3. "Zone 5 Spray Ring Cracking", Item D-92; Zone 5 spray ring relocated downstream to eliminate autoignition. Also included is the 6 point bolt-on retention feature per ECP 279026 and L-96394.
4. "Afterburner Tailcone Burning", Item D-93; Tailcone rear I.D. coated with magnesium zirconate to eliminate burning.
5. "Multi-nozzle Burner Durability", Item B-17; Centertubes of M.E.R.L. 711 material installed to reduce burning, and louvers dimpled downstream of crossover tubes to reduce warping.

### 11.2.2 Vibratory Stress And Temperature Survey

Blade Set No. 2 was installed in TF30-P-9 Engine X-433-26 to undergo testing directed toward determining the vibratory stress characteristics and radial temperature profile of the third-stage BORSIC®/aluminum fan blades under simulated altitude conditions. The blades were first tested to determine the stress and performance characteristics at various inlet conditions. They were then subjected to a 10-hour endurance test at Mn 1.2, sea-level conditions and a 120-hour endurance test at Mn 2.2, 56,000-feet altitude, inlet conditions.

The results of the tests indicated that the blade stress levels measured at simulated altitude conditions within the engine flight envelope were acceptable. High nonintegral stresses were observed outside of the flight envelope, just off idle speed, but were considered to be a test stand-connected acoustic rumble.

#### 11.2.2.1 Blade Instrumentation

Ten of the 36 composite blades tested were instrumented.

Twenty six M-M WD-DY-126-AD-350-B-87 foil strain gages were installed with M-610 adhesive. Figure 11.2-5 shows the installation, while Table 11.2-IV presents information about the strain gage locations and lists the blades to which they were attached. The intermediate leads of five mil nickel-clad copper were silver soldered to the manufacturers gage leads and routed down the airfoil. The lead was then spliced to Kapton wire using GA-60 adhesive for precoat and overcoat. These leads were then ducted to the slip ring.

**TABLE 11.2-IV**  
**STRAIN GAGE SUMMARY**  
**THIRD-STAGE FAN BLADE SIMULATED FLIGHT TEST**  
**Gage Type WD-DY-125AD-350-**

Gage Number	Gage Location	Blade S/N	Disk Slot Number
1	RMT-CX	178	1
2	RTE-CC		
3	RLE-CC		
4	TMT-CX		
5	RMT-CS	175	36
6	RTE-CC		
7	RLE-CC		
8	TMT-CX		
9	RMT-CX	179	5
10	RTE-CC		
11	RLE-CC		
12	15% MT-CX45°		
13	RMT-CX	171	8
14	RTE-CC		
15	RLE-CC		
16	15% MT-CX45°		

TABLE 11.2-IV (Cont'd.)

<u>Gage Number</u>	<u>Gage Location</u>	<u>Blade S/N</u>	<u>Disk Slot Number</u>
17	RMT-CX	182	9
18	RTE-CC		
19	RLE-CC		
20	15% MT-CX-45°		
21	TMT-CX	180	19
22	RLE-CC		
23	RMT-CX-45°		
24	TMT-CX	169	12
25	RLE-CX		
26	RMT-CX-45°		

RMT = root maximum thickness

RLE = root leading edge

CC = concave

RTE = root trailing edge

TMT = tip maximum thickness

CX = convex

In addition to the strain gages, ten five-mil chromel/alumel ungrounded thermocouples with tackwelded junctions were installed using GA-60 adhesive. Figure 11.2-6 shows how the thermocouples were installed while Table 11.2-V lists the blades to which they were attached and their locations. The thermocouples were routed down the airfoil using GA-60 cement for precoat and overcoat, where they were spliced to chromel/alumel duplex by tackwelding. The wires were then ducted to the slip ring.

TABLE 11.2-V  
THERMOCOUPLE SUMMARY  
THIRD-STAGE FAN BLADE SIMULATED FLIGHT TEST

## Type 5 Mil C/A

<u>Thermocouple</u>	<u>T/C Location</u>	<u>Blade S/N</u>	<u>Disk Slot No.</u>
A	MS-MC-CC	169	12
B	½" R-MC-CC	176	2
C	MS-MC-CC		
D	½" T-MC-CC		
E	½" R-MC-CC	167	3
F	MS-CC-CC		
G	½" T-MC-CC		
H	½" R-MC-CC	181	18
I	MS-MC-CC		
J	½" R-MC-CC		

MS = mid span

R = root

MC = mid chord

T = tip

A No. 16 Aeroquip hose with manifold was used to duct air to help cool the sliring cavity during the heated runs. Four chromel/alumel cable duct thermocouples and two CEC 4-118 velocity transducers were installed to monitor the sliring and cable environment. Thermocouples and velocity pickups to monitor slip ring operation were also installed.

#### 11.2.2.2 Test Sequence

Following an instrumentation check run at static, sea-level conditions, the test was conducted in accordance with the procedures presented in paragraph 11.2.3 of this document. To summarize, the engine ran 31-hours to conduct the stress survey (Mn 1.2, sea level; Mn 0.7, 33,000 ft.; and Mn 2.2, 56,000 ft.); 39-hours to set altitude conditions; 10-hours at Mn 1.2, sea level conditions; and 120-hours at Mn 2.2, 56,000 ft.

#### 11.2.2.3 Test Results

The results of the preliminary vibratory stress survey conducted at sea-level static conditions on 22 February 1973 are presented in Table 11.2-VI.

TABLE 11.2-VI  
MAXIMUM STRESSES AT SEA LEVEL STATIC CONDITIONS

Strain Gage Number	Gage Location*	Stress (psi)	Order/Frequency	N <sub>1</sub> Speed (rpm)
25	RLE-CC	6,000	2E	5650
5	RMT-CX	4,700	2E	5700
10	RTE-CC	3,700	16E	9100
21	TMT-CX	3,800	44E	6750

\* RLE = root leading edge, RMT = root maximum thickness  
RTE = root trailing edge, TMT = Tip maximum thickness  
CC = concave surface XC = convex surface

Figure 11.2-7 are plots of representative stresses versus fan speed.

The maximum vibratory stresses which occurred at significant engine operating conditions during the altitude stress survey conducted on X-210 stand from 10 April through 25 April 1973 are presented in Figure 11.2-8. Table 11.2-VII presents a summary of the maximum stresses encountered during the tests as indicated by the highest reading strain gage while Table 11.1-VIII presents the maximum airfoil temperatures measured at military thrust. The gage was mounted on the blade's concave surface at the root leading edge.

TABLE II.2-VII

BORSIC ALUMINUM THIRD-STAGE BLADES MAX STRESS SUMMARY  
TF30 ENGINE X-433-26 IN X-210 STAND ALTITUDE RUNNING

S/G Record	Test Condition	Simulated Fit. Cond.			Inlet	Engine Operation	Overall Stress ~ ksi	Freq. ~ Hz	Nodal Diameter ~ E	N RPM	Comments
		P <sub>T</sub> INLET	T <sub>INLET</sub>	Mn							
229	Atmos	55° F	0.0	S/L	Clean	Accel. Idle to Mil	7.5 4.0	2	5700 4	7600 2	
231	35.3 psia	208°F	1.2	S/L	Clean	Accel. Idle to Mil	28 19	165 165	6500 7500	7500	High non integral stress occurs between 6500 - 7500 RPM Freq. of stress indicated forced vibration below 1st mode
234	35.3 psia	208°F	1.2	S/L	Clean	Decel/Accel Thru Full A/B	18.6 25.0	165 165	6700	7100	High stress same as above - apparently induced by test stand
236	35.3 psia	208°F	1.2	S/L	Clean	Accel	29.6	165	7400	7600	Inlet conditions stabilized
237	35.3 psia	208°F	1.2	S/L	Clean	Decel	16 23.2 7.2 6.0	165 165 165 165	6500 +4 2 2	7400 8300 9500	165 Hz stress predominates 15 ksi, 4E @ 9 ksi This is stress at max. speed - not a peak
245	Atmos	308°F	2.2	\$6,000	Clean	Accel Idle to Mil	9.2 3.1 4.0 2.8 2.8 2.8	260-300 260-300 260-300 260-300 260-300 260-300	7550	8700	Stress at max rpm - Not a peak 4 pulses to 40 ksi - Steady stress 2.8 ksi
246	Atmos	308°F	2.2	\$6,000	Clean	Decel to Idle	9.5 3.0	4 2	7500 8800		
990	35 psia	208°F	1.2	S/L	6.3A	Accel - Decel	11.2 12.3	4 4	7400 7400	6400	Test Stand induced stress - See Above
993	5.9 psia	-30°F	0.7	33,000	58D	Accel Idle to Mil	3.4 5.5	2 4	5700 7800		This is not peaked - idle is above 2E peak
994	5.9 psia	-30°F	0.7	33,000	58D	Decel Mil to Idle	3.4 4.8 7.7	6 2 4	4600 5600 7750		
061	5.9 psia	-30°F	0.7	33,000	Clean	At Mil Power Zone 1 Zone 2 Zone 3 Zone 4 Zone 5	1.0 10.5 3.0 3.0 3.0 3.0				Steady stress level Transient - at 10Hz and 250 Hz (first bending mode peak stress) >20 ksi

**TABLE 11.2-VIII**  
**MAXIMUM AIRFOIL TEMPERATURES MEASURED**  
**AT MILITARY THRUST**

Simulated Conditions		Inlet	Tip	Mean Section	Root
Altitude (ft)	MN	Temperature °F	(T/C)	°F	(T/C) °F
Sea Level	1.2	208	(D)	390	(F) 323 (H) 293
56,000	2.2	308	(D)	467	(C) 424 (B) 406
33,000	0.7	-30	(D)	266	(C) 214 (B) 194

Table 11.2-IX presents the slirping bearing and cavity maximum temperatures recorded at military thrust during the testing.

AD-A055 891

PRATT AND WHITNEY AIRCRAFT GROUP WEST PALM BEACH FL G--ETC F/G 1/3  
TF30 THIRD-STAGE COMPOSITE FAN BLADE SERVICE PROGRAM. (U)

MAY 78 D G RANDALL

F33657-70-C-0624

NL

UNCLASSIFIED

PWA-5141

4 of 4

AD  
A055 891



END  
DATE  
FILMED  
8-78  
DDC

**TABLE 11.2-IX**  
**MAXIMUM SLIP RING BEARING AND CAVITY TEMPERATURES**  
**AT MILITARY THRUST**

Simulated Conditions		Inlet	S/R Bearing	S/R Cavity
Altitude (ft)	Mn	Temperature (°F)	(°F)	(°F)
Sea Level	1.2	208	104	100
56,000	2.2	308	116	116
33,000	0.7	-30	104	97

Table 11.2-X presents the maximum levels in displacement ( $\pm$  mils peak, 40 Hz to 440 Hz) for the leadwire tube which carried the cables out from the slip ring.

**TABLE 11.2-X**  
**DUCTING CABLE DISPLACEMENT**

Pickup Location	N <sub>1</sub> Speed (rpm)	O/A ( $\pm$ Mils)	1E <sub>T</sub> ( $\pm$ Mils)	1E <sub>H</sub> ( $\pm$ Mils)
Elbow, Vertical	9250	1.8	1.5	0.5
Elbow, Horizontal	9400	3.2	2.8	0.7

#### 11.2.2.4 Analysis of Data

Co-Quad analysis of the RLE-CC strain gages was accomplished to determine the mode shape of the high nonintegral stresses which occurred. Phasing results show that the data satisfies conditions for an eight nodal diameter wave traveling rearward. The frequency of the response was less than the third-stage blade first bending mode and is attributed to an acoustic rumble heard in the stand during this operating condition.

#### 11.2.2.5 Regions of High Stress

During this series of tests two regions of high stress were observed which merit special discussion.

In the first region observed, fluctuating stresses on the order of 25,000 to 30,000 psi occurred over a speed range of 6,500 to 7,500 rpm at Mach No. 1.2, sea level simulated operating conditions. The frequency of blade vibration was non-integral between 115 and 160 Hz, which is approximately 30 Hz below the third stage first coupled mode frequency. The first coupled mode frequency has been experimentally verified as 175 Hz at 5600 rpm, which, with centrifugal stiffening, would give a frequency of 195 to 210 Hz between 6500 and 7500 rpm. It is concluded that this high stress region is a forced vibration (since the blade normal mode is substantially higher in frequency) and not flutter, and is associated with test stand engine coupling conditions or transients. The fact that a "rumbling" was heard in the control room at the time the stresses were high also suggests that the vibration is due to stand conditions.

It is felt that this high stress is of negligible concern for engine operation in the airplane, because it is apparently a phenomenon associated with the test stand and in addition at sea level, Mach number 1.2, the engine will not be operating in the speed range where the high stress was observed.

The second area of high stress on third-stage blades meriting special comment is the transient peak which occurred during Zone 1 afterburner light while simulating Mach number of 0.7 at 33,000 feet altitude. This transient occurred only during Zone 1 light and high stress persisted for approximately 2.5 seconds, and reached levels on the order of 25,000 psi. Close examination of the pulse revealed that it is comprised of five separate pulses, each approximately 0.3 seconds in duration with low stress periods in between. Two components of frequency were present in these spikes, blade first bending approximately 250 Hz at a level of 15,000 to 16,000 psi and, a very low frequency 8 to 10 Hz at a level estimated to be 20,000 to 25,000 psi. The low frequency component also appears on engine linear vibration pickups and fan duct static pressure pickups.

There are no stress transients associated with lighting the other four zones of afterburning.

#### 11.2.3 Altitude Endurance Testing

This section outlines the altitude endurance testing at Mn 1.2 and 2.2 conditions conducted on the TF30-P-9 third-stage BORSIC®/aluminum fan blades designed and fabricated under this program. These tests were required by Contract F-33657-70-C-0624.

A composite fan blade design review meeting held on 12 February 1973 resulted in some additions to the original program in order to incorporate distortion screen runs at Mn 1.2, sea level and Mn 0.7, 40,000 feet. The revised altitude program is presented in the subsequent paragraphs of this document.

#### 11.2.3.1 Test Procedures (Altitude Endurance Testing)

The engine was built to the TF30-P-9 configuration in order to run Mach 1.2 and Mach 2.2 endurance testing on the BORSIC®/aluminum composite material third-stage fan blades in accordance with the requirements of Contract F-33657-70-C-0624. In addition, a sea level functional and performance checkout was conducted before the engine was delivered to the altitude facility (X-210 stand). During all running, the composite blade strain gages were monitored.

In order to complete this running, the following sequence was used:

- Normal Operating Procedures
- Stand Preparation and Mount
- Checkout Procedures
- Sea Level Performance Calibration
- Altitude Endurance Program

##### 11.2.3.1.1 Normal Operating Procedures

1. All adjustments and work was recorded on the operators log sheets including all incidents of the test such as leaks, vibration, or any other irregular functioning of the engine or components.
2. The following procedure was used for all starts:
  - a. Set starter air pressure at 50-60 psig measured at inlet to starter.
  - b. Energize engine starter.
  - c. 750-800 rpm  $N_2$  - ignition switch on.
  - d. 2500 rpm  $N_2$  - throttle to idle.
  - e. Max.  $T_{t5}$  - 1300°F
  - f. Check for oil pressure indication within 10 seconds.
  - g. Engine starter switch-off (when start is assured) 7000-7500  $N_2$ .
  - h. Ignition switch - ARS position.
  - i. Nozzle position indicator - check for open.
  - j. Take an idle reading.

PRATT & WHITNEY AIRCRAFT GROUP

3. The following check procedure was used for starts after lay-up:
  - a. Check exhaust nozzle operation as power lever is slowly moved off idle. Nozzle should actuate at  $22^\circ +1^\circ$  PLA.
  - b. Make a slow accel and check that the 12th bleeds close.
  - c. Check seventh bleed operation between 8000 and 8500  $N_1$  observed.
  - d. Continue the slow acceleration to mil power noting any abnormalities in vibration, main oil pressure, and breather pressure.
4. Wet and dry bulb temperature and true barometer were read every hour, except every 3 hours while on endurance.
5. Oil samples were taken at convenient intervals during the test.
6. For all power lever movements the power lever was advanced or retarded as applicable, in not more than 1 second.

11.2.3.1.2 Stand Preparation and Mount

1. This test was run with a blunt nose, coarse bellmouth and inlet screen at sea level and modified as necessary at altitude.
2. T/C's were installed on the inlet screen.
3. A full barrel of oil, PMC 9874, was available at the stand.
4. Fuel used was MIL-J-5161 Grade I (JP4C).
5. Four fuel flow turbine meters (Cox) were used on this test.

2-2" Cox

2-1/4" Cox

The following parameters were recorded on a continuous tape monitor multiplex system (Mars):

<u>Parameter</u>	<u>Range</u>	<u>Remarks</u>
Time of Day		
$N_1$	0-11000 rpm	
$N_2$	0-16000 rpm	
Vibration (inlet case)	4 mils/in	
Vibration (diffuser case)	4 mils/in	
Vibration (rear case)	4 mils/in	

<u>Parameter</u>	<u>Range</u>	<u>Remarks</u>
$P_{s4.5}$	0-200 psig	
$W_f$ (High Range)	2" Cox Meter	
PLA	0° - 120°	
Thrust	0-25000 lbs.	Transducer at load cell
$T_{t5}$	0-2300°F	Potentiometer inside Brown Indicator
$P_b$	0-300 psig	
Nozzle Position	Open-Closed	
Main Oil Pressure	0-60 psig	

6. AiResearch starter Model ATS100-232 was used.
7. All stand fuel filters were cleaned prior to running.

#### Mount

1. The engine was mounted per mount sheet left hand side with 2° - 22° tilt and 5° rotation sea level and 2° 22' tilt and 0° rotation at altitude.
2. A blunt nose coarse bellmouth and inlet screen was installed.
3. The engine oil tank was filled with 5 gal of PMC 9874 oil and the batch number and supplier were recorded. The sight glass was calibrated. One half gallon oil was taken as a sample from barrel at stand for complete MDL analysis.
4. Two 3/4" fuel flow meters (Cox) were installed between the main fuel control discharge and the main fuel oil cooler inlet.
5. Two 2" fuel flow turbine meters (Cox) were installed at the stand filter discharge in the main fuel line.
6. An exhaust nozzle position indicator was installed and calibrated for "open" and "closed".
7. Six  $P_{t2}$  probes were installed P/N 403104 SKL-39451 (sea level only).
8. T/C's were installed on the inlet screen.
9. Vibration pickups were installed.
10. The specific gravity setting on the fuel control and A/B meter was set on JP4C.
11. All instrumentation was installed per the instrumentation sheet.
12. Inflight trim motors were hooked up.

11.2.3.1.3 Sea Level Check Out Procedures

1. All adjustments and work were recorded on operator's log sheet. Operators log sheet was carbon backed starting with the trim.
2. All stand fuel filters were vented and full of fuel.
3. The engine was motored and the fuel system pressurized with the ignition off long enough to establish a constant oil pressure and purge the fuel system of air. A leak check was made.
4. The engine was motored without pressurizing the fuel system to dry the engine.

Prior to starting the engine, appropriate personnel were notified to record the initial start and all transient running

5. The engine was started per normal procedures (paragraph 11.2.3.1).
6. An idle reading was taken.
7. Inspect engine for leaks at idle.
8. The engine was checked per normal procedures (paragraph 11.2.3.1).
9. A slow accel to 10,000 lb.  $F_n$  was made noting any abnormalities in vibration main oil pressure and breather pressure. Transient running was recorded.

NOTE:  $F_n$  stability to be  $\pm 1\%$ .

10. A full instrumentation reading was taken.
11. Turbine cooling pressure was checked.  
 $P_{s4.5}/P_{s4} = .65 \pm .02$ .
12. Main oil temperature automatic regulation was checked.
13. Check corrected main oil pressure differential. Should be  $45 \pm 5$  psig at normal rated and above.
14. Cox meter fuel flow agreement was checked to be within one percent.
15. Engine was slowly advanced to military (PLA  $65^\circ$  to  $68^\circ$ ). Military trim curve  $T_{15}$  was not exceeded. Military trim down was adjusted if necessary with in-flight trim motor.

16. A full instrumentation reading was taken.
17. Check afterburner operation to Max Zone 5.
18. Shut down and repair bad instrumentation.
19. Thrustmeter was calibrated from 0-25,000 lbs.

#### 11.2.3.1.4 Performance Calibration

1. Station 2 and Station 3 instrumentation was installed.
2. Suppression in Mid Zone 3 was rechecked.
3. Full data readings were taken at the following points (the points were stabilized seven minutes before read and wet and dry bulb thermometer and barometer were taken every hour).
  - a. Idle
  - b. Min 12th bleeds closed.
  - c. 6000  $F_n$
  - d. 8000  $F_n$
  - e. 10,000  $F_n$
  - f. 11,000  $F_n$
  - g. 12,000  $F_n$
  - h. Mil trim
  - i. Min Z-1
  - j. Mid Z-3
  - k. Max Z-5
4. When calibration was completed and data checked, the engine was shut down and pulled to prepare for installation in X-210 capsule.

#### 11.2.3.1.5 Altitude Running Program

1. With slip ring cooling air on and strain gage monitor on, the engine was windmilled and checked for leaks.

2. The engine was started and a full idle reading taken. Recording strain gages were started.
3. The engine was shut down and instrumentation repaired where necessary.
4. A slow acceleration to military was made and mil trim was checked. Any abnormalities were noted.
5. Acceleration to maximum Zone 5 was accomplished and a suppression check made.
6. The capsule was closed, the engine started and accelerated to military while setting Mach 2.2, 60,000 feet, conditions of 245°F inlet air at 14.7 psia and  $P_{t7}/P_{ejector}$  of 2.3 minimum in order to warm up duct work and deceleration to idle. Make a 30 second acceleration and 30 second deceleration from idle to military and back to idle while holding Mach 2.2 conditions. NOTE: The accel/decel would have to be extended longer than 30 seconds if conditions could not be maintained that quickly.
7. Mach 1.2 sea-level conditions of 208°F inlet air at 35.3 psia and  $P_{t7}/P_{ejector}$  of 2.4 minimum were set. Recording strain gages were started. A 30 second (if possible) acceleration to military and a 30 second (if possible) deceleration to idle were made. Equipment was cooled and shut down.
8. A distortion spider and distortion screen No. 58D (Mach 0.7, 40,000 feet) was installed. The engine was started and conditions of Mach 0.7, 40,000 feet, of -31°F inlet air at 3.78 psia and  $P_{ejector}$  of 2.72 psia were set. Recording strain gages were started and a 30 second (if possible) acceleration to military and 30 second (if possible) deceleration to idle were made. Equipment was cooled and shut down.
9. The Mach 0.7, 40,000 feet, distortion screen was removed and Mach 1.2 sea level distortion screen (screen No. 63A) was installed. The engine was started and conditions of Mach 1.2 sea level of 208°F inlet air at 35.3 psia and  $P_{t7}/P_{ejector}$  of 2.4 minimum were set. Recording strain gages were started and a 30 second (if possible) acceleration to military and 30 second (if possible) deceleration to idle while holding conditions were made. Equipment was cooled and shut down.
10. The slip ring setup, distortion screen and spider, and strain gage P.T.O. cover were removed.
11. The capsule was closed, the engine started and accelerated to military while Mach 1.2 sea-level conditions of 208°F inlet air at 35.3 psia with  $P_{t7}/P_{ejector}$  of 2.4 minimum were set.
- 12.\* 6.25 hours at military power were run as shown in Figure 11.2-9.
- 13.\* A/B was lighted, the same conditions as Item #11 were set and the engine was run 6.25 hours at maximum Zone 5. (Figure 11.2-9).

14. Mach 2.2 conditions were set as shown in Figure 11.2-10.
15. 25 cycles of Mach 2.2 endurance (Figure 11.2-10) were run.
16. The engine was shut down for third-stage fan blade inspection and decision on additional running of 70 hours at Mach 2.2 conditions.
17. Testing was resumed and a total of 120-hours at Mach 2.2 conditions was completed.

\* Items 12 and 13 were combined into 10.5-hours testing at military power.

#### 11.2.4 Destructive Examination of Engine Test Blade

After a fan case tip rub occurred during engine operation, seven BORSIC®/aluminum fan blades were found to have cracks just above the titanium root. Two blades had cracks of reasonable size; the remaining five exhibited smaller cracks. The cracks were discovered by means of fluorescent penetrant and visual inspection. The blades were removed from the engine and a comprehensive examination was scheduled. As the damage to the two blades having the larger cracks was similar, the examination was conducted primarily on Blade E-184.

The examination showed that material properties and general structure were consistent with requirements. Fiber breakage on the convex side was generally superficial and confined to surface ply. Fiber breakage on the concave side was due to over-stressing in operation, and extended through the cross plies but did not extend into the longitudinal central fibers.

The fabrication data compiled for these two blades was reviewed and indicated that both the raw material and fabricating process were completely acceptable. Quality assurance data, presented in Table 11.2-XI, indicated that the fiber used in Blade E-184 had axial tensile strengths exceeding 425,000 psi and a hot pressed density of 2.67 gram per cubic centimeter.

TABLE 11.2-XI  
QUALITY ASSURANCE DATA  
SERVICE BLADE E-184

Density:	2.668 gm/cm <sup>3</sup>
Union Carbide Tape Lot:	3004-91
Monotape strength:	
Fiber Lot (a):	425,000 psi      425,000 psi avg
	425,000 psi
Fiber Lot (b):	427,000 psi      452,000 psi avg
	477,000 psi

#### 11.2.4.1 General Condition of Blade

As shown in Figure 11.2-11 damage was incurred at the trailing edge tip due to contact with the fan case. Minor localized deformation and fiber breakage was observed.

A crack in the aluminum surface layer extended about one-half inch on both the convex and concave sides from the leading edge, as shown in Figures 11.2-12 and 11.2-13, just above the horizontal plane edge of the titanium root blocks. No other defects were observed.

The titanium root blocks were significantly misaligned at the upstream end of the blade as shown in Figure 11.2-14. Deformation of plies just above the root blocks was also observed.

#### 11.2.4.2 Determining Fiber Breakage By Leaching

Before leaching, a 3/8-inch section of the leading edge was removed for microexamination as shown in Figure 11.2-15. The aluminum surface layer and underlying matrix material was progressively removed by acid leaching so that each fiber layer would be exposed. It was then possible to measure the crack length in each fiber layer.

The crack length from the cut surface was measured for each ply on both the convex and concave sides, and is shown in Figures 11.2-15 and 11.2-16. Damage to the first ply was slightly more extensive than indicated on the aluminum surface. The degree of damage decreased in each subsequent inner ply, and was more severe on the concave side, which is consistent with the stress distribution due to the tip rub.

Figure 11.2-17 indicates the more moderate damage on the convex side first ply layer. There was no damage in any layers beneath the second layer. Some random fiber breakage away from the crack was observed on the convex side, attributable to the fabrication process.

Figure 11.2-18 indicates the more extensive cracking on the concave side. Similar fiber breakage in the alternate cross plies was observed in decreasing extent until the eighth layer, as indicated in Figure 11.2-16. Although some cracking is reported in layers eight and nine, the proximity of the damage to the cut surface may indicate the cause was the sectioning process. Figure 11.2-19 shows the first longitudinal fiber layer; slight damage is indicated near the saw cut surface in a plane slightly above the dominant fracture plane of the cross plies.

#### 11.2.4.3 Microexamination

Examination of the longitudinal surface plane of the leading edge through the surface fracture region indicated a consistent crack pattern to that determined by leaching. Damage was more severe on the concave side than the convex, but did not extend into the longitudinal plies. While there was slight evidence of matrix cracking, it was not considered indicative of any failure mode other than stressing beyond the ultimate tensile strength.

### 11.2.5 Nondestructive Inspection

After the 200-hour altitude/supersonic test program, Blade Set No. 2 was non-destructively inspected. The results of the inspection paralleled those of Blade Set No. 1 after the 100-hour sea-level static endurance test which were described in paragraph 11.1 of this report. Four blades of Set No. 2 exhibited leading edge cracks in the fillet area, the longest being 5/16 inch. This data is presented in Table 11.2-XII.

Table 11.2-XIII presents the frequency history of the blades. Except for the seven blades which were damaged in the tip rub experience, the frequency losses were modest and well within the blade design limits.

The blade tip chord angles were not charted prior to the test, but post-test results are presented in Table 11.2-XIV. Of the seven blades charted, five of the blades are within tolerance, and of the other two, the worst is less than half a degree out of tolerance.

TABLE 11.2-XII  
X-RAY RESULTS  
SET NO. 2 AFTER 200 HOURS  
(Fillet Area Cracks Only)

Blade No.	Pretest	Post test
168	None	1/16 inch LE
175	None	5/16 inch LE
190	None	1/8 inch LE
199	None	5/16 inch LE 1/4 inch TE

TABLE 11.2-XIII

## NATURAL FREQUENCIES

SET NO. 2 AFTER 200 HOURS OF SUPERSONIC/ALTITUDE ENGINE TESTS

Blade No.	1st Bending			2nd Bending			1st Torsion			
	Pretest	Post test	% Change	Pretest	Post test	% Change	Pretest	Post test	% Change	
87	144	168	4.2	462	439	5.0	983	970	1.3	
114	143	142	0.7	462	455	1.5	989	991	+0.2	
115	144	141	2.1	459	458	0.2	967	967	0.0	
155	139	138	0.7	438	445	+1.5	957	963	+0.6	
167	139	138	0.7	447	437	2.2	966	968	+0.2	
168	141	138	2.1	456	443	2.8	970	1037	+6.2	
169	137	135	1.5	449	437	2.6	946	949	+0.3	
170	137	135	1.5	450	440	2.2	941	941	0.0	
171	138	137	0.7	449	445	0.9	974	974	0.0	
175	141	140	0.7	456	446	2.2	974	975	0.1	
176	143	141	1.5	460	452	1.7	976	973	0.5	
178	139	138	0.7	452	443	1.9	965	964	0.1	
179	140	140	0.0	460	452	1.7	964	956	0.8	
180	139	138	0.7	456	446	2.2	955	954	0.1	
182	137	136	0.7	449	440	1.9	945	951	0.6	
183	141	139	1.5	455	443	2.6	965	964	0.1	
186	136	139	+2.1	447	450	+0.7	937	967	+3.2	
187	136	134	1.5	443	434	1.9	941	942	+0.1	
188	140	138	1.5	455	444	2.4	967	965	0.2	
189	137	137	0.0	445	436	1.9	950	950	0.0	
190	139	137	1.5	455	442	2.8	964	961	0.3	
191	137	136	0.7	447	436	2.4	949	947	0.2	
192	138	137	1.5	447	436	2.4	962	962	0.0	
193	136	135	0.7	444	432	2.6	945	947	+0.2	
195	138	136	1.5	447	436	2.4	947	947	0.0	
197	139	138	0.7	453	444	1.9	957	955	0.2	
198	142	141	0.7	454	448	1.0	996	1054	+5.5	
199	139	138	0.7	453	445	1.7	957	960	+0.3	
200	136	134	1.5	440	425	2.8	937	940	+0.3	
Avg. % Change						1.9			+0.4	
*	194	136	137	+0.7	433	442	+2.2	930	942	+1.3
	201	135	136	+1.5	429	438	+1.9	920	931	+1.2
	205	133	132	0.7	429	428	0.2	928	933	+0.5
	206	133	134	+0.7	427	435	+0.7	915	926	+1.2
	212	233	133	0.0	425	434	+1.9	917	926	+0.9
	223	138	138	0.0	435	442	+1.7	947	960	+1.3
	225	140	141	+0.7	443	451	+1.7	960	971	+1.2
	Avg. % Change								+1.1	

TABLE II.2-XIII (Cont'd.)

Blade No.	Pretest	1st Bending			2nd Bending			1st Torsion		
		Post test	% Change	Pretest	Post test	% Change	Pretest	Post test	% Change	
** 82	141	—	—	447	—	—	961	—	—	
85	140	—	—	443	—	—	941	—	—	
89	143	—	—	457	—	—	985	—	—	
148	140	—	—	461	—	—	972	—	—	
163	139	135	2.9	451	421	6.6	944	927	1.8	
184	139	134	3.6	452	424	6.1	952	936	1.7	
196	139	—	—	455	—	—	967	—	—	
Avg. % Change		3.3			6.4			1.8		

\* Replacement blades following tip rub (60 hours).

\*\* Blades removed after 60 hours.

B/P Tol.      1st bending mode  $130 \pm 15$  cycles/sec  
 2nd bending mode 410 min cycles/sec  
 1st torsion mode 850 min cycles/sec

TABLE 11.2-XIV  
 TIP STATION CHORD ANGLE  
 BLADE SET NO. 2 AFTER 200 HOURS

B/P Tol.  $19^\circ 58' - 21^\circ 22'$ 

Blade No.	Post Test
194	$21^\circ 0'$
201	$21^\circ 46'$
205	$19^\circ 46'$
206	$20^\circ 0'$
212	$20^\circ 38'$
223	$20^\circ 24'$
225	$20^\circ 52'$
Avg.	$20^\circ 38'$

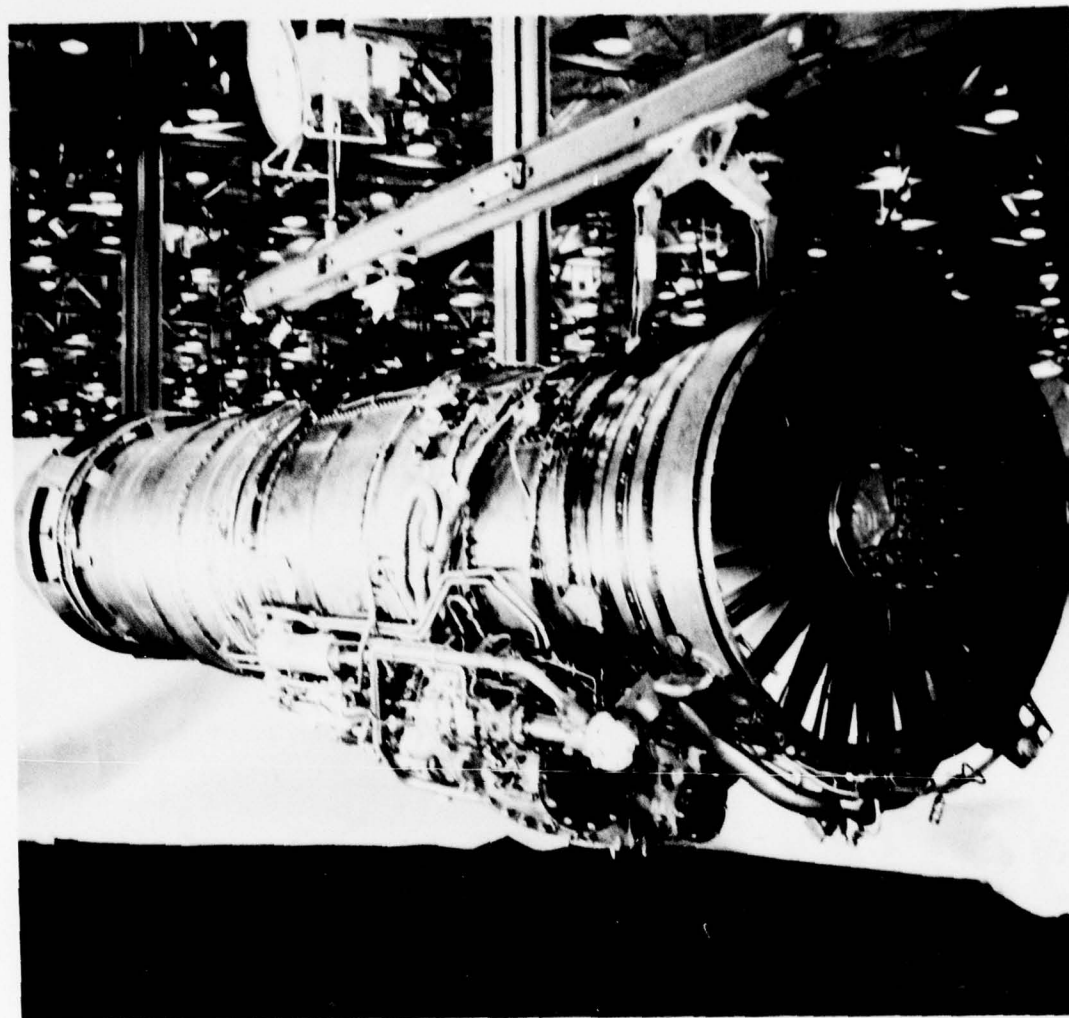
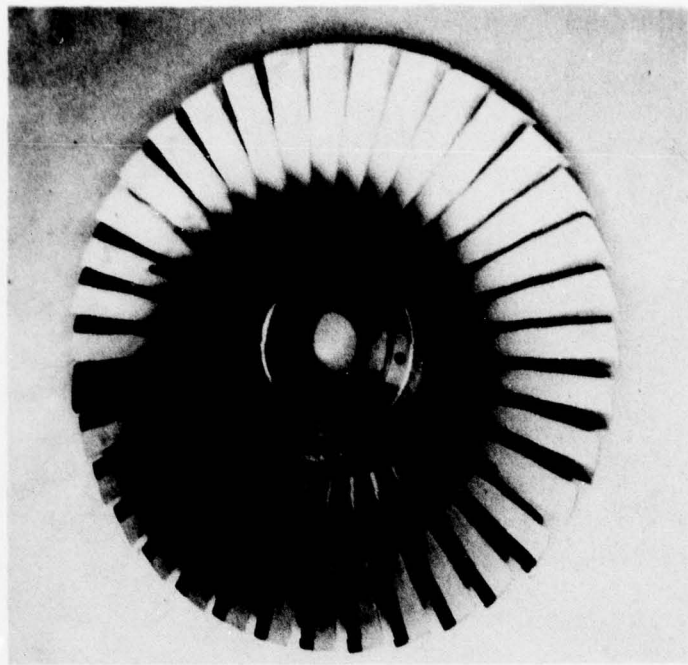
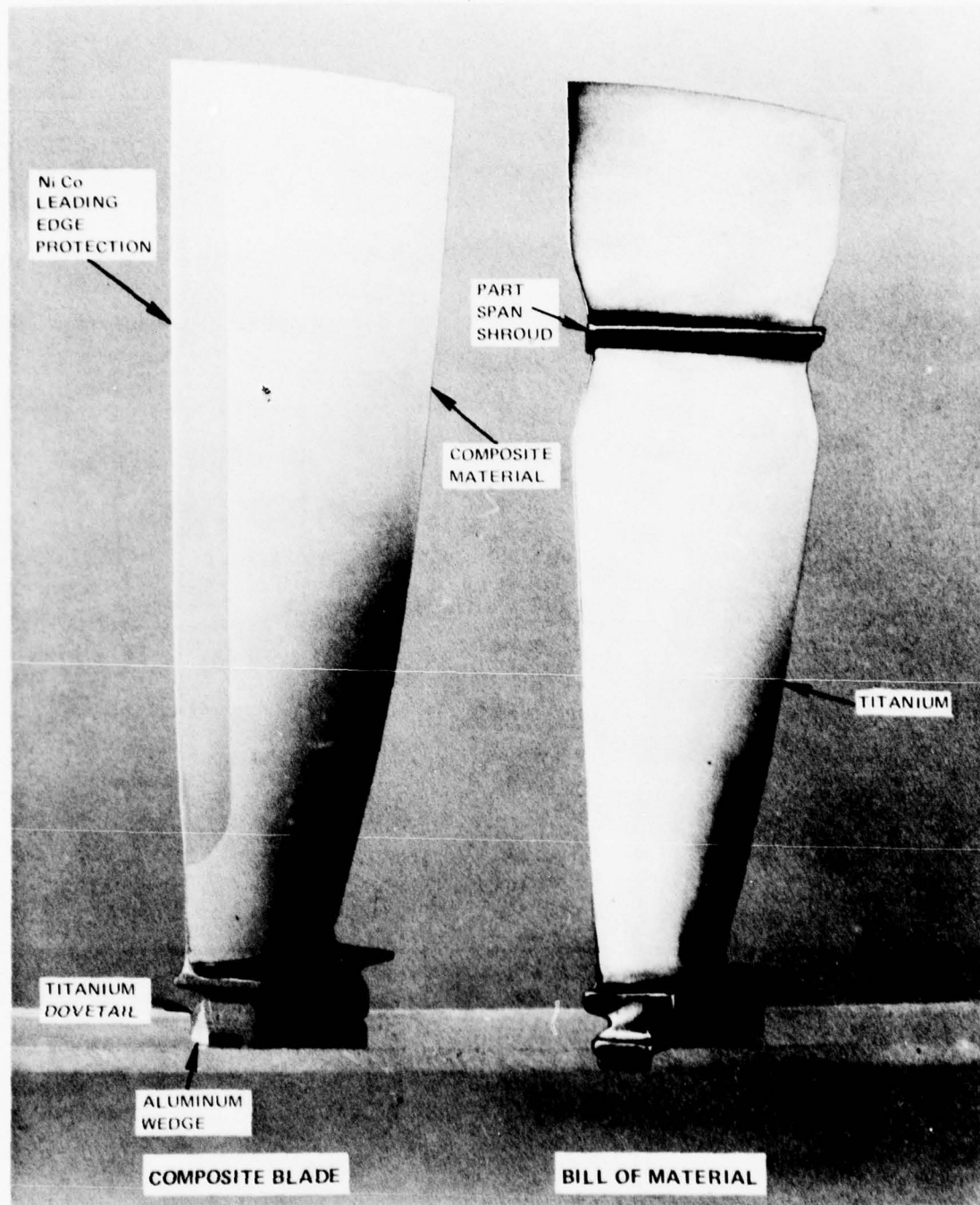


Figure 11.0-1 *The Vehicle for Conducting Engine Environmental Tests on BORSIC®/Aluminum Fan Blades Was a TF30 P-9 Engine*



*Figure 11.0-2 Blade Set No. 2 Used in the Supersonic/Altitude Test Program*



Figures 11.1-1 Comparison of the BORSIC®/Aluminum TF30-P-9 Third Stage Fan Blade With the B/M Titanium Fan Blade



Figure 11.1-2 Pratt & Whitney Aircraft TF30-P-9 Engine

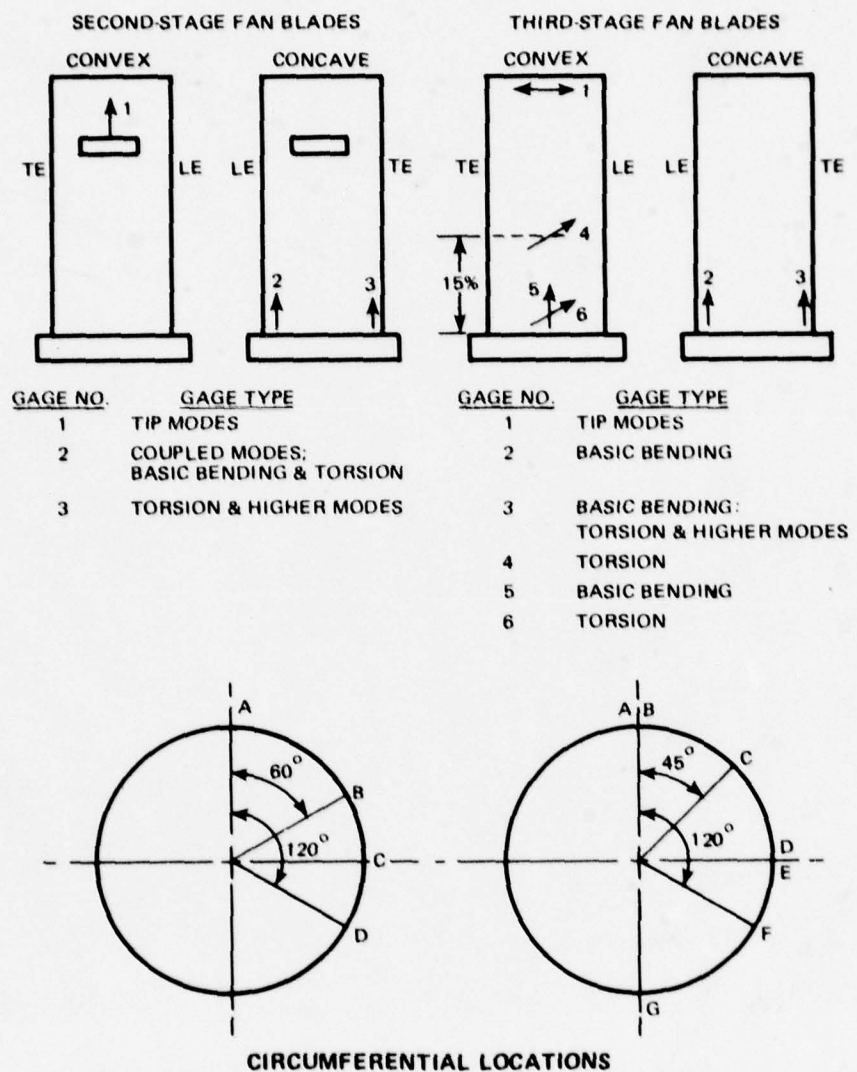


Figure 11.1-3 Schematic Showing Location and Type of Strain-Gage Instrumentation on Second- and Third-Stage Fan Blades for Sea-Level Engine Environment Test

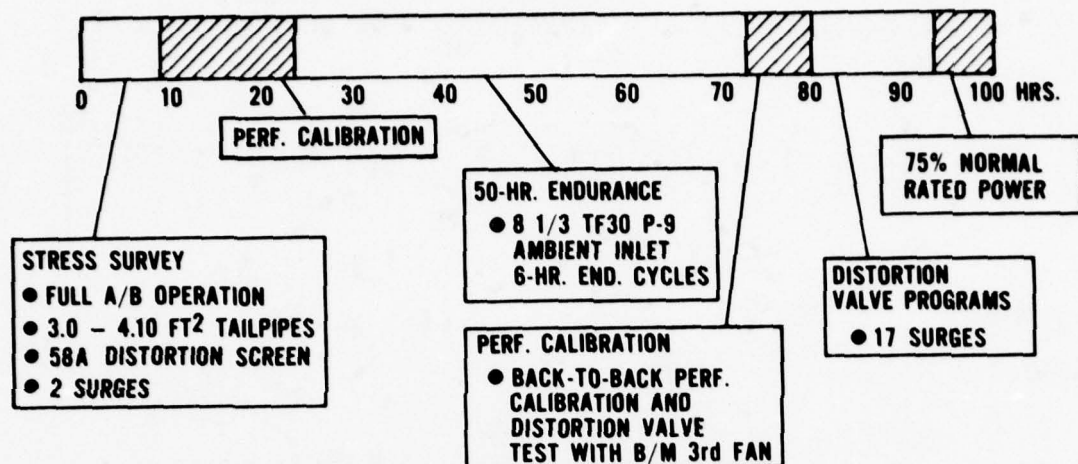


Figure 11.1-4 Schedule for 100-Hour Subsonic Engine Test Program (Blade Set No. 1)

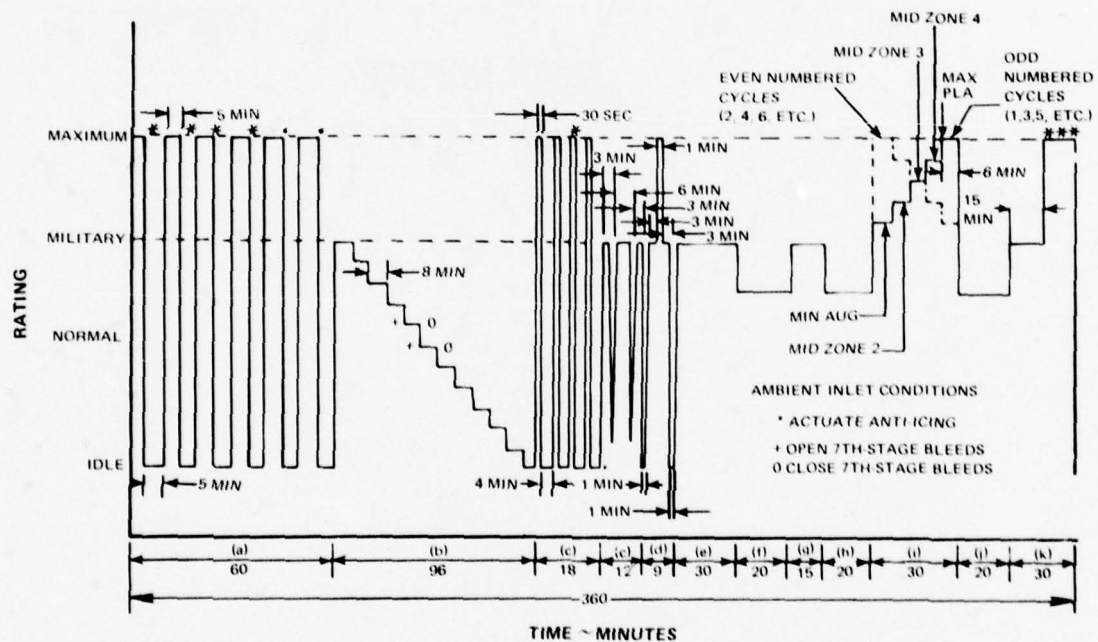


Figure 11.1-5 TF30-P-9 Six-Hour Endurance Cycle

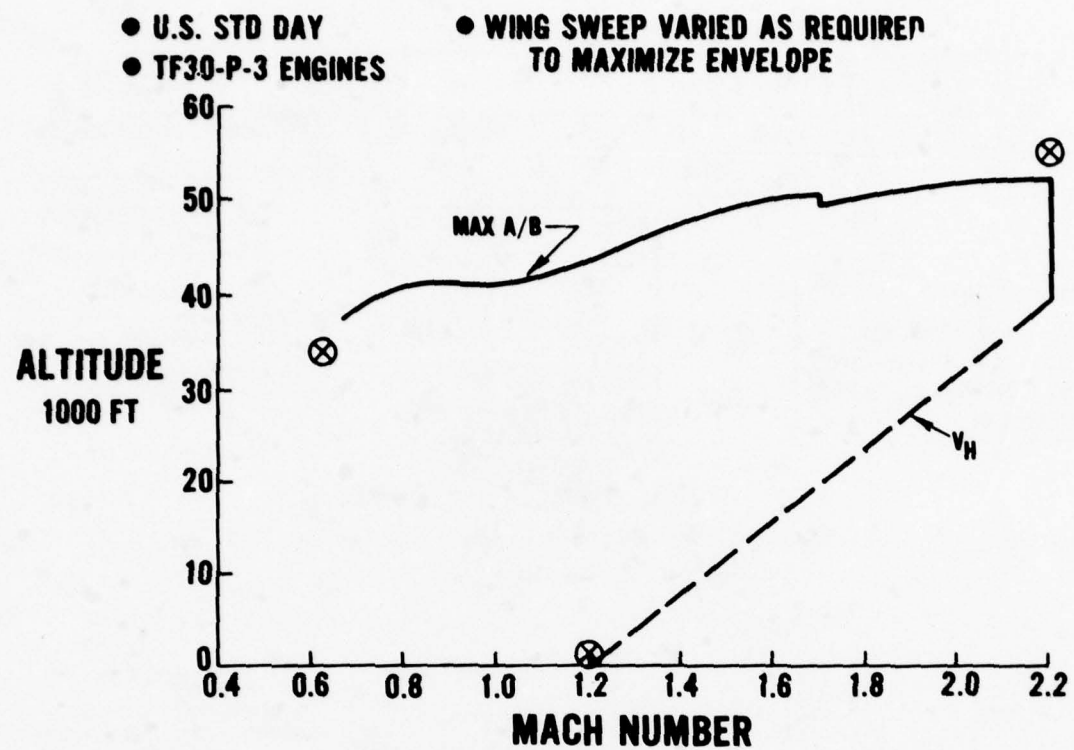


Figure 11.2-1 Flight Envelope of the F-111A Aircraft

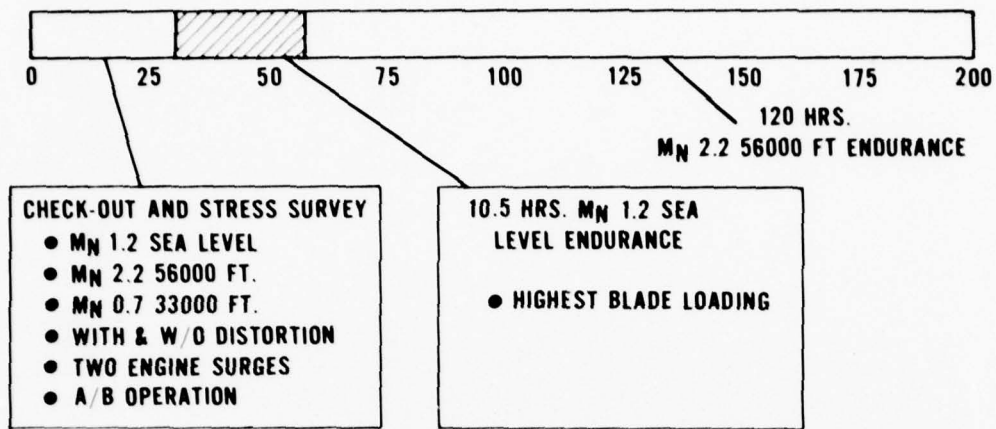


Figure 11.2-2 The 200-Hour Supersonic/Altitude Test Program in Which Blade Set No. 2 Was Used

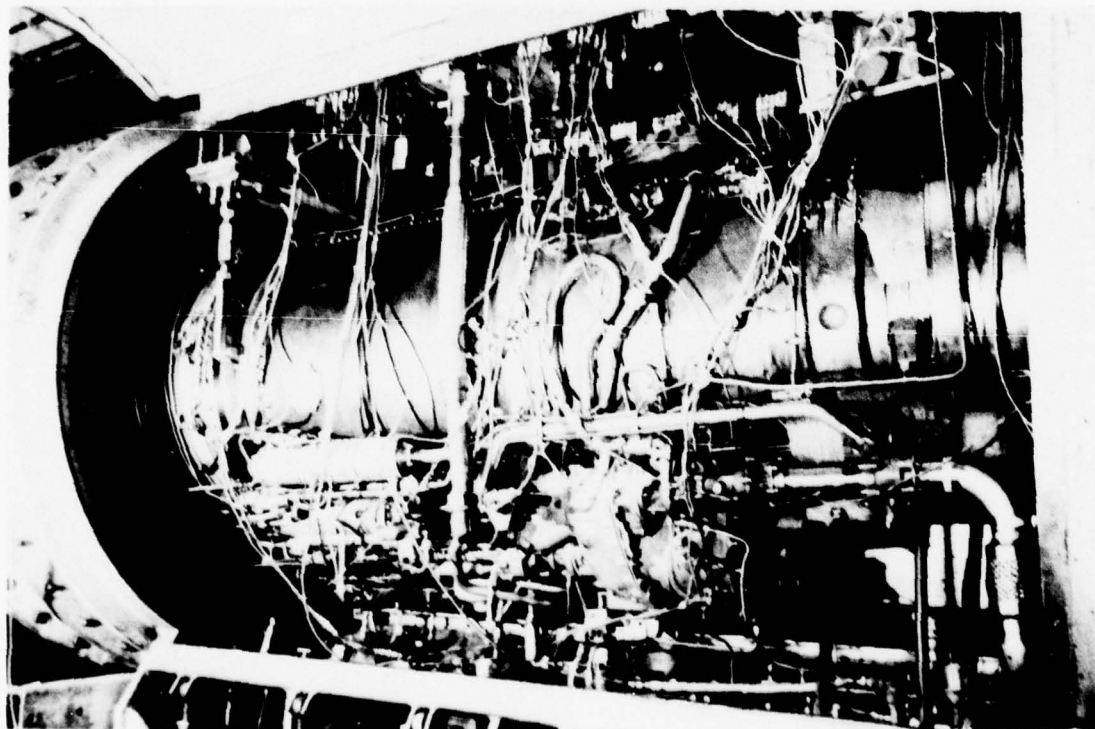


Figure 11.2-3 TF30-P-9 Engine Installed in X-210 Test Stand

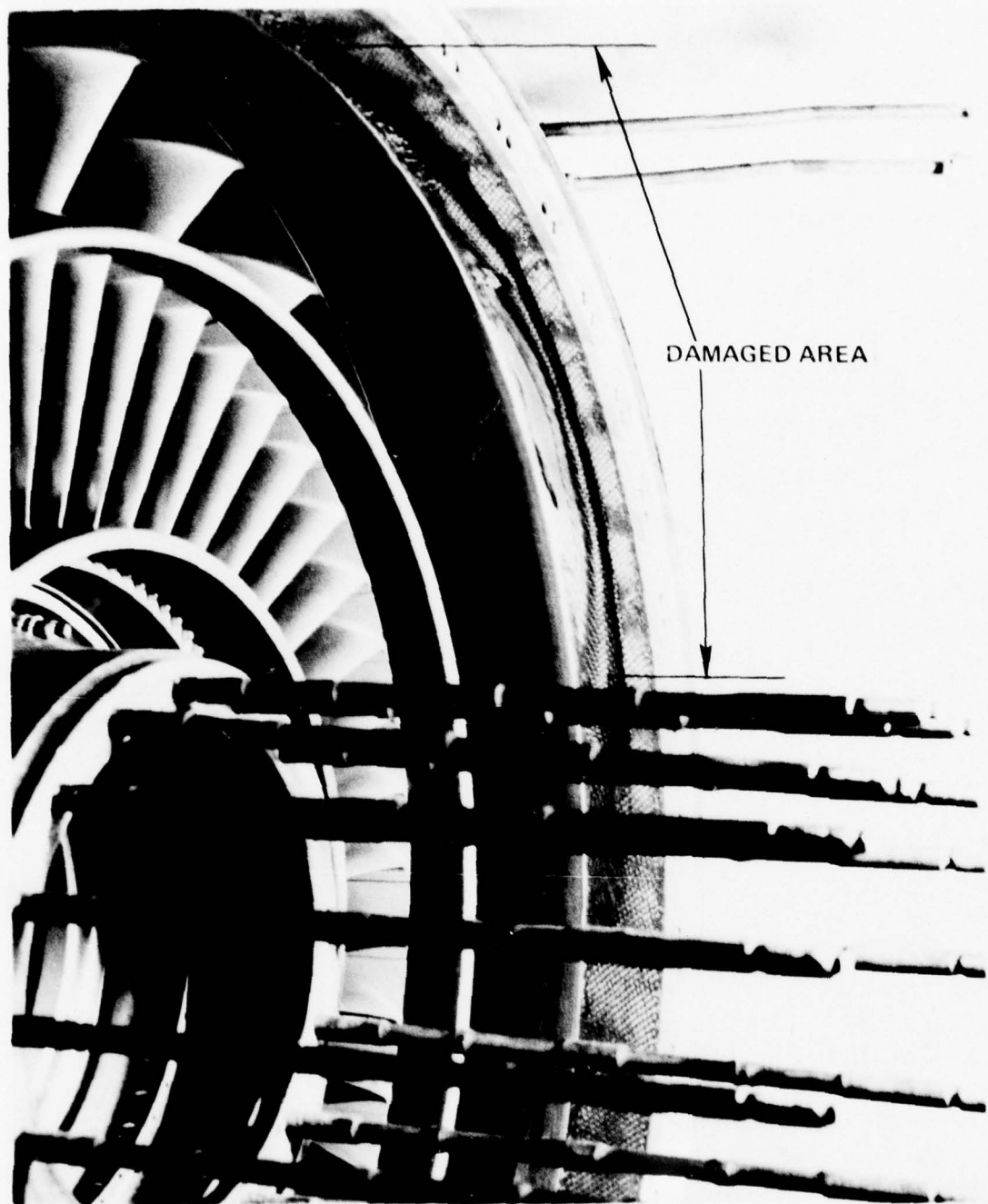


Figure 11.2.4 - 0.090-Inch Deep Tip Rub Area on TE30-P-9 Engine Fan Case

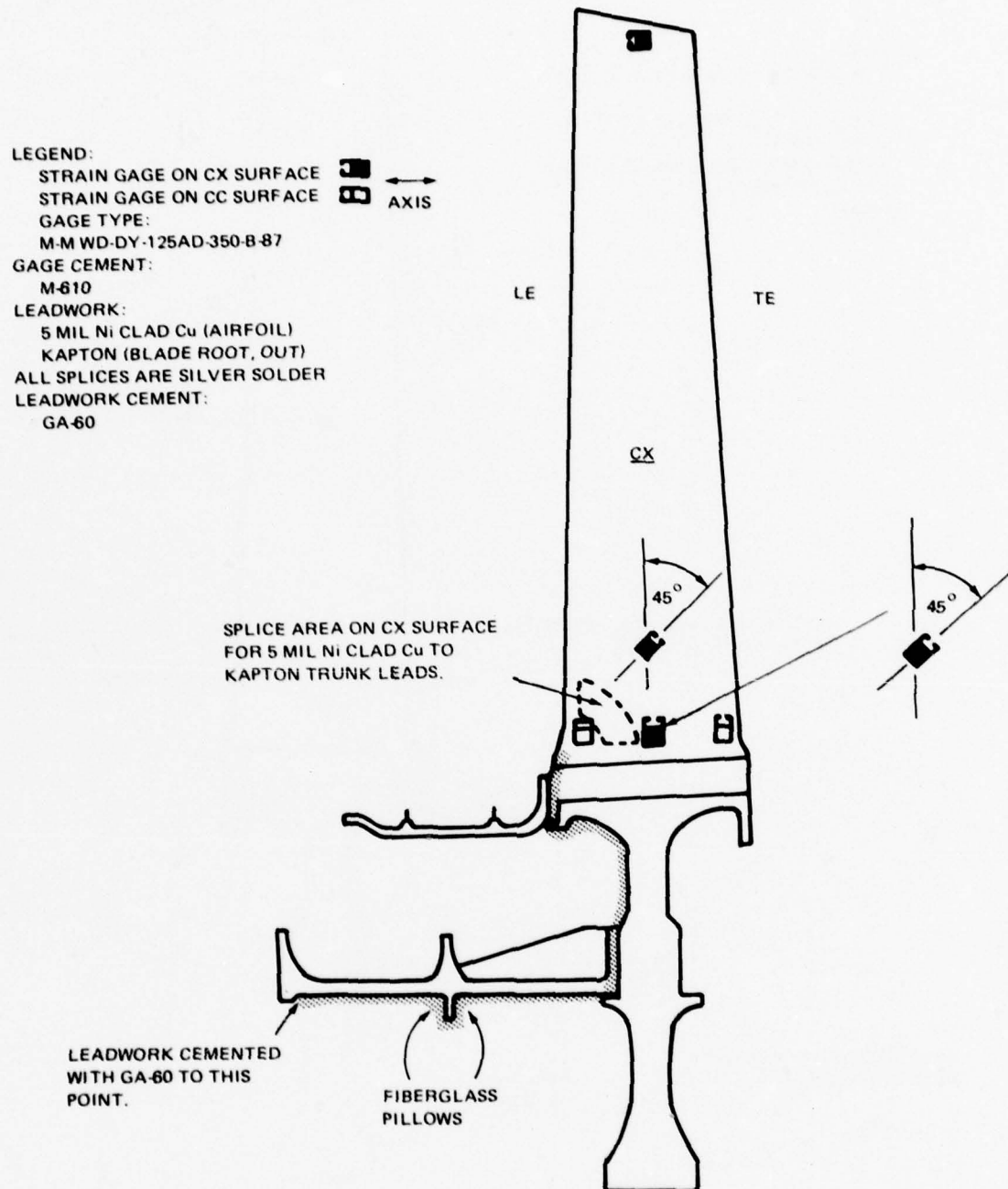


Figure 11.2-5 Installation of Strain-Gage Instrumentation on BORSIC®/Aluminum Third-Stage Fan Blades

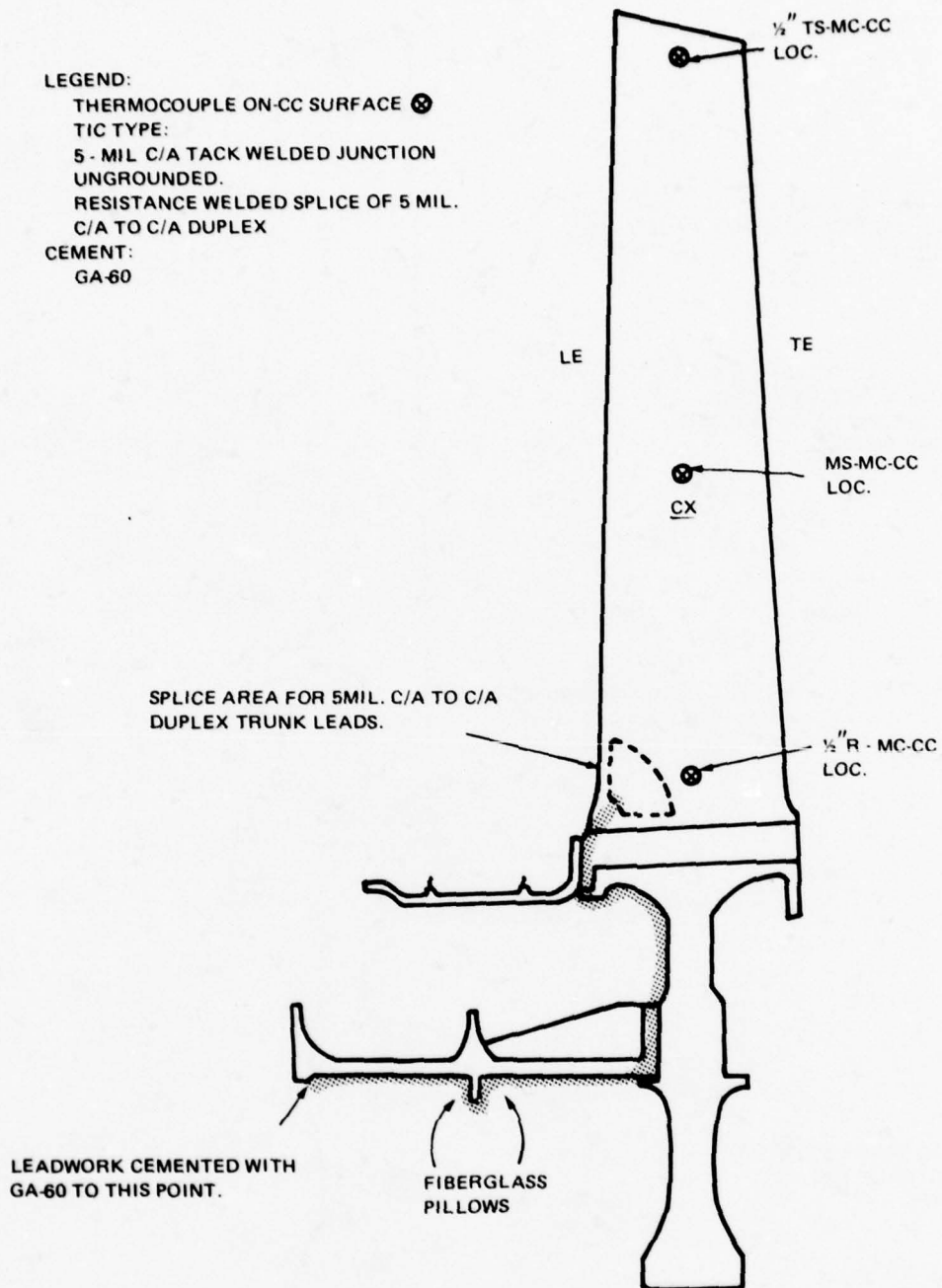


Figure 11.2-6 Installation of Thermocouple Instrumentation on BORSIC®/Aluminum Third-Stage Fan Blades

PRATT & WHITNEY AIRCRAFT GROUP

VIBRATORY STRESS SURVEY

ENGINE X-433-26

TEST STAND X-231

TEST DATE 2-22-73

TITLE INSTRUMENTATION CHECK OUT RUN

COND. CLEAN INLET, TEMP -45°F, ALT = SEA LEVEL,  $M_N$  = STATIC

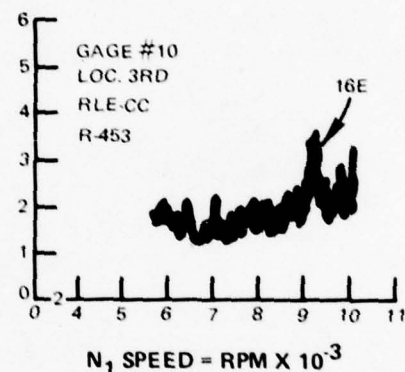
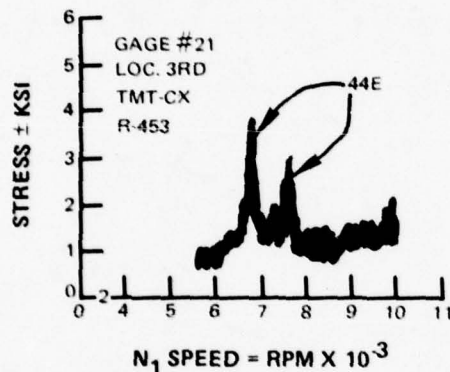
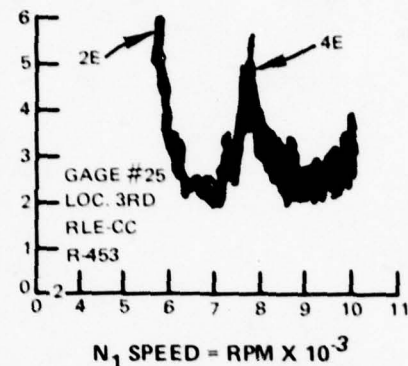
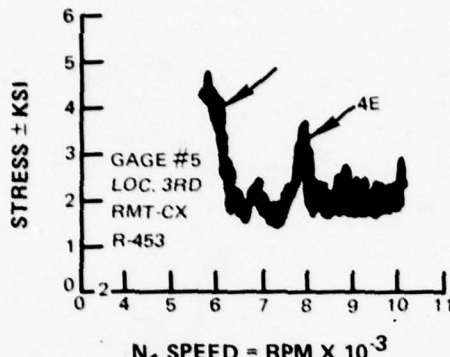


Figure 11.2-7 Data From the Preliminary Stress Survey Yielded the Data for These Plots of Representative Stress Versus Fan Speed

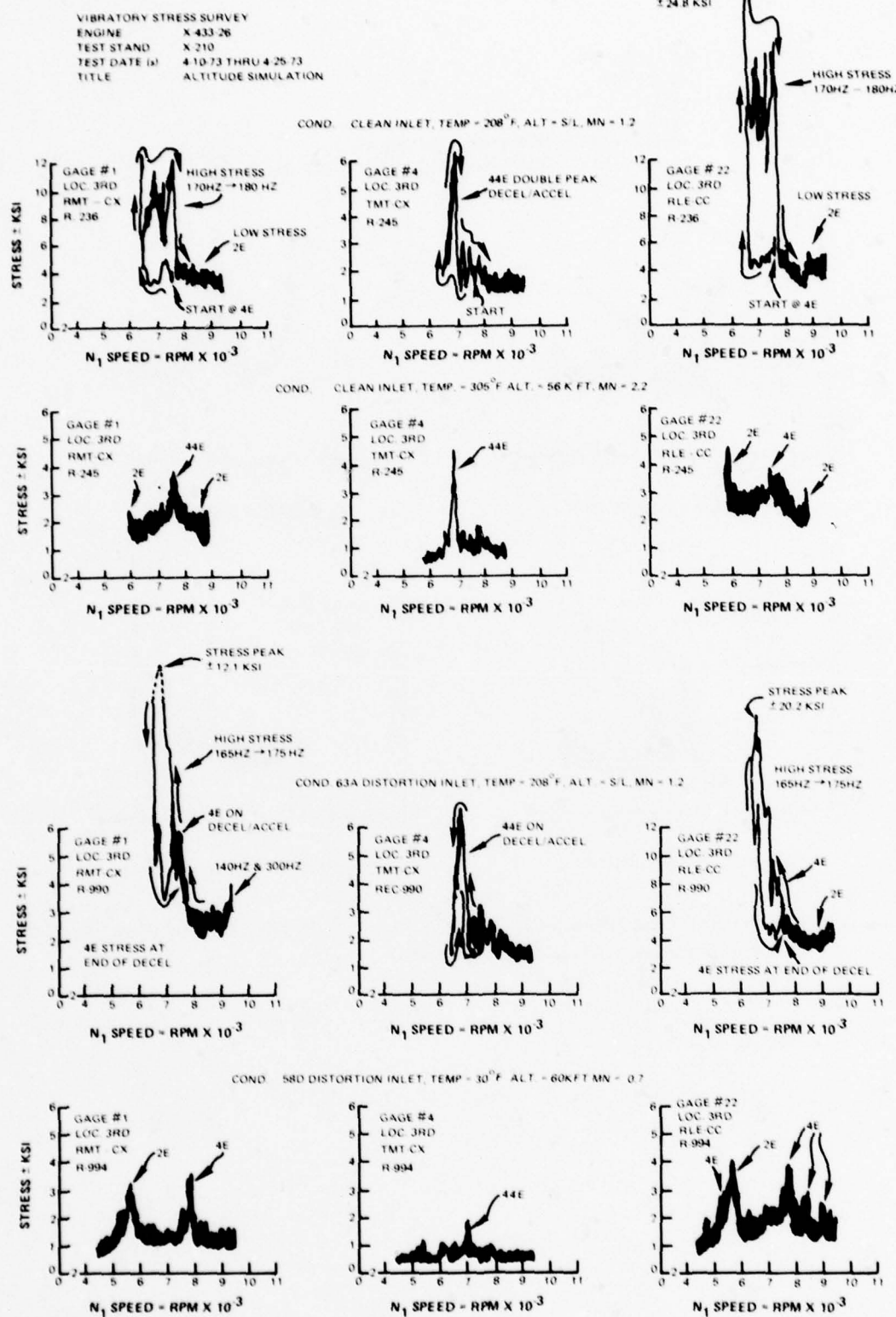


Figure 11.2-8 Maximum Vibratory Stresses Which Occurred at Significant Engine Operating Conditions During Altitude Stress Survey

**ENDURANCE**

X-433-26

208°F (97.8°C) INLET AIR

35.3 PSIA

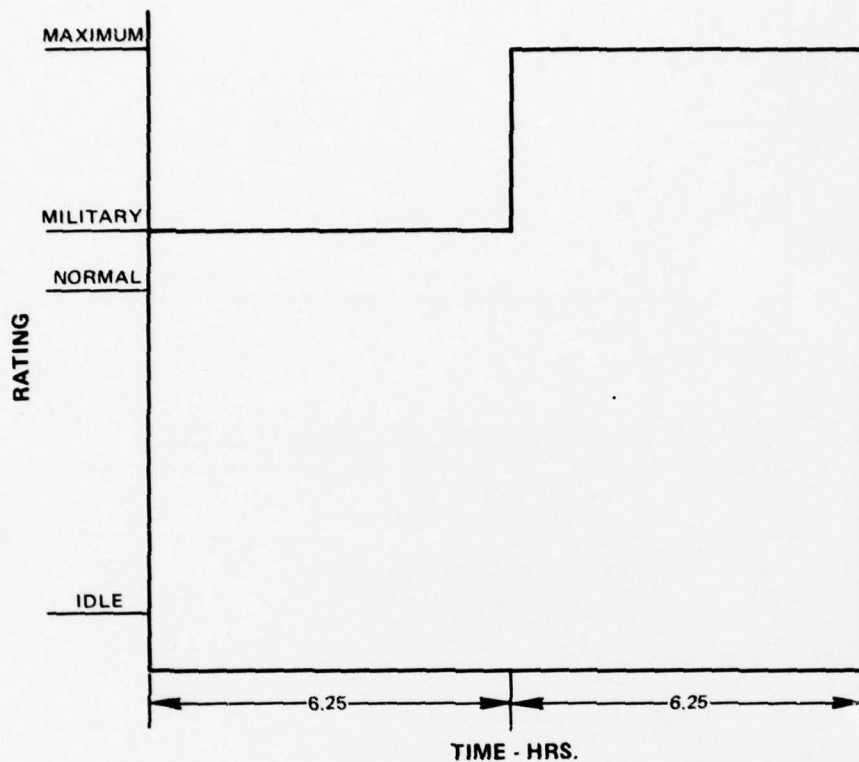


*Figure 11.2-9 The Schedule for Running Military and Maximum Endurance Tests. This Schedule Was Subsequently Changed to Encompass Approximately 10.5-Hours of Military Power*

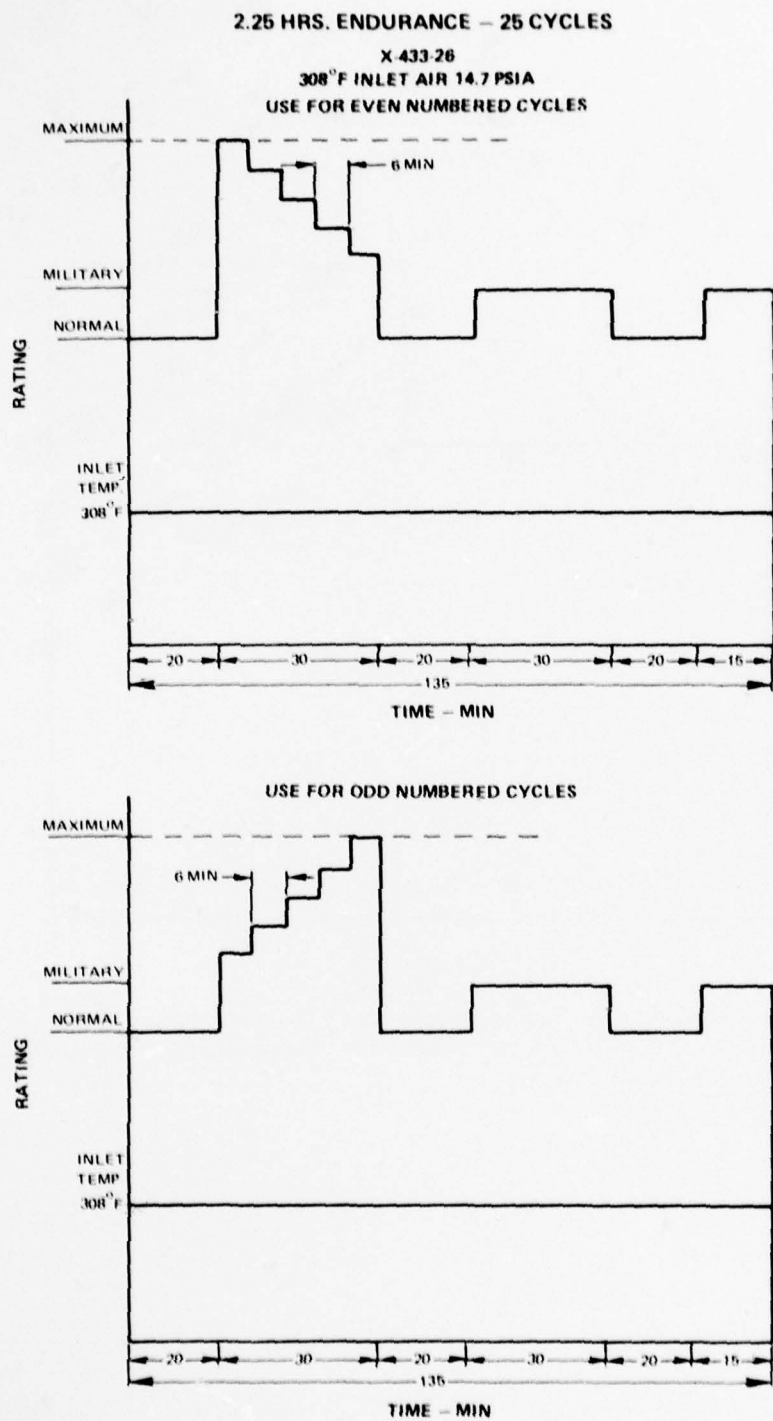
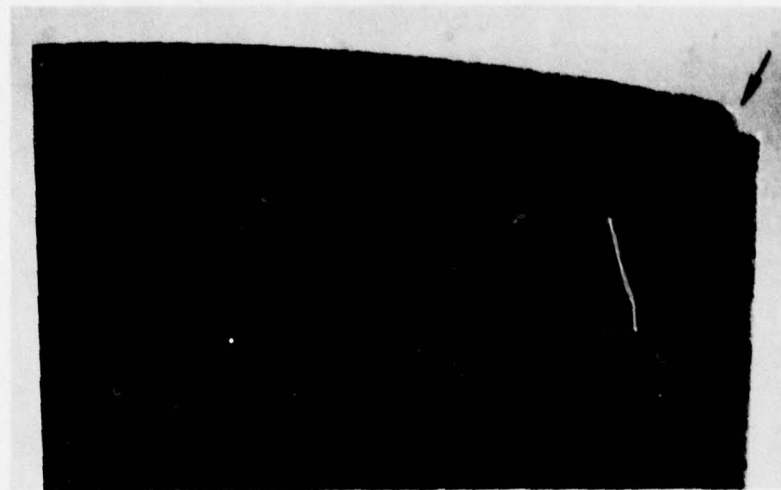
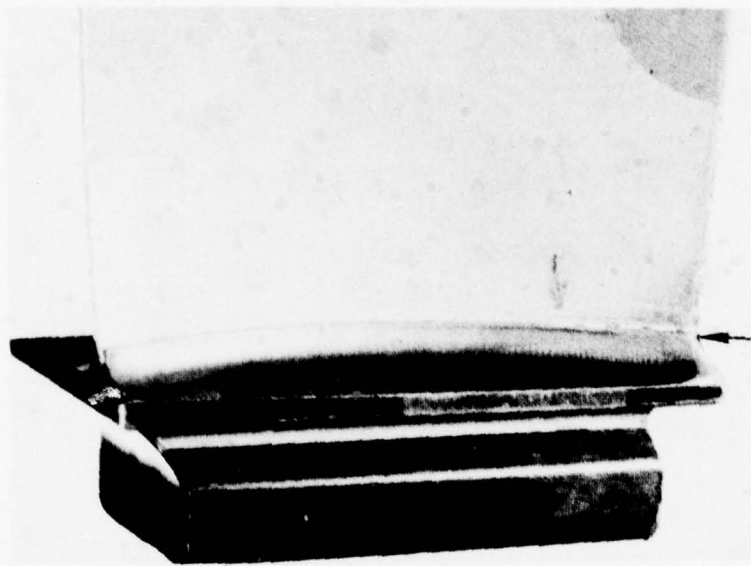


Figure 11.2-10 The Cycle Schedule for Conducting the Mn 2.2 Endurance Portion of the Supersonic/Altitude Tests



*Figure 11.2-11 Damaged Area at Blade Tip Convex Side, Due to Rubbing Contact With Compressor Case*



*Figure 11.2-12 Location of Crack at Concave Side of Airfoil Root*

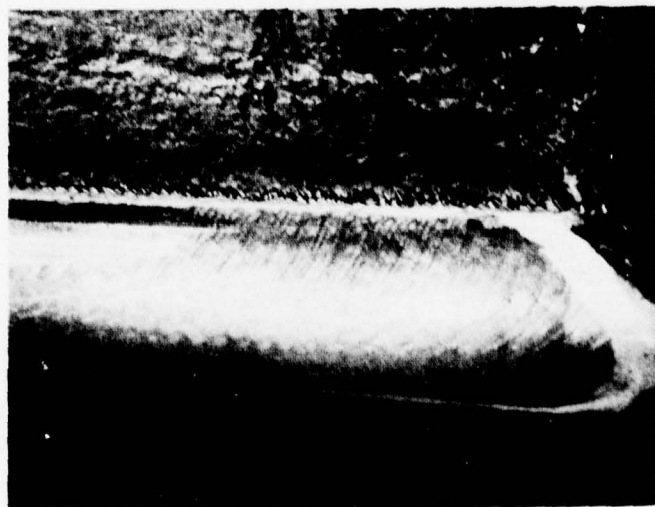


*Figure 11.2-13 Close-Up View of Crack at Concave Side of Root, Crack Extends Around Leading Edge to Convex Side*

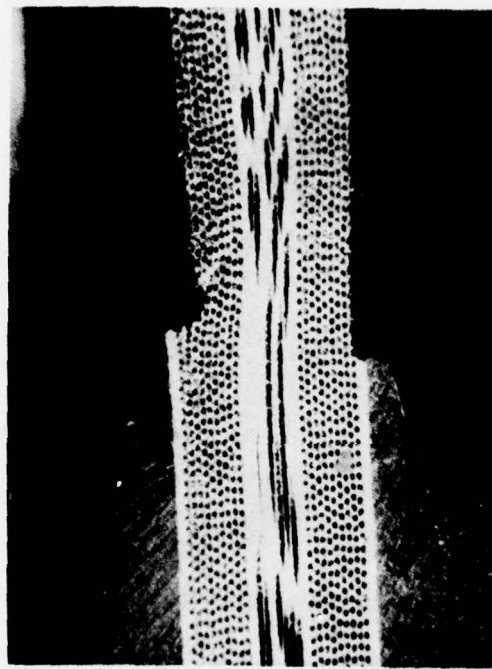


Figure 11.2-14 Vertical Plane Cross-Sectional View Shows the Misalignment of Root Blocks Toward the Leading Edge Area of the Blade as Well as Deformation of Plies Just Above Root Blocks

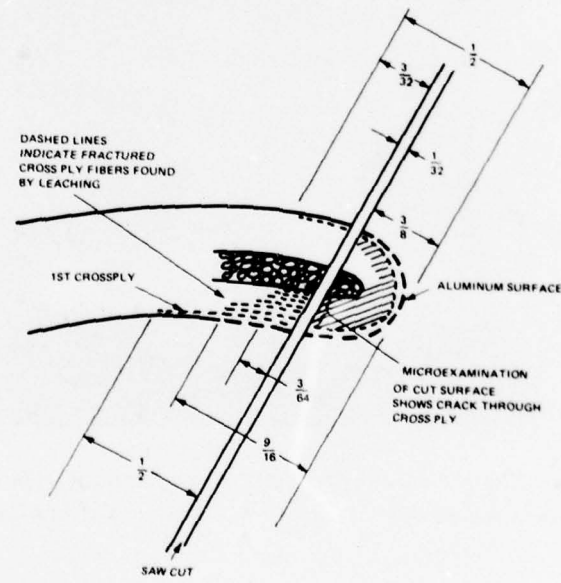


Figure 11.2-15 Nominal Dimensions of Sections Examined by Microexamination and Leaching/Crossply Removal; Dashed Lines Represent the Extent of Damage Due to Overstressing at the Blade Root; Shaded Area Indicates Probable Damage in Microsection

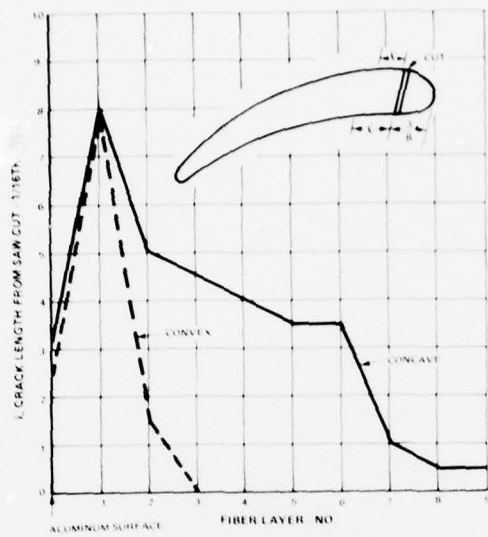


Figure 11.2-16 Correlation of Crack Length and Fiber Layer on Concave Side of Blade

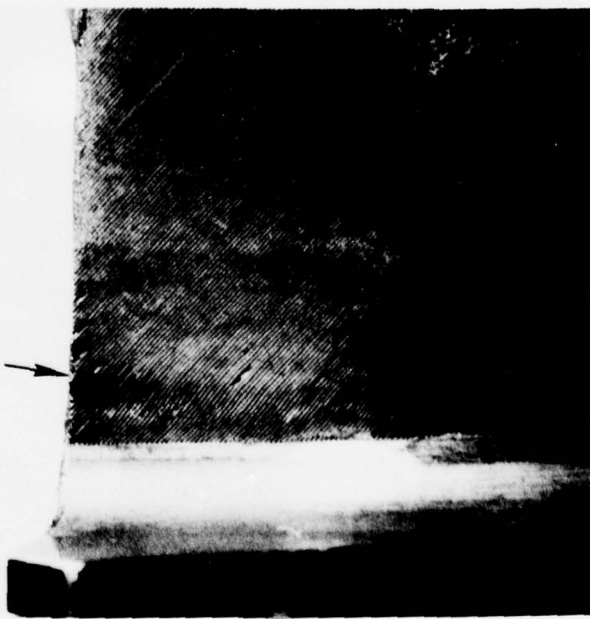
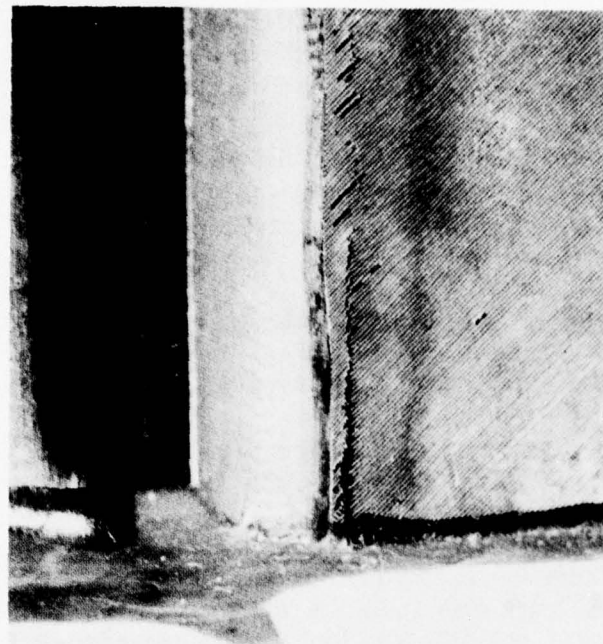
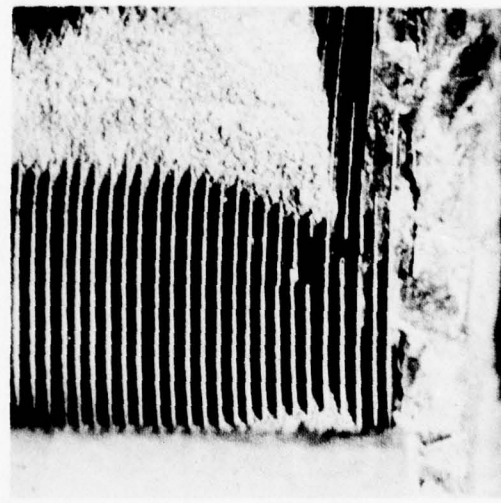


Figure 11.2-17 Convex Side of Blade With Surface Aluminum Layer Removed Shows Relatively Little Damage (Arrow) and Damage Was Limited to First Crossply Layer



*Figure 11.2-18 Fractured Fibers in First Crossply of Concave Side After Leaching and Removing Leading Edge Pieces; Damage Was More Extensive Than on Convex Side*



*Figure 11.2-19 First Longitudinal Fiber Layer on Concave Side Shows Only Slight Damage Above Plane of Dominant Crack*

## 12.0 AIRCRAFT FLIGHT EVALUATION PROGRAM

### 12.1 SUMMARY

During the period August 1975 to December 1976, a full set of TF30-P-9 3rd stage BORSIC®/aluminum fan blades was flown in service in two different F111-D aircraft operating out of Edwards AFB, California. The blade set used for this flight evaluation program was assembled from blades previously tested in an experimental engine program at Pratt & Whitney Aircraft, East Hartford, Conn., and described in Sections 11.1 and 11.2 of this report. Prior to the flight program, the high-time blades had experienced 364 hours in ground engine testing.

In the flight program, the blade set amassed an additional 184 hours in 90 flights, bringing the high-time blades up to 548 hours of engine operation. During this time, no blade failure was encountered. There were no restrictions imposed on the aircraft flight envelope.

After 184 hours of flight operation, a routine borescope inspection revealed surface cracks on some of the blades in the root area. The rotor was then removed and shipped to P&WA for a full inspection.

This inspection (both nondestructive and destructive) revealed that several blades did have visual cracks in the root area, which were confined to the surface region of the blades. However, because of the presence of the cracks, a decision was made to terminate the flight program.

This program constitutes the first successful flight experience with composite fan blades in this country, and has built confidence in government and industry that composites are a technically feasible aircraft engine material.

### 12.2 INTRODUCTION

Under AF Contract F33657-70-C-0624, initiated in July 1970, TF30-P-9 3rd stage BORSIC®/aluminum fan blades were developed and evaluated in experimental (ground) engine tests. The experimental engine test program, encompassing 564 hours of sea level and altitude testing on two full sets of blades, was successfully completed in August 1973; by January 1974, the decision had been made to fabricate and test two additional blade sets in F111 aircraft at Edwards AFB. A contract modification to that effect was issued in October 1974.

In the first quarter of 1975, P&WA discovered that the BORSIC®/aluminum raw material purchased for the flight hardware exhibited serious strength deficiencies, even though it had been purchased to the same specifications\* and from the same vendors as the previously acceptable material used in the experimental portion of the program. Several weeks of extensive investigations failed to reveal the source or the solution of this problem, and in April 1975 a decision was made to utilize previously tested blades in the flight program, and not to pursue a new materials/fabrication effort.

\*The original specifications covered both filament strength minimums and plasma-sprayed tape minimums. However, since two different vendors were involved (one for filament, one for tape) it was virtually impossible to obtain a firm guarantee on the strength of the final product. In future programs this same problem may recur, and can be avoided only if one vendor will accept responsibility for the properties of the final product.

As a result, the blades from the previously tested engine sets (72 in all) were segregated and reinspected to P&WA production delivery standards. Of these 72 blades, 41 were accepted for the flight program. These provided one full rotor set of 36 blades, plus 5 spares.

These blades, plus a new disk, seal, and blade locks, were assembled, balanced, and shipped to Edwards AFB on June 24, 1975. This rotor was then installed in an F111-D aircraft at Edwards as a Class II modification, and first flown on August 4, 1975. In March 1976, the engine with the composite blades was removed and reinstalled in a different F111-D aircraft and continued flying until December 1976 for a total of about 17 months. The details of this USAF-conducted flight are not contained herein, but will be in a separate ASD technical report.

During this period, a total of 184.1 flight hours in 90 separate flights was accumulated, with no problems attributable to the composite blades. Since the blades were not new, a requirement of periodic 25-hour borescope inspections of the blades had been imposed by P&WA. No restrictions on the aircraft flight envelope were imposed, however.

After flight No. 90, the borescope inspection revealed apparent surface cracks on some blades in the root region. Since an engine overhaul was nearly due, it was decided to remove the stage at this time and inspect the blades, particularly to investigate the apparent cracks.

The engine was removed and the 3rd rotor shipped to P&WA, East Hartford, where it was received in early February 1977. The rotor was disassembled and all parts were inspected, including destructive examination of two of the composite blades. This bench inspection revealed all parts, including blades, to be in good condition with the exception of cracks in the root-area. These cracks were visible under magnification on approximately 2/3 of the blades. However, destructive examination revealed that the cracks did not penetrate beyond the surface area of the blades.

Since there is no accurate method of predicting the propagation rate of cracks in this type of materials, and thus the remaining blade life, it was decided to terminate the flight program at that point.

This section describes in more detail the pre-flight blade inspection and selection procedures, the flight program, and the post-flight inspection procedures and results.

### 12.3 PRE-FLIGHT QUALITY ASSURANCE

Two full sets of TF30-P-9 3rd stage BORSIC®/aluminum fan blades, totaling 72 blades, had been previously tested at P&WA in experimental engines. Set No. 1 had experienced a total of 364 hours at sea-level conditions, and set No. 2 had experienced 200 hours at altitude conditions (Section 11).

Of these 72 blades, a total of 16 blades had developed visual surface cracks in the root area (Section 11). These 16 blades were immediately rejected for the flight program. An additional 6 blades were rejected because the outer aluminum surface had been accidentally removed in a stripping operation, resulting in a significant loss of frequency. An additional 3 blades could not be located at that time.

At this point, 47 blades were still available for the flight set, and were submitted to the P&WA Quality Engineering Department for Q/A to production delivery standards (see Appendix B, Quality Plan). Under this plan, all blades were reinspected to production delivery standards; these included X-ray, ultrasonic C-scan, dimensional, and visual inspections.

Of the 47 final candidate blades, one was rejected by X-ray, one by ultrasonic C-scan, two by dimensional, and one by visual inspection. In addition, a review of frequency loss as a result of previous engine testing resulted in rejection of one blade. As a result, 41 blades were accepted and certified to production delivery standards and stamped with the appropriate symbol (Flying W).

Table 12.3-I lists the blades rejected and the reasons therefor; Table 12.3-II lists the blades accepted and shipped to Edwards AFB.

Other rotor parts (disk, 2-3 airseal, and blade locks) were inspected to similar standards. The 3rd rotor was then assembled and balanced, and shipped to Edwards AFB. The rotor parts list was as follows:

<u>Part</u>	<u>P/N</u>
2-3 Air Seal	713246
3rd Stage Disk	712703
*3rd Stage Fan Blades (36)	713603
3rd Stage Blade Locks (36)	661920

\*Five Spare fan blades (P/N 713603) were also supplied. See Table D-II for blade serial numbers.

Also supplied to Edwards were blade weights, including spares (Table 12.3-II), and Field Inspection, Removal, and Repair Guidelines (para. 12.4) developed specifically under this program for the composite fan blades. Figure 12-1 shows the rotor as received at Edwards; Figure 12-2 shows the B/M 3rd rotor which it replaced.

The final item supplied to Edwards was the location and design of a borescope port modification (L-99469) to the 2nd stator assembly. This modification, done at Edwards, is shown in Figure 12-3, and allowed on-the-wing borescope inspection of the 3rd stage blades at periodic intervals.

TABLE 12.3-I  
REJECTED BLADES FROM SET NOS. 1 AND 2

<u>Blade No.</u>	<u>Set No.</u>	<u>Reason for Rejection</u>
81	1	Cracks in fillet area
105	1	
109	1	
111	1	
126	1	
130	1	
144	1	
145	1	
156	1	
157	1	
162	1	
165	1	
168	2	
175	2	
190	2	
199	2	
79	1	Aluminum surface replaced with epoxy; high frequency loss after engine test.
95	1	
107	1	
110	1	
119	1	
123	1	

TABLE 12.3-I (Cont'd)

<u>Blade No.</u>	<u>Set No.</u>	<u>Reason for Rejection</u>
*144	1	Aluminum surface replaced with epoxy; high frequency loss after engine test.
*145	1	Aluminum surface replaced with epoxy; high frequency loss after engine test.
137	1	Local delamination (C-scan)
99	1	Excessive bow (dimensional)
106	1	Excessive bow (dimensional)
174	2	LE tip damage (visual)
160	1	Crack (X-ray)
87	2	Frequency loss
172	2	Could not be located
179	2	Could not be located
188	2	Could not be located

TABLE 12.3-II  
FLIGHT QUALITY BLADES FROM SET NOS. 1 AND 2

<u>Installed</u>							
<u>S/N</u>	<u>Wt. (oz.)</u>	<u>S/N</u>	<u>Wt. (oz.)</u>	<u>S/N</u>	<u>Wt. (oz.)</u>	<u>S/N</u>	<u>Wt. (oz.)</u>
195	6.70	80	6.70	167	6.70	178	6.70
121	6.68	161	6.68	116	6.68	187	6.68
205	6.67	182	6.67	170	6.67	212	6.66
131	6.65	181	6.65	128	6.58	192	6.65
103	6.63	169	6.62	223	6.65	155	6.62
139	6.58	120	6.59	114	6.64	183	6.62
98	6.74	194	6.74	201	6.75	158	6.74
86	6.73	197	6.73	225	6.72	176	6.73
200	6.72	193	6.71	189	6.72	180	6.72

SPARES

<u>S/N</u>	<u>Wt. (oz.)</u>
127	6.55
143	6.81
206	6.78
133	6.70
171	6.90

## 12.4 FIELD INSPECTION PROCEDURES AND REWORK LIMITS FOR TF30-P-9 3RD STAGE BORSIC®/ALUMINUM FAN ROTOR

(The following guidelines were supplied to Edwards AFB in connection with the Flight Evaluation Program.)

References: (1) Contract F-33657-70-C-0624

This rotor assembly consists of the following details:

<u>P/N</u>	<u>Name</u>	<u>Number in Assy</u>
713603	Blade	36
661920	Blade Lock	36
713703	3rd Disk	1
713246	2-3 Airseal	1

### General Instructions:

Following installation in an aircraft at Edwards AFB, the 3rd stage blades should be visually inspected with a one-half inch or less diameter borescope through the engine port provided. This will familiarize the inspector with the mechanics of the procedure and the general appearance of the blades.

It is required that the blades be inspected with a borescope after engine test stand checkout, and also on a noninterference basis after each of the first ten flights of the aircraft, with the following exceptions:

- (1) Turnaround flights shall be considered as a single flight.
- (2) Multiple flights on a given day shall be considered as a single flight.

Subsequently, if no significant damage is observed, the frequency of this inspection procedure may be lowered to once every 25 hours of engine operation. After a total of 200 hours of engine operation, the blades must be removed from the engine and inspected on the bench.

### Damage and Rework Limits:

Blades - For the purpose of establishing damage and rework limits, the blade is divided into seven areas (Figure 12-4).

Maximum allowable blended nick or crack limits are listed in Table 12.4-1.

TABLE 12.4-I

Maximum Allowable Blended Crack or Nick Limits

Blade Area	Stage 3	
A		5/16"R
B		1/32"RB
C		5/32"D
D		1/8" D
E		1/8" D
F	Nick -	1/16"D Crack-None
G	Nick -	1/32"RB Crack-None
H		1/32"RB

R - Radius

D - Depth

RB - Round  
Bottom

In addition, visible cracks in the nickel-cobalt LE (Areas A, C, D, H) are allowable with no limit on length or number. If any such crack is wide enough to expose the composite substrate, it is cause for removal. No repair is allowed in this case.

Conventional metal-working tooling may be used to blend nicks or cracks, such as fine files, hand grinding wheels, stones, or emery cloth.

Area F leading edge may erode significantly. This is allowable, subject to the nick limits above, providing it does not exceed 1/16" depth.

At the 200-hr. bench inspection, X-ray and 10X visual examinations are required.

Since the number of spares is limited, blades may be replaced singly. The replacement blade must match the weight of the replaced blade within .03 oz.

**Disk and Seal** - The disk and seal are conventional titanium parts, and are subject to the same assembly procedures and damage rework limits as the P-9 B/M parts.

**Blade Locks** - The blade locks are required to be fluorescent penetrant inspected at the 200-hr. bench inspection. Any crack will be cause for removal; no repair allowed.

## Deviations to T. O. 2J-TF30-36

## Applicable to Composite 3rd Stage Fan

<u>Page No.</u>	<u>Item No.</u>	<u>Revision</u>
8-3	54	Change .092 .104 To .094 .108 .114
3-38	3-54a	Eliminate this item; refer to "Inspection Procedures and Rework Limits"
3-38	3-54b	Eliminate "After blending, fluorescent penetrant inspect blades"
3-38	3-54d CAUTION NOTE	Change "Surface finish shall be comparable to new blade" to "Surface finish shall be comparable to tip end of new blade"
3-38A	3-54j	Change 2nd sentence to read: "Coating must not be stripped; reapply over old coating if more than ten percent is missing from load bearing surfaces"
3-40	Entire	Eliminate: Refer to "Inspection Procedures and Rework Limits"
3-42	3-55 NOTE:	Eliminate: Refer to "Inspection Procedures and Rework Limits"
3-42	3-55f	Add: "3rd stage composite blades have separate blade locks"

## 12.5 FLIGHT PROGRAM

Upon receipt at Edwards AFB, the composite 3rd rotor was installed in the right engine of F111-D-3 (A/C 68-087, engine P676591). The first flight of the aircraft occurred on August 4, 1975.

The only requirements peculiar to the composite stage were that the blades be visually inspected at 25-hour intervals (which coincided with on-the-wing inspection of the 2-3 air seal), and that the blades also be bench inspected after a maximum of 200 hours of operation. No limitations on the aircraft flight envelope were imposed.

F111-D-3 experienced various problems not associated with the 3rd rotor, and accumulated only 12 flights (19 hours) between August 1975 and March 1976 (Figure 12-5). At that time, the engine incorporating the composite blades was installed in F111-D-1 (A/C 68-085). This aircraft accumulated 78 flights (165.1 hours) between March 1976 and December 1976 for a total of 90 flights, 184.1 hours, in the two aircraft. No blade-related problems were encountered during this time.

At the 184.1 hour point, a regularly scheduled borescope inspection of the blades revealed crack indications on some blades in the root area. From the description of the borescope operator, these indications were seen only on blades which had strain-gage cement in the root area, which obscured the actual airfoil surface (Figure 12-6). Since the engine was nearly due for overhaul, and since there was no way of determining the extent of these cracks on-the-wing, a decision was made to pull the 3rd rotor at that time and thoroughly inspect the blades on the bench.

The flight envelope explored during the program described above included Mach Nos. to 2.2 and altitudes to 50,000 ft. Most of the flight hours were at cruise or military power, but did include approximately 300 afterburner lights (which stress the 3rd stage blades to a reasonably high level). No engine surges were encountered in the flight program.

## 12.6 POST FLIGHT INSPECTION

On February 10, 1977, the carton containing the 3rd rotor and spare blades was opened at East Hartford in the presence of NAVPRO personnel. There was no apparent shipping damage to the parts.

The rotor was removed from the carton and photographed (Figures 12-7, 8). The visual appearance of the blades was excellent, with no evidence of erosion or dovetail bearing surface galling. Six blades had a very slight nick or dent at the LE tip, probably caused by some form of FOD. Also, a few blades exhibited radial surface scratches, possibly caused by inadvertent rubbing of the borescope on the airfoil during on-the-wing inspection. Neither of these types of damage would affect blade structural integrity.

### 12.6.1 Weight Loss

The rotor was disassembled and the blades and blade locks were individually weighed. The blade locks had zero weight loss, while the blades had an average weight loss of .01 oz. on an average blade weight of 6.7 oz., or 0.15%. The maximum weight loss of any individual blade was .02 oz., or 0.3%. This slight weight loss is presumed to be the result of erosion of the aluminum surface of the airfoil.

### 12.6.2 Visual Inspection

All of the blades were then inspected visually at 10X-20X magnification. It was discovered that 25 out of the 36 flight blades exhibited chordwise surface cracks just above the platform fillet (Figures 12-10, 11), very similar to those developed during the ground engine testing. All cracks were present at the LE concave side, with a few extending around to the convex side. The cracks shown in Figures 12-10, 11 are on blade E-169, and are visually the most severe.

The flight blades can be grouped into 3 categories, as follows:

Set No. 1 (12 blades) - Tested for 364 hours at sea-level conditions, including 264 hours of cyclic endurance testing.

Set No. 2 (18 blades) - Tested for 200 hours at altitude conditions, including a severe tip rub (Sect. 11).

Set No. 2a (6 blades) - Replacement blades for Set No. 2 after tip rub occurred.

The post-flight cracked blades can be grouped accordingly as follows:

Set No. 1 - 7 out of 12 blades cracked.

Set No. 2 - 18 out of 18 cracked. (Apparently the severe tip rub experienced during ground tests caused undetected structural distress which ultimately caused all blades to develop cracks during the flight program.)

Set No. 2a - 0 out of 6 cracked.

It should be emphasized, however, that the majority of the cracks were visually very minor, and that subsequent destructive examination of the most extensive crack, on blade E-169 (see below), revealed that the cracks were confined to the surface cross-ply, and did not extend into the radial-ply core of the blade. This damage was slightly less severe than that caused by the tip rub of Set No. 2a, above; wherein the worst blade exhibited crack damage extending through all nine of the cross-ply, but remained structurally intact through continued engine operation.

A second indication of structural distress was found on 12 blades at the base of the dovetail (Figure 12-9). This took the form of relative displacement of the composite portion of the dovetail with respect to the root pads and wedge. It might best be described as a shear yielding of the composite airfoil root. In most blades affected, it was very minor, but in two blades it was measurable. These two blades were E-169 and E-176. The maximum measured deformation in these two blades was 2.3 mils in blade E-169, and 1.7 mils in blade E-176 (Figure 12-9).

### 12.6.3 X-Ray

All test blades were X-rayed, and results were negative. Two X-ray techniques were employed. First, a standard overall X-ray shot of each blade, identical to that used for inspection for flight qualification; second, a high resolution shot of the fillet area only where the visual cracks existed. In neither case were the visual cracks detectable on the X-rays.

### 12.6.4 Dimensional

Blade untwist as a result of flight experience was measured on 6 blades (Table 12.6-I). These blades were selected because pre-flight data was available. Table 12.6-I shows that two blades (E-201 and E-205) were slightly out of tolerance (in different directions) both before and after flight testing, and that the average permanent untwist incurred in the flight program was 12', with a maximum of 26' for blade E-223.

### 12.6.5 Natural Frequency

Table 12.6-II presents the average frequency losses in first bending, second bending, and first torsion modes, segregated for blade sets 1, 2 and 2a (see above). Apparent increases in frequency are presumed to be the result of experimental error in frequency measurement. These blades were retested several times, with no change in the results.

The most significant observations that can be drawn from Table 12.6-II are the comparatively large 2B frequency loss for the tip-rub blades (Set No. 2), and the negligible loss for all blades in the first torsional mode (which controls flutter).

Table 12.6-III presents the worst individual blade frequency losses, all from Set No. 2. As noted, no blades were outside of B/P frequency limits, either before or after testing.

### 12.6.6 Destructive Examination

The blade exhibiting the worst cracks (visually), E-169, was selected for destructive examination to determine the depth of the cracks. As shown in Figures 12-10 and 12-11, the blade had a surface crack on the concave surface extending from leading edge to approximately 40% chord, and a second crack on the convex surface extending from 25% chord to 50% chord.

These cracks were investigated by progressively leaching the aluminum matrix away from the filaments, one ply at a time. The leaching agent used was a 50% solution of HC1. As each successive cross-ply layer was exposed, it was photographed. There are 9 crossplies on each surface; the leaching operation was continued until all 9 layers were exposed, down to the radial core.

Figures 12-12 and 12-13 depict the 2nd ply layer on each blade surface (concave and convex), and clearly show the cracks, which are in effect many successive fracture filaments. Figures 12-14 and 12-15 depict the 7th ply layer on each surface, and show that a continuous crack no longer exists. The 8th and 9th cross-ply layers confirmed this, as well as the 1st radial ply layer.

TABLE 12.6-I  
BLADE PERMANENT UNTWIST

<u>Blade No.</u>	<u>Tip Chord Angle</u>		<u>Δ</u>
	<u>Pre-Flight</u>	<u>Post-Flight</u>	
194	21°0'	21°5'	5'
*201	21°46'	21°55'	9'
*205	19°46'	19°50'	4'
212	20°38'	20°50'	12'
223	20°24'	20°50'	26'
225	<u>20°52'</u>	<u>21°5'</u>	<u>13'</u>
Avg.	20°44'	20°56	12'
Nominal B/P	-	20°40'	
B/P Tolerance	-	19°58' - 21°22'	

\*Out of tolerance

TABLE 12.6-II  
AVERAGE BLADE FREQUENCY LOSS

BLADE FREQUENCY LOSS - %	TOTAL BLADE LIFE			FLIGHT TEST ONLY					
	(INCLUDING FLIGHT TEST)			1B	2B	1T	1B	2B	1T
<b>TOTAL BLADE SET - (36)</b>		1.0	2.2	+0.2*			0.3	0.7	0
SET NO. 1 - (12)		1.2	1.2	0.2			0.6	+1.1	+0.1
SET NO. 2 - TIP RUB (18)		1.2	4.0	+0.1			0.3	1.4	0
SET NO. 2a - (6)		+0.4	0.3	+1.1			0	1.8	0

\*Plus values indicate a frequency increase. These values have been rechecked, and are considered to be within the range of experimental error.

TABLE 12.6-III  
WORST BLADE FREQUENCY LOSS

1B	4~	2.8%	(BLADE 176)
2B	23~	5.0%	(BLADE 183)
1T	8~	0.85%	(BLADE 193)

(ALL FROM SET NO. 2)

No blades were out of B/P frequency limits, either before or after test.

The results of this investigation closely parallel those of Blade E-184, which exhibited similar cracking following the tip-rub of Set No. 2 (Section 11.2.5). In both cases, the cracks disappeared before reaching the radial-ply core.

#### 12.6.7 Conclusions

- The BORSIC®/aluminum blade performance was excellent throughout the 184 hour flight evaluation program. Weight loss, frequency degradation, and dimensional effects (untwist) were insignificant.
- The visual cracks in the root area were confined to the surface cross-ply layers and probably did not jeopardize the structural integrity of the blades.
- In future blade development, the use of cross-plies should be avoided, if possible, in order to minimize fabrication damage which may induce local cracks. This type of local damage has been observed in high-resolution x-rays, which are then highly magnified in order to become visible.
- The shear yielding in the root attachment (Section 2.6.2) can most plausibly be attributed to a "weak" bond between the root pads and the composite structure. Since ultrasonic C-scan cannot currently define a "weak" bond (only a lack of bonding) the most practical solution would appear to be to design for lower shear stresses, or to develop an NDI technique to quantify bond strength.

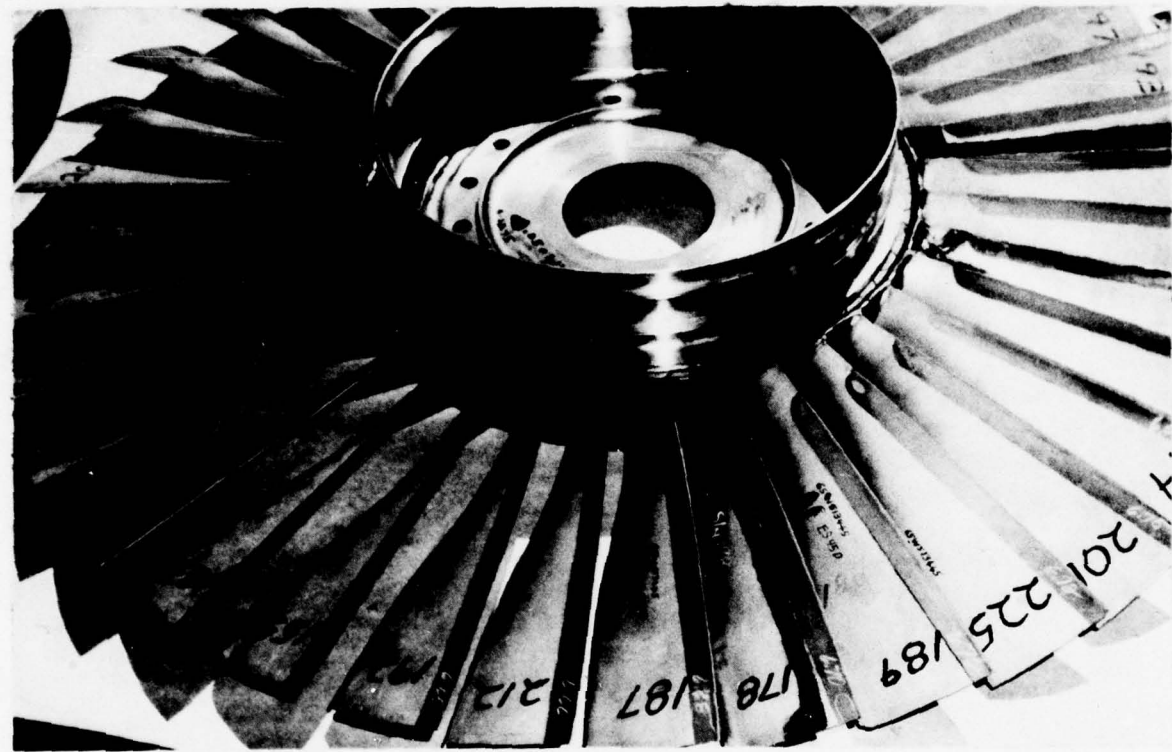


Figure 12-1 TF30P-9 3rd Rotor Assembly as Received at Edwards AFB Prior to Installation in F111-D Aircraft (BORSIC®/Aluminum Blades)

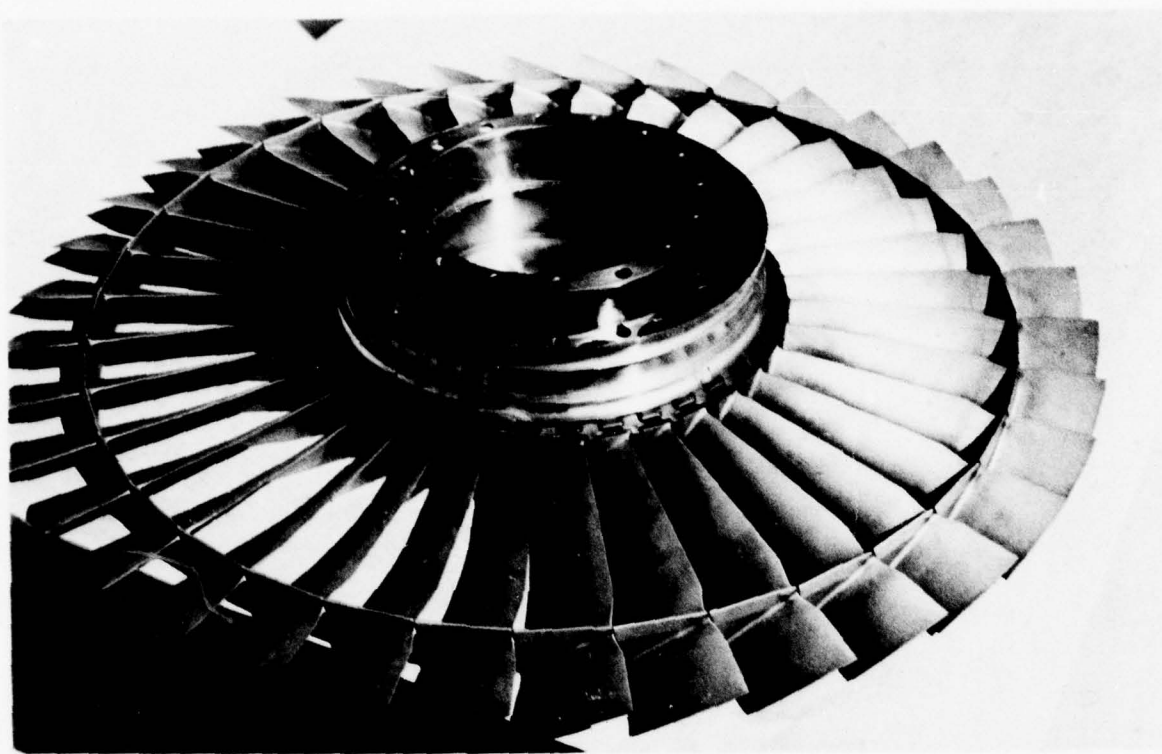


Figure 12-2 Bill-of-Material TF30P-9 3rd Rotor Assembly (Titanium Alloy Blades)

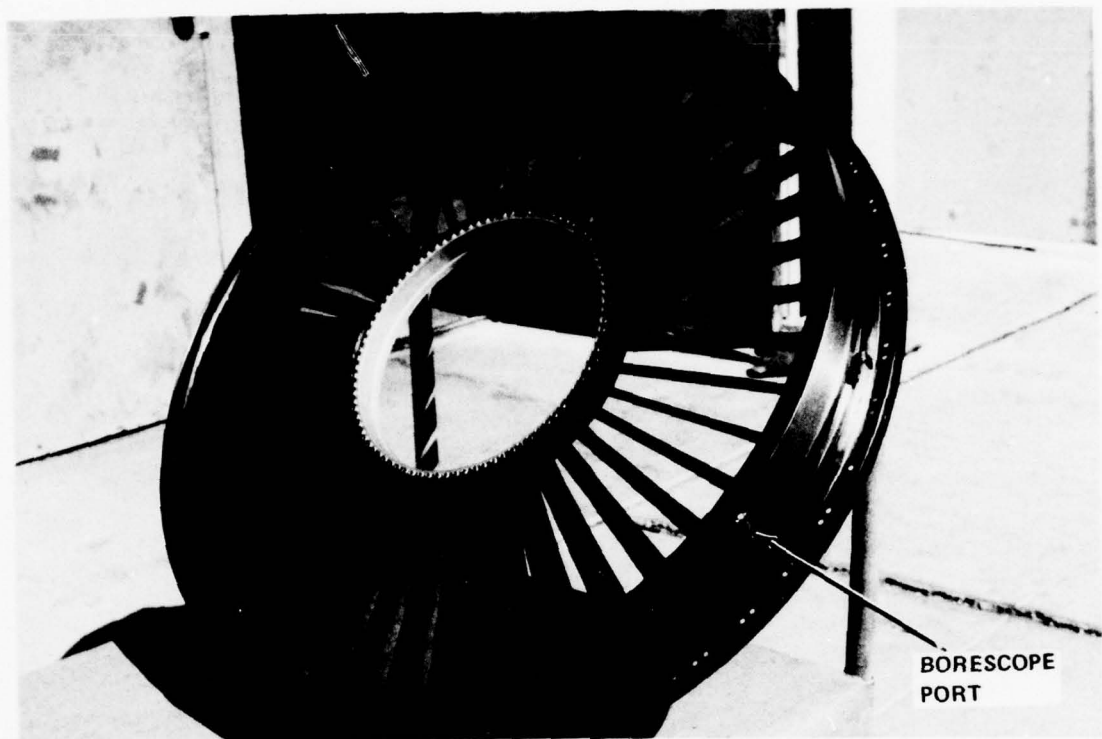


Figure 12-3 TF30P-9 2nd Stator Assembly With Borescope Inspection Port

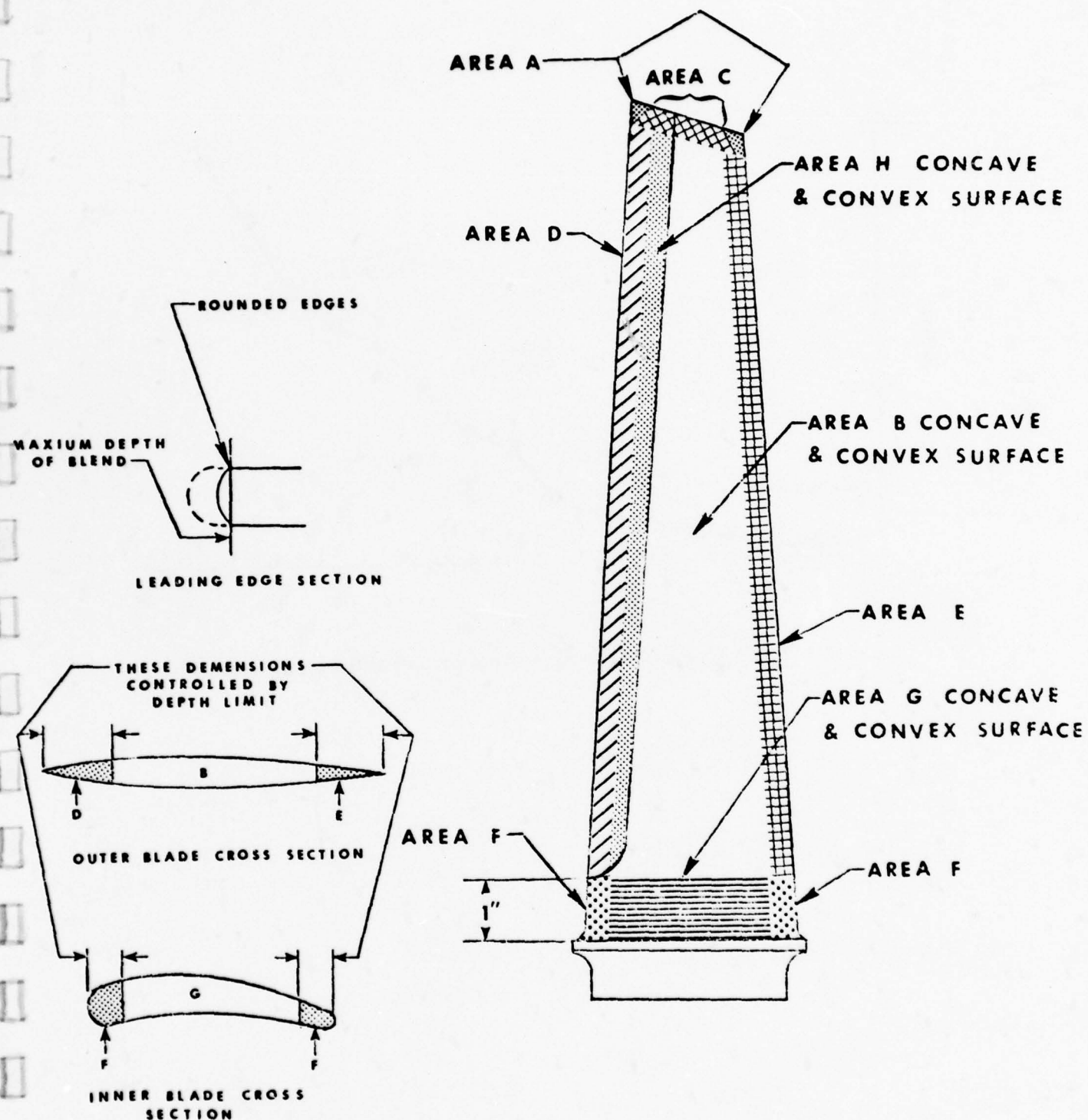


Figure 12-4 Areas Used to Establish Damage and Rework Limits

PRATT & WHITNEY AIRCRAFT GROUP

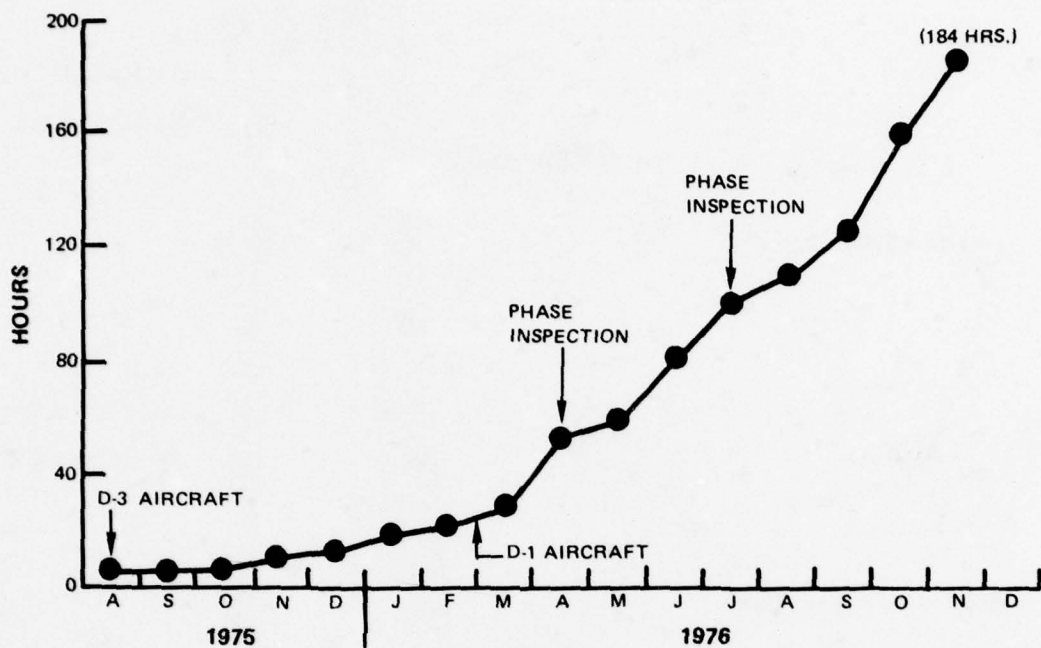
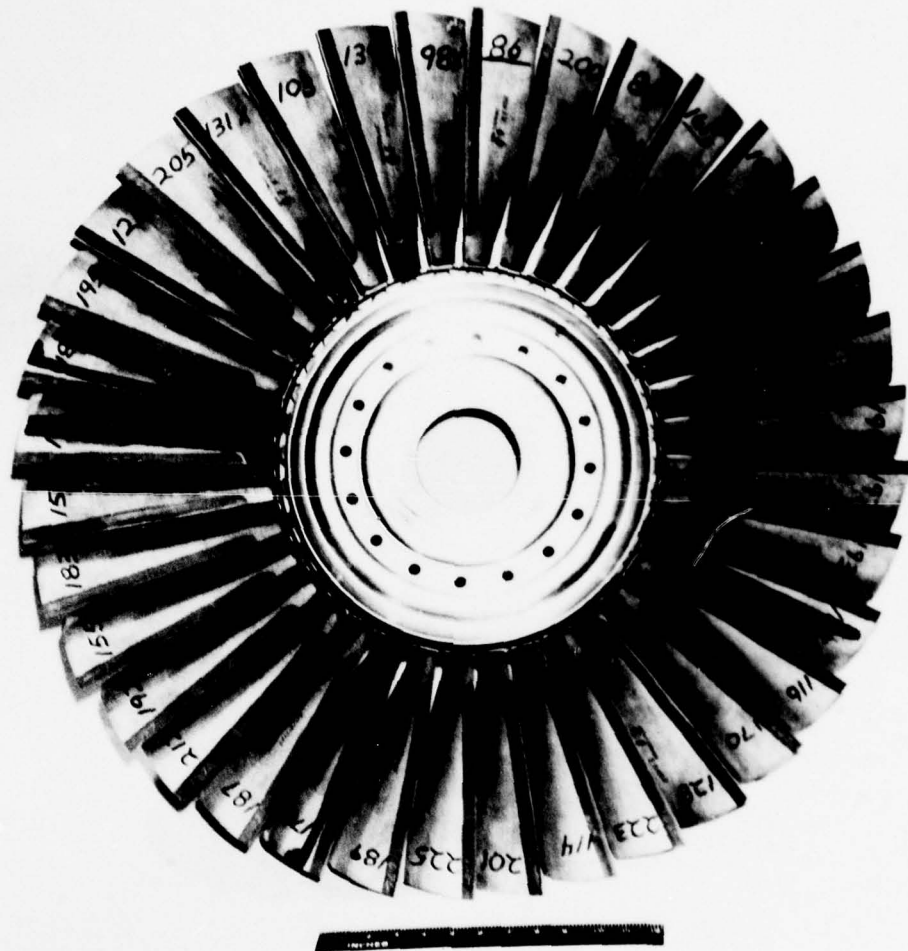


Figure 12-5 TF30 Composite Fan Flight Program (Cumulative Hours by Month)

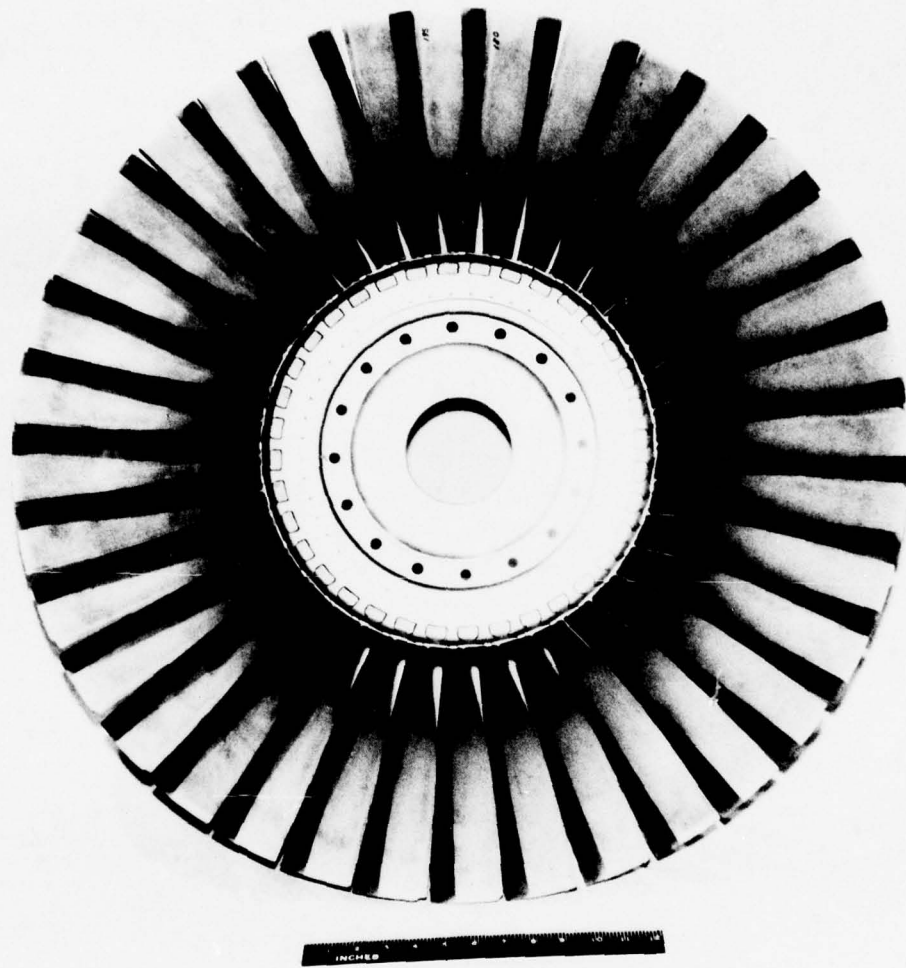


Figure 12-6 TF30P-9 BORSIC®/Aluminum Fan Blades After 184-Hr. F111-D Flight Program (Front View)



TOTAL FLIGHT HOURS - 184

Figure 12-7 TF30P-9 3rd Rotor After Removal From F111-D Aircraft (Front View)



TOTAL FLIGHT HOURS - 184

Figure 12-8 TF30P-9 3rd Rotor After Removal From F111-D Aircraft (Rear View)

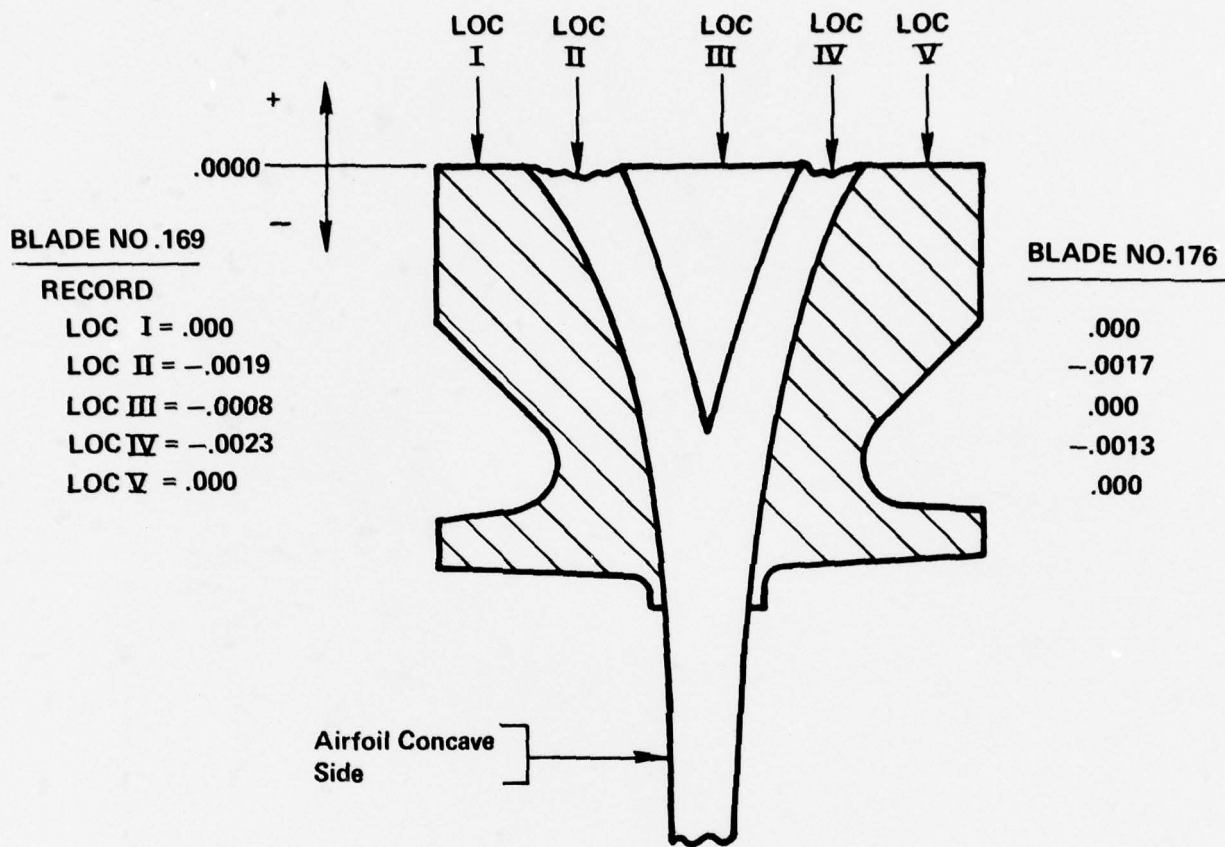


Figure 12-9 Root Deformation



Figure 12-10 Concave (Pressure) Surface of Blade E-169 as Removed From F111-D Aircraft

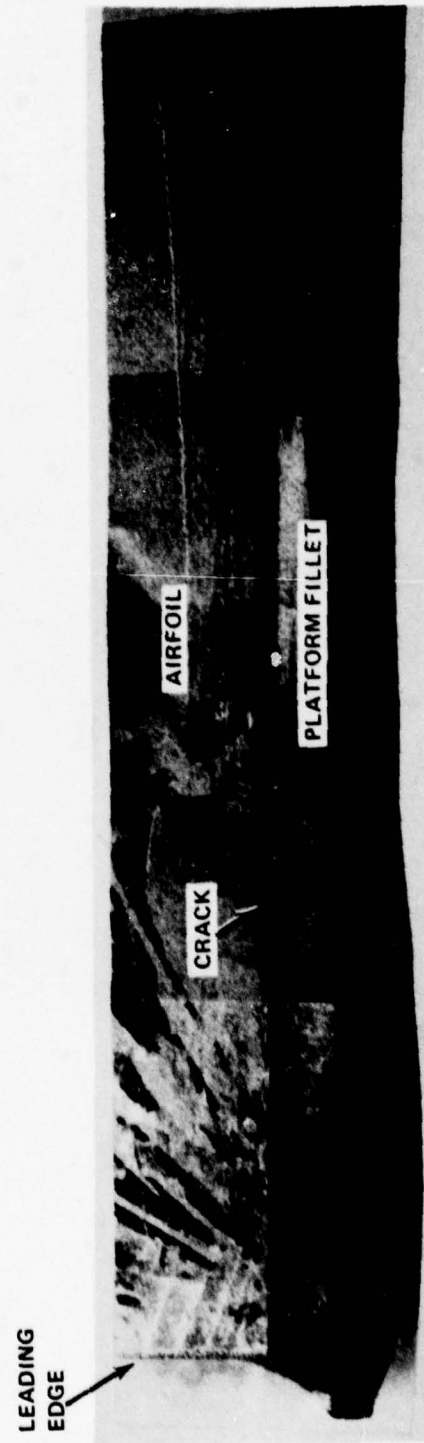


Figure 12-11 Convex (Suction) Surface of Blade E-169 as Removed from F111-D Aircraft



Figure 12-12 Concave (Pressure) Surface of Blade E-169 with 2nd Ply Layer Exposed

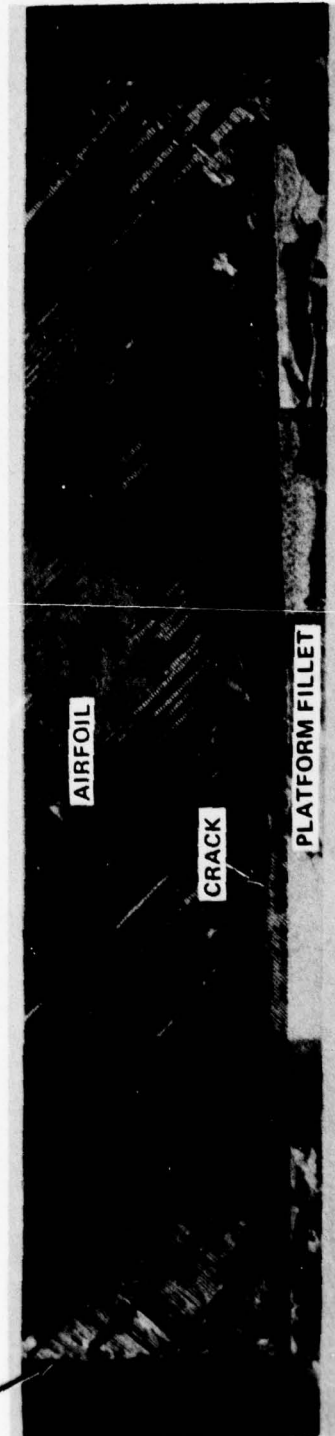
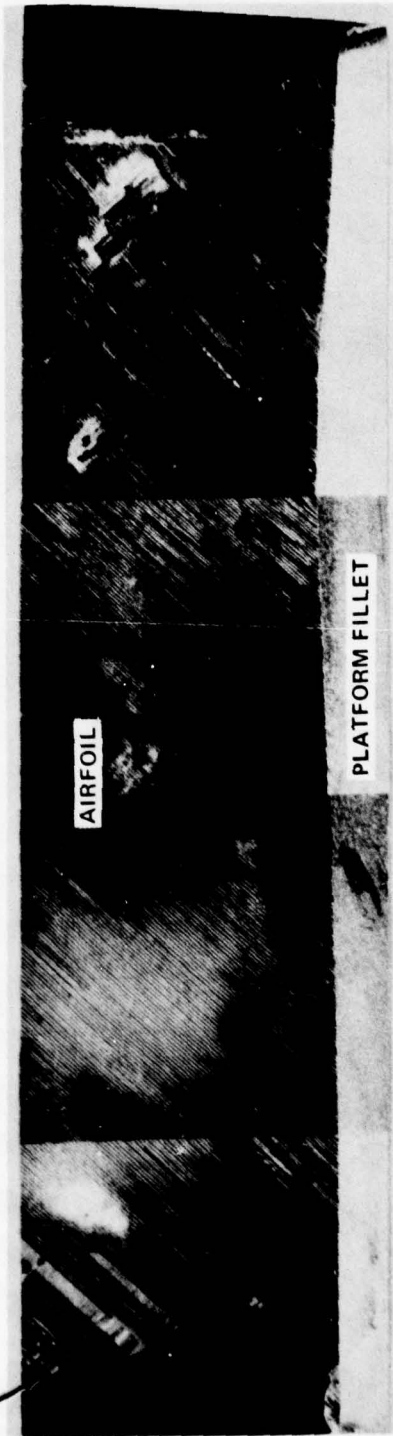


Figure 12-13 Convex (Suction) Surface of Blade E-169 with 2nd Ply Layer Exposed



*Figure 12-14 Concave (Pressure) Surface of Blade E-169 with 7th Ply Layer Exposed*

LEADING  
EDGE



*Figure 12-15 Convex (Suction) Surface of Blade E-169 with 7th Ply Layer Exposed*

## APPENDIX A

## BLADE MANUFACTURING LEARNING CURVE

The curve of Figure A-1 represents our blade manufacturing experience in this program. It is based on bonding blades individually, but finish machining them in lots of 12 each. The hump in the curve is a result of a root pad machining problem, which slowed down the blade manufacturing flow for several weeks.

The man-hours plotted represent ply cutting, detail machining, layup, bonding, finish machining, leading edge plating, and normal inspection. The raw material cost per blade was approximately \$300 throughout the life of the program.

No reliable production cost estimates are available at this time for future blades of this type.

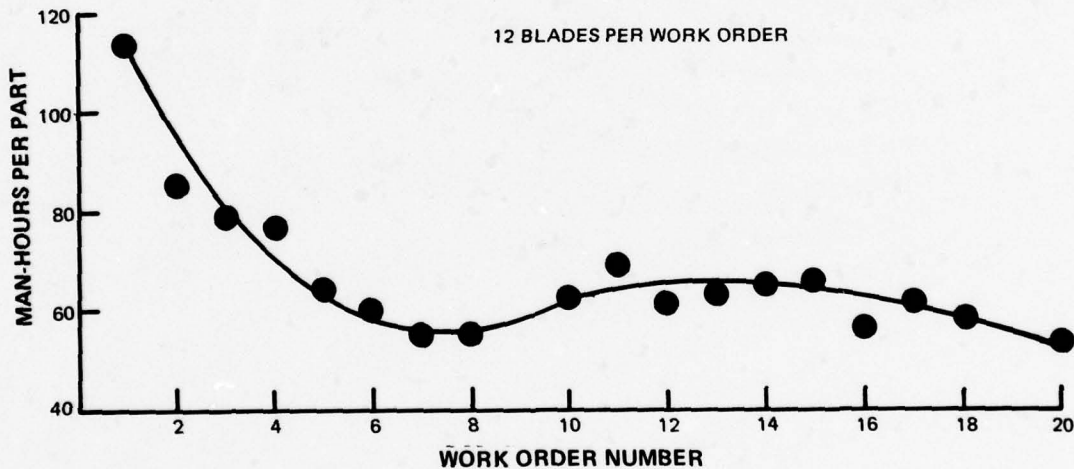


Figure A-1 Manufacturing Learning Curve for TF30P-9 3rd Stage BORSIC®/Aluminum Fan Blades

## APPENDIX B

### QUALITY CONTROL PLAN FOR TF30 COMPOSITE FAN BLADES

#### B.1 INTRODUCTION

Contract requirements included submission of a quality control plan prior to initiation of the flight program. The quality control plan described in this appendix evolved from those requirements, and was put into effect prior to the flight evaluation program described in Section 12 of this report. Basically, the plan incorporates all of the pertinent NDI procedures established during the Phase I blade development program; applied through approved P&WA "Production Delivery" procedures to meet production delivery standards. This means that all material and finished parts will be subjected to quality procedures equivalent to those employed for production items. Briefly, this entails release of all material by the Materials Control Laboratory (MCL) and certification that the finished parts are of flight quality by stamping them with the "Flying W" emblem.

Since no new blades were manufactured for the flight program (Section 12.2), the previously manufactured and tested blades must be reinspected by the Quality Control department to production delivery standards, with proper documentation of the results. Where certain in-process inspection procedures cannot be repeated, the previous laboratory inspection results will be reviewed and approved by the Quality Control department.

The material and blades previously manufactured for the ground engine test program were inspected for quality by the Materials Engineering and Research Laboratory (MERL), with the exception of X-ray, dimensional, and FPI. MERL will continue to perform this function, with the additional control of having the Quality Control department approve the procedures and equipment used, and witness the testing. Also, standard QC documentation of the test results will be generated.

Any significant deviations will be noted in an LDOW (Laboratory Deviation or Waiver) which must be signed off by Design, Materials Engineering, Production Engineering, and ASD before the material or part can be accepted.

The noncomposite adapting parts (3rd disk, 2-3 air seal, and blade locks) will utilize material released by MCL, and will be inspected to B/P requirements for dimensional control, surface finish, etc. In addition, the 3rd disks will be proofspun to 14,000 RPM (33% overspeed) as required on the drawing.

Blades that were fabricated earlier in the program will be placed on QR (Quality Review) and will be certified by that group prior to being incorporated into the flight hardware.

Enclosed are a description of the NDI techniques recommended for the blades, the fiber and tape material specifications PWA 437 and 438 and the NDI standards to be applied to the material and parts. These standards are equivalent to those followed in the ground engine test program.

In summary, the parts and material will meet or exceed the quality of those used in the ground engine test program; in addition, they will be subjected to standard P&WA production quality control methods.

## B.2 ESTABLISHMENT OF NDI PROCEDURES

The experience gained in developing reliable nondestructive inspection techniques for advanced composite materials and substantiated through bench and engine testing has resulted in the establishment of NDI procedures which fulfill the requirements of Item 3A, Phase II\* of Contract No. F33657-70-C-0624. The comprehensiveness of these techniques and procedures assures a high probability of detecting advanced composite blade defects which could adversely affect operating performance.

### B.2.1 Summary of Inspection Technique Evaluation

The following ten inspection techniques, having been thoroughly evaluated and proved effective, were incorporated into the established NDI procedures:

- 1 Airfoil ultrasonic C-scan inspection
- 2 Root ultrasonic C-scan inspection
- 3 Contact ultrasonic inspection (edges and fillet region)
- 4 Airfoil X-ray inspection
- 5 Natural frequency determination
- 6 Density determination
- 7 Fluorescent penetrant inspection
- 8 Dimensional inspection (on a random sampling basis)
- 9 115 percent speed proof spin test
- 10 Visual inspection

\*“The contractor shall complete the development of the NDI/quality control criteria initiated under Item 6A of Phase I of this work statement. Such effort shall establish NDI techniques and quality control criteria for production fan blades.”

Three additional inspection techniques were evaluated during the program, found to be deficient, and not recommended for use. They are:

- 1 Ultrasonic inspection with wheel units (more easily accomplished by C-scan techniques)
- 2 Electrical conductivity (provided local indication of volume percent of fiber, but this data was considered extraneous)
- 3 Acoustic emission (results could not be correlated with blade quality)

One other technique, eddy current inspection, has proved to be useful in detecting cracks in blades. Although not a production type technique, eddy current inspection is a valuable supplement to X-ray and visual inspection of fan blades during maintenance or service checks.

### **B.2.2 Recommended NDI Techniques**

The listed techniques are based on completed work which provides the experience for selecting the ten most effective NDI procedures. A discussion of the procedures and results of each is presented below.

#### **B.2.2.1 Airfoil C-Scan**

Using this technique, delamination and porosity flaws as small as about 0.25 inch diameter can be reliably detected.

The apparatus required, shown in Figure B-1, consists of a blade positioning system, a standard immersion tank, an automatic scanner, a data recording instrument, and an ultrasonic pulser/receiver which is the transducer and supplies the information to the data recorder in the form of an analog electrical signal.

In the blade positioning system used, a blade follower is placed in contact with a dummy or pattern so that it is perpendicular to the blade surface. The transducer is placed on the blade under inspection at the same relative location as the follower such that the sonic transmission is always perpendicular to the test specimen surface. The dummy blade is rotated and the rotation is transmitted through a timing belt to the blade under test. The resulting motion of the blade follower is transmitted to the transducer, thereby keeping the sonic waves perpendicular to the test blade surface. As each full rotation of the blade is completed, a carriage automatically indexes this follower and transducer forward on the blade.

The SIL transmitter used in this technique is 0.50 inch diameter while a 0.50 inch diameter SIL receiver, masked to .187 inch diameter, is used. The operating frequency is 2.25 MHz.

This inspection technique has exhibited the required resolution, in addition to having the advantages of being able to vary the sensitivity by varying recorder amplification and providing a permanent inspection record.

#### B.2.2.2 Root C-Scan

This inspection technique is used to ascertain that satisfactory bonds between the aluminum wedge and the composite, and the titanium alloy root pad and the composite have been achieved. In addition to detecting unbonded areas, it is also able to detect broken fibers at the wedge tip as well.

The equipment used is essentially similar to that described in the preceding section, Airfoil C-Scan. However, the SIL receiver is 0.25 inch diameter and is masked to a 0.06 inch diameter. The operating frequency is 5.0 MHz. Figure B-2 shows the equipment in use.

#### B.2.2.3 Contact Ultrasonic Through-Transmission

Although more time consuming and subject to operator interpretation, this method of inspection provides a comprehensive means of inspecting the blade leading edge, trailing edge and airfoil sections immediately adjacent to the root. It, like the C-scan technique, detects porosity, bond, and lamination defects.

The apparatus, shown in Figure B-3, consists of two 0.25 inch diameter ultrasonic transducers, each fitted with plastic adapters on the contact face. A strip chart recorder is also used to provide a permanent record of the inspection. The system operates at a frequency of 5 MHz. The transducers are placed in contact with and on opposite sides of the blade. Attenuation of the signal through the blade indicates the presence of a flaw.

#### B.2.2.4 Airfoil X-Ray

Radiographic inspection has demonstrated the capability to detect a single skewed fiber, cut fibers in a ten-ply build-up, a 0.375 inch diameter hole in a single ply of a 30-ply build-up, inclusions, matrix-rich areas, buckled fibers, and as few as five broken plies in the root and fillet areas. As such, it is the most powerful inspection tool used in the program.

The extra-sensitive radiographic techniques developed in this program include using extra fine grain film with high contrast and definition values, and positioning the airfoil relative to the X-ray beam so as to minimize geometric distortion. Kilovoltages were kept as low as practical to maximize subject contrast. Lead filters placed in front of the film in the film holder filtered out X-ray scatter which would be detrimental to radiographic sensitivity. Because of the varying thickness and complex geometry of the blades, eleven separate exposures were required to achieve maximum contrast and minimum distortion. A 14 inch x 17 inch film is used; magnifications as high as 20X are required to permit reliable radiographic inspection of the fibers.

#### B.2.2.5 Determining Natural Frequency

Measurement of blade natural frequency in first and second bending and first torsional modes is performed on all blades. This is done at low amplitudes on a shake table. All blades are evaluated relative to established values (first bending = 130 + 15 Hz, second bending<sub>min</sub> = 410 Hz, first torsional<sub>min</sub> = 850 Hz).

#### B.2.2.6 Density Measurement

Every part is weighed, and its volume determined by water displacement. The resulting average density calculation reveals the level of compaction attained in the pressing operation. The range of average density for all airfoils fabricated was 2.64 to 2.70 grams/cc. One hundred percent compaction would result in a density of approximately 2.70 grams/cc. An average density below 2.64 grams/cc is cause for rejection.

#### B.2.2.7 Fluorescent Penetrant Inspection (FPI)

The blades are fluorescent penetrant inspected using Magnaflux Corporation's ZL-30 penetrant (Zyglo). Only the root bearing surface region can be effectively examined by this method. The ends and the bottom of the root have exposed fibers which hold the penetrant, indicating defects when none exist.

#### B.2.2.8 Dimensional Inspection

Blade root form is inspection dimensionally by shadowgraph and other conventional means. Airfoils are dimensionally inspected by using a New England Plotter, which provides a 10X profile at any desired spanwise station.

#### B.2.2.9 Proof Spin Test

The established proof spin test for these blades consists of accelerating the blades individually to  $12,150 \pm 25$  rpm at room temperature in a vacuum spin pit five times.

The value of 12,150 rpm is slightly in excess of the required 115 percent of the redline speed for the TF30-P-9 fan (10,550 rpm).

#### B.2.2.10 Visual Inspection

Visual inspection, primarily in the root fillet area, is used to reveal local areas of poor compaction or surface fiber damage. Magnification of 10X - 20X is required for effective inspection.

The causes for rejecting engine test blades are summarized in Table B-I. The eight blades rejected for poor bonding were all deficient in the root region - no airfoils exhibited poor bonding or delamination. Figure B-4 shows an example of an extremely poor root bond readily detected by C-scan. The total acceptance rate for all blades was over 92 percent.

Table B-II presents the minor variations that occurred in density, frequency, and weight of the blades. These figures are based on the first engine set of 36 blades. Subsequent blade sets indicated a similar uniformity of end product.

PRATT & WHITNEY AIRCRAFT GROUP

TABLE B-I

**SUMMARY OF INSPECTION RESULTS**  
**TF30-P-9 Advanced Composite Third-Stage Fan Blades**

Total Number of Blades Fabricated	246
Number Accepted	227
Acceptance Rate	92.3%
Number Rejected	19
<i>Cause of Rejection</i>	
Inadequate Natural Frequency	4
Poor Bond (C-Scan Detected)	8
Cracks (X-Ray Detected)	1
Processing Errors	6

TABLE B-II

**VARIATION OF BLADE DENSITY, FREQUENCY, AND WEIGHT**  
**(Based on Engine Test Set No. 1 – 36 Blades)**

Parameter	Variation
Density	± 0.4 %
Frequency	
First Bending	± 3.6 %
Second Bending	± 3.4 %
First Torsional	± 2.9 %
Weight	± 1.9 %

### B.3 QUALITY CONTROL STANDARDS FOR TF30 COMPOSITE FAN BLADES

#### INTRODUCTION

Based on the experience gained from this program, the following QC standards have been established by P&WA and approved by USAF. These standards specifically apply to TF30 3rd stage flight quality blades, but can be extrapolated in general to future blades of other configurations, and ultimately to production blades. Obviously, some of the specific numbers quoted below may change depending on the material used or the specific blade design requirements; but in general the standards are considered to be applicable to any future B/Al fan blade.

##### 1. Material QC - Plasma Sprayed Tape

Material received in 5' x 15" sheets. Two tape tensile test per fiber lot in each sheet.

Minimum acceptable strength - 340 ksi (based on load/filament area).

Strength less than 340 ksi requires manufacture of 1½" x 4" x 10 layer panel.

Minimum average tensile strength of panel - 140 ksi (three tests).

100% inspection for:

Volume percent of fiber

Unbond - none allowed

Missing, crossed over, or broken fibers - none allowed

Wrinkled foil - none allowed

No. fibers per inch

Fiber diameter

Weight per unit area

Specification PWA 437 will apply.

##### II. Blade NDI

A. Natural frequency in 1B, 2B, 1T - specified on B/P.

B. Density - 2.64 g/cc minimum

C. FPI (root only) - no indications allowed

D. Root "C" scan -

1. 95% bond overall
2. No extensive indications at fillet

E. Airfoil "C" scan - no delaminations greater than ¼" diameter

F. X-ray -

1. No cracks, broken fibers, or inclusion up to 1" from fillet.
2. No cracks greater than  $\frac{1}{4}$ " in remainder of airfoil.

G. Proof Spin - Five cycles to 12,150 rpm.

H. Visual - no significant surface defects in the fillet area, as revealed by a 20x examination.

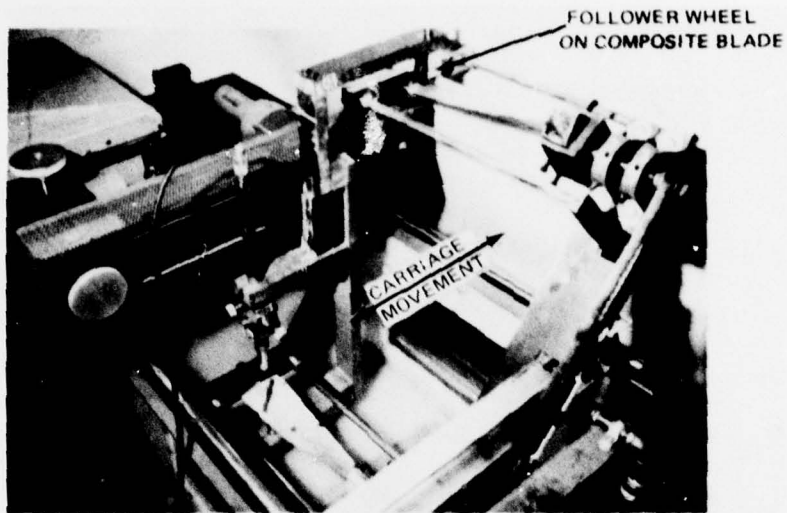


Figure B-1 Modified Fixture For Ultrasonic C-Scanning of Composite Airfoils

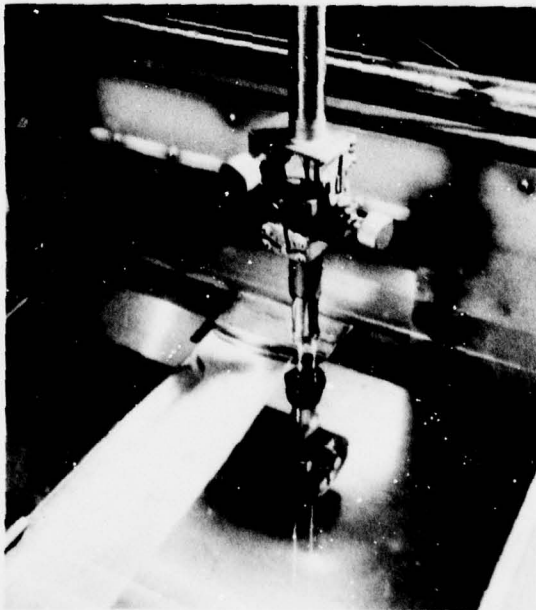


Figure B-2 Root Sections Ultrasonically Inspected by Through-Transmission Using  $\frac{1}{2}$ " Diameter Transmitter With  $\frac{1}{4}$ " Diameter Receiver Masked to  $\frac{1}{32}$ " Diameter. Operating Frequency is 5.0 MHZ.

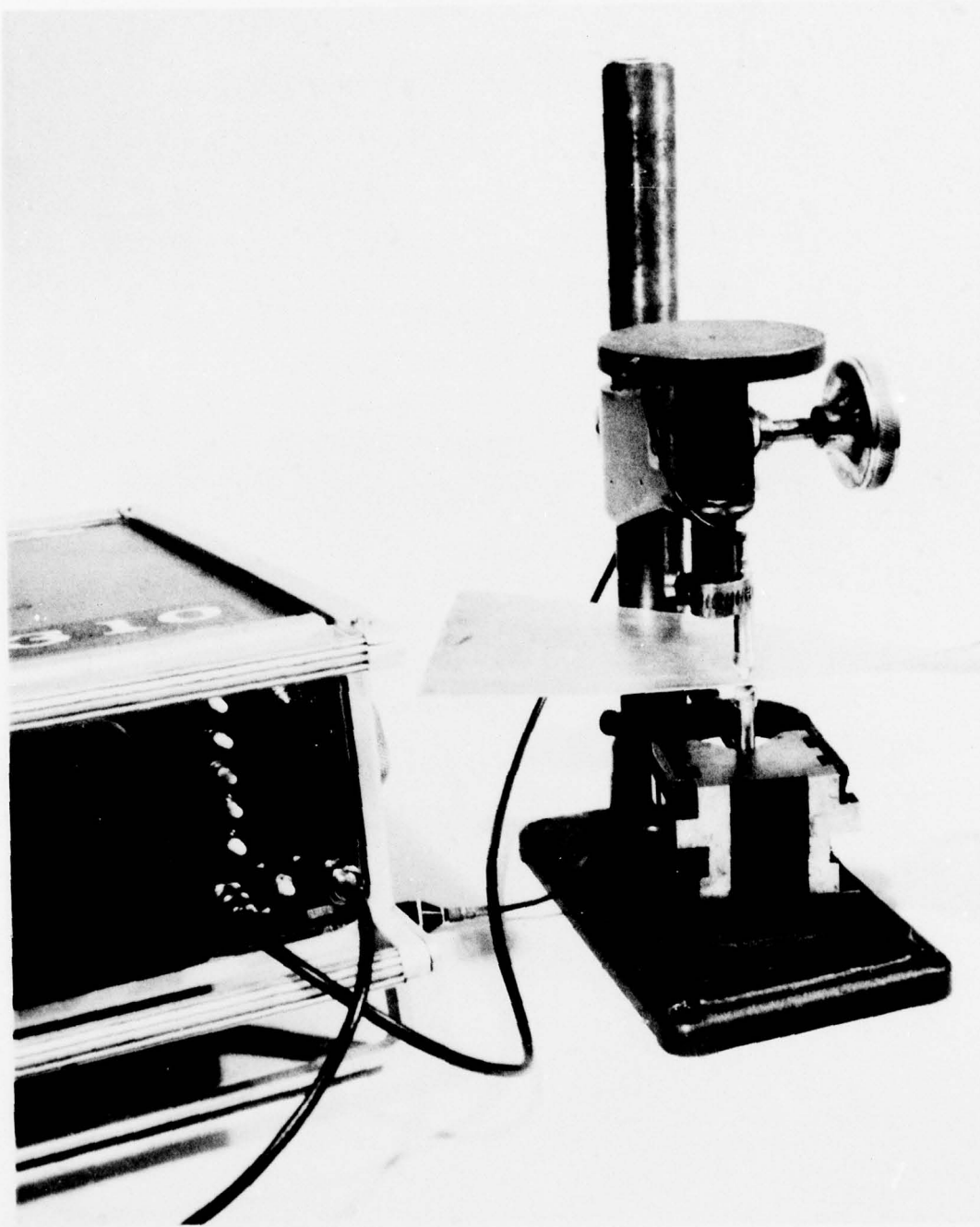


Figure B-3      *Areas Near Blade Leading Edge, Trailing Edge, and Adjacent to Root Are Inspected With This Ultrasonic Through Transmission Equipment*

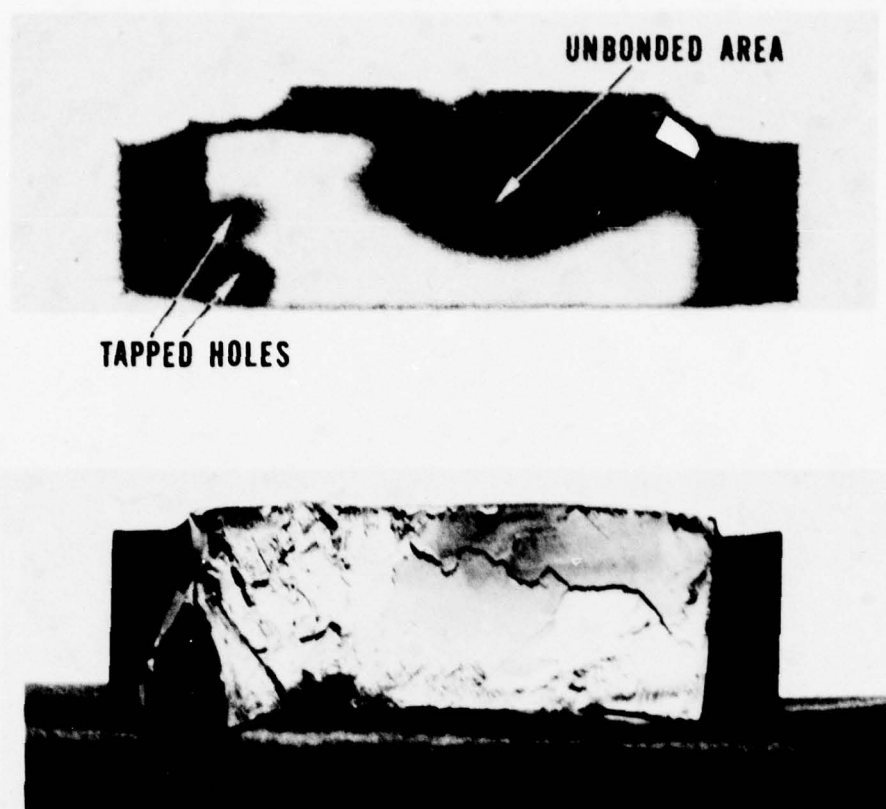


Figure B-4      *Example of Root Bond Defect Readily Detected By C-Scan Inspection*

Pratt &  
Whitney  
Aircraft

DIVISION OF UNITED AIRCRAFT CORPORATION

U  
AP&WA  
SPECIFICATION  
(DEVELOPMENT)

PWA 437

REVISION	D
ISSUED	5/20/69
REVISED	9/28/70

BORSIC<sup>®</sup> - ALUMINUM TAPE  
Silicon Carbide Coated Boron Filament - Aluminum Alloy Matrix

1. ACKNOWLEDGMENT: Vendor shall mention this specification number and its revision letter in all quotations and when acknowledging purchase orders.

2. PURPOSE: Primarily for compressor components operating up to 600 F.

3. TECHNICAL REQUIREMENTS: Unless otherwise specified:

3.1 Material:

3.1.1 Product shall be furnished as tape consisting of silicon carbide coated boron filaments, meeting the requirements of the latest issue of PWA 438-1, affixed to aluminum foil by procedures indicated by the following, as applicable.

3.1.1.1 When "PWA 437-1" is Specified on the Drawing: Fabrication shall be accomplished by plasma spraying using AA 6061 aluminum powder.

3.1.1.2 When "PWA 437-2" is Specified on the Drawing: Fabrication shall be accomplished by sandwiching between two sheets of AA 6061 aluminum foil and diffusion bonding.

3.1.2 Aluminum alloy matrix shall constitute 50  $\pm$  3 Vol % of the tape product, and shall conform to the composition listed in the latest issue of AMS 4025.

3.1.3 Tape shall be of uniform thickness and shall contain 175  $\pm$  5 equally spaced filaments per inch of width. Filaments shall be aligned so as not to intersect one another.

3.1.4 Filament splices shall be limited to 10 per 6 ft of tape length. No splice shall occur within 1 in. in any direction from any other splice.

3.1.5 Tape Width: Shall conform to the following:

Percentage of Shipment	Widths, in.	
	min	max
50	15	--
50	6	--

3.1.6 Tape Length: Not less than 5 feet.

3.1.7 Tape Weight: 0.210  $\pm$  0.005 g per sq. inch.

3.2 Properties: Each lot of tape shall conform to the following when tested by procedures agreed upon by purchaser and vendor.

3.2.1 Test Material: Tape representative of each lot shall be pressed into a ten layer, parallel filament, laminate under the following conditions:

Temperature:	1040 F $\pm$ 10
Vacuum:	10 <sup>-4</sup> Torr. or lower
Time and Pressure:	1.5 hr at 5000 psi

Code Ident No. 77445

THIS PAGE IS BEST QUALITY PRACTICABLE  
FROM COPY FURNISHED TO DDG

PWA	437
REVISION	D

3.2.2 Laminate Properties: Test specimens cut from material prepared as in 3.2.1 shall meet the following:

3.2.2.1 Tensile Strength, psi, min

Filaments parallel to applied load:	140,000
Filaments perpendicular to applied load:	9,000

3.2.2.2 Tensile Modulus, psi x 10<sup>6</sup>, min

Filaments parallel to applied load:	31.0
-------------------------------------	------

4. QUALITY:

4.1 The product shall be uniform in quality and condition, and free from foreign materials, knots, misalignment and from internal and external imperfections.

4.2 Visual standards shall be as specified on the purchase order.

5. CONTROL: Metallurgical control and control of shipments shall be in accordance with the latest issue of PWA 300.

6. IDENTIFICATION: Unless otherwise specified, each length of material shall be identified by attached removable tags using characters not less than 3/8 in. in height, which will not be obliterated by normal handling. Each tag shall be legibly marked to give the following information:

BORSIC®-ALUMINUM TAPE

PWA 437-D

PURCHASE ORDER NUMBER \_\_\_\_\_

MANUFACTURER'S IDENTIFICATION \_\_\_\_\_

QUANTITY OF TAPES \_\_\_\_\_

AREAS OF EACH TAPE, SQ FT \_\_\_\_\_

TAPE WEIGHT, g per sq inch \_\_\_\_\_

FILAMENT LOT NO. \_\_\_\_\_

FILAMENT DIA., mils \_\_\_\_\_

TENSILE STRENGTH, psi min \_\_\_\_\_

7. PACKAGING: Sheets of plasma sprayed or diffusion bonded material shall be protected during shipment and storage by interleaving with polyethylene liners not less than 0.004 in. in thickness and otherwise protected against permanent distortion and against damage from exposure to weather or any normal hazard. Plasma sprayed material when supplied in rolls shall be subject to these packaging requirements, and the diameter of each roll shall not be less than 10 inches.

8. APPROVAL:

8.1 Material shall be procured only from sources approved by Pratt & Whitney Aircraft Engineering Department.

8.2 Vendor shall use the same ingredients, manufacturing procedures, and methods of inspection for production material as for approved sample material. If necessary to make any change vendor shall obtain written permission from purchaser prior to incorporating such change.

9. REJECTIONS: Material not conforming to this specification or to authorized modifications will be subject to rejection.

Code Ident No. 77445

Pratt &  
Whitney  
Aircraft

DIVISION OF UNITED AIRCRAFT CORPORATION

P&WA  
SPECIFICATION  
(DEVELOPMENT)PWA 438  
REVISION A  
ISSUED 10/16/67  
REVISED 1/25/70

## FILAMENTS, BORSIC® AND BORON

1. ACKNOWLEDGMENT: Vendor shall mention this specification number and its revision letter in all quotations and when acknowledging purchase orders.
2. FORM: Filament consisting of boron deposited on tungsten wire approximately 0.0005 in. dia., and either coated with silicon carbide to a thickness not less than 0.0001 in. or uncoated, as designated by the following suffix numbers:

Suffix

1	coated	(Borsic®)
2	uncoated	(Boron)

3. APPLICATION: Primarily for structural reinforcement of plastic or metallic matrices.

4. TECHNICAL REQUIREMENTS:

- 4.1 Splices: Unless otherwise specified, minimum distance between splices shall be 1000 feet. Type and method of splicing shall be as agreed upon by purchaser and vendor.

- 4.2 Properties: Product shall be capable of meeting requirements of 4.2.1 and 4.2.2. Not less than 10 specimens from each production run shall be made available for test to determine conformance to 4.2.1 and 4.2.2. A production run shall consist of filament produced continuously by a single reactor.

- 4.2.1 Tensile Strength: Shall be determined statistically, testing to an acceptable quality level of 10.00.

- 4.2.1.1 Values shall be determined using a 1 in. gage length and a crosshead speed not exceeding 0.25 in. per minute.

- 4.2.1.2 Acceptability of filament testing shall be determined by the application of following formula to tensile test results as specified in NOTE 1.

$$K(K_1 \text{ or } K_2) = \frac{\bar{x} - 335,000}{v}$$

where  $\bar{x}$  = average tensile strength

v = the difference between the highest and lowest tensile strength values

NOTE 1

- a. Test 4 specimens. If "K" is 0.276 or greater, tensile properties are acceptable.
- b. If "K" is less than 0.276, 3 additional specimens shall be tested for tensile strength, and "K" for the 7 tests shall be determined. If this value is 0.266 or greater, tensile properties are acceptable.
- c. If "K" (determined for 7 tests) is less than 0.266, 3 remaining specimens shall be tested for tensile strength.

THIS PAGE IS BEST QUALITY PRACTICABLE  
FROM COPY FURNISHED TO DDC

PWA	438
REVISION	A

d. For the group of 10 tests, the first 5 specimens shall be placed in one group and  $K_1$  determined by the formula.  $K_2$  shall be determined for the other 5 specimens.  $K$  shall then be:

$$K = \frac{K_1 + K_2}{2}$$

e. If "K" for the entire group is 0.341 or greater, tensile properties are acceptable. If "K" is less than 0.341, production run has failed to meet the tensile strength requirements.

4.2.2 Modulus of Elasticity: Filament shall have minimum average modulus of elasticity of 55,000,000 psi. Modulus of elasticity shall be determined by stress-strain measurements of not less than 4 specimens taken from each production run. Specimens shall have gage length not less than 10 inches.

5. QUALITY: The filament shall be uniform in quality and condition, clean, and free from voids and foreign materials.

6. SIZE AND TOLERANCES: Unless otherwise specified, Boron filament diameter shall be 0.0039 in.  $\pm 0.0002$ , and Borsic<sup>®</sup> filament diameter shall be 0.00425 in.  $\pm 0.00015$ , as determined optically or by a method agreed upon by purchaser and vendor.

7. PACKAGING: Unless otherwise specified, filament shall be wound on spools and, when necessary, interleaved with paper. Winding shall be uniform and provide for proper unreeling. The spools shall be encased in suitable containers to protect the filament during shipment. Materials used for spools and packaging shall have no deleterious effect upon the product.

8. IDENTIFICATION: Unless otherwise ordered, each spool and container shall have a label or tag attached giving the purchase order number, material specification number, spool number, manufacturer's identification, and quantity in feet.

9. APPROVAL:

9.1 Material shall be procured only from sources approved by Pratt and Whitney Aircraft Engineering Department.

9.2 Vendor shall use the same manufacturing processes for production material as for approved sample material. If necessary to make any change in ingredients, finish or processing, vendor shall obtain written permission from Pratt and Whitney Aircraft Engineering Department prior to incorporating such change.

10. REJECTION: Material not conforming to this specification or to authorized modifications will be subject to rejection.

Code Ident No. 77445

## APPENDIX C

### PROGRAM REVIEWS

Paragraphs 11.3.1 and 11.3.2 of this document present the reports of Pratt & Whitney Aircraft and Air Force program reviews conducted in February and September 1973, respectively.

#### **P&WA REVIEW OF TF30 COMPOSITE FAN BLADE PROGRAM – FEBRUARY, 1973**

A BORSIC®/aluminum composite third stage TF30 fan blade has been under development on Air Force contract since 1970. Development has reached the point where a set of blades has successfully completed 100 hours of engine testing as part of a qualification program leading to eventual flight test in an F-111 aircraft. A review was requested to consider questions posed by the Air Force concerning suitability of the blades for flight test, adequacy of the engine ground test program for flight qualification and possible need for flight envelope restrictions or special flight test requirements.

#### **Conclusion**

If the composite blades successfully complete the presently planned FOD and engine test programs, with the additional tests noted in the recommendations, they should be qualified for flight test without restrictions or special requirements. With the recommended additional tests the engine test program would appear to cover adequately the blade stress and vibration exposure over the whole flight envelope.

#### **Recommendations**

To round out the flight envelope stress and vibration survey, the engine test program should be changed to include testing with inlet distortion and afterburner lighting at the sea-level dash and at the high altitude, low Mach No. (highest  $N_1/\sqrt{\theta_2}$ ) flight points. This testing is needed to check out 2E vibration and possible high speed flutter stresses.

It is recommended, for the flight hardware parts, that a full review be made of the in-process inspection which applies to the transition area from the titanium root block to the airfoil to improve the assurance of the boron fiber integrity in that region. Also, a review should be made of the post-spin inspection procedure of the transition area to assure that any defects caused or aggravated during spin are found and the parts rejected.

It is suggested that rig and engine tests be conducted to determine the blade tip rubbing characteristics.

It is also suggested that some FOD damaged blades with a blend repair equal to that allowed for comparable titanium blades be run in the engine during the "piggy-back" testing to check their survivability.

#### Discussion

The blade in question is a shroudless version of the TF30 P-9 third stage fan blade. It is 40% lighter than the B/M titanium blade. The airfoil is constructed of BORSIC®/aluminum plies, oriented radially in the core and  $\pm 45^\circ$  in the shell. The fibers are retained in a titanium root dovetail block by an aluminum wedge. The whole assembly is diffusion bonded together. Leading edge FOD protection is provided by a plated-on Ni/Co sheath. Maximum operating temperature is 450°F.

The evaluation program includes:

- Fabrication of 268 blades (36/set).
- Extensive bench testing of blades (including FOD).
- Development of NDI techniques.
- 680 hours of engine testing on 3 blade sets

- 100 hours subsonic (completed 1/11/73)
- 130 hours supersonic (sea level and altitude)
- 450 hours "piggyback" on routine TF30 testing.

The 100 hour engine test program just completed included:

- Stress surveys
- Performance calibrations
- 50 hour endurance
- Afterburner operation
- Distortion valve testing
- 19 surges

Bench testing included:

- Generation of blade Goodman diagram
- Titanium root tests

Salt corrosion  
Bending fatigue  
Thermal fatigue  
Combined stress fatigue  
Spin testing

Ni/Co leading edge tests

Bending fatigue  
Thermal fatigue  
Salt corrosion  
Ballistic impact  
Drop-weight test  
Spin pit erosion and FOD

Overspeed spin tests of all blades (120%  $N_1$ )  
Spin pit FOD tests with sand, gravel, 1" ice balls  
Blade NDI of various kinds.

Engine vibration surveys showed that the observed blade natural frequencies agreed reasonably well with predictions but were a little higher. Aside from surge, no stresses appeared to be of concern for the conditions tested. Surge stresses seemed to be similar to those for metal blades.

The most noticeable vibratory stresses occurred in 2E at about 5500 RPM and in a non-integral order (possibly flutter) at 10,000 RPM with distortion. This was about the maximum speed tested and stress was increasing with speed. It, therefore, seems essential to check the maximum speed encountered in flight (max.  $N_1/\sqrt{\theta_2}$ ), which occurs at high altitude and low flight Mach no., for the suspected flutter stress, and the high density sea-level dash point for maximum 2E stress. Both tests should include afterburner lighting and appropriate inlet distortion. If vibratory stresses are acceptable at these two conditions, the blade should be capable of flight testing over the whole aircraft flight envelope without restriction.

The major problem area which has been experienced to date in this blade and similar blading made under the ACE program is the transition from the titanium root block to the airfoil. It is suggested, for the flight hardware, that a full review be made of the in-process inspection of this area to assure the boron fiber integrity. Any minor errors in the ply layup prior to bonding could lead to fiber damage. Increased scrutiny of the manufacturing process at this stage of fabrication could possibly improve the reliability of the parts.

A similar review of the post-spin inspection procedure for the root transition area is also recommended to assure finding any defects caused or aggravated by the spin test.

PRATT & WHITNEY AIRCRAFT GROUP

With regard to FOD testing, it was felt that this is to some extent "one-shot" testing and that it would be desirable to see how damaged, but aerodynamically repairable, blades would survive in normal usage following FOD damage. It is recommended that some blades with a blend repair equal to that allowed for a comparable titanium blade be included in the "piggy-back" engine testing.

A further question arose concerning what happens when BORSIC®/aluminum blades rub the casing - whether this is a simple abrasive action or whether some detrimental reaction occurs in the blades. It is suggested that this be checked in a rig, preferably with strain-gaged blading, and then some long blades be installed in the test engine.

**Review Participants**

Reviewers:	L. Beckett	Advanced Tech. Programs
	A. Hiegel	FRDC Project
	W. Owczarski	MERL
	G. Parks	JT8 Project
	E. Sciegel	TF30 Project
	F. Smakula	Compressor Design
	R. Spaulding	Structures Design
	W. Doll	Chairman of Review Board

**Other Participants:**

K. Boll	Mechanical Components/Structures T&R
D. Randall	Composite Blade Program Manager
S. Blecherman	Advanced Tech. Programs
L. Friedrich	MERL
A. Alver	Structures T&R
G. Fulton	Structures T&R
R. Liss	Structures T&R
H. Stargardter	Structures T&R
R. Doak	Structures T&R
T. Kusnierz	Structures T&R

**AIR FORCE REVIEW OF TF30 COMPOSITE FAN BLADE INSPECTION RESULTS**

On September 27-28, 1973, the below listed Air Force personnel visited P&WA to review the NDI results on two sets of Borsic-aluminum fan blades which had undergone 564 hours of engine testing.

Matt Chopin	ASD
Will Taylor	ASD
Floyd Evans	F111 SPO
Ted Norbut	APL
John Rhodehamel	AFML
Lee Gulley	AFML
Bill Schulz	AFML

PRATT & WHITNEY AIRCRAFT GROUP

Set No. 1 had experienced 364 hours of sea-level testing including stress survey, distortion, performance, and 314 hours of endurance testing. Set No. 2 had experienced 200 hours of altitude testing, including a stress survey with and without distortion at sea-level Mn 1.2; 56,000 ft., Mn 2.2; and 33,000 ft. Mn 0.7; plus 130 hours of endurance; sea-level ram (10 hours) and Mn 2.2 56,000 ft. (120 hours)

The significant points established at the meeting were:

1. The engine test program established that the blade can operate throughout the entire flight envelope of the P9 engine with no limitations.
2. Blade natural frequencies, dimensional stability, and general appearance were excellent.
3. Twelve blades of Set No. 1 (364 hours, Tables X and Y) and 4 blades of Set No. 2 (200 hours) showed x-ray indications at the airfoil LE just above the root. These appear to be cracks, with a maximum length of 3/8 inch.
4. The effect of these apparent cracks on blade life is not known at this time. Past experience has shown that this composite material is not nearly as notch sensitive as titanium.
5. If blades of this type are to be evaluated in a flight program, we must be able to inspect the blades at intervals no greater than 200 hours, on the bench.
6. It would be very desirable to build up more ground engine test time on these blades to determine the significance of the LE cracks, and to approach more closely the current 750 TBO of the P9 engine.

In my judgement, the blades have demonstrated their structural integrity in a tough ground engine test program, and despite the x-ray indications are ready for service evaluation. The only stipulation I would require is to be able to inspect the blades at 200 hour intervals.

A thorough review of the x-ray results is now being conducted by NDI personnel (Frank Vicki), and a meeting is scheduled on Monday, October 22 to review these. It is recommended that no final decisions be made concerning the blades until that review is completed.

D. G. Randall

**Pratt & Whitney Aircraft Recommendation**

As a result of the preceding review sessions, a letter was written by Mr. W. G. Taylor, TF30 Program Manager, to Mr. P. Gagaris, ASD. This letter expressed the company's position concerning flight evaluation of the composite third-stage blades, and is reproduced below.

October 31, 1973

VIA: Naval Plant Representative  
Pratt & Whitney Aircraft  
400 Main Street  
East Hartford, Connecticut 06108

TO: United States Air Force  
Air Force Systems Command  
Aeronautical Systems Division  
Wright-Patterson Air Force Base  
Dayton, Ohio 45433

ATTENTION: SD-111KD (Mr. P. Gagaris)

SUBJECT: Borsic-Aluminum Fan Blade Program, Contract F33657-70-C-0624

REFERENCES: (a) Meeting of Air Force and P&WA personnel at East Hartford 9/27-9/28/73 concerning the subject program.  
(b) Telcon between Mr. M. Chopin, ASD, and Mr. W. G. Taylor, P&WA, 10/19/73.

1. The Reference (a) meeting included personnel from ASD, AFML, and F111 SPO. The purpose of the meeting was to review all inspection data on two sets of TF30-P-9 third stage Borsic-aluminum fan blades which had undergone a total of 564 hours of engine testing, both sea level and supersonic.
2. It was established at the meeting that several of the blades exhibited X-ray indications of small cracks, but were otherwise undamaged.
3. It is the contractor's judgment that the TF30-P-9 third stage Borsic-aluminum fan blade has reasonable structural integrity based on testing conducted to date and, as discussed in the reference (b) telephone conversation, is suitable for flight evaluation in an F-111 aircraft. However, in view of the presence of the X-ray indications noted above, the contractor recommends that if a flight evaluation is conducted the blades be inspected at 200 hour intervals to determine if these indications are progressing at an unacceptable rate.

UNITED AIRCRAFT CORPORATION

Pratt &amp; Whitney Aircraft Division

W. G. Taylor  
TF30 Program Manager

bbg

cc: Mr. M. Chopin - ASD  
ENJEA